REDUCED BIS(IMINO)PYRIDINE IRON AND MANGANESE COMPLEXES: ELECTRONIC STRUCTURE, REACTIVITY COMPARISONS AND SYNTHESIS OF AN IRON CARBENE

A Dissertation

Presented to the Faculty of the Graduate School

of Cornell University

In Partial Fulfillment of the Requirements for the Degree of

Doctor of Philosophy

by

Sarah Kathleen Russell

May 2011

REDUCED BIS(IMINO)PYRIDINE IRON AND MANGANESE COMPLEXES: ELECTRONIC STRUCTURE, REACTIVITY COMPARISONS AND SYNTHESIS OF AN IRON CARBENE

Sarah Kathleen Russell, Ph. D.

Cornell University 2011

The synthesis, electronic structures and reactivity of bis(imino)pyridine iron and manganese complexes were investigated. A series of dimeric bis(imino)pyridine iron dinitrogen compounds was prepared by reduction of the corresponding iron dihalide complexes with sodium naphthalenide. The dinitrogen compounds were shown to have electronic structures similar to the monomeric bis(imino)pyridine iron bis(dinitrogen) compound, (^{iPr}PDI)Fe(N_2). Evaluation of the catalytic olefin hydrogenation activity of the new dinitrogen compounds revealed a significant improvement in rate over (^{iPr}PDI)Fe(N_2), which was attributed to the smaller substituents on the bis(imino)pyridine aryl groups. The reactivity of the bis(imino)pyridine iron dinitrogen compounds with diazoalkanes was investigated. For all of the iron dinitrogen compounds, diazoalkane N-N bond cleavage was observed with monosubstituted diazoalkanes. Addition of diphenyldiazomethane to smaller bis(imino)pyridine iron dinitrogen compounds furnished bis(imino)pyridine iron carbene complexes. A combination of ^{1}H NMR, Mössbauer and X-ray absorption spectroscopies, SQUID magnetometry and X-ray diffraction was used to propose several possible electronic structures for the bis(imino)pyridine iron carbene complexes. The spectroscopic data most strongly supported an electronic structure having an intermediate spin iron(III) center and a one-electron reduced bis(imino)pyridine chelate. The bis(imino)pyridine iron carbene complexes underwent carbene transfer to carbon monoxide and aryl azides, but not

cyclopropanation or olefin metathesis reactions. The bis(imino)pyridine iron dinitrogen compounds were also found to be competent catalysts for carbon-carbon bond forming catalysis. Addition of ethylene to butadiene in the presence of 5 mol% iron catalyst resulted in a [2π + 2π] cycloaddition to furnish vinylcyclobutane, while addition of ethylene to isoprene under the same conditions resulted in 1,4-hydrovinylation to yield 5-methyl-1,4-hexadiene. Under similar reaction conditions, $[(^{Me}PDI)Fe(N_2)]_2(\mu_2\text{-}N_2)$ also catalyzed the cycloisomerization of 1,5-hexadiene. Finally, syntheses of variations of the bis(imino)pyridine iron dinitrogen compounds were investigated. Reduction of a bis(aldimino)pyridine iron dibromide did not afford an iron dinitrogen compound, but instead gave a diiron compound. Modeling variable temperature SQUID data for this compound provided experimental evidence for the redox activity of the bis(aldimino)pyridine ligand. The reduction of a bis(imino)pyridine manganese dichloride also did not afford a dinitrogen complex, but instead resulted in a bis(tetrahydrofuran) compound.

BIOGRAPHICAL SKETCH

Sarah Kathleen Russell was born and raised in Arlington Heights, Illinois. She attended South Middle School and Rolling Meadows High School where she developed an interest in science, particularly chemistry, through the guidance of several energetic teachers and the participation in Science Olympiad. After graduating high school in 2002, she moved to Northfield, Minnesota to attend Carleton College. At Carleton, Sarah had the opportunity to do research with Professor Gretchen Hofmeister, studying the kinetics of the titanium-catalyzed ring opening polymerization of lactide. Upon graduating from Carleton in 2006, she moved to Ithaca, New York to pursue her graduate studies at Cornell University. In December, 2006, she joined Paul Chirik's lab where she investigated the reduction of different bis(imino)pyridine metal compounds and the reactivity and electronic structure of a bis(imino)pyridine iron carbene complex.

My parents

&

My grandparents

ACKNOWLEDGMENTS

I would like to thank Prof. Paul Chirik for giving me the opportunity to develop my skills as a chemist and for providing direction to my chemistry when I was unsure of where it was going. I have learned a lot about chemistry and also a lot about myself these past four and a half years. Also, thank you to my committee members, Prof. Pete Wolczanski and Prof. Bruce Ganem for their insightful criticisms and knowledge. I would like to especially thank Pete, who through classes and lit lunch, has provided me with a solid foundation in inorganic chemistry and shown me how to be a critical scientist. Emil Lobkovsky and Thomas Weyhermüller, especially Emil, deserve credit for solving all of the crystal structures in this work. Thank you to Dave Wise for fixing all of my broken glassware, to Ivan Keresztes for help with my NMR questions and to Prof. Serena DeBeer for collecting XAS data.

There are several members of the Chirik group, both past and present, that I would like to thank. Doris was the person I could always go to with questions, and even though she was "not an iron person," she would always try to answer them and take the time to help. Thank you to Kevin for providing much-needed humor and for talking to me while at the rotovap. Jon Darmon has been a good friend since our days in the windowless box-of-an office; thank you for doing everything that no one else wanted to do. Thank you to Amanda for collecting data for me in Mülheim, to Chantal for collecting XAS data and to Carsten for helping with my attempts to model and interpret said data. To my boxmates – Crisita, Scott, David, Amanda and Brad – thank you for your knowledge and help over the years. Crisita deserves a special thank you for taking good care of our box and for always making me smile. I am lucky to have two awesome classmates, Aaron and Don. Thank you both for all the help throughout grad school – from early morning Chem 605 homework sessions to

being the “old people” in the lab. Finally, Aaron has been my best friend these past five years, I would not have made it here without him. Thank you for your help, your patience and the hot chocolates.

This thesis is dedicated to my family for their love and support over the years; I would not have gotten this far academically without them. My grandparents showed me the value of hard work and education, and were always there with hugs and words of encouragement. To my brothers, Eric and Colin, thank you for the phone calls and laughter. Thank you to my parents for their advice, comfort and support these past five years. Most importantly, thank you for the little pushes when I needed them and also for reminding me that there is a world outside of the lab.

TABLE OF CONTENTS

Chapter 2: N-N Bond Cleavage of Diazoalkanes by Bis(imino)pyridine Iron Dinitrogen Complexes

Chapter 3: Synthesis, Electronic Structure and Reactivity of Bis(imino)pyridine Iron Carbene Complexes

Chapter 4: Synthesis, Electronic Structure and Reactivity of Reduced Bis(aldimino)pyridine Iron Compounds

Chapter 5: Carbon-Carbon Bond Forming Reactions Catalyzed by Reduced Bis(imino)pyridine Iron Complexes

Chapter 6: Synthesis and Electronic Structure Investigation of Reduced Bis(imino)pyridine Manganese Complexes

LIST OF FIGURES

LIST OF TABLES

CHAPTER 1

SYNTHESIS AND REACTIVITY OF REDUCED ARYL-SUBSTITUTED BIS(IMINO)PYRIDINE IRON COMPOUNDS [*]

1.1 Abstract

A series of reduced bis(imino)pyridine iron complexes, $[(^{Ar}PDI)Fe(N_2)]_2(\mu_2\text{-}N_2)$ (^{Ar}PDI = 2,6-(*Ar*N=CMe)$_2C_5H_3N$; *Ar* = 2,6-Et_2-C_6H_3 (^{Et}PDI), 2,6-Me_2-C_6H_3 (^{Me}PDI), 2-^{i}Pr-6-Me-C_6H_3 ($^{iPr,Me}PDI$)) was prepared by treatment of the corresponding dihalide complexes with a catalytic amount of sodium naphthalenide under a dinitrogen atmosphere. The asymmetrically substituted bis(imino)pyridine iron dinitrogen compound, *rac/meso*-$[(^{Me,iPr}PDI)Fe(N_2)]_2(\mu_2\text{-}N_2)$ was also prepared under 1 atmosphere of N_2 using excess 0.5% sodium amalgam. The dinitrogen compounds were characterized using a combination of ^{1}H NMR, ^{13}C NMR and infrared spectroscopies and X-ray crystallography. Several neutral ligand compounds were also synthesized and the electronic structures established and compared to their previously reported diisopropyl bis(imino)pyridine iron counterparts. A bis(imino)pyridine iron olefin compound was prepared by reduction of *rac/meso*-($^{2\text{-}iPr}PDI)FeBr_2$ with two equivalents of 0.5% sodium amalgam in the presence of excess isoprene and characterized by NMR and Mössbauer spectroscopy. The newly prepared bis(imino)pyridine iron dinitrogen compounds and bis(imino)pyridine iron olefin compound were evaluated for the catalytic hydrogenation of olefins. All of reported compounds were found to be more active hydrogenation catalysts than the previously reported monomeric $(^{iPr}PDI)Fe(N_2)_2$ and allowed expansion of the scope of bis(imino)pyridine iron hydrogenation.

[*] Parts of this chapter have been taken from: Russell, S. K.; Darmon, J. M.; Lobkovsky, E.; Chirik, P. J. *Inorg. Chem.* **2010**, *49*, 2782-2792.

1.2 Introduction

The hydrogenation of olefins and ketones catalyzed by homogeneous transition metal compounds is one of the most well-studied and widely applied transformations in organic synthesis. Since Wilkinson's discovery of $(Ph_3P)_3RhCl$ over four decades ago,[1] precious metal catalysts based on rhodium, iridium and ruthenium have been widely studied and have resulted in several commercial processes for the synthesis of pharmaceuticals as well as fine and commodity chemicals.[2] The environmental and cost advantages of iron have renewed interest in using earth abundant elements as alternatives to precious metal catalysts for organic and commodity chemical synthesis.[3,4,5]

Aryl-substituted bis(imino)pyridine ligands have become popular since Brookhart's[6] and Gibson's[7] independent reports of ethylene and α-olefin polymerization with the methylaluminoxane (MAO) activated bis(imino)pyridine iron and cobalt dichlorides (^{R}PDI)$FeCl_2$ and (^{R}PDI)$CoCl_2$ (^{R}PDI = 2,6-(*Ar*N=CMe)$_2C_5H_3N$; *Ar* = 2,6-R_2-C_6H_3 (R = ^{i}Pr, Et, Me); 2,4,6-Me_3-C_6H_2, 2-R-C_6H_4 (R = ^{i}Pr, ^{t}Bu), etc.). In polymerization as well as several other organic transformations, the redox-activity of the bis(imino)pyridine chelate, defined as the ability to undergo reversible transfer of one to three electrons with the metal, appears to be a key ingredient for high activity catalysts.[8,9,10,11] This class of ligand has been used to support dinitrogen complexes of vanadium,[12] chromium,[13] cobalt[14,15] and ruthenium.[16]

In 2004, our laboratory reported the synthesis of the bis(imino)pyridine iron bis(dinitrogen) compound, (^{iPr}PDI)Fe$(N_2)_2$ (^{iPr}PDI = 2,6-(2,6-$^{i}Pr_2$-C_6H_3N=CMe)$_2C_5H_3N$) (Figure 1.1).[17] This pre-catalyst exhibits rich catalytic chemistry including the hydrogenation,[17,18] hydrosilylation[17] and [2π + 2π] cycloisomerization[19] of olefins and the hydrogen-mediated reductive cyclization of

enynes and diynes.[20] In all cases, substrate scope is limited and much work has been devoted to discovering improved version of the bis(imino)pyridine iron bis(dinitrogen) complex. Shortly thereafter, in 2006, our laboratory reported the synthesis of (^{iPr}BPDI)Fe(N_2)$_2$ (^{iPr}BPDI = 2,6-(2,6-^{i}Pr$_2$-C_6H_3N=CPh)$_2$$C_5H_3$N), where the imine methyl groups have been replaced by phenyl rings (Figure 1.1).[21] This complex showed improved catalytic hydrogenation activity compared to (^{iPr}PDI)Fe(N_2)$_2$; however, η^6-coordination of both the imine phenyl ring and the diisopropyl aryl group were identified as catalyst deactivation pathways, preventing (^{iPr}BPDI)Fe(N_2)$_2$ from being a viable catalyst.[21] Gambarotta and coworkers have subsequently reported the synthesis of a family of anionic iron dinitrogen complexes following treatment of (^{iPr}PDI)$FeCl_2$ with various amounts of NaH.[22]

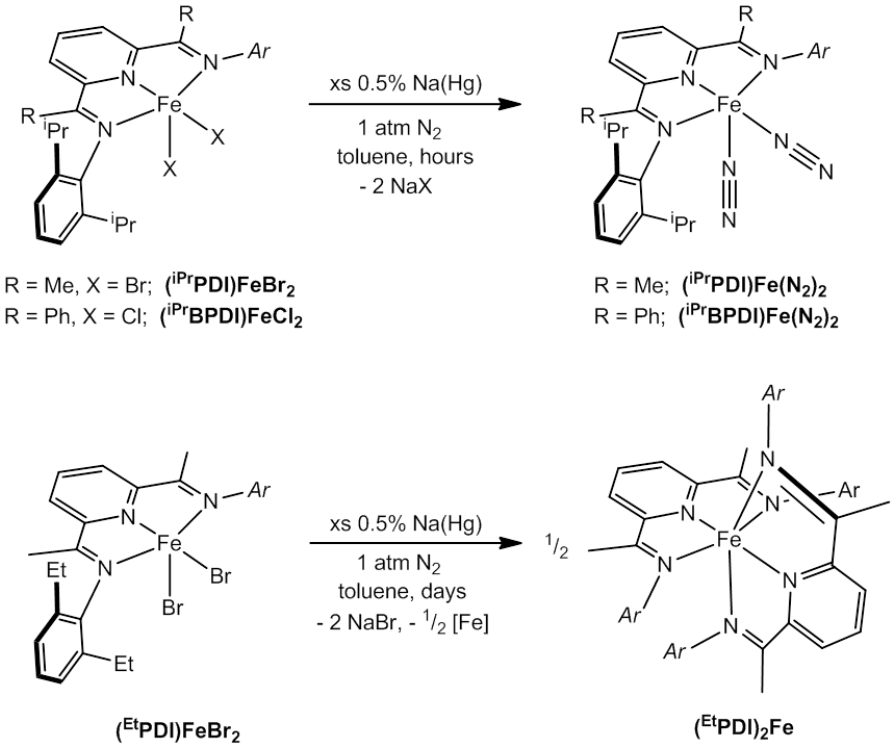

Figure 1.1 Sodium amalgam reduction of bis(imino)pyridine iron dihalides with varying degrees of steric protection.

One of the attractive features of bis(imino)pyridine ligands is their modularity and the ease with which new ligands can be accessed from the condensation of the appropriate amine or aniline with 2,6-diacetylpyridine.[23,24] This modularity offers a myriad of possibilities for new bis(imino)pyridine iron dinitrogen compounds with improved catalytic properties compared to (^{iPr}PDI)Fe(N_2)$_2$ and (^{iPr}BPDI)Fe(N_2)$_2$. Unfortunately, attempts to prepare bis(imino)pyridine iron dinitrogen compounds with smaller aryl groups or alkyl groups on the imine nitrogen have been unsuccessful.[25] Stirring (^{Et}PDI)$FeBr_2$ with excess 0.5% sodium amalgam under a dinitrogen atmosphere did not yield the desired dinitrogen complex. Instead, the catalytically inactive bis(chelate) iron species, (^{Et}PDI)$_2$Fe, was isolated. Similar outcomes were observed for alkyl-substituted bis(imino)pyridine and bis(oxazoline) iron complexes where sodium amalgam reduction of (^{R}APDI)$FeBr_2$ (^{R}APDI = 2,6-(R-N=CMe)$_2C_5H_3N$; R = C_6H_{11}, ^{i}Pr) or (^{iPr}Pybox)$FeCl_2$ also yielded bis(chelate) iron complexes, (^{R}APDI)$_2$Fe and (^{iPr}Pybox)$_2$Fe, respectively.[26]

1.3 Synthesis of Bis(imino)pyridine Iron Dinitrogen Compounds

Because the previously established reduction conditions (excess 0.5% sodium amalgam, toluene or pentane, 1 atm N_2)[17] used to synthesize (^{iPr}PDI)Fe(N_2)$_2$ yielded iron bis(chelate) complexes for bis(imino)pyridine iron dihalide compounds with aryl substituents smaller than 2,6-diisopropyl[25] (Figure 1.1), different reduction methods were studied in an effort to prepare new bis(imino)pyridine iron dinitrogen compounds. Stirring a THF slurry of (^{Et}PDI)$FeBr_2$ with 2 equivalents of sodium naphthalenide under a dinitrogen atmosphere for one hour furnished the iron dinitrogen complex, [(^{Et}PDI)Fe(N_2)]$_2$(μ_2-N_2) as dark green needles in modest (49%) yield. Unfortunately, the naphthalene byproduct was difficult to remove without concurrent decomposition of the iron dinitrogen compound. Because naphthalene was

both consumed and formed during the reduction, one alternative to removing excess naphthalene after the reduction was to reduce the amount used initially.

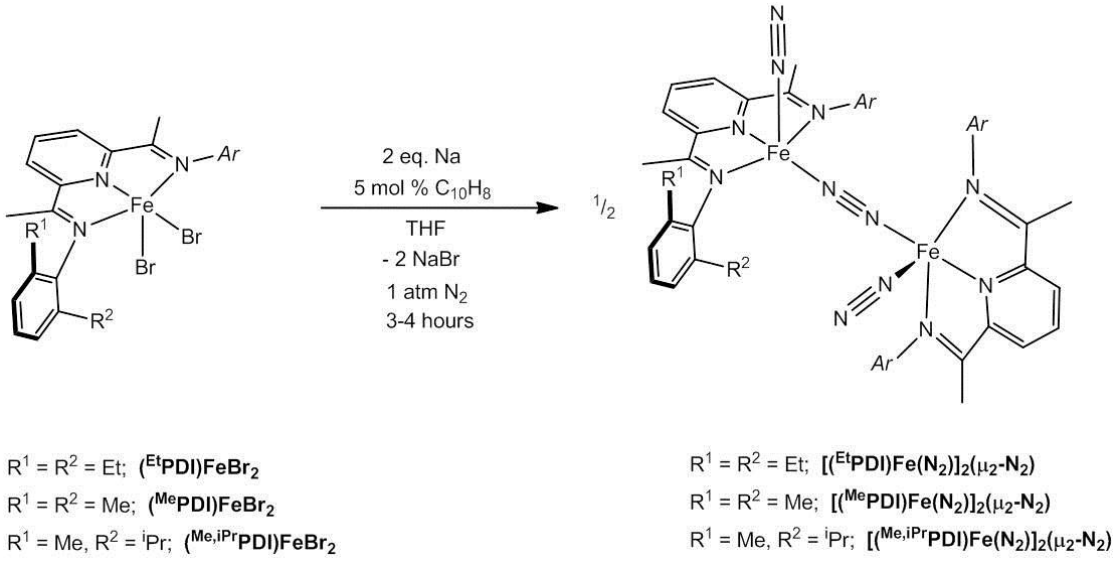

Figure 1.2 Synthesis of bis(imino)pyridine iron dinitrogen complexes by reduction with catalytic sodium naphthalenide.

Stirring a THF slurry of $(^{Et}PDI)FeBr_2$ with 2 equivalents of sodium and 5 mol% naphthalene under a dinitrogen atmosphere for 3 to 4 hours, followed by solvent removal, extraction into diethyl ether and recrystallization at -35°C produced $[(^{Et}PDI)Fe(N_2)]_2(\mu_2\text{-}N_2)$ in 61% yield. Similarly, reduction of $(^{Me}PDI)FeBr_2$ and *rac/meso*-$(^{Me,iPr}PDI)FeBr_2$ with 2 equivalents of sodium and catalytic naphthalene followed by recrystallization from diethyl ether furnished the corresponding iron dinitrogen compounds, $[(^{Me}PDI)Fe(N_2)]_2(\mu_2\text{-}N_2)$ and $[(^{Me,iPr}PDI)Fe(N_2)]_2(\mu_2\text{-}N_2)$, in 69% and 37% yield, respectively (Figure 1.2). Interestingly, the non-symmetrically substituted dinitrogen compound, $[(^{Me,iPr}PDI)Fe(N_2)]_2(\mu_2\text{-}N_2)$, was also prepared from reduction of *rac/meso*-$(^{Me,iPr}PDI)FeBr_2$ with excess 0.5% sodium amalgam in toluene

in moderate yields (43%) with no evidence for formation of the bis(chelate) compound.

Cámpora and coworkers have reported that (^{Me,iPr}PDI)$FeBr_2$ is isolated as a 9:1 mixture of *rac* and *meso* diasteromers.[27] This result suggests that the dinitrogen complex, [(^{Me,iPr}PDI)Fe(N_2)]$_2$(μ_2-N_2), is also a mixture of isomers. Because of line broadening, the ^{1}H NMR spectrum of the dinitrogen compound is uninformative in identifying the presence of isomers. Both infrared and Mössbauer spectroscopy provided spectra consistent with only one compound. Addition of excess carbon monoxide to a benzene-d_6 solution of [(^{Me,iPr}PDI)Fe(N_2)]$_2$(μ_2-N_2), isolated from either sodium naphthalenide or sodium amalgam reduction, resulted in observation of a 4:1 mixture of two isomers of the monomeric bis(imino)pyridine iron dicarbonyl compound, (^{Me,iPr}PDI)Fe$(CO)_2$. This result suggests that the dinitrogen compound exists as more than one isomer; however, the identity of the two isomers of (^{Me,iPr}PDI)Fe$(CO)_2$ could not be assigned based on ^{1}H NMR spectroscopy so it is unknown whether the *rac* isomer remains the major species and if epimerization takes place during reduction or upon the addition of carbon monoxide.

With the success of the sodium naphthalenide reduction conditions for smaller 2,6-substituted aryl bis(imino)pyridine iron compounds, a wider variety of substitutions on the chelate was explored. Unfortunately, for all other aryl-substitutions studied the reductions did not proceed cleanly and no dinitrogen compounds were isolated. Iron compounds containing bis(imino)pyridine rings with only a single *ortho*-substituent, such as *rac/meso*-($^{2\text{-}iPr}$PDI)$FeBr_2$ ($^{2\text{-}iPr}$PDI = 2,6-((2-^{i}Pr-C_6H_4)N=CMe)$_2C_5H_3N$) and *rac/meso*-($^{2\text{-}tBu}$PDI)$FeBr_2$ ($^{2\text{-}tBu}$PDI = 2,6-((2-^{t}Bu-C_6H_4)N=CMe)$_2C_5H_3N$), produced a mixture of unidentifiable products when subjected to both catalytic or stoichiometric sodium naphthalenide reduction conditions. Even the additional steric protection of a second tert-butyl group as in *rac/meso*-($^{2,5\text{-}}$

^{tBu}PDI)FeBr$_2$ ($^{2,5\text{-}tBu}$PDI = 2,6-((2,5-^{t}Bu$_2$-C$_6$H$_3$)N=CMe)$_2$C$_5$H$_3$N) did not aid in the formation of a dinitrogen compound. Similarly, reduction of iron compounds containing no ortho substituents on the aryl rings, such as (^{3,5Me}PDI)FeBr$_2$ (^{3,5Me}PDI = 2,6-((3,5-Me$_2$-C$_6$H$_3$)N=CMe)$_2$C$_5$H$_3$N) and ($^{4\text{-}OMe}$PDI)FeBr$_2$ ($^{4\text{-}OMe}$PDI = 2,6-((4-OMe-C$_6$H$_4$)N=CMe)$_2$C$_5$H$_3$N), resulted in intractable mixtures. Both alkyl substituted bis(imino)pyridine iron compounds that were studied, (^{iPr}APDI)FeBr$_2$ and (^{Cy}APDI)FeBr$_2$, also failed to yield dinitrogen compounds, instead forming the corresponding bis(chelate) complexes. All of the specific iron compounds that were studied are shown in Figure 1.3. These results suggest that the steric protection from the 2,6-substituents on the aryl rings of the bis(imino)chelate are important to the formation and stability of bis(imino)iron dinitrogen complexes when accessed by sodium naphthalenide reduction.

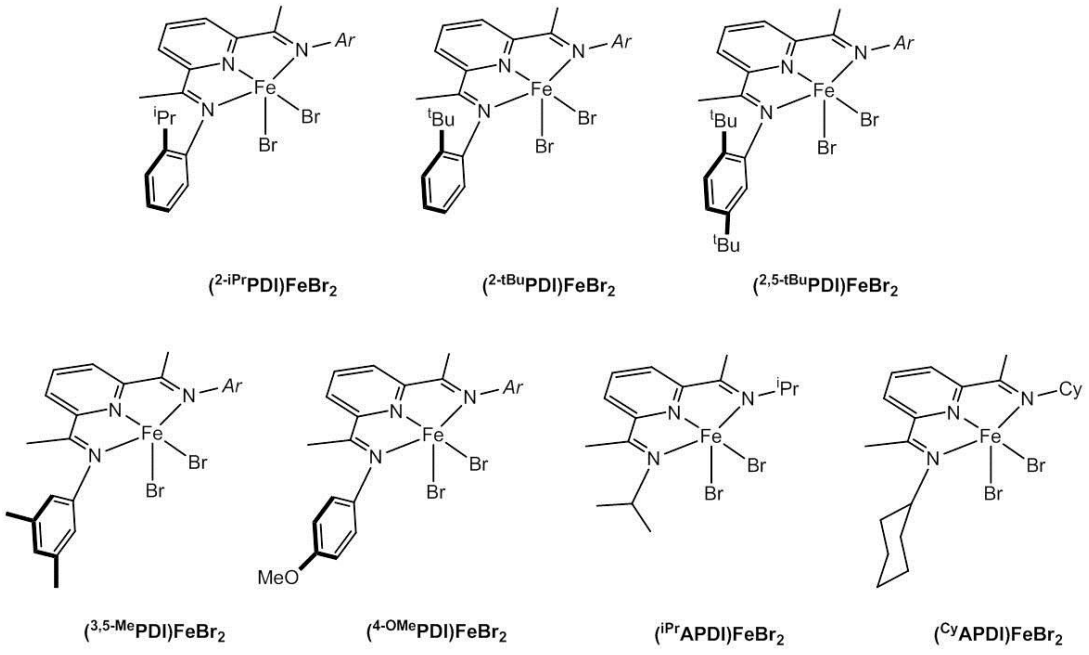

Figure 1.3 Aryl- and alkyl-substituted bis(imino)pyridine iron dibromides that failed to yield a dinitrogen compound upon sodium naphthalenide reduction.

All of the dimeric iron dinitrogen compounds exhibit very similar infrared spectra with relatively high stretching frequencies for the terminal dinitrogen ligands (Table 1.1). The symmetric and asymmetric stretching frequencies for the dimers are separated by only 15 to 20 cm^{-1}, considerably less than the 80 cm^{-1} separation for monomeric (^{iPr}PDI)Fe(N_2)$_2$. No stretches were identified that could easily be assigned to the bridging N_2 ligand which may be a result of a centrosymmetric structure in solution. Recently, Berry and coworkers reported the observation of the bridging N_2 stretch around 1856 cm^{-1} in [^{Me}PDI)Ru]$_2$(μ_2-N_2) compounds.[16]

Table 1.1 Infrared stretching frequencies of bis(imino)pyridine iron dinitrogen compounds recorded in a toluene solution.

Compound	**ν(N≡N) (cm^{-1})**
(^{iPr}PDI)Fe(N_2)$_2$	2122, 2058
[(^{Me,iPr}PDI)Fe(N_2)]$_2$(μ_2-N_2)	2099, 2084
[(^{Et}PDI)Fe(N_2)]$_2$(μ_2-N_2)	2101, 2086
[(^{Me}PDI)Fe(N_2)]$_2$(μ_2-N_2)	2102, 2085

Toepler pump experiments were conducted on [(^{Me}PDI)Fe(N_2)]$_2$(μ_2-N_2) and [(^{Et}PDI)Fe(N_2)]$_2$(μ_2-N_2) to quantify the amount of dinitrogen per molecule. Addition of $PbCl_2$ to [(^{Me}PDI)Fe(N_2)]$_2$(μ_2-N_2) yielded 2.9 equivalents of N_2 per two iron centers (97% of the expected total), indicating that the bulk of the sample contained dimers with three N_2 ligands and two iron centers. The same Toepler pump experiment for [(^{Et}PDI)Fe(N_2)]$_2$(μ_2-N_2) yielded only 2.6 equivalents of N_2 per two iron centers. Analysis of the sample by Mössbauer spectroscopy (*vide infra*) prior to addition of $PbCl_2$ showed a 9:1 mixture of dimers with 3 dinitrogen ligands and 1 dinitrogen ligand, respectively. With respect to this mixture, 93% of the expected total of N_2 gas was collected. The dinitrogen compound with 3 N_2 ligands, [(^{Et}PDI)Fe(N_2)]$_2$(μ_2-N_2), was also isolated exclusively, as evidenced by Mössbauer spectroscopy (*vide infra*).

The Toepler pump experiment for this particular sample yielded 2.9 equivalents of N_2 per two iron centers.

Although each dinitrogen compound is diamagnetic, the benzene-d_6 ^{1}H NMR spectra at 20 °C are broad and featureless. The methyl-substituted dinitrogen compound, [(^{Me}PDI)Fe(N_2)]$_2$(μ_2-N_2), displays the most informative ^{1}H NMR spectrum, allowing for peak assignment (Figure 1.4). The number of peaks consistent with a C_{2v} molecule was observed, indicating interchange of the bridging and terminal N_2 ligands on the NMR timescale. Notably, the resonance for the imine methyl group of this compound appears at 1.78 ppm, in contrast to the downfield value of 13.61 ppm observed for (^{iPr}PDI)Fe(N_2)$_2$.[17]

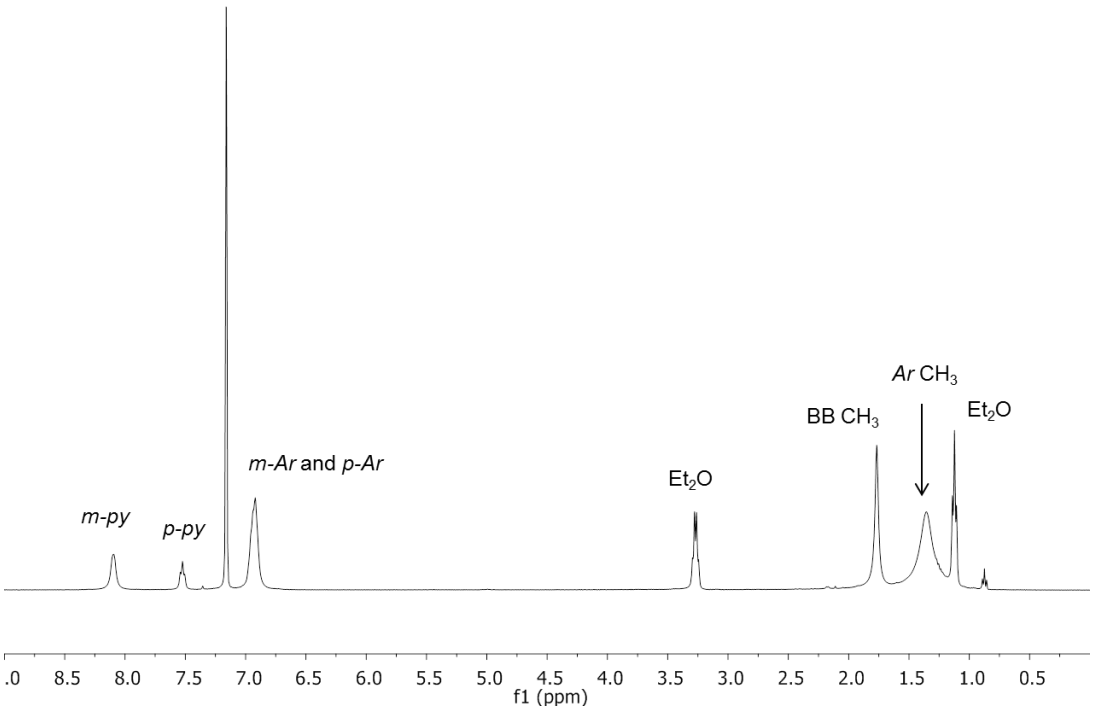

Figure 1.4 ^{1}H NMR spectrum of [(^{Me}PDI)Fe(N_2)]$_2$(μ_2-N_2) in benzene-d_6 at 20 °C.

The ^{1}H NMR spectra of [(^{Et}PDI)Fe(N_2)]$_2$(μ_2-N_2) and [(^{Me,iPr}PDI)Fe(N_2)]$_2$(μ_2-N_2) exhibit broader peaks and are less facile to assign than that of [(^{Me}PDI)Fe(N_2)]$_2$(μ_2-N_2). As with [(^{Me}PDI)Fe(N_2)]$_2$(μ_2-N_2), however, the resonances in each spectrum fall within the range from 0 ppm to 10 ppm in contrast to the 15 ppm range found for (^{iPr}PDI)Fe(N_2)$_2$.[17] The broadening of the ^{1}H NMR spectra is likely due in part to interchange of the terminal and bridging N_2 ligands on the NMR time scale through a fluxional process. Each iron center is five coordinate and can undergo a Berry pseudorotation, or similar process, which would exchange the axial and basal N_2 ligands.[28] When the spectra were collected under vacuum, all peaks disappeared suggesting that exchange of the terminal N_2 ligands with free N_2 molecules also occurs. Re-exposure to a dinitrogen atmosphere resulted in reappearance of the previously observed resonances, although with decreased intensities, suggesting that some decomposition occured.

Variable temperature ^{1}H NMR experiments were conducted on [(^{Et}PDI)Fe(N_2)]$_2$(μ_2-N_2) in benzene-d_6 (Figure 1.5, 20 to 70 °C) and toluene-d_8 (Figure 1.6, -60 to 20 °C). As the sample was cooled, the number of peaks increased which indicates inequivalency within the dimer. Peaks that can likely be assigned to the ethyl CH_2 groups of the aryl rings appear by -40°C, and the number of peaks assignable to methyl groups of the bis(imino)pyridine ligand increase and sharpen slightly. The peaks in the aromatic region also sharpen and separate from each other. Unfortunately none of the peaks sharpen enough such that coupling is observed. At higher temperatures, from 20°C to 80°C, the resonances for the bis(imino)pyridine also sharpen, though still not enough to observe any splitting.

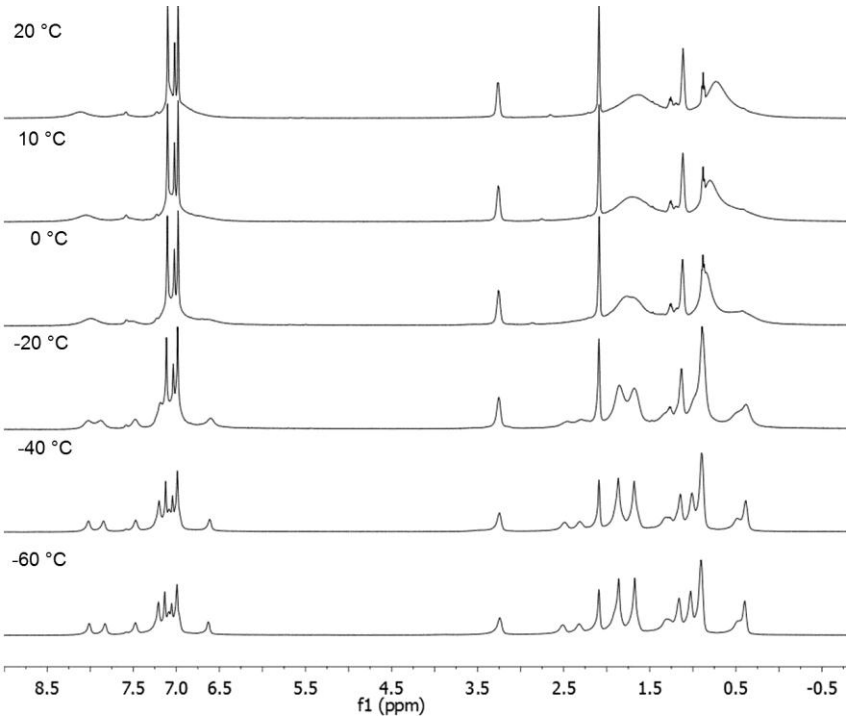

Figure 1.5 Variable temperature ^{1}H NMR of [(^{Et}PDI)Fe(N_2)]$_2$(μ_2-N_2) in benzene-d_6.

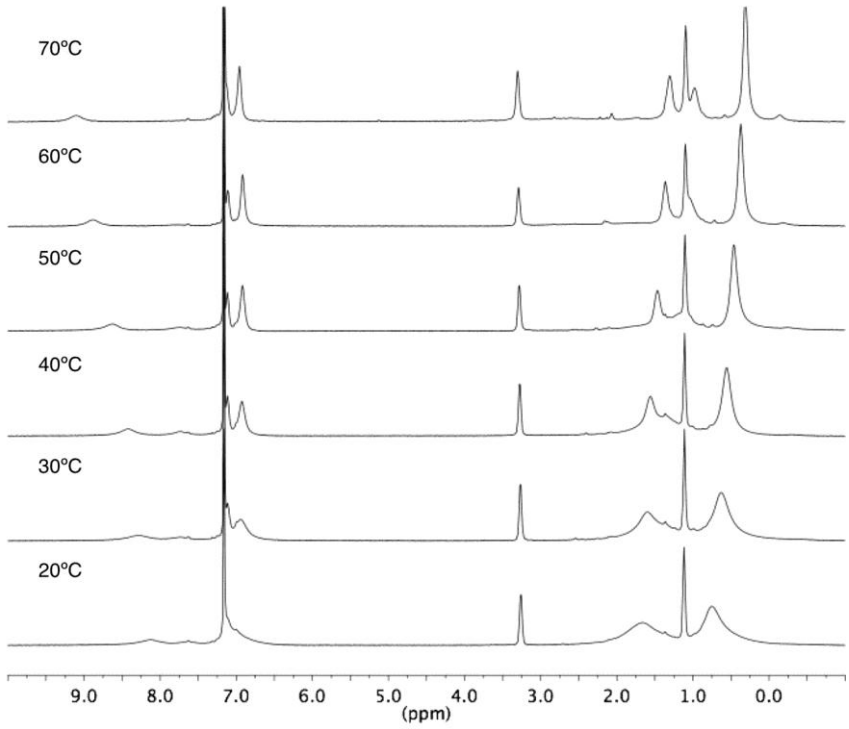

Figure 1.6 Variable temperature ^{1}H NMR of [(^{Et}PDI)Fe(N_2)]$_2$(μ_2-N_2) in toluene-d_8.

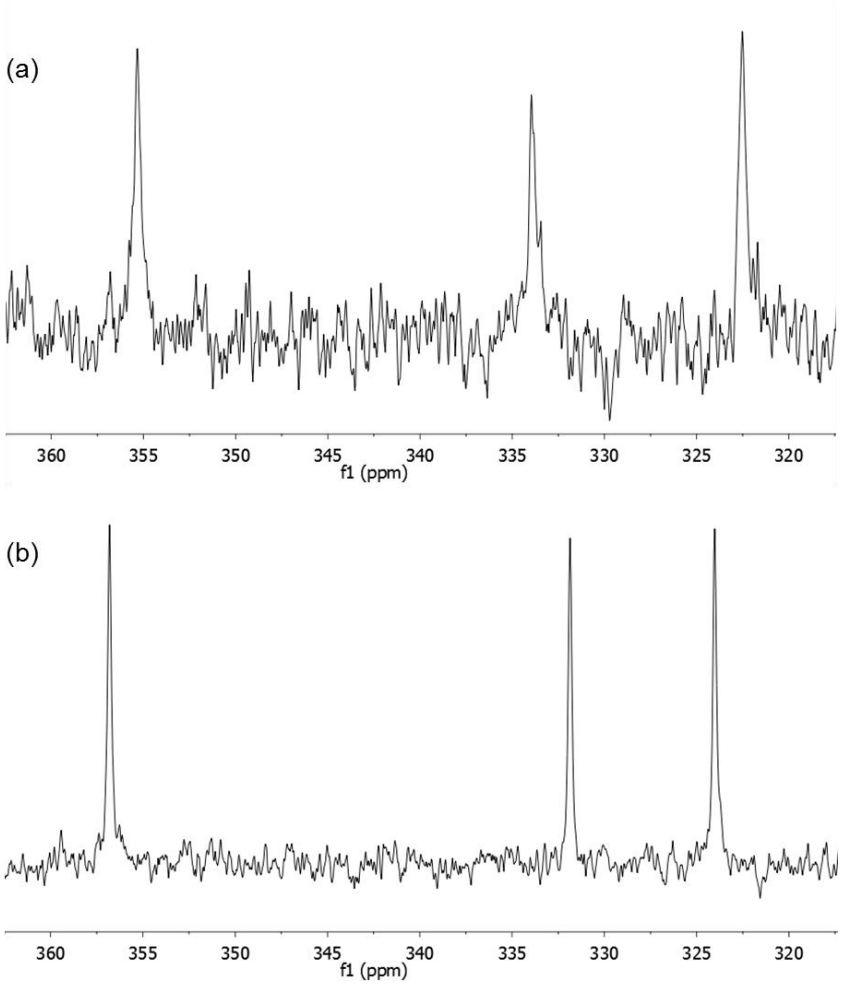

Figure 1.7 ^{15}N NMR spectra of (a) $[(^{Me}PDI)Fe(N_2)]_2(\mu_2\text{-}N_2)$ and (b) $[(^{Et}PDI)Fe(N_2)]_2(\mu_2\text{-}N_2)$ in toluene-d_8 at -80°C.

The new dinitrogen compounds were also investigated by ^{15}N NMR spectroscopy. Treatment of both $[(^{Me}PDI)Fe(N_2)]_2(\mu_2\text{-}N_2)$ and $[(^{Et}PDI)Fe(N_2)]_2(\mu_2\text{-}N_2)$ with excess $^{15}N_2$ gas in toluene-d_8 resulted in incorporation of $^{15}N_2$ into both the terminal and bridging positions of the dimers, providing further evidence for the lability of the dinitrogen ligands. The ^{15}N NMR spectra of $[(^{Me}PDI)Fe(N_2)]_2(\mu_2\text{-}N_2)$ and $[(^{Et}PDI)Fe(N_2)]_2(\mu_2\text{-}N_2)$ in toluene-d_8 were recorded at -80°C and each exhibited three broad singlets consistent with two terminal and one bridging dinitrogen ligand

(Figure 1.7). For [(^{Me}PDI)Fe(N_2)]$_2$(μ_2-N_2) the peaks appeared at -322.4, -334.2 and -355.5 ppm while for [(^{Et}PDI)Fe(N_2)]$_2$(μ_2-N_2) the peaks appeared at -324.1, -331.5 and -356.7 ppm. For comparison, the ^{15}N NMR spectrum of (^{iPr}PDI)Fe(N_2)$_2$ exhibits two broad singlets at -324.1 and -355.1 ppm. The lack of coupling information due to broadness prevents accurate assignment of the peaks; however, with respect to the shifts of (^{iPr}PDI)Fe(N_2)$_2$ it seems likely that the peaks centered around -324 and -355 ppm correspond to the terminal N_2 ligands. The broadening of peaks has previously been observed in phosphine-ligated iron dinitrogen compounds.[29] Like the ^{1}H NMR spectra, removal of the dinitrogen headspace resulted in disappearance of the peaks and exposure to $^{15}N_2$ allowed the peaks to again be observed.

In contrast to the previously isolated monomeric (^{iPr}PDI)Fe(N_2)$_2$, each of the new dinitrogen compounds were isolated as dimers. The ethyl-substituted compound, [(^{Et}PDI)Fe(N_2)]$_2$(μ_2-N_2), was crystallized from diethyl ether and characterized by X-ray diffraction (Figure 1.8). The metrical parameters for [(^{Et}PDI)Fe(N_2)]$_2$(μ_2-N_2) are reported in Table 1.2 along with the corresponding data of (^{iPr}PDI)Fe(N_2)$_2$[17] for comparison. The molecular geometry around each iron center in [(^{Et}PDI)Fe(N_2)]$_2$(μ_2-N_2) is best described as distorted square pyramidal with the bridging dinitrogen ligand occupying the apical position on one iron center and a basal position on the second iron center.

The iron-nitrogen bond distances of 1.929(3), 1.926(3), 1.923(3) and 1.932(3) Å for the Fe-N_{imine} bonds and 1.818(3) and 1.834(2) Å for the Fe-$N_{pyridine}$ bonds are indicative of a low or intermediate spin ferrous center.[30] The Fe-N distances to the bridging N_2 ligand are 1.873(3) and 1.879(3) Å, slightly longer than the Fe-N distances of 1.849(3) and 1.837(3) Å to the terminal N_2 ligands. The N-N bond distance of 1.137(3) Å for the bridging N_2 ligand shows little activation from coordination to two iron centers. The N_{imine}-C_{inime} distances of 1.328(4), 1.318(4),

1.328(4) and 1.331(4) Å are consistent with a two electron reduced chelate and are, with one exception, statistically indistinguishable from the corresponding distances in (^{iPr}PDI)Fe(N_2)$_2$. The C_{imine}-$C_{pyridine}$ distances of the dimer, 1.410(5), 1.406(4), 1.423(4) and 1.400(4) Å, are more contracted than in (^{iPr}PDI)Fe(N_2)$_2$ and are again consistent with two electron reduction of the chelate.

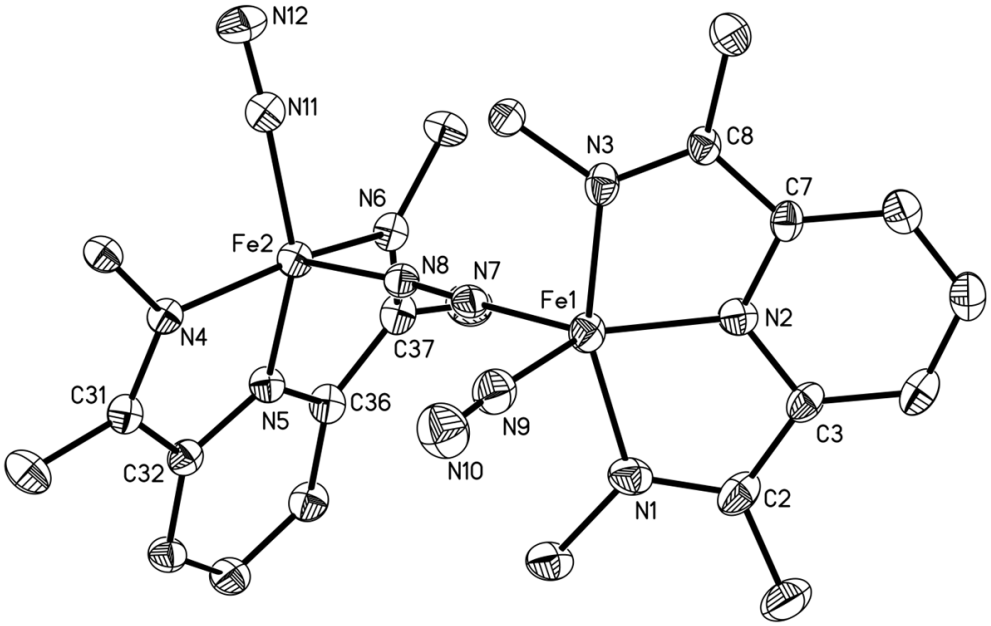

Figure 1.8 Solid state structure of [(^{Et}PDI)Fe(N_2)]$_2$(μ_2-N_2) at 30% probability ellipsoids. Hydrogen atoms and aryl groups omitted for clarity.

Table 1.2 Selected bond distances (Å) and angles (°) for $[(^{Et}PDI)Fe(N_2)]_2(\mu_2\text{-}N_2)$. The values for $(^{iPr}PDI)Fe(N_2)_2$ are included for comparison.[17]

	$[(^{Et}PDI)Fe(N_2)]_2(N_2)$	**$(^{iPr}PDI)Fe(N_2)_2$**
Fe(1)-N(1)	1.929(3)	1.9473(16)
Fe(1)-N(2)	1.818(3)	1.8362(14)
Fe(1)-N(3)	1.926(3)	1.9452(16)
Fe(1)-N(7)	1.873(3)	1.8800(19)
Fe(1)-N(9)	1.849(3)	1.8341(16)
Fe(2)-N(4)	1.923(3)	
Fe(2)-N(5)	1.834(2)	
Fe(2)-N(6)	1.932(3)	
Fe(2)-N(8)	1.879(3)	
Fe(2)-N(11)	1.837(3)	
N(1)-C(2)	1.328(4)	1.333(2)
N(3)-C(8)	1.318(4)	1.332(2)
N(4)-C(31)	1.328(4)	
N(6)-C(37)	1.331(4)	
C(2)-C(3)	1.410(5)	1.427(2)
C(7)-C(8)	1.406(4)	1.428(3)
C(31)-C(32)	1.423(4)	
C(36)-C(37)	1.400(4)	
N(2)-Fe(1)-N(7)	135.96(12)	159.09(8)
N(2)-Fe(1)-N(9)	130.21(13)	102.89(7)
N(7)-Fe(1)-N(9)	93.82(13)	98.02(8)
N(5)-Fe(2)-N(11)	149.01(12)	
N(5)-Fe(2)-N(8)	114.04(11)	
N(8)-Fe(2)-N(11)	96.95(12)	

The dinitrogen compounds were also studied by zero-field ^{57}Fe Mössbauer spectroscopy. Parameters for the dimeric dinitrogen compounds are given in Table 1.3 along with the parameters for (^{iPr}PDI)Fe(N_2)$_2$ and (^{iPr}PDI)FeN_2 for comparison.[17] In each case, a dimer with three N_2 ligands was cleanly isolated (Figure 1.9). The parameters for these compounds are all similar to the parameters for five-coordinate (^{iPr}PDI)Fe(N_2)$_2$ with isomer shifts (δ) between 0.37 and 0.39 mm/s and quadrupole splittings (ΔE_Q) between 0.49 and 0.53 mm/s. In the case of the ethylated bis(imino)pyridine compound, the dimer with only one bridging N_2 ligand was also observed. Dissolution of [(^{Et}PDI)Fe(N_2)]$_2$(μ_2-N_2) in diethyl ether followed by removal of solvent resulted in loss of some terminal dinitrogen ligands and observation of [(^{Et}PDI)Fe]$_2$(μ_2-N_2) as a mixture with [(^{Et}PDI)Fe(N_2)]$_2$(μ_2-N_2) (Figure 1.9). The parameters for [(^{Et}PDI)Fe]$_2$(μ_2-N_2) are consistent with the four coordinate dinitrogen compound, (^{iPr}PDI)FeN_2, with slightly lower isomer shifts and larger quadrupole splittings than their five-coordinate counterparts. The differences in the values of the quadrupole splittings are likely due to a change in electric field gradient arising from different ordering, and hence population, of the cloverleaf d-orbitals and the d_{z2} orbital between the two coordination numbers; however, additional spectroscopic and computational studies are required to support this assertion.

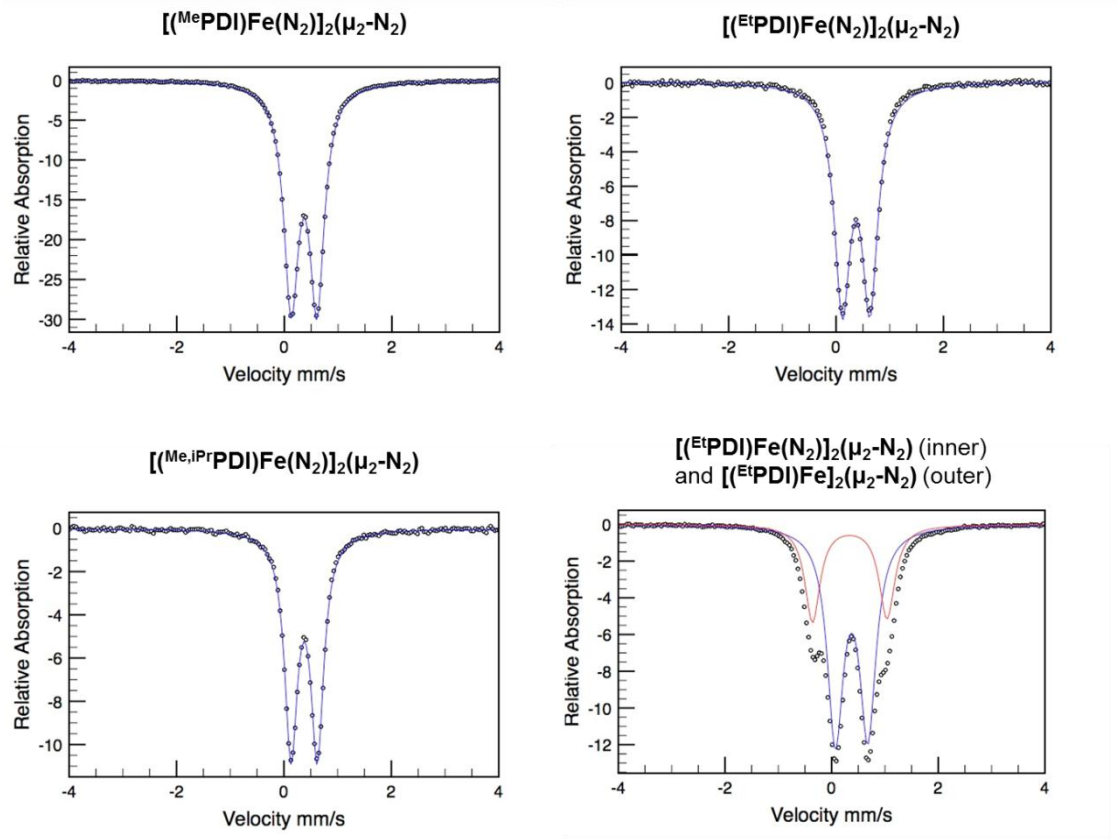

Figure 1.9 Zero-field ^{57}Fe Mössbauer spectra of dimeric bis(imino)pyridine iron dinitrogen compounds collected at 80K.

Table 1.3 Zero-field ^{57}Fe Mössbauer parameters for bis(imino)pyridine iron dinitrogen complexes. Values for (^{iPr}PDI)Fe(N_2)$_2$ and (^{iPr}PDI)FeN_2 taken from reference 17.

Compound	δ (mm/s)	ΔE_Q (mm/s)
(^{iPr}PDI)Fe(N_2)$_2$	0.39	0.53
(^{iPr}PDI)Fe(N_2)	0.38	1.72
[(^{Et}PDI)Fe(N_2)]$_2$(μ$_2$-N_2)	0.37	0.51
[(^{Et}PDI)Fe]$_2$(μ$_2$-N_2)	0.33	1.50
[(^{Me}PDI)Fe(N_2)]$_2$(μ$_2$-N_2)	0.37	0.49
[(^{Me,iPr}PDI)Fe(N_2)]$_2$(μ$_2$-N_2)	0.38	0.49

For both the dimers with five-coordinate and four coordinate iron centers, the Mössbauer parameters are consistent with intermediate spin iron(II) complexes.[9b,30] Together with the bond distances from the crystal structure of $[(^{Et}PDI)Fe(N_2)]_2(\mu_2\text{-}N_2)$, these parameters establish an electronic structure of a doubly reduced bis(imino)pyridine chelate ($S_{PDI} = 1$) antiferromagnetically coupled to an intermediate spin Fe(II) ($S_{Fe} = 1$) for each half of a dimer, giving an overall $S = 0$ compound. The similarity of electronic structures between the dimeric and monomeric dinitrogen compounds implies that the dimerization occurs due to the reduced steric protection of the iron center as the substituents of the aryl rings are decreased.

1.4 Reactivity of Dimeric Bis(imino)pyridine Iron Dinitrogen Compounds

The reactivity of the dimeric bis(imino)pyridine dinitrogen compounds with several neutral ligands was studied to compare the electronic structures of the resulting bis(imino)pyridine iron compounds with the corresponding known isopropyl substituted compounds. The diisopropyl bis(imino)pyridine iron N,N-dimethyl-4-aminopyridine compound, (^{iPr}PDI)Fe(DMAP) has been well characterized and studied.[9b] Therefore, the analogous compounds of the smaller PDI ligands were synthesized. Addition of one equivalent of DMAP to $[(^{Et}PDI)Fe(N_2)]_2(\mu_2\text{-}N_2)$ in diethyl ether followed by solvent removal furnished red-brown solid (^{Et}PDI)Fe(DMAP) in quantitative yield. Similarly, (^{Me}PDI)Fe(DMAP) was synthesized from addition of one equivalent of DMAP to $[(^{Me}PDI)Fe(N_2)]_2(\mu_2\text{-}N_2)$ (Figure 1.10).

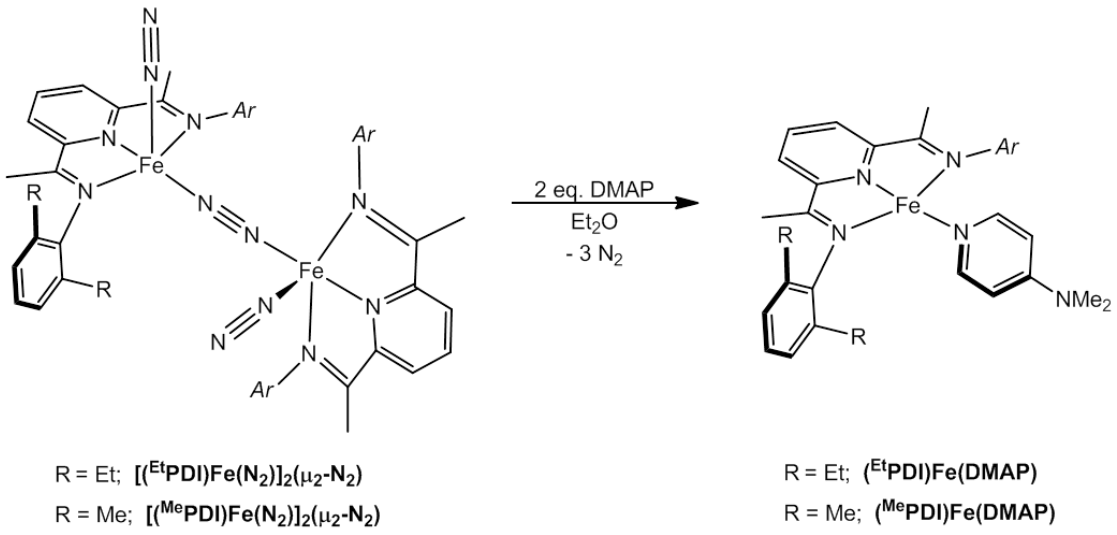

Figure 1.10 Synthesis of (^{Et}PDI)Fe(DMAP) and (^{Me}PDI)Fe(DMAP) from the corresponding bis(imino)pyridine iron dinitrogen compounds.

Like (^{iPr}PDI)Fe(DMAP), both (^{Et}PDI)Fe(DMAP) and (^{Me}PDI)Fe(DMAP) exhibit features consistent with temperature independent magnetism in their ^{1}H NMR spectra. The imine methyl group resonances of (^{Et}PDI)Fe(DMAP) and (^{Me}PDI)Fe(DMAP) appear at -5.59 and 5.79 ppm while the *meta*-pyridine resonances are shifted upfield to 12.06 and 11.94 ppm, respectively. The corresponding values for (^{iPr}PDI)Fe(DMAP) are -5.85 and 12.42 ppm.[9b] The only notable difference between the bis(imino)pyridine iron N,N-dimethyl-4-aminopyridine compounds by ^{1}H NMR spectroscopy is that the resonances for the DMAP hydrogens and the in-plane hydrogens of the chelate are broadened for (^{Et}PDI)Fe(DMAP) and (^{Me}PDI)Fe(DMAP), suggesting that a smaller steric environment around the iron center allows movement of the DMAP ligand in solution.

Zero-field ^{57}Fe Mössbauer spectroscopy was also used to study the electronic structures of (^{Et}PDI)Fe(DMAP) and (^{Me}PDI)Fe(DMAP). Representative spectra are presented in Figure 1.11 and the corresponding parameters are reported in Table 1.4

along with those of (^{iPr}PDI)Fe(DMAP)[9b] for comparison. As expected from the similarities in the ^{1}H NMR spectra, the three bis(imino)pyridine iron N,N-4-dimethylaminopyridine compounds all have similar Mössbauer parameters. As the steric bulk of the aryl groups decreases from isopropyl to methyl groups, the isomer shift (δ) decreases from 0.31 mm/s to 0.27 mm/s and the quadrupole splitting (ΔE_Q) increases from 1.94 mm/s to 2.24 mm/s, respectively. The similarities between the Mössbauer parameters of (^{Et}PDI)Fe(DMAP), (^{Me}PDI)Fe(DMAP) and (^{iPr}PDI)Fe(DMAP) suggest that the electronic structures of (^{Et}PDI)Fe(DMAP) and (^{Me}PDI)Fe(DMAP) are best described as intermediate spin iron(II) center antiferromagnetically coupled to a triplet bis(imino)pyridine chelate.[9b]

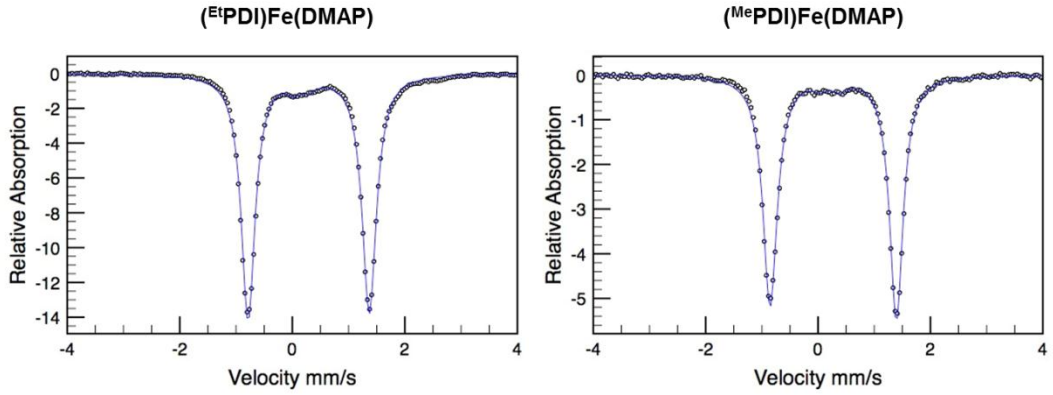

Figure 1.11 Zero-field ^{57}Fe Mössbauer spectra of (^{Et}PDI)Fe(DMAP) and (^{Me}PDI)Fe(DMAP).

Table 1.4 Zero-field ^{57}Fe Mössbauer parameters for (^{iPr}PDI)Fe(DMAP)[9b], (^{Et}PDI)Fe(DMAP) and (^{Me}PDI)Fe(DMAP).

Compound	δ (mm/s)	ΔE_Q (mm/s)
(^{iPr}PDI)Fe(DMAP)	0.31	1.94
(^{Et}PDI)Fe(DMAP)	0.29	2.15
(^{Me}PDI)Fe(DMAP)	0.27	2.24

The bis(imino)pyridine iron tetrahydrofuran complex, (^{Et}PDI)Fe(THF), was prepared to verify that it is not present as an impurity in the dinitrogen compound, [(^{Et}PDI)Fe(N_2)]$_2$(μ_2-N_2). Stirring [(^{Et}PDI)Fe(N_2)]$_2$(μ_2-N_2) in a 2:1 pentane/THF mixture for 10 minutes followed by removal of the solvent afforded (^{Et}PDI)Fe(THF) as a red-brown powder. As expected for a bis(imino)pyridine iron compound with a weak field neutral ligand, the ^{1}H NMR spectrum of (^{Et}PDI)Fe(THF) exhibits contributions from temperature independent paramagnetism.[30] The imine methyl peak is shifted upfield to -6.32 ppm while the *meta*-pyridine peak is shifted downfield to 12.36 ppm. Integration of the ^{1}H NMR resonances indicates that (^{Et}PDI)Fe(THF) contains only one coordinated THF ligand. The THF compound was also studied by zero-field ^{57}Fe Mössbauer spectroscopy (Figure 1.12) and the quadruopole splitting (ΔE_Q) value of 2.04 mm/s is consistent with a four-coordinate iron center (see Tables 1.3 and 1.4). The isomer shift (δ) of 0.39 mm/s suggests that (^{Et}PDI)Fe(THF) has a similar electronic structure to the dinitrogen compounds.

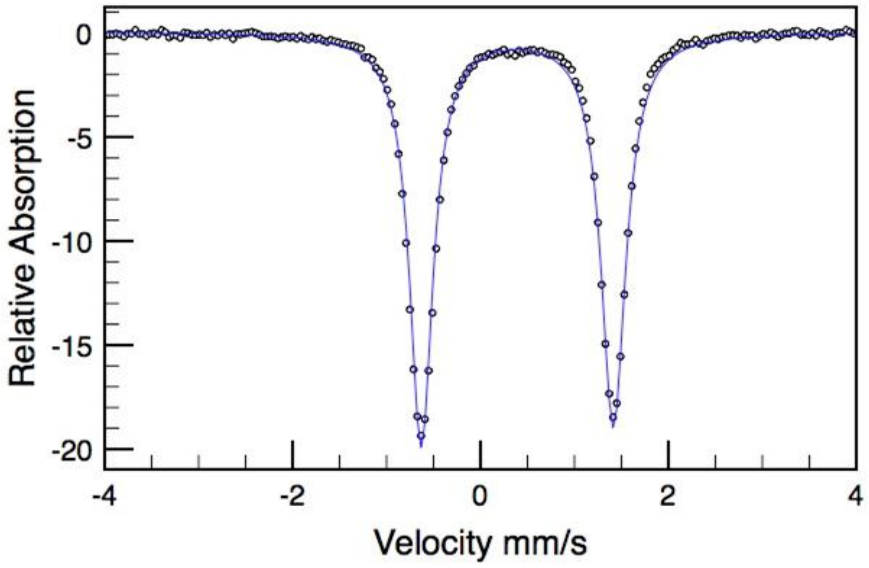

Figure 1.12 Zero-field ^{57}Fe Mössbauer spectrum of (^{Et}PDI)Fe(THF); δ = 0.39 mm/s, ΔE_Q = 2.04 mm/s.

Because the new bis(imino)pyridine iron dinitrogen compounds were targeted as potential olefin hydrogenation catalysts, the reaction of $[(^{Et}PDI)Fe(N_2)]_2(\mu_2\text{-}N_2)$ and $[(^{Et}PDI)Fe(N_2)]_2(\mu_2\text{-}N_2)$ with dihydrogen were studied. The monomeric bis(dinitrogen) compound $(^{iPr}PDI)Fe(N_2)_2$ is known to react with H_2 to form the bis(imino)pyridine iron dihydrogen complex, $(^{iPr}PDI)Fe(H_2)$, which converts back to the dinitrogen compound when exposed to an N_2 atmosphere.[17] The dihydrogen compound exhibits a very similar ^{1}H NMR spectrum to $(^{iPr}PDI)Fe(N_2)_2$, but with subtle shifts for the in-plane hydrogens of the chelate.

Exposing a benzene-d_6 solution of either $[(^{Et}PDI)Fe(N_2)]_2(\mu_2\text{-}N_2)$ or $[(^{Et}PDI)Fe(N_2)]_2(\mu_2\text{-}N_2)$ to an atmosphere of H_2 resulted in a slight color change of the solution to brown. Observation of the reaction by ^{1}H NMR spectrum showed that all resonances for the dinitrogen compounds disappeared, but no new ones for a product grew into the spectrum. Removing the H_2 headspace of the J Young tube and exposing the solution to a dinitrogen atmosphere did not result in a color change back to the red-brown color of the dinitrogen compounds. However, inspection of the solution by IR spectroscopy revealed weak bands centered around 2100 cm^{-1} indicating that at least some of the corresponding dimeric iron dinitrogen compound with terminal N_2 ligands was formed. Unfortunately, because a band for the bridging N_2 has not been easily identified in the IR spectrum, it is difficult to ascertain how much dinitrogen compound is actually reformed. Inspection of the solution by ^{1}H NMR spectroscopy after exposure to N_2 revealed peaks for the corresponding dimeric dinitrogen compound; however, the peaks were much less intense than before H_2 addition.

1.5 Synthesis of a Bis(imino)pyridine Iron Butadiene Complex

Bis(imino)pyridine iron butadiene complexes have been shown to be useful catalytic precursors for olefin hydrogenation.[31] Both (^{iPr}PDI)Fe(η^4-C_4H_6)[19] and (^{Et}PDI)Fe(η^4-C_4H_6)[31] have been previously prepared by reduction of the corresponding bis(imino)pyridine iron dihalide compound with excess 0.5% sodium amalgam and excess 1,3-butadiene. The diisopropyl-aryl butadiene compound, (^{iPr}PDI)Fe(η^4-C_4H_6), was also characterized by X-ray diffraction and exhibits unusual *trans*-butadiene ligand coordination. Because of the catalytic performance of (^{iPr}PDI)Fe(η^4-C_4H_6) and (^{Et}PDI)Fe(η^4-C_4H_6), the dimethyl-aryl bis(imino)pyridine derivative was targeted as a potential hydrogenation catalyst.

Stirring a pentane slurry of (^{Me}PDI)$FeBr_2$ with excess 0.5% sodium amalgam and ten equivalents of 1,3-butadiene for 24 hours followed by filtration and recrystallization from diethyl ether furnished red (^{Me}PDI)Fe(η^4-C_4H_6) in 61% yield (Figure 1.13). The benzene-d_6 ^{1}H NMR spectrum of (^{Me}PDI)Fe(η^4-C_4H_6) exhibits the number of peaks consistent with a C_s symmetric molecule in solution. Interestingly, the imine methyl group resonance of (^{Me}PDI)Fe(η^4-C_4H_6) appears close to the value of the free bis(imino)pyridine ligand indicating little to no contribution from temperature independent paramagnetism,[30] unlike other neutral ligand compounds that were studied. The resonances of the butadiene ligand appear at approximately the same chemical shifts with the same splitting patterns as in (^{iPr}PDI)Fe(η^4-C_4H_6) suggesting that the butadiene ligand in (^{Me}PDI)Fe(η^4-C_4H_6) is also in an unusual *trans* conformation.[19,32]

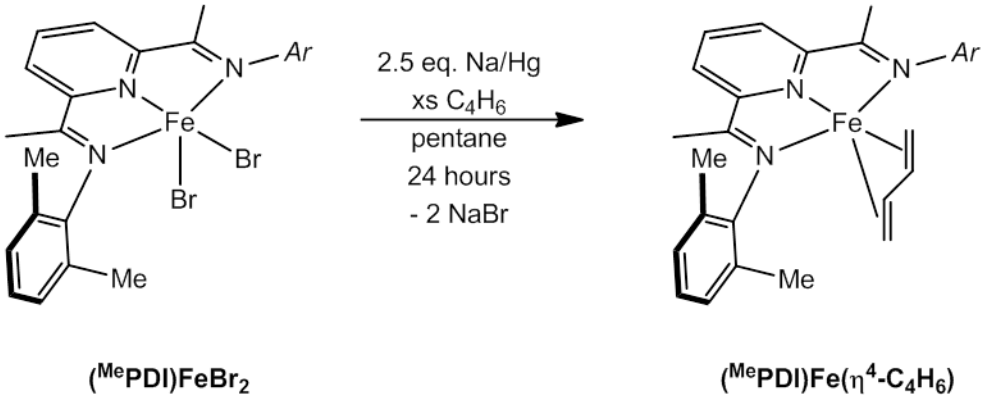

Figure 1.13 Synthesis of (^{Me}PDI)Fe(η^4-C_4H_6).

The three butadiene compounds were also studied by zero-field ^{57}Fe Mössbauer spectroscopy. Neither (^{iPr}PDI)Fe(η^4-C_4H_6) nor (^{Et}PDI)Fe(η^4-C_4H_6) had been previously studied by Mössbauer spectroscopy so data were collected on all three compounds. Representative spectra are presented in Figure 1.14 and the corresponding parameters reported in Table 1.5. The bis(imino)pyridine iron butadiene compounds all have very similar isomer shifts (δ) and quadrupole splittings (ΔE_Q), providing further evidence for the same overall structure with a *trans*-coordinated butadiene ligand. Furthermore, the Mössbauer parameters are similar to those reported for the five-coordinate iron centers in both the monomeric and dimeric bis(imino)pyridine iron dinitrogen compounds. The isomer shifts, coupled with the bond distances from the crystal structure of (^{iPr}PDI)Fe(η^4-C_4H_6), which are consistent with a doubly reduced bis(imino)pyridine chelate,[30] support an electronic structure of an intermediate spin ferrous center antiferromagnetically coupled to a triplet diradical bis(imino)pyridine ligand. Because no features consistent with contributions from temperature idependent paramagnetism were present in the ^{1}H NMR spectrum, the triplet excited state must be much higher in energy than the singlet ground state.[30]

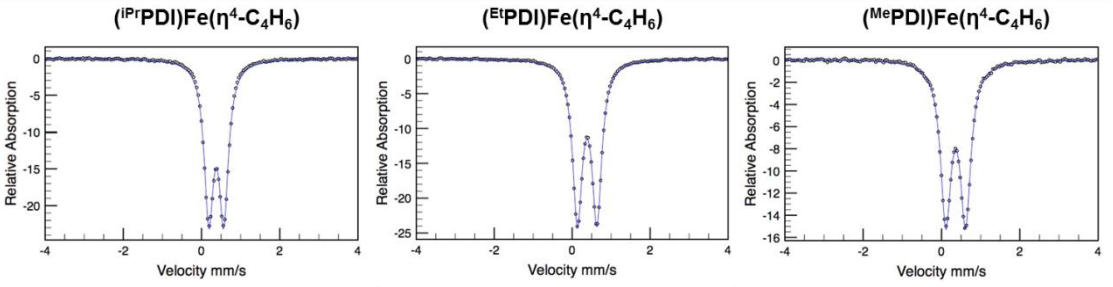

Figure 1.14 Zero-field ^{57}Fe Mössbauer spectra of (^{iPr}PDI)Fe(η^4-C_4H_6), (^{Et}PDI)Fe(η^4-C_4H_6) and (^{Me}PDI)Fe(η^4-C_4H_6) at 80K.

Table 1.5 Zero-field ^{57}Fe Mössbauer parameters for (^{iPr}PDI)Fe(η^4-C_4H_6), (^{Et}PDI)Fe(η^4-C_4H_6) and (^{Me}PDI)Fe(η^4-C_4H_6).

Compound	δ (mm/s)	ΔE_Q (mm/s)
(^{iPr}PDI)Fe(η^4-C_4H_6)	0.38	0.38
(^{Et}PDI)Fe(η^4-C_4H_6)	0.38	0.50
(^{Me}PDI)Fe(η^4-C_4H_6)	0.36	0.50

1.6 Synthesis and Reactivity of a Bis(imino)pyridine Iron Intramolecular Olefin Compound

As presented in Section 1.3, sodium naphthalenide reduction of *rac/meso*-($^{2\text{-}iPr}$PDI)$FeBr_2$ ($^{2\text{-}iPr}$PDI = 2,6-((2-^{i}Pr-C_6H_4)N=CMe)$_2C_5H_3N$) resulted in an intractable mixture of products instead of the desired bis(imino)pyridine iron dinitrogen compound. Because of the success in synthesizing bis(imino)pyridine iron butadiene compounds with smaller bis(imino)pyridine ligands, the same method was attempted with *rac/meso*-($^{2\text{-}iPr}$PDI)$FeBr_2$. Unfortunately, stirring a toluene slurry of *rac/meso*-($^{2\text{-}iPr}$PDI)$FeBr_2$ and 2.5 equivalents of 0.5 % sodium amalgam with 10 equivalents of butadiene resulted in formation of a brown viscous substance. Hypothesizing that the material was poly(butadiene), a slightly more hindered diene, isoprene, was explored. Stirring a toluene slurry of ($^{2\text{-}iPr}$PDI)$FeBr_2$ with 2.5 equivalents of 0.5 % sodium

amalgam and 4 equivalents of isoprene furnished a brown solid. Recrystallizing the solid from diethyl ether at - 35°C afforded the putative bis(imino)pyridine iron olefin compound, ($^{2\text{-iPr,iPropenyl}}$PDI)Fe (Figure 1.15). No band for an N-N stretch was observed in the benzene-d_6 infrared spectrum indicating that N_2 does not coordinate to the iron center.

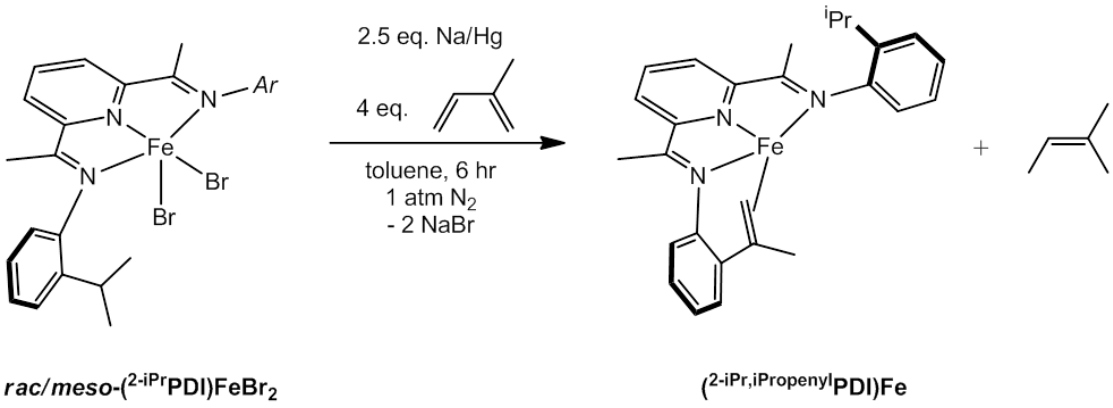

Figure 1.15 Synthesis of ($^{2\text{-iPr,iPropenyl}}$PDI)Fe.

Performing the reaction on a small scale with 2 equivalents of isoprene in a minimal amount of benzene-d_6 followed by analysis of the volatiles by ^{1}H NMR spectroscopy revealed an approximately 1:1 mixture of unreacted isoprene to 2-methyl-2-butene as well as trace amounts of 2-methyl-1-butene in solution. The observation of these organic byproducts suggests that the reduced [($^{2\text{-iPr}}$PDI)Fe] species in solution coordinates isoprene then undergoes a transfer dehydrogenation forming first 2-methyl-1-butene and ($^{2\text{-iPr,iPropenyl}}$PDI)Fe. The terminal alkene is isomerized to the 2-methyl-2-butene by either ($^{2\text{-iPr,iPropenyl}}$PDI)Fe or another reduced [($^{2\text{-iPr}}$PDI)Fe] species in solution.

The ^{1}H NMR spectrum of ($^{2\text{-iPr,iPropenyl}}$PDI)Fe exhibits the number of peaks consistent with C_1 symmetry. The presence of only one intact isopropyl group is supported by observation of only two upfield doublets in the benzene-d_6 ^{1}H NMR

spectrum corresponding to one methyl group each. The dehydrogenated isopropyl group appears as a singlet at 1.12 ppm for the methyl group and two singlets at 2.50 and 2.70 ppm for the two olefinic hydrogens. Two resonances for aryl protons are shifted upfield to 5.66 and 6.27 ppm, suggesting possible interaction between the iron center and part of an aryl group or κ^2-coordination of the bis(imino)pyridine chelate.

The presence of an olefin on one aryl group was also supported by addition of water or carbon monoxide to ($^{2\text{-iPr,iPropenyl}}$PDI)Fe (Figure 1.16). Decomposition of the bis(imino)pyridine iron olefin compound with H_2O and investigation of the free ligand by ^{1}H NMR spectroscopy revealed two resonances at 5.04 and 5.11 ppm for the olefinic hydrogens. Addition of one atmosphere of carbon monoxide to ($^{2\text{-iPr,iPropenyl}}$PDI)Fe resulted in an immediate color change to green. Observation of the green solution by ^{1}H NMR spectroscopy revealed the formation of at least two new C_1 symmetric diamagnetic products, presumably two different isomers of the bis(imino)pyridine iron dicarbonyl compound with a dehydrogenated ligand. The infrared spectrum of this solution displayed only two strong bands for carbonyl stretches at 1964 and 1906 cm^{-1}.

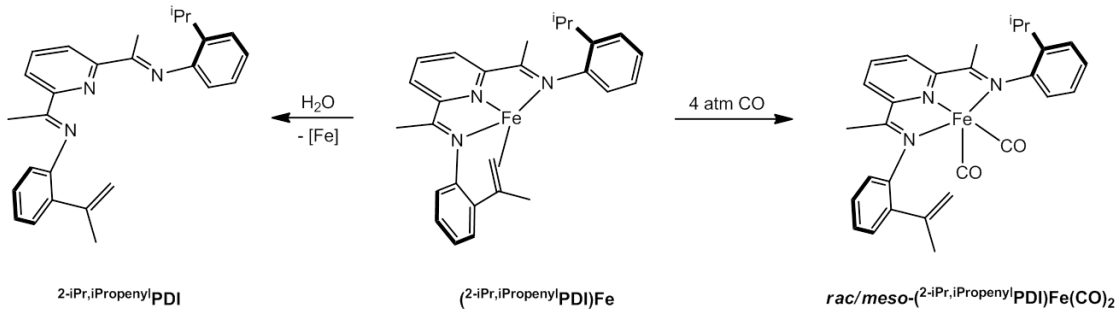

Figure 1.16 Addition of H_2O and CO to ($^{2\text{-iPr,iPropenyl}}$PDI)Fe.

Addition of one atmosphere of H_2 to a benzene-d_6 solution of ($^{2\text{-iPr,iPropenyl}}$PDI)Fe resulted in complete conversion to a new diamagnetic bis(imino)pyridine iron compound after about 2 hours. The ^{1}H NMR spectrum of this new compound is broad and spans from -6 ppm to 11 ppm, indicating a contribution from temperature independent paramagnetism.[9b] The identity of the hydrogenated compound has not yet been assigned; however, the most reasonable candidate is the bis(imino)pyridine iron dihydrogen compound, ($^{2\text{-iPr}}$PDI)Fe$(H_2)_2$, as is seen with addition of H_2 to (^{iPr}PDI)Fe$(N_2)_2$ (Figure 1.17).[17] A second possibility is the η^6-benzene compound, but based on previously reported η^6-arene bis(imino)pyridine compounds, this would be an 18 electron compound and not exhibit contributions from temperature independent paramagnetism.[16,21]

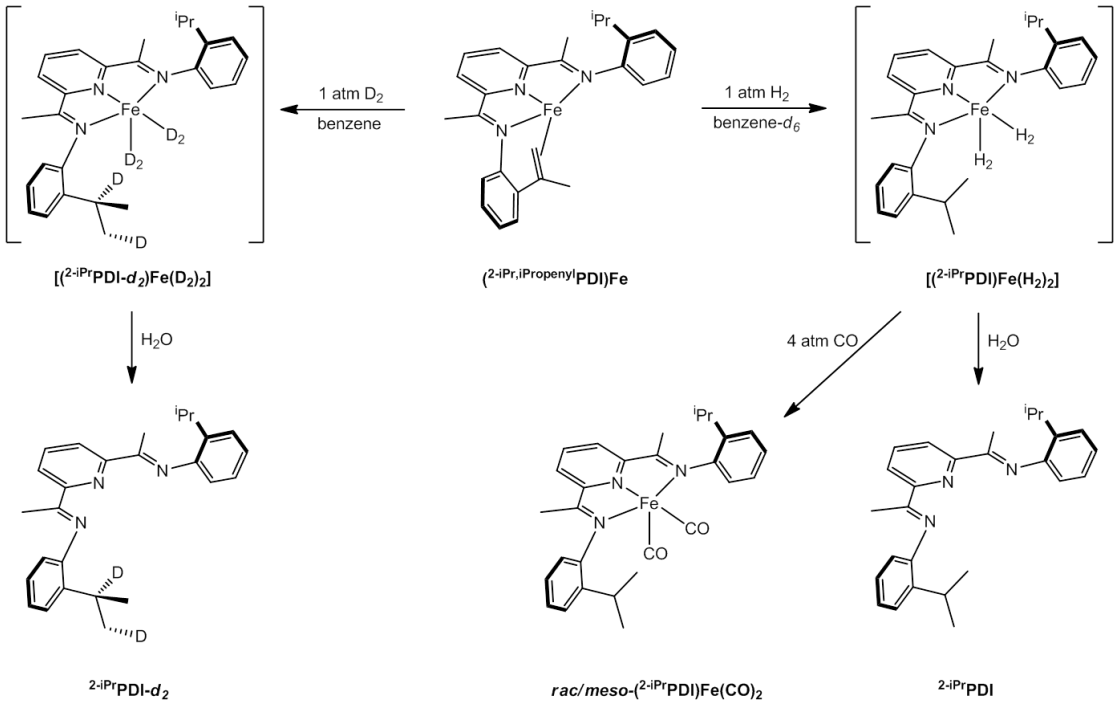

Figure 1.17 Hydrogenation of the bis(imino)pyridine ligand in ($^{2\text{-iPr,iPropenyl}}$PDI)Fe.

Addition of H_2O to the putative dihydrogen compound and analysis of the free ligand by ^1H NMR established that the dehydrogenated ligand of ($^{2\text{-iPr,iPropenyl}}$PDI)Fe was hydrogenated back to $^{2\text{-iPr}}$PDI (Figure 1.17). Addition of one atmosphere of D_2 to ($^{2\text{-iPr,iPropenyl}}$PDI)Fe followed by addition of H_2O and analysis of the free ligand by ^2H NMR furnished $^{2\text{-iPr}}$PDI with deuterium incorporation into both the isopropyl methine and methyl groups (Figure 1.17). Further confirmation of the hydrogenation of the $^{2\text{-iPr,iPropenyl}}$PDI ligand was obtained by addition of one atmosphere of CO to the hydrogenation product which afforded primarily one isomer of *rac/meso*-($^{2\text{-iPr}}$PDI)Fe$(CO)_2$, with carbonyl stretching frequencies of 1964 and 1902 cm^{-1} (Figure 1.17).

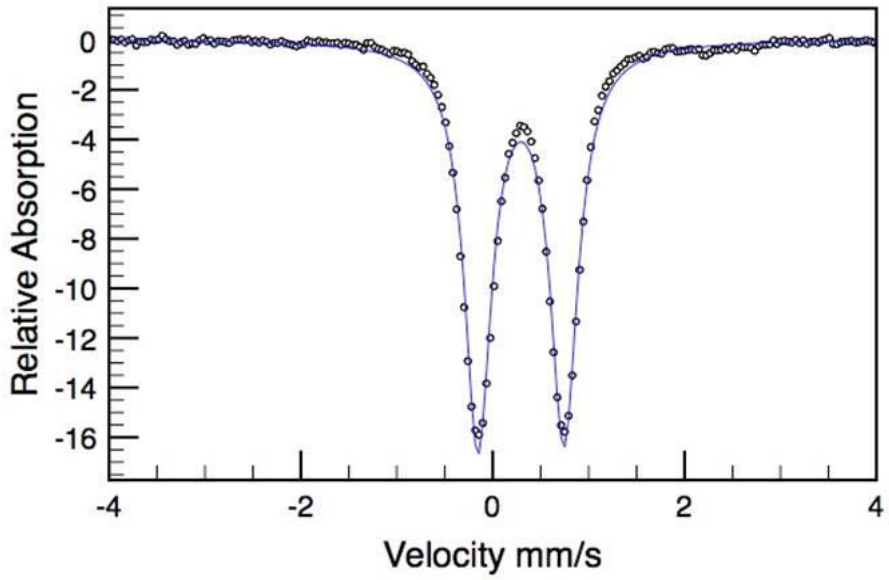

Figure 1.18 Zero-field ^{57}Fe Mössbauer spectrum of ($^{2\text{-iPr,iPropenyl}}$PDI)Fe collected at 80K; $\delta = 0.29$ mm/s, $\Delta E_Q = \left|0.90\right|$ mm/s.

The bis(imino)pyridine iron intramolecular olefin compound was also studied by zero-field ^{57}Fe Mössbauer spectroscopy (Figure 1.18). The isomer shift (δ) of 0.29 mm/s is slightly lower than that of other reduced bis(imino)pyridine iron compounds,

such as the dinitrogen and butadiene compounds, which all have isomer shifts closer to 0.40 mm/s. Despite this difference, the isomer shift of ($^{2\text{-iPr,iPropenyl}}$PDI)Fe is still consistent with an intermediate spin iron(II) compound. When considered in the context of the afore mentioned reduced bis(imino)pyridine iron compounds, the quadrupole splitting (ΔE_Q) of 0.90 mm/s is more consistent with a five coordinate iron center suggesting that there is a more complicated geometry than just an intramolecular olefin coordination. However, a crystal structure is needed to justify these claims.

1.7 Catalytic Olefin Hydrogenations

It has been shown previously that (^{iPr}PDI)Fe(N_2)$_2$ is an effective pre-catalyst for the hydrogenation of terminal, gem and disubstituted olefins.[17,18] However, presumably because of steric hindrance from the aryl isopropyl groups, tri- and tetrasubstituted olefins are not effectively hydrogenated by this catalyst. The one known exception to this is the hydrogenation of ethyl-3-methylbut-2-enoate which at 5 mol% (^{iPr}PDI)Fe(N_2)$_2$ in benzene-d_6 is hydrogenated to ethyl-3-methylbutanoate at 50% conversion after 24 hours under 4 atmospheres of H_2.[18] At longer reaction times, a maximum 65% conversion is reached and the iron complex undergoes competitive deactivation by irreversible C-O bond cleavage.

The dimeric dinitrogen compounds and the olefin compound were evaluated for the catalytic hydrogenation of ethyl-3-methylbut-2-enoate under the same conditions as (^{iPr}PDI)Fe(N_2)$_2$. Standard conditions employed a 0.92 M solution of the substrate in benzene-d_6, 5 mol% of iron pre-catalyst (2.5 mol% of the dimer) and 4 atmospheres of H_2 at 23°C. Each reaction was run to >95% conversion in order to compare the catalytic activity of the dinitrogen precatalysts. The results are presented in Table 1.6. Reducing the size of the substituents on the aryl groups greatly affects

the activity of the dinitrogen precatalysts. Removing a methyl group from each isopropyl substituent, going from (^{iPr}PDI)Fe(N_2)$_2$ to [(^{Et}PDI)Fe(N_2)]$_2$(μ_2-N_2), allowed the reaction to reach complete conversion in 10 hours. Similarly, changing one of the isopropyl groups to a methyl group, going from (^{iPr}PDI)Fe(N_2)$_2$ to [(^{Me,iPr}PDI)Fe(N_2)]$_2$(μ_2-N_2), decreased the reaction time to 5 hours. The most active dinitrogen compound studied was [(^{Me}PDI)Fe(N_2)]$_2$(μ_2-N_2), for which the time to reach >95% conversion was only 1.5 hours; however, the most active catalyst by far was ($^{2\text{-}iPr,iPropenyl}$PDI)Fe, which reached >95 % conversion in less than 30 minutes.

Table 1.6. Comparison of reduced aryl-substituted bis(imino)pyridine iron compounds for the catalytic hydrogenation of ethyl-3-methylbut-2-enoate.

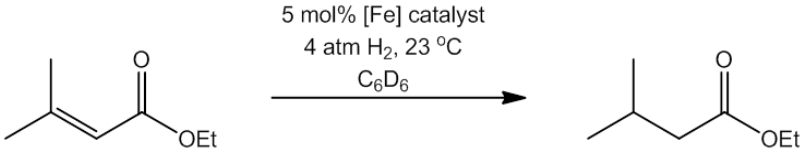

Catalyst	Time (hrs)[a]
(^{iPr}PDI)Fe(N_2)$_2$	50% (24 hrs)
[(^{Et}PDI)Fe(N_2)]$_2$(μ_2-N_2)	10
[(^{Me,iPr}PDI)Fe(N_2)]$_2$(μ_2-N_2)	5
[(^{Me}PDI)Fe(N_2)]$_2$(μ_2-N_2)	1.5
($^{2\text{-}iPr,iPropenyl}$PDI)Fe	0.5

[a] Time required to reach >95% conversion as judged by ^{1}H NMR spectroscopy. Conditions: 5.0 mol% [Fe], 0.92 M substrate in benzene-d_6 solution, 4 atm H_2, 23 °C.

These improved results for a carboxylated trisubstituted olefin inspired attempts at broadening the scope of the catalytic hydrogenations to unactivated alkenes and even tetrasubstituted olefins. The specific olefins that were screened are

shown in Figure 1.19. Trimethylethylene, *trans*-methylstilbene, and tetramethylethylene were all investigated using the same conditions as for ethyl-3-methylbut-2-enoate. No turnover was observed for any substrate with the dimeric dinitrogen compounds or ($^{2\text{-iPr,iPropenyl}}$PDI)Fe. In case the carbonyl group of ethyl-3-methylbut-2-enoate was helping the catalysis by coordinating to the iron center prior to olefin hydrogenation, diethylisopropylidenemalonate was also tested. Again, no conversion with any pre-catalyst was observed.

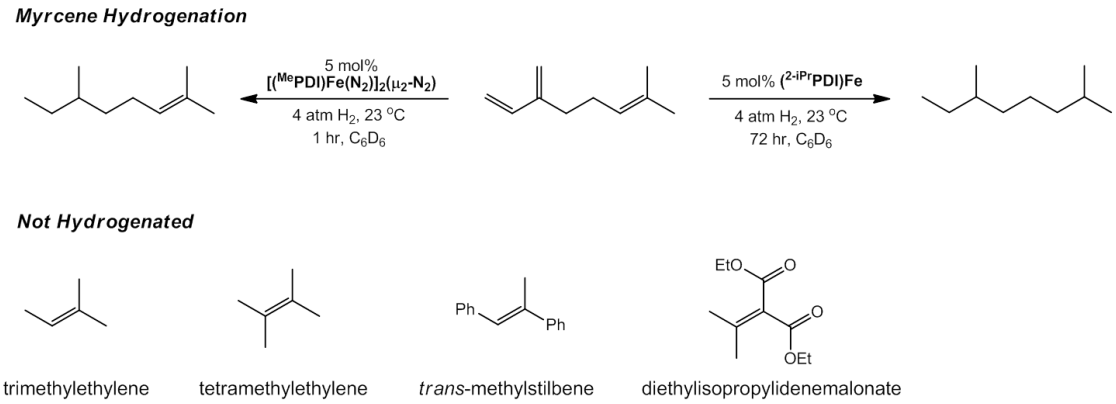

Figure 1.19 Scope of bis(imino)pyridine iron-catalyzed olefin hydrogenation.

One substrate that did yield interesting hydrogenation activity was myrcene. Not surprisingly, the dinitrogen compounds catalyzed the hydrogenation of the conjugated diene portion of myrcene but did not touch the trisubstituted olefin. In contrast to the dinitrogen compounds, ($^{2\text{-iPr,iPropenyl}}$PDI)Fe proved to be an active catalyst for the complete hydrogenation of myrcene. Under the standard conditions of a 0.92 M solution of substrate in benzene-d_6, 5 mol% of iron and 4 atmospheres of H_2 at 23°C, myrcene was successfully hydrogenated to >95% conversion in 72 hours. The major hydrogenation product, 2,6-dimethyloctane, was identified by GCMS and comparison to an authentic sample by ^{1}H NMR and ^{13}C NMR spectroscopy.

Unfortunately, the hydrogenation was not clean and trace amounts of other unidentified hydrocarbons were also observed.

1.8 Conclusions

The dimeric bis(imino)pyridine iron dinitrogen compounds, $[(^{Et}PDI)Fe(N_2)]_2(\mu_2\text{-}N_2)$, $[(^{Me}PDI)Fe(N_2)]_2(\mu_2\text{-}N_2)$ and $[(^{Me,iPr}PDI)Fe(N_2)]_2(\mu_2\text{-}N_2)$ were prepared by reduction of the corresponding bis(imino)pyridine iron dibromide with sodium and a catalytic amount of naphthalene in tetrahydrofuran. Toepler experiments, IR spectroscopy and X-ray diffraction established a dimeric structure with one bridging and two terminal N_2 ligands. The crystal structure of $[(^{Et}PDI)Fe(N_2)]_2(\mu_2\text{-}N_2)$ also establishes two electron reduction of each chelate in the dimer. The ^1H NMR spectra of the diamagnetic dinitrogen compounds are broad and differ from that of the monomeric analog, $(^{iPr}PDI)Fe(N_2)_2$, in that no contribution from temperature independent paramagnetism was observed. However, Mössbauer spectroscopy of each dimeric dinitrogen compound established a similar electronic structure that previously reported for $(^{iPr}PDI)Fe(N_2)_2$. Taking all spectroscopy into account, though formally iron(0) compounds, the dimeric dinitrogen compounds are best described as having intermediate spin iron(II) centers antiferromagnetically coupled to doubly reduced bis(imino)pyridine chelates. Because the dimeric iron dinitrogen compounds do not exhibit spectroscopic features consistent with temperature independent paramagnetism, it is likely that the triplet excited state is higher in energy relative to that of $(^{iPr}PDI)Fe(N_2)_2$.

To further study electronic and steric differences between the different bis(imino)pyridine ligands, the neutral ligand iron compounds, $(^{R}PDI)Fe(DMAP)$ and $(^{R}PDI)Fe(\eta^4\text{-}C_4H_6)$ (R = Et, Me), were prepared and studied by NMR and Mössbauer spectroscopy. In both cases, the diethyl-aryl and dimethyl-aryl substituted

bis(imino)pyridine iron compounds displayed very similar spectroscopic features to the previously reported diisopropyl-aryl bis(imino)pyridine iron N,N-4-dimethylaminopyridine and 1,3-butadiene compounds, (^{iPr}PDI)Fe(DMAP) and (^{iPr}PDI)Fe(η^4-C_4H_6), respectively.

A new bis(imino)pyridine iron intramolecular olefin complex, ($^{2\text{-}iPr,iPropenyl}$PDI)Fe, was prepared by reduction of ($^{2\text{-}iPr}$PDI)$FeBr_2$ with 0.5% sodium amalgam in the presence of isoprene. Analysis of the reaction volatiles showed formation of 2-methyl-2-butene, consistent with a transfer hydrogenation from one isopropyl aryl substituent of the bis(imino)pyridine ligand to one equivalent of isoprene. The diamagnetic olefin compound was studied by Mössbauer spectroscopy and displays parameters consistent with the intermediate spin iron(II) centers observed for other reduced bis(imino)pyridine iron compounds.

Each new reduced bis(imino)pyridine iron compound was assayed for the catalytic hydrogenation of ethyl-3-methylbut-2-enoate. Of the nitrogen compounds, as the aryl-group substituents decreased in size, the hydrogenation activity increased, and the species with the smallest aryl-substituent, [(^{Me}PDI)Fe(N_2)]$_2$(μ_2-N_2), displayed the greatest improvement over the original pre-catalyst, (^{iPr}PDI)Fe(N_2)$_2$. As expected from the trend, ($^{2\text{-}iPr,iPropenyl}$PDI)Fe was the most active hydrogenation pre-catalyst of the group, hydrogenating ethyl-3-methylbut-2-enoate to >99% conversion in under 30 minutes. The olefin compound also catalyzed the complete hydrogenation of myrcene to 2,6-dimethyloctane, a rare example of hydrogenation of a trisubstituted olefin by a bis(imino)pyridine iron compound.

1.8 Experimental Procedures

General Considerations. All air- and moisture-sensitive manipulations were carried out using standard vacuum line, Schlenk, and cannula techniques or in an MBraun

inert atmosphere dry box containing an atmosphere of purified nitrogen. Solvents for air- and moisture-sensitive manipulations were initially dried and deoxygenated using literature procedures. Benzene-d_6 was purchased from Cambridge Isotope Laboratories and dried over 4 Å molecular sieves. The complexes (^{Me}PDI)$FeBr_2$, (^{Et}PDI)$FeBr_2$, (^{Me,iPr}PDI)$FeBr_2$ and *rac/meso*-($^{2\text{-}iPr}$PDI)$FeBr_2$ were prepared according to the literature procedure for (^{iPr}PDI)$FeBr_2$.[5b] Naphthalene was purchased from Sigma Aldrich, dried over CaH_2 as a toluene solution and recrystallized from THF. N,N-4-dimethylaminopyridine was purchased from Acros Organics and dried on the high vacuum line overnight. Cyclohexene and 1,3-butadiene were purchased from Sigma Aldrich and dried over $LiAlH_4$. Ethyl-3-methylbut-2-enoate and isoprene were purchased from Sigma Aldrich and dried over CaH_2.

^{1}H NMR spectra were recorded on Varian Mercury 300, Inova 400, 500, and 600 spectrometers operating at 299.76, 399.78, 500.62, and 599.78 MHz, respectively. ^{13}C NMR spectra were recorded on an Inova 500 spectrometer operating at 125.893 MHz. All ^{1}H and ^{13}C NMR chemical shifts are reported relative to $SiMe_4$ using the ^{1}H (residual) and ^{13}C chemical shifts of the solvent as a secondary standard. For diamagnetic complexes, many assignments were made based on COSY and HSQC NMR experiments. Solution magnetic moments were determined by Evans method using a ferrocene standard and are the average value of at least two independent measurements. Gouy balance measurements were performed with a Johnson Matthey instrument that was calibrated with $HgCo(SCN)_4$. Peak widths at half heights are reported for paramagnetically broadened and shifted resonances. Infrared spectra were collected on a Thermo Nicolet spectrometer. Elemental analyses were performed at Robertson Microlit Laboratories, Inc., in Madison, NJ.

Single crystals suitable for X-ray diffraction were coated with polyisobutylene oil in a drybox, transferred to a nylon loop and then quickly transferred to the

goniometer head of a Bruker X8 APEX2 diffractometer equipped with a molybdenum X-ray tube (λ = 0.71073 Å). Preliminary data revealed the crystal system. A hemisphere routine was used for data collection and determination of lattice constants. The space group was identified and the data were processed using the Bruker SAINT+ program and corrected for absorption using SADABS. The structures were solved using direct methods (SHELXS) completed by subsequent Fourier synthesis and refined by full-matrix least-squares procedures.

Zero-field ^{57}Fe Mössbauer spectra were recorded on a SEE Co. Mössbauer spectrometer (MS4) at 80 K in constant acceleration mode. ^{57}Co/Rh was used as the radiation source. WMOSS software was used for the quantitative evaluation of the spectral parameters (least-squares fitting to Lorentzain peaks). The minimum experimental line widths were 0.23 mm/s. The temperature of the sample was controlled by a Janis Research Co. CCS-850 He/N_2 cryostat within and accuracy of ± 0.3 K. Isomer shifts were determined relative to α-iron at 298 K.

Preparation of [(^{Me}PDI)Fe(N_2)]$_2$(μ_2-N_2). A 100 mL round bottom flask was charged with 1.00 g (^{Me}PDI)FeBr_2 (1.71 mmol), 0.081 g sodium metal (3.50 mmol, 2.1 equivalents) and 0.011 g of naphthalene (0.085 mmol, 0.05 equivalents). To the flask was added approximately 20 mL of THF and the resulting reaction mixture was stirred for 3-4 hours. During this time, the solution changed color from blue to green to red-brown. After reduction was complete (indicated by the formation of the red solution), the THF was removed *in vacuo*. The resulting solid was dissolved in diethyl ether and filtered through celite. The filtrate was collected and concentrated and stored at -35 ºC yielding 0.550 g (69 %) of a dark brown solid identified as [(^{Me}PDI)Fe(N_2)]$_2$(μ_2-N_2). Analysis for $C_{50}H_{54}N_{12}Fe$: Calc. C, 64.25; H, 5.82; N, 17.98. Found C, 63.87; H, 6.19; N, 17.80. ^{1}H NMR (benzene-d_6, 20°C): δ = 1.35 (bs, 24H, Ar CH_3), 1.78 (bs, 12H,

C(CH_3)), 6.92 (bs, 12H, *m*- and *p*-*Ar*), 7.52 (bs, 2H, *p*-*py*), 8.10 (bs, 4H, *m*-*py*). ^{13}C NMR (benzene-d_6, 20°C): δ = 16.17 (*Ar C*CH_3), 19.50 (C(*C*H_3)), 115.92 (*m*- or *p*- *py*), 125.35 (*m*- or *p*- *Ar*) , 130.93 (*m*- or *p*- *Ar*), 148.76 (*m*- or *p*- *py*), 153.05, 3 peaks not located. ^{15}N NMR (toluene-d_8, -80°C) δ = -355.5 (bs), -334.2 (bs), -322.4 (bs). IR(toluene): $\nu(N_2)$ = 2102, 2085 cm^{-1}.

Preparation of [(^{Et}PDI)Fe(N_2)]$_2$(μ_2-N_2). The compound was prepared in a similar manner to [(^{Me}PDI)Fe(N_2)]$_2$(μ_2-N_2) with 1.00 g (1.56 mmol) (^{Et}PDI)$FeBr_2$, 0.073 g (3.20 mmol) sodium metal and 0.010 g (0.078 mmol) of naphthalene. Following recrystallization from diethyl ether at -35 ºC, 0.500 g (61% yield) of [(^{Et}PDI)Fe(N_2)]$_2$(μ_2-N_2) were isolated as dark green needles. Crystals suitable for X-ray analysis were grown from a pentane/ether solution. Analysis for $C_{58}H_{70}N_{12}Fe_2$: Calc. C, 66.54; H, 6.74; N, 16.05. Found C, 66.27; H, 7.10; N, 15.65. ^{1}H NMR (benzene-d_6, 20 °C): δ = 0.72 (bs, 24H, CH_2CH_3), 1.65 (bs, 28H, C(CH_3)) and CH_2CH_3), 7.04 (bm, 12H, *m*- and *p*-*Ar*), 7.64 (bs, 2H, *p*-*py*), 8.16 (bs, 4H, *m*-*py*). ^{13}C NMR (benzene-d_6, 20 °C): δ = 14.79 (CH_2CH_3), 18.07 (C(*C*H_3)), 24.68 (CH_2CH_3), 117.04 (*m*- or *p*- *py*), 125.77 (*m*- or *p*- *Ar*), 126.19 (*m*- or *p*- *Ar*), 135.94 (*m*- or *p*- *py*), 4 peaks not located. ^{15}N NMR (toluene-d_8, -80 °C) δ = -356.7 (bs), -331.5 (bs), -324.1 (bs). IR (toluene): $\nu(N_2)$ = 2101, 2086 cm^{-1}.

Preparation of [(^{Me,iPr}PDI)Fe(N_2)]$_2$(μ_2-N_2). The compound was prepared in a similar manner to [(^{Me}PDI)Fe(N_2)]$_2$(μ_2-N_2) with 1.00 g (1.56 mmol) of (^{Me,iPr}PDI)$FeBr_2$, 0.073 g (3.20 mmol) sodium metal and 0.10 g (0.078 mmol) of naphthalene. Following recrystallization from diethyl ether at -35 ºC, 0.304 g (37%) of [(^{Me,iPr}PDI)Fe(N_2)]$_2$(μ-N_2) was isolated as a dark solid. ^{1}H NMR (benzene-d_6, 20 °C): δ = 0.71 (bs, 24H, CH(CH_3)$_2$), 0.80 – 2.50 (bm, 28H, C(CH_3) and *Ar*-CH_3 and C*H*(CH_3)$_2$), 6.50 – 7.30

(bm, 12H, *m*- and *p*- *Ar*), 7.50 (bs, 2H, *p-py*), 8.00 (bs, 4H, *m-py*). ^{13}C NMR (benzene-d_6, 20 °C): δ = 23.48, 25.61, 27.98, 30.58, 118.19, 123.84, 125.93, 129.61, 141.75, 151.21. IR (toluene): $\nu(N_2)$ = 2099, 2084 cm^{-1}.

Alternate preparation of [(^{Me,iPr}PDI)Fe(N_2)]$_2$(μ_2-N_2). A 250 mL round bottom was charged with 43.02 g (214.4 mmol) of mercury and approximately 70 mL of toluene. With stirring, 0.215 g (9.36 mmol) of sodium metal was added to the flask and the resulting mixture stirred for 10 minutes. To this was added 1.00 g (1.56 mmol) of (^{MeiPr}PDI)$FeBr_2$ and the resulting reaction mixture was stirred for 16 hours. After this time, the dark solution was filtered through celite and the toluene removed *in vacuo*. Recrystallization from diethyl ether at -35 °C afforded 0.350 g (43%) of a dark red solid identified as [(^{Me,iPr}PDI)Fe(N_2)]$_2$(μ-N_2).

Preparation of (^{Et}PDI)Fe(DMAP). A 20 mL scintillation vial was charged with 0.130 g (0.12 mmol) of [(^{Et}PDI)Fe(N_2)]$_2$(μ-N_2) and approximately 10 mL of diethyl ether. To the vial was added a diethyl ether solution of N,N-4-dimethylamino-pyridine (0.030 g, 0.25 mmol) resulting in bubbling and a color change to red. The solution was filtered through celite, concentrated and cooled to -35 °C to afford 0.103 g (69%) of a red solid identified as (^{Et}PDI)Fe(DMAP). ^{1}H NMR (benzene-d_6, 20 °C) δ = -5.59 (br s, 6H, C(CH_3)), 0.74 (t, 7.6 Hz, 12H, CH_2CH_3), 1.53 (q, 7.6 Hz, 4H, CH_2CH_3), 1.87 (br s, 6H, DMAP N(CH_3)$_2$), 2.04 (q, 7.6 Hz, 4H, CH_2CH_3), 5.12 (br s, 2H, DMAP *meta*-CH), 5.60 (br, s, 2H, DMAP *ortho*-CH), 7.09 (d, 7.6 Hz, 4H, *m-Ar*), 7.49 (t, 7.6 Hz, 2H, *p-Ar*), 8.99 (br s, 1H, *p-py*), 12.06 (br s, 2H, *m-py*).

Preparation of (^{Me}PDI)Fe(DMAP). A 20 mL scintillation vial was charged with 0.130 g (0.14 mmol) of [(^{Me}PDI)Fe(N_2)]$_2$(μ-N_2) and approximately 10 mL of diethyl

ether. To the vial was added a diethyl ether solution of N,N-4-dimethylamino-pyridine (0.034 g, 0.28 mmol) resulting in bubbling and a color change to red. The solution was filtered through celite, concentrated and cooled to -35 °C to afford 0.111 g (84%) of a red solid identified as (^{Me}PDI)Fe(DMAP). ^{1}H NMR (benzene-d_6, 20 °C) δ = -5.79 (br s, 6H, C(C*H*$_3$)), 1.49 (s, 12H, *Ar* C*H*$_3$), 1.82 (br s, 6H, DMAP N(C*H*$_3$)$_2$), 5.16 (br s, 2H, DMAP *meta*-CH), 5.47 (br, s, 2H, DMAP *ortho*-CH), 6.90 (d, 7.6 Hz, 4H, *m-Ar*), 7.28 (t, 7.6 Hz, 2H, *p-Ar*), 8.83 (br s, 1H, *p-py*), 11.94 (br s, 2H, *m-py*).

Preparation of (^{Et}PDI)Fe(THF). A 20 mL scintillation vial was charged with 0.100 g (0.096 mmol) of [(^{Et}PDI)Fe(N$_2$)]$_2$(μ$_2$-N$_2$), approximately 7 mL of pentane and approximately 3 mL of THF. The resulting red-brown solution was stirred for 10 minutes. The solution was filtered through celite and all volatiles removed to yield 0.100 g (95%) of a red-brown powder identified as (^{Et}PDI)Fe(THF). Analysis for $C_{33}H_{41}N_3O_1Fe$: Calc. C, 71.86; H, 7.49; N, 7.62. Found C, 71.58; H, 7.48; N, 7.51. ^{1}H NMR (benzene-d_6, 20 °C) δ = -6.32 (s, 6H, C(C*H*$_3$)), 0.70 (t, 7.6 Hz, 12H, CH$_2$C*H*$_3$), 1.02 (bs, 4H, THF C*H*$_2$), 1.52 (q, 7.6 Hz, 4H, C*H*$_2$CH$_3$), 1.90 (q, 7.6 Hz, 4H, C*H*$_2$CH$_3$), 2.40 (bs, 4H, THF OC*H*$_2$), 7.12 (d, 7.6 Hz, 4H, *m-Ar*), 7.61 (t, 7.6 Hz, 2H, *p-Ar*), 8.89 (t, 7.6 Hz, 1H, *p-py*), 12.36 (d, 7.6 Hz, 2H, *m-py*). ^{13}C NMR (benzene-d_6, 20 °C) δ = 13.87 (CH$_2$*C*H$_3$), 24.01 (*C*H$_2$CH$_3$), 25.83 (*C*H$_2$CH$_3$), 26.94 (THF *C*H$_2$), 68.85 (THF O*C*H$_2$), 102.80 (*m-py*), 124.33 (*p-Ar*), 125.97 (*m-Ar*), 131.60 (*p-py*), quaternary carbons not located.

Preparation of (^{Me}PDI)Fe(η^4-C$_4$H$_6$). A thick walled glass vessel was charged with 31.43 g (156.7 mmol) of mercury, approximately 30 mL of pentane and a stir bar. Sodium metal (.157 g, 6.83 mmol) was added to the vessel. The resulting slurry was allowed to stir for 10 minutes to amalgamate then 0.800 g (1.37 mmol) of solid

(^{Me}PDI)$FeBr_2$ was added to the vessel. The vessel was brought out of the dry box and submerged in liquid nitrogen. On the high vacuum line, the vessel was evacuated and 2500 mmHg (13.7 mmol, 10 eq) of butadiene was added via calibrated gas bulb. The reaction mixture was stirred for 24 hours at room temperature during which the solution changed from blue to green to orange. After 24 hours, unreacted butadiene was removed on the high vacuum line and the vessel was brought back into the dry box. The orange solution was decanted away from the amalgam and filtered through celite. Diethyl ether was used to extract the remaining product and also filtered through celite. Recrystallization from a diethyl ether solution at -35°C afforded 0.398 g (0.83 mmol, 61%) of a red solid identified as (^{Me}PDI)Fe(η^4-C_4H_6). Analysis for $C_{29}H_{33}N_3Fe$: Calc. C, 72.65; H, 6.94; N, 8.76. Found C, 72.83; H, 6.77; N, 8.52. ^{1}H NMR (benzene-d_6, 20 °C): δ = 1.29 (s, 6H, C(C*H*$_3$) or *Ar*-C*H*$_3$), 1.58 (s, 6H, C(C*H*$_3$) or *Ar*-C*H*$_3$), 1.70 (s, 6H, C(C*H*$_3$) or *Ar*-C*H*$_3$), 2.76 (bs, 2H, *cis*-butadiene), 3.39 (d, 12.0 Hz, 2H, *trans*-butadiene), 4.58 (bs, 2H, butadiene-C*H*'s), 6.85 (m, 6H, *m-Ar* and *p-Ar*), 7.48 (t, 7.6 Hz, 1H, *p-py*), 8.07 (d, 7.6 Hz, 2H, *m-py*). ^{13}C NMR (benzene-d_6, 20 °C): δ = 17.33 (C(*C*H$_3$) or *Ar*-*C*H$_3$), 18.18 (C(*C*H$_3$) or *Ar*-*C*H$_3$), 19.30 (C(*C*H$_3$) or *Ar*-*C*H$_3$), 63.29 (butadiene *C*H$_2$), 103.46 (butadiene *C*H), 117.25 (*p-py*), 117.33 (*m-py*), 125.48 (*m*- and *p-Ar*), 130.44, 150.61, 150.95, 152.30 (quaternary carbons).

Preparation of ($^{2\text{-iPr,iPropenyl}}$PDI)Fe. A 100 mL round bottom flask was charged with 9.0 g (45 mmol) of mercury and approximately 5 mL of toluene. Sodium metal (0.045 g, 1.20 mmol) was added to the flask in pieces. The sodium amalgam was stirred for 10 minutes then 0.280 g (4.11 mmol, 4 eq.) of isoprene were added to the solution followed immediately by 0.600 g (0.98 mmol) of solid *rac/meso*-($^{2\text{-iPr}}$PDI)$FeBr_2$ and approximately 10 mL of toluene. The reaction was stirred for approximately 4 hours during which time the color changed from blue to green to brown. The solution was

filtered through celite and the amalgam washed with diethyl ether. Removal of the solvent followed by recrystallization from diethyl ether at -35 °C afforded 0.314 g (71%) of a brown crystalline solid identified as ($^{2\text{-iPr,iPropenyl}}$PDI)Fe. ^{1}H NMR (benzene-d_6, 20 °C): δ = 0.83 (d, 6.8 Hz, 3H, CH(CH_3)$_2$), 1.00 (d, 6.8 Hz, 3H, CH(CH_3)$_2$), 1.12 (s, 3H, *Ar* C(CH_3)), 1,49 (s, 3H, N=C(CH_3)), 2.08 (s, 3H, N=C(CH_3)), 2.23 (sept, 6.8 Hz, 1H, C*H*(CH$_3$)$_2$), 2.50 (s, 1H, *Ar* C=CH_2), 2.70 (s, 1H, *Ar* C=CH_2), 5.66 (d, 7.6 Hz, 1H, *o-Ar*), 6.27 (t, 7.6 Hz, 1H, *m-Ar*), 6.86 (t, 7.6 Hz, 1H, *m-Ar*), 6.96 (m, 2H, *m-Ar* and *p-Ar*), 7.13 (t, 7.6 Hz, 1H, *p-Ar*), 7.19 (d, 7.6 Hz, 1H, *m-Ar*), 7.43 (t, 7.6 Hz, 1H, *p-py*), 7.46 (d, 7.6 Hz, 1H, *o-Ar*), 7.96 (d, 7.6 Hz, 1H, *m-py*), 8.00 (d, 7.6 Hz, 1H, *m-py*). ^{13}C NMR (benzene-d_6, 20 °C): δ = 17.36 (N=*C*H$_3$), 18.04 (N=C(*C*H$_3$)), 20.56 (*Ar* C(*C*H$_3$)), 25.03 (*Ar* CH(*C*H$_3$)$_2$), 25.23 (*Ar* CH(*C*H$_3$)$_2$), 27.21 (*Ar C*H(CH$_3$)$_2$), 58.63 (*Ar* C=*C*H$_2$), 79.48 (quaternary carbon), 116.32 (*p-py*), 117.95 (*m-py*), 118.60 (*m-py*), 119.34 (*m-Ar* or *p-Ar*), 123.92 (*m-Ar*), 124.56 (*o-Ar*), 125.19 (*m-Ar* or *p-Ar*), 125.31 (*m-Ar* or *p-Ar*), 125.36 (*m-Ar*), 126.35 (*m-Ar* or *p-Ar*), 127.54 (*o-Ar*), 129.66, 140.15, 145.34, 149.12, 150.18, 151.31, 152.33, 156.87 (quaternary carbons).

Observation of $^{\text{2-iPr,iPropenyl}}$PDI. ^{1}H NMR (benzene-$d_6$, 20 °C): δ = 1.20 (d, 6.8 Hz, 12H, CH(CH_3)$_2$), 2.08 (dd, 5.6 Hz and 0.80 Hz, 3H, *Ar* C(CH_3)), 2.30 (s, 3H, imine C(CH_3)), 2.31 (s, 3H, imine C(CH_3)), 3.18 (sept, 6.8 Hz, 1H, C*H*(CH$_3$)$_2$), 5.04 (m, 1H, C=CH_2), 5.11 (m, 1H, C=CH_2), 6.30 (dd, 7.6 Hz and 1.6 Hz, 1H, *o-Ar*), 6.71 (dd, 7.6 Hz and 1.6 Hz, 1H, *o-Ar*), 7.00 (td, 7.6 Hz and 1.6 Hz, 1H, *m-Ar*), 7.08 (td, 7.6 Hz and 1.6 Hz, 1H, *m-Ar*), 7.12 (dd, 7.6 Hz and 1.6 Hz, 1H, *m-Ar*), 7.16 (dd, 7.6 Hz and 1.6 Hz, 1H, *m-Ar*), 7.24 (t, 7.6 Hz, 1H, *p-py*), 7.29 (dd, 7.6 Hz and 1.6 Hz, 1H, *p-Ar*), 7.33 (dd, 7.6 Hz and 1.6 Hz, 1H, *p-Ar*), 8.41 (dd, 7.6 Hz, 1.6 Hz, *m-py*), 8.43 (dd, 7.6 Hz and 1.6 Hz, *m-py*).

Observation of ($^{2\text{-iPr}}$PDI)Fe(H_2)$_2$. A J Young tube containing 0.015 g (0.033 mmol) of ($^{2\text{-iPr,iPropenyl}}$PDI)Fe in benzene-$d_6$ was frozen in liquid nitrogen and evacuated on the high vacuum line. One atmosphere of H_2 was added with the tube still at liquid nitrogen temperature. The tube was warmed to room temperature and allowed to sit for approximately 2 hours. No color change was observed, but analysis of the solution revealed formation of a new diamagnetic product, tentatively identified as ($^{2\text{-iPr}}$PDI)Fe(H_2)$_2$. ^{1}H NMR (benzene-d_6, 20 °C): δ = -5.71 (bs, 3H, N=C(C*H*$_3$) or *Ar* CH(C*H*$_3$)$_2$), -2.29 (bs, 3H, N=C(C*H*$_3$) or *Ar* CH(C*H*$_3$)$_2$), 2.52 (bs, 8H, N=C(C*H*$_3$) or *Ar* CH(C*H*$_3$)$_2$ and *Ar* C*H*(CH$_3$)$_2$), 2.71 (bs, 3H, N=C(C*H*$_3$) or *Ar* CH(C*H*$_3$)$_2$), 3.94 (bs, 3H, N=C(C*H*$_3$) or *Ar* CH(C*H*$_3$)$_2$), 5.63 (bs, 1H, *Ar* or *py*), 5.84 (bs, 1H, *Ar* or *py*), 6.09 (bs, 1H, *Ar* or *py*), 6.48 (bs, 1H, *Ar* or *py*), 6.53 (bs, 1H, *Ar* or *py*), 7.09 (bs, 1H, *Ar* or *py*), 8.26 (bs, 1H, *Ar* or *py*), 8.30 (bs, 1H, *Ar* or *py*), 8.76 (bs, 1H, *Ar* or *py*), 10.45 (bs, 1H, *Ar* or *py*).

Observation of rac/meso-($^{2\text{-iPr}}$PDI)Fe(CO)$_2$. One atmosphere of carbon monoxide was added to a J Young tube containing a benzene-d_6 solution of 0.15 g (0.033 mmol) of ($^{2\text{-iPr}}$PDI)Fe(H_2)$_2$ at liquid nitrogen temperature. The solution was warmed to room temperature and the solution turned green immediately. ^{1}H NMR (benzene-d_6, 20 °C): Major isomer, δ = 0.91 (d, 6.8 Hz, 6H, CH(C*H*$_3$)$_2$), 1.22 (d, 6.8 Hz, 6H, CH(C*H*$_3$)$_2$), 2.06 (s, 6H, C(C*H*$_3$)), 2.64 (sept, 6.8 Hz, 2H, C*H*(CH$_3$)$_2$), 7.05 (m, 4H, *Ar*), 7.21 (t, 7.6 Hz, 1H, *p-py*), 7.28 (m, 2H, *Ar*), 7.69 (d, 7.6 Hz, 2H, *m-py*); Minor isomer, δ = 0.95 (d, 6.8 Hz, 6H, CH(C*H*$_3$)$_2$), 1.33 (d, 6.8 Hz, 6H, CH(C*H*$_3$)$_2$), 2.07 (s, 6H, C(C*H*$_3$)), 2.76 (sept, 6.8 Hz, 2H, C*H*(CH$_3$)$_2$), 7.70 (d, 7.6 Hz, 2H, *m-py*), *Ar* and *p-py* resonances located under major isomer peaks. IR (benzene-d_6): ν(CO) 1964, 1902 cm^{-1}.

General Procedure for Catalytic Olefin Hydrogenation. In a typical experiment, a thick-walled glass vessel was charged with a solution containing 0.016 mmol of the desired iron compound in 0.65 g (7.72 mmol) of benzene-d_6 and a magnetic stir bar. The vessel was placed in a liquid nitrogen cooled cold well for 20 minutes. Once the solution was frozen, 0.081 g (0.63 mmol) of substrate was layered on the reaction mixture. The vessel was taken out of the dry box and transferred to a high vacuum line while continuously submerged in liquid nitrogen. Following evacuation of the dinitrogen atmosphere, 1 atmosphere of dihydrogen was admitted at 80 K. the solution was then thawed and stirred at ambient temperature. At the desired reaction time, the vessel was vented of dihydrogen and exposed to air. Decomposed iron compound was removed by filtration through celite and the filtrate collected into an NMR tube. Conversions were determined by integrating the CH_2 peak of the ester ethyl group of the reactant against the corresponding peak of the product.

REFERENCES

[1] Osborn, J. A.; Jardine, F. H.; Young, J. F.; Wilkinson, G. *J. Chem. Soc. A* **1966**, 1711.

[2] Enthaler, S.; Junge, K.; Beller, M. *Angew. Chem., Int. Ed.* **2008**, *47*, 3317.

[3] Bolm, C.; Legros, J.; Le-Paith, J.; Zani, L. *Chem. Rev.* **2004**, *104*, 6217.

[4] Correa, A.; Mancheño, O. G.; Bolm, C. *Chem. Soc. Rev.* **2008**, *37*, 1108.

[5] Sherry, B. D.; Fürstner, A. *Acc. Chem. Res.* **2008**, *41*, 1500.

[6] (a) Small, B. M.; Brookhart, M. *J. Am. Chem. Soc.* **1998**, *120*, 7143. (b) Small, B. L.; Brookhart, M.; Bennett, A. M. A. *J. Am. Chem. Soc.* **1998**, *120*, 4049.

[7] (a) Britovsek, G. J. P.; Gibson, V. C.; Kimberley, B. S.; Maddox, S. J.; Solan, G. A.; White, A. J. P.; Williams, D. J. *Chem. Commun.* **1998**, 849. (b) Britovsek, G. J. P.; Bruce, M.; Gibson, V. C.; Kimberely, B. S.; Maddox, P. J.; Mastroianni, S.; McTavish, S. J.; Redshaw, C.; Solan, G. A.; Strömberg, S.; White, A. J. P.; Williams, D. J. *J. Am. Soc.* **1999**, *121*, 8728.

[8] Trovitch, R. J.; Lobkovsky, E.; Chirik, P. J. *Inorg. Chem.* **2006**, *45*, 7252.

[9] (a) Knijnenburg, Q.; Gambarotta, S.; Budzelaar, P. H. M. *Dalton Trans.* **2006**, 5442. (b) Bart, S. C.; Chlopek, K.; Bill, E.; Bouwkamp, M. W.; Lobkovsky, E.; Neese, F.; Wieghardt, K.; Chirik, P. J. *J. Am. Chem. Soc.* **2006**, *128*, 13901.

[10] Butin, K. P.; Beloglazkina, E. K.; Zyk, N. V. *Russ. Chem. Rev.* **2005**, *74*, 531.

[11] Knijnenburg, Q.; Hetterscheid, D.; Kooistra, T. M.; Budzelaar, P. H. M. *Eur. J. Inorg. Chem.* **2004**, 1204.

[12] Vidyaratne, I.; Gambarotta, S.; Korobkov, I.; Budzelaar, P. H. M. *Inorg. Chem.* **2005**, *44*, 1187.

[13] Vidyaratne, I.; Scott, J.; Gambarotta, S.; Budzelaar, P. H. M. *Inorg. Chem.* **2007**, *46*, 7040.

[14] Gibson, V. C.; Humphries, M. J.; Tellmann, K. P.; Wass, D. F.; White, A. J. P.; Williams, D. J. *Chem. Commun.* **2001**, 2252.

[15] Bowman, A. C.; Milsmann, C.; Atienza, C. C. H.; Lobkovsky, E.; Wieghardt, K.; Chirik, P. J. *J. Am. Chem. Soc.* **2010**, *132*, 1676.

[16] Gallagher, M.; Wieder, N. L.; Dioumaev, V. K.; Carroll, P. J.; Berry, D. H. *Organometallics* **2010**, *29*, 591.

[17] Bart, S. C.; Lobkovsky, E.; Chirik, P. J. *J. Am. Chem. Soc.* **2004**, *126*, 13794.

[18] Trovitch, R. J.; Lobkovsky, E.; Bill, E.; Chirik, P. J. *Organometallics* **2008**, *27*, 1470.

[19] Bouwkamp, M. W.; Bowman, A. C.; Lobkovsky, E.; Chirik, P. J. *J. Am. Chem. Soc.* **2006**, *128*, 13340.

[20] Sylvester, K. T.; Chirik, P.J. *J. Am. Chem. Soc.* **2009**, *131*, 8772.

[21] Archer, A. M.; Bouwkamp, M. W.; Cortez, M. –P.; Lobkovsky, E.; Chirik, P. J. *Organometallics* **2006**, *25*, 4269.

[22] Scott, J.; Vidyaratne, I.; Korobkov, I; Gambarotta, S.; Budzelaar, P. H. M. *Inorg. Chem.* **2008**, *47*, 896.

[23] Gibson, V. C.; Redshaw, C.; Solan, G. A. *Chem. Rev.* **2007**, *107*, 1745.

[24] Matsugi, T.; Fujita, T. *Chem. Soc. Rev.* **2008**, *37*, 1264.

[25] Wile, B. M.; Trovitch, R. J.; Bart, S. C.; Tondreau, A. M.; Lobkovsky, E.; Milsmann, C.; Bill, E.; Wieghardt, K.; Chirik, P. J. *Inorg. Chem.* **2009**, *48*, 4190.

[26] Tondreau, A. M.; Darmon, J. M.; Wile, B. M.; Floyd, S. K.; Lobkovsky, E.; Chirik, P. J. *Organometallics* **2009**, *28*, 3928.

[27] Cámpora, J.; Cartes, M. Á.; Rodriguez-Delgado, A.; Naz, A. M.; Palma, P.; Pérez, C. M. *Inorg. Chem.* **2009**, *48*, 3679.

[28] Meutterties, E. L. *Acc. Chem. Res.* **1970**, *3*, 266.

[29] Field, L. D.; Hazari, N.; Li, H. L.; Luck, I. J. *Magn. Reson. Chem.* **2003**, *41*, 709.

[30] Bart, S. C.; Lobkovsky, E.; Bill, E.; Wieghardt, K.; Chirik, P. J. *Inorg. Chem.* **2007**, *46*, 7055.

[31] Archer, A. M., *Masters Thesis*, Cornell University, 2006.

[32] (a) Norman, D. W.; Ferguson, M. J.; McDonald, R.; Stryker, J. M. *Organometallics* **2006**, *25*, 2705. (b) Bachler, v.; Grevels, R. –W.; Kerpen, K. Olbrich, G.; Schaffner, K. *Organometallics* **2003**, *22*, 1696.

CHAPTER 2

N-N BOND CLEAVAGE OF DIAZOALKANES BY BIS(IMINO)PYRIDINE IRON DINITROGEN COMPLEXES*

2.1 Abstract

Addition of monosubstituted diazoalkanes, N_2CHR^1 (R^1 = Ph, 4-Me-C_6H_4, 2,4,6-Me_3-C_6H_2, 2-OMe-C_6H_4, 2-O^{i}Pr-C_6H_4, C_6H_{11}, ^{t}Bu), to bis(imino)pyridine iron dinitrogen complexes, (^{R}PDI)Fe$(N_2)_2$ (^{R}PDI = 2,6-(2,6-R_2-C_6H_3-N=CMe)$_2C_5H_3N$; R = ^{i}Pr) and [(^{R}PDI)Fe(N_2)]$_2(\mu_2$-$N_2)$ (R = Et, Me) resulted in formation of the corresponding bis(imino)pyridine iron nitrile and imine compounds, (^{R}PDI)FeNCR^1 and (^{R}PDI)FeNHCHR^1, respectively, via cleavage of the diazoalkane N-N bond. Mechanistic studies suggest initial formation of a highly reactive transient bis(imino)pyridine iron alkylidene complex which quickly undergoes a [4π + 2π] cycloaddition with a second equivalent of diazoalkane to form a metallacycle. A 1,3-hydrogen shift followed by retrocycloaddition yield the observed iron complexes. Deuterium labeling studies support the 1,3-hydrogen shift as the rate determining step in the proposed pathway. The bis(imino)pyridine iron dinitrogen complexes also facilitated cleavage of the N-N bond of benzaldazine, providing additional support for the proposed mechanism. Addition of the disubstituted diazoalkane, phenyldiazoethane (N_2C(Me)Ph), to (^{iPr}PDI)Fe$(N_2)_2$ resulted in the formation of a diazoalkane complex. The same diazoalkane reacted with the smaller bis(imino)pyridine iron dinitrogen complexes, [(^{Et}PDI)Fe(N_2)]$_2(\mu_2$-$N_2)$ and [(^{Me}PDI)Fe(N_2)]$_2(\mu_2$-$N_2)$ to furnish stable iron azine complexes.

* Parts of this chapter have been taken from (a) Russell, S. K.; Lobkovsky, E.; Chirik, P. J. *J. Am. Chem. Soc.* **2009**, *131*, 36-37. Copyright 2009 American Chemical Society.

2.2 Introduction

The reactivity of diazoalkanes with first row transition metals is of long-standing interest due to the utility of carbene transfer reactions in organic synthesis[1] and the intermediacy of $M{=}CR_2$ species in olefin metathesis.[2] Diazoalkanes have also been used as mimics of dinitrogen to understand N_2 coordination and functionalization.[3] Motivated by the economic and environmental advantages of base metals as alternatives to established precious metal catalysts,[4] coupled with the role of iron in nitrogen-fixing bacteria,[5] the coordination chemistry of diazoalkanes with reduced iron complexes is of fundamental and practical interest.

Several iron porphyrin and related macrocyclic complexes have been shown to react with select diazoalkanes in catalytic cyclopropanation reactions.[6,7] Woo and coworkers have reported that several iron(II) tetraarylporphyrin complexes are efficient catalysts for the cyclopropanation of olefins with ethyl diazoacetate as well as aryldiazomethanes (Figure 2.1).[6a,6b] In 2002, they reported several chiral iron(II) porphyrin and tetraaza macrocycles were described that catalyze the cyclopropanation of styrene with diazoacetates with high diastereoselectivities and yields but with modest enantioselectvities.[6c] Shortly thereafter, in 2003, Edulji and Nguyen reported a series of air-stable μ-oxo-bis[(salen)iron(III)] complexes that catalyze the cyclopropanation of olefins with ethyl diazoacetate in good yields.[7]

Woo and coworkers have also shown that the iron(III) porphyrin complex, Fe(TPP)Cl (TPP = 5,10,15,20-tetraphenylporphyrinato), is a precatalyst for olefination reactions[8] as well as N-H[9] and C-H[10] bond insertions (Figure 2.1). Using ethyl diazoacetate with a stoichiometric amount of triphenylphosphine and 0.1 to 2 mol% catalyst loadings, catalytic olefinations of both aromatic and aliphatic aldehydes were observed in greater than 85% yields with over 90% selectivity for the corresponding *E*-olefin isomer.[8] Carbene insertion from ethyl diazoacetate into aliphatic and

aromatic amine N-H bonds also proceeded with greater than 85 % yields using 1 mol % catalyst.[9] Similarly, 2 mol% loadings of (TPP)FeCl catalyzed benzylic and ring C-H bond insertions by carbene fragments transferred from several methyl diazoacetates in greater than 70 % yields.[10] In contrast, insertion of diazoalkanes into the Fe-P bonds of tetrahedral $(R_3P)_2FeCl_2$ compounds has been reported to yield the corresponding catalytically inactive phosphazine derivatives.[11]

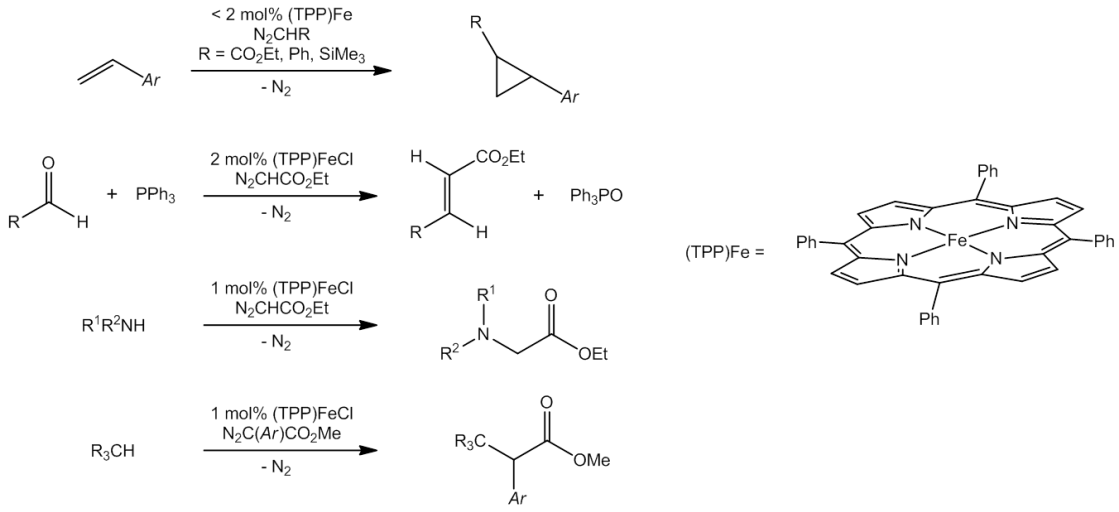

Figure 2.1 Examples of organic transformations of diazoalkanes catalyzed by an iron porphyrin complex.

Our laboratory has previously reported the synthesis and characterization of the bis(imino)pyridine iron η^1-diazoalkane complex, (^{iPr}PDI)$FeN_2CHSiMe_3$.[12] Addition of one atmosphere of H_2 to (^{iPr}PDI)$FeN_2CHSiMe_3$ induces diazoalkane N-N and N-C bond cleavage to yield the corresponding bis(imino)pyridine iron ammonia complex, (^{iPr}PDI)$FeNH_3$ and $SiMe_4$. The diazoalkane complex is thermally unstable in solution at 23°C, slowly and quantitatively converting to an NMR silent intramolecular bis(imino)pyridine iron olefin compound with concomitant loss of $SiMe_4$ (Figure 2.2). These reactions demonstrate that the bis(imino)pyridine iron

framework has the ability to produce interesting and potentially useful chemistry with diazoalkane substrates.

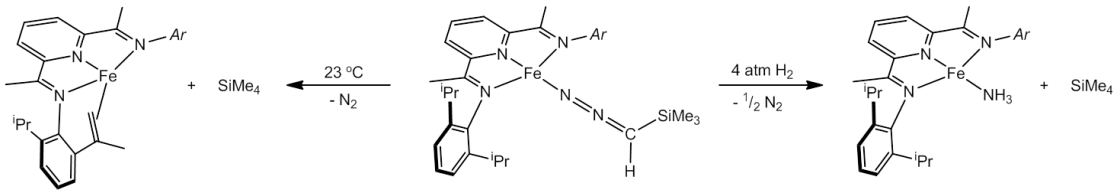

Figure 2.2 Hydrogenative N-N and N-C diazoalkane bond cleavage and intramolecular C-H activation with (^{iPr}PDI)FeN_2CHSiMe_3.

2.3 Addition of Mono-substituted Diazoalkanes

Addition of one equivalent of phenyldiazomethane, N_2CHPh, to a benzene-d_6 solution of the bis(imino)pyridine iron bis(dinitrogen) complex, (^{iPr}PDI)Fe$(N_2)_2$, resulted in immediate and quantitative conversion to an equimolar mixture of two new products accompanied by a color change from green to blue-green. A combination of ^{1}H NMR, ^{13}C NMR and infrared spectroscopies identified these new compounds as the bis(imino)pyridine iron benzonitrile and benzaldimine compounds, (^{iPr}PDI)FeNCPh and (^{iPr}PDI)FeNHCHPh, respectively, arising from N-N bond cleavage of phenyldiazomethane (Figure 2.3). Performing the reaction in a sealed vessel allowed quantification by Toepler pump of the gas released following addition of the diazoalkane. Approximately 2.4 equivalents of N_2 were collected, consistent with loss of two equivalents of N_2 from (^{iPr}PDI)Fe$(N_2)_2$ and half an equivalent of N_2 from the diazoalkane.

The bis(imino)pyridine iron benzonitrile compound, (^{iPr}PDI)FeNCPh, was independently prepared by addition of one equivalent of benzonitrile to (^{iPr}PDI)Fe$(N_2)_2$ (Figure 2.4). The ^{1}H NMR spectrum of (^{iPr}PDI)FeNCPh exhibits features consistent with temperature independent paramagnetism.[13] The resonance for

the imine methyl group was located -0.12 ppm and the *meta*- and *para*-pyridine protons were found at 11.32 and 9.10 ppm, respectively. These peaks did not shift significantly upon heating or cooling the compound in toluene-d_8. The C≡N stretch in the infrared spectrum appears at 2169 cm^{-1}, red-shifted from the free nitrile stretching frequency at 2230 cm^{-1}, indicating some amount of electron density donation into the π* orbitals of the nitrile from the iron center.

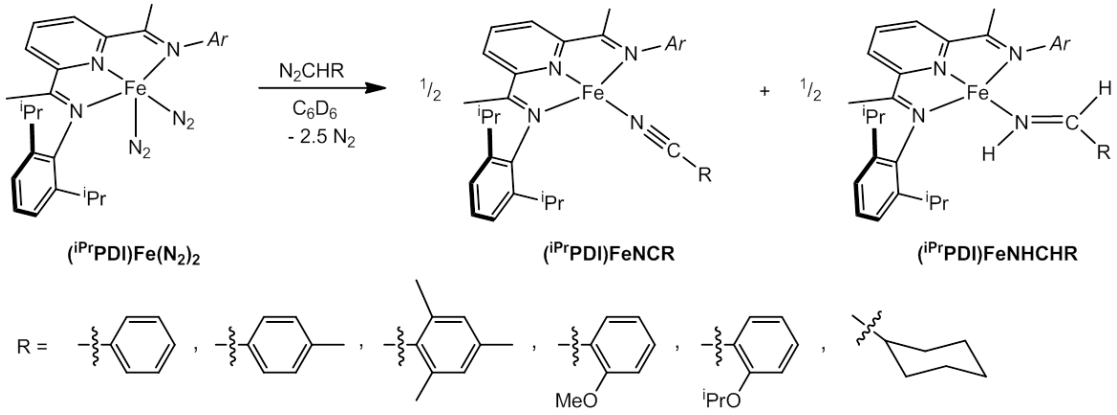

Figure 2.3 Scope of diazoalkane N-N bond cleavage with (^{iPr}PDI)Fe(N_2)$_2$.

The bis(imino)pyridine iron benzaldimine compound, (^{iPr}PDI)FeNHCHPh, was independently synthesized from addition of one atmosphere of H_2 to isolated (^{iPr}PDI)FeNCPh (Figure 2.4). After six hours at room temperature, the solution had changed from blue-green to emerald green, indicating formation of the benzaldimine compound. Like the bis(imino)pyridine iron benzonitrile compound, (^{iPr}PDI)FeNHCHPh, also has a ^{1}H NMR spectrum which exhibits features consistent with temperature independent paramagnetism.[13] The imine methyl group in this case is shifted farther upfield to -2.82 ppm, while the *meta*- and *para*-pyridine peaks appear at 11.16 and 9.10 ppm, respectively. As with (^{iPr}PDI)FeNCPh, these chemical shifts do not change upon heating to 60 °C or cooling to -60 °C. One notable feature of the ^{1}H NMR spectrum of (^{iPr}PDI)FeNHCHPh is the pair of doublets at 3.74 and 17.95

ppm ($^3J_{H\text{-}H}$ = 21.6 Hz) in benzene-d_6, corresponding to the C-H and N-H, respectively, of the coordinated imine. The assignment of these peaks was confirmed by a ^{1}H, ^{13}C HSQC NMR experiment and isotopic labeling with D_2 gas. The infrared N-H stretching frequency of the coordinated imine appears at 3142 cm^{-1} in pentane. Upon labeling with D_2 gas, the N-D stretching frequency appeared at 2248 cm^{-1}, close to the expected value of 2292 cm^{-1}. The formation of (^{iPr}PDI)FeNDCDPh was also confirmed by ^{2}H NMR spectroscopy, where two peaks were observed at 3.74 and 17.93 ppm for the coordinated imine C-D and N-D resonances, respectively.

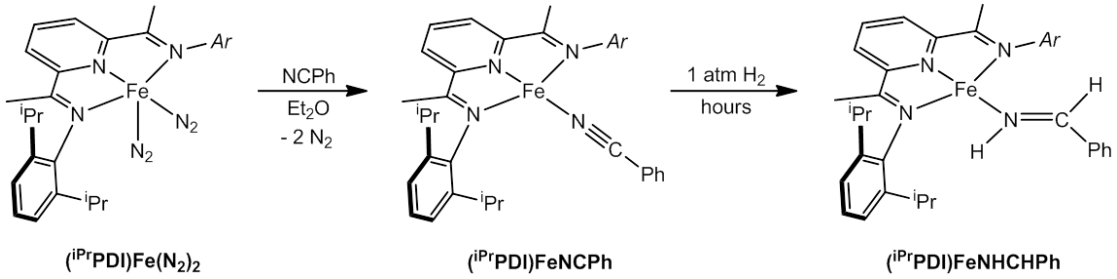

Figure 2.4 Independent syntheses of (^{iPr}PDI)FeNCPh and (^{iPr}PDI)FeNHCHPh.

The bis(imino)pyridine iron benzaldimine compound, (^{iPr}PDI)FeNHCHPh, was characterized by X-ray crystallography (Figure 2.5). Selected bond distances and angles are reported in Table 2.1. The X-ray data was of sufficient quality such that all of the hydrogen atoms were located in the difference map, establishing a *trans* orientation of the coordinated imine, consistent with the large ^3J coupling constant observed by solution ^{1}H NMR spectroscopy. The molecular geometry of (^{iPr}PDI)FeNHCHPh is essentially planar with the sum of the angles about iron equal to 359.18(14)°. The distortions in the bond distances of the bis(imino)pyridine chelate are consistent with two electron reduction with elongated N_{imine}-C_{imine} bond distances of 1.356(2) and 1.350(2) Å and contracted C_{imine}-$C_{pyridine}$ bond distances of 1.412(2)

and 1.411(3) Å. The Fe-N bond distances to the bis(imino)pyridine chelate and to the coordinated imine ligand indicate an intermediate spin iron center. The benzaldimine ligand shows little distortion from coordination to the iron center with a C-N bond distance of 1.278(4) Å, consistent with a double bond.

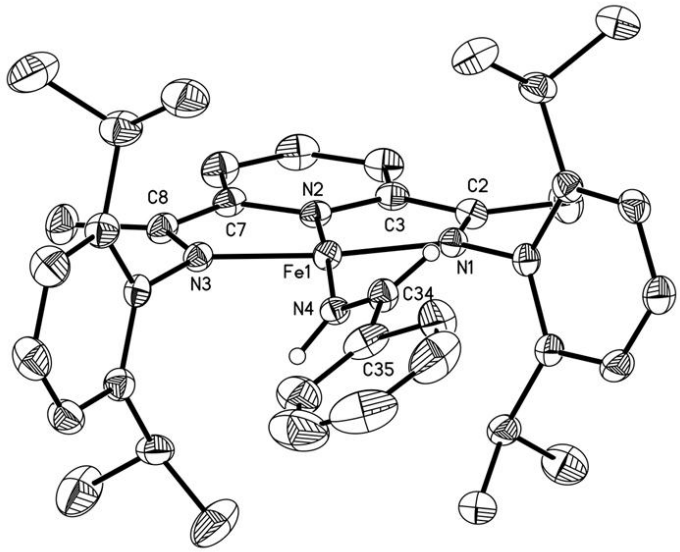

Figure 2.5 Solid state structure of (^{iPr}PDI)FeNHCHPh at 30 % probability ellipsoids. Hydrogen atoms, except those on the imine, omitted for clarity.

Table 2.1 Selected bond distances (Å) and angles (°) for (^{iPr}PDI)FeNHCHPh.

Fe(1)-N(1)	1.9015(14)	N(1)-C(2)	1.356(2)
Fe(1)-N(2)	1.8302(13)	N(3)-C(8)	1.350(2)
Fe(1)-N(3)	1.8961(14)	C(2)-C(3)	1.412(2)
Fe(1)-N(4)	1.938(2)	C(7)-C(8)	1.411(3)
N(4)-C(34)	1.278(4)	Fe(1)-N(4)-C(34)	134.1(2)
		N(4)-C(34)-C(35)	122.9(3)

Continued exposure of (^{iPr}PDI)FeNHCHPh to one atmosphere of H_2 in benzene-d_6 yielded the iron benzylamine complex, (^{iPr}PDI)FeNH_2CH_2Ph, after one week (Figure 2.6). This compound was independently synthesized by addition of one equivalent of benzylamine to (^{iPr}PDI)Fe$(N_2)_2$ resulting in a color change from green to red. Analogous to bis(imino)pyridine iron amine compounds, (^{iPr}PDI)FeNH_3[12] and (^{iPr}PDI)Fe$NH_2CH_2CH{=}CH_2$),[14] this compound also exhibits ^{1}H NMR spectroscopic features consistent with temperature independent paramagnetism.[13] The imine methyl resonance is shifted upfield to -6.11 ppm and the *meta*- and *para*-pyridine peaks are shifted downfield to 12.08 and 8.77 ppm, respectively. The N-H infrared stretching frequencies are 3245 and 3304 cm^{-1}.

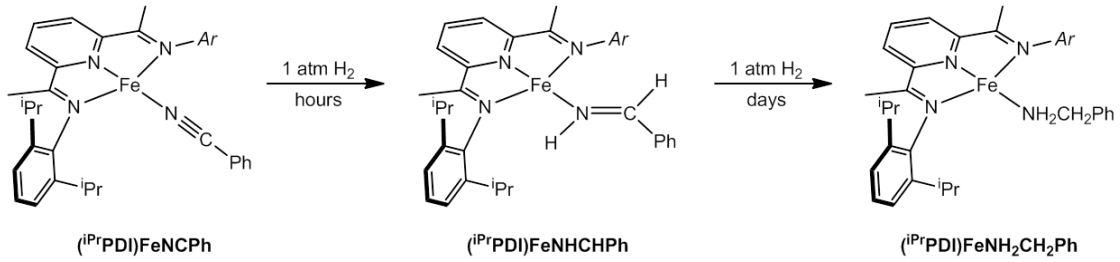

Figure 2.6 Hydrogenation of (^{iPr}PDI)FeNCPh to (^{iPr}PDI)FeNH_2CH_2Ph.

The scope of N-N bond cleavage was studied with a series of monosubstituted diazoalkanes. Steric effects were investigated with the addition of N_2CH(4-Me-C_6H_4) and N_2CH(2,4,6-$Me_3C_6H_2$) to (^{iPr}PDI)Fe$(N_2)_2$ and electronic effects with addition of $N_2CH(C_6H_{11})$. In each case, rapid and quantitative conversion to the corresponding bis(imino)pyridine iron nitrile and imine complexes was observed (Figure 2.3). All of the bis(imino)pyridine iron nitrile and imine complexes exhibit NMR and infrared spectroscopic features similar to (^{iPr}PDI)FeNCPh and (^{iPr}PDI)FeNHCHPh.

One monosubstituted diazoalkane that gave a slightly different result when added to (^{iPr}PDI)Fe$(N_2)_2$ was N_2CH^tBu. In this case, the corresponding

bis(imino)pyridine iron nitrile and imine compounds, (^{iPr}PDI)FeNC^{t}Bu and (^{iPr}PDI)FeNHCH^{t}Bu, were formed, but a third product, identified as the bis(imino)pyridine iron diazoalkane compound, (^{iPr}PDI)FeN_2CH^{t}Bu, was obtained in approximately 60% yield (Figure 2.7). The diazoalkane compound, (^{iPr}PDI)FeN_2CH^{t}Bu, exhibits a characteristic infrared N-N stretching frequency of 2043 cm^{-1} for the coordinated diazoalkane. The ^{1}H NMR spectrum is sharp and shows the number of peaks consistent with a C_{2v} symmetric molecule, indicating that in solution the diazoalkane ligand is likely η^1-coordinated allowing free rotation about the Fe-N_{diazo} bond. In analogy to the previously reported trimethylsilyl substituted diazoalkane compound, (^{iPr}PDI)FeN_2CHSiMe_3,[12] (^{iPr}PDI)FeN_2CH^{t}Bu also exhibits temperature independent paramagnetism in its ^{1}H NMR spectrum, with the imine methyl group shifted upfield to 0.20 ppm.

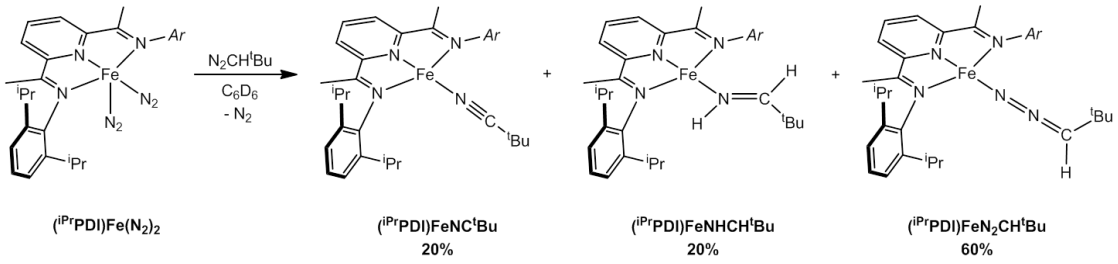

Figure 2.7 Addition of $N_2CH^{t}Bu$ to (^{iPr}PDI)Fe$(N_2)_2$ to yield (^{iPr}PDI)FeNC^{t}Bu, (^{iPr}PDI)FeNHCH^{t}Bu and (^{iPr}PDI)FeN_2CH^{t}Bu.

The *tert*-butyl substituted diazoalkane compound, (^{iPr}PDI)FeN_2CH^{t}Bu, exhibited similar reactivity to (^{iPr}PDI)FeN_2CHSiMe_3, which has an η^1-coordinated diazoalkane ligand.[12] In solution (^{iPr}PDI)FeN_2CHSiMe_3 is thermally unstable, converting quantitatively to the intramolecular bis(imino)pyridine iron olefin compound with concomitant loss of $SiMe_4$ (Figure 2.2). Similarly, in benzene-d_6 at 23°C, (^{iPr}PDI)FeN_2CH^{t}Bu converted completely to the same NMR-silent

intramolecular olefin compound and one equivalent of neopentane. Also, addition of one atmosphere of H_2 to (^{iPr}PDI)FeN_2CH^tBu resulted in N-N and N-C hydrogenative cleavage to yield previously characterized (^{iPr}PDI)FeNH_3 and neopentane. Interestingly, the diazoalkane compound, (^{iPr}PDI)FeN_2CH^tBu, did not convert to (^{iPr}PDI)FeNC^{t}Bu and (^{iPr}PDI)FeNHCH^tBu, indicating that it is not an intermediate on the path for N-N bond cleavage.

To further study the scope of the N-N bond cleavage reaction, phenyldiazomethane was added to bis(imino)pyridine iron dinitrogen compounds with smaller aryl substituents. Addition of N_2CHPh to both [(^{Et}PDI)Fe$(N_2)]_2(\mu_2$-$N_2)$ and [(^{Me}PDI)Fe$(N_2)]_2(\mu_2$-$N_2)$ resulted in immediate and quantitative conversion to the corresponding bis(imino)pyridine iron benzonitrile and benzaldimine compounds. Because the reactivity of (^{iPr}PDI)Fe$(N_2)_2$ is better understood than the reactivity of the dimeric dinitrogen compounds, the mechanism of the N-N bond cleavage reaction was probed only with (^{iPr}PDI)Fe$(N_2)_2$.

2.4 Deuterium Labeling and Mechanistic Studies of N-N Bond Cleavage

Several additional experiments were performed to help elucidate the mechanism of diazoalkane N-N bond cleavage by bis(imino)pyridine iron dinitrogen compounds. Addition of 0.5 equivalents of benzaldazine, PhHC=N-N=CHPh, to (^{iPr}PDI)Fe$(N_2)_2$ resulted in immediate conversion to (^{iPr}PDI)FeNCPh and (^{iPr}PDI)FeNHCHPh. Symmetric azine N-N bond cleavage to form two M-N=CR_2 species is well-documented.[15] Triiron dodecacarbonyl has been shown to cleave ketazine substrates to form bis(μ_2-ketoiminato)-(bis)tricarbonyliron complexes.[16] In contrast to the reaction with ketazines, addition of benzaldazine to $Fe_3(CO)_{12}$ did not result in N-N bond cleavage. Instead, *ortho*-proton rearrangement to the azomethine carbon and the metallization of the phenyl ring was observed.[17]

In 2003, Milstein and coworkers reported the first metal-promoted nonsymmetrical cleavage of the N-N bond of benzaldazine with a PCP-pincer rhodium(I) dinitrogen complex.[18] Addition of benzaldazine to (PCP)Rh(N_2) led to the formation of the (PCP)Rh benzonitrile and benzaldimine compounds, the latter of which is unstable in toluene solution at room temperature and decomposed to unidentified products. When an excess of benzaldazine was added to the rhodium compound catalytic N-N bond cleavage was observed to produce free benzonitrile and benzaldimine.

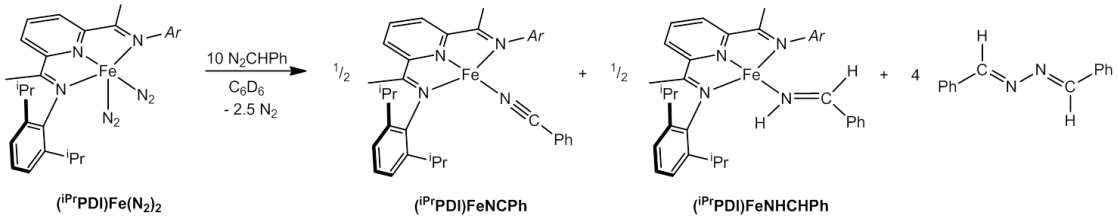

Figure 2.8 Catalytic formation of benzaldazine by (^{iPr}PDI)Fe(N_2)$_2$.

Although (^{iPr}PDI)Fe(N_2)$_2$ does not catalytically cleave the N-N bond of azines, the bis(imino)pyridine iron dinitrogen compound does couple diazoalkanes to form azines catalytically. Addition of 10 equivalents of phenyldiazomethane to (^{iPr}PDI)Fe(N_2)$_2$ resulted in formation of the expected N-N bond cleavage products, (^{iPr}PDI)FeNCPh and (^{iPr}PDI)FeNHCHPh, as well as free benzaldazine (Figure 2.8). Treatment of the product mixture with 10 additional equivalents of phenyldiazomethane produced more benzaldazine, demonstrating the catalytic competence of (^{iPr}PDI)Fe(N_2)$_2$ as well as one, or both, of (^{iPr}PDI)FeNCPh and (^{iPr}PDI)FeNHCHPh for the conversion of diazoalkanes to azine. Catalytic formation of azines from diazoalkanes has also been reported for a ruthenium pyridine bis(oxazoline) compound[19] and for a tridentate tantalum(V) complex.[20] A crossover

experiment was performed where a mixture of 5 equivalents of N_2CHPh and 5 equivalents of $N_2CH(4\text{-Me-}C_6H_4)$ in benzene-d_6 was added to a benzene-d_6 solution of (^{iPr}PDI)Fe(N_2)$_2$. All four expected N-N bond cleavage products as well as the three possible azine products, PhHC=N-N=CHPh, PhHC=N-N=CH(4-Me-C_6H_4) and (4-Me-C_6H_4)HC=N-N=CH(4-Me-C_6H_4), were observed. The three azines were observed in approximately a 1:1:1 mixture as determined by ^{1}H NMR spectroscopy and GC-MS.

An isotopic labeling experiment was conducted with deuterated phenyldiazomethane to investigate the rate determining step of N-N bond cleavage. Addition of N_2CDPh to (^{iPr}PDI)Fe(N_2)$_2$ in benzene-d_6 resulted in clean conversion to (^{iPr}PDI)FeNCPh and (^{iPr}PDI)FeNDCDPh with no evidence for deuterium incorporation into the bis(imino)pyridine chelate of either compound. The formation of (^{iPr}PDI)FeNDCDPh was confirmed by comparison to an independently prepared sample from D_2 addition to (^{iPr}PDI)FeNCPh. Monitoring the reaction by ^{1}H and ^{2}H NMR spectroscopy in benzene at 23°C over the course of minutes revealed the formation of a C_s symmetric intermediate (Figure 2.9) with a half-life of approximately 15 minutes, which was not detected when the reaction was performed with natural abundance N_2CHPh. The intermediate has a ^{2}H NMR resonance located at 5.20 ppm in benzene and no discernible N-N or N-D stretching frequency in the infrared spectrum. Performing the reaction with an internal ferrocene standard showed that 2 completely converts to (^{iPr}PDI)FeNCPh and (^{iPr}PDI)FeNDCDPh in under an hour, confirming its assignment as an intermediate on the N-N bond cleavage pathway. Unfortunately, the intermediate cannot be conclusively identified; however, based on the limited data, the likely possibilities are either the bis(imino)pyridine iron benzylidene, [(^{iPr}PDI)Fe=CDPh] or the metallacycle, (^{iPr}PDI)Fe(PhDCNNCDPh). Regardless of the identity of the intermediate, the fact that an intermediate was not

observed with natural abundance phenyldiazomethane suggests that the rate determining step of N-N bond cleavage is a C-H(D) bond breaking event.

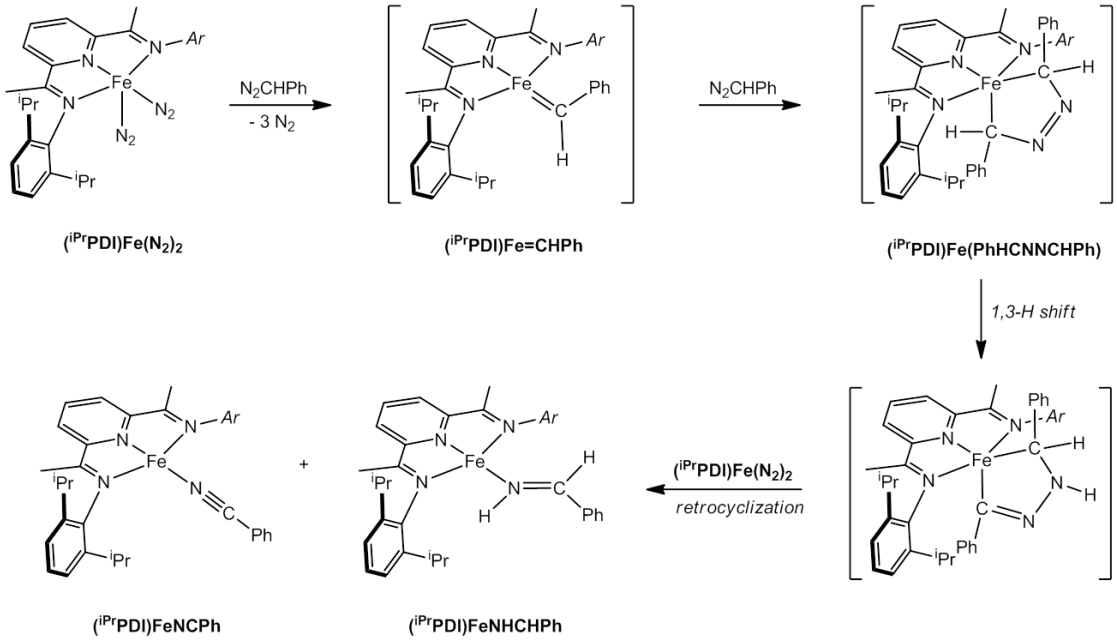

Figure 2.9 Proposed mechanism for diazoalkane N-N bond cleavage by (^{iPr}PDI)Fe(N_2)$_2$.

Taking all of these studies into account, a proposed mechanism for the N-N bond cleavage of mono-substituted diazoalkanes is presented in Figure 2.9 using N_2CHPh as a model substrate. The mechanism begins with the formation of the bis(imino)pyridine iron alkylidene, [(^{iPr}PDI)Fe=CHPh], arising from nucleophilic attack of (^{iPr}PDI)Fe(N_2)$_2$ on the diazoalkane carbon. The transient iron alkylidene then undergoes a rapid [4π + 2π] cycloaddition with a second equivalent of diazoalkane to generate the bis(imino)pyridine iron azine compound, (^{iPr}PDI)Fe(PhDCNNCDPh), which likely was the observed intermediate with N_2CDPh. A rate-determining 1,3-hydrogen shift followed by retrocyclization forms the separate nitrile and imine entities. Finally, a linkage isomerization to form the observed iron-nitrogen bonds of

the products and capture of either free nitrile or imine by an additional bis(imino)pyridine iron species occurs to yield (^{iPr}PDI)FeNCPh and (^{iPr}PDI)FeNHCHPh.

Because the initial goal of adding diazoalkanes to bis(imino)pyridine iron dinitrogen complexes was to form a bis(imino)pyridine iron alkylidene, several attempts were made to observe or trap putative [(^{iPr}PDI)Fe=CHPh] formed during the N-N bond cleavage pathway. Reaction conditions were systematically varied in hopes of preventing metallacycle formation. Slow or inverse addition of diazoalkane to (^{iPr}PDI)Fe(N_2)$_2$ and running the reaction at low temperatures still resulted in immediate N-N bond cleavage with no evidence for any intermediates. Addition of diazoalkane in the presence of external trapping reagents such norbornene, isoprene, styrene, acetophenone, benzaldehyde, pyridine or 4 atmospheres of H_2 also had no effect on the product distribution.

Attempts at intramolecular trapping were also unsuccessful. The *ortho*-alkoxy substituted diazoalkanes, N_2CH(2-OMe-C_6H_4) and N_2CH(2-O-^{i}Pr-C_6H_4), popularized by Hoveyda and co-workers,[21] were added to (^{iPr}PDI)Fe(N_2)$_2$ in hopes of stabilizing the transient alkylidene through Lewis base coordination of the *ortho*-alkoxy oxygen atom. Although the bis(imino)pyridine iron alkylidene could not be trapped, the fact that the diazoalkane compound, (^{iPr}PDI)FeN_2CH^{t}Bu, does not react with excess diazoalkane to form the corresponding N-N bond cleavage products suggests that the reaction pathway must go through a different initial step, likely the formation of an iron alkylidene.

2.5 Addition of Disubstituted Diazoalkanes

In order to isolate a bis(imino)pyridine iron alkylidene, the diazoalkane N-N bond cleavage pathway has to be disrupted. One method of preventing N-N bond

cleavage would be to inhibit metallacycle formation by increasing the size of the diazoalkane substituents. A second approach would be to prevent the opportunity for 1,3-hydrogen atom migration by replacing the hydrogen atom with an alkyl or aryl group. This way, even if metallacycle formation occurs, it may be reversible, allowing for more facile trapping of the intermediate alkylidene. To address both of these issues, the disubstituted diazoalkane, phenyldiazoethane, $N_2C(Me)Ph$, was synthesized and its reaction with several bis(imino)pyridine iron dinitrogen compounds was studied.

Addition of one equivalent of $N_2C(Me)Ph$ to a diethyl ether solution of (^{iPr}PDI)Fe(N_2)$_2$ resulted in immediate formation of the blue-green bis(imino)pyridine iron diazoalkane compound, (^{iPr}PDI)FeN_2C(Me)Ph (Figure 2.10). Analogous to other bis(imino)pyridine iron diazoalkane complexes, (^{iPr}PDI)FeN_2C(Me)Ph has a diagnostic infrared N-N stretching frequency at 2045 cm^{-1}. The ^{1}H NMR spectrum of (^{iPr}PDI)FeN_2C(Me)Ph exhibits the number of peaks for a C_{2v} symmetric molecule in solution, indicating that either the diazoalkane ligand comes on and off the metal center or that the diazoalkane can rotate freely about the Fe-N bond on the NMR timescale. Similar to the spectra of the other bis(imino)pyridine iron η^1-diazoalkane compounds, the ^{1}H NMR spectrum of (^{iPr}PDI)FeN_2C(Me)Ph exhibits temperature independent paramagnetism, with the imine methyl group shifted upfield to 0.01 ppm.

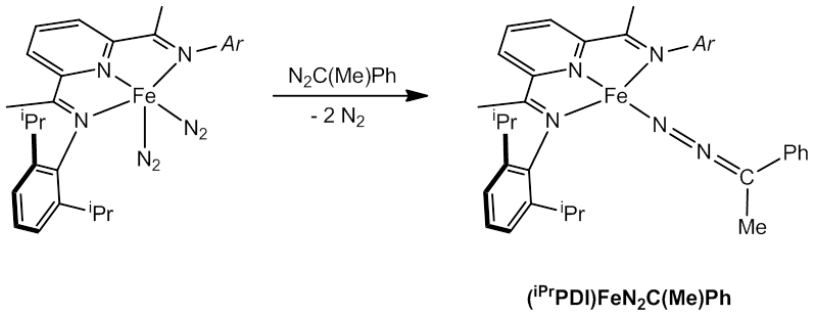

Figure 2.10 Synthesis of (^{iPr}PDI)FeN_2C(Me)Ph from addition of $N_2C(Me)Ph$ to (^{iPr}PDI)Fe(N_2)$_2$.

Decreasing the size of the substituents on the bis(imino)pyridine aryl rings led to different reactivity with phenyldiazoethane. Addition of one equivalent per iron center of $N_2C(Me)Ph$ to either $[(^{Et}PDI)Fe(N_2)]_2(\mu_2\text{-}N_2)$ or $[(^{Me}PDI)Fe(N_2)]_2(\mu_2\text{-}N_2)$ resulted in formation of new diamagnetic bis(imino)pyridine iron compounds, but an approximately equal amount of the starting dinitrogen compound was still present. Increasing the amount of added diazoalkane to two equivalents per iron center resulted in complete conversion to the previously observed diamagnetic product, identified as the corresponding bis(imino)pyridine iron azine compound, $(^{R}PDI)Fe(Ph(Me)CNNC(Me)Ph)$ (R = Et, Me) (Figure 2.11).

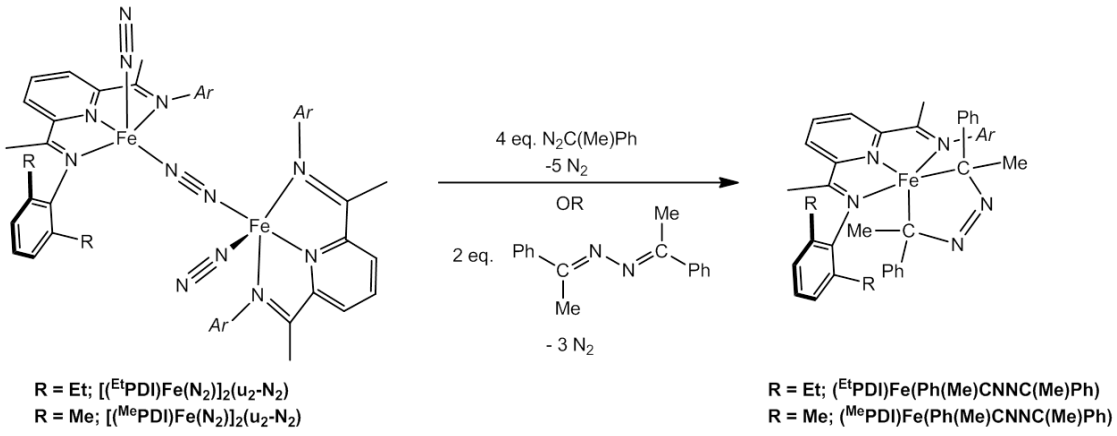

Figure 2.11 Syntheses of bis(imino)pyridine iron azine complexes, $(^{R}PDI)Fe(Ph(Me)CNNC(Me)Ph)$ (R = Et, Me).

The azine compounds were independently prepared from addition of acetophenone azine to the corresponding dinitrogen compound (Figure 2.11). The ^1H NMR spectra of both azine compounds exhibit the number of peaks consistent with C_{2v} symmetry. The spectra for both compounds also exhibit little evidence of contributions from temperature independent paramagnetism, with the imine methyl groups appearing at 1.87 and 1.83 ppm in $(^{Et}PDI)Fe(Ph(Me)CNNC(Me)Ph)$ and

(^{Me}PDI)Fe(Ph(Me)CNNC(Me)Ph), respectively. The peaks for (^{Et}PDI)Fe(Ph(Me)CNNC(Me)Ph) are sharp and exhibit coupling while those for the methylated compound are broad, suggesting that the reduced steric hindrance of ^{Me}PDI allows for a dynamic process to occur in solution.

Surprisingly, the symmetry of both (^{Et}PDI)Fe(Ph(Me)CNNC(Me)Ph) and (^{Me}PDI)Fe(Ph(Me)CNNC(Me)Ph) observed in solution is different from that of the postulated intermediate azine complex, 2, observed from addition of N_2CDPh to (^{iPr}PDI)Fe(N_2)$_2$. While the acetophenone azine complexes have C_{2v} symmetry in a benzene-d_6 solution, 2 appears to have C_s symmetry under the same conditions. The difference in symmetry between the compounds suggests that either the mechanism for diazoalkane N-N bond cleavage is more complicated than what is proposed in Section 2.4 or that the observed intermediate, 2, is not the azine compound as proposed. Another possibility is that the steric difference between a deuterium and a methyl substituent on the sp^2 carbon causes a change in coordination mode of the azine ligand or in how tightly the azine ligand coordinates to the iron center. A situation in which the azine ligand dissociates and recoordinates faster than the NMR time scale could cause the observed C_{2v} symmetry. Similarly, the change in size of the bis(imino)pyridine aryl substituents may also result in changes in coordination.

The formation of the azine complexes from N_2C(Me)Ph with the smaller bis(imino)pyridine ligands provides support for the proposed mechanism of diazoalkane N-N bond cleavage of monosubstituted diazoalkanes. While the change from a hydrogen to a methyl group as the second substituent on the diazoalkane did not provide enough steric hindrance to prohibit metallacycle formation, it did inhibit the 1,3-hydrogen migration path.

2.6 Conclusions

The addition of phenyldiazomethane, N_2CHPh, to the bis(imino)pyridine iron dinitrogen compound (^{iPr}PDI)Fe$(N_2)_2$ resulted in formation of a 1:1 ratio of the corresponding iron benzonitrile compound, (^{iPr}PDI)FeNCPh, and the iron benzaldimine compound, (^{iPr}PDI)FeNHCHPh. Mechanistic studies suggest initial formation of a transient bis(imino)iron alkylidene species which undergoes a rapid [4π + 2π] cycloaddition with a second equivalent of diazoalkane to form an iron metallacycle. The metallacycle then undergoes a 1,3-hydrogen shift followed by a retrocyclization to yield the observed iron nitrile and imine complexes. Performing the addition with labeled phenyldiazomethane, N_2CDPh, allowed observation of the intermediate 2 on the N-N bond cleavage pathway, putatively assigned as the bis(imino)pyridine iron metallacycle, (^{iPr}PDI)Fe(PhDCNNCDPh). The deuterium labeling studies also support the 1,3-hydrogen shift as the rate determining step in the proposed mechanism.

Altering the steric or electronic environment of the diazoalkane substrate by investigating substituted phenyldiazomethanes (e.g $N_2CH(4\text{-}Me\text{-}C_6H_4)$ and $N_2CH(2,4,6\text{-}Me_3\text{-}C_6H_2)$), and cyclohexyldiazomethane ($N_2CH(C_6H_{11})$), respectively, did not change the products of the reaction. The product distribution was only altered when *tert*-butyl diazomethane was studied. Addition of N_2CH^tBu to (^{iPr}PDI)Fe$(N_2)_2$ resulted in formation of the bis(imino)pyridine iron diazoalkane compound, (^{iPr}PDI)FeN_2CH^tBu, as well as the nitrile and imine compounds. The diazoalkane compound does not convert to the nitrile and imine compounds indicating that this species is not on the pathway of N-N bond cleavage and that the putative bis(imino)pyridine iron alkylidene likely forms from direct reaction of the iron center with the diazoalkane carbene carbon. The observation of (^{iPr}PDI)FeN_2CH^tBu also

suggests that as the steric bulk of the diazoalkane increases, the ability to form the iron alkylidene decreases and coordination of the diazoalkane becomes competitive.

Addition of a disubstituted diazoalkane, $N_2C(Me)Ph$, to (^{iPr}PDI)Fe$(N_2)_2$ furnished the bis(imino)pyridine iron diazoalkane compound (^{iPr}PDI)FeN_2C(Me)Ph. Decreasing the size of the aryl substituents on the bis(imino)pyridine ligand to ethyl or methyl resulted in formation of the corresponding iron azine complexes, (^{Et}PDI)Fe(Ph(Me)CNNC(Me)Ph) and (^{Me}PDI)Fe(Ph(Me)CNNC(Me)Ph), and provides further support for the proposed mechanism of N-N bond cleavage. Most importantly, the observation of the azine compounds and the N-N bond cleavage reaction suggest that the formation of a isolable bis(imino)pyridine iron alkylidene may be possible under the appropriate conditions.

2.7 Experimental Procedures

General Considerations. All air- and moisture-sensitive manipulations were carried out using standard vacuum line, Schlenk and cannula techniques or in an MBraun inert atmosphere dry box containing an atmosphere of purified nitrogen. Solvents for air- and moisture-sensitive manipulations were initially dried and deoxygenated using literature procedures.[22] Hydrogen and deuterium gas were passed through a column containing manganese oxide supported on vermiculite and 4 Å molecular sieves before admission to the high vacuum line. Benzene-d_6 and toluene-d_8 were purchased from Cambridge Isotope Laboratories and dried over 4 Å molecular sieves or titanocene, respectively. (^{iPr}PDI)Fe$(N_2)_2$,[23] [(^{Et}PDI)Fe(N_2)]$_2(\mu_2$-$N_2)$[24] and [(^{Me}PDI)Fe(N_2)]$_2(\mu_2$-$N_2)$[24] were prepared according to literature procedures. Phenyldiazomethane, tolyldiazomethane, mesityldiazomethane, cyclohexyldiazomethane and *tert*-butyldiazomethane were prepared as described previously by vacuum pyrolysis of the corresponding tosylhydrazone salts at 90 - 110 °C.[25] (2-methoxyphenyl)-diazomethane

and (2-isopropoxyphenyl)-diazomethane were synthesized according to literature procedure.[21] Phenyldiazomethane-d_1 was prepared from tosylhydrazone-d_3[26] and benzaldehyde-d_1 according to a modified literature procedure.[27] 1-Phenyldiazoethane was synthesized according to literature procedure.[28] Acetophenone azine was purchased from Sigma Aldrich and dried on the high vacuum line for 16 hours.

^{1}H NMR spectra were recorded on Varian Mercury 300, Inova 400, 500, and 600 spectrometers operating at 299.76, 399.78, 500.62, and 599.78 MHz, respectively. ^{2}H NMR spectra were recorded at 20 ºC on an Inova 400, 500, and 600 MHz spectrometers operating at 61.37, 76.85, and 92.07 MHz, respectively. All ^{1}H chemical shifts are reported relative to $SiMe_4$ using the ^{1}H (residual) shift of the solvent as a secondary standard. Elemental analyses were performed at Robertson Microlit Laboratories, Inc., in Madison, NJ.

Single crystals suitable for X-ray diffraction were coated with polyisobutylene oil in a drybox, transferred to a nylon loop and then quickly transferred to the goniometer head of a Bruker X8 APEX2 diffractometer equipped with a molybdenum X-ray tube (λ = 0.71073 Å). Preliminary data revealed the crystal system. A hemisphere routine was used for data collection and determination of lattice constants. The space group was identified and the data were processed using the Bruker SAINT+ program and corrected for absorption using SADABS. The structures were solved using direct methods (SHELXS) completed by subsequent Fourier synthesis and refined by full-matrix least-squares procedures.

Preparation of (^{iPr}PDI)FeNCPh. A 20-mL scintillation vial was charged with 0.057 g (0.097 mmol) of (^{iPr}PDI)Fe(N_2)$_2$ and approximately 10 mL diethyl ether forming a green solution. A solution containing 0.010 g (0.097 mmol) benzonitrile in 5 mL diethyl ether was added to the vial resulting in an immediate color change to green.

The resulting solution was stirred for approximately 45 minutes after which time the volatiles were removed in vacuo yielding 0.059 g (95%) of a green solid identified as (^{iPr}PDI)FeNCPh. Analysis for $C_{40}H_{48}N_4Fe$: Calc. C, 75.46; H, 7.60; N, 8.80. Found C, 75.43; H, 7.66; N, 8.41. ^{1}H NMR (benzene-d_6): δ = -0.72 (d, 6.8 Hz, 12H, CH(CH_3)$_2$), -0.12 (s, 6H, C(CH_3)), 1.47 (d, 6.8 Hz, 12H, CH(CH_3)$_2$), 2.38 (sept, 6.8 Hz, 4H, CH(CH$_3$)$_2$), 6.08 (t, 7.6 Hz, 1H, *p*-Ph), 6.18 (d, 7.2 Hz, 2H, *o*-Ph), 7.07 (t, 7.6 Hz, 2H, *m*-Ph), 7.66 (d, 8 Hz, 4H, *m*-Ar), 7.98 (t, 7.6 Hz, 2H, *p*-Ar), 9.10 (t, 1H, 7.6, *p*-pyr), 11.32 (d, 2H, 7.6, *m*-pyr). ^{13}C NMR (benzene-d_6): δ = 24.26 (CH(*C*H$_3$)$_2$), 26.84 (CH(*C*H$_3$)$_2$), 35.32(*C*H(CH$_3$)$_2$), 95.96 (*m*-pyr), 124.16 (*p*-Ar), 124.89 (*o*-Ph), 125.36 (*m*-Ar), 129.46 (*m*-Ph and *p*-Ph), 145.32 (*p*-pyr), 151.58, 160.76, 172.95. IR (pentane): ν(C≡N) 2169 cm^{-1}.

Preparation of (^{iPr}PDI)FeNHCHPh. A thick-walled glass vessel was charged with 0.050 g (0.079 mmol) of (^{iPr}PDI)FeNCPh and approximately 20 mL diethyl ether forming a blue-green solution. The vessel was submerged in liquid nitrogen and evacuated on the high vacuum line. Four atmospheres of H_2 were added and the contents of the vessel warmed to room temperature. The solution was stirred for 6 hours after which time the volatiles were removed *in vacuo* yielding 0.046 g (91%) of an emerald green solid identified as (^{iPr}PDI)FeNHCHPh. Analysis for $C_{40}H_{50}N_4Fe$: Calc. C, 75.22; H, 7.89; N, 8.77. Found C, 74.91; H, 7.73; N, 8.81. ^{1}H NMR (benzene-d_6): δ = -2.82 (s, 6H, C(CH_3)), -0.55 (d, 6.8 Hz, 12H, CH(CH_3)$_2$), 1.27 (d, 6.8 Hz, 12H, CH(CH_3)$_2$), 2.56 (sept, 6.8 Hz, 4H, CH(CH$_3$)$_2$), 3.74 (d, 22 Hz, 1H, NHCHPh), 6.70 (t, 8 Hz, 1H, *p*-Ph), 6.78 (d, 8 Hz, 2H, *o*-Ph), 7.42 (d, 8 Hz, 4H, *m*-Ar), 7.80 (t, 8 Hz, 2H, *p*-Ar), 9.10 (t, 1H, 7.6, *p*-pyr), 11.16 (d, 2H, 7.6, *m*-pyr), 17.95 (d, 21.6 Hz, 1H, NHCHPh), *m*-Ph resonance not located. ^{13}C NMR (benzene-d_6): δ = 24.23 (CH(*C*H$_3$)$_2$), 24.44 (CH(*C*H$_3$)$_2$), 30.0 (C(*C*H$_3$)), 30.62 (*C*H(CH$_3$)$_2$), 102.31 (*m*-

pyr), 125.04 (*m*-, *p*-Ar), 128.50 (*o*- and *m*-*Ph*), 132.3 (*p*-*Ph*) 140.46 (*p*-pyr), 141.00, 161.02, 170.10 (NH*C*HPh), 175.24, 176.45. IR (pentane): ν (N-H) 3241 cm^{-1}.

Preparation of (^{iPr}PDI)FeNH$_2$CH$_2$Ph. A 20-mL scintillation vial was charged with 0.051 g (0.086 mmol) of (^{iPr}PDI)Fe(N_2)$_2$ and 10 mL pentane forming a green solution. A solution of 0.009 g (0.086 mmol) of benzylamine in 3 mL pentane was prepared and added to the vial resulting in an immediate color change to red-brown. The reaction mixture was stirred for approximately 45 minutes after which time the volatiles were removed *in vacuo* yielding 0.052 g (94%) of a dark solid identified as (^{iPr}PDI)FeNH$_2$CH$_2$Ph. Analysis for $C_{40}H_{52}N_4Fe$: Calc. C, 74.98; H, 8.18; N, 8.74. Found C, 75.16; H, 7.89; N, 8.77. ^{1}H NMR (benzene-d_6): δ = -6.11 (s, 6H, C(C*H*$_3$)), -0.36 (d, 6.8 Hz, 12H, CH(C*H*$_3$)$_2$), 0.25 (d, 5.6 Hz, 12H, CH(C*H*$_3$)$_2$), 2.07 (t, 8 Hz, 2H, NH$_2$C*H*$_2$Ph), 2.79 (sept, 6.8 Hz, 4H, C*H*(CH$_3$)$_2$), 5.12 (t, 8 Hz, 2H, N*H*$_2$CH$_2$Ph), 6.76 (d, 7.6 Hz, 2H, *o*-Ph), 7.01 (t, 7.2 Hz, 1H, *p*-Ph), 7.12 (d, 7.6 Hz, 2H, *m*-Ph), 7.32 (d, 8 Hz, 4H, *m*-Ar), 7.75 (t, 7.6 Hz, 2H, *p*-Ar), 8.77 (t, 7.2 Hz, 1H, *p*-pyr), 12.08 (d, 7.2 Hz, 2H, *m*-pyr). ^{13}C NMR (benzene-d_6): δ = 23.16 (CH(*C*H$_3$)$_2$), 24.32 (CH(*C*H$_3$)$_2$), 28.54 (*C*H(CH$_3$)$_2$), 48.19 (NH$_2$*C*H$_2$Ph), 103.06 (*m*-pyr), 124.64 (*m*-Ar), 125.21 (*p*-Ar), 129.56 (*o*-Ph), 136.84 (*m*-Ph and *p*-Ph), 140.12 (*p*-pyr), 142.26, 164.91, 165.46, 189.67. IR (pentane): ν (N-H) 3304 cm^{-1}, 3245 cm^{-1}.

Preparation of (^{iPr}PDI)FeNC(4-Me-C$_6$H$_4$). This compound was prepared in a similar manner to (^{iPr}PDI)FeNCPh with 0.047 g (0.079 mmol) of (^{iPr}PDI)Fe(N_2)$_2$ and 0.009 g (0.079 mmol) of p-tolunitrile to yield 0.048 g (92%) of a green solid identified as (^{iPr}PDI)FeNC(4-Me-C_6H_4). ^{1}H NMR (benzene-d_6): δ = -1.55 (s, 6H, C(*CH*$_3$)), -0.64 (d, 6.8 Hz, 12H, CH*(CH*$_3$*)*$_2$), 1.49 (d, 6.8 Hz, 12H, CH*(CH*$_3$*)*$_2$), 2.42 (s, 3H, tol CH_3), 2.61 (sept, 6.8 Hz, 4H, C*H*(CH$_3$)$_2$), 6.22 (d, 7.6 Hz, 2H, *m*-tol), 6.77 (d, 7.6 Hz, 2H, *o*-

tol), 7.66 (d, 7.6 Hz, 4H, *m*-Ar), 8.00 (t, 7.6 Hz, 2H, *p*-Ar), 9.33 (t, 7.6 Hz, 1H, *p*-pyr), 11.32 (d, 7.6 Hz, 2H, *m*-pyr). ^{13}C NMR (benzene-d_6): δ = 24.30 (CH(*C*H$_3$)$_2$), 26.16 (CH(*C*H$_3$)$_2$), 26.51 (tol *C*H$_3$), 33.71 (*C*H(CH$_3$)$_2$), 99.36 (*m*-pyr), 124.28 (*p*-Ar), 125.19 (*m*-Ar), 128.68 (tol CH) 143.72 (*p*-pyr), 161.57, 173.44 192.03. IR (pentane): ν (C≡N) 2173 cm^{-1}.

Preparation of (^{iPr}PDI)FeNHCH(4-Me-C$_6$H$_4$). This compound was prepared in an similar manner to (^{iPr}PDI)FeNHCHPh with 0.048 g (0.073) of (^{iPr}PDI)FeNC(4-Me-C$_6$H$_4$) and four atmospheres of H_2 to yield 0.041 g (86%) of a green solid identified as (^{iPr}PDI)FeNHCH(4-Me-C$_6$H$_4$). ^{1}H NMR (benzene-d_6): δ = -3.45 (s, 6H, C(*CH$_3$*)), -0.52 (d, 6.8 Hz, 12H, CH*(CH$_3$)$_2$*), 1.29 (d, 6.8 Hz, 12H, CH*(CH$_3$)$_2$*), 2.11 (s, 3H, tol CH$_3$), 2.67 (sept, 6.8 Hz, 4H, C*H*(CH$_3$)$_2$), 4.04 (d, 21.2 Hz, 1H, NHC*H*(tol)), 6.95 (d, 7.6 Hz, 2H, *m*-tol), 7.44 (d, 7.6 Hz, 2H, *o*-tol), 7.65 (d, 7.6 Hz, 4H, *m*-Ar), 7.83 (t, 7.6 Hz, 2H, *p*-Ar), 9.14 (t, 7.6 Hz, 1H, *p*-pyr), 11.29 (d, 7.6 Hz, 2H, *m*-pyr), 17.42 (d, 21.6 Hz, 1H, N*H*CH(tol)). ^{13}C NMR (benzene-d_6): δ = 24.18 (CH(*C*H$_3$)$_2$), 24.24 (CH(*C*H$_3$)$_2$), 27.16 (tol *C*H$_3$), 30.41 (*C*H(CH$_3$)$_2$), 102.46 (*m*-pyr), 124.93 (*m*-Ar), 125.05 (*p*-Ar), 140.01 (*p*-pyr), 140.90 (tol *C*H), 142.81 (tol *C*H), 148.75, 162.24, 175.52, 178.10, NH*C*H(tol) not located. IR (pentane): ν (N-H) 3241 cm^{-1}.

Preparation of (^{iPr}PDI)FeNC(2,4,6-Me$_3$-C$_6$H$_2$). This compound was prepared in a similar manner to (^{iPr}PDI)FeNCPh with 0.044 g (0.075 mmol) of (^{iPr}PDI)Fe(N$_2$)$_2$ and 0.011 g (0.076 mmol) of 2,4,6-trimethylbenzonitrile to yield 0.047 g (97%) of a green solid identified as (^{iPr}PDI)FeNC(2,4,6-Me$_3$-C$_6$H$_2$). Analysis for C$_{43}$H$_{45}$N$_4$Fe: Calc. C, 75.64; H, 7.97; N, 8.21. Found C, 75.24; H, 7.85; N, 8.02. ^{1}H NMR (benzene-d_6): δ = -3.03 (s, 6H, C(*CH$_3$*)), -0.56 (d, 6.8 Hz, 12H, CH*(CH$_3$)$_2$*), 1.46 (d, 6.8 Hz, 12H, CH*(CH$_3$)$_2$*), 1.59 (s, 6H, mes *o*-CH$_3$), 1.76 (s, 3H, mes *p*-CH$_3$), 2.76 (sept, 6.8 Hz, 4H,

C*H*(CH_3)$_2$), 6.43 (s, 2H, *m*-mes), 7.49 (d, 7.6 Hz, 4H, *m*-Ar), 7.81 (t, 7.6 Hz, 2H, *p*-Ar), 9.49 (t, 7.6 Hz, 1H, *p*-pyr), 11.46 (d, 7.6 Hz, 2H, *m*-pyr). ^{13}C NMR (benzene-d_6): δ = 23.57 (CH(*C*H_3)$_2$), 23.97 (CH(*C*H_3)$_2$), 24.07 (mes *C*H_3), 25.25 (mes *C*H_3), 33.00 (*C*H(CH_3)$_2$), 99.93 (*m*-pyr), 124.56 (*p*-Ar), 125.13 (*m*-Ar), 142.03 (*p*-pyr), 164.18, 180.52, 190.86. IR (pentane): ν (N≡C) 2170 cm^{-1}.

Preparation of (^{iPr}PDI)FeNHCH(2,4,6-Me_3-C_6H_2). This compound was prepared in a similar manner to (^{iPr}PDI)FeNHCHPh with 0.035 g (0.052 mmol) (^{iPr}PDI)FeNC(2,4,6-Me_3-C_6H_2) and four atmospheres of H_2 to yield 0.029 g (84%) of a green solid identified as (^{iPr}PDI)FeNHCH(2,4,6-Me_3-C_6H_2). Analysis for $C_{43}H_{47}N_4Fe$: Calc. C, 75.42; H, 8.24; N, 8.18. Found C, 75.27; H, 7.89; N, 7.87. ^{1}H NMR (benzene-d_6): δ = -4.17 (s, 6H, C(*CH*$_3$)), -0.40 (d, 6.8 Hz, 12H, CH(*CH*$_3$)$_2$), 1.29 (d, 6.8 Hz, 12H, CH(*CH*$_3$)$_2$), 1.78 (s, 3H, Mes *p*-CH_3), 1.86 (s, 6H, Mes *o*-CH_3), 2.70 (sept, 6.8 Hz, 4H, C*H*(CH_3)$_2$), 5.41 (d, 22.0 Hz, 1H, NHC*H*(Mes)), 6.49 (s, 2H, *m*-Mes), 7.28 (d, 7.6 Hz, 4H, *m*-Ar), 7.62 (t, 7.6 Hz, 2H, *p*-Ar), 9.14 (t, 7.6 Hz, 1H, *p*-pyr), 11.42 (d, 7.6 Hz, 2H, *m*-pyr), 16.59 (d, 22.0 Hz, 1H, N*H*CH(Mes)). ^{13}C NMR (benzene-d_6): δ = 23.57 (CH(*C*H_3)$_2$), 23.97 (CH(*C*H_3)$_2$), 24.07 (mes *C*H_3), 25.25 (mes *C*H_3), 29.99 (*C*H(CH_3)$_2$), 103.09 (*m*-pyr), 124.66 (*m*-Ar), 124.96 (*p*-Ar), 131.90 (mes CH), 139.17 (*p*-pyr), 163.06, 179.21, NH*C*H(mes) not located. IR (pentane): ν(N-H) 3241 cm^{-1}.

Preparation of (^{iPr}PDI)FeNC(C_6H_{11}). This compound was prepared in a similar manner to (^{iPr}PDI)FeNCPh with 0.022 g (0.037 mmol) of (^{iPr}PDI)Fe(N_2)$_2$ and 0.004 g (0.037 mmol) of cyclohexylnitrile to yield 0.023g (96%) of a green solid identified as (^{iPr}PDI)FeNC(C_6H_{11}). Analysis for $C_{40}H_{53}N_4Fe$: Calc. C, 74.29; H, 8.42; N, 8.66. Found C, 73.88; H, 8.06; N, 8.36. ^{1}H NMR (benzene-d_6): δ = -4.41 (s, 6H, C(C*H*$_3$)), -

0.59 (d, 6.8 Hz, 12H, CH(C*H*$_3$)$_2$), 0.80-1.06 (m, 10H, *Cy*), 1.46 (d, 6.8 Hz, 12H, CH(C*H*$_3$)$_2$), 2.98 (sept, 6.8 Hz, 4H, C*H*(CH$_3$)$_2$), 7.45 (d, 7.6 Hz, 4H, *m*-Ar), 7.80 (t, 7.6 Hz, 2H, *p*-Ar), 9.52 (t, 7.6 Hz, 1H, *p*-pyr), 11.48 (d, 7.6 Hz, 2H, *m*-pyr). ^{13}C NMR (benzene-d_6): δ = 23.80 (Cy), 24.13 (CH(*C*H$_3$)$_2$), 24.99 (CH(*C*H$_3$)$_2$), 25.38 (Cy), 29.61 (Cy), 30.16 (Cy), 31.56 (*C*H(CH$_3$)$_2$), 33.18 (C(CH$_3$)), 101.65 (*m*-pyr), 124.32 (*p*-Ar), 124.52 (*m*-Ar), 139.83 (*p*-pyr), 144.23, 165.75, 183.06, 184.79, 205.10. IR (pentane): ν (N≡C) 2218 cm^{-1}.

Preparation of (^{iPr}PDI)FeNHCH(C$_6$H$_{11}$). This compound was prepared in a similar manner to (^{iPr}PDI)FeNHCHPh with 0.60 g (0.093 mmol) of (^{iPr}PDI)FeNC(C$_6$H$_{11}$) and four atmospheres of H$_2$ to yield 0.054 g (90%) of a green solid identified as (^{iPr}PDI)FeNHCH(C$_6$H$_{11}$). Analysis for C$_{40}$H$_{55}$N$_4$Fe: Calc. C, 74.51; H, 8.75; N, 8.69. Found C, 74.24; H, 8.55; N, 8.71. ^{1}H NMR (benzene-d_6): δ = -5.12 (s, 6H, C(C*H*$_3$)), -0.47 (d, 6.8 Hz, 12H, CH(C*H*$_3$)$_2$), 1.31 (d, 6.8 Hz, 12H, CH(C*H*$_3$)$_2$), 1.52-1.85 (m, 10H, *Cy*), 2.88 (sept, 6.8 Hz, 4H, C*H*(CH$_3$)$_2$), 4.45 (dd, 22.0 Hz, 1H, NHC*H*(Cy)), 7.32 (d, 7.6 Hz, 4H, *m*-Ar), 7.68 (t, 7.6 Hz, 2H, *p*-Ar), 9.08 (t, 7.6 Hz, 1H, *p*-pyr), 11.74 (d, 7.6 Hz, 2H, *m*-pyr), 14.54 (d, 22.0 Hz, 1H, N*H*CH(Cy)). ^{13}C NMR (benzene-d_6): δ = 23.79 (CH(*C*H$_3$)$_2$), 24.11 (CH(*C*H$_3$)$_2$), 25.58 (Cy), 28.42 (Cy), 28.78 (Cy), 29.15 (Cy), 29.50 (*C*H(CH$_3$)$_2$), 29.62 (Cy), 102.78 (*m*-pyr), 124.31 (*m*-Ar), 124.52 (*p*-Ar), 137.78 (*p*-py), 140.85, 142.87, 156.72, 171.13, 179.91. IR (pentane): ν (N-H) 3247 cm^{-1}.

Preparation of (^{iPr}PDI)FeNC^{t}Bu. This compound was prepared in a similar manner to (^{iPr}PDI)FeNCPh with 0.078 g (0.13 mmol) of (^{iPr}PDI)Fe(N$_2$)$_2$ and 0.011 g (0.13 mmol) of trimethylacetonitrile to yield 0.078 g (98%) of a green solid identified as (^{iPr}PDI)FeNC^{t}Bu. Analysis for C$_{40}$H$_{52}$N$_4$Fe: Calc. C, 73.53; H, 8.44; N, 9.03. Found

C, 73.35; H, 8.26; N, 8.73. ^{1}H NMR (benzene-d_6): δ = -4.35 (s, 6H, C(CH_3)), -0.62 (d, 6.8 Hz, 12H, CH(CH_3)$_2$), 0.57 (s, 9H, NC(CH_3)$_3$), 1.46 (d, 6.8 Hz, 12H, CH(CH_3)$_2$), 2.96 (sept, 6.8 Hz, 4H, C*H*(CH$_3$)$_2$), 7.44 (d, 7.6 Hz, 4H, *m*-Ar), 7.78 (t, 7.6 Hz, 2H, *p*-Ar), 9.52 (t, 7.6 Hz, 1H, *p*-pyr), 11.47 (d, 7.6 Hz, 2H, *m*-pyr). ^{13}C NMR (benzene-d_6): δ = 24.13 (C(*C*H$_3$)$_3$), 25.04 CH(*C*H$_3$)$_2$), 28.43 CH(*C*H$_3$)$_2$), 31.62 *C*H(CH$_3$)$_2$), 101.51 (*m*-pyr), 124.33 (*p*-Ar), 124.50 (*m*-Ar), 139.95 (*p*-pyr), 144.41, 166.08, 182.90, 185.45, 209.88. IR (pentane): ν (N≡C) 2224 cm^{-1}.

Preparation of (^{iPr}PDI)FeNHCH^{t}Bu. This compound was prepared in a similar manner to (^{iPr}PDI)FeNHCHPh with 0.060 g (0.097 mmol) of (^{iPr}PDI)FeNC^{t}Bu and four atmospheres of H_2 to yield 0.058 g (96%) of a green solid identified as (^{iPr}PDI)FeNHCH^{t}Bu. Analysis for $C_{40}H_{50}N_4Fe$: Calc. C, 73.29; H, 8.74; N, 9.00. Found C, 72.94; H, 8.52; N, 9.04. ^{1}H NMR (benzene-d_6): δ = -5.23 (s, 6H, C(CH_3)), -0.50 (d, 6.8 Hz, 12H, CH(CH_3)$_2$), 0.51 (s, 9H, NC(CH_3)$_3$), 1.30 (d, 6.8 Hz, 12H, CH(CH_3)$_2$), 2.88 (sept, 6.8 Hz, 4H, C*H*(CH$_3$)$_2$), 4.35 (d, 22.4 Hz, 1H, NHC*H*C(CH$_3$)$_3$), 7.31 (d, 7.6 Hz, 4H, *m*-Ar), 7.69 (t, 7.6 Hz, 2H, *p*-Ar), 9.09 (t, 7.6 Hz, 1H, *p*-pyr), 11.81 (d, 7.6 Hz, 2H, *m*-pyr), 14.45 (d, 22.8 Hz, 1H, N*H*CHC(CH$_3$)$_3$). ^{13}C NMR (benzene-d_6): δ = 23.79 (C(*C*H$_3$)$_3$), 26.29 (CH(*C*H$_3$)$_2$), 29.17 (*C*H(CH$_3$)$_2$), 29.59 (CH(*C*H$_3$)$_2$), 102.60 (*m*-pyr), 123.91 (*p*-Ar), 124.40 (*m*-Ar), 137.62 (*p*-pyr), 141.34, 164.55, 172.08, 184.22, NH*C*H(CH$_3$)$_3$ not located. IR (pentane): ν (N-H) 3242 cm^{-1}.

Observation of (^{iPr}PDI)FeN$_2$CH^{t}Bu. ^{1}H NMR (benzene-d_6): δ = 0.20 (s, 6H, C(CH_3)), 0.51 (d, 6.8 Hz, 12H, CH(CH_3)$_2$), 0.75 (s, 9H, N$_2$CH(CH_3)$_3$), 1.18 (d, 6.8 Hz, 12H, CH(CH_3)$_2$), 2.99 (sept, 6.8 Hz, 4H, C*H*(CH$_3$)$_2$), 7.30 (d, 7.6 Hz, 4H, *m*-Ar), 7.46 (t, 7.6 Hz, 2H, *p*-Ar), 8.35 (d, 7.6 Hz, 1H, *p*-pyr), 8.44 (d, 7.6 Hz, 2H, *m*-pyr). IR (pentane): ν (N=N) 2043 cm^{-1}.

Characterization of (^{iPr}PDI)FeNC(2-OMe-C_6H_4). ^{1}H NMR (benzene-d_6): δ = -1.81 (s, 6H, C(*CH*$_3$)), -0.48 (d, 6.8 Hz, 12H, CH*(CH*$_3$*)*$_2$), 1.45 (d, 6.8 Hz, 12H, CH*(CH*$_3$*)*$_2$), 2.71 (sept, 6.8 Hz, 4H, C*H*(CH$_3$)$_2$), 3.03 (s, 3H, *o*-OCH$_3$), (d, 7.6 Hz, 1H, *ortho* to OCH$_3$), 6.43 (t, 7.6 Hz, 1H, *para* to OCH$_3$), 6.54 (d, 7.6 Hz, 1H, *meta* to OCH$_3$), 6.69 (t, 7.6 Hz, 1H, *ortho* to C≡N) 7.56 (d, 7.6 Hz, 4H, *m*-Ar), 7.86 (t, 7.6 Hz, 2H, *p*-Ar), 9.34 (t, 7.6 Hz, 1H, *p*-pyr), 11.30 (d, 7.6 Hz, 2H, *m*-pyr). ^{13}C NMR (benzene-d_6): δ = 23.55 (CH(*C*H$_3$)$_2$), 24.21 (CH(*C*H$_3$)$_2$), 25.96 (*C*H(CH$_3$)$_2$), 55.64 (O*C*H$_3$), 99.06 (*m*-pyr), 112.15 (OCH$_3$*Ph*), 121.86 (OCH$_3$*Ph*), 124.31 (*m*-Ar), 125.24 (*p*-Ar), 129.84 (OCH$_3$*Ph*), 130.88 (OCH$_3$*Ph*), 143.31 (*p*-pyr), 157.47, 162.57, 176.92, 179.52, 195.64.

Characterization of (^{iPr}PDI)FeNHCH(2-OMe-C_6H_4). ^{1}H NMR (benzene-d_6): δ = -3.97 (s, 6H, C(*CH*$_3$)), -0.32 (d, 6.8 Hz, 12H, CH*(CH*$_3$*)*$_2$), 1.30 (d, 6.8 Hz, 12H, CH*(CH*$_3$*)*$_2$), 2.72 (sept, 6.8 Hz, 4H, C*H*(CH$_3$)$_2$), 3.16 (s, 3H, *o*-OCH$_3$), 5.20 (d, 20.8 Hz, 1H, NHC*H*(*o*-OMePh)), 6.22 (d, 7.6 Hz, 1H, *ortho* to OCH$_3$), 6.67 (t, 7.6 Hz, 1H, *para* to OCH$_3$), 6.83 (d, 7.6 Hz, 1H, *meta* to OCH$_3$), 6.93 (t, 7.6 Hz, 1H, *ortho* to C≡N) 7.31 (d, 7.6 Hz, 4H, *m*-Ar), 7.65 (t, 7.6 Hz, 2H, *p*-Ar), 9.15 (t, 7.6 Hz, 1H, *p*-pyr), 11.25 (d, 7.6 Hz, 2H, *m*-pyr), 16.66 (d, 20.8 Hz, 1H, N*H*CH(*o*-OMePh)). ^{13}C NMR (benzene-d_6): δ = 23.54 (CH(*C*H$_3$)$_2$), 24.20 (CH(*C*H$_3$)$_2$), 29.82 (*C*H(CH$_3$)$_2$), 55.64 (O*C*H$_3$), 103.12 (*m*-pyr), 112.09 (OCH$_3$*Ph*), 121.85 (OCH$_3$*Ph*), 124.54 (*m*-Ar), 124.87 (*p*-Ar), 129.84 (OCH$_3$*Ph*), 130.88 (OCH$_3$*Ph*), 138.98 (*p*-pyr), 139.66, 157.49, 160.31, 162.55, 170.43, NH*C*H(*o*-OCH$_3$) not located.

Characterization of (^{iPr}PDI)FeNC(2-O^{i}Pr-C_6H_4). ^{1}H NMR (benzene-d_6): δ = -2.74 (s, 6H, C(*CH*$_3$)), -0.55 (d, 6.8 Hz, 12H, CH*(CH*$_3$*)*$_2$), 0.89 (d, 6.8 Hz, 3H, *o*-O^{i}Pr CH$_3$), 1.47 (d, 6.8 Hz, 12H, CH*(CH*$_3$*)*$_2$), 2.92 (sept, 6.8 Hz, 4H, C*H*(CH$_3$)$_2$), 3.95 (sept, 6.8

Hz, 1H, *o*-O^{i}Pr CH), 6.21 (d, 7.6 Hz, 1H, O^{i}Pr*Ph*), 6.87 (t, 7.6 Hz, 1H, O^{i}Pr*Ph*), 7.01 (t, 7.6 Hz, 1H, O^{i}Pr*Ph*), 7.23 (d, 7.6 Hz, 1H, O^{i}Pr*Ph*), 7.51 (d, 7.6 Hz, 4H, *m*-Ar), 7.79 (t, 7.6 Hz, 2H, *p*-Ar), 9.50 (t, 7.6 Hz, 1H, *p*-pyr), 11.37 (d, 7.6 Hz, 2H, *m*-pyr). ^{13}C NMR (benzene-d_6): δ = 21.82 (OCH(*C*H$_3$)$_2$), 23.75 (CH(*C*H$_3$)$_2$), 24.22 (CH(*C*H$_3$)$_2$), 33.07 (*C*H(CH$_3$)$_2$), 34.60 (C(*C*H$_3$), 71.18 (O*C*H(CH$_3$)$_2$), 99.28 (*m*-pyr), 114.29 (O^{i}Pr*Ph*), 121.73 (O^{i}Pr*Ph*), 124.69 (*m*-Ar), 125.15 (*p*-Ar), 125.88 (O^{i}Pr*Ph*), 130.27 (O^{i}Pr*Ph*), 142.18 (*p*-pyr), 154.83, 162.47, 169.45, 178.31, 191.83.

Characterization of (^{iPr}PDI)FeNHCH(2-O^{i}Pr-C$_6$H$_4$). ^{1}H NMR (benzene-d_6): δ = -3.85 (s, 6H, C(*CH$_3$*)), -0.32 (d, 6.8 Hz, 12H, CH*(CH$_3$)$_2$*), 0.94 (d, 6.8 Hz, 3H, *o*-O^{i}Pr CH$_3$), 1.29 (d, 6.8 Hz, 12H, CH*(CH$_3$)$_2$*), 2.78 (sept, 6.8 Hz, 4H, C*H*(CH$_3$)$_2$), 3.95 (sept, 6.8 Hz, 1H, O^{i}Pr CH), 5.96 (d, 22 Hz, 1H, NHC*H*(O^{i}Pr*Ph*)), 6.26 (d, 7.6 Hz, 1H, O^{i}Pr*Ph*), 6.80 (t, 7.6 Hz, 1H, O^{i}Pr*Ph*), 6.97 (t, 7.6 Hz, 1H, O^{i}Pr*Ph*), 7.23 (d, 7.6 Hz, 1H, O^{i}Pr*Ph*), 7.35 (d, 7.6 Hz, 4H, *m*-Ar), 7.64 (t, 7.6 Hz, 2H, *p*-Ar), 9.17 (t, 7.6 Hz, 1H, *p*-pyr), 11.08 (d, 7.6 Hz, 2H, *m*-pyr), 16.38 (d, 22 Hz, 1H, N*H*CH(*o*-O^{i}PrPh)). ^{13}C NMR (benzene-d_6): δ = 22.14 (OCH(*C*H$_3$)$_2$), 23.75 (CH(*C*H$_3$)$_2$), 24.22 (CH(*C*H$_3$)$_2$), 29.77 (*C*H(CH$_3$)$_2$), 31.70 (C(*C*H$_3$), 70.07 (O*C*H(CH$_3$)$_2$), 103.60 (*m*-pyr), 114.29 (O^{i}Pr*Ph*), 121.73 (O^{i}Pr*Ph*), 124.73 (*m*-Ar), 125.32 (*p*-Ar), 125.88 (O^{i}Pr*Ph*), 130.27 (O^{i}Pr*Ph*), 139.01 (*p*-pyr), 154.82, 162.47, 169.62, 178.31, NH*C*H(*o*-O^{i}PrPh) not located.

Preparation of (^{Et}PDI)FeNCPh. A 20 mL scintillation vial was charged with 0.200 g (0.19 mmol) of [(^{Et}PDI)Fe(N$_2$)]$_2$(μ$_2$-N$_2$) and approximately 5 mL of pentane. A pentane solution of NCPh (0.039 g, 0.38 mmol) was added to the vial resulting in bubbling and immediate color change to green. The solution was stirred for 5 minutes then filtered and concentrated. Recrystallization from pentane at -35°C yielded .060 g

(54%) of a green solid identified as (^{Et}PDI)FeNCPh. Analysis for $C_{36}H_{40}N_4Fe$: Calc. C, 73.97; H, 6.90; N, 9.58. Found C, 73.78; H, 6.64; N, 9.18. ^{1}H NMR (benzene-d_6): δ = -1.02 (s, 6H, C(C*H*$_3$)), -0.16 (t, 7.6 Hz, 12H, CH$_2$C*H*$_3$), 1.81 (m, 7.6 Hz, 4H, C*H*$_2$CH$_3$), 1.96 (m, 7.6 Hz, 4H, C*H*$_2$CH$_3$), 6.99 (m, 5H, *Ph*), 7.55 (d, 7.6 Hz, 4H, *m-Ar*), 7.86 (t, 7.6 Hz, 2H, *p-Ar*), 9.26 (t, 7.6 Hz, 1H, *p-py*), 11.26 (d, 7.6 Hz, 2H, *m-py*). ^{13}C NMR (benzene-d_6): δ = 17.79 (CH$_2$*C*H$_3$), 22.75 (C(*C*H$_3$)), 27.06 (*C*H$_2$CH$_3$), 31.67 (*C*H$_2$CH$_3$), 98.73 (*m-py*), 123.79 (*p-Ar*), 126.65 (*Ph*), 127.46 (*m-Ar*), 130.32 (*Ph*), 132.66 (*Ph*), 138.59 (*p-py*), quaternary carbons not located. IR(pentane): ν(NC) 2151 cm^{-1}.

Preparation of (^{Et}PDI)FeNHCHPh. A thick-walled glass vessel was charged with 0.050 g (0.086 mmol) of (^{Et}PDI)FeNCPh and approximately 10 mL of pentane forming a green solution. The vessel was submerged in liquid nitrogen and evacuated on the high vacuum line. Four atmospheres of H_2 were added and the contents of the vessel warmed to room temperature. The solution was stirred for 3 hours after which time the volatiles were removed *in vacuo* yielding 0.044 g (0.075 mmol, 88%) of a green solid identified as (^{Et}PDI)FeNHCHPh. Analysis for $C_{36}H_{42}N_4Fe$: Calc. C, 73.97; H, 6.90; N, 9.58. Found C, 73.45; H, 6.89; N, 9.68. ^{1}H NMR (benzene-d_6): δ = -3.60 (s, 6H, C(C*H*$_3$)), 0.10 (t, 7.6 Hz, 12H, CH$_2$C*H*$_3$), 1.81 (m, 7.6 Hz, 4H, C*H*$_2$CH$_3$), 2.05 (m, 7.6 Hz, 4H, C*H*$_2$CH$_3$), 4.71 (d, 20.8 Hz, 1H, NHC*H*Ph), 6.99 (m, 5H, *Ph*), 7.31 (d, 7.6 Hz, 4H, *m-Ar*), 7.67 (t, 7.6 Hz, 2H, *p-Ar*), 9.19 (t, 7.6 Hz, 1H, *p-py*), 11.05 (d, 7.6 Hz, 2H, *m-py*), 16.35 (d, 21.6 Hz, 1H, N*H*CHPh). ^{13}C NMR (benzene-d_6): δ = 15.07 (CH$_2$*C*H$_3$), 27.07 (*C*H$_2$CH$_3$), 31.14 (*C*H$_2$CH$_3$), 31.41 (C(*C*H$_3$)), 103.62 (*m-py*), 124.60 (*p-Ar*), 126.65 (*Ph*), 127.37 (*m-Ar*), 129.57 (*Ph*), 134.68 (*Ph*), 139.29 (*p-py*), quaternary carbons not located. IR(pentane): ν(NH) 3245 cm^{-1}.

Observation of Intermediate 2. A 20-mL scintillation vial was charged with 0.010 g (0.017 mmol) of (^{iPr}PDI)Fe(N_2)$_2$ and approximately 0.50 mL of C_6D_6. A second vial was charged with 0.002 g (0.017 mmol) of N_2CDPh and approximately 0.20 mL of C_6D_6. The phenyldiazomethane solution was then added to the (^{iPr}PDI)Fe(N_2)$_2$ solution resulting in a color change to yellow-green and formation of intermediate 2. Data for 2: ^{1}H NMR (benzene-d_6): δ = 0.67 (d, 6.8 Hz, 6H, CH(C*H*$_3$)$_2$), 0.78 (d, 6.8 Hz, 6H, CH(C*H*$_3$)$_2$, 1.01 (d, 6.8 Hz, 6H, CH(C*H*$_3$)$_2$), 1.30 (d, 6.8 Hz, 6H, CH(C*H*$_3$)$_2$), 1.62 (sept, 6.8 Hz, 2H, C*H*(CH$_3$)$_2$), 1.97 (s, 6H, C(C*H*$_3$)), 3.09 (sept, 6.8 Hz, 2H, C*H*(CH$_3$)$_2$), 6.92 (m, 7.6 Hz, 7H), 7.33 (t, 7.6 Hz, 5H), 7.41 (d, 7.6 Hz, 2H), 7.79 (d, 7.6 Hz, 3H), 8.30 (d, 7.6 Hz, 2H). ^{2}H NMR (benzene): δ = 5.20.

Preparation of (^{iPr}PDI)FeN$_2$C(Me)Ph. A 20 mL scintillation vial was charged with 0.200 g (0.34 mmol) of (^{iPr}PDI)Fe(N_2)$_2$ and approximately 10 mL of pentane. A pentane solution of N_2CMePh (0.45 g, 0.34 mmol) was added to the vial resulting in vigorous bubbling and immediate color change to blue-green. The solution was stirred for 20 minutes then filtered and concentrated. Recrystallization from pentane at -35°C yielded 0.98 g (0.14 mmol, 43%) of a green solid identified as (^{iPr}PDI)FeN$_2$C(Me)Ph. Analysis for $C_{41}H_{51}N_5Fe$: Calc. C, 73.53; H, 7.68; N, 10.46. Found C, 73.59; H, 8.02; N, 10.37. ^{1}H NMR (benzene-d_6): δ = 0.01 (s, 6H, C(C*H*$_3$)), 0.57 (d, 7.0 Hz, 12H, CH(C*H*$_3$)$_2$), 1.14 (d, 7.0 Hz, 12H, CH(C*H*$_3$)$_2$), 2.47 (s, 3H, N$_2$(C*H*$_3$)Ph), 2.97 (q, 7.0 Hz, 4H, C*H*(CH$_3$)$_2$), 6.39 (d, 8.0 Hz, 2H, *o-Ph*), 6.66 (t, 8.0 Hz, 1H, *p-Ph*), 7.28 (t, 8.0 Hz, 2H, *p-Ar* or *m-Ph*), 7.35 (d, 8.0 Hz, 4H, *m-Ar*), 7.51 (t, 8.0 Hz, 2H, *p-Ar* or *m-Ph*), 8.34 (d, 7.0 Hz, 2H, *m-py*), 8.69 (t, 7.0 Hz, 1H, *p-py*). ^{13}C NMR (benzene-d_6): δ = 14.63 (N$_2$C(*C*H$_3$)Ph), 22.97 (C(*C*H$_3$)), 23.90 (CH(*C*H$_3$)$_2$), 24.48 (CH(*C*H$_3$)$_2$), 28.71 (*C*H(CH$_3$)$_2$), 121.91 (*m-py*), 123.11 (*p-py*), 124.31 (*m-Ar*), 126.72 (*o-Ph*), 126.79 (*p-*

Ph), 126.94 (*p-Ar*), 127.34 (*m-Ph*), 141.83, 146.12, 151.52, 158.45 (quaternary carbons). IR(pentane): ν(NN) 2045 cm^{-1}.

Preparation of (^{Et}PDI)Fe(Ph(Me)CNNC(Me)Ph). A 20 mL scintillation vial was charged with 0.200 g (0.19 mmol) of [(^{Et}PDI)Fe(N_2)]$_2$(μ_2-N_2) and approximately 10 mL of diethyl ether. A solution of acetophenone azine (0.90 g, 0.38 mmol, 2 eq) in 5 mL of diethyl ether was added to the vial resulting in vigorous bubbling and immediate color change from red to brown. Stirring the solution for 5 minutes followed by removal of the solvent *in vacuo* yielded 0.268 g (0.37 mmol, 98%) of a brown solid identified as (^{Et}PDI)Fe(Ph(Me)CNNC(Me)Ph). Analysis for $C_{45}H_{51}N_5Fe$: Calc. C, 75.30; H, 7.16; N, 9.76. Found C, 75.03; H, 7.08; N, 9.57. ^{1}H NMR (benzene-d_6): δ = 0.80 (t, 7.6 Hz, 12H, CH_2CH_3), 1.45 (s, 6H, azine CH_3), 1.81 (m, 7.6 Hz, 4H, CH_2CH_3), 1.87 (s, 6H, C(CH_3)), 2.07 (m, 7.6 Hz, 4H, CH_2CH_3), 6.81 (d, 7.6 Hz, 4H, *m-Ar*), 6.90 (t, 7.6 Hz, 2H, *p-Ar*), 7.38 (m, 8.0 Hz, 5H, *p-py* and *m-Ph*), 7.76 (d, 8.0 Hz, 2H, *m-py*), 8.02 (d, 8.0 Hz, 4H, *o-Ph*), *p-Ph signal under benzene peak.* ^{13}C NMR (benzene-d_6): δ = 13.60 (CH_2CH_3), 16.75 (azine CH_3 and C(CH_3)), 24.06 (CH_2CH_3), 116.73 (*p-py*), 121.14 (*m-py*), 125.13 (*m-Ar*), 125.77 (*p-Ar*), 127.01 (*o-Ph*), 127.33 (*p-Ph*), 128.01 (*m-Ph*), 135.57, 139.42, 148.90, 157.15, 162.25, 166.63 (quaternary carbons).

Preparation of (^{Me}PDI)Fe(Ph(Me)CNNC(Me)Ph). A 20 mL scintillation vial was charged with 0.200 g (0.21 mmol) of [(^{Me}PDI)Fe(N_2)]$_2$(μ_2-N_2) and approximately 10 mL of diethyl ether. A solution of acetophenone azine (0.101 g, 0.43 mmol) in 5 mL of diethyl ether was added to the vial resulting in vigorous bubbling and immediate color change from red to brown. Stirring the solution for 5 minutes followed by removal of the solvent *in vacuo* yielded 0.255 g (0.38 mmol, 90%) of a brown solid

identified as (^{Me}PDI)Fe(Ph(Me)CNNC(Me)Ph). Analysis for $C_{41}H_{43}N_5Fe$: Calc. C, 74.43; H, 6.55; N, 10.58. Found C, 73.99; H, 6.63; N, 10.45. ^{1}H NMR (benzene-d_6): δ = 1.54 (bs, 18H, Ar CH_3 and azine CH_3), 1.83 (bs, 6H, C(CH_3)), 6.68 (bs, 6H, *m-Ar* and *p-Ar*), 7.38 (bs, 5H, *p-py* and *m-Ph*), 7.75 (bs, 2H, *m-py*), 8.07 (bs, 4H, *o-Ph*), *p-Ph signal under benzene peak*. ^{13}C NMR (benzene-d_6): δ = 15.98 (azine CH$_3$ and C(CH$_3$)), 18.99 (Ar CH$_3$), 116.29 (*p-py*), 121.19 (*m-py*), 125.34 (*m-Ar* and *p-Ar*), 126.98 (*o-Ph*), 127.34 (*p-Ph*), 130.19 (*m-Ph*), 133.37, 139.20, 149.62, 156.68, 161.76, 166.20 (quaternary carbons).

REFERENCES

[1] (a) Kirmse, W. *Angew. Chem., Int. Ed.* **2003**, *42*, 1088. (b) Doyle, M. P.; Forbes, D. C. *Chem. Rev.* **1998**, *98*, 911. (c) Dartiguenave, M.; Menu, M. J.; Dyedier, E.; Dartiguenave, Y.; Siebald, H. *Coord. Chem. Rev.*, **1998**, *178-180*, 623.

[2] (a) Grubbs, R. H. *Angew. Chem., Int. Ed.* **2006**, *45*, 3760. (b) Schrock, R. R. *Angew. Chem., Int. Ed.* **2006**, *45*, 3748.

[3] (a) Hidai, M.; Aramaki, S.; Yoshida, K.; Komida, T.; Takahashi, T.; Uchida, Y.; Mizobe, Y. *J. Am. Chem. Soc.* **1986**, *108*, 1562. (b) Hidai, M.; Mizobe, Y. *Can. J. Chem.* **2005**, *83*, 358. (c) Schramm, K. D.; Ibers, J. A. *Inorg. Chem.* **1980**, *19*, 1231.

[4] Enthaler, S.; Junge, K.; Beller, M. *Angew. Chem., Int. Ed.* **2008**, *47*, 3317.

[5] Barney, B. M.; Lukoyanov, D.; Yang, T. C.; Dean, D. R.; Hoffman, B. M.; Seefelt, L. C. *Proc. Natl. Acad. Sci. U.S.A.* **2006**, *103*, 17113.

[6] (a) Wolf, J. R.; Hamaker, C. G.; Djukic, J. –P.; Kodadek, T.; Woo, L. K. *J. Am. Chem. Soc.* **1995**, *117*, 9194. (b) Hamaker, C. G.; Mirafzal, G. A.; Woo, L. K. *Organometallics* **2001**, *20*, 5171. (c) Du, G.; Andrioletti, B.; Rose, E.; Woo, L. K. *Organometallics* **2002**, *21*, 4490.

[7] Edulji, S. K.; Nguyen, S. T. *Organometallics* **2003**, *22*, 3374.

[8] Cheng, G.; Mirafzal, G. A.; Woo, L. K. *Organometallics* **2003**, *22*, 1468.

[9] Baumann, L. K.; Mbuvi, H. M.; Du, G.; Woo, L. K. *Organometallics* **2007**, *26*, 3995.

[10] Mbuvi, H. M.; Woo, L. K. *Organometallics* **2008**, *27*, 637.

[11] Louie, J.; Grubbs, R. H. *Organometallics* **2001**, *20*, 481.

[12] Bart, S. C.; Bowman, A. C.; Lobkovsky, E.; Chirik, P. J. *J. Am. Chem. Soc.* **2007**, *129*, 7212.

[13] (a) Bart, S. C.; Chlopek, K.; Bill, E.; Bouwkamp, M. W.; Lobkovsky, E.; Neese, f.; Wieghardt, K.; Chirik, P. J. *J. Am. Chem. Soc.* **2006**, *128*, 13901. (b) Bart, S. C.; Lobkovsky, E.; Bill, E.; Wieghardt, K.; Chirik, P. J. *Inorg. Chem.* **2007**, *46*, 7055.

[14] Trovitch, R. J.; Lobkovsky, E.; Bill, E.; Chirik, P. J. *Organometallics* **2008**, *27*, 1470-1478.

[15] (a) Rep, M.; Kaagman, J.-W. F.; Elsevier, C. J.; Sedmera, P.; Hiller, J.; Thewalt, U.; Horacek, M.; Mach, K. *J. Organomet. Chem.* **2000**, *597*, 146. (b) Ohff, A.; Zippel, T.; Arndt, P.; Spannenberg, A.; Kempe, R.; Rosenthal, U. *Organometallics*, **1998**, *17*, 1649. (c) Zippel, T.; Arndt, P.; Ohff, A.; Spannenberg, A.; Kempe, R.; Rosenthal, U. *Organometallics* **1998**, *17*, 4429.

[16] (a) Bright, D.; Mills, O. S. *Chem. Commun.* **1967**, *5*, 245-246. (b) Zimniak, A.; Bakalarski, G. *J. Mol. Struct.* **2001**, *597*, 211.

[17] (a) Nametkin, N. S.; Tyurin, v. D.; Trusov, V. V.; Nekhaev, A. I.; Batsanov, A. S.; Struchkov, Yu. T. *J. Organomet. Chem.* **302**, 243-248. (b) Zachara, J.; Zimniak, A. *Acta Cryst. C54* **1998**, 353-355.

[18] Cohen, R.; Rybtchinski, B.; Gandelman, M.; Shimon, L. J. W.; Martin, J. M. L.; Milstein, D. *Angew. Chem., Int. Ed.* **2003**, *42*, 1949.

[19] Park, S. B.; Hishiyama, H.; Itoh, Y.; Itoh, K. *J. Chem. Soc., Chem. Commun.* **1994**, 1315.

[20] Zarkesh, R. A.; Heyduk, A. F. *Organometallics* **2009**, *28*, 6629.

[21] Kingsbury, J. S.; Harrity, J. P. A.; Bonitatebus, Jr., P. J.; Hoveyda, A. H. *J. Am. Chem. Soc.* **1999**, *121*, 791.

[22] Pangborn, A.B.; Giardello, M.A.; Grubbs, R.H.; Rosen, R.K.; Timmers, F.J. *Organometallics* **1996**, *15*, 1518.

[23] Bart, S. C.; Lobkovsky, E.; Chirik, P. J. *J. Am. Chem. Soc.* **2004**, *126*, 13794.

[24] Russell, S. K.; Darmon, J. M.; Lobkovsky, E.; Chirik, P. J. *Inorg. Chem.* **2010**, *49*, 2782.

[25] Kaufman, G. M.; Smith, J. A.; Vander Stouw, G. G.; Shechter, H. *J. Am. Chem. Soc.*, **1965**, *87*, 935.

[26] Schwab, F. C.; Brandolini, A. J. *Macromolecules*, **1989**, *22*, 2538.

[27] McMahon, R. J.; Abelt, C. J.; Chapman, O. L.; Johnson, J. W.; Kreil, C. L.; LeRoux, J. P.; Mooring, A. M.; West, P. R. *J. Am. Chem. Soc.*, **1987**, *109*, 2456.

[28] Çelebi, S.; Leyva, S.; Modarelli, D. A.; Platz, M. S. *J. Am. Chem. Soc.* **1993**, *115*, 8613.

CHAPTER 3

SYNTHESIS, ELECTRONIC STRUCTURE AND REACTIVITY OF BIS(IMINO)PYRIDINE IRON CARBENE COMPLEXES

3.1 Abstract

Two bis(imino)pyridine iron carbene species, (^{Et}PDI)FeCPh$_2$ and (^{Me}PDI)FeCPh$_2$ (^{R}PDI = 2,6-(2,6-R$_2$-C$_6$H$_3$-N=CMe)$_2$C$_5$H$_3$N; R = Et, Me), were synthesized by addition of diphenyldiazomethane to the corresponding dinitrogen compounds, [(^{R}PDI)Fe(N$_2$)]$_2$(μ_2-N$_2$). The iron carbene species were studied by ^{1}H NMR, Mössbauer and XAS spectroscopies, SQUID magnetometry and X-ray diffraction. The spectroscopic data are consistent with several different electronic structure possibilities. The two most reasonable proposals are: (a) an intermediate spin iron(III) center antiferromagnetically coupled to a one-electron reduced bis(imino)pyridine chelate with a triplet, X$_2$-type carbene, and (b) an intermediate spin iron(II) center antiferromagnetically coupled to a one-electron reduced chelate with a ferromagnetically interacting carbene radical. Both (^{Et}PDI)FeCPh$_2$ and (^{Me}PDI)FeCPh$_2$ react with H$_2$ to furnish diphenylmethane and the corresponding iron dihydrogen compounds. While (^{Et}PDI)FeCPh$_2$ is thermally unstable in solution, converting to diphenylmethane and the intramolecular olefin compound overnight, (^{Me}PDI)FeCPh$_2$ remains unchanged in benzene solution for weeks. Addition of carbon monoxide or 2,4,6-trimethylphenyl azide to (^{Me}PDI)FeCPh$_2$ induced carbene transfer and furnished diphenylketene and the N-mesityl-substituted diphenylketimine, respectively. Unfortunately, (^{Me}PDI)FeCPh$_2$ was not active as a pre-catalyst for cyclopropanation reactions or for ring opening or ring closing olefin metathesis.

3.2 Introduction

Transition metal carbene complexes are one of the most useful stoichiometric and catalytic tools in organic chemistry as they are employed in olefination and cyclopropanation reactions as well as olefin metathesis.[1] Olefin metathesis has been called "the most powerful carbon-carbon bond breaking and making reaction in chemical synthesis"[2] and accordingly high accolades have been awarded for its development.[3,4,5] A variety of catalyst families have been established,[2,6,7,8] the most popular of which being the ruthenium-based Grubbs family of catalysts (Figure 3.1).[7,9]

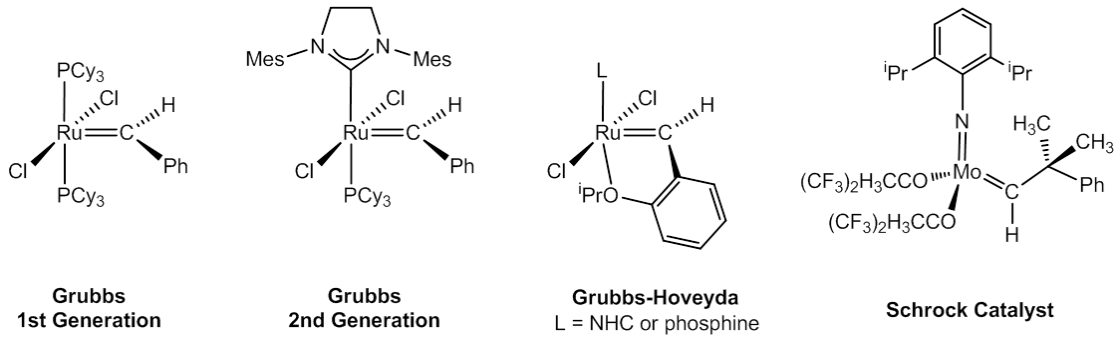

Figure 3.1 Synthetically useful olefin metathesis catalysts.

Along with being synthetically useful, transition metal carbene complexes exhibit unique electronic structures depending on the type of carbene as well as the ancillary ligands coordinated to the metal center. There are two limiting classes of carbene ligand: the Fischer-type, singlet carbenes and the Schrock-type, triplet carbenes. Fischer-type carbenes typically contain a heteroatom and an electrophilic carbene carbon, while Schrock-type carbenes are primarily hydrocarbon in nature and contain a nucleophilic carbene carbon.[1,10] The Grubbs catalysts do not fall into either of these categories as they have been described as ruthenium(II) compounds with electrophilic carbene ligands, but are not Fischer carbene complexes.[11] This unusual

electronic structure is thought to contribute to the ability of these compounds to catalyze olefin metathesis. In light of this, several theoretical[12,13] and spectroscopic[14,15] studies are on-going to investigate the nature of these catalysts.

Examples of iron carbene complexes date back to the 1960's;[16] however, many of the first examples were transient and only characterized at low temperatures.[17] These initial examples were primarily cyclopentadienyl-based, half-sandwich, cationic iron complexes with electrophilic carbene ligands.[18,19] Around 1980, Jones and coworkers reported the synthesis and crystallographic characterization of two η^1-cycloheptatrienylidene iron complexes, $[(\eta^5\text{-}C_5H_5)(\eta^1\text{-}C_7H_6)Fe(CO)_2][PF_6]$ and $[(\eta^5\text{-}C_5H_5)(\eta^1\text{-}C_{11}H_8)Fe(CO)_2][PF_6]$, which have iron-carbon bond lengths of 1.979(3) and 1.996(2) Å, respectively.[19,20] Since then several examples of crystallographically characterized terminal iron carbene complexes have been reported. In 1996, Lapinte and coworkers reported the isolation of $[(C_5Me_5)Fe(dppe)(=C(H)Me)][OTf]$, which has an iron-carbon bond length of 1.787(8) Å.[21] Shortly thereafter, in 1997, Guerchais and coworkers reported the synthesis and characterization of a series of $(\eta^2\text{-}C,X)$ chelate arylcarbene iron complexes, one of which was crystallographically characterized.[22] The iron-carbon bond length in $[(C_5Me_5)Fe(CO)\{\eta^2\text{-}C(OMe)C_6H_4\text{-}o\text{-}Cl\}][OTf]$ is 1.857(6) Å. Figure 3.2 presents examples of crystallographically characterized iron carbene complexes with their respective iron-carbon bond lengths.

While the first examples of iron carbene compounds were primarily cyclopentadienyl-based, half-sandwich complexes, more recent investigations have focused on macrocyclic[23] and porphyrin[24,25,26] supported systems. Again, like the earlier examples, many of the iron carbene complexes are unstable and cannot be observed, but instead are proposed as intermediates in organic transformations.[25,26] In contrast to these species, Floriani and coworkers isolated and crystallographically characterized an iron carbene stabilized by a tetramethyldibenzotetraazaannulene

(tmtaa) ligand, (tmtaa)$FeCPh_2$, with an iron-carbon bond length of 1.794(3) Å (Figure 3.2).[23] Similarly, Che and coworkers reported the crystal structures of two porphyrin-based iron carbene compounds, (TPFPP)$FeCPh_2$ and (TPFPP)$Fe(CPh_2)$(MeIm) (Figure 3.2; TPFPP = *meso*-tetrakis(pentafluorophenyl)porphyrinato dianion; MeIm = *N*-methylimidazole), with iron-carbon bond lengths of 1.794(3) Å and 1.827(5) Å, respectively.[24]

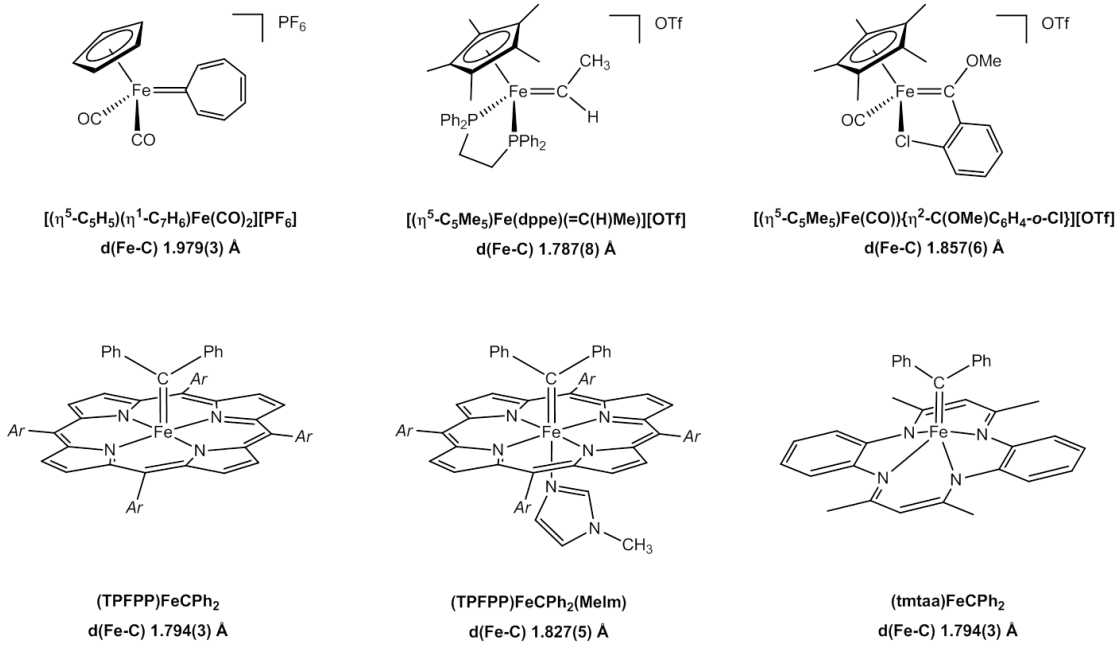

Figure 3.2 Crystallographically characterized iron carbene complexes and their iron-carbon bond lengths.

Bis(imino)pyridine ligands (^{R}PDI = 2,6-(2,6-R-C_6H_3-N=CMe)$_2C_5H_3N$); R= ^{i}Pr, Et, Me, etc.) have become popular in the last two decades because of their ease of synthesis,[27] electronic[28] and structural modularity,[29,30] and ability to support a range of transition metal and alkali metal ions,[31] including several dinitrogen complexes.[32,33,34,35,36] The ability of the π-system of the bis(imino)pyridine chelate to undergo reversible transfer of one to three electrons with the metal center[37,38,39,40] has

allowed for the isolation of metal-carbon and metal-nitrogen multiple bonded species. In 2000, Bianchini and coworkers reported the bis(imino)pyridine ruthenium carbene compound, *trans*-(^{Cy}PDI)$RuCl_2$(=$CHCO_2Et$), from the addition of ethyldiazoacetate to *cis*- or *trans*-(^{Cy}PDI)$RuCl_2$(η^2-C_2H_4) and demonstrated its catalytic activity in cyclopropanation reactions.[41]

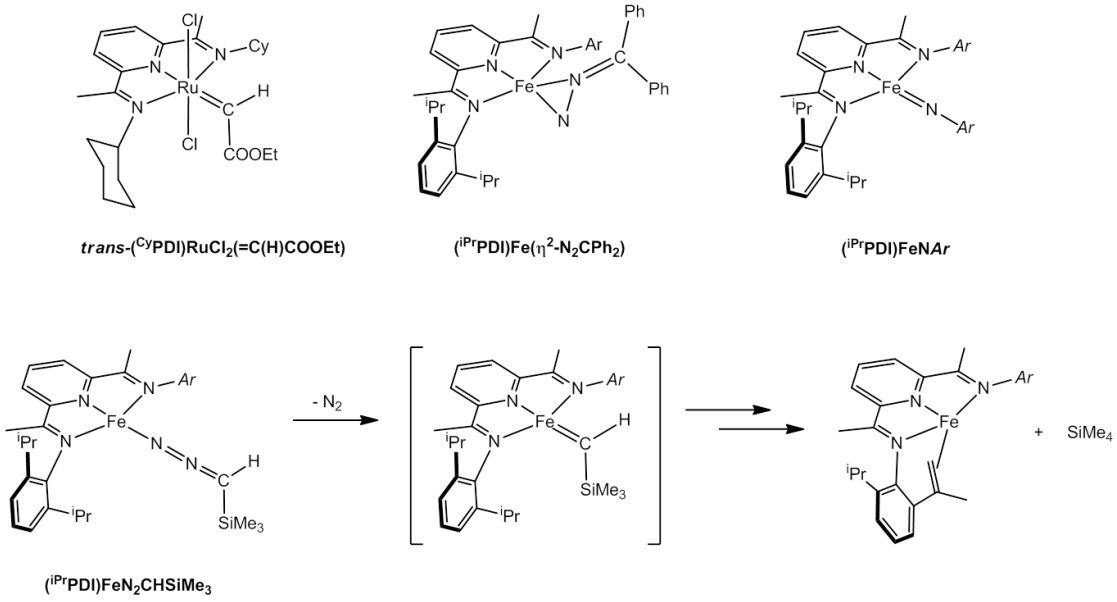

Figure 3.3 Bis(imino)pyridine-based inspirations for an iron carbene.

Previous studies from our laboratory suggest that a bis(imino)pyridine iron carbene can be synthesized. Investigation of the bis(imino)pyridine iron η^1-diazoalkane complex, (^{iPr}PDI)$FeN_2CHSiMe_3$, revealed that it is thermally unstable in solution at 23°C and slowly and quantitatively converts to an NMR silent intramolecular bis(imino)pyridine iron olefin compound with concomitant loss of $SiMe_4$.[42] The pathway for this transformation is proposed to go through an iron carbene species (Figure 3.3). Bis(imino)pyridine iron induced diazoalkane N-N bond cleavage observed for other monosubstituted diazoalkanes is also proposed to proceed

through a transient iron carbene species. The bis(imino)pyridine iron η^2-diazoalkane complex, (^{iPr}PDI)Fe(η^2-N_2CPh_2), has been synthesized and characterized by our laboratory.[43] While this compound is thermally stable, the η^2-coordination of the diazoalkane ligand in this compound demonstrates a potential for new reactivity with the iron center. Finally, our laboratory has previously reported the synthesis and characterization of a family of bis(imino)pyridine iron aryl imides which exhibit hydrogenation and nitrene transfer activity and show that the bis(imino)pyridine ligand framework on iron can support multiply-bonded species.[44]

3.3 Synthesis of Bis(imino)pyridine Iron Carbene Complexes

The intriguing η^2-coordination of diphenyldiazomethane in (^{iPr}PDI)Fe(η^2-N_2CPh_2) led to the investigation of this diazoalkane with other bis(imino)pyridine iron dinitrogen compounds. Complexes with smaller aryl substituents on the bis(imino)pyridine chelates were targeted under the hypothesis that the bulky isopropyl groups were inhibiting the ability of the iron center to reach the potential carbene carbon. Addition of one equivalent of diphenyldiazomethane, N_2CPh_2, to a diethyl ether solution of [(^{R}PDI)Fe(N_2)]$_2$(μ_2-N_2) (^{R}PDI = 2,6-(2,6-R_2-C_6H_3-N=CMe)$_2C_5H_3N$; R = Et, Me) furnished the green-brown bis(imino)pyridine iron carbene species, (^{Et}PDI)FeCPh_2 and (^{Me}PDI)FeCPh_2 (Figure 3.4). Investigation of the products by infrared spectroscopy revealed the absence of an N-N stretch confirming loss of N_2 and coordination of only the carbene fragment to the iron center. Addition of H_2O to a benzene-d_6 solution of either compound followed by removal of the iron products and analysis of the organic species in solution established a 1:1 ratio of the corresponding bis(imino)pyridine ligand and diphenylmethane (CH_2Ph_2). For comparsion, decomposition of the η^2-bound diazoalkane compound,

(^{iPr}PDI)Fe(N_2CPh_2), results in an approximately 1:1 ratio of ^{iPr}PDI to N_2CPh_2 with no appreciable amount of CH_2Ph_2 observed by ^{1}H NMR spectroscopy.

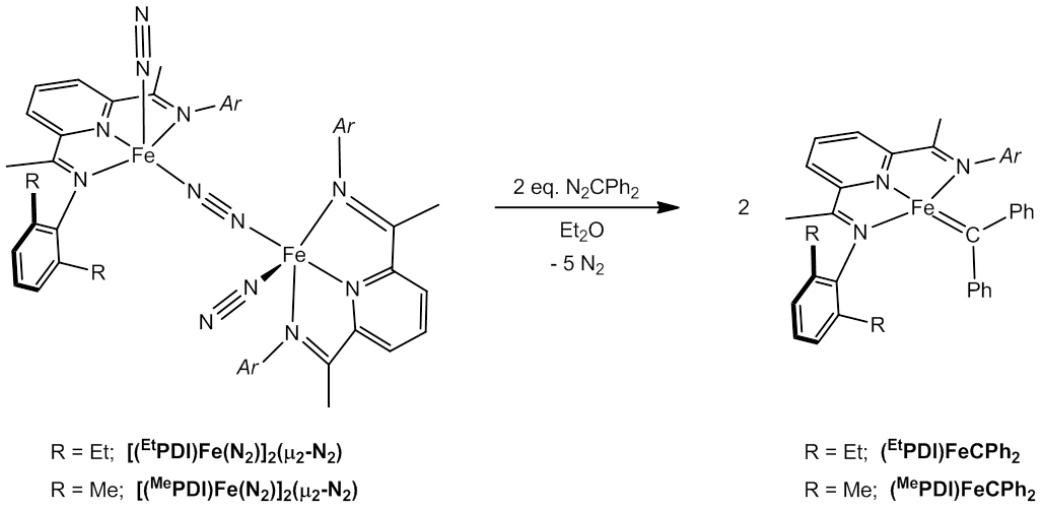

Figure 3.4 Synthesis of bis(imino)pyridine iron carbene compounds.

The benzene-d_6 ^{1}H NMR spectra of the paramagnetic iron carbene compounds are quite similar to each other and both exhibit the number of peaks consistent with a C_{2v} symmetric molecule in solution. Representative ^{1}H NMR spectra of (^{Et}PDI)FeCPh$_2$ and (^{Me}PDI)FeCPh$_2$ recorded in benzene-d_6 at 20°C are presented in Figure 3.5. The resonances for (^{Et}PDI)FeCPh$_2$ span a range of almost 250 ppm while those for (^{Me}PDI)FeCPh$_2$ are spread over only about 200 ppm. One unusual feature present in both ^{1}H NMR spectra is the upfield peak centered around -27 ppm (^{Et}PDI)FeCPh$_2$ and -24 ppm for (^{Me}PDI)FeCPh$_2$ which integrates to four protons and corresponds to one of the carbene phenyl resonances. The other resonances for the phenyl groups appear much more downfield between 50 and 120 ppm.

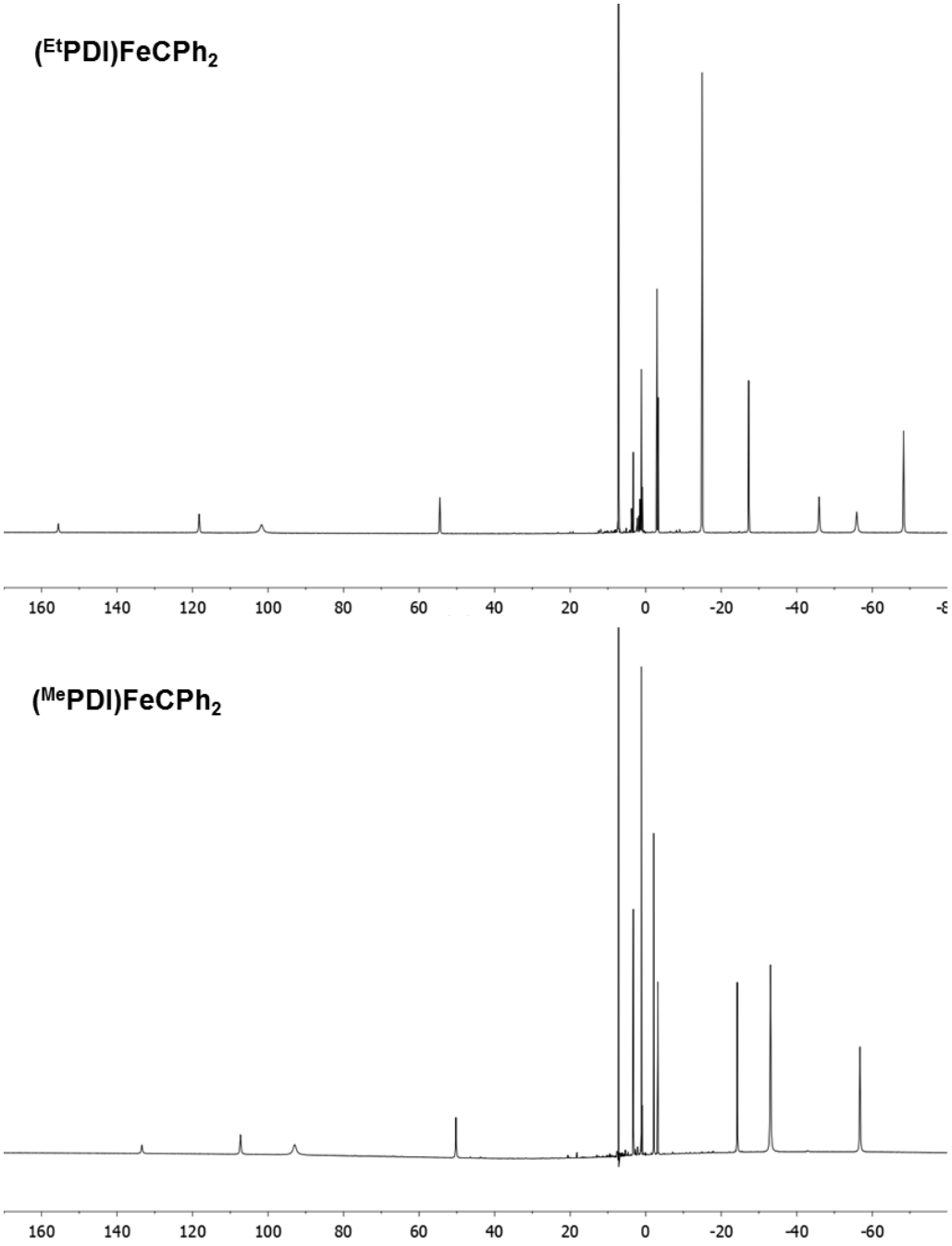

Figure 3.5 Representative ^{1}H NMR spectra of (^{Et}PDI)FeCPh$_2$ and (^{Me}PDI)FeCPh$_2$ recorded in benzene-d_6 at 20 °C.

Single crystals of (^{Et}PDI)FeCPh$_2$ suitable for X-ray diffraction were grown from a concentrated diethyl ether solution at -35 °C. A representative solid state structure is presented in Figure 3.6 and selected bond distances and angles are reported in Table 3.1. The chelate bond distances in (^{Et}PDI)FeCPh$_2$ are consistent with one-electron reduction.[38] The N_{imine}-C_{imine} distances of 1.330(3) and 1.322(2) Å and the C_{imine}-C_{ipso} distances of 1.432(3) and 1.436(3) Å fall well within the range of values accepted for a monoanionic bis(imino)pyridine chelate.[38] The relatively long Fe-N_{PDI} bond lengths allow for the possibility that (^{Et}PDI)FeCPh$_2$ contains a high spin iron center, but also may be a result of the iron center deviating from the chelate plane by 0.647 Å.

The most notable feature of the solid state structure of (^{Et}PDI)FeCPh$_2$ is that the carbene fragment is canted significantly out of the iron-chelate plane. The N(2)-Fe(1)-C(30) angle of 147.82(8)° is reminiscent of the deviation from planarity seen for the bis(imino)pyridine iron aryl imide compounds, (^{iPr}PDI)FeN(2,4,6-Me_3-C_6H_2) and (^{iPr}PDI)FeN(2,6-$^{i}Pr_2$-C_6H_3) which have $N_{pyridine}$-Fe-N_{imide} angles of 154.75(7)° and 138.79(7)°, respectively.[44] The iron aryl imide compounds are assigned as having intermediate spin iron(III) centers antiferromagnetically coupled to mono-reduced bis(imino)pyridine chelates. Their unusual geometry was suggested to be a result of the alleviation of σ* character in the d_{z2} orbital stemming from interaction of the torus with an sp hybrid of the imido nitrogen.

The Fe-$C_{carbene}$ bond length of 1.921(2) Å is fairly long relative to previously characterized macrocyclic and Cp-based iron carbene compounds which have Fe-$C_{carbene}$ bond lengths between 1.787(8) and 1.996(2) Å.[16-26] The bis(imino)pyridine iron monoalkyl, (^{Et}PDI)Fe$CH_2C(CH_3)_3$, has also been structurally characterized and exhibits a similar deviation from planarity with a $N_{pyridine}$-Fe-C_{alkyl} angle of 142.24(14)° and a Fe-C_{alkyl} bond distance of 2.036(4) Å.[45] Comparing these two Fe-C

bond lengths suggests that the Fe-$C_{carbene}$ bond in (^{Et}PDI)FeCPh$_2$ is consistent with a double bond. One explanation for the unusually long Fe-$C_{carbene}$ bond is the fact that the carbene fragment is canted out of the plane.

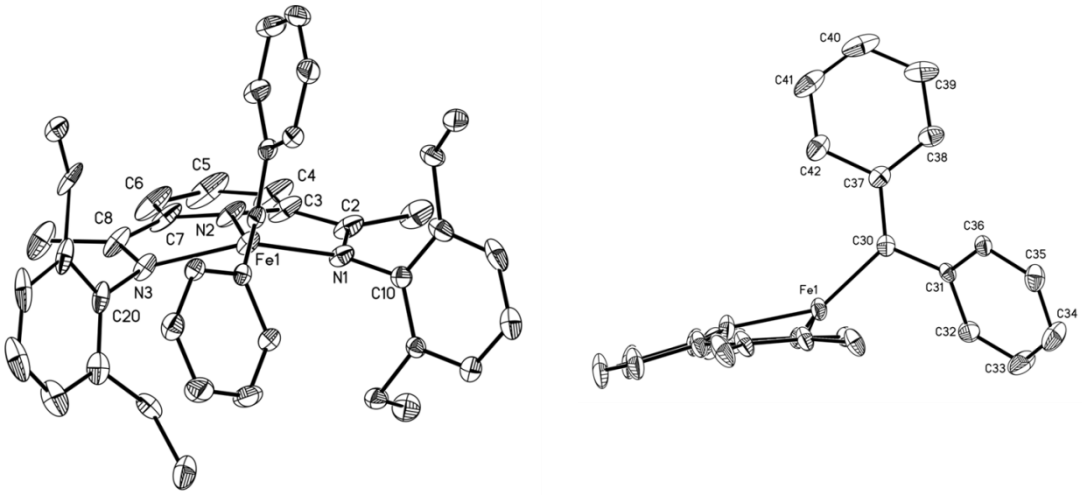

Figure 3.6 Solid state structure of (^{Et}PDI)FeCPh$_2$ at 30% probability ellipsoids. Hydrogen atoms omitted for clarity.

Table 3.1 Selected bond lengths (Å) and angles (°) for (^{Et}PDI)FeCPh$_2$.

Fe(1)-N(1)	2.047(2)	N(2)-Fe(1)-C(30)	147.82(8)
Fe(1)-N(2)	1.955(2)	Fe(1)-C(30)-C(31)	112.31(13)
Fe(1)-N(3)	2.093(2)	Fe(1)-C(30)-C(37)	127.52(14)
Fe(1)-C(30)	1.921(2)	C(31)-C(30)-C(37)	119.87(17)
N(1)-C(2)	1.330(3)	N(1)-Fe(1)-N(3)	140.43(7)
N(3)-C(8)	1.322(2)		
C(2)-C(3)	1.432(3)	Deviation of Fe(1) from N(1), N(2), N(3) plane	0.647
C(7)-C(8)	1.436(3)		

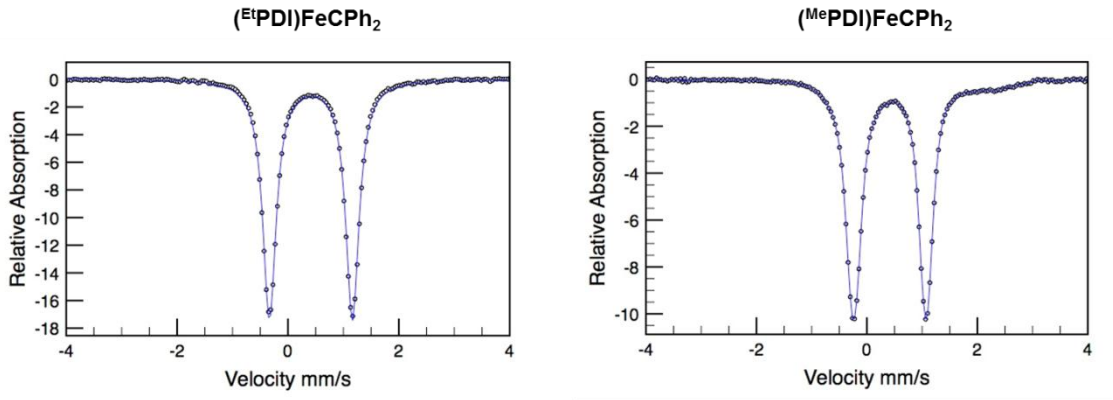

Figure 3.7 Zero-field ^{57}Fe Mössbauer spectra of (^{Et}PDI)FeCPh$_2$ (left, δ = 0.41 mm/s and ΔE_Q = 1.50 mm/s) and (^{Me}PDI)FeCPh$_2$ (right, δ = 0.41 mm/s and ΔE_Q = 1.31 mm/s) collected at 80K.

The bis(imino)pyridine iron carbene complexes were also studied by zero-field ^{57}Fe Mössbauer spectroscopy. Representative spectra for both compounds are presented in Figure 3.7. Both (^{Et}PDI)FeCPh$_2$ and (^{Me}PDI)FeCPh$_2$ have an isomer shift (δ) of 0.41 mm/s and similar quadrupole splittings (ΔE_Q) of 1.50 mm/s and 1.31 mm/s, respectively. Discussion on the interpretation of these values is presented in Section 3.4. Importantly, the Mössbauer spectra demonstrate that these compounds can be isolated cleanly, within the detection limit of these experiments, which suggests that any unusual spectroscopic features are likely a result of the compounds, not of impurities.

3.4 Electronic Structure Investigations of Bis(imino)pyridine Iron Carbene Complexes

As evidenced by their ^{1}H NMR spectra, the bis(imino)pyridine iron carbene complexes are paramagnetic. Solid state magnetic susceptibility balance (MSB) measurements on (^{Et}PDI)FeCPh$_2$ and (^{Me}PDI)FeCPh$_2$ were performed and yielded

average effective magnetic moments of 3.2 μ_B and 3.4 μ_B at 23 °C, respectively. Both ^{1}H NMR and zero-field ^{57}Fe Mössbauer spectroscopies suggest that (^{Et}PDI)FeCPh$_2$ and (^{Me}PDI)FeCPh$_2$ exhibit very similar electronic and structural characteristics to each other in solution and in the solid state. Because of the similarities and because (^{Et}PDI)FeCPh$_2$ is not thermally stable (*vide infra*), further experimental investigations into the electronic structure of a bis(imino)pyridine iron carbene were performed with (^{Me}PDI)FeCPh$_2$.

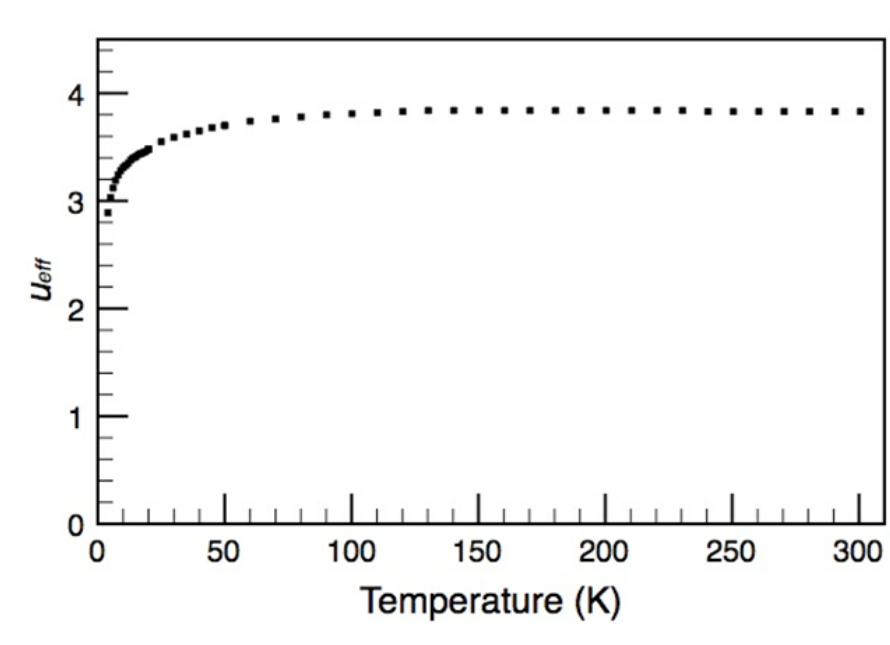

Figure 3.8 Representative SQUID magnetometry data for (^{Me}PDI)FeCPh$_2$.

The magnetic moment of (^{Me}PDI)FeCPh$_2$ was further investigated in both the solution and solid state. The room temperature solution magnetic moment was measured to be 3.0 μ_B by Evans method (23 °C). Both the Evans method and magnetic susceptibility balance data are consistent with an S = 1 ground state for (^{Me}PDI)FeCPh$_2$. SQUID magnetrometry data were also collected on several independently prepared samples of (^{Me}PDI)FeCPh$_2$ and a representative trace is shown

in Figure 3.8. The average room temperature μ_{eff} predicted by the SQUID measurements is 3.8 μ_B, slightly higher than the moments observed by magnetic susceptibility balance and Evans method. As of this moment, the origin of the discrepancy in measured magnetic moment between the data collected on the magnetic susceptibility balance (MSB) and that collected by SQUID is unknown. Both experiments were conducted on solid, crystalline samples judged pure by ^{1}H NMR and/or Mössbauer spectroscopy.

Table 3.2 Mössbauer parameters for selected bis(imino)pyridine iron compounds.

Compound	δ (mm/s)	$\lvert \Delta E_Q \rvert$ (mm/s)
$(^{Et}PDI)FeCPh_2$	0.41	1.50
$(^{Me}PDI)FeCPh_2$	0.41	1.31
$(^{iPr}PDI)FeN(2,6\text{-}^{i}Pr_2\text{-}C_6H_3)$	0.30	+ 1.08
$(^{iPr}PDI)FeN(2,4,6\text{-}Me_3\text{-}C_6H_2)$	0.30	1.34
$(^{iPr}PDI)FeCH_2CMe_3$	0.57	1.16
$(^{Et}PDI)FeCH_2CMe_3$	0.56	1.13
$(^{iPr}PDI)FeCH_2SiMe_3$	0.54	1.55

This Mössbauer isomer shifts of 0.41 mm/s for both bis(imino)pyridine iron carbene compounds are consistent with low or intermediate spin iron(II) and low, intermediate or high spin iron(III).[46] Relative to previously reported bis(imino)pyridine iron compounds, these isomer shifts are most similar to those observed for the bis(imino)pyridine iron dinitrogen compounds and several other neutral ligand compounds, which are proposed to contain intermediate spin iron(II) centers.[34,47] However, the iron carbene compounds have one-electron reduced bis(imino)pyridine chelates, while the dinitrogen and neutral ligand compounds all contain two-electron reduced chelates which may complicate a comparison between

the two sets of compounds. Also, many neutral ligand compounds either have five-coordinate iron centers or are planar four-coordinate compounds. In contrast to this, the solid state geometry of (^{Et}PDI)FeCPh$_2$ deviates significantly from planarity. Both the bis(imino)pyridine iron aryl imides[44] and monoalkyls[45,48] are assigned as having one-electron reduced chelates and are also four-coordinate iron compounds with ligands canted out of the chelate plane. Table 3.2 presents the isomer shift and quadrupole splitting parameters for several iron aryl imide and monoalkyl compounds.

The bis(imino)pyridine iron aryl imide compounds, (^{iPr}PDI)FeN(2,6-^{i}Pr$_2$-C$_6$H$_3$) and (^{iPr}PDI)FeN(2,4,6-Me$_3$-C$_6$H$_2$), both have isomer shifts of 0.30 mm/s and quadrupole splittings of + 1.08 mm/s and $\left|1.34\right|$ mm/s, respectively.[44] The electronic structures of these compounds are best described as intermediate spin iron(III) centers antiferromagnetically coupled to mono-reduced bis(imino)pyridine chelates.[44] In contrast, the bis(imino)pyridine iron monoalkyl compounds are best portrayed as high spin iron(II) centers antiferromagnetically coupled to mono-reduced chelates and have isomer shifts between 0.54 mm/s and 0.57 mm/s and quadrupole splittings ranging from $\left|1.13\right|$ mm/s to $\left|1.55\right|$ mm/s.[45,48] The quadrupole splitting parameters of the iron carbenes, aryl imides and monoalkyls are all very similar; perhaps not surprising given that they all have similar deviations from planarity. The isomer shifts of (^{Et}PDI)FeCPh$_2$ and (^{Me}PDI)FeCPh$_2$ are more similar to those of the iron aryl imides than the alkyls, suggesting that iron(III) is a plausible description of the iron center in the carbene compounds.

Iron K-edge X-ray absorption spectroscopy was also performed on (^{Me}PDI)FeCPh$_2$. A representative spectrum for (^{Me}PDI)FeCPh$_2$ plotted against (^{iPr}PDI)FeN(2,6-^{i}Pr$_2$-C$_6$H$_3$) and (^{iPr}PDI)FeCH$_2$CMe$_3$ for comparison, is presented in Figure 3.9 and an expansion of the pre-edge is presented in Figure 3.10. The pre-edge feature of the spectrum is typically used to assign the iron oxidation state and a

difference of 1 eV per change in oxidation state is usually observed.[49] The iron monoalkyl, (^{iPr}PDI)FeCH$_2$CMe$_3$, is described as high spin iron(II) and accordingly displays a pre-edge value of 7111.8 eV. However, the intermediate spin iron(III) aryl imide, (^{iPr}PDI)FeN(2,6-^{i}Pr$_2$-C$_6$H$_3$), has a pre-edge value of 7112.0 eV, which deviates from the trend of 1 eV per oxidation state unit. The measured pre-edge value for (^{Me}PDI)FeCPh$_2$ is 7111.8 eV, which is consistent with both the iron(II) and iron(III) measurements. As the pre-edge energy can be affected by coordination number and ligand field strength of the ligands, the inflection point of the rising-edge can also provide insight into the oxidation state of the iron center.[49] The inflection point of the rising edge of the iron carbene compound appears to be most similar to that of the aryl imides, providing support for an iron(III) oxidation state in (^{Me}PDI)FeCPh$_2$.

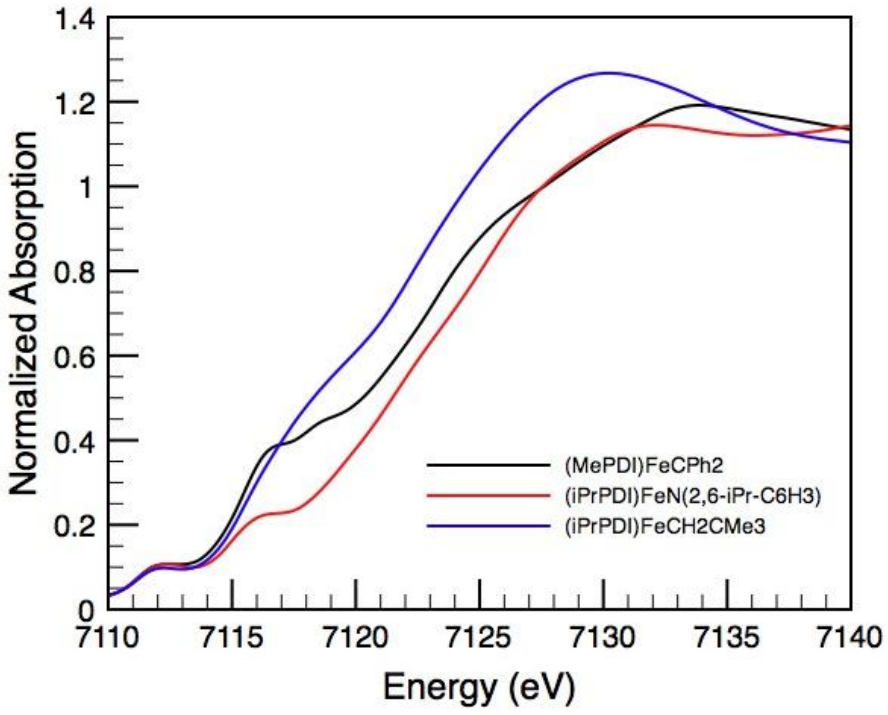

Figure 3.9 Iron K-edge data.

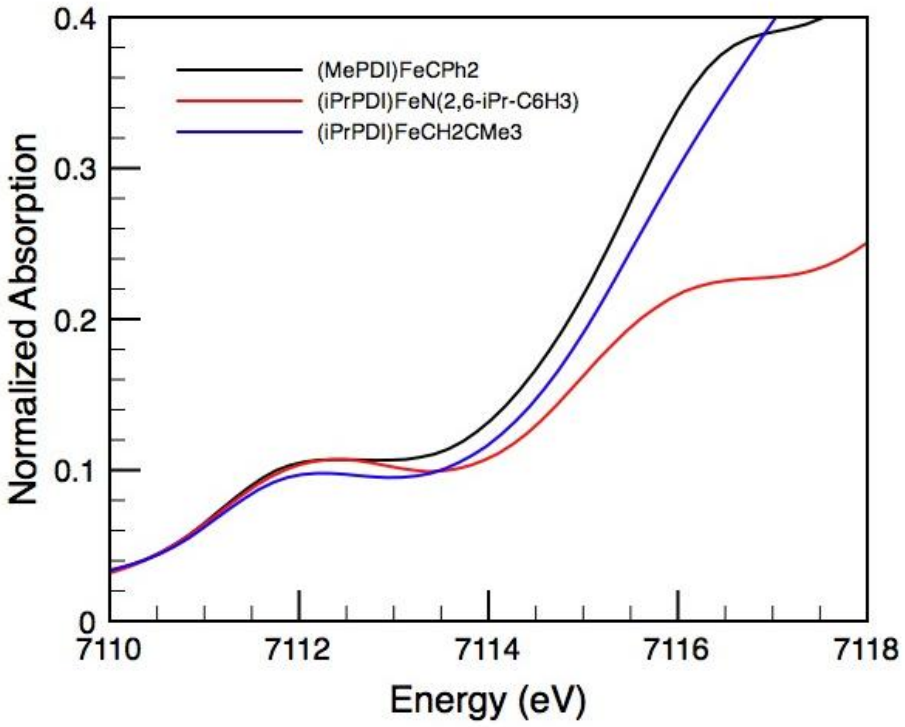

Figure 3.10 Pre-edge feature of the iron K-edge data.

Carbene ligands are generally grouped into two limiting cases: triplet, X_2-type carbenes or singlet, L-type carbenes.[1] Typically, singlet, or Fischer-type, carbenes contain at least one electronegative substituent, such as a heteroatom, while triplet, or Schrock-type, carbenes have primarily alkyl groups or hydrogen atoms as substituents. Based on these descriptions, the diphenylcarbene fragment is most likely to be an X_2-type, dianionic, ligand. However, de Bruin and coworkers recently reported the observation of a cobalt porphyrin carbene compound by EPR and used the spectroscopic and computational data to suggest that the carbene fragment is best described as a carbon-centered radical, rather than as a typical singlet or triplet carbene (Figure 3.11).[50] Because the cobalt carbene is derived from addition of ethyldiazoacetate, they propose that it is described as a one-electron reduced Fischer-type carbene.

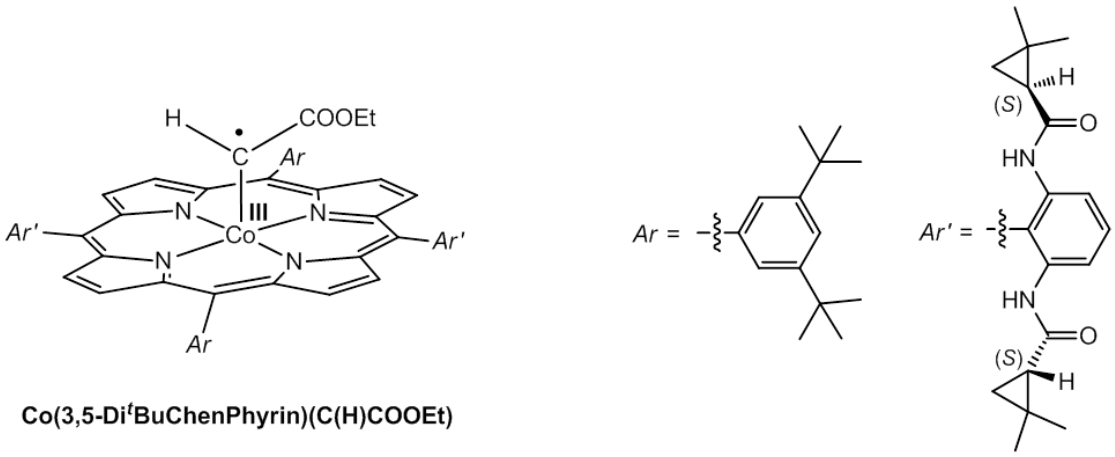

Figure 3.11 Carbon-centered radical on a cobalt porphyrin carbene complex.

Taking into account all of the spectroscopic and magnetic data as well as the possibilities for the carbene fragment, several electronic structures can be proposed for the bis(imino)pyridine iron carbene complexes. These proposals are shown in Figure 3.12 and all adhere to the restraint of a one-electron reduced bis(imino)pyridine chelate and an overall $S = 1$ ground state. If the carbene ligand exists as a singlet carbene then the compound must contain a high spin iron(I) ion antiferromagnetically coupled to the monoreduced chelate (Proposal A). An iron compound with a triplet carbene ligand yields Proposal B with an intermediate spin iron(III) center antiferromagnetically coupled to a monoreduced chelate, the same electronic structure proposed for the bis(imino)pyridine aryl imide compounds. The final two proposed structures contain iron(II) centers and carbon centered carbene radicals. Proposal C contains a high spin iron(II) center antiferromagnetically coupled to both a carbene radical and a monoreduced chelate while Proposal D contains an intermediate spin iron(II) center antiferromagnetically coupled to a monoreduced chelate, but not coupled to the carbene radical.

Proposal A

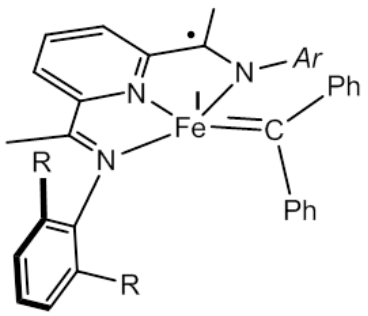

L-type, singlet carbene

High Spin Fe(I)	$S_{Fe} = {}^3/_2$
$[^{iPr}PDI]^{1-}$	$S_{PDI} = {}^1/_2$
	$S_{total} = 1$

Proposal B

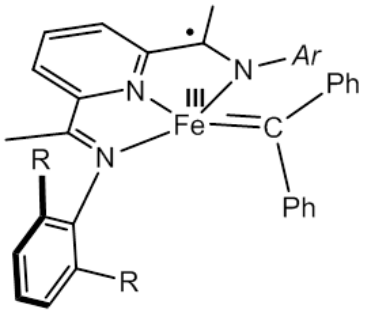

X_2-type, triplet carbene

Int. Spin Fe(III)	$S_{Fe} = {}^3/_2$
$[^{iPr}PDI]^{1-}$	$S_{PDI} = {}^1/_2$
	$S_{total} = 1$

Proposal C

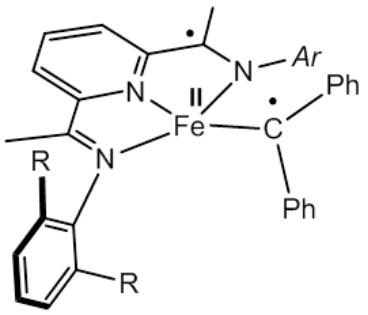

carbene radical

High Spin Fe(II)	$S_{Fe} = 2$
$[^{iPr}PDI]^{1-}$	$S_{PDI} = {}^1/_2$
$[CPh_2]^{1-}$	$S_{CPh2} = {}^1/_2$
	$S_{total} = 1$

Proposal D

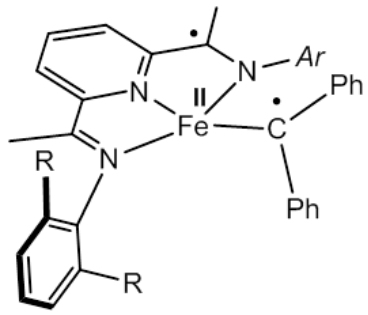

carbene radical

Int. Spin Fe(II)	$S_{Fe} = 1$
$[^{iPr}PDI]^{1-}$	$S_{PDI} = {}^1/_2$
$[CPh_2]^{1-}$	$S_{CPh2} = {}^1/_2$
	$S_{total} = 1$

Figure 3.12 Possible electronic structures for the bis(imino)pyridine iron carbene complexes.

Proposal A and Proposal C are inconsistent with the Mössbauer isomer shift observed for (^{Et}PDI)FeCPh$_2$ and (^{Me}PDI)FeCPh$_2$ as both high spin iron(I) and iron(II) are expected to have much higher isomer shifts than 0.41 mm/s;[46] however, the long F-N_{PDI} bond lengths in the solid state structure of (^{Et}PDI)FeCPh$_2$ do suggest contributions from a high spin iron center. On the other hand, proposals B and D are both supported by the Mössbauer parameters as an isomer shift of 0.41 mm/s falls in the range of values expected for both intermediate spin iron(III) and iron(II) oxidation states. The iron K-edge data is also consistent with either an iron(II) or iron(III) center, possibly favoring an iron(III) description based on the inflection point of the rising edge. Proposal D would also explain the relatively long Fe-$C_{carbene}$ bond because it has a Fe-C single bond instead of a double bond. Based on the spectroscopic data, Proposal A can be ruled out, but other than that it is difficult to assign the actual electronic structure of the bis(imino)pyridine iron carbene compounds.

Overall, the spectroscopic data provide the most support for Proposal B, the analogous electronic structure to the bis(imino)pyridine iron aryl imides. Also consistent with this proposal, the reactivity of (^{Me}PDI)FeCPh$_2$ is similar to that reported for the iron aryl imide compounds (*vide infra*). Based on this, the electronic structure of the bis(imino)pyridine iron carbene complexes is best described as an intermediate spin iron(III) center (S_{Fe} = $^3/_2$) antiferromagnetically coupled to a singly reduced chelate (S_{PDI} = ½) yielding an overall S = 1 ground state. In this description, the carbene ligand is best described as a triplet, X_2-type carbene.

3.5 Reactivity of Bis(imino)pyridine Iron Carbene Complexes

Although (^{Et}PDI)FeCPh$_2$ and (^{Me}PDI)FeCPh$_2$ have similar electronic structures, (^{Me}PDI)FeCPh$_2$ is stable in solution for weeks while (^{Et}PDI)FeCPh$_2$

decomposes within a day. Monitoring a benzene-d_6 solution of (^{Et}PDI)FeCPh$_2$ by ^{1}H NMR spectroscopy over the course of 16 hours at room temperature established the disappearance of the peaks associated with (^{Et}PDI)FeCPh$_2$ and the appearance of new aromatic resonances and a singlet at 3.75 ppm consistent with diphenylmethane. No peaks for a [(^{Et}PDI)Fe] species were observed indicating that the new compound was NMR silent. It has been documented that the substituents on the aryl rings of bis(imino)pyridine ligands can participate in transfer hydrogenation reactions with coordinated substrates.[44,51] For example, the η^1-diazoalkane compound, (^{iPr}PDI)FeN$_2$CHSiMe$_3$, is thermally unstable and undergoes transfer hydrogenation in solution overnight to form an NMR silent intramolecular iron olefin compound and SiMe$_4$ (Figure 3.3).[44] Therefore, it is likely that the NMR silent product observed in the decomposition of the iron carbene compound is a similar intramolecular iron olefin compound (Figure 3.13).

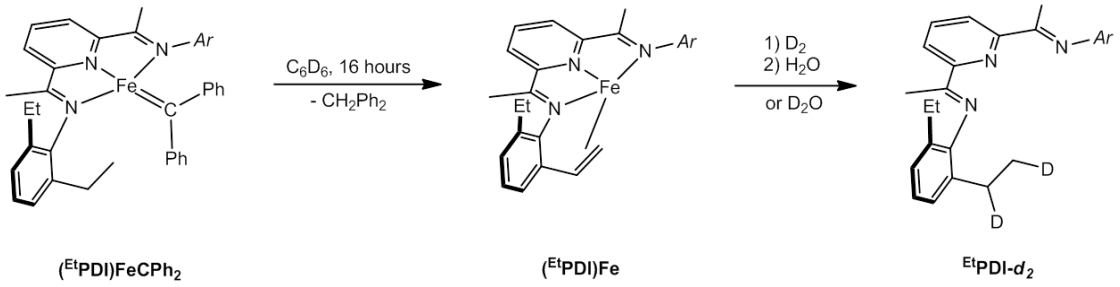

Figure 3.13 Transfer hydrogenation from the aryl substituents of (^{Et}PDI)FeCPh$_2$ across the Fe-C bond.

The proposed intramolecular iron olefin compound was characterized by degradation experiments (Figure 3.12). Addition of D_2O to the NMR silent material followed by analysis of the ^{2}H NMR spectrum revealed deuterium incorporation into the ethyl methylene and methyl positions in approximately a 1:1 ratio. Similarly, addition of D_2 gas followed by decomposition with H_2O and analysis of the free ligand

by ^{2}H NMR also resulted in deuterium incorporation in the methylene and methyl positions of the aryl ethyl substituents. The results from these two experiments support the presence of a dehydrogenated aryl substituent in the NMR silent species.

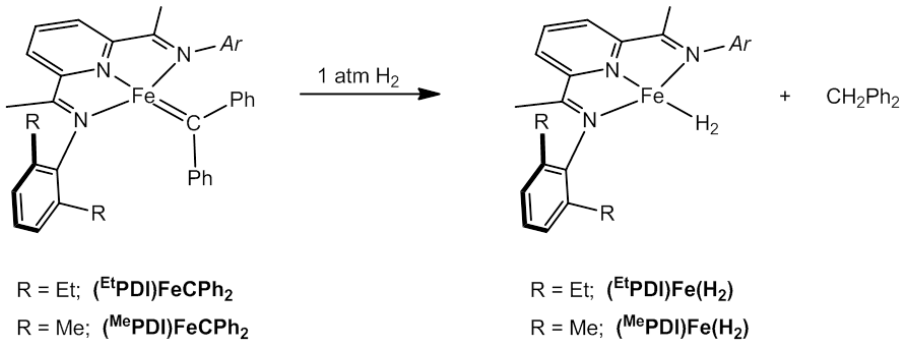

Figure 3.14 Addition of H_2 to bis(imino)pyridine iron carbene complexes.

The bis(imino)pyridine iron carbene compounds both undergo hydrogenative Fe-C bond cleavage to form CH_2Ph_2 (Figure 3.14) and the corresponding bis(imino)pyridine iron dihydrogen compounds discussed in Chapter 1. When D_2 gas is added to a solution of either iron carbene compound, d_2-diphenylmethane, CD_2Ph_2, is observed by ^{2}H NMR spectroscopy. This reactivity is very similar to that observed for the bis(imino)pyridine iron aryl imide complexes, where addition of H_2 furnished the free aniline and $(^{iPr}PDI)Fe(H_2)_2$,[44] further support for a similar electronic structure between the two groups of compounds. Because $(^{Et}PDI)FeCPh_2$ is thermally unstable, all other reactivity studies were conducted with $(^{Me}PDI)FeCPh_2$ to avoid any competing decomposition pathways.

Addition of 1 atmosphere of CO to a benzene-d_6 solution of (^{Me}PDI)FeCPh$_2$ resulted in carbene transfer and formation of diphenylketene and the bis(imino)pyridine iron dicarbonyl compound, (^{Me}PDI)Fe(CO)$_2$ (Figure 3.14). Diphenylketene was identified by comparison of NMR and IR spectra with those of an authentic sample. The bis(imino)pyridine iron aryl imide compounds also exhibit similar reactivity as addition of 1 atmosphere of CO to (^{iPr}PDI)FeN*Ar* results in nitrene transfer to afford the corresponding isocyanate and (^{iPr}PDI)Fe(CO)$_2$.[44] In a related reaction, upon addition of two equivalents of 2,4,6-trimethylphenyl azide to (^{Me}PDI)FeCPh$_2$, carbene transfer was again observed and the resulting products were the bis(imino)pyridine iron imide, (^{Me}PDI)FeN(2,4,6-Me$_3$-C$_6$H$_2$), and the free ketimine, Ph$_2$C=N(2,4,6-Me$_3$-C$_6$H$_2$) (Figure 3.15). This reactivity has also been observed by Hillhouse and coworkers for a bis(phosphine) nickel diphenylcarbene complex, (dtbpe)NiCPh$_2$.[52]

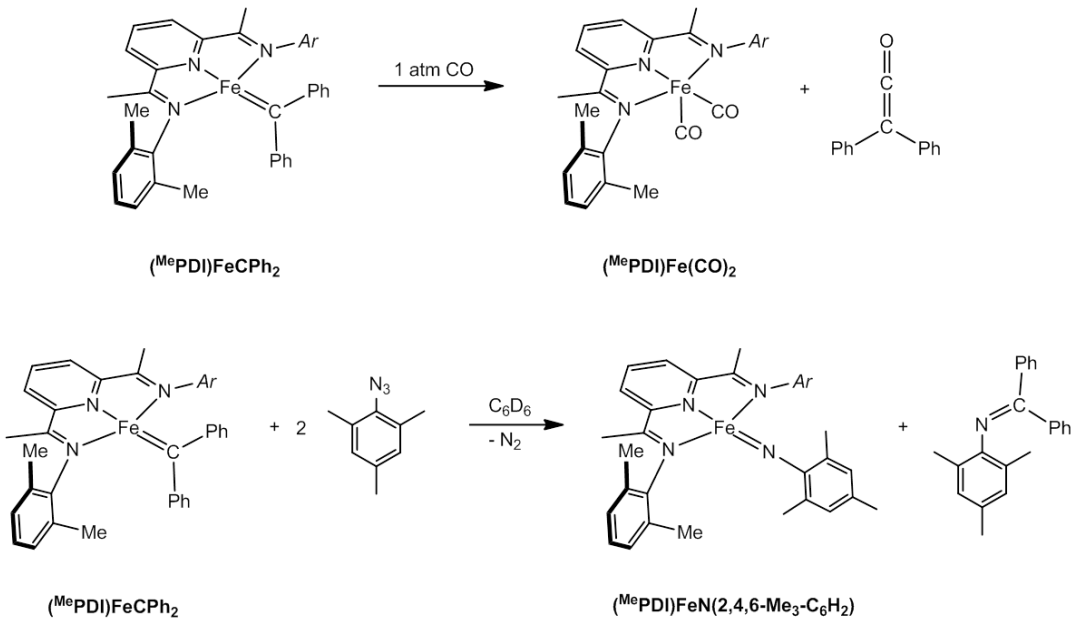

Figure 3.15 Addition of CO and 2,4,6-trimethylphenyl azide to (^{Me}PDI)FeCPh$_2$.

The bis(imino)pyridine iron carbene complex, (^{Me}PDI)FeCPh$_2$, was also screened as a pre-catalyst for olefination and cyclopropanation reactions as well as for olefin metathesis. Unfortunately, none of the attempted reactions yielded any catalytic or stoichiometric activity. Addition of two equivalents of benzaldehyde, acetophenone or acetone to a benzene-d_6 solution of (^{Me}PDI)FeCPh$_2$ all resulted in no reaction after 24 hours at room temperature. The cyclopropanation reactivity was tested by addition of styrene and ethylene, both of which also produced no reaction after 24 hours at room temperature. Finally, 10 equivalents of norbornene and diethyl diallyl malonate were separately added to benzene-d_6 solutions of (^{Me}PDI)FeCPh$_2$ and stirred at room temperature for 24 hours to assay potential ring opening and ring closing metathesis activity, respectively. Unfortunately, no reaction was observed for either substrate. In all cases, heating to 85 °C resulted in decomposition of the iron compound and no observation of the desired products.

3.6 Conclusions

Two bis(imino)pyridine iron diphenylcarbene complexes, (^{Et}PDI)FeCPh$_2$ and (^{Me}PDI)FeCPh$_2$, were synthesized by addition of 2 equivalents of diphenyldiazomethane to [(^{Et}PDI)Fe(N$_2$)]$_2$(μ_2-N$_2$) and [(^{Me}PDI)Fe(N$_2$)]$_2$(μ_2-N$_2$), respectively. Both iron carbene compounds were characterized by ^{1}H NMR and Mössbauer spectroscopies and shown to have very similar electronic structures. X-ray diffraction data were collected on (^{Et}PDI)FeCPh$_2$ and established a one-electron reduced chelate. Like the bis(imino)pyridine iron aryl imide complexes, the solid state geometry of (^{Et}PDI)FeCPh$_2$ deviates from planarity with the carbene fragment canted significantly out of the iron-chelate plane.

Solution and solid state magnetic data were collected on (^{Me}PDI)FeCPh$_2$ and established an S = 1 ground state for the iron carbene complex at 23 °C. Variable

temperature SQUID magnetometry data was also collected on (^{Me}PDI)FeCPh$_2$ and reproducibly exhibits an unusually high average effective magnetic moment of 3.8 μ_B for an S = 1 ground state. Several different electronic structures were proposed for the bis(imino)pyridine iron carbene complexes. The spectroscopic data and observed reactivity of (^{Me}PDI)FeCPh$_2$ best support an electronic structure analogous to the bis(imino)pyridine iron aryl imides compounds with an intermediate spin iron(III) center antiferromagnetically coupled to a one-electron reduced chelate. In this case the carbene ligand is described as a triplet, X_2-type carbene. However, contributions from other electronic structure descriptions are also possible.

The bis(imino)pyridine iron carbene complexes both react with H_2 and H_2O to furnish diphenylmethane and the corresponding dihydrogen compounds or rust, respectively. While (^{Et}PDI)FeCPh$_2$ is thermally stable in solution for weeks, (^{Et}PDI)FeCPh$_2$ decomposes over 16 hours at room temperature to afford diphenylmethane and an NMR silent iron compound which proved difficult to isolate and characterize. Degradation studies of this new compound strongly suggest that it is the intramolecular bis(imino)pyridine iron olefin compound. When 1 atmosphere of carbon monoxide or 2 equivalents of 2,4,6-trimethylphenyl azide were added to (^{Me}PDI)FeCPh$_2$, carbene transfer was observed to afford diphenylketene and N-mesityl diphenylketimine. Unfortunately, no cyclopropanation or olefin metathesis reactivity was observed for (^{Me}PDI)FeCPh$_2$ under several different reaction conditions.

3.7 Experimental Procedures

General Considerations. All air- and moisture-sensitive manipulations were carried out using standard vacuum line, Schlenk, and cannula techniques or in an MBraun inert atmosphere dry box containing an atmosphere of purified nitrogen. Solvents for air- and moisture-sensitive manipulations were initially dried and deoxygenated using

literature procedures.[53] Benzene-d_6 was purchased from Cambridge Isotope Laboratories and dried over 4 Å molecular sieves. Diphenyldiazomethane[54] and 2,4,6-trimethylphenyl azide[55] were prepared according to literature procedure. The compounds: $[(^{Et}PDI)Fe(N_2)]_2(\mu_2\text{-}N_2)$ and $[(^{Me}PDI)Fe(N_2)]_2(\mu_2\text{-}N_2)$ were prepared according to literature procedure.[34a]

^1H NMR spectra were recorded on Varian Mercury 300, Inova 400, 500, and 600 spectrometers operating at 299.76, 399.78, 500.62, and 599.78 MHz, respectively. ^{13}C NMR spectra were recorded on an Inova 500 spectrometer operating at 125.893 MHz. All ^1H and ^{13}C NMR chemical shifts are reported relative to $SiMe_4$ using the ^1H (residual) and ^{13}C chemical shifts of the solvent as a secondary standard. Peak widths at half heights are reported for paramagnetically broadened and shifted resonances. For diamagnetic complexes, many assignments were made based on COSY and HSQC NMR experiments. Solution magnetic moments were determined by Evans method[56] using a ferrocene standard and are the average value of at least two independent measurements. Magnetic susceptibility balance measurements were performed with a Johnson Matthey instrument that was calibrated with $HgCo(SCN)_4$. Infrared spectra were collected on a Thermo Nicolet spectrometer. Elemental analyses were performed at Robertson Microlit Laboratories, Inc., in Madison, NJ.

Single crystals suitable for X-ray diffraction were coated with polyisobutylene oil in a drybox, transferred to a nylon loop and then quickly transferred to the goniometer head of a Bruker X8 APEX2 diffractometer equipped with a molybdenum X-ray tube (λ = 0.71073 Å). Preliminary data revealed the crystal system. A hemisphere routine was used for data collection and determination of lattice constants. The space group was identified and the data were processed using the Bruker SAINT+ program and corrected for absorption using SADABS. The structures were solved

using direct methods (SHELXS) completed by subsequent Fourier synthesis and refined by full-matrix least-squares procedures.

SQUID magnetization data of crystalline powdered samples were recorded with a SQUID magnetometer (Quantum Design) at 10 kOe between 5 and 300 K for all samples. Values of the magnetic susceptibility were corrected for the underlying diamagnetic increment by using tabulated Pascal constants and the effect of the blank sample holders (gelatin capsule/straw). Samples used for magnetization measurement were recrystallized multiple times and checked for chemical composition by ^{1}H NMR spectroscopy. The program julX written by E. Bill was used for (elements of) the simulation and analysis of magnetic susceptibility data.[57]

Zero-field ^{57}Fe Mössbauer spectra were recorded on a SEE Co. Mössbauer spectrometer (MS4) at 80 K in constant acceleration mode. ^{57}Co/Rh was used as the radiation source. WMOSS software was used for the quantitative evaluation of the spectral parameters (least-squares fitting to Lorentzain peaks). The minimum experimental line widths were 0.23 mm/s. The temperature of the sample was controlled by a Janis Research Co. CCS-850 He/N_2 cryostat within and accuracy of ± 0.3 K. Isomer shifts were determined relative to α-iron at 298 K.

Preparation of (^{Et}PDI)Fe(CPh_2). A 20 mL scintillation vial was charged with 0.200 g (0.191 mmol) of [(^{Et}PDI)Fe(N_2)]$_2$(μ_2-N_2) and approximately 10 mL of diethyl ether. A solution of diphenyldiazomethane (0.074 g, 0.382 mmol) in 5 mL of diethyl ether was added to the vial resulting in vigorous bubbling and a color change from brown to green. Removal of the solvent *in vacuo* yielded 0.240 g (0.371 mmol, 97%) of a green solid identified as (^{Et}PDI)Fe(CPh_2). Crystals suitable for X-ray analysis were grown from a pentane solution. Analysis for $C_{42}H_{45}N_3Fe$: Calc. C, 77.89; H, 7.00; N, 6.49. Found C, 77.67; H, 7.17; N, 6.38. Magnetic susceptibility: μ_{eff} = 3.2 μ_B (benzene-*d*$_6$,

20 °C); 3.2 μ_B (magnetic susceptibility balance, 23 °C). ^{1}H NMR (benzene-d_6, 20 °C): δ = -68.32 (72.38 Hz, 6H, C(CH_3)), -55.88 (177.9 Hz, 4H, CH_2CH$_3$), -45.91 (107.3 Hz, 4H, CH_2CH$_3$), -27.30 (29.33 Hz, 4H, Ph), -14.96 (24.67 Hz, 12H, CH$_2$CH_3), -3.32 (18.58 Hz, 2H, *p-Ar*), -3.00 (17.32 Hz, 4H, *m-Ar*), 54.45 (50.61 Hz, 2H, *m-py* or *Ph*), 101.72 (432.6 Hz, 4H, *Ph*), 118.22 (124.5 Hz, 2H, *m-py* or *Ph*), 155.56 (150.3 Hz, 1H, *p-py*).

Preparation of (^{Me}PDI)Fe(CPh$_2$). A 20 mL scintillation vial was charged with 0.200 g (0.214 mmol) of [^{Me}PDIFe(N$_2$)]$_2$(μ_2-N$_2$) and approximately 10 mL of diethyl ether. A solution of diphenyldiazomethane (0.083g, 0.428 mmol) in diethyl ether was added to the vial resulting in vigorous bubbling and a color change from brown to green. Removal of the solvent *in vacuo* yielded 0.238 g (0.402 mmol, 94%) of a green solid identified as (^{Me}PDI)Fe(CPh$_2$). Analysis for $C_{38}H_{37}N_3Fe$: Calc. C, 77.15; H, 6.30; N, 7.10. Found C, 76.93; H, 6.39; N, 6.86. Magnetic susceptibility: μ_{eff} = 3.0 μ_B (benzene-d_6, 20 °C), μ_{eff} = 3.4 μ_B (Gouy balance, 23 °C), μ_{eff} = 4.1 μ_B (SQUID). ^{1}H NMR (benzene-d_6, 20 °C): δ = -56.76 (64.90 Hz, 6H, C(CH_3)), -33.07 (71.57 Hz, 12H, Ar CH_3), -24.27 (26.89 Hz, 4H, *Ph*), -3.23 (16.47 Hz, 2H, *p-Ar*), -2.15 (16.12 Hz, 4H, *m-Ar*), 50.23 (49.01 Hz, 2H, *m-py* or *Ph*), 92.96 (350.1 Hz, 4H, *Ph*), 107.28 (104.5 Hz, 2H, *m-py* or *Ph*), 133.40 (123.8 Hz, 1H, *p-py*).

Independent preparation of (^{Me}PDI)FeN(2,4,6-Me$_3$C$_6$H$_2$). A 20 mL-scintillation vial was charged with 0.200 g (0.21 mmol) of [^{Me}PDIFe(N$_2$)]$_2$(μ_2-N$_2$) and approximately 10 mL of diethyl ether. A solution of 2,4,6-trimethylphenyl azide (0.068 g, 0.43 mmol) in diethyl ether was added to the vial resulting in vigorous bubbling and a color change from brown to dark blue. Romoval of the solvent yielded .167 g (70 %) of a dark blue solid identified as (^{Me}PDI)FeN(2,4,6-Me$_3$C$_6$H$_2$).

Magnetic susceptibility: μ_{eff} = 3.0 μ_B (Gouy balance, 296K). ^{1}H NMR (benzene-d_6, 20 °C): δ = -109.44 (43.45 Hz, 6H, C(CH_3)), -19.67 (32.30 Hz, 12H, Ar CH_3), 0.88 (14.52 Hz, 6H, mes o-CH_3), 7.41 (21.66 Hz, 2H, mes C*H*), 45.54 (26.45 Hz, 4H, *m-Ar*), 98.20 (31.85 Hz, 2H, *p-Ar*), 125.40 (66.30 Hz, 2H, *m-py*), 239.18 (169.73 Hz, 1H, *p-py*).

REFERENCES

[1] Collman, J. P.; Hegedus, L. S.; Norton, J. R.; Finke, R. G. *Principles and Applications of Organotransition Metal Chemistry*, 2nd Ed. University Science, 1987.

[2] Romero, P. E.; Piers, W. E.; McDonald, R. *Angew. Chem. Int. Ed.* **2004**, *43*, 6161.

[3] Chauvin, Y. *Angew. Chem. Int. Ed.* **2006**, *45*, 3740.

[4] Schrock, R. R. *Angew. Chem. Int. Ed.* **2006**, *45*, 3748.

[5] Grubbs, R. H. *Angew. Chem. Int. Ed.* **2006**, *45*, 3760.

[6] (a) Blanc, R.; Thivolle-Cazat, J.; Basset, J. –M.; Copéret, C.; Hock, A. S.; Tonzetich, Z. J.; Sinha, A.; Schrock, R. R. *J. Am. Chem. Soc.* **2007**, *129*, 1044. (b) Schrock, R. R. *J. Chem. Soc., Dalton Trans.* **2001**, 2541.

[7] (a) Schwab, P.; Grubbs, R. H.; Ziller, J. W. *J. Am. Chem. Soc.* **1996**, *118*, 100. (b)Schwab, P.; France, M. B.; Ziller, J. W.; Grubbs, R. H. *Angew. Chem. Int. Ed.* **1995**, *34*, 2039.

[8] Bieniek, M.; Michrowska, A.; Usanov, D. L.; Grela, K. *Chem. Eur. J.* **2008**, *14*, 806.

[9] (a) Vougioukalakis, G. C.; Grubbs, R. H. *Chem. Rev.* **2010**, *110*, 1746. (b) Trnka, T. M.; Grubbs, R. H. *Acc. Chem. Res.* **2001**, *34*, 18.

[10] Esteruelas, M. A.; González, A. I.; López, A. M.; Oñate, E. *Organometallics* **2003**, *22*, 414.

[11] (a) Wu, Z.; Nguyen, S. T.; Grubbs, R. H.; Ziller, J. W. *J. Am. Chem. Soc.* **1995**, *117*, 5503. (b) Nguyen, S. T.; Johnson, L. K.; Grubbs, R. H. *J. Am. Chem. Soc.* **1992**, *114*, 3974.

[12] (a) Adlhart, C.; Chen, P. *Angew. Chem. Int. Ed.* **2002**, *41*, 4484. (b) Adlhart, C.; Chen, P. *Helv. Chim. Acta* **2003**, *86*, 941.

[13] Krapp, A.; Pandey, K. K.; Frenking, G. *J. Am. Chem. Soc.* **2007**, *129*, 7596.

[14] Wong, C. Y.; Chan, M. C. W.; Zhu, N.; Che, C. M. *Organometallics* **2004**, *23*, 2263.

[15] (a) Getty, K.; Delgado-Jaime, M. U.; Kennepohl, P. *Inorg. Chim. Acta* **2008**, *361*, 1059. (b) Getty, K.; Delgado-Jaime, M. U.; Kennepohl, P. *J. Am. Chem. Soc.* **2007**, *129*, 15774.

[16] Jolly, P. W.; Pettit, R. *J. Am. Chem. Soc.* **1966**, *88*, 5044.

[17] (a) Brookhart, M.; Studabaker, W. B.; Humphrey, M. B. *Organometallics* **1989**, *8*, 132. (b) Guerchais, V.; Lapinte, C. *J. Chem. Soc., Chem. Commun.* **1986**, 663. (c) Casey, C. P.; Miles, W. H.; Tukada, H.; O'Connor, J. M. *J. Am. Chem. Soc.* **1982**, *104*, 3761. (d) Brookhart, M.; Tucker, J. R.; Flood, T. C.; Jensen, J. *J. Am. Chem. Soc.* **1980**, *102*, 1203. (e) Brookhart, M.; Nelson, G. O. *J. Am. Chem. Soc.* **1977**, *99*, 6099.

[18] Guerchais, V. *Eur. J. Inorg. Chem.* **2002**, 783.

[19] Riley, P. E.; Davies, R. E.; Allison, N. T.; Jones, W. M. *Inorg. Chem.* **1982**, *21*, 1321.

[20] Allison, N. T.; Kawada, Y.; Jones, W. M. *J. Am. Chem. Soc.* **1978**, *100*, 5224.

[21] Mahias, V.; Cron, S.; Toupet, L.; Lapinte, C. *Organometallics* **1996**, *15*, 5399.

[22] Poignant, g.; Nlate, S.; Geurchais, V. *Organometallics* **1997**, *16*, 124.

[23] Klose, A.; Solari, E.; Floriani, C.; Re, N.; Chiesi-Villa, A.; Rizzoli, C. *Chem. Commun.* **1997**, 2297.

[24] Li, Y.; Huang, J. –S.; Zhou, Z. –Y.; Che, C. –M.; You, X. –Z. *J. Am. Chem. Soc.* **2002**, *124*, 13185.

[25] (a) Wolf, J. R.; Hamaker, C. G.; Djukic, J. –P.; Kodadek, T.; Woo, L. K. *J. Am. Chem. Soc.* **1995**, *117*, 9194. (b) Hamaker, C. G.; Mirafzal, G. A.; Woo, L. K. *Organometallics* **2001**, *20*, 5171. (c) Du, G.; Andrioletti, B.; Rose, E.; Woo, L. K. *Organometallics* **2002**, *21*, 4490. (d) Baumann, L. K.; Mbuvi, H. M.; Du, G.; Woo, L. K. *Organometallics* **2007**, *26*, 3995. (e) Mbuvi, H. M.; Woo, L. K. *Organometallics* **2008**, *27*, 637. (f) Cheng, G.; Mirafzal, G. A.; Woo, L. K. *Organometallics* **2003**, *22*, 1468.

[26] Edulji, S. K.; Nguyen, S. T. *Organometallics* **2003**, *22*, 3374.

[27] (a) Kleigrewe, N.; Steffen, W.; Blömker, T.; Kehr, G.; Fröhlich, R.; Wibbeling, B.; Erker, G.; Wasilke, J. –C.; Wu, G.; Bazan, G. C. *J. Am. Chem. Soc.* **2005**, *127*, 13955. (b) Bianchini, C.; Giambastiani, G.; Rios, I. G.; Mantovani, G.; Meli, A.; Segarra, A. M. *Coord. Chem. Rev.* **2006**, *250*, 1391.

[28] Zu, D.; Budzelaar, P. H. M. *Organometallics* **2008**, *27*, 2699.

[29] Gibson, V. C.; Redshaw, C.; Solan, G. A. *Chem. Rev.* **2007**, *107*, 1745.

[30] Matsugi, T.; Fujita, T. *Chem. Soc. Rev.* **2008**, *37*, 1264.

[31] Blackmore, I. J.; Gibson, V. C.; Hitchcock, P. B.; Rees, C. W.; Williams, D. J.; White, A. J. P. *J. Am. Chem. Soc.* **2005**, *127*, 6012.

[32] Vanadium: Vidyaratne, E.; Gambarotta, S.; Korobkov, E.; Budzelaar, P. H. M. *Inorg. Chem.* **2005**, *44*, 1187.

[33] Chromium: Vidyaratne, I.; Scott, j.; Bambarotta, S.; Budzelaar, P. H. M. *Inorg. Chem.* **2007**, *46*, 7040.

[34] Iron: (a) Russell, S. K.; Darmon, J. M.; Lobkovsky, E.; Chirik, P. J. *Inorg. Chem.* **2010**, *49*, 2782. (b) Bart, S. C.; Lobkovsky, E.; Chirik, P. J. *J. Am. Chem. Soc.* **2004**, *126*, 13794.

[35] Cobalt: (a) Bowman, A. C.; Milsmann, C.; Atienza, C. C. H.; Lobkovsky, E.; Wieghardt, K.; Chirik, P. J. *J. Am. Chem. Soc.* **2010**, *132*, 1676. (b) Gibson, V. C.; Humphries, M. J.; Tellmann, K. P.; Wass, D. F.; White, A. J. P.; Williams, D. J. *Chem. Commun.* **2001**, 2252.

[36] Ruthenium: Gallagher, M.; Wieder, N. L.; Dioumaev, V. K.; Carroll, P. J.; Berry, D. H. *Organometallics* **2010**, *29*, 591.

[37] Trovitch, R. J.; Lobkovsky, E.; Chirik, P. J. *Inorg. Chem.* **2006**, *45*, 7252.

[38] (a) Knijnenburg, Q.; Gambarotta, S.; Budzelaar, P. H. M. *Dalton Trans.* **2006**, 5442. (b) Bart, S. C.; Chlopek, K.; Bill, E.; Bouwkamp, M. W.; Lobkovsky, E.; Neese, F.; Wieghardt, K.; Chirik, P. J. *J. Am. Chem. Soc.* **2006**, *128*, 13901.

[39] Butin, K. P.; Beloglazkina, E. K.; Zyk, N. V. *Russ. Chem. Rev.* **2005**, *74*, 531.

[40] Knijnenburg, Q.; Hetterscheid, D.; Kooistra, T. M.; Budzelaar, P. H. M. *Eur. J. Inorg. Chem.* **2004**, 1204.

[41] Bianchini, C.; Lee, H. M. *Organometallics* **2000**, *19*, 1833.

[42] Bart, S. C.; Bowman, A. C.; Lobkovsky, E.; Chirik, P. J. *J. Am. Chem. Soc.* **2007**, *129*, 7212.

[43] Bart, S. C. *Ph. D. Thesis*, Cornell University, 2006.

[44] Bart, S. C.; Lobkovsky, E.; Bill, E.; Chirik, P. J. *J. Am. Chem. Soc.* **2006**, *128*, 5302.

[45] Fernández, I.; Trovitch, R. J.; Lobkovsky, E.; Chirik, P. J. *Organometallics* **2008**, *27*, 109.

[46] Gütlich, P. In *Topics in Applied Physics*; Gonser, U., Ed.; Springer: New York, 1975; vol. 5, p. 68.

[47] Bart, S. C.; Lobkovsky, E.; Bill, E.; Wieghardt, K. Chirik, P. C. *Inorg. Chem.* **2007**, *46*, 7055.

[48] Tondreau, A. M.; Milsmann, C.; Patrick, A. D.; Hoyt, H. M.; Lobkovsky, E.; Wieghardt, K.; Chirik, P. J. *J. Am. Chem. Soc.* **2010**, *132*, 15046.

[49] Westre, T. E.; Kennepohl, P.; DeWitt, J. G.; Hedman, B.; Hodgson, K. O.; Solomon, E. I. *J. Am. Chem. Soc.* **1997**, *119*, 6297.

[50] Dzik, W. I.; Xu, X.; Zhang, X. P.; Reek, J. N. H.; de Bruin, B. *J. Am. Chem. Soc.* **2010**, *132*, 10891.

[51] Sylvester, K. T.; Chirik, P.J. *J. Am. Chem. Soc.* **2009**, *131*, 8772.

[52] Mindiola, D. J.; Hillhouse, G. L. *J. Am. Chem. Soc.* **2002**, *124*, 9976.

[53] Pangborn, A. B.; Giardello, M. A.; Grubbs, R. H.; Rosen, R. K.; Timmers, F. J. *Organometallics* **1996**, *15*, 1518.

[54] Miller, J. B. *J. Org. Chem.* **1959**, *24*, 560.

[55] Lui, Q.; Tor, Y. *Org. Lett.* **2003**, *5*, 2571.

[56] Sur, S. K. *J. Mag. Res.* **1989**, *82*, 169-173.

[57] http://ewww.mpi-muelheim.mpg.de/bac/logins/bill/julX_en.php

CHAPTER 4

SYNTHESIS, ELECTRONIC STRUCTURE AND REACTIVITY OF REDUCED BIS(ALDIMINO)PYRIDINE IRON COMPOUNDS*

4.1 Abstract

A variety of bis(aldimino)pyridine iron compounds was synthesized for the purpose of comparing electronic structure and reactivity of the resulting compounds with their related bis(imino)pyridine iron derivatives. Reduction of the bis(aldimino)pyridine iron dibromide, (^{iPr}PDAI)FeBr$_2$ (^{iPr}PDAI = 2,6-(2,6-^{i}Pr$_2$-C$_6$H$_3$-N=CH)$_2$C$_5$H$_3$N), with two equivalents of 0.5 % sodium amalgam in a toluene solution under one atmosphere of N_2 furnished the η^6-toluene compound, (^{iPr}PDAI)Fe(η^6-C$_7$H$_8$). Cooling a pentane or diethyl ether solution of (^{iPr}PDAI)Fe(η^6-C$_7$H$_8$) to -35 °C results in loss of the η^6-toluene ligand and affords the bis(aldimino)pyridine iron compound, [(^{iPr}PDAI)Fe]$_2$. The dimeric iron compound was characterized by ^{1}H NMR and Mössbauer spectroscopies, X-ray crystallography and SQUID magnetrometry. SQUID magnetometry established two non-interacting high spin ferrous centers each coupled to a triplet dianionic bis(aldimino)pyridine chelate. The two-electron reduction of (^{iPr}PDAI)FeBr$_2$ with two equivalents of sodium amalgam in the presence of 1,3-butadiene furnished (^{iPr}PDAI)Fe(η^4-C$_4$H$_6$), which serves as a pre-catalyst for olefin hydrogenations and [$2\pi + 2\pi$] α,ω-diene cycloaddition reactions. The bis(aldimino)pyridine iron neutral ligand compounds, (^{iPr}PDAI)Fe(DMAP) and (^{iPr}PDAI)Fe(CO)$_2$, were also prepared and characterized by X-ray crystallography and by NMR and Mössbauer spectroscopies, and their electronic structures compared to

* Parts of this chapter have been taken from: Russell, S. K.; Milsmann, C.; Lobkovsky, E.; Weyhermüller; Chirik, P. J. *Inorg. Chem.* **2011**, *50*, 3159. Copyright 2011 American Chemical Society.

the known ketimine-based iron derivatives. Similarly, two bis(aldimino)pyridine iron imide compounds, (^{iPr}PDAI)FeN(2,4,6-Me_3-C_6H_2) and (^{iPr}PDAI)FeN^{1}Ad, were synthesized and their electronic structures and reactivities relative to the bis(imino)pyridine iron derivatives were studied.

4.2 Introduction

Replacing precious metals with more sustainable, abundant and potentially non-toxic iron compounds in homogeneous catalysis is an area of widespread interest and the number of reactions that proceed with high activity and selectivity continues to grow.[1] Much of this recent activity has been inspired by Brookhart and Gibson's independent reports of ethylene and α-olefin polymerization with the methylaluminoxane (MAO) activated aryl-substituted bis(imino)pyridine iron dichlorides (^{R}PDI)$FeCl_2$ (^{R}PDI = 2,6-(*Ar*N=CMe)$_2C_5H_3N$; *Ar* = 2,6-R_2-C_6H_3 (R = ^{i}Pr, Et, Me); 2,4,6-Me_3-C_6H_2, 2-R-C_6H_4 (R = ^{i}Pr, ^{t}Bu), etc.).[2,3] Our research laboratory has reported that the two electron reduction of several of these compounds furnished the corresponding bis(imino)pyridine iron dinitrogen complexes, (^{iPr}PDI)Fe$(N_2)_2$ [4] and [(^{R}PDI)Fe(N_2)]$_2$(μ_2-N_2) (R = Et; R = Me; R = Me, ^{i}Pr) (Figure 4.1).[5] These compounds serve as efficient pre-catalysts for the hydrogenation of olefins[4,5,6] and alkynes[4], the hydrosilylation of olefins,[4] ketones and aldehydes,[7] the [2π + 2π] cycloisomerization of dienes[8] and the hydrogenative cyclization of enynes and diynes.[9]

A notable feature of the bis(imino)pyridine ligand framework is its ability to accept and transfer up to three electrons from the metal center.[10,11] This redox-activity of the bis(imino)pyridine chelate [12,13,14,15] gives rise to unusual electronic structures of aryl-substituted bis(imino)pyridine iron dinitrogen and related neutral ligand

compounds.[16,17] The redox-activity of bis(imino)pyridine ligands has been shown to be general for many transition metals[18,19,20,21,22] as well as main group alkali metals. [23]

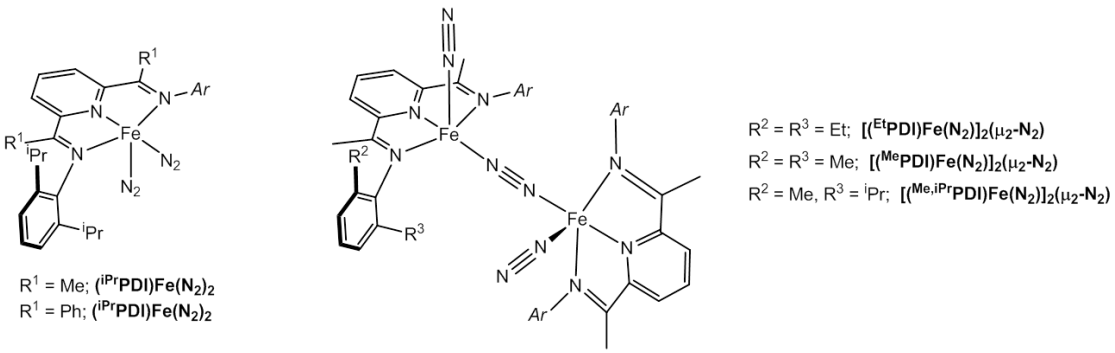

Figure 4.1 Bis(imino)pyridine iron dinitrogen complexes and their shorthand designations.

The presence of ligand centered radicals in the bis(imino)pyridine π-system suggests that modifications in the plane of the chelate may alter the electronic structure and consequently the reactivity of related iron compounds. For this reason, our research laboratory has explored modifications of the bis(imino)pyridine ligand architecture. Previous studies have demonstrated that replacing the imine methyl groups with phenyl rings, *e.g.* (^{iPr}PDI)Fe(N_2)$_2$ versus (^{iPr}BPDI)Fe(N_2)$_2$ (^{iPr}BPDI = 2,6-((2,6-$^{i}Pr_2$-C_6H_3)N=CPh)$_2$$C_5H_3N$) (Figure 4.1), makes the chelate more electron withdrawing, resulting in a more electrophilic iron center.[5,24,] The phenylated iron bis(dinitrogen) compound is a more active 1-hexene hydrogenation catalyst than (^{iPr}PDI)Fe(N_2)$_2$, but the increased reactivity also results in shorter catalyst lifetimes because of irreversible intramolecular arene coordination.

Bis(aldimino)pyridine iron dichloride compounds have previously been studied alongside their analogous bis(imino)pyridine iron dichloride compounds for ethylene polymerization by several groups.[3b,25,26] In all cases, lower activities and molecular weights of polymer are observed for bis(aldimino)pryidine iron dichlorides. Gibson

and coworkers have reported that the ketimine-based iron precatalysts produced productivities between 5340 and 20600 g/mmol•h•bar while the related aldimine-based iron catalysts had lower productivities between 305 and 560 g/mmol•h•bar.[3b] The difference in activities between closely related compounds such as (^{iPr}PDI)$FeCl_2$ and (^{iPr}PDAI)$FeCl_2$ suggests that a subtle change in the tridentate ligand framework can create a substantial change in the steric protection or electronic structure, or both, of the iron compound.

4.3 Reduction chemistry of (^{iPr}PDAI)$FeBr_2$.

Stirring a toluene slurry of (^{iPr}PDAI)$FeBr_2$ with 2 equivalents of 0.5 % sodium amalgam under a dinitrogen atmosphere followed by filtration and removal of the solvent furnished a brown solid identified as the bis(aldimino)pyridine iron η^6-toluene compound, (^{iPr}PDAI)Fe(η^6-C_7H_8) (Figure 4.2). The ^{1}H NMR spectrum of (^{iPr}PDAI)Fe(η^6-C_7H_8) in cyclohexane-d_{12} exhibits the number of peaks consistent with a C_s symmetric molecule indicating that the iron center is coordinated by a κ^2-bis(aldimino)pyridine chelate. The C_s symmetry is revealed by the presence of four isopropyl methyl doublets, two isopropyl methine septets and two imine proton singlets. The resonances for the aromatic protons of the coordinated toluene molecule are shifted considerably upfield to 5.92, 4.87 and 4.80 ppm for the *para*-, *ortho*- and *meta*- positions, respectively.

Berry and coworkers have reported a related structure in bis(imino)pyridine ruthenium chemistry using the 2,6-dimethyl aryl (^{Me}PDI = 2,6-((2,6-Me_2-C_6H_3)N=CMe)$_2C_5H_3N$) variant of the ligand.[27] They showed that treatment of (^{Me}PDI)$RuCl_2$(η^2-C_2H_4) with triethylsilane in either toluene or benzene leads to the formation of the corresponding κ^2-bis(imino)pyridine ruthenium η^6-arene compounds, (^{Me}PDI)Ru(η^6-C_6H_6) and (^{Me}PDI)Ru(η^6-C_7H_8). The η^6-toluene ligand of

(^{Me}PDI)Ru(η^6-C_7H_8) is labile and when the compound is stirred in hexane under a dinitrogen atmosphere at room temperature for several days, the toluene ligand is displaced by N_2, forming the bridged bis(imino)pyridine ruthenium dinitrogen compound, [(^{Me}PDI)Ru]$_2$(μ_2-N_2).

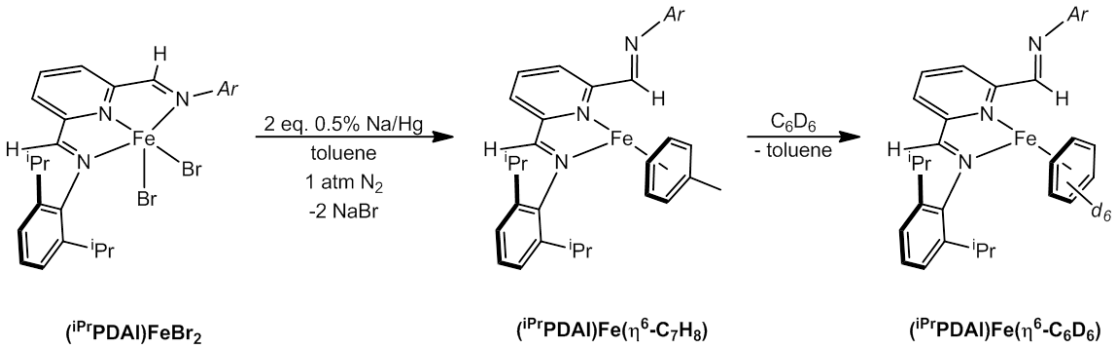

Figure 4.2 Synthesis of (^{iPr}PDAI)Fe(η^6-C_7H_8) and (^{iPr}PDAI)Fe(η^6-C_6D_6).

Our laboratory has also reported η^6-arene coordination in related bis(imino)pyridine iron chemistry.[5,24] Allowing (^{iPr}BPDI)Fe(N_2)$_2$ and [(^{Me}BPDI)Fe(N_2)]$_2$(μ_2-N_2) to stand for hours in solution resulted in formation of two intramolecular η^6-arene compounds, (^{R}BPDI)Fe(η^6-aryl) and (^{R}BPDI)Fe(η^6-phenyl) (Figure 4.3). Unlike the ruthenium example, both (^{R}BPDI)Fe(η^6-aryl) and (^{R}BPDI)Fe(η^6-phenyl) are thermally stable compounds and do not undergo loss of the η^6-arene ligands even at high temperatures. In all the iron and ruthenium examples, the κ^2-coordination mode serves to maintain an 18 electron count at the metal center as well as provides steric relief for the molecule. Also in both cases, the bond length distortions in the bis(imino)pyridine chelate are consistent with two-electron reduction suggesting that the metal centers are best described as iron(II) and ruthenium(II).

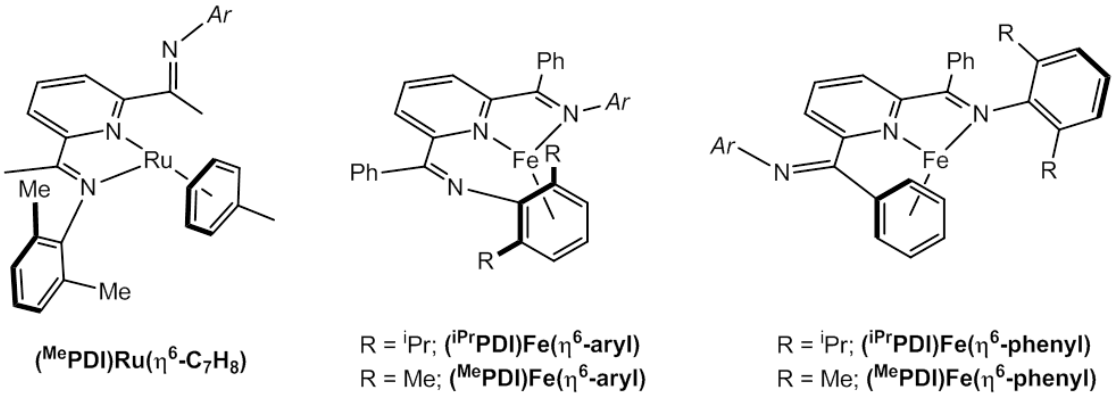

(^{Me}PDI)Ru(η^6-C_7H_8)

R = ^{i}Pr; (^{iPr}PDI)Fe(η^6-aryl)
R = Me; (^{Me}PDI)Fe(η^6-aryl)

R = ^{i}Pr; (^{iPr}PDI)Fe(η^6-phenyl)
R = Me; (^{Me}PDI)Fe(η^6-phenyl)

Figure 4.3 Examples of η^6-arene bis(imino)pyridine compounds.

The bis(aldimino)pyridine iron η^6-toluene compound acts more like the related bis(imino)pyridine ruthenium η^6-toluene compound than the intramolecular η^6-arene iron examples. Like (^{Me}PDI)Ru(η^6-C_7H_8), placing (^{iPr}PDAI)Fe(η^6-C_7H_8) in a benzene-d_6 solution resulted in the η^6-toluene compound quickly and quantitatively converting to the corresponding η^6-benzene compound, (^{iPr}PDAI)Fe(η^6-C_6D_6) with release of one equivalent of toluene (Figure 4.2). As expected, the benzene-d_6 ^{1}H NMR spectrum of (^{iPr}PDAI)Fe(η^6-C_6D_6) exhibits the number of peaks consistent with a C_s symmetric molecule and a κ^2-bis(aldimino)pyridine chelate. The lability of the toluene ligand in (^{iPr}PDAI)Fe(η^6-C_7H_8) was also probed in a nonaromatic solvent. Addition of one equivalent of C_6H_6 to a cyclohexane-d_{12} solution of (^{iPr}PDAI)Fe(η^6-C_7H_8) resulted in displacement of toluene and quantitative formation of (^{iPr}PDAI)Fe(η^6-C_6H_6). The bis(aldimino)pyridine iron η^6-benzene compound could also be prepared by stirring a benzene slurry of (^{iPr}PDAI)$FeBr_2$ with two equivalents of 0.5 % sodium amalgam.

Recrystallization of either (^{iPr}PDAI)Fe(η^6-C_7H_8) or (^{iPr}PDAI)Fe(η^6-C_6H_6) from a diethyl ether or a toluene/pentane mixture at -35 °C furnished brown crystals identified as the dimeric iron bis(aldimino)pyridine compound, [(^{iPr}PDAI)Fe]$_2$ in

moderate yields. The dimer was also synthesized by reduction of (^{iPr}PDAI)FeBr$_2$ with 2 equivalents of sodium and 0.05 equivalents of naphthalene in THF followed by recrystallization from diethyl ether (Figure 4.4).

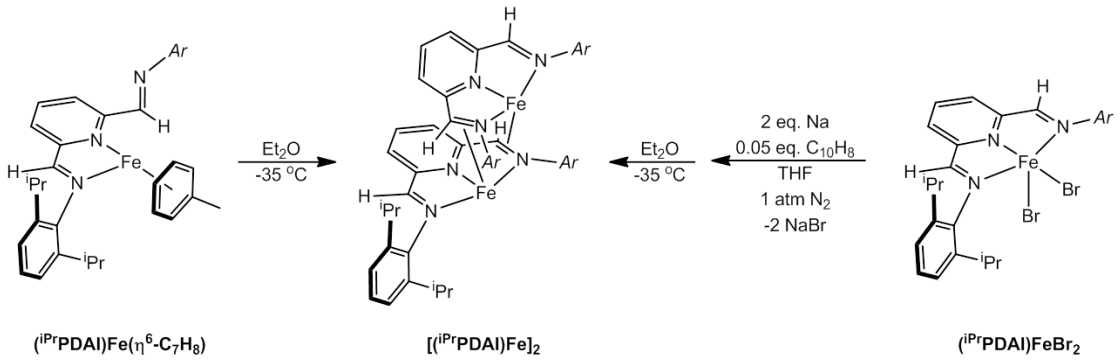

Figure 4.4 Syntheses of [(^{iPr}PDAI)Fe]$_2$.

The identity of [(^{iPr}PDAI)Fe]$_2$ was established by X-ray diffraction and a representation of the solid state structure is presented in Figure 4.5. For chelate bond distance comparison, the crystal structure of the free bis(aldimino)pyridine ligand, ^{iPr}PDAI, was also determined. Selected bond distances for both structures are presented in Table 4.1. The crystallographic data for [(^{iPr}PDAI)Fe]$_2$ established a bimetallic diiron compound with a metal-metal distance of 2.8047(5) Å. A C_2 axis of symmetry passes through the midpoint of the two iron atoms and relates each monomeric subunit of the dimer. Each iron atom is five coordinate, ligated by a κ^3-bis(aldimino)pyridine chelate and a η^2-imine arm from the second bis(aldimino)pyridine iron subunit. The π-interaction with the imine ligand results in deviation of the iron center from the κ^3-chelate plane by about 20°.

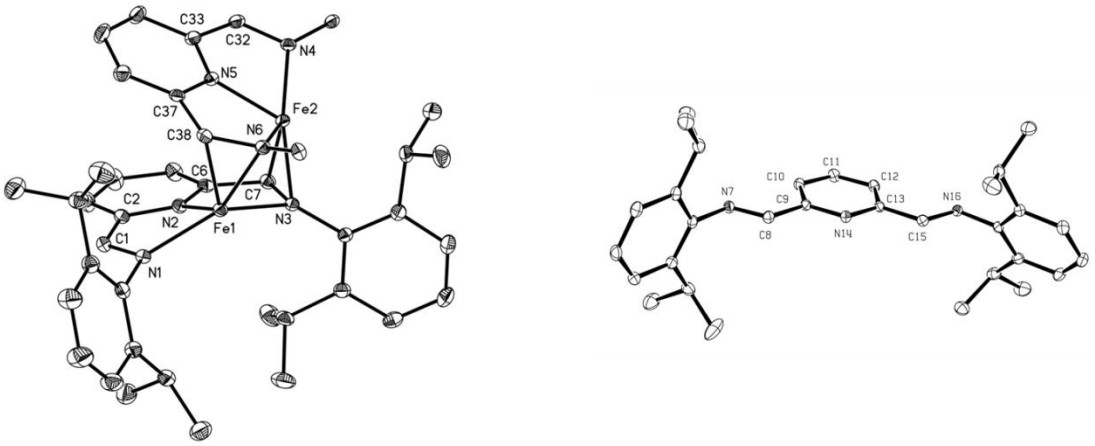

Figure 4.5 Left: Solid state structure of $[(^{iPr}PDAI)Fe]_2$ at 30 % probability ellipsoids. Hydrogen atoms and two aryl groups omitted for clarity. Right: Solid state structure of $^{iPr}PDAI$ at 30 % probability ellipsoids. Hydrogen atoms omitted for clarity.

As is well established with bis(imino)pyridine compounds[16,28] and in the chemistry of other redox-active ligands,[29,30,31,32] distortions in bond distances of the chelate signal non-innocence and participation of the bis(imino)pyridine in the electronic structure of the compound. Because of the unusual coordination mode of the chelating ligands in the dimeric iron structure, bond distortions of bis(α-iminopyridine) metal compounds[30] as well as those for bis(imino)pyridine iron compounds[16,28] were considered when assigning the oxidation state of the bis(aldimino)pyridine in $[(^{iPr}PDAI)Fe]_2$. The C_{imine}-N_{imine} and C_{imine}-$C_{pyridine}$ bond distances of each the ligand half that is not coordinated to the second iron center are consistent with one electron reduction. The imines that are not involved in the π-interaction with the second metal, N(1)-C(1) and N(4)-C(32), are elongated from the free ligand to 1.326(3) and 1.322(3) Å, respectively. The corresponding C_{imine}-C_{ipso} distances, C(1)-C(2) and C(32)-C(33), are contracted to 1.410(3) and 1.412(3) Å, respectively. The η^2-coordinated imine arms show even greater bond elongation with N(3)-C(7) and N(6)-C(38) both having a bond distance of 1.392(3) Å, consistent with

a one electron reduction of the imine arm due to backbonding from the iron center. The bond distances of each bis(aldimino)pyridine ligand are consistent with overall two electron reduction of the chelate.[16,28,30]

Table 4.1 Selected bond distances (Å) for [(^{iPr}PDAI)Fe]$_2$ and ^{iPr}PDAI.

	[(^{iPr}PDAI)Fe]$_2$	**^{iPr}PDAI**[a]
Fe(1)-N(1)	2.127(2)	
Fe(1)-N(2)	1.967(2)	
Fe(1)-N(3)	2.272(2)	
Fe(1)-N(6)	1.984(2)	
Fe(1)-C(38)	2.085(2)	
Fe(2)-N(4)	2.1489(19)	
Fe(2)-N(5)	1.967(2)	
Fe(2)-N(6)	2.2640(19)	
Fe(2)-N(3)	1.9827(19)	
Fe(2)-C(7)	2.076(2)	
N(1)-C(1)	1.326(3)	1.265(2)
N(3)-C(7)	1.392(3)	1.265(2)
N(4)-C(32)	1.322(3)	
N(6)-C(38)	1.392(3)	
C(1)-C(2)	1.410(3)	1.475(2)
C(6)-C(7)	1.454(4)	1.476(2)
C(32)-C(33)	1.412(3)	
C(37)-C(38)	1.447(3)	
Fe(1)-Fe(2) distance	2.8047(5)	

[a] ^{iPr}PDAI distances placed with corresponding bonds in [(^{iPr}PDAI)Fe]$_2$, not by atom labels.

Analysis of $[(^{iPr}PDAI)Fe]_2$ by ^1H NMR spectroscopy confirms that the dimeric structure is preserved in a benzene-d_6 solution. The spectrum exhibits 21 of the expected 23 peaks distributed over a 280 ppm range consistent with a C_2 symmetric dimer. The large number of peaks is due to the complete asymmetry of each monomeric bis(aldimino)pyridine iron subunit. If the dimer dissociated in solution the expected product would be the η^6-benzene compound; however, no evidence for $(^{iPr}PDAI)Fe(\eta^6\text{-}C_6D_6)$ was observed in solution at 23 °C after 24 hours.

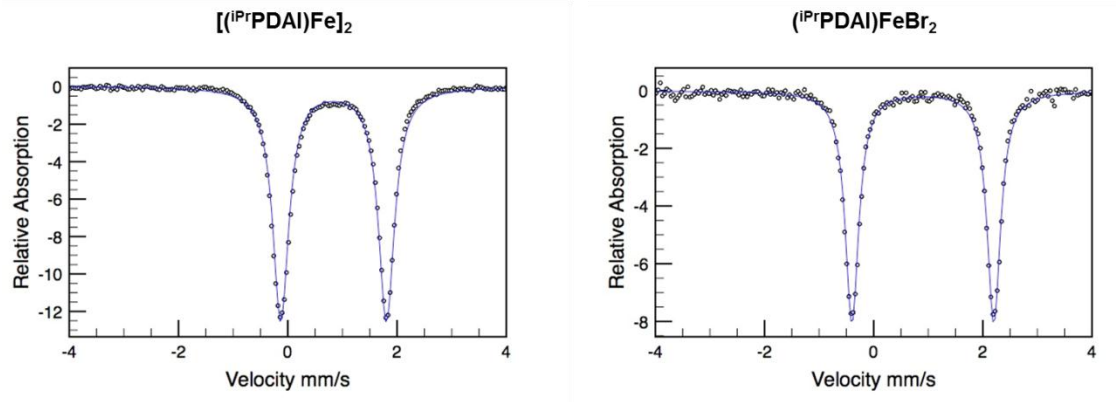

Figure 4.6 Zero-field ^{57}Fe Mössbauer spectra of $[(^{iPr}PDAI)Fe]_2$ (δ = 0.84 mm/s, ΔE_Q = │1.93│ mm/s) and $(^{iPr}PDAI)FeBr_2$ (δ = 0.90 mm/s, ΔE_Q = │2.60│ mm/s) collected at 80 K.

The electronic structure of $[(^{iPr}PDAI)Fe]_2$ was studied by zero-field Mössbauer spectroscopy at 80 K. A representative spectrum is presented in Figure 4.6. Fitting the experimental data yielded an isomer shift (δ) of 0.84 mm/s and a quadrupole splitting (ΔE_Q) of │1.93│ mm/s. The presences of only one relatively sharp quadrupole doublet indicates that the iron centers of the dimer are equivalent. The zero field Mössbauer spectrum of $(^{iPr}PDAI)FeBr_2$ was also collected as an example of a bis(aldimino)pyridine high spin iron(II) compound for comparsion. The isomer shift (δ) of 0.90 mm/s for $(^{iPr}PDAI)FeBr_2$ is similar to the value measured for the dimer, providing further evidence that $[(^{iPr}PDAI)Fe]_2$ contains high spin iron(II) centers.

As indicated by the large peak dispersion of chemical shifts in the benzene-d_6 ^{1}H NMR spectrum, [(^{iPr}PDAI)Fe]$_2$ is a paramagnetic compound. A solution (benzene-d_6, Evans method, 20 °C) magnetic moment of 4.7 μ_B was measured for the overall molecule while a slightly lower value of 4.2 μ_B was measured in the solid state by magnetic susceptibility balance at 23 °C. The unusual structural motif observed in the solid state structure of [(^{iPr}PDAI)Fe]$_2$ prompted a more detailed investigation of the magnetochemistry to determine the degree of electronic communication between the two iron centers bearing redox-active ligands.

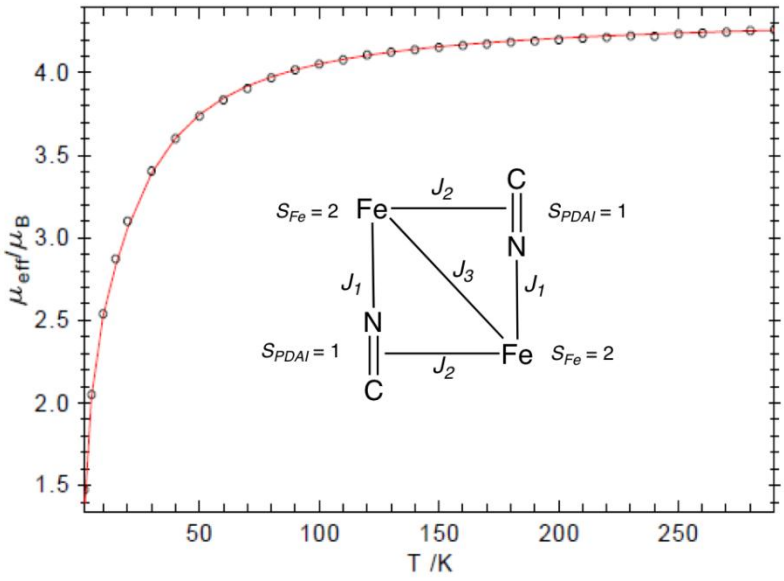

Figure 4.7 Variable temperature SQUID magnetic data for [(^{iPr}PDAI)Fe]$_2$.

The solid state magnetic behavior of [(^{iPr}PDAI)Fe]$_2$ was studied by SQUID magnetometry and the temperature dependence of the effective magnetic moment, μ_{eff}, is shown in Figure 4.7. From 100 - 300 K, μ_{eff} is almost temperature independent and reaches a value of 4.3 μ_B at 300 K, consistent with the magnetic moment of 4.2 μ_B measured at 296 K by magnetic susceptibility balance. Below 100 K, μ_{eff} decreases monotonically from 4.1 μ_B at 100 K to 1.5 μ_B at 2 K. The room temperature value of

μ_{eff} is very close to the spin-only value of 4.0 μ_B for two weakly interacting spins of S = 1. Based on this information, the data were initially modeled[33] with each [(^{iPr}PDAI)Fe] subunit as a separate S = 1 system. While this model readily reproduced the high-temperature region of the data using electronic g values of g = 2.15, all attempts to fit the temperature dependence in the low-temperature region produced simulation parameters that were physically meaningless.

The best fit resulted in a very small isotropic coupling constant, J, of -1.315 cm^{-1}, which is likely too small for a doubly bridged molecule, and the obtained zero field splitting parameter, $|D|$ = 104 cm^{-1}, is much larger than reported values for other high spin Fe(II) compounds.[34,35,36,37] To date, the largest axial zero-field splitting for a high-spin iron(II) complex, $|D|$ = 50 cm^{-1}, was reported by Münck, Holland and coworkers for a three-coordinate β-diketiminate iron methyl complex.[37] Chang, Long and coworkers have reported similar values for a family of trigonal pyramidal iron(II) complexes.[36] The large axial zero-field splitting parameters in these compounds can be explained by the particular symmetry of the complexes, which leads to an almost orbitally degernerate ground state with unquenched orbital angular momentum. In contrast, the symmetry about the iron centers in [(^{iPr}PDAI)Fe]$_2$ is significantly lower. The unusual simulation parameters with respect to the symmetry of [(^{iPr}PDAI)Fe]$_2$ led to investigations of a more complicated spin system for the molecule.

The Mössbauer data and metrical parameters of the solid state structure of [(^{iPr}PDAI)Fe]$_2$ establish two equivalent high spin Fe(II) centers and two [^{iPr}PDAI]$^{2-}$ chelates, respectively. It has been well established[16] that bis(imino)pyridine ligands in their doubly reduced dianionic form possess nearly degenerate singlet (S = 0) and triplet states (S = 1), which have both been identified in coordination compounds.[16,20] Therefore, each high spin Fe(II) center (S_{Fe} = 2) and each [^{iPr}PDAI]$^{2-}$ ligand (S_{PDAI} = 1)

were treated as separate entities, yielding a total of 4 spin centers. The coupling scheme for such a four-spin system in the given geometry and symmetry is presented in the inset in Figure 4.7. Although all coupling pathways are, in principle, antiferromagnetic in nature, metal-ligand (J_1 and J_2) and metal-metal (J_3) coupling represent competing pathways for the alignment of the spins on the iron centers. Because of the symmetry of the system, the number of independent parameters was significantly reduced by assuming equivalent *g* and *D* values for the two iron centers. To further limit the number of fit parameters, g-anisotropy and zero-field splitting were neglected for the ligands ($g_{PDAI} = 2.00$; $D_{PDAI} = 0$ cm^{-1}), which is in good agreement with the small deviations from the *g* value of the free electron and the small zero-field splitting parameters typically observed in organic triplet diradicals. [38,39] The best fit obtained by this model agreed well with the experimental data over the whole temperature range and produced simulation parameters of $|D_{Fe}| = 10$ cm^{-1}, $g_{Fe} = 2.11$, $J_1 = -1000$ cm^{-1}, $J_2 = -147$ cm^{-1}, $J_3 = -103$ cm^{-1}.

To further substantiate this model, multiple-field variable-temperature measurements were performed at 1, 4 and 7 Tesla. The obtained isofield magnetization curves were successfully modeled using the above-mentioned parameters (Figure 4.8). However, this solution is not unique and other satisfactory fits to the data were also obtained with different sets of simulation parameters. An analysis of the error surface upon variation of J_2 vs J_3 (all other parameters constant) revealed that even under these strongly constrained conditions, no unique solution can be identified because multiple minima of similar goodness of fit can be found (Figure 4.9). Somewhat surprisingly, the values for J_2 and J_3 are also strongly dependent on the magnitude of J_1 (an increase in J_1 leads to an increase in J_2 and J_3) despite the strength of the antiferromagnetic interaction between the iron and the tridentate ligand in each half of the dimer which precludes an experimental determination of J_1 by

magnetic susceptibility measurements in the accessible temperature range. Although this increases the error of the other variables, the qualitative model remains intact.

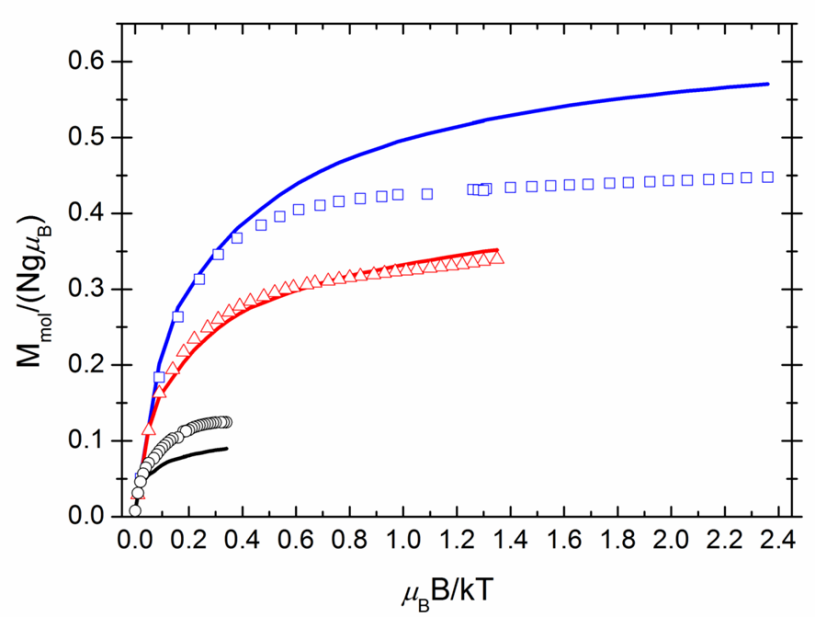

Figure 4.8 Multiple-field variable-temperature measurement of magnetization for $[(^{iPr}PDAI)Fe]_2$. The solid lines represent spin Hamiltonian simulations obtained with $|D_{Fe}|$ = 10.0 cm^{-1}, g_{Fe} = 2.11, J_1 = -1000 cm^{-1}, J_2 = -147 cm^{-1}, J_3 = -103 cm^{-1}.

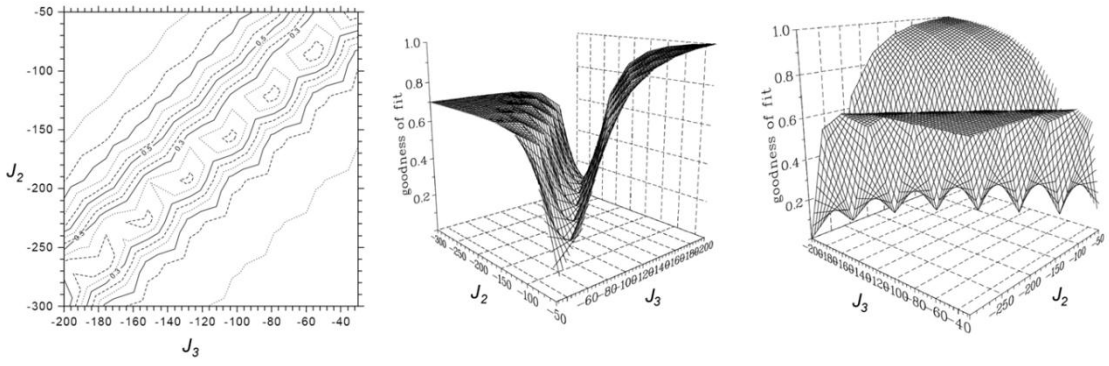

Figure 4.9 Error surface plots for spin Hamiltonian simulations upon variation of J_2 vs. J_3. All other simulation parameters were kept constant ($|D_{Fe}|$ = 10.0 cm^{-1}, g_{Fe} = 2.11, J_1 = -1000 cm^{-1}).

Very strong antiferromagnetic coupling between each of the high-spin Fe(II) ions with its chelating $[^{iPr}PDAI]^{2-}$ ligand, in agreement with previous results for the ketimine-substituted analogues,[16,20] results in two essentially uncoupled $S = 1$ monomeric subunits at high temperatures (100 - 300 K). At lower temperatures, weaker antiferromagnetic coupling between the two subunits gives rise to lower magnetic moments and accounts for the temperature dependence of μ_{eff}. In contrast to J_1 and J_2, which describe the direct magnetic interactions between paramagnetic metal ($S = 2$) and ligand ($S = 1$) fragments, the metal-metal interaction, J_3, is mediated via a superexchange pathway. Nevertheless, J_3 is essential within the proposed four-spin coupling model. All simulations, employing only the direct interactions J_1 and J_2 resulted in slightly lower fit quality and required large axial zero-field splitting parameters (> 50 cm-1) for the iron centers in addition to ferromagnetic coupling constants J_2. Because of the competing coupling pathways J_2 and J_3, the effective coupling between the two halves of the dimer is weak, and the compound is paramagnetic over the whole temperature range, despite the sizable antiferromagnetic coupling constants (> 100 cm^{-1}). In combination with the failure of the simple two spin model to reproduce the low-temperature region of the data within reasonable parameters, this model provides strong experimental evidence for the presence of a diradical bis(imino)pyridine ligand coordinated in its triplet state.

4.4 Electronic Structure Comparison to Bis(imino)pyridine Iron Complexes

To directly compare the electronic structures and ultimately the catalytic activities of reduced bis(aldimino)pyridine iron compounds with their more studied bis(imino)pyridine iron counterparts, several compounds with the same metal-ligand combinations were synthesized. Bis(imino)pyridine iron butadiene compounds are relatively straightforward to prepare and have been shown to be competent pre-

catalysts for olefin hydrogenation. Additionally, the solid state structure of (^{iPr}PDI)Fe(η^4-C_4H_6) established an unusual *trans* geometry of the butadiene ligand bound to the metal.[8] For these reasons, the bis(aldimino)pyridine iron butadiene compound was identified as a target compound. Stirring a pentane slurry of (^{iPr}PDAI)$FeBr_2$ with excess 0.5 % sodium amalgam and 1,3-butadiene (10 equivalents) followed by filtration and recrystallization from diethyl ether at -35 °C furnished (^{iPr}PDAI)Fe(η^4-C_4H_6) as a brown solid in 70 % yield (Figure 4.10).

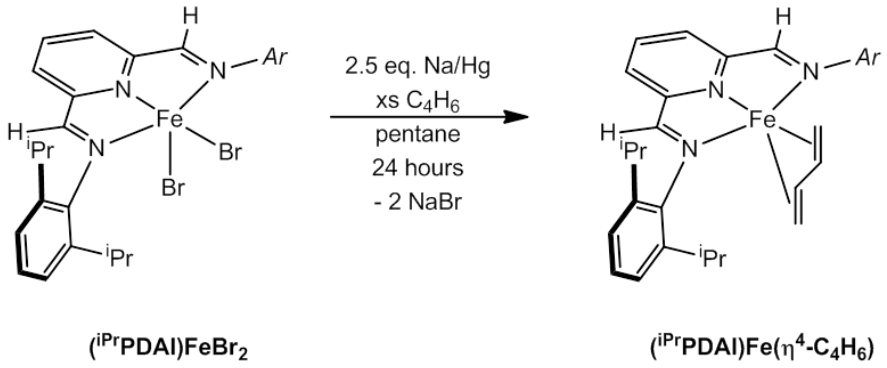

Figure 4.10 Synthesis of (^{iPr}PDAI)Fe(η^4-C_4H_6).

The benzene-d_6 ^{1}H NMR spectrum of (^{iPr}PDAI)Fe(η^4-C_4H_6) at 20 °C displays the number of peaks consistent with a C_2 symmetric molecule. Assignment of the peaks was possible; however, all of the resonances are broad suggesting a dynamic process on the time scale of the spectroscopic experiment. To investigate this dynamic processes further, ^{1}H NMR spectra were collected over a range of temperatures from -80 to 80 °C. Cooling a toluene-d_8 solution of (^{iPr}PDAI)Fe(η^4-C_4H_6) to temperatures below -20 °C resulted in a sharpening of the bis(aldimino)pyridine resonances, but those of the butadiene ligand remained slightly broadened (Figure 4.11). Warming the sample above 40 °C produced the number of bis(aldimino)pyridine resonances consistent with a C_{2v} symmetric molecule and only

two observable butadiene peaks. These observations suggest that the dynamic process involves dissociation and recoordination of the butadiene ligand.

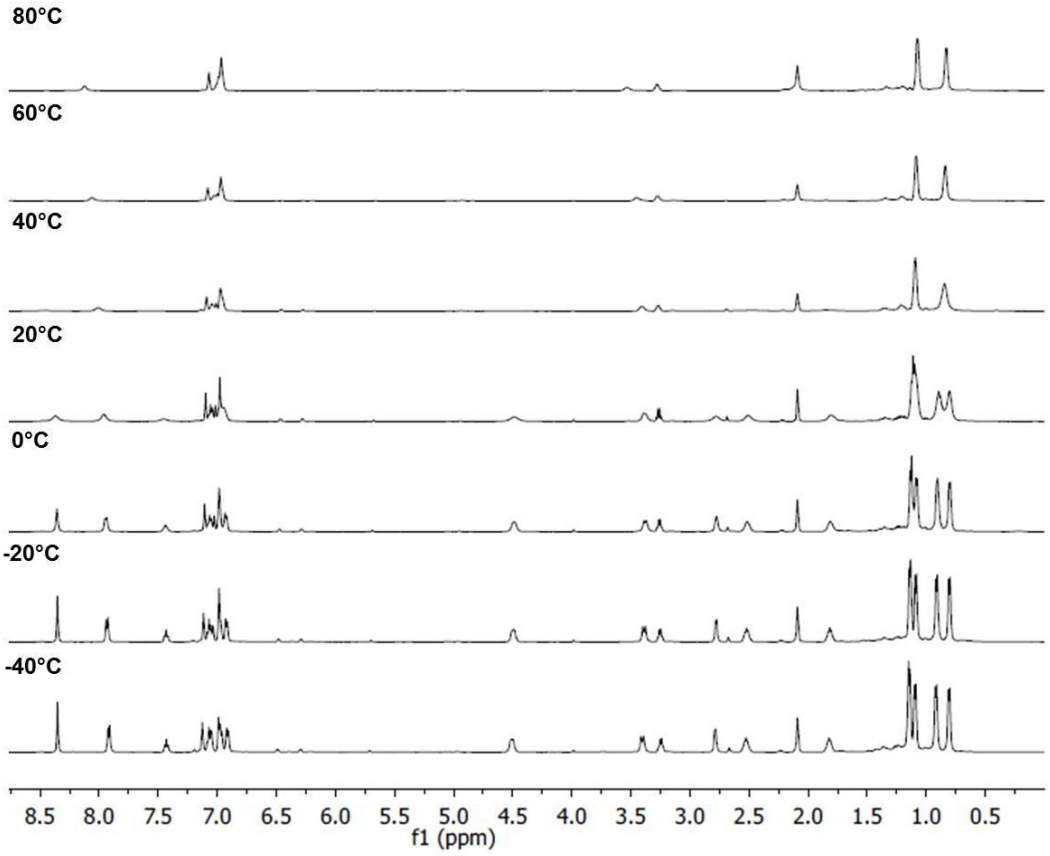

Figure 4.11 Variable temperature ^{1}H NMR spectroscopy of (^{iPr}PDAI)Fe(η^4-C_4H_6) collected in toluene-d_8.

The dynamic behavior of the butadiene ligand in (^{iPr}PDAI)Fe(η^4-C_4H_6) prompted similar variable temperature studies on the previously reported ketimine analog, (^{iPr}PDI)Fe(η^4-C_4H_6) (Figure 4.12). The toluene-d_8 solution ^{1}H NMR spectrum of (^{iPr}PDI)Fe(η^4-C_4H_6) at 20 °C exhibits the number of peaks consistent with C_2 symmetry but, unlike (^{iPr}PDAI)Fe(η^4-C_4H_6), all of the bis(imino)pyridine resonances are sharp. Warming the sample of (^{iPr}PDI)Fe(η^4-C_4H_6) to 40 °C resulted in broadening of all resonances to produce a spectrum similar to the one observed for

(^{iPr}PDAI)Fe(η^4-C_4H_6) at 20 °C. These results indicate a higher barrier for dissociation and recoordination of the butadiene ligand in the ketimine substituted compound compared to the aldimine analog.

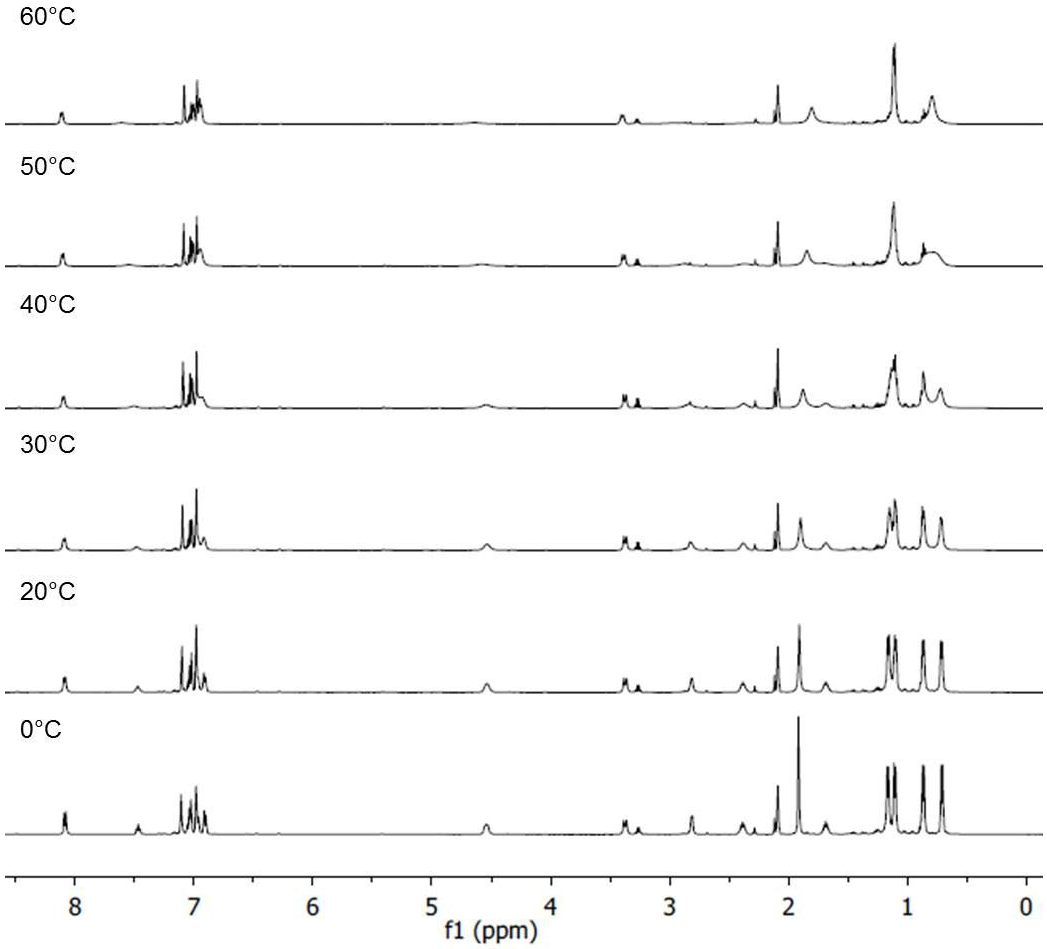

Figure 4.12 Variable ^{1}H NMR spectroscopy on (^{iPr}PDI)Fe(η^4-C_4H_6) collected in toluene-d_8.

Single crystals of (^{iPr}PDAI)Fe(η^4-C_4H_6) suitable for X-ray diffraction were grown from a concentrated hexane solution at -35 °C. A representation of the solid state molecular structure is presented in Figure 4.13 and selected bond distances are reported in Table 4.2 along with corresponding distances from (^{iPr}PDI)Fe(η^4-C_4H_6). Like the ketimine analog, the butadiene ligand in (^{iPr}PDAI)Fe(η^4-C_4H_6) also

coordinates in a relatively unusual *trans* geometry.[8,40] The bond distances of the bis(aldimino)pyridine chelate are consistent with two electron reduction and are overall similar to those of (^{iPr}PDI)Fe(η^4-C_4H_6). The N_{imine}-C_{imine} bond distances of 1.329(3) and 1.333(3) Å are slightly longer than in (^{iPr}PDI)Fe(η^4-C_4H_6) while the C_{imine}-C_{ipso} bond distances of 1.410(3) and 1.402(3) Å are slightly shorter than the ketimine compound. The doubly reduced chelate and short Fe-N bond distances suggest an intermediate spin ferrous center. The butadiene ligand of (^{iPr}PDAI)Fe(η^4-C_4H_6) is less symmetrically bound to the iron center with one shorter and one longer Fe-C_{CH2} bond in comparison to (^{iPr}PDI)Fe(η^4-C_4H_6) which has two very similar Fe-C_{CH2} bond distances. The difference in steric environment about the iron center can be seen by comparing the Fe-N_{imine}-C_{Ar} angles of (^{iPr}PDAI)Fe(η^4-C_4H_6) versus (^{iPr}PDI)Fe(η^4-C_4H_6). The angles of the aldimine-supported iron compound are 129.74(14) ° and 130.76(13) ° which are significantly larger than the corresponding angles of 127.78(6) ° and 126.35(6) ° in the ketimine-supported iron compound.

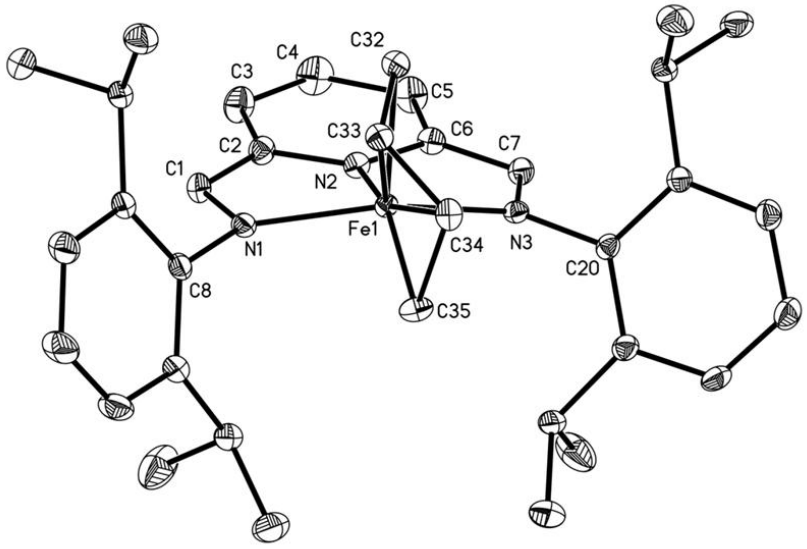

Figure 4.13 Solid state structure of (^{iPr}PDAI)Fe(η^4-C_4H_6) at 30 % probability ellipsoids. Hydrogen atoms omitted for clarity.

Table 4.2 Selected bond distances (Å) and angles (°) for (^{iPr}PDAI)Fe(η^4-C_4H_6) and (^{iPr}PDI)Fe(η^4-C_4H_6).[8]

	(^{iPr}PDAI)Fe(η^4-C_4H_6)	**(^{iPr}PDI)Fe(η^4-C_4H_6)**
Fe-$N_{pyridine}$	1.8523(17)	1.8411(7)
Fe-N_{imine}	1.9657(17), 1.9728(18)	2.0049(7), 1.9656(7)
Fe-C_{CH2}	2.129(18), 2.240(14)	2.1785(9), 2.196(1)
Fe-C_{CH}	2.041(3), 2.055(3)	2.0496(9), 2.0565(8)
N_{imine}-C_{imine}	1.329(3), 1.333(3)	1.3324(11), 1.3718(11)
C_{imine}-C_{ipso}	1.410(3), 1.402(3)	1.4219(12), 1.4136(12)
C_{ipso}-$N_{pyridine}$	1.366(3), 1.377(3)	1.3718(11), 1.3768(11)
C_{CH2}-C_{CH}	1.388(11), 1.385(9)	1.388(2), 1.392(1)
C_{CH}-C_{CH}	1.425(6)	1.429(1)
Fe-N_{imine}-C_{Ar}	129.74(14), 130.76(13)	127.78(6), 126.35(6)

The relative electronic structures of (^{iPr}PDAI)Fe(η^4-C_4H_6) and (^{iPr}PDI)Fe(η^4-C_4H_6) were also studied by zero-field ^{57}Fe Mössbauer spectroscopy. Representative spectra are reported in Figure 4.14. An isomer shift (δ) of 0.37 mm/s and a quadrupole splitting (ΔE_Q) of $\left|0.73\right|$ mm/s were measured for (^{iPr}PDAI)Fe(η^4-C_4H_6). The ketimine compound, (^{iPr}PDI)Fe(η^4-C_4H_6), has an almost identical isomer shift (δ) of 0.38 mm/s, but a slightly different quadrupole splitting ($\Delta E_Q = \left|0.38\right|$ mm/s). The isomer shifts of both compounds are consistent with an intermediate spin iron(II) center.[16,17] The quadrupole splitting reflects the electric field gradient and symmetry of the molecule. Taking into account the slight differences in the crystal structures, (^{iPr}PDAI)Fe(η^4-C_4H_6) and (^{iPr}PDI)Fe(η^4-C_4H_6) may be expected to have different quadrupole splittings; however, the crystal structure data and Mössbauer parameters

for each compound are consistent with an intermediate spin ferrous center antiferromagnetically coupled to a doubly reduced chelate.[16,17]

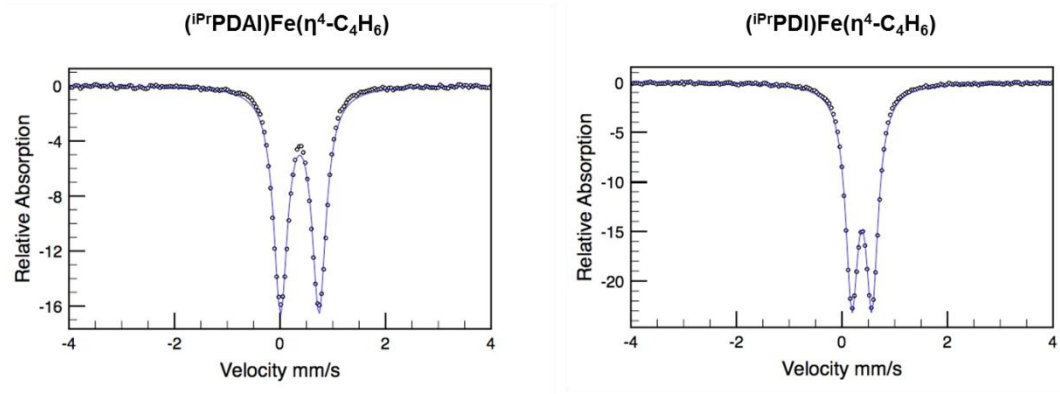

Figure 4.14 Zero-field ^{57}Fe Mössbauer spectra of (^{iPr}PDAI)Fe(η^4-C_4H_6) (left, δ = 0.37 mm/s, ΔE_Q = │0.73│ mm/s) and (^{iPr}PDI)Fe(η^4-C_4H_6) (right, (δ = 0.38 mm/s, ΔE_Q = │0.38│ mm/s) collected at 80K.

One of the most well-studied bis(imino)pyridine iron compounds is the N,N-dimethyl-4-aminopyridine compound, (^{iPr}PDI)Fe(DMAP).[16] For this reason, the bis(aldimino)pyridine analog was targeted as a compound to further explore any possible electronic structure differences between bis(imino)pyridine iron and bis(aldimino)pyridine iron compounds. The synthesis of (^{iPr}PDAI)Fe(DMAP) was accomplished by addition of one equivalent of N,N-4-dimethylaminopyridine to (^{iPr}PDAI)Fe(η^4-C_4H_6) in diethyl ether (Figure 4.15). After removal of the solvent, (^{iPr}PDAI)Fe(DMAP) was isolated as a brown powder in 95% yield.

The benzene-d_6 ^{1}H NMR spectrum of diamagnetic (^{iPr}PDI)Fe(DMAP) exhibits unusual shifts of the in-plane chelate resonances that signal contribution from temperature independent paramagnetism arising from mixing of singlet and triplet states via spin orbit coupling. The peak for the imine methyl group is shifted upfield to -5.85 ppm and the *meta*- and *para*- pyridine hydrogen peaks are shifted downfield to 12.42 and 9.04 ppm, respectively.[16] The benzene-d_6 ^{1}H NMR spectrum of

(^{iPr}PDAI)Fe(DMAP) exhibits the number of peaks consistent with an idealized C_2 symmetric molecule as well as contributions from temperature independent paramagnetism. Like the ketimine derivative, the in-plane hydrogens of the chelate are shifted from the diamagnetic reference values of the free ligand. For reference, the corresponding value for the aldimine hydrogen in ^{iPr}PDAI is 8.54 ppm, and the *meta*- and *para*- pyridine resonances appear at 8.30 and 7.19 ppm, respectively. The aldimine hydrogen and *meta*- and *para*- pyridine hydrogen resonances are each shifted downfield to 17.16, 12.66 and 8.50 ppm, respectively. Variable temperature ^{1}H NMR spectroscopy on (^{iPr}PDAI)Fe(DMAP) in toluene-d_8 showed little change in the chemical shifts of the bis(aldimino)pyridine chelate. For example, the aldimine hydrogen peak moves approximately 4 ppm over a 120 °C range, shifting from 18.95 ppm at -40 °C to 14.68 ppm at 80 ° C.

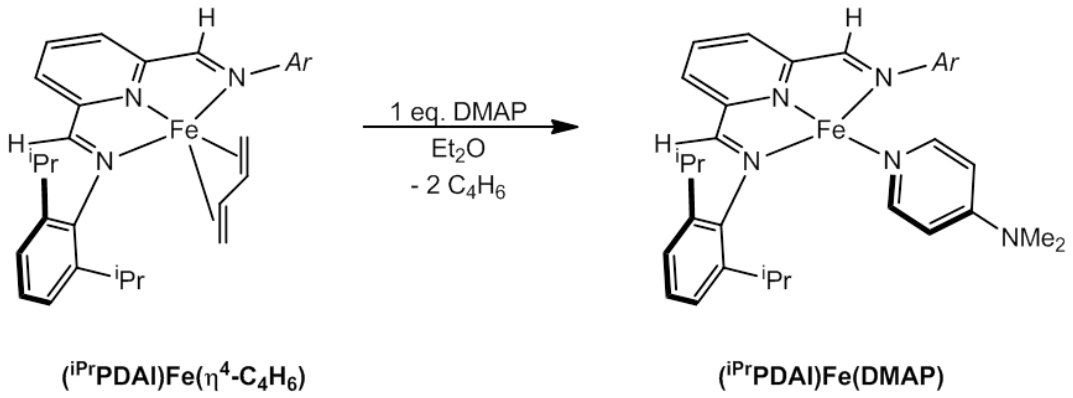

Figure 4.15 Synthesis of (^{iPr}PDAI)Fe(DMAP).

Single crystals of (^{iPr}PDAI)Fe(DMAP) suitable for X-ray diffraction were grown from a diethyl ether solution at -35 °C. Two molecules are present in the asymmetric unit and differ by the direction of rotation of the DMAP ligand relative to the iron-chelate plane. A representation of the solid state structure is shown in Figure 4.16. Selected bond distances and angles for both molecules of the asymmetric unit

along with the corresponding values from (^{iPr}PDI)Fe(DMAP) for comparison are reported in Table 4.3. The overall geometry of both molecules of (^{iPr}PDAI)Fe(DMAP) is best described as idealized square planar with the plane of the DMAP ligand at angles of 53.78(6)° and 55.36(6)° relative to the iron-chelate plane. The same angle for (^{iPr}PDI)Fe(DMAP) is 50.36(10)°.

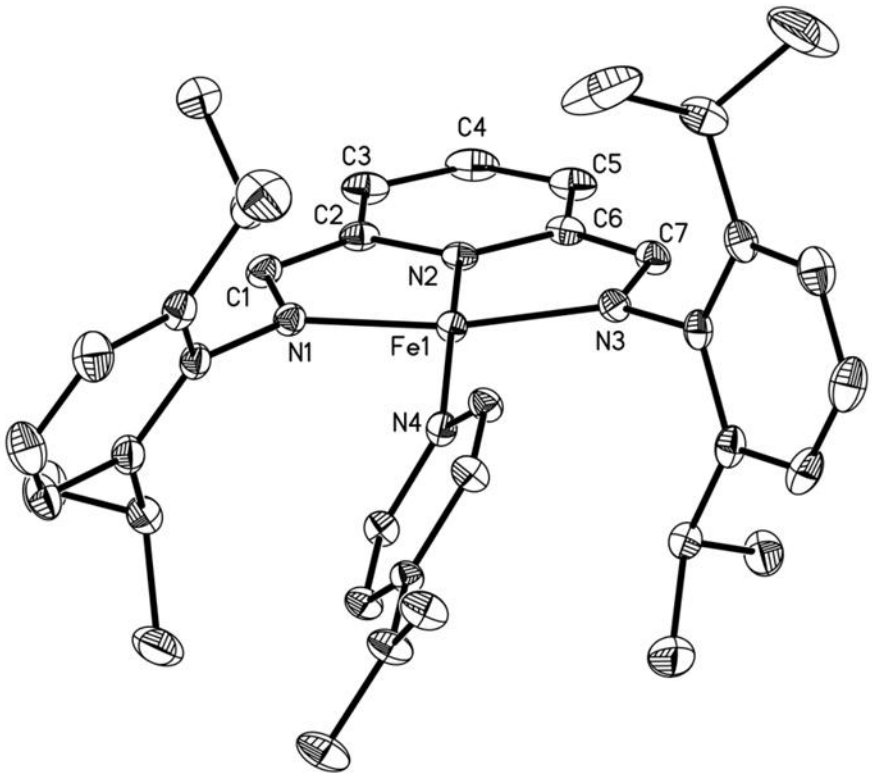

Figure 4.16 Solid state structure of (^{iPr}PDAI)Fe(DMAP) with 30% probability ellipsoids. Hydrogen atoms omitted for clarity.

Table 4.3 Selected bond distances (Å) and angles (°) for both molecules of (^{iPr}PDAI)Fe(DMAP) and (^{iPr}PDI)Fe(DMAP).[16]

	(^{iPr}PDAI)Fe(DMAP)	**(^{iPr}PDI)Fe(DMAP)**
Fe-$N_{pyridine}$	1.8357(19)	1.821(3)
	1.8330(17)	
Fe-N_{imine}	1.904(2), 1.922(2)	1.908(3), 1.943(3)
	1.889(2), 1.917(2)	
Fe-N_{DMAP}	1.978(2)	1.979(3)
	1.9850(19)	
N_{imine}-C_{imine}	1.339(3), 1.355(3)	1.350(5), 1.358(5)
	1.349(3), 1.343(3)	
C_{imine}-C_{ipso}	1.407(4), 1.406(4)	1.414(5), 1.406(5)
	1.406(3), 1.406(3)	
Fe-N_{imine}-C_{Ar}	127.59(16),127.52(16)	126.2(3), 125.7(2)
	125.80(15), 125.83(15)	

The bond distances in the solid state structure of (^{iPr}PDAI)Fe(DMAP) are consistent with two electron reduction of the chelate and an intermediate spin ferrous center. The N_{imine}-C_{imine} bond lengths in one molecule of (^{iPr}PDAI)Fe(DMAP) of 1.339(3) and 1.355(3) Å and the corresponding values of the second molecule, 1.349(3) and 1.343(3) Å are elongated from both the free ligand and the uncoordinated half of [(^{iPr}PDAI)Fe]$_2$ (Table 4.1) which is assigned as mono-reduced. The C_{imine}-C_{ipso} bond distances of (^{iPr}PDAI)Fe(DMAP) are correspondingly contracted compared to ^{iPr}PDAI and [(^{iPr}PDAI)Fe]$_2$. The distortions observed in (^{iPr}PDAI)Fe(DMAP) are comparable to those observed for (^{iPr}PDI)Fe(DMAP) which has an electronic structure best described as an intermediate spin iron(II) center antiferromagnetically couple to a bis(imino)pyridine diradical dianion.[16]

As with the butadiene compound, the zero-field ^{57}Fe Mössbauer spectrum of (^{iPr}PDAI)Fe(DMAP) was collected (Figure 4.17) and the parameters compared to those previously reported for (^{iPr}PDI)Fe(DMAP).[16] The isomer shift (δ) of (^{iPr}PDI)Fe(DMAP) is 0.31 mm/s and the quadrupole splitting (ΔE_Q) is + 1.94 mm/s. The parameters for (^{iPr}PDAI)Fe(DMAP), δ = 0.30 mm/s and ΔE_Q = │2.04│ mm/s, are almost identical to those of (^{iPr}PDI)Fe(DMAP) indicating similar electronic structures for the ketimine and aldimine compounds.

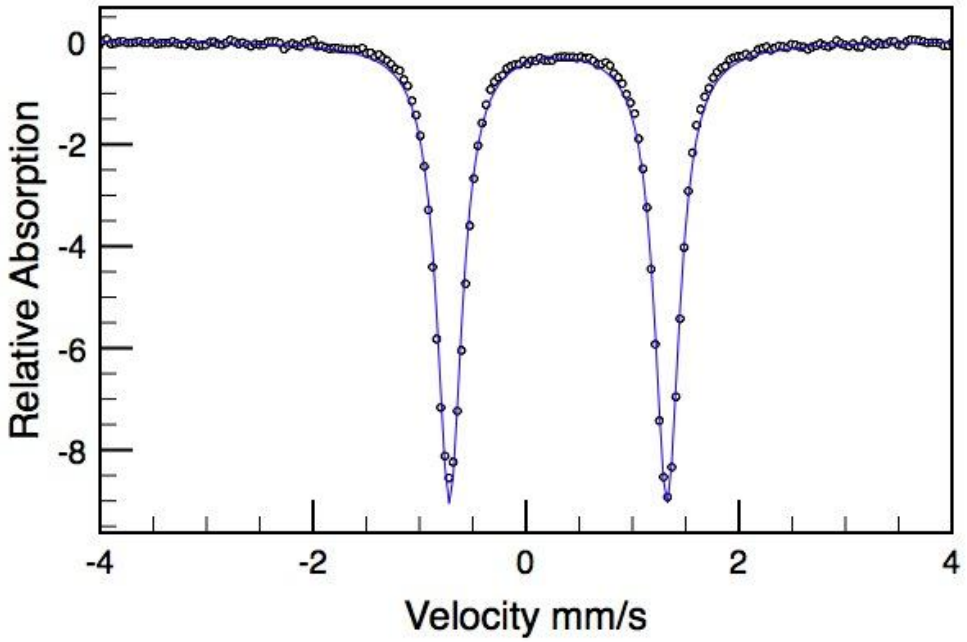

Figure 4.17 Zero-field ^{57}Fe Mössbauer spectrum of (^{iPr}PDAI)Fe(DMAP) collected at 80K; δ = 0.30 mm/s, ΔE_Q = │2.04│ mm/s.

Because of the ease of synthesis of bis(imino)pyridine iron dicarbonyl compounds, the corresponding bis(aldimino)pyridine iron dicarbonyl compound, (^{iPr}PDAI)Fe(CO)$_2$ was also synthesized. Reduction of (^{iPr}PDAI)FeBr$_2$ in toluene with excess 0.5% sodium amalgam under four atmospheres of carbon monoxide followed by filtration and recrystallization from diethyl ether at -35 °C furnished green

(^{iPr}PDAI)Fe(CO)$_2$ in 69 % yield (Figure 4.18). The dicarbonyl compound could also be prepared by addition of excess CO to any of the previously discussed bis(aldimino)pyridine iron neutral ligand complexes including the dimer.

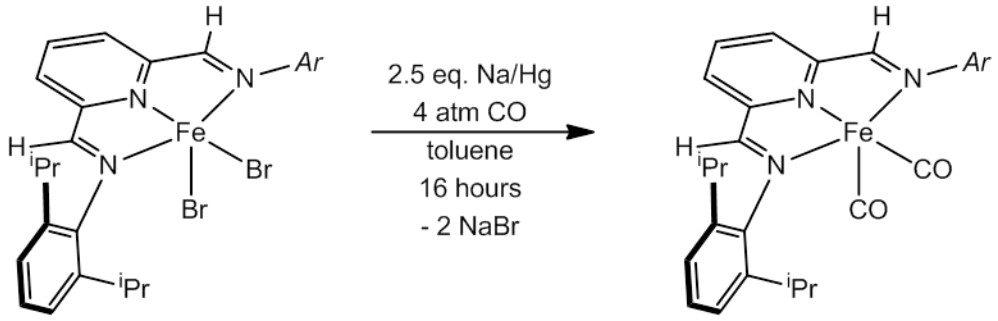

(^{iPr}PDAI)FeBr$_2$ **(^{iPr}PDAI)Fe(CO)$_2$**

Figure 4.18 Synthesis of (^{iPr}PDAI)Fe(CO)$_2$.

The dicarbonyl compound was characterized by NMR and IR spectroscopies. The pentane solution IR spectrum of (^{iPr}PDAI)Fe(CO)$_2$ exhibits two strong bands centered at 1981 and 1925 cm^{-1}, which are at higher energies than those of (^{iPr}PDI)Fe(CO)$_2$ which appear at 1974 and 1914 cm^{-1}.[4] As expected, this difference demonstrates that the ketimine compound has a slightly more electron-rich iron center than the aldimine compound. The benzene-d_6 ^{1}H NMR spectrum of (^{iPr}PDAI)Fe(CO)$_2$ exhibits the number of peaks consistent with a C_{2v} symmetric molecule in solution, consistent with rapid exchange of the carbonyl ligands on the NMR timescale.

The electronic structure of (^{iPr}PDAI)Fe(CO)$_2$ was also studied by zero-field ^{57}Fe Mössbauer spectroscopy (Figure 4.19) and compared to (^{iPr}PDI)Fe(CO)$_2$. The ketimine compound (^{iPr}PDI)Fe(CO)$_2$ has an isomer shift (δ) of 0.03 mm/s and a quadrupole splitting (ΔE_Q) of $\left|1.17\right|$ mm/s. The aldimine compound, (^{iPr}PDAI)Fe(CO)$_2$, has very similar parameters with an isomer shift (δ) of 0.01 mm/s and a quadrupole splitting (ΔE_Q) of $\left|1.15\right|$ mm/s. The almost identical Mössbauer

parameters suggest that (^{iPr}PDAI)Fe(CO)$_2$ has the same electronic structure as (^{iPr}PDI)Fe(CO)$_2$.[16,17]

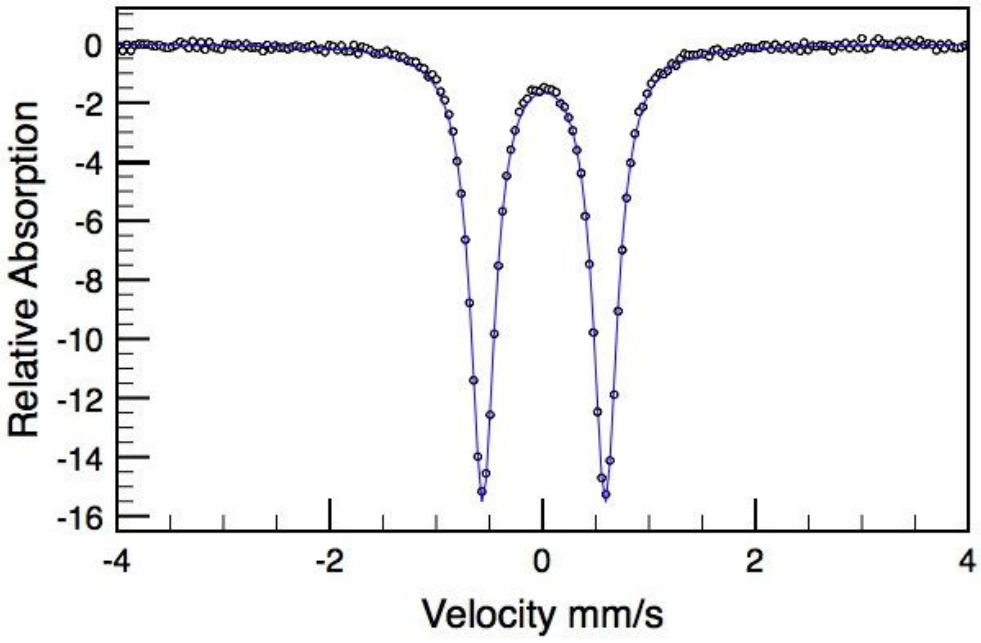

Figure 4.19 Zero-field ^{57}Fe Mössbauer spectrum of (^{iPr}PDAI)Fe(CO)$_2$ collected at 80K; δ = 0.01 mm/s, ΔE_Q = $\left|1.15\right|$ mm/s

The comparison of the three bis(aldimino)pyridine iron neutral ligand compounds, (^{iPr}PDAI)Fe(η^4-C$_4$H$_6$), (^{iPr}PDAI)Fe(DMAP) and (^{iPr}PDAI)Fe(CO)$_2$, to their bis(imino)pyridine iron counterparts shows that there is very little difference between the two chelate frameworks. Comparison of crystal structures and Mössbauer and ^{1}H NMR spectra show little difference in electronic structure between ketimine and aldimine-supported iron compounds with the same neutral ligand. The only difference between the chelate structures was observed in the IR spectrum of the dicarbonyl compounds where the carbonyl stretching frequencies establish a slightly more electron-rich iron center for the ketimine compound, (^{iPr}PDI)Fe(CO)$_2$.

4.5 Catalytic Olefin Hydrogenation

Bis(imino)pyridine iron dinitrogen complexes have been shown to be active catalysts for olefin hydrogenation,[4,5,6,24] hydrosilylation,[4,7,24] and cycloisomerization reactions.[8,9] The compounds with less sterically hindered iron centers have been shown to be more active precatalysts for olefin hydrogenations than their bulkier counterparts.[5] The formation of the bis(aldimino)pyridine iron η^6-arene compounds as well as isolation of $[(^{iPr}PDAI)Fe]_2$ suggest that the aldimine framework provides less steric protection for the iron center than the corresponding ketimine ligand. For this reason, several bis(aldimino)pyridine iron compounds were screened for the catalytic hydrogenations of cyclohexene and ethyl-3-methylbut-2-eonate.

The first compound studied was the dimer $[(^{iPr}PDAI)Fe]$ which unfortunately did not exhibit any hydrogenation activity for cyclohexene or ethyl-3-methylbut-2-eonate even after several days. Observing the addition of a stoichiometric amount of either substrate to $[(^{iPr}PDAI)Fe]$ by ^1H NMR spectroscopy showed that the dimer remains intact and is unreactive towards both the olefin and ester groups of the substrates. Similarly, addition of one atmosphere of H_2 to $[(^{iPr}PDAI)Fe]$ also did not result in any reaction even after 24 hours, demonstrating that the dimer requires stronger ligands to break it apart and that it does not dissociate in solution to an active catalyst.

Bis(imino)pyridine iron butadiene compounds have been shown to be active precatalysts for olefin hydrogenation, oftenr with significant induction periods.[41] Because of this, the next compound screened for hydrogenation activity was $(^{iPr}PDAI)Fe(\eta^4\text{-}C_4H_6)$. For direct comparison, $(^{iPr}PDAI)Fe(\eta^4\text{-}C_4H_6)$ and $(^{iPr}PDI)Fe(\eta^4\text{-}C_4H_6)$ were run in side-by-side reactions. The hydrogenation of cyclohexene was run at room temperature with 5 mol% catalyst in a benzene-d_6 solution under 4 atmospheres of H_2 (Figure 4.20) and the conversion to product

determined by ^{1}H NMR spectroscopy. The ketimine compound, (^{iPr}PDI)Fe(η^4-C_4H_6), reached > 99% conversion in under one hour while the aldimine compound, (^{iPr}PDAI)Fe(η^4-C_4H_6), produced only 28% conversion after 4 hours, 82 % conversion after 16 hours and required 24 hours for > 99% conversion.

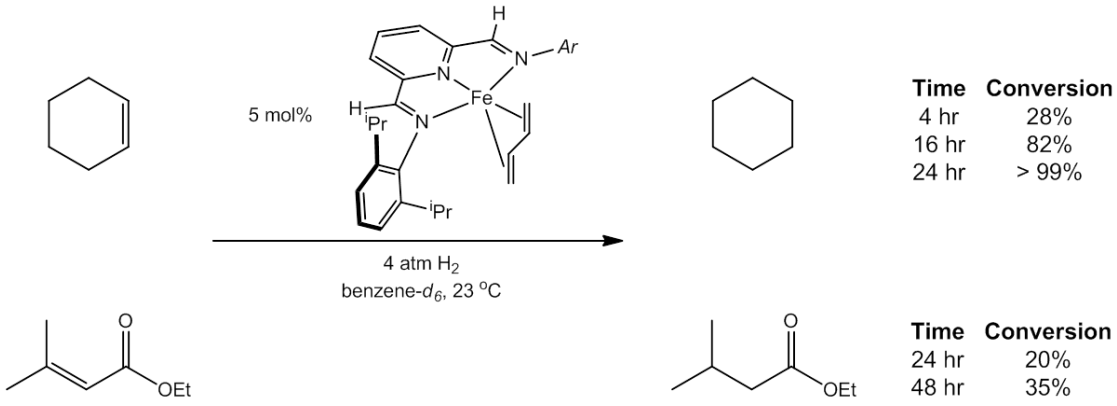

Figure 4.20 Catalytic hydrogenation of cyclohexene and ethyl-3-methylbut-2-enoate with (^{iPr}PDAI)Fe(η^4-C_4H_6).

Similarly, (^{iPr}PDAI)Fe(η^4-C_4H_6) was a far less active catalyst for the hydrogenation of ethyl-3-methylbut-2-enoate than (^{iPr}PDI)Fe(η^4-C_4H_6). Like the cyclohexene reactions, the hydrogenation of the trisubstituted olefin was run at room temperature with 5 mol% catalyst in benzene-d_6 under 4 atmospheres of H_2 (Figure 4.20). The ketimine-substituted precatalyst, (^{iPr}PDI)Fe(η^4-C_4H_6), yielded 60 % conversion after 24 hours while the aldimine-substituted precatalyst, (^{iPr}PDAI)Fe(η^4-C_4H_6), produced only 20 % conversion after the same amount of time. For comparison, the related bis(imino)pyridine iron bis(dinitrogen) compound, (^{iPr}PDI)Fe(N_2)$_2$, is reported to reach 65 % conversion after 24 hours after which time the iron is deactivated by irreversible C-O bond cleavage. Running the reaction with (^{iPr}PDAI)Fe(η^4-C_4H_6) as a catalyst for 48 hours improved the conversion to 35 %, but

no additional conversion was observed at longer reaction times, suggesting that C-O bond cleavage may become competitive for this pre-catalyst.

Additional studies were conducted to determine the origin of the poor catalytic performance of (^{iPr}PDAI)Fe(η^4-C_4H_6). Analysis of the iron compound by ^{1}H NMR spectroscopy following catalytic hydrogenation of cyclohexene revealed formation of the η^6-benzene compound, (^{iPr}PDAI)Fe(η^6-C_6D_6), along with several other unidentified (both diamagnetic and paramagnetic) iron compounds. A catalyst recycling experiment was also performed in which the hydrogenation of cyclohexene by (^{iPr}PDAI)Fe(η^4-C_4H_6) was run in benzene-d_6 to > 95% conversion. The reaction was then recharged with another 20 equivalents of cyclohexene and 4 atmospheres of H_2. After 16 hours, 40 % conversion was observed, indicating that a substantial amount of the original catalyst had been deactivated during the first hydrogenation cycle.

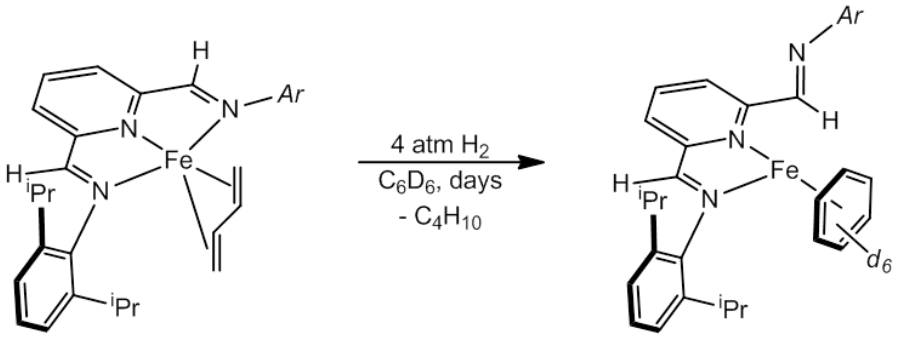

Figure 4.21 Hydrogenative conversion of (^{iPr}PDAI)Fe(η^4-C_4H_6) to (^{iPr}PDAI)Fe(η^6-C_6D_6).

Treatment of a benzene-d_6 solution of (^{iPr}PDAI)Fe(η^4-C_4H_6) with 4 atmospheres of H_2 resulted in loss of butane and formation of the iron η^6-benzene compound, (^{iPr}PDAI)Fe(η^6-C_6D_6), over the course of days at 23 °C (Figure 4.21).

Under the same conditions, (^{iPr}PDI)Fe(η^4-C_4H_6) undergoes complete conversion to the bis(imino)pyridine iron dihydrogen compound, (^{iPr}PDI)Fe(η^2-H_2) within 16 hours. These results suggest that the difference in hydrogenation activity between the two complexes likely results from the slower initiation of the aldimine iron butadiene compound relative to the ketimine analog. In this case, the more open coordination sphere around the iron center in the aldimine complex does not improve catalytic activity, but rather inhibits it by enabling competing decomposition pathways and slowing activation of the precatalyst.

4.6 Addition of Azides

A variety of terminal bis(imino)pyridine iron aryl and alkyl imides have been previously reported by our research group.[42,43] The bis(imino)pyridine iron aryl-imido compounds,[37] (^{iPr}PDI)FeN*Ar* (*Ar* = 2,6-$^{i}Pr_2$-C_6H_3, 2,6-Et_2-C_6H_3, 2,5-$^{t}Bu_2$-C_6H_3, 2,4,6-$Me_3C_6H_2$), are paramagnetic and most exhibit unique catalytic hydrogenation activity, furnishing the corresponding aniline and bis(imino)pyridine iron dihydrogen complex, (^{iPr}PDI)Fe(η^2-H_2). Two of the bis(imino)pyridine iron aryl-imido complexes, (^{iPr}PDI)FeN(2,6-$^{i}Pr_2$-C_6H_3) and (^{iPr}PDI)FeN(2,4,6-$Me_3C_6H_2$) have been crystallographically characterized. The most notable feature of these compounds is that the imide substituent is lifted significantly out of the iron-chelate plane. For (^{iPr}PDI)FeN(2,6-$^{i}Pr_2$-C_6H_3), the observed $N_{pyridine}$-Fe-N_{imide} angle is 138.79(7)°, while for (^{iPr}PDI)FeN(2,4,6-$Me_3C_6H_2$) a less distorted angle of 154.75(7)° was observed. Because it has been shown that the iron center in bis(aldimino)pyridine compounds is less sterically hindered than in the respective bis(imino)pyridine compounds, an aldimine-supported iron aryl-imide complex may allow for a more planar iron imide fragment and C-H bond activation chemistry.

In contrast to the paramagnetic bis(imino)pyridine iron aryl-imide complexes, the alkyl-imide compound (^{iPr}PDI)FeN(^{1}Ad) is diamagnetic and exhibits very different reactivity.[38] The alkyl-imide compound is unreactive toward H_2, but undergoes intramolecular C-H bond activation of the imine methyl groups to afford the bis(enamide)pyridine iron amine compound, (^{iPr}PDEA)FeNH_2^{1}Ad (^{iPr}PDEA = 2,6-(2,6-^{i}Pr$_2$-C_6H_3NC=CH_2)$_2$$C_5H_3$N) (Figure 4.22). Because the bis(aldimino)pyridine ligand framework does not have the imine methyl groups available for C-H bond activation, the corresponding aldimine-supported iron alkyl-imide complex was targeted as a potentially thermally stable diamagnetic iron imide compound.

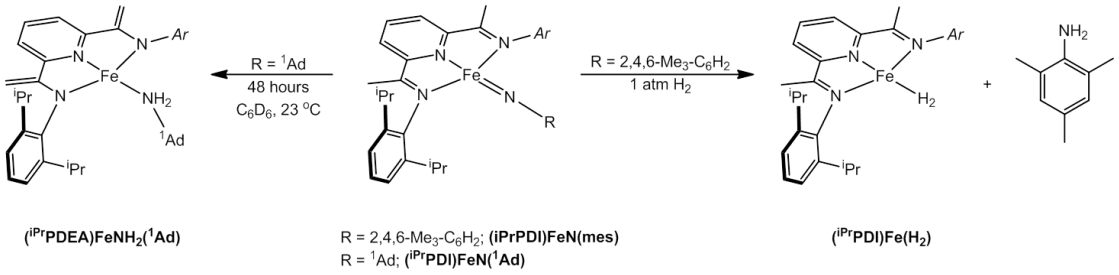

Figure 4.22 Previously reported bis(imino)pyridine iron imide compounds and their differing reactivities.

Addition of one equivalent of 2,4,6-trimethylphenyl azide to a diethyl ether solution of (^{iPr}PDAI)Fe(η^4-C_4H_6) resulted in bubbling and a color change from brown to dark blue. Filtration and recrystallization from diethyl ether at -35 °C furnished the bis(aldimino)pyridine iron aryl-imide compound (^{iPr}PDAI)FeN(2,4,6-Me_3-C_6H_2) (Figure 4.23). Like its ketimine counterpart, (^{iPr}PDAI)FeN(2,4,6-Me_3-C_6H_2) is paramagnetic with a magnetic moment of μ_{eff} = 2.7 μ_B, corresponding to an overall S = 1 spin state. The ^{1}H NMR spectrum is also consistent with a paramagnetic compound with a peak range from -40 ppm to 290 ppm, similar to that observed for (^{iPr}PDI)FeN(2,4,6-Me_3-C_6H_2).[37] The reactivity of (^{iPr}PDAI)Fe(2,4,6-Me_3-C_6H_2) also

mirrors that of the ketimine-based iron imide in that (^{iPr}PDAI)Fe(2,4,6-Me_3-C_6H_2) is unreactive towards H_2, but reacts with CO to form (^{iPr}PDAI)Fe$(CO)_2$ and one equivalent of 2,4,6-trimethylphenyl isocyanate.

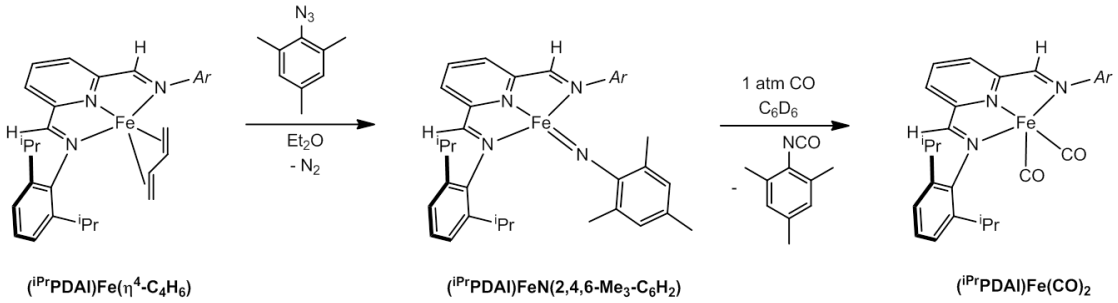

Figure 4.23 Synthesis and reactivity of (^{iPr}PDAI)FeN(2,4,6-Me_3-C_6H_2).

Single crystals of (^{iPr}PDAI)FeN(2,4,6-Me_3-C_6H_2) suitable for X-ray diffraction were grown from a concentrated pentane solution at -35 °C. A representation of the solid state structure is presented in Figure 4.24 and metrical parameters are reported in Table 4.4, along with those of (^{iPr}PDI)FeN(2,4,6-Me_3-C_6H_2) for comparison. Notably, the molecular geometry of (^{iPr}PDAI)FeN(2,4,6-Me_3-C_6H_2) is significantly deviated from planarity with a $N_{pyridine}$-Fe-N_{imide} angle of 175.79(13)°. This distortion is similar to the one observed in (^{iPr}PDI)FeN(2,4,6-Me_3-C_6H_2), where the $N_{pyridine}$-Fe-N_{imide} angle is 159.00(13)°.[37] An overlay of the solid state structures of (^{iPr}PDAI)FeN(2,4,6-Me_3-C_6H_2) and (^{iPr}PDI)FeN(2,4,6-Me_3-C_6H_2) is presented in Figure 4.25. As in (^{iPr}PDI)FeN(2,4,6-Me_3-C_6H_2), the iron is lifted out of the plane of the chelate, but by a lesser amount. The short Fe-$N_{pyridine}$ and Fe-N_{imine} bond distances of 1.860(1) and 1.916(1) and 1.932(1) Å, respectively, in (^{iPr}PDAI)FeN(2,4,6-Me_3-C_6H_2) are consistent with an intermediate or low spin iron center. These Fe-N_{PDAI} distances are shorter than those reported for (^{iPr}PDI)FeN(2,4,6-Me_3-C_6H_2). Accordingly, the Fe-N_{imide} distance of the aldimine-based iron imide is also shorter at 1.673(1) Å compared

to 1.717(3) Å for the ketimine version; however, this bond length is still longer than those observed for the bis(imino)pyridine iron alkyl imides.[38]

The bond distances of the ^{iPr}PDAI chelate are most consistent with two electron reduction. The N_{imine}-C_{imine} bond distances of 1.330(1) Å and 1.331(1) Å are comparable to those reported for (^{iPr}PDAI)Fe(η^4-C_4H_6) (1.329(3) Å and 1.333(3) Å), but shorter than those in (^{iPr}PDAI)Fe(DMAP). Both (^{iPr}PDAI)Fe(η^4-C_4H_6) and (^{iPr}PDAI)Fe(DMAP) are suggested to be intermediate spin iron(II) compounds with doubly reduced ^{iPr}PDAI chelates. The C_{imine}-C_{ipso} bond distances of 1.413(2) Å and 1.412(2) Å in (^{iPr}PDAI)FeN(2,4,6-Me_3-C_6H_2) are also suggestive of two electron reduction. Although these distances are slightly longer than those reported for (^{iPr}PDAI)Fe(η^4-C_4H_6) and (^{iPr}PDAI)Fe(DMAP), they are significantly shorter than the corresponding distances in (^{iPr}PDI)FeN(2,4,6-Me_3-C_6H_2).

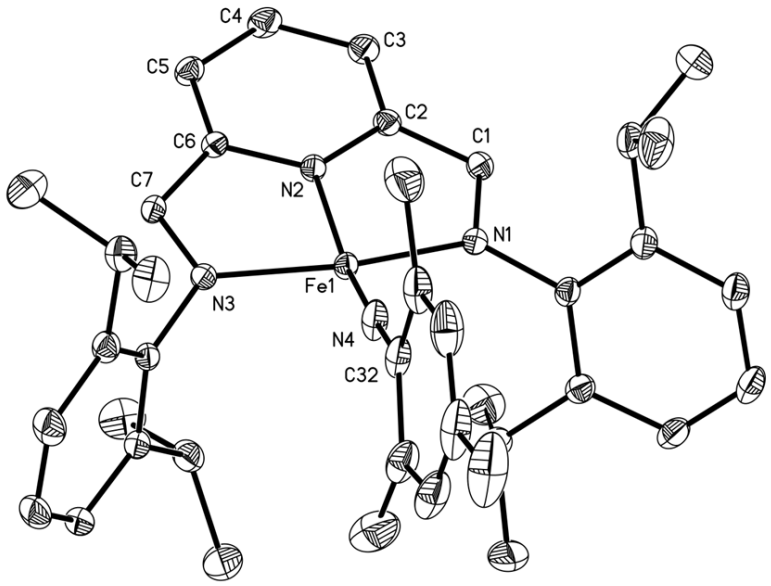

Figure 4.24 Solid state structure of (^{iPr}PDAI)FeN(2,4,6-Me_3-C_6H_2) at 30% probability ellipsoids. Hydrogen atoms omitted for clarity.

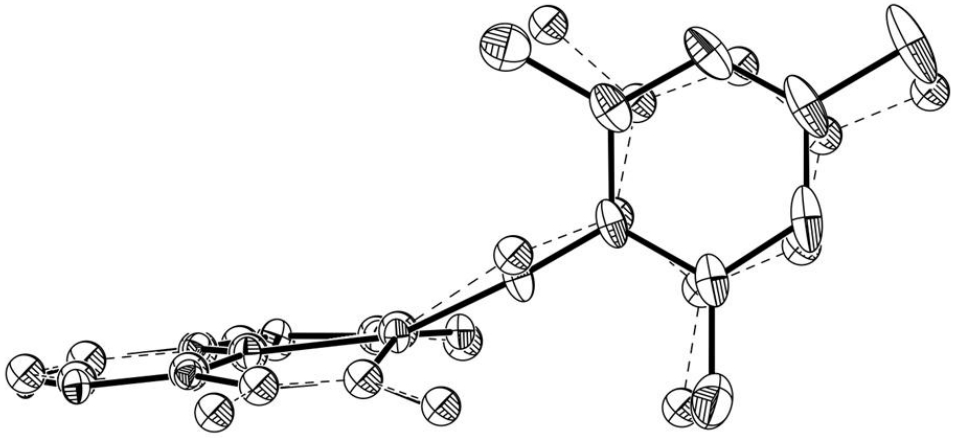

Figure 4.25 Overlay of (^{iPr}PDAI)FeN(2,4,6-Me_3-C_6H_2) (solid bonds) and (^{iPr}PDI)FeN(2,4,6-Me_3-C_6H_2) (dotted bonds) at 30% probability ellipsoids. Hydrogen atoms and aryl groups omitted for clarity.

Table 4.4 Selected bond lengths (Å) and angles (°) for (^{iPr}PDAI)FeN(2,4,6-Me_3-C_6H_2) and (^{iPr}PDI)FeN(2,4,6-Me_3-C_6H_2).[37]

	(^{iPr}PDAI)Fe N(2,4,6-Me_3-C_6H_2)	**(^{iPr}PDI)Fe N(2,4,6-Me_3-C_6H_2)**
Fe-$N_{pyridine}$	1.860(1)	1.872(1)
Fe-N_{imine}	1.916(1), 1.932(1)	2.011(1), 1.977(1)
Fe-N_{imide}	1.673(1)	1.717(2)
N_{imine}-C_{imine}	1.330(1), 1.331(1)	1.321(2), 1.334(2)
C_{imine}-C_{ipso}	1.413(2), 1.412(2)	1.436(2), 1.426(2)
N_{py}-Fe-N_{imide}	160.64(6)	154.75(7)
Fe-N_{imide}-C_{imide}	175.79(13)	159.00(13)
Fe deviation from N(1), N(2), N(3) plane	0.2776	0.3386

The bis(aldimino)pyridine iron aryl-imide, (^{iPr}PDAI)FeN(2,4,6-Me_3-C_6H_2), was also studied by zero-field ^{57}Fe Mössbauer spectroscopy and representative spectra

are shown in Figure 4.26. At 80K, the isomer shift (δ) of 0.03 mm/s is significantly different from the isomer shift of 0.30 mm/s reported for the ketimine-based derivative at the same temperature,[38] while the quadrupole splitting parameters of both imide compounds, ΔE_Q = │1.21│ mm/s for (^{iPr}PDAI)FeN(2,4,6-Me_3-C_6H_2) and ΔE_Q = │1.34│ mm/s for (^{iPr}PDI)FeN(2,4,6-Me_3-C_6H_2), are very similar. The isomer shift of (^{iPr}PDAI)FeN(2,4,6-Me_3-C_6H_2) is quite similar to that of the ketimine-based iron alkyl imide, (^{iPr}PDI)FeN(^{1}Ad), which has an isomer shift of 0.04 mm/s. Because of the unexpectedly low isomer shift for (^{iPr}PDAI)FeN(2,4,6-Me_3-C_6H_2), spin-crossover behavior was investigated by variable temperature Mössbauer spectroscopy. The spectrum collected at 293 K the same isomer shift of δ = 0.03 mm/s as did the spectrum collected at 80K, disfavoring a spin-crossover phenomenon. However, SQUID magnetometry data is needed to support this conclusion.

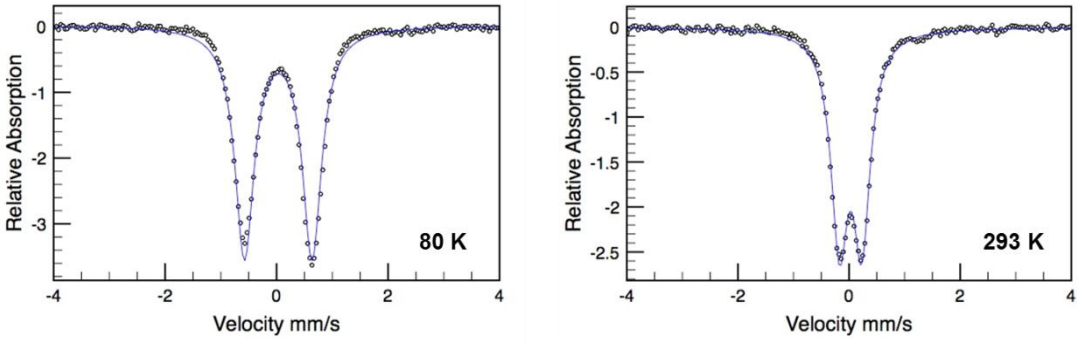

Figure 4.26 Zero-field ^{57}Fe Mössbauer spectra of (^{iPr}PDAI)FeN(2,4,6-Me_3-C_6H_2) at 80K (left, δ = 0.03 mm/s, ΔE_Q = │1.21│ mm/s) and 293K (right, δ = 0.03 mm/s, ΔE_Q = │0.40│ mm/s).

The difference in isomer shifts between the ketimine and aldimine-based iron aryl-imide compounds suggests that (^{iPr}PDAI)FeN(2,4,6-Me_3-C_6H_2) has a different solid-state electronic structure than (^{iPr}PDI)FeN(2,4,6-Me_3-C_6H_2). The electronic structure of the bis(imino)pyridine iron aryl-imide compound is reported as an

intermediate spin iron(III) center ($S_{Fe} = {}^3/_2$) antiferromagnetically coupled to a PDI-ligand centered radical ($S_{PDI} = ½$). Based on the Mössbauer parameters, magnetic moment and crystal structure metrics, (^{iPr}PDAI)FeN(2,4,6-Me_3-C_6H_2) appears to have an electronic structure more similar to the ketimine-based alkyl imides rather than the aryl-imides. One possible electronic structure that is consistent with the spectroscopic and X-ray data is a low-spin iron(IV) center ($S_{Fe} = 0$) with a triplet diradical bis(imino)pyridine chelate ($S = 1$) which would yield the observed $S = 1$ ground state; however, more evidence from SQUID and computational studies is needed to support this proposal.

The bis(aldimino)pyridine iron alkyl-imide was synthesized starting from the dimer, [(^{iPr}PDAI)Fe]$_2$. Slow addition of two equivalents of 1-adamantyl azide to a dilute diethyl ether solution of [(^{iPr}PDAI)Fe]$_2$ resulted in a gradual color change from brown to bright purple. Filtration followed by recrystallization from pentane at -35 °C afforded the bis(aldimino)pyridine iron alkyl-imide compound (^{iPr}PDAI)FeN(^{1}Ad) (Figure 4.27). The benzene-d_6 ^{1}H NMR spectrum of (^{iPr}PDAI)FeN(^{1}Ad) exhibits proton coupling indicative of a diamagnetic compound and the number of peaks consistent with a C_{2v} symmetric molecule in solution. Compared to the bis(imino)pyridine iron 1-adamantyl imide compound, the peak range for (^{iPr}PDAI)FeN(^{1}Ad) is much smaller. The chemical shift range for (^{iPr}PDAI)FeN(^{1}Ad) spans only about 15 ppm compared to the 45 ppm range for (^{iPr}PDI)FeN(^{1}Ad). The chemical shifts of the in-plane hydrogens of the chelate are only slightly shifted from their diamagnetic reference values. For example, the aldimine hydrogen resonance of (^{iPr}PDAI)FeN(^{1}Ad) appears at 13.30 ppm, shifted from 8.54 ppm in ^{iPr}PDAI. The *meta*- and *para*- pyridine hydrogen resonances are shifted only a small amount to 9.50 ppm and 9.83 ppm, respectively. The *meta*- and *para*- pyridine hydrogen resonances for ^{iPr}PDAI appear at 8.30 and 7.19 ppm, respectively.

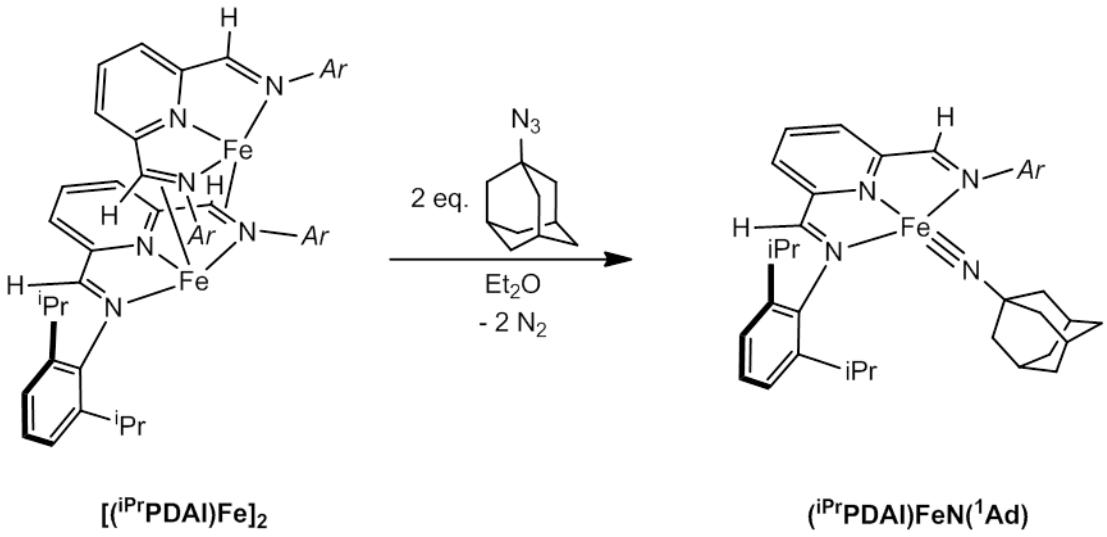

Figure 4.27 Synthesis of (^{iPr}PDAI)FeN(^{1}Ad).

The bis(aldimino)pyridine iron 1-adamantyl imide compound was also studied by zero-field ^{57}Fe Mössbauer spectroscopy and a representative spectrum is presented in Figure 4.28. The isomer shift (δ) of -0.01 mm/s and the quadrupole splitting (ΔE_Q) of $\left|2.42\right|$ mm/s are very similar to the reported values of δ = 0.04 mm/s and ΔE_Q = -2.38 mm/s for (^{iPr}PDI)FeN(^{1}Ad). The similarities in Mössbauer parameters and ^{1}H NMR spectra between (^{iPr}PDAI)FeN(^{1}Ad) and (^{iPr}PDI)FeN(^{1}Ad) suggest that the aldimine-substituted compound has the same electronic structure as the previously prepared ketimine-derivative.

The bis(aldimino)pyridine iron 1-adamantyl imide also exhibits reactivity similar to the bis(imino)pyridine iron analog. Like the ketimine-based derivative, (^{iPr}PDAI)FeN(^{1}Ad) is unreactive towards hydrogen. However, unlike (^{iPr}PDI)FeN(^{1}Ad), (^{iPr}PDAI)FeN(^{1}Ad) is stable in solution for days at room temperature with no evidence for any intramolecular C-H bond activation. Because Mössbauer and ^{1}H NMR spectroscopy suggest that (^{iPr}PDAI)FeN(^{1}Ad) has a similar

electronic structure to (^{iPr}PDI)FeN(^{1}Ad), the possibility for intermolecular C-H bond activation by (^{iPr}PDAI)FeN(^{1}Ad) was explored. Unfortunately, substrates with weak C-H bonds such as 1,4-cyclohexadiene, toluene and dihydroanthracene did not react at room temperature with (^{iPr}PDAI)FeN(^{1}Ad) after 24 hours in solution. Heating the reactions to 85 °C only resulted in decomposition of (^{iPr}PDAI)FeN(^{1}Ad).

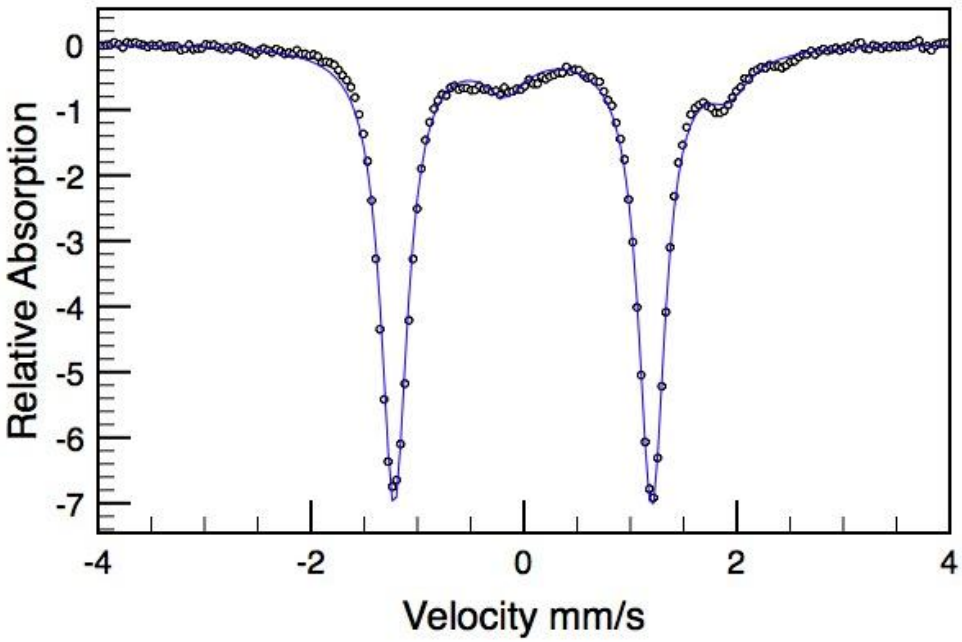

Figure 4.28 Zero-field ^{57}Fe Mössbauer spectrum for (^{iPr}PDI)FeN(^{1}Ad) collected at 80K; δ = -0.01 mm/s, ΔE_Q = $\left|2.42\right|$ mm/s.

4.7 Conclusions

The reduction chemistry of the bis(aldimino)pyridine iron dibromide, (^{iPr}PDAI)$FeBr_2$, was studied and several compounds not known in bis(imino)pyridine iron chemistry were observed. Reduction of (^{iPr}PDAI)$FeBr_2$ with 2 equivalents of 0.5% sodium amalgam in an arene solvent, such as toluene or benzene, furnished the respective bis(aldimino)pyridine iron η^6-arene compounds, (^{iPr}PDAI)Fe(η^6-C_7H_8) and (^{iPr}PDAI)Fe(η^6-C_6H_6), which both converted to the η^6-benzene compound,

(^{iPr}PDAI)Fe(η^6-C_6D_6), when dissolved in benzene-d_6. In a pentane or diethyl ether solution at -35 °C (^{iPr}PDAI)Fe(η^6-C_7H_8) and (^{iPr}PDAI)Fe(η^6-C_6H_6) lost the η^6-arene ligand and furnished the dimeric bis(aldimino)pyridine iron compound, [(^{iPr}PDAI)Fe]$_2$. Mössbauer and ^{1}H NMR spectroscopy, X-ray diffraction and SQUID magnetometry establish a diiron compound with two non-interacting high spin iron(II) centers each antiferromagnetically coupled to a triplet dianionic bis(aldimino)pyridine chelate. Both arene coordination and dimerization instead of dinitrogen coordination contrast the known chemistry for analogous ketimine-substituted bis(imino)pyridine iron compounds and suggest that the iron center in the aldimine derivatives is less sterically protected.

Two electron reduction of (^{iPr}PDAI)FeBr$_2$ in the presence of 1,3-butadiene furnished (^{iPr}PDAI)Fe(η^4-C_4H_6). The reactivity and electronic structure of (^{iPr}PDAI)Fe(η^4-C_4H_6) were studied with Mössbauer and ^{1}H NMR spectroscopies and X-ray crystallography and compared to those of the ketimine-based derivative. The bis(aldimino)pyridine iron butadiene compound was shown to be a pre-catalyst for olefin hydrogenation and [$2\pi + 2\pi$] cycloaddition, but less active than its ketimine-based analog. Two other bis(aldimino)pyridine iron neutral ligand compounds, (^{iPr}PDAI)Fe(DMAP) and (^{iPr}PDAI)Fe(CO)$_2$, were prepared and their electronic structures also studied by Mössbauer, ^{1}H NMR and infrared spectroscopy as well as X-ray crystallography. All three bis(aldimino)pyridine iron neutral ligand compounds exhibited very similar electronic structures to their bis(imino)pyridine iron derivatives, suggesting that any difference in reactivity between the families of compounds is derived from steric differences about the iron center.

Finally, two bis(aldimino)pyridine iron imide compounds, (^{iPr}PDAI)FeN(2,4,6-Me_3-C_6H_2) and (^{iPr}PDAI)FeN(^{1}Ad), were prepared and studied by NMR and Mössbauer spectroscopy and for (^{iPr}PDAI)FeN(2,4,6-Me_3-C_6H_2), X-ray diffraction.

The two aldimine-based iron imides appear to have similar electronic structures to each other and to the ketimie-based alkyl imide, (^{iPr}PDI)FeN(^{1}Ad). Unlike its ketimine analog, (^{iPr}PDAI)FeN(^{1}Ad) is thermally stable and does not appear to readily react with weak C-H bonds.

4.8 Experimental Procedures

General Considerations. All air- and moisture-sensitive manipulations were carried out using standard vacuum line, Schlenk, and cannula techniques or in an MBraun inert atmosphere dry box containing an atmosphere of purified nitrogen. Solvents for air- and moisture-sensitive manipulations were initially dried and deoxygenated using literature procedures.[44] Benzene-d_6 was purchased from Cambridge Isotope Laboratories and dried over 4 Å molecular sieves. N,N-dimethyl-4-aminopyridine and 1-adamantyl azide were purchased from Acros and dried on a high-vacuum line overnight. 1,3-butadiene was purchased from Sigma Aldrich and dried over lithium aluminum hydride. 2,6-(2,6-^{i}Pr$_2$-C$_6$H$_3$-N=CH)$_2$C$_5$H$_3$N (^{iPr}PDAI) was prepared according to literature procedure.[3b] 2,4,6-trimethylphenyl azide was prepared according to literature procedure.[45]

^{1}H NMR spectra were recorded on Varian Mercury 300, Inova 400, 500, and 600 spectrometers operating at 299.76, 399.78, 500.62, and 599.78 MHz, respectively. ^{13}C NMR spectra were recorded on an Inova 500 spectrometer operating at 125.893 MHz. All ^{1}H and ^{13}C NMR chemical shifts are reported relative to SiMe$_4$ using the ^{1}H (residual) and ^{13}C chemical shifts of the solvent as a secondary standard. Peak widths at half heights are reported for paramagnetically broadened and shifted resonances. For diamagnetic complexes, many assignments were made based on COSY and HSQC NMR experiments. Solution magnetic moments were determined by Evans method[46] using a ferrocene standard and are the average value of at least two

independent measurements. Magnetic susceptibility balance measurements were performed with a Johnson Matthey instrument that was calibrated with $HgCo(SCN)_4$. Infrared spectra were collected on a Thermo Nicolet spectrometer. Elemental analyses were performed at Robertson Microlit Laboratories, Inc., in Madison, NJ.

Single crystals suitable for X-ray diffraction were coated with polyisobutylene oil in a drybox, transferred to a nylon loop and then quickly transferred to the goniometer head of a Bruker X8 APEX2 diffractometer equipped with a molybdenum X-ray tube (λ = 0.71073 Å). Preliminary data revealed the crystal system. A hemisphere routine was used for data collection and determination of lattice constants. The space group was identified and the data were processed using the Bruker SAINT+ program and corrected for absorption using SADABS. The structures were solved using direct methods (SHELXS) completed by subsequent Fourier synthesis and refined by full-matrix least-squares procedures.

SQUID magnetization data of crystalline powdered samples were recorded with a SQUID magnetometer (Quantum Design) at 10 kOe between 5 and 300 K for all samples. Values of the magnetic susceptibility were corrected for the underlying diamagnetic increment by using tabulated Pascal constants and the effect of the blank sample holders (gelatin capsule/straw). Samples used for magnetization measurement were recrystallized multiple times and checked for chemical composition by ^{1}H NMR spectroscopy. The program julX written by E. Bill was used for (elements of) the simulation and analysis of magnetic susceptibility data.[47]

Zero-field ^{57}Fe Mössbauer spectra were recorded on a SEE Co. Mössbauer spectrometer (MS4) at 80 K in constant acceleration mode. $^{57}Co/Rh$ was used as the radiation source. WMOSS software was used for the quantitative evaluation of the spectral parameters (least-squares fitting to Lorentzain peaks). The minimum experimental line widths were 0.23 mm/s. The temperature of the sample was

controlled by a Janis Research Co. CCS-850 He/N_2 cryostat within and accuracy of ± 0.3 K. Isomer shifts were determined relative to α-iron at 298 K.

Preparation of (^{iPr}PDAI)FeBr$_2$. A 100 mL round bottom flask was charged with 1.55 g (3.42 mmol) of ^{iPr}PDAI and 0.736 g (3.41 mmol) of $FeBr_2$. Approximately 20 mL of THF was added and the resulting reaction mixture was stirred for 16 hours producing a green solution. Pentane (50 mL) was then added to the flask and blue solid precipitated. The solid was collected by filtration and yielded 2.12 g (93%) of a dark blue powder identified as (^{iPr}PDAI)$FeBr_2$. ^{1}H NMR (CD_2Cl_2): δ = -8.07 (22 Hz), -0.67 (156 Hz, 24H, CH(C*H*$_3$)$_2$), 1.55 (9 Hz) 1.82 (14 Hz), 3.69 (14 Hz), 14.71 (24 Hz), 59.88 (44 Hz).

Preparation of (^{iPr}PDAI)Fe(η^6-C$_7$H$_8$). A 100 mL round bottom flask was charged with 9.0 g (45 mmol) of mercury and approximately 15 mL of toluene. Sodium metal (0.045 g, 1.96 mmol) was added and the slurry was amalgamated for 10 minutes. Solid (^{iPr}PDAI)$FeBr_2$ (0.500 g, 0.747 mmol) was added followed by approximately 5 mL of diethyl ether. Within 10 minutes the color of the solution changed from blue to green to brown. Approximately two minutes after the color had reached a constant brown color, the solution was decanted from the amalgam and then filtered through celite. The amalgam was washed with pentane and the wash filtered through celite. Removal of all solvent and collection of the crude material yielded 0.365 g (81%) of a brown solid identified as (^{iPr}PDAI)Fe(η^6-C_7H_8). ^{1}H NMR (cyclohexane-*d*$_{12}$): δ = 0.94 (d, 6.8 Hz, 6H, CH(C*H*$_3$)$_2$), 1.31 (d, 6.8 Hz, 12H, CH(C*H*$_3$)$_2$), 1.48 (d, 6.8 Hz, 6H, CH(C*H*$_3$)$_2$), 2.36 (s, 3H, toluene C*H*$_3$), 3.32 (sept, 6.8 Hz, 2H, C*H*(CH$_3$)$_2$), 3.40 (sept, 6.8 Hz, 2H, C*H*(CH$_3$)$_2$), 4.80 (t, 6.0 Hz, 2H, toluene *m*-C*H*), 4.87 (d, 6.0 Hz, 2H, toluene *o*-C*H*), 5.92 (t, 6.0 Hz, 1H, toluene *p*-C*H*), 6.74 (d, 8.0 Hz, 1H, *m-py*), 6.83 (t,

8.0 Hz, 1H, *p-py*), 7.22 (m, 7H, N=C*H* and *Ar*) , 7.39 (d, 8.0 Hz, 1H, *m-py*), 9.60 (s, 1H, N=C*H*). Dissolution in C_6D_6 resulted in immediate displacement of the η^6-bound toluene ligand with a molecule of C_6D_6 and formation of (^{iPr}PDAI)Fe(η^6-C_6D_6) and one equivalent of free toluene.

Preparation of (^{iPr}PDAI)Fe(η^6-C_6H_6). This compound was prepared in a similar manner to (^{iPr}PDAI)Fe(η^6-C_7H_8) with 0.500 g (0.747 mmol) of (^{iPr}PDAI), 0.45 g Na in 9.0 g of Na and approximately 15 mL of benzene. This procedure yielded 0.341 g (78%) of a brown solid identified as (^{iPr}PDAI)Fe(η^6-C_6H_6). ^{1}H NMR (benzene-d_6): δ = 0.93 (d, 6.8 Hz, 6H, CH(CH_3)$_2$), 1.32 (d, 6.8 Hz, 12H, CH(CH_3)$_2$), 1.37 (d, 6.8 Hz, 6H, CH(CH_3)$_2$), 3.44 (q, 6.8 Hz, 2H, C*H*(CH$_3$)$_2$), 3.55 (q, 6.8 Hz, 2H, C*H*(CH$_3$)$_2$), 6.57 (d, 8.0 Hz, 1H, *m-py*), 6.76 (t, 8.0 Hz, 1H, *p-py*), 7.27 (m, 7H, N=C*H* and *Ar*) , 7.74 (d, 8.0 Hz, 1H, *m-py*), 9.69 (s, 1H, N=C*H*). ^{13}C NMR (benzene-d_6): δ = 23.43 (CH(*C*H$_3$)$_2$), 24.34 (CH(*C*H$_3$)$_2$), 27.29 (CH(*C*H$_3$)$_2$), 28.32 (*C*H(CH$_3$)$_2$), 28.83 (*C*H(CH$_3$)$_2$), 118.30 (*m-py*), 120.72 (*m-py*), 123.56 (*Ar*), 124.16 (*Ar*), 125.48 (*Ar*), 127.17 (*Ar*), 127.73 (*p-py*), 128.92 (*Ar*), 138.72, 141.73, 141.87, 148.90, 150.18, 155.41, 160.77 (quaternary carbons), 164.93 (N=*C*H), one N=*C*H peak not located.

Preparation of [(^{iPr}PDAI)Fe]$_2$. The arene complex, (^{iPr}PDAI)Fe(η^6-C_7H_8), was generated as described above with 0.500 g (0.747 mmol) of (^{iPr}PDAI)FeBr$_2$, 0.045 g (1.96 mmol) of sodium metal and 9.00 g (44.9 mmol) of mercury. The resulting crude solid was dissolved in diethyl ether and stored at -35°C overnight. The solution turned green-brown and a crystalline solid formed. The crystals were collected and dried and yielded 0.165 g (43%) of a brown solid identified as [(^{iPr}PDAI)Fe]$_2$. Crystals suitable for X-ray diffraction were grown from a concentrated diethyl ether solution at -35°C. Analysis for $C_{62}H_{78}N_6Fe_2$: Calc. C, 73.08; H, 7.71; N, 8.25. Found C, 73.16; H, 7.76;

N, 7.83. Magnetic susceptibility: μ_{eff} = 4.7 μ_B (Evans Method, 293K), μ_{eff} = 4.2 μ_B (Magnetic susceptibility balance, 296K), μ_{eff} = 4.3 μ_B (SQUID, 300K). ^{1}H NMR (benzene-d_6): δ = -63.59 (50 Hz), -15.43 (15 Hz), -9.82 (42 Hz), -9.76 (26 Hz), -8.58 (13 Hz), -8.18 (20 Hz), -2.25 (17 Hz), -1.86 (17 Hz), -1.60 (22 Hz), 3.93 (19 Hz), 5.01 (16 Hz), 7.55 (21 Hz), 16.62 (15 Hz), 18.26 (106 Hz), 25.86 (25 Hz), 28.03 (18 Hz), 38.95 (25 Hz), 103.76 (27 Hz), 113.62 (35 Hz), 187.33 (158 Hz), 209.28 (61 Hz).

Preparation of (^{iPr}PDAI)Fe(η^4-C_4H_6). A thick-walled glass vessel was charged with 15.00 g (74.78 mmol) of mercury, approximately 30 mL of pentane and a stir bar. Sodium metal (0.075 g, 3.26 mmol) was added to the vessel. The resulting slurry was stirred for 20 minutes to amalgamate then 0.750 g (1.12 mmol) of solid (^{iPr}PDAI)$FeBr_2$ was added to the vessel. The vessel was transferred out of the dry box and submerged in liquid nitrogen. On the high vacuum line, the vessel was evacuated and 2000 mm Hg (10.77 mmol, ~10 eq, in 5 x 400 mm portions) of butadiene was added via calibrated gas bulb. The reaction mixture was stirred for 24 hours at room temperature during which time the solution changed from blue to orange. After 24 hours the excess butadiene was removed on the high vacuum line and the vessel was brought back into the dry box. The orange solution was decanted away from the amalgam and filtered through celite. The remaining product was extracted into diethyl ether and also filtered through celite. Recrystallization from a diethyl ether solution at -35°C yielded 0.440 g (70%) of a brown solid identified as (^{iPr}PDAI)Fe(η^4-C_4H_6). Crystals suitable for X-ray diffraction were grown from a concentrated hexane solution at -35 °C. Analysis for $C_{35}H_{45}N_3Fe$: Calc. C, 74.59; H, 8.05; N, 7.46. Found C, 73.70; H, 8.51; N, 7.42. ^{1}H NMR (benzene-d_6, 20°C): δ = 0.80 (bs, 6H, CH(C*H*$_3$)$_2$), 0.88 (bs, 6H, CH(C*H*$_3$)$_2$), 1.12 (bs, 12H, CH(C*H*$_3$)$_2$), 1.86 (bs, 2H, C*H*(CH$_3$)$_2$), 2.54 (bs, 2H, C*H*(CH$_3$)$_2$), 2.94 (bs, 2H, C_4H_6 C*H*$_2$), 3.54 (bs, 2H, C_4H_6

CH_2), 4.59 (bs, 2H, C_4H_6 CH), 6.99 (bs, 6H, *m*- and *p- Ar*), 7.48 (bs, 1H, *p-py*), 7.95 (bs, 2H, *m-py*), 8.43 (bs, 2H, N=CH). ^{1}H NMR (toluene-d_8, -40° C): δ = 0.80 (d, 6.5 Hz, 6H, CH(CH_3)$_2$), 0.91 (d, 6.5 Hz, 6H, CH(CH_3)$_2$), 1.09 (d, 6.5 Hz, 6H, CH(CH_3)$_2$), 1.14 (d, 6.5 Hz, 6H, CH(CH_3)$_2$), 1.82 (sept, 6.5 Hz, 2H, CH(CH$_3$)$_2$), 2.52 (sept, 6.5 Hz, 2H, CH(CH$_3$)$_2$), 2.78 (m, 2H, C_4H_6 CH_2), 3.39 (d, 12 Hz, 2H, C_4H_6 CH_2), 4.49 (m, 2H, C_4H_6 CH), 6.92 (d, 7.0 Hz, 2H, *m-Ar*), 6.97 (d, 7.0 Hz, 2H *m-Ar*), 7.11 (t, 2H, 7.0 Hz, *p-Ar*), 7.43 (t, 7.5 Hz, 1H, *p-py*), 7.95 (d, 7.5 Hz, 2H, *m-py*), 8.35 (s, 2H, N=CH). ^{13}C NMR (benzene-d_6, 20°C): δ = 22.79 (CH(*C*H$_3$)$_2$), 27.02 (CH(*C*H$_3$)$_2$), 27.44 (CH(*C*H$_3$)$_2$), 28.10 (*C*H(CH$_3$)$_2$), 28.65 (*C*H(CH$_3$)$_2$), 64.69 (C_4H_6 *C*H$_2$), 104.54 (C_4H_6 *C*H), 118.19 (*m-py*), 123.80 (*m-Ar*), 127.14 (*p-Ar*), 139.00, 147.89, 149.93 (quaternary carbons), 151.07 (N=*C*H), *p-py* not located.

Preparation of (^{iPr}PDAI)Fe(CO)$_2$. A thick-walled glass vessel was charged with 9.0 g (44.8 mmol) of mercury and approximately 10 mL of toluene. Sodium metal (0.045 g, 1.96 mmol) was added in pieces and the slurry amalgamated for 10 minutes. Solid (^{iPr}PDAI)FeBr$_2$ (0.500 g, 0.747 mmol) and approximately 10 mL more of toluene were added to the vessel. The vessel was immediately brought out of the drybox and submerged in liquid nitrogen. Four atmospheres of CO were added to the vessel at liquid nitrogen temperature. The reaction was then warmed to room temperature and stirred for 16 hours during which time the color changed from blue to green. The excess CO was removed and the amalgam washed with diethyl ether and filtered through celite. Recrystallization of the crude solid from pentane furnished 0.303 g (76%) of a green solid identified as (^{iPr}PDAI)Fe(CO)$_2$. Analysis for $C_{33}H_{39}N_3O_2Fe$: Calc. C, 70.09; H, 6.95; N, 7.43. Found C, 69.89; H, 6.95; N, 7.41. ^{1}H NMR (benzene-d_6): δ = 1.01 (d, 6.8 Hz, 12H, CH(CH_3)$_2$), 1.38 (d, 6.8 Hz, 12H, CH(CH_3)$_2$), 2.90 (quint, 6.8 Hz, 4 Hz, CH(CH$_3$)$_2$), 7.16 (m, 6 Hz, *m*- and *p-Ar* and *p-py*), 7.62 (d,

7.6 Hz, 2H, *m-py*), 8.20 (s, 2H, N=C*H*). ^{13}C NMR (benzene-d_6): δ = 23.29 (CH(*C*H$_3$)$_2$), 27.66 (CH(*C*H$_3$)$_2$), 28.40 (*C*H(CH$_3$)$_2$), 119.41 (*m-py*), 121.92 (*p-py*), 123.86 (*m-Ar*), 127.65 (*p-Ar*), 141.39, 145.56, 150.58 (quaternary carbons), 152.88 (N=*C*H). IR(pentane): ν(CO) 1925, 1981 cm^{-1}.

Preparation of (^{iPr}PDAI)Fe(DMAP). A 20 mL scintillation vial was charged with 0.140 g (0.248 mmol) of (^{iPr}PDAI)Fe(η^4-C$_4$H$_6$) and approximately 8 mL of diethyl ether. In a second vial, 0.030 g (0.248 mmol) of DMAP was dissolved in approximately 7 mL of diethyl ether. The DMAP solution was then added to the first vial resulting in a change in color from orange to brown. Filtration through celite and removal of the solvent yielded 0.147 g (95%) of a brown solid identified as (^{iPr}PDAI)Fe(DMAP). Crystals suitable for X-ray analysis were grown from a concentrated solution of diethyl ether at -35 °C. Analysis for C$_{38}$H$_{49}$N$_5$Fe: Calc. C, 72.25; H, 7.82; N, 11.09. Found C, 71.89; H, 7.59; N, 10.92. ^{1}H NMR (benzene-d_6): δ = 0.24 (bs, 6H, CH(C*H$_3$*)$_2$), 0.25 (bs, 6H, CH(C*H$_3$*)$_2$), 1.22 (bs, 16H, CH(C*H$_3$*)$_2$ and C*H*(CH$_3$)$_2$), 1.90 (bs, 6H, DMAP N(CH$_3$), 5.96 (bs, 2H, DMAP C*H*), 6.82 (bs, 2H, DMAP C*H*), 7.12 (d, 7.6 Hz, 4H, *m-Ar*), 7.59 (t, 7.6 Hz, 2H, *p-Ar*), 8.50 (t, 7.6 Hz, 1H, *p-py*), 12.66 (bs, 2H, *m-py*), 17.16 (bs, 2H, N=C*H*). ^{13}C NMR (benzene-d_6): δ = 22.91 (CH(*C*H$_3$)$_2$), 24.51 (CH(*C*H$_3$)$_2$), 33.07 (*C*H(CH$_3$)$_2$), 38.18 (DMAP N(*C*H$_3$)$_2$), 97.10 (DMAP *m-C*H), 110.08 (*m-py*), 123.80, 124.19, 124.67, 127.13, 139.10, 152.13, 163.52, 178.39.

Preparation of (^{iPr}PDAI)FeN(2,4,6-Me$_3$-C$_6$H$_2$). A 20 mL scintillation vial was charged with 0.105 g (0.19 mmol) of (^{iPr}PDAI)Fe(η^4-C$_4$H$_6$) and approximately 10 mL of diethyl ether. A solution of 2,4,6-trimethylphenyl azide (0.030 g, 0.19 mmol) in 3 mL of diethyl ether was added to the vial resulting in bubbling and a color change

from brown to dark blue. The solution was filtered through celite, concentrated and cooled to -35 °C to afford 0.077 g (65%) of a dark blue rectangular crystals solid identified as (^{iPr}PDAI)FeN(2,4,6-Me_3-C_6H_2). Analysis for $C_{40}H_{50}N_4Fe$: Calc. C, 74.75; H, 7.84; N, 8.72. Found C, 74.61; H, 7.93; N, 8.57. Magnetic susceptibility: μ_{eff} = 2.7 μ_B (Magnetic susceptibility balance, 23 °C). ^{1}H NMR (benzene-d_6): δ = -32.79 (95 Hz), -3.39 (9.0 Hz, CH(CH_3)$_2$), -1.93 (12 Hz, CH(CH_3)$_2$), 1.76 (7.1 Hz), 1.78 (7.3 Hz), 35.52 (15 Hz), 75.91 (46 Hz), 77.26 (28 Hz), 104.43 (59 Hz), 198.68 (160 Hz), 289.01 (320 Hz).

Preparation of (^{iPr}PDAI)FeN^{1}Ad. A 100 mL round bottom flask was charged with 0.100 g (0.098 mmol) of [(^{iPr}PDAI)Fe]$_2$ and approximately 20 mL of diethyl ether, resulting in a brown solution. A solution of 0.034 g (0.196 mmol) of 1-adamantyl azide in 10 mL of diethyl ether was added dropwise to the flask, resulting in a slow color change of the solution from brown to purple. The solution was stirred for 20 minutes then filtered through celite. The purple solution was concentrated and cooled to -35 °C to afford 0.065 g (50%) of a purple crystalline solid identified as (^{iPr}PDAI)FeN(^{1}Ad). Analysis for $C_{41}H_{54}N_4Fe$: Calc. C, 74.75; H, 8.26; N, 8.51. Found C, 74.49; H, 8.17; N, 8.30. ^{1}H NMR (benzene-d_6): δ = 0.70 (d, 6.4 Hz, 12H, CH(CH_3)$_2$), 0.82 (d, 6.4 Hz, 12H, CH(CH_3)$_2$), 1.27 (sept, 6.4 Hz, 4 H, C*H*(CH$_3$)$_2$), 1.41 (br s, 6H, adamantyl CH_2), 1.70 (d, 12 Hz, 3H, adamantyl CH_2), 1.88 (d, 12 Hz, 3H, adamantyl CH_2), 3.20 (br s, 3H, adamantyl CH_2), 6.92 (d, 8.0 Hz, 4H, *m-Ar*), 7.28 (t, 8.0 Hz, 2H, *p-Ar*), 9.50 (d, 7.6 Hz, 2H, *m-py*), 9.83 (t, 7.6 Hz, 1H, *p-py*), 13.30 (s, 2H, N=C*H*). ^{13}C NMR (benzene-d_6): 23.87 (*C*H(CH$_3$)$_2$), 23.97 (CH(*C*H$_3$)$_2$), 30.57 (adamantyl), 31.40 (CH(*C*H$_3$)$_2$), 38.02 (adamantyl), 39.01 (adamantyl), 117.36 (*m-py*), 121.25 (*p-py*), 123.90 (*m-Ar*), 126.43 (*p-Ar*), 133.81, 137.70 (N=*C*H), 148.88, 163.64, 168.34 (quaternary carbons)

REFERENCES

[1] For recent reviews see: (a) Bolm, C.; Legros, J.; Paith, J. L.; Zani, L. *Chem. Rev.* **2004**, *104*, 6217. (b) Enthaler, S.; Junge, K.; Beller, M. *Angew. Chem. Int. Ed.* **2008**, *47*, 3317. (c) Correa, A.; Mancheño, O. G.; Bolm, C. *Chem. Soc. Rev.* **2008**, *37*, 1108. d) Sherry, B. D.; Fürstner, A. *Acc. Chem. Res.* **2008**, *41*, 1500. (d) Bauer, E. B. *Curr. Org. Chem.* **2008**, *12*, 1341. (e) Enthaler, S.; Junge, K.; Beller, M. *Angew. Chem. Int. Ed.* **2008**, *47*, 3317. (f) Gaillard, S.; Renaud, J. L. *ChemSusChem.* **2008**, *1*, 505. (g) Sarhan, A. A. O.; Bolm, C. *Chem. Soc. Rev.* **2009**, *38*, 2730. (h) Czaplik, W. M.; Mayer, M.; Cvengros, J.; von Wangelin, J. *ChemSusChem.* **2009**, *2*, 396. (i) Liu, L. X. *Curr. Org. Chem.* **2010**, *14*, 1099.

[2] (a) Small, B. M.; Brookhart, M. *J. Am. Chem. Soc.* **1998**, *120*, 7143. (b) Small, B. L.; Brookhart, M.; Bennett, A. M. A. *J. Am. Chem. Soc.* **1998**, *120*, 4049.

[3] (a) Britovsek, G. J. P.; Gibson, V. C.; Kimberley, B. S.; Maddox, S. J.; Solan, G. A.; White, A. J. P.; Williams, D. J. *Chem. Commun.* **1998**, 849. (b) Britovsek, G. J. P.; Bruce, M.; Gibson, V. C.; Kimberely, B. S.; Maddox, P. J.; Mastroianni, S.; McTavish, S. J.; Redshaw, C.; Solan, G. A.; Strömberg, S.; White, A. J. P.; Williams, D. J. *J. Am. Soc.* **1999**, *121*, 8728.

[4] Bart, S. C.; Lobkovsky, E.; Chirik, P. J. *J. Am. Chem. Soc.* **2004**, *126*, 13794.

[5] Russell, S. K.; Darmon, J. M.; Lobkovsky, E.; Chirik, P. J. *Inorg. Chem.* **2010**, *49*, 2782.

[6] Trovitch, R. J.; Lobkovsky, E.; Bill, E.; Chirik, P. J. *Organometallics* **2008**, *27*, 1470.

[7] Tondreau, A. M.; Lobkovsky, E.; Chirik, P.J. *Org. Lett.* **2008**, *10*, 2789.

[8] Bouwkamp, M. W.; Bowman, A. C.; Lobkovsky, E.; Chirik, P. J. *J. Am. Chem. Soc.* **2006**, *128*, 13340.

[9] Sylvester, K. T.; Chirik, P. J. *J. Am. Chem. Soc.* **2009**, *131*, 8772.

[10] Knijnenburg, Q.; Gambarotta, S.; Budzelaar, P. H. M. *Dalton Trans.* **2006**, 5442.

[11] Chirik, P. J.; Wieghardt, K. *Science* **2010**, *327*, 794.

[12] Kuwabara, I. H.; Comninos, F. C. M.; Pardini, V. L.; Viertler, H.; Toma, H. E. *Electrochim. Acta* **1994**, *39*, 2401.

[13] Toma, H. E.; Chavez-Gil, T. E. *Inorg. Chim. Acta* **1997**, *257*, 197.

[14] de Bruin, B.; Bill, E.; Bothe, E.; Weyhermüller, T.; Wieghardt, K. *Inorg. Chem.* **2000**, *39*, 2936.

[15] Budzelaar, P. H. M.; de Bruin, B.; Gal, A. W.; Wieghardt, K.; van Lenthe, J. H. *Inorg. Chem.* **2001**, *40*, 4649.

[16] Bart, S. C.; Chlopek, K.; Bill, E.; Bouwkamp, M. W.; Lobkovsky, E.; Neese, F.; Wieghardt, K.; Chirik, P.J. *J. Am. Chem. Soc.* **2006**, *128*, 13901.

[17] Bart, S. C. Lobkovsky, E.; Bill, E.; Wieghardt, K.; Chirik, P. J. *Inorg. Chem.* **2007**, *46*, 7055.

[18] Vanadium: Vidyaratne, E.; Gambarotta, S.; Korobkov, E.; Budzelaar, P. H. M. *Inorg. Chem.* **2005**, *44*, 1187.

[19] Chromium: Vidyaratne, I.; Scott, j.; Bambarotta, S.; Budzelaar, P. H. M. *Inorg. Chem.* **2007**, *46*, 7040.

[20] Manganese: Reardon, D.; Aharonian, G.; Gambarotta, S.; Yap, G. P. A. *Organometallics* **2002**, *21*, 786.

[21] Cobalt: (a) Bowman, A. C.; Milsmann, C.; Atienza, C. C. H.; Lobkovsky, E.; Wieghardt, K.; Chirik, P. J. *J. Am. Chem. Soc.* **2010**, *132*, 1676. (b) Gibson, V. C.; Humphries, M. J.; Tellmann, K. P.; Wass, D. F.; White, A. J. P.; Williams, D. J. *Chem. Commun.* **2001**, 2252.

[22] Ruthenium: Gallagher, M.; Wieder, N. L.; Dioumaev, V. K.; Carroll, P. J.; Berry, D. H. *Organometallics* **2010**, *29*, 591.

[23] Blackmore, I. J.; Gibson, V. C.; Hitchcock, P. B.; Rees, C. W.; Williams, D. J.; White, A. J. P. *J. Am. Chem. Soc.* **2005**, *127*, 6012.

[24] Archer, A. M.; Bouwkamp, M. W.; Cortez, M. –P.; Lobkovsky, E.; Chirik, P. J. *Organometallics* **2006**, *25*, 4269.

[25] Britovsek, G. J. P.; Mastroianni, S.; Solan, G. A.; Baugh, S. P. D.; Redshaw, C.; Gibson, V. C.; White, A. J. P.; Williams, D. J.; Elsegood, M. R. J. *Chem. Eur. J.* **2000**, *6*, 2221.

[26] Small, B. L.; Brookhart, M. *Macromolecules* **1999**, *32*, 2120.

[27] Gallagher, M.; Wieder, N. L.; Dioumaev, V. K.; Carroll, P. J.; Berry, D. H. *Organometallics* **2010**, *29*, 591.

[28] Knijnenburg, Q.; Gambarotta, S.; Budzelaar, P. H. M. *Dalton Trans.* **2006**, 5442.

[29] Chaudhuri, P.; Wieghardt, K. *Prog. Inorg. Chem.* **2001**, *50*, 151.

[30] Lu, C. C.; Bill, E.; Weyhermüller, T.; Bothe, E.; Weighardt, K. *J. Am. Chem. Soc.* **2008**, *130*, 3181.

[31] Rochford, J.; Tsai, M. K.; Szaida, D. J.; Boyer, J. L.; Muckerman, J. T.; Fujita, E. *Inorg. Chem.* **2010**, *49*, 860.

[32] Blackmore, K. J.; Sly, M. B.; Haneline, M. R.; Ziller, J. W.; Heyduk, A. F. *Inorg. Chem.* **2008**, *47*, 10522.

[33] Modeled by Carsten Milsmann.

[34] Khusniyarov, M. M.; Weyhermüller, T.; Bill, E.; Wieghardt, K. *J. Am. Chem. Soc.* **2008**, *131*, 1208.

[35] (a) Hu, C.; Noll, B. C.; Schulz, C. E.; Scheidt, W. R. *Inorg. Chem.* **2010**, *ASAP*. (b) Hu, C.; Sulok, C. D.; Paulat, F.; Lehnert, N.; Twigg, A. I.; Hendrich, M. P.; Schulz, C. E.; Scheidt, W. R. *J. Am. Chem. Soc.* **2010**, *132*, 3737.

[36] Freedman, D. E.; Harman, W. H.; Harris, T. D.; Long, G. J.; Chang, C. J.; Long, J. R. *J. Am. Chem. Soc.* **2010**, *132*, 1224.

[37] Andres, H.; Bominaar, E. L.; Smith, J. M.; Eckert, N. A.; Holland, P. L.; Münck, E. *J. Am. Chem. Soc.* **2002**, *124*, 3012.

[38] Borden, W. T.; Iwamura, H.; Berson, J. A. *Acc. Chem. Res.* **1994**, *27*, 109.

[39] Neuhaus, P.; Grote, D.; Sander, W. *J. Am. Chem. Soc.* **2008**, *130*, 2993.

[40] (a) Norman, D. W.; Ferguson, J. J.; McDonald, R.; Stryker, J. M. *Organometallics* **2006**, *25*, 2705. (b) Bachler, V.; Grevels, F. –W.; Kerpen, K.; Olbrich, G.; Schaffner, K. *Organometallics* **2003**, *22*, 1696.

[41] Archer, A. M. *Masters Thesis*, Cornell University, 2006.

[42] Bart, S. C.; Lobkovsky, E.; Bill, E.; Chirik, P. J. *J. Am. Chem. Soc.* **2006**, *128*, 5302.

[43] Bowman, A. C. *Ph.D. Thesis*, Cornell University, 2010.

[44] Pangborn, A. B.; Giardello, M. A.; Grubbs, R. H.; Rosen, R. K.; Timmers, F. J. *Organometallics* **1996**, *15*, 1518.

[45] Lui, Q.; Tor, Y. *Org. Lett.* **2003**, *5*, 2571.

[46] Sur, S. K. *J. Mag. Res.* **1989**, *82*, 169-173.

[47] http://ewww.mpi-muelheim.mpg.de/bac/logins/bill/julX_en.php

CHAPTER 5

CARBON-CARBON BOND FORMING REACTIONS CATALYZED BY REDUCED BIS(IMINO)PYRIDINE IRON COMPOUNDS

5.1 Abstract

The addition of ethylene to 1,3-dienes catalyzed by a series of bis(imino)pyridine iron dinitrogen compounds, (^{R}PDI)Fe(N_2)$_2$ (^{R}PDI = 2,6-(2,6-R_2-C_6H_3-N=CMe)$_2$$C_5H_3N$; R = ^{i}Pr) and [(^{R}PDI)Fe(N_2)]$_2$(N_2) (^{R}PDI = 2,6-(2,6-R_2-C_6H_3-N=CMe)$_2$$C_5H_3N$; R = Et, Me), was studied. Depending on the substitution pattern of the diene and of the aryl groups of the bis(imino)pyridine iron dinitrogen compound, different outcomes were observed. For the case of butadiene and ethylene, a formal intermolecular [2π+2 π] cycloaddition furnished vinylcyclobutane. An intermediate on the catalytic pathway, the bis(imino)pyridine iron alkyl allyl compound (^{Me}PDI)Fe((CH$_2$)$_3$(CH)$_2$CH$_2$), was isolated and characterized by NMR and Mössbauer spectroscopies and X-ray diffraction. The metallacycle was shown to be catalytically competent for the transformation of butadiene and ethylene to vinylcyclobutane. Labeling studies with ethylene-d_4 and *cis*-d_2-ethylene were performed and are consistent with a formal [2+2] addition for butadiene plus ethylene. For the reaction of isoprene and ethylene different products were observed when different bis(imino)pyridine iron dinitrogen compounds were used. With [(^{Et}PDI)Fe(N_2)]$_2$(N_2) and [(^{Me}PDI)Fe(N_2]$_2$(N_2) formal 1,4-hydrovinylation produced 5-methyl-1,4-hexadiene; however, with (^{iPr}PDI)Fe(N_2)$_2$ the isomerized diene, 2-methyl-2,4-hexadiene, was the observed product. In another carbon-carbon bond forming reaction, the cycloisomerization of 1,5-hexadiene to methylenecyclopentane by bis(imino)pyridine iron dinitrogen compounds was also studied. In all cases, deuterium isotopic labeling studies were performed to gather mechanistic insight.

5.2 Introduction

Transition metal-mediated carbon-carbon bond forming reactions have attracted considerable interest because of their potential for use in small molecule synthesis as well as industrial processes. Hydrovinylation, the formal addition of a carbon-hydrogen bond from a vinyl group to an olefin, represents an atom-economical, stereoselective example of a carbon-carbon bond forming reaction using abundant starting materials.[1] Depending on the nature of the olefin, several different outcomes are possible. Hydrovinylation of an unconjugated olefin leads to formal 1,2-addition of the vinylic C-H bond across the olefin.[2,3,4,5,6,7,8,9,10] When the substrate is a 1,3 diene, either 1,2-addition across one double bond[11] or 1,4-addition across the conjugated diene can be observed.[12,13] Most hydrovinylation reactions have relied on nickel[2,3,4,11] and palladium[6] based catalysts, although examples of ruthenium,[7] rhodium[8] and iridium[9] catalysts have also been reported. However, as concerns about sustainability and the environment grow, interest in replacing precious metal catalysts with more abundant, relatively non-toxic metals also increases. Recently, several reports of cobalt-catalyzed hydrovinylation reactions,[12,13] including the asymmetric hydrovinylation of unactivated linear 1,3-dienes,[13] have been reported.

Iron compounds have also been shown to be efficient catalysts for carbon-carbon bond forming reactions.[14,15,16,17] In the 1960's, Hata reported the addition of ethylene to several 1,3-dienes catalyzed by an $Fe(acac)_3/Et_3Al$ mixture in an autoclave at ethylene pressures greater than 500 psi.[18] When the diene was 1,3-butadiene, *cis*-1,4-hexadiene was formed exclusively. However, when asymmetric dienes were used, both possible regioisomers of the corresponding products were formed. For example, the reaction of ethylene and isoprene afforded an approximately 1:1 mixture of 4-methyl-1,4-hexadiene and 5-methyl-1,4-hexadiene. In the 1980's, Takacs and coworkers reported that the addition of allylic ethers to several 1,3-dienes results in

formal [4 + 4] ene reactions across the diene or net 1,4 insertion of the diene into a C-H bond of the allylic ether when 2,2'-bipyridine was added to the $Fe(acac)_3/Et_3Al$ mixture.[19] In 1985, tom Dieck and coworkers reported the dimerization and trimerization of 1,3-butadiene to yield vinylcyclohexene and cycloctadiene using iron diimine catalysts.[20]

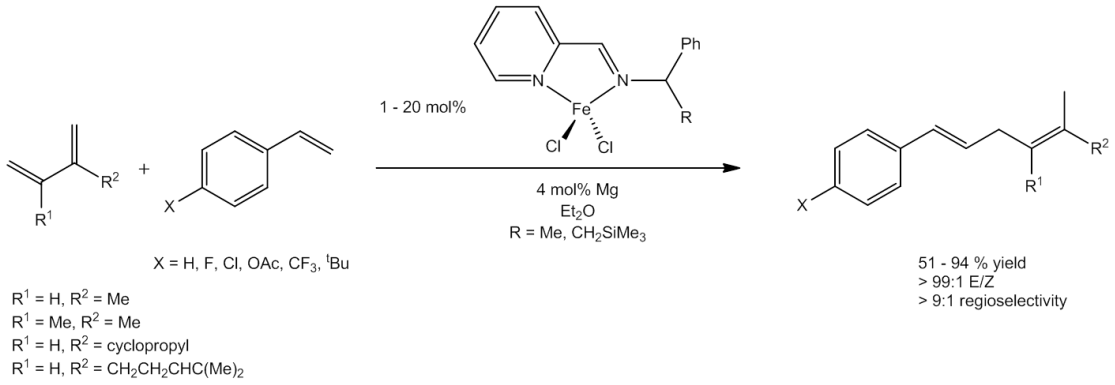

Figure 5.1 Iminopyridine iron-catalyzed 1,4-hydrovinylation.

More recently, Ritter and coworkers have demonstrated iron-catalyzed 1,4-hydrovinylation reactions using two well defined iron(II) iminopyridine dichloride pre-catalysts (Figure 5.1).[21] Activating the iron pre-catalysts with magnesium metal in the presence of a 1,3-diene and a styrene derivative afforded the *E*-isomer of the corresponding linear 1,4-diene addition product. Labeling experiments supported formal 1,4-addition of the α-olefin to the 1,3-diene. The proposed mechanism for this reaction begins with reduction of the iron(II) pre-catalyst, allowing for coordination of the diene and styrene to the iron center. Oxidative coupling forms an iron(II) alkyl allyl complex which undergoes a π-σ rearrangement followed by β-hydrogen elimination to afford an iron(II) alkyl hydride complex. Reductive elimination from this species furnishes the 1,4-hexadiene.

The bis(imino)pyridine iron bis(dinitrogen) compound, (^{iPr}PDI)Fe(N_2)$_2$,[22] has been shown to catalyze the [2π + 2π] cycloisomerization of α,ω-dienes to form a family of bicycle[0.2.3]heptane derivatives .[23] The iron catalyst is tolerant of amine and ester groups, and cyclizes the hydrocarbon 1,6-heptadiene efficiently. Also reported was the cyclization of 1,5-hexadiene by the bis(imino)pyridine iron dihydrogen compound, (^{iPr}PDI)Fe(η^2-H_2)$_2$, to methylenecyclopentane.[22] Accordingly, the bis(dinitrogen) complex (^{iPr}PDI)Fe(N_2)$_2$ catalyzes the same cyclization of 1,5-hexadiene under 0.5 atmospheres of H_2; however, the hydrogenation products, n-hexane and methylcyclopentane, were also formed. Because of their improved catalytic olefin hydrogenation activities,[24] the dimeric bis(imino)pyridine iron dinitrogen compounds with smaller aryl substituents were screened as catalysts for several C-C bond forming reactions.

5.3 Formal [2π + 2π] Addition of Butadiene and Ethylene

The three symmetrically 2,6-disubstituted dinitrogen complexes, [(^{Me}PDI)Fe(N_2)]$_2$(μ_2-N_2), [(^{Et}PDI)Fe(N_2)]$_2$(μ_2-N_2) and (^{iPr}PDI)Fe(N_2)$_2$ (^{R}PDI = 2,6-(2,6-R_2-C_6H_3-N=CMe)$_2$$C_5H_3N$; R = Me, Et, ^{i}Pr), were screened as catalysts for the addition of ethylene to butadiene. Exposing an equimolar mixture of butadiene and ethylene to 2.5 mol% [(^{Me}PDI)Fe(N_2)]$_2$(μ_2-N_2) in benzene-d_6 for 16 hours resulted in complete conversion of the starting materials to vinylcyclobutane and not the expected 1,4-hydrovinylation product, 1,4-hexadiene (Figure 5.2). Under the same reaction conditions, [(^{Et}PDI)Fe(N_2)]$_2$(μ_2-N_2) and (^{iPr}PDI)Fe(N_2)$_2$ required 16 and 24 hours to reach completion, respectively. In all three cases, vinylcyclobutane was the only addition product formed, and no evidence for 1,4-hexadiene was observed. For [(^{Et}PDI)Fe(N_2)]$_2$(μ_2-N_2) and (^{iPr}PDI)Fe(N_2)$_2$, small amounts of ethane were also

observed by ^{1}H NMR, suggesting that transfer hydrogenation from the bis(imino)pyridine ligand to ethylene also occurs.[25]

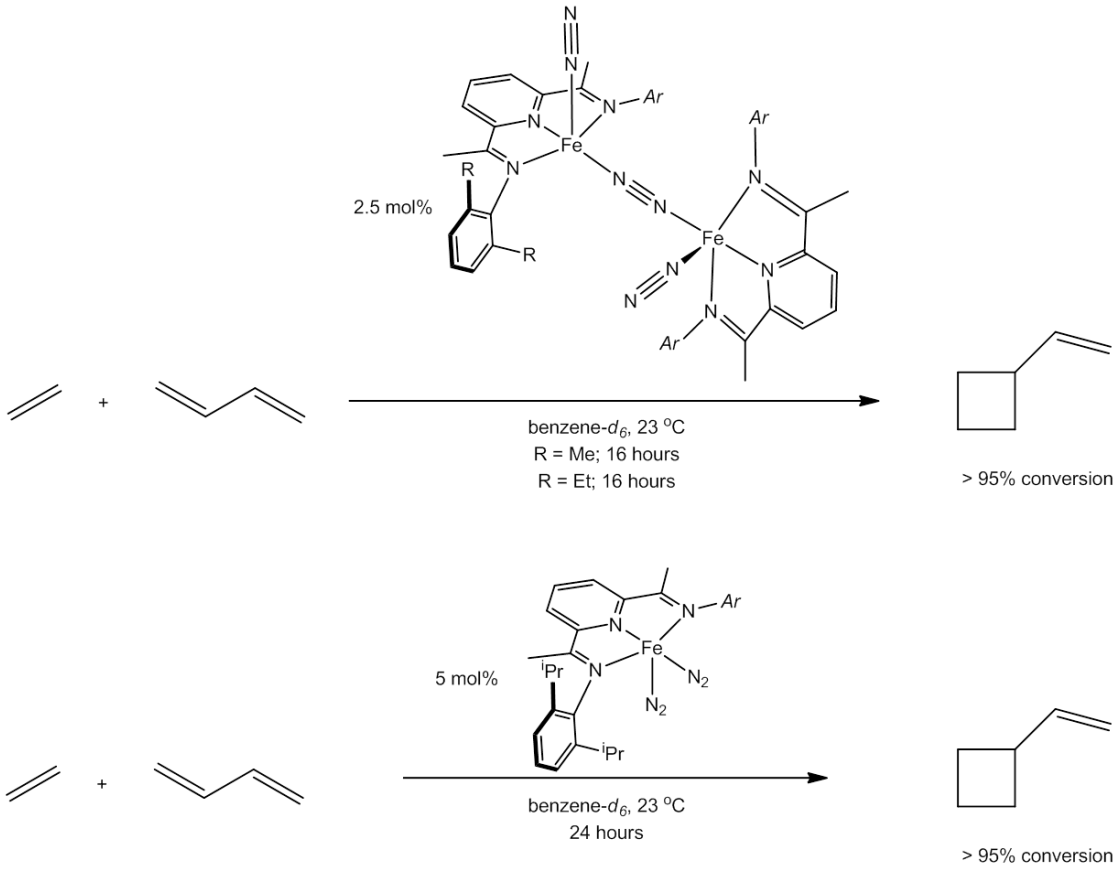

Figure 5.2 Transformation of butadiene and ethylene to vinylcyclobutane catalyzed by bis(imino)pyridine iron dinitrogen and butadiene compounds.

The corresponding bis(imino)pyridine iron η^4-butadiene compounds, (^{R}PDI)Fe(η^4-C_4H_6) (R = Me, Et, ^{i}Pr), were also competent catalysts for the formation of vinylcyclobutane and exhibited the same reaction times as their dinitrogen counterparts. This similarity was expected as addition of butadiene to the bis(imino)pyridine iron dinitrogen compounds affords the butadiene derivative immediately.[22] Because the bis(imino)pyridine iron butadiene compounds proved to

be viable catalysts, the aldimine-based iron butadiene compound was also screened. Exposing an equimolar mixture of butadiene and ethylene to 5 mol% (^{iPr}PDAI)Fe(η^4-C_4H_6) (^{iPr}PDAI = 2,6-(2,6-$^{i}Pr_2$-C_6H_3-N=CH)$_2C_5H_3N$) in benzene-d_6 resulted in complete conversion of the starting materials to vinylcylobutane in 48 hours. As with [(^{Et}PDI)Fe(N_2)]$_2$(μ_2-N_2) and (^{iPr}PDI)Fe(N_2)$_2$, a small amount of ethane was also observed with the product.

The product, vinylcyclobutane, was characterized by NMR spectroscopy and mass spectrometry. The benzene-d_6 ^{1}H NMR spectrum of vinylcyclobutane exhibits a multiplet at 2.80 for the allylic proton as well as characteristic resonances for the α-olefin. The ^{13}C NMR spectrum confirms the presence of only three inequivalent sp^3-carbon atoms, consistent with a four-membered ring. Mass spectrometry was also obtained on the organic product and an m/z value of 82.14 was obtained.

Although 1,4-hexadiene was not observed as a product of the addition of butadiene and ethylene for any of the catalysts screened, one possible mechanism for the formation of vinylcyclobutane involves first the 1,4-addition of ethylene to butadiene to afford 1,4-hexadiene, followed by a rapid cycloisomerization to form the observed product. To test the viability of this pathway, 1,4-hexadiene was stirred under a dinitrogen atmosphere with 2.5 mol% [(^{Me}PDI)Fe(N_2)]$_2$(μ_2-N_2) in benzene-d_6 for 16 hours. Examination of the organic product by ^{1}H NMR showed starting material and 2,4-hexadiene in an approximately 1:1 ratio. This isomerization is not surprising as (^{iPr}PDI)Fe(N_2)$_2$ has been reported to isomerize 1-hexene, likely by an iron allyl hydride mechanism.[22] No evidence of any vinylcyclobutane was observed, ruling out 1,4-addition followed by cycloisomerization as a possible mechanism.

In order to provide some mechanistic insight on the formal [2+2] cycloaddition of butadiene and ethylene, attempts at observation of an intermediate were made. Addition of three equivalents of ethylene to a benzene-d_6 solution of (^{Me}PDI)Fe(η^4-

C_4H_6) resulted in a color change of the solution to yellow and observation of a new diamagnetic C_1 symmetric product. Repeating the reaction on a larger scale in diethyl ether allowed isolation of the bis(imino)pyridine iron alkyl allyl complex, (^{Me}PDI)Fe($(CH_2)_3(CH)_2CH_2$) (Figure 5.3). The C_1 symmetry of (^{Me}PDI)Fe($(CH_2)_3(CH)_2CH_2$) is evident in the ^{1}H NMR spectrum by the presence of six singlets between 1.20 and 2.05 ppm, one for each aryl and imine methyl group. The fact that these peaks, along with the *meta*-pyridine resonances at 7.80 and 8.00 ppm, are very close to their diamagnetic reference values indicates very little contribution from temperature independent paramagnetism, and hence, a low-lying triplet excited state, in (^{Me}PDI)Fe($(CH_2)_3(CH)_2CH_2$).[26] The resonances for the two hydrogen atoms of the methylene group directly attached to the iron center appear upfield at -0.12 and 0.43 ppm and the remaining resonances of the hydrocarbon chain appear between 1.82 and 5.80 ppm.

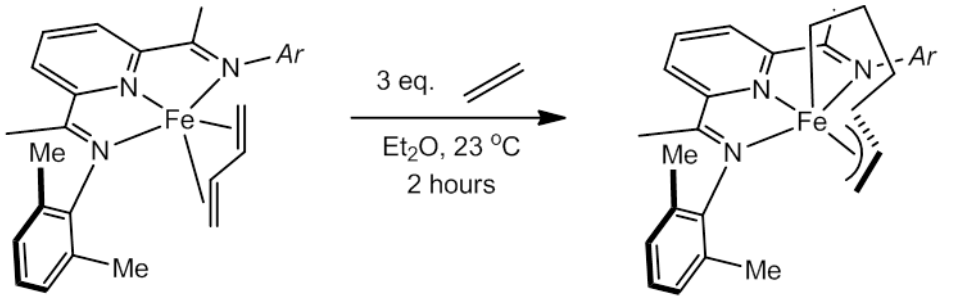

(^{Me}PDI)Fe(C_4H_6) (^{Me}PDI)Fe($(CH_2)_3(CH)_2CH_2$)

Figure 5.3 Synthesis of (^{Me}PDI)Fe($(CH_2)_3(CH)_2CH_2$).

Single crystals of (^{Me}PDI)Fe($(CH_2)_3(CH)_2CH_2$) suitable for X-ray diffraction were obtained from a concentrated diethyl ether solution at -35 °C. A representative solid state structure is presented in Figure 5.4 and selected bond lengths and angles are

reported in Table 5.1. The solid state geometry of (^{Me}PDI)Fe($(CH_2)_3(CH)_2CH_2$) is best described as square pyramidal with the chelate and the center carbon of the coordinated allyl in the basal plane and the alkyl-coordinated end of the hydrocarbon group in the apical position. The short Fe-N chelate distances indicate that the iron center in the metallacycle is likely either intermediate or low spin. A bis(imino)pyridine iron allyl complex, (^{iPr}PDI)Fe(CH_2CHCH_2), has been previously reported and the Fe-C bond distances of 2.155(4), 2.074(3) and 2.151(3) Å are similar to the Fe(1)-C(29), Fe(1)-C(30) and Fe(1)-C(31) distances of 2.155(5), 2.096(4) and 2.149(2), respectively.[27] Similarly, several bis(imino)pyridine iron mono- and dialkyl complexes have been crystallographically characterized and the Fe(1)-C(26) bond length of 2.080(2) Å falls within the range of observed Fe-C bond lengths.[28]

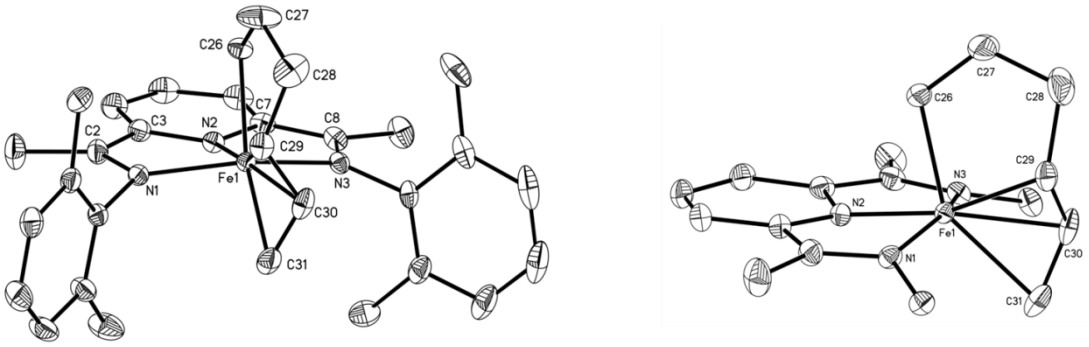

Figure 5.4 Solid state structure of (^{Me}PDI)Fe($(CH_2)_3(CH)_2CH_2$) at 30% probability ellipsoids. Hydrogen atoms omitted for clarity.

It has been well-documented that the bond distortions in the bis(imino)pyridine chelate are diagnostic of redox-activity.[29] The N_{imine}-C_{imine} and C_{imine}-C_{ipso} bond distances in (^{Me}PDI)Fe($(CH_2)_3(CH)_2CH_2$) are most consistent with a two-electron reduced chelate. The N(1)-C(2) and N(3)-C(8) bonds are elongated to 1.333(2) and 1.330(2) Å, respectively, while the C(2)-C(3) and C(7)-C(8) bond are contracted to 1.419(3) and 1.417(3) Å, respectively.

Table 5.1 Selected bond distances (Å) and angles (°) for (^{Me}PDI)Fe((CH$_2$)$_3$(CH)$_2$CH$_2$).

Fe(1)-N(1)	1.990(2)	C(26)-C(27)	1.505(3)
Fe(1)-N(2)	1.841(1)	C(27)-C(28)	1.453(4)
Fe(1)-N(3)	1.979(2)	C(28)-C(29)	1.524(7)
Fe(1)-C(26)	2.080(2)	C(29)-C(30)	1.372(10)
Fe(1)-C(29)	2.155(5)	C(30)-C(31)	1.341(6)
Fe(1)-C(30)	2.096(4)		
Fe(1)-C(31)	2.149(2)	N(2)-Fe(1)-C(26)	84.13(7)
N(1)-C(2)	1.333(2)	N(2)-Fe(1)-C(30)	164.03(17)
N(3)-C(8)	1.330(2)	C(26)-Fe(1)-C(30)	107.00(17)
C(2)-C(3)	1.419(3)		
C(7)-C(8)	1.417(3)	Fe deviation from N(1), N(2), N(3) plane	0.259

The bis(imino)pyridine iron alkyl allyl compound was also studied by zero-field ^{57}Fe Mössbauer spectroscopy and a representative spectrum is presented in Figure 5.5. The narrow quadrupole splitting (ΔE_Q) of $\left|0.63\right|$ mm/s is similar to that reported for (^{Me}PDI)Fe(η^4-C$_4$H$_6$), suggesting that the two compounds have similar electron distributions. The isomer shift (δ) of 0.27 mm/s is very similar to the isomer shift of 0.28 mm/s observed for the bis(imino)pyridine iron dialkyl, (^{iPr}PDI)FeCH$_2$SiMe$_3$, which is described as having an iron(III) center.[30] Based on the crystal structure parameters, (^{Me}PDI)Fe((CH$_2$)$_3$(CH)$_2$CH$_2$) should be described as a low or intermediate spin iron(IV) center with a doubly reduced chelate and two X-type ligands. However, a better description of the electron structure is likely a resonance

structure between an iron(II) compound and an iron(IV) compound. This would result in an isomer shift consistent with an iron(III) center.

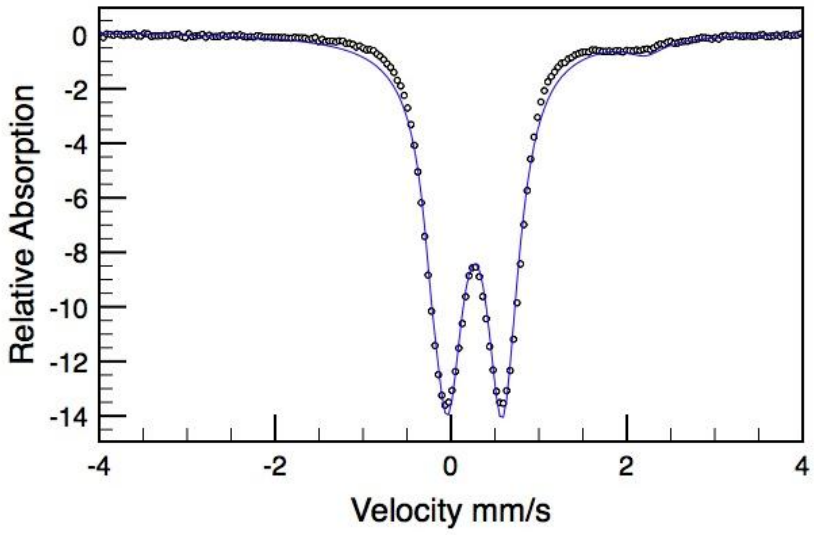

Figure 5.5 Zero-field ^{57}Fe Mössbauer spectrum of (^{Me}PDI)Fe((CH$_2$)$_3$(CH)$_2$CH$_2$) collected at 80K; δ = 0.27 mm/s, ΔE_Q = $\left|0.65\right|$ mm/s.

The thermal stability of (^{Me}PDI)Fe((CH$_2$)$_3$(CH)$_2$CH$_2$) was evaluated by allowing a benzene-d_6 solution of the metallacycle to stand at 23 °C for several days under a dinitrogen atmosphere. Observation by ^{1}H NMR spectroscopy over this time period demonstrated that the metallacycle slowly lost ethylene and converted back to (^{Me}PDI)Fe(η^4-C$_4$H$_6$) with no production of vinylcyclobutane. Warming a benzene-d_6 solution of (^{Me}PDI)Fe((CH$_2$)$_3$(CH)$_2$CH$_2$) to 65 ºC for 16 hours resulted in decomposition of the iron compound with no vinylcyclobutane observed by ^{1}H NMR spectroscopy. These experiments establish that C-C reductive elimination to form vinylcyclobutane does not proceed directly from (^{Me}PDI)Fe((CH$_2$)$_3$(CH)$_2$CH$_2$).

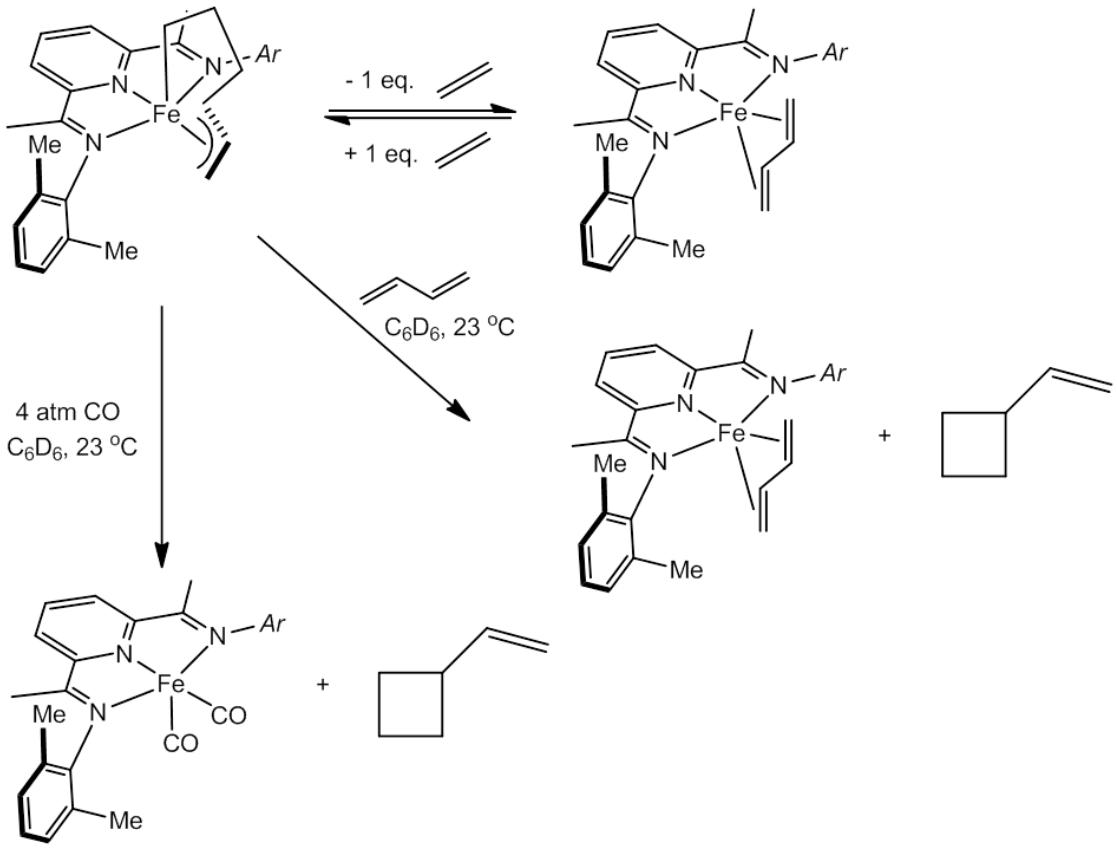

Figure 5.6 Reactivity of (^{Me}PDI)Fe((CH$_2$)$_3$(CH)$_2$CH$_2$).

The lack of thermal reductive elimination from (^{Me}PDI)Fe((CH$_2$)$_3$(CH)$_2$CH$_2$) prompted exploration of ligand-induced pathways. Addition of one atmosphere of carbon monoxide to a benzene-*d*$_6$ solution of (^{Me}PDI)Fe((CH$_2$)$_3$(CH)$_2$CH$_2$) cleanly induced C-C bond formation and generated vinylcyclobutane and the iron dicarbonyl compound, (^{Me}PDI)Fe(CO)$_2$.[24] Hydrogenation (1 atm, 16 hours, 23 ºC) of (^{Me}PDI)Fe((CH$_2$)$_3$(CH)$_2$CH$_2$) produced a similar outcome as ethylcyclobutane was observed, consistent with the initial formation of vinylcyclobutane followed by rapid alkene hydrogenation.[16] In chemistry more relevant to catalytic turnover, treatment of (^{Me}PDI)Fe((CH$_2$)$_3$(CH)$_2$CH$_2$) with excess butadiene also liberated vinylcyclobutane

with concomitant formation of the iron butadiene compound, (^{Me}PDI)Fe(η^4-C_4H_6) (Figure 5.6).

Deuterium labeling studies were performed to gain insight into the mechanism of the reaction and to evaluate the involvement of the bis(imino)pyridine ligand during the reaction. Characterization of the volatiles of the reaction of 1,3-butadiene and ethylene-d_4 in benzene-d_6 with 2.5 mol% [(^{Me}PDI)Fe(N_2)]$_2$(μ_2-N_2) after 16 hours yielded vinylcyclobutane-d_4 where the deuterium label was only present in the 2 and 3 positions of the cyclobutane ring (Figure 5.7). The products of the reaction were studied by ^{1}H, ^{2}H and ^{13}C NMR spectroscopy. The four inequivalent deuterium atoms of the cyclobutane ring appeared as four separate peaks between 1.50 and 2.00 ppm in the benzene ^{2}H NMR spectrum. Accordingly, these peaks are diminished in the benzene-d_6 ^{1}H NMR spectrum. The resonances for the corresponding carbons of the cyclobutane ring at 19.10 and 28.84 ppm show splitting from J^1 couplings to two distinct deuterium atoms to the point that the peak at 28.84 ppm is about half its original intensity and the peak at 19.10 ppm is broadened into the baseline.

The formal [$2\pi + 2\pi$] reaction was also performed with *cis*-d_2-ethylene to investigate the possibility of scrambling during the catalysis which would indicate formation of a transient iron-hydride species. Investigation of the volatiles of the reaction of 1,3-butadiene and *cis*-d_2-ethylene in benzene-d_6 with 2.5 mol% [(^{Me}PDI)Fe(N_2)]$_2$(μ_2-N_2) after 16 hours showed vinylcyclobutane-d_2 where the deuterium label is only present in the 2 and 3 positions of the cyclobutane ring (Figure 5.7). Similar to the ethylene-d_4 experiment, the ^{2}H NMR spectrum of the products shows four resonances for the same four positions of the cyclobutane ring. This potentially arises from the lack of facial selectivity for addition of the ethylene molecule to butadiene, yielding both possible diasteromers where the deuterium atoms remain *cis*. Alternatively, if scrambling did occur, the two diastereomers of *trans*-2,3-

d_2-vinylcyclobutane would also produce the same ^{2}H NMR spectrum. Unfortunately, because of overlap of the proton signal in the ^{1}H NMR, it is difficult to measure coupling constants to provide a better picture of the *cis/trans* arrangement of the remaining hydrogens.

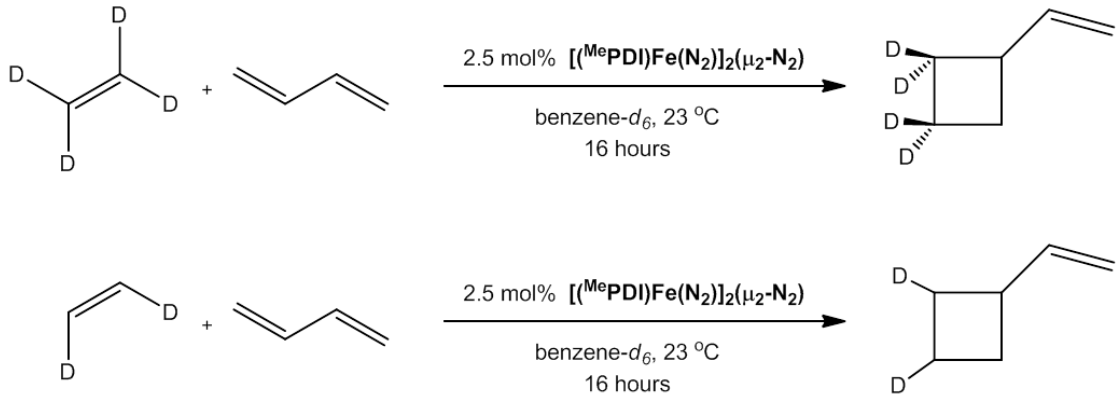

Figure 5.7 Labeling studies with ethylene-d_4 and *cis*-d_2-ethylene.

Notably, in both labeling experiments, deuterium incorporation into the aryl methyl groups of the ^{Me}PDI ligand was observed. This indicates that aryl substituent cyclometallation occurs during catalytic turnover. To further study the deuterium incorporation, 3 equivalents of C_2D_4 were added to (^{Me}PDI)Fe($(CH_2)_3(CH)_2CH_2$) and the reaction monitored by ^{1}H and ^{2}H NMR. Deuterium incorporation was observed in the C(α) and C(β) positions of the metallacycle as well as in the aryl methyl substituents within the first 15 minutes. In a control experiment, 3 equivalents of C_2D_4 were added to [(^{Me}PDI)FeN_2]$_2$(μ_2-N_2) and, again, analysis of the the ^{1}H and ^{2}H NMR spectra after 15 minutes revealed incorporation into the aryl methyl substituents, demonstrating that cyclometallation can occur from the corresponding iron ethylene compound as well.

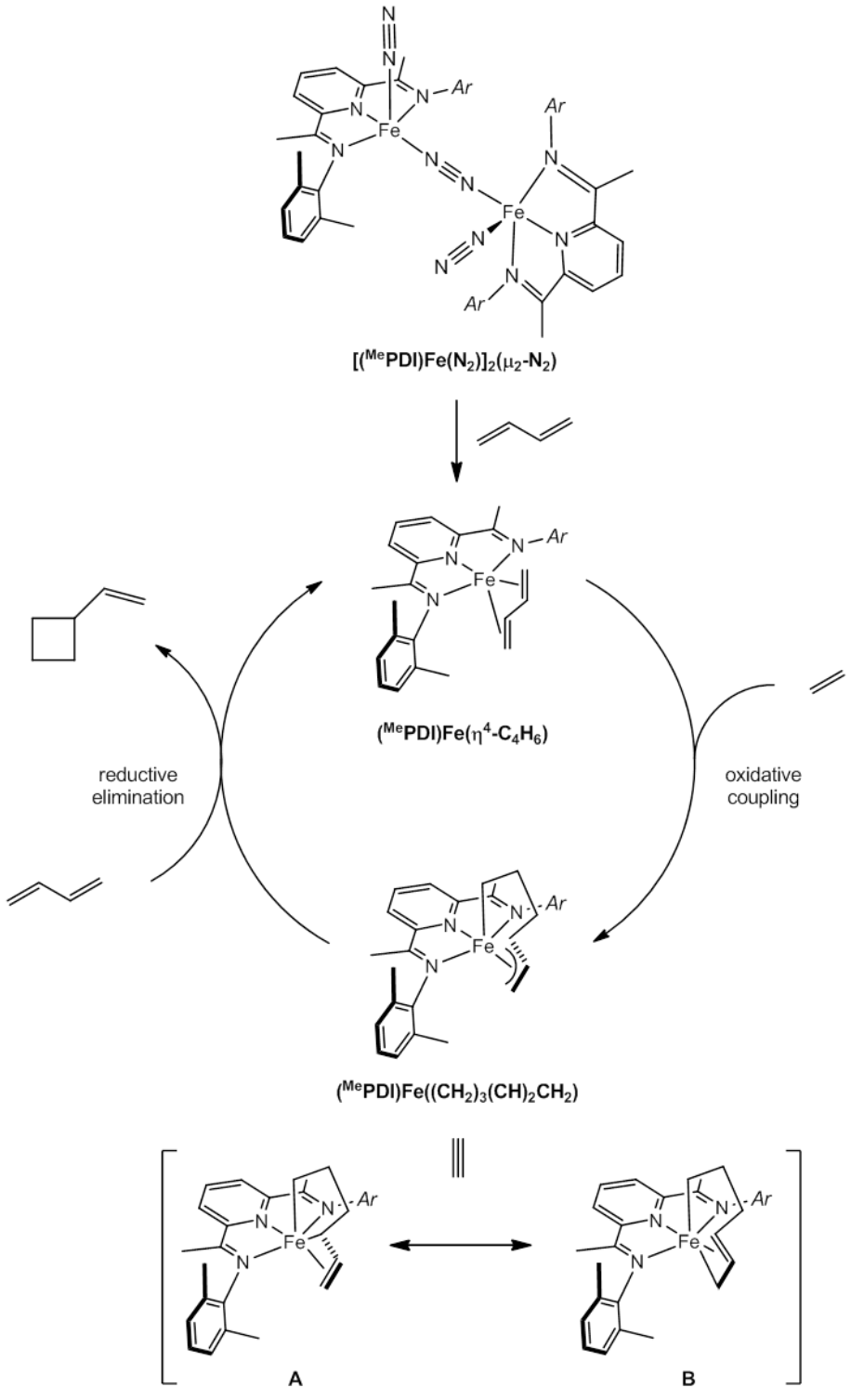

Figure 5.8 Proposed catalytic cycle for formation of vinylcyclobutane.

A proposed catalytic cycle for the transformation of butadiene and ethylene to vinylcyclobutane is presented in Figure 5.8. First, the N_2 ligands in $[(^{Me}PDI)Fe(N_2)]_2(\mu_2\text{-}N_2)$ are displaced by butadiene, forming $(^{Me}PDI)Fe(\eta^4\text{-}C_4H_6)$. The next step is likely ethylene coordination to the iron center, possibly with either a change from η^4 to η^2-coordination of the butadiene ligand or κ^3 to κ^2-coordination of the bis(imino)pyridine chelate ligand. The observed intermediate, $(^{Me}PDI)Fe((CH_2)_3(CH)_2CH_2)$, is formed by iron-promoted oxidative coupling of ethylene and butadiene, which is also proposed by Ritter in the mechanism for 1,4-hydrovinylation.[21] Excess butadiene in solution then induces reductive elimination from resonance structure **A** of the alkyl allyl complex and furnishes vinylcyclobutane and reforms $(^{Me}PDI)Fe(\eta^4\text{-}C_4H_6)$. Monitoring the reaction by ^1H NMR spectroscopy reveals only the organic starting materials and products and $(^{Me}PDI)Fe((CH_2)_3(CH)_2CH_2)$. This observation and the fact that the iron alkyl allyl compound is relatively stable in solution suggest that the final reductive elimination is the turnover limiting step and is caused by the coordination of external ligands such as butadiene and carbon monoxide.

5.4 1,4-Hydrovinylation of Isoprene with Ethylene

Because of the interesting chemistry observed with butadiene and ethylene catalyzed by bis(imino)pyridine iron compounds, studies into the scope of the reaction were performed. Changing the diene from butadiene to isoprene (2-methyl-butadiene) and performing the catalytic reaction under the same conditions produced different results. Exposure of an equimolar mixture of isoprene and ethylene to 2.5 mol% $[(^{Me}PDI)Fe(N_2)]_2(\mu_2\text{-}N_2)$ in benzene-d_6 for 16 hours resulted in complete conversion to one new organic product. Analysis of the volatiles by NMR spectroscopy and mass spectrometry revealed the identity of the product to be 5-methyl-1,4-hexadiene from

1,4-addition of ethylene to isoprene (Figure 5.9). This is consistent with the major product observed by Ritter in the iron-catalyzed 1,4-hydrovinylation reaction of styrene and isoprene and carbon-carbon bond formation at the least hindered olefin in isoprene.[21] No evidence for 4-methyl-1,4-hexadiene, the regioisomer from carbon-carbon bond formation at the germinal olefin of isoprene, was observed by NMR spectroscopy. In an attempt to isolate the pure hydrocarbon product without residual solvent or iron species, the catalysis was performed in neat isoprene. Addition of a slight excess of ethylene to a thick-walled glass vessel charged with isoprene and 0.3 mol% [(^{Me}PDI)Fe(N_2)]$_2$(μ_2-N_2) followed by stirring the solution for 20 hours at 23 °C and transfer of the volatiles to a separate glass vessel afforded clean 5-methyl-1,4-hexadiene in near quantitative yield.

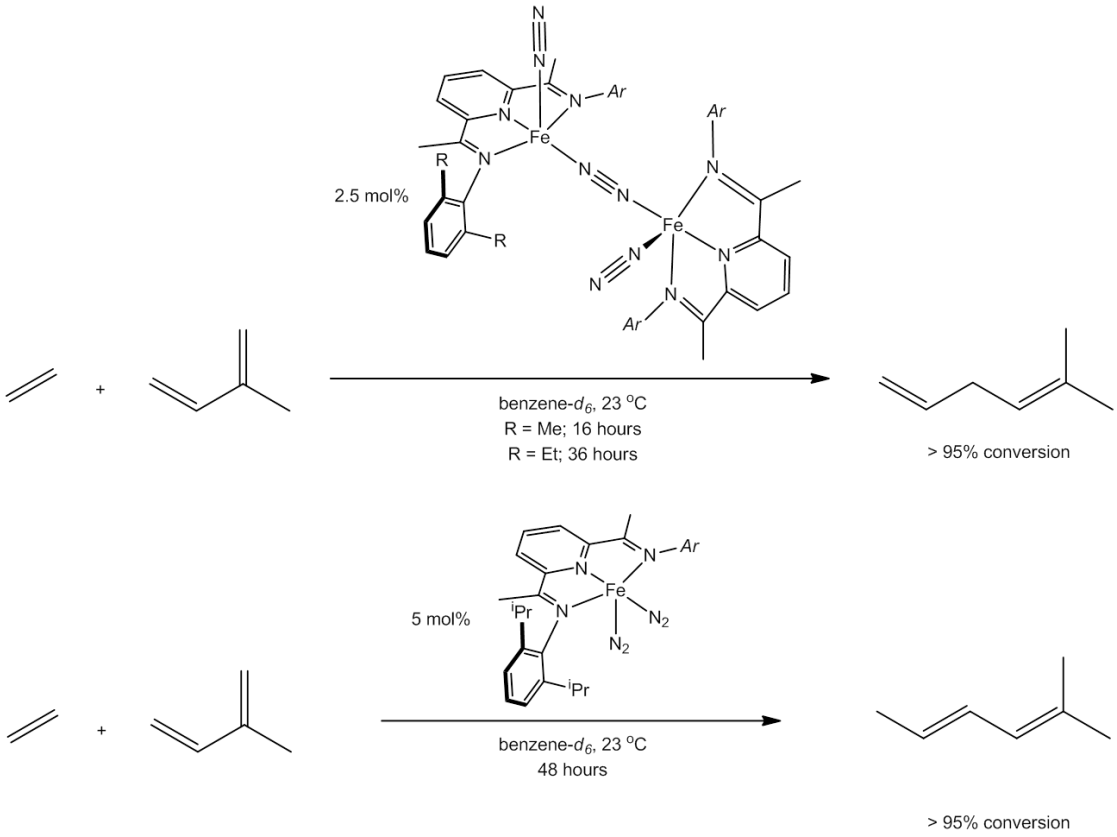

Figure 5.9 1,4-Hydrovinylation of isoprene catalyzed by bis(imino)pyridine iron dinitrogen compounds.

The larger bis(imino)pyridine iron dinitrogen compounds, [(^{Et}PDI)Fe(N_2)]$_2$(μ_2-N_2) and (^{iPr}PDI)Fe(N_2)$_2$, were also screened for the addition of ethylene to isoprene. Performing the reaction with 2.5 mol% [(^{Et}PDI)Fe(N_2)]$_2$(μ_2-N_2) in benzene-d_6 furnished 5-methyl-1,4-hexadiene in near quantitative yield after 36 hours at room temperature. Under the same reaction conditions, (^{iPr}PDI)Fe(N_2)$_2$ reached >95% conversion after 48 hours, but yielded a different product. Analysis of the volatiles from the (^{iPr}PDI)Fe(N_2)$_2$-catalyzed reaction revealed formation of exclusively the conjugated isomer, 2-methyl-2,4-hexadiene (Figure 5.9). To determine how the observed product was formed, isolated 5-methyl-1,4-hexadiene was added to **(^{iPr}PDI)Fe(N_2)$_2$** in benzene-d_6 and the reaction was monitored by ^{1}H NMR. Checking the reaction after one hour revealed that all of the 5-methyl-1,4-hexadiene had been isomerized to 2-methyl-2,4-hexadiene, suggesting that 5-methyl-1,4-hexadiene is the initial product formed, but is then rapidly isomerized by the bis(imino)pyridine iron species in solution (Figure 5.10).

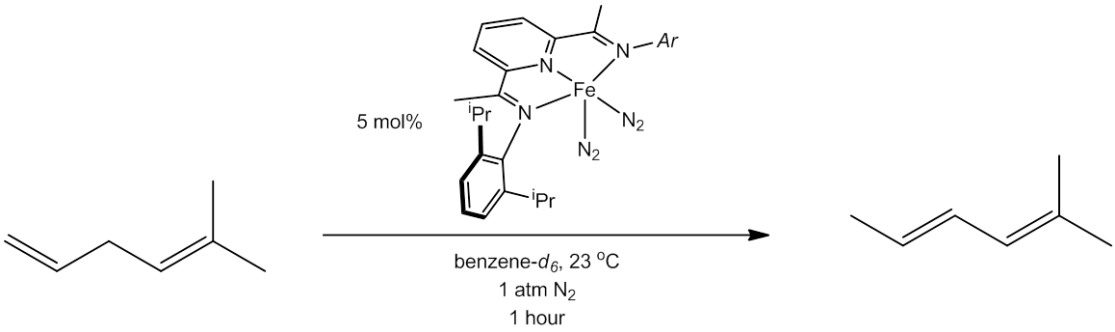

Figure 5.10 Isomerization of 5-methyl-1,4-hexadiene to 2-methyl-2,4-hexadiene by (^{iPr}PDI)Fe(N_2)$_2$.

Deuterium labeling experiments were performed to provide some mechanistic insight into 5-methyl-1,4-hexadiene formation. Analysis of the volatiles of the

reaction of ethylene-d_4 and isoprene catalyzed by 2.5 mol% [(^{Me}PDI)Fe(N_2)$_2$]$_2$(μ_2-N_2) by ^{1}H, ^{2}H and ^{13}C NMR spectroscopy revealed formation of 5-methyl-1,4-hexadiene as well as several minor, as yet, unidentified products. As expected from the proposed mechanism (*vide infra*) deuterium incorporation was observed in all three positions of the terminal olefin as well as in one methyl group (Figure 5.11). Analysis of the bis(imino)pyridine ligand by ^{2}H NMR spectroscopy revealed no deuterium incorporation into the aryl methyl groups. In contrast to this, when a similar deuterium labeling experiment was performed with (^{iPr}PDI)Fe(N_2)$_2$ as the pre-catalyst, significant deuterium incorporation into the isopropyl methyl groups was observed. This scrambling likely occurred during the isomerization of the initial 5-methyl-1,4-hexadiene to the observed product as some scrambling was also observed in the 3 position of the 2-methyl-2,4-hexadiene (Figure 5.11).

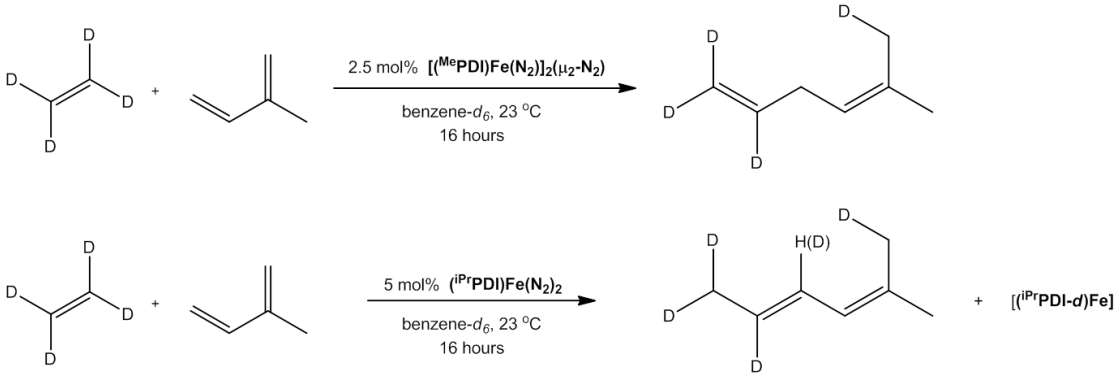

Figure 5.11 Deuterium labeling experiments with ethylene-d_4 and isoprene.

The proposed catalytic cycle for the [(^{Me}PDI)Fe(N_2)$_2$]$_2$(μ_2-N_2) catalyzed transformation is shown in Figure 5.12, and is similar to the one proposed by Ritter for iron-catalyzed 1,4-hydrovinylation reactions. As in the proposal for vinylcyclobutane formation, the first step is likely displacement of the dinitrogen ligands by the diene, isoprene. Ethylene then coordinates to the iron center and an oxidative coupling

reaction produces intermediate **1**, the methylated analog of (^{Me}PDI)Fe((CH$_2$)$_3$(CH)$_2$CH$_2$). The pathway now deviates from that of vinylcyclobutane formation and instead of reductive elimination, **1** undergoes a β-hydrogen elimination to form the iron allyl hydride, **2**. Several factors may play a part in the diverging pathways. For vinylcyclobutane formation, there is evidence that the reductive elimination is induced by butadiene coordination. The extra methyl group in isoprene relative to butadiene may cause enough steric hindrance on both intermediate **1** and on the incoming isoprene molecule that β-hydrogen elimination becomes competitive. A σ,π-rearrangement isomerizes intermediate **2** to **3**, and from **3** a reductive elimination forms the observed organic product.

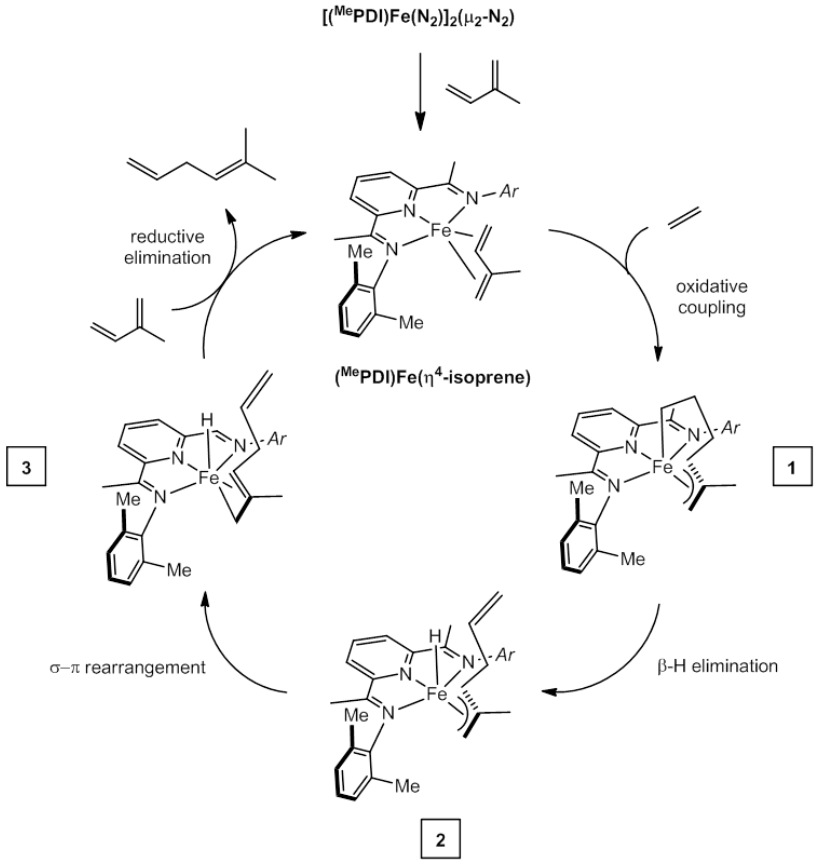

Figure 5.12 Proposed catalytic cycle for the formation of 5-methyl-1,4-hexadiene by iron-catalyzed 1,4-hydrovinylation.

5.5 Catalytic Cyclization of 1,5-Hexadiene

While investigating reactions involving dienes, the cycloisomerization reaction of 1,5-hexadiene to form methylenecyclopentane was observed. Ziegler first reported the observation of this reaction in 1956 when he noted that dialkyl aluminum hydride reagents catalyzed the formation of methylenecyclopentane from 1,5-hexadiene during polymerization attempts.[31] Since then, this reaction has been studied using catalysts based on Al,[31,32,33] Ti,[34,35] Zr,[36,37] and Ni[38,39] compounds. However, in most cases the reaction rate is slow, high temperatures are needed and unwanted products (dimers, oligomers, polymers) are formed.[38]

In 2006, our laboratory reported the cycloisomerization of 1,5-hexadiene with (^{iPr}PDI)Fe(N_2)$_2$ in the presence of 0.5 atmospheres of H_2.[23] Investigation of the reaction of 1,5-hexadiene with (^{iPr}PDI)Fe(N_2)$_2$ in the absence of H_2 revealed clean cycloisomerization to methylenecyclopentane within 10 hours in > 95% conversion (Figure 5.13). Increasing the temperature of the reaction to 45 °C with 5 mol% (^{iPr}PDI)Fe(N_2)$_2$ resulted in complete conversion after only 2 hours. With [(^{Et}PDI)FeN_2]$_2$(μ_2-N_2) as the catalyst, the reaction reached only 60% conversion after 24 hours. A longer reaction time (48 hours) did not result in any further conversion.

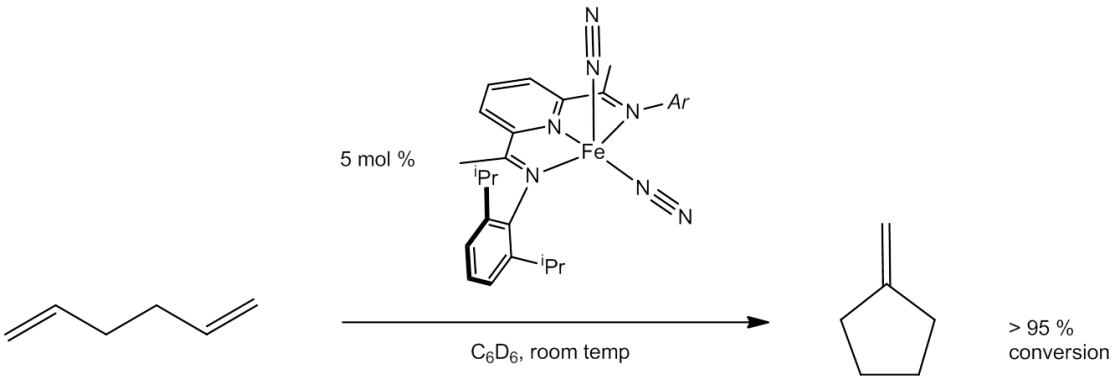

Figure 5.13 Catalytic cycloisomerization of 1,5-hexadiene by (^{iPr}PDI)Fe(N_2)$_2$.

Addition of 40 equivalents of 1,5-hexadiene to [(^{Me}PDI)Fe(N_2)]$_2$(μ_2-N_2) (5 mol% [Fe]) resulted in about 80% conversion of the diene after 8 hours. Allowing the reaction to run longer did not result in any further conversion. Of the 80% conversion, approximately 65% of the product was methylenecyclopentane and 15% was 2,4-hexadiene. Heating the reaction to 45°C increased the rate, but did not drive the reaction to completion or alter the ratio of products. A bis(imino)pyridine iron compound was observed during the course of the reaction which was identified as the 2,4-hexadiene adduct, (^{Me}PDI)Fe(η^4-C_6H_{10}). This compound was shown to be catalytically active for the cycloisomerization of 1,5-hexadiene, although at diminished rates (62% conversion after 24 hours) suggesting that coordination of the conjugated diene to the iron center inhibits methylenecyclopentane formation. Addition of 2,4-hexadiene under the same conditions does not result in formation of methylenecyclopentane, providing further evidence that the internal diene is a byproduct of the reaction and not on the path to the desired product.

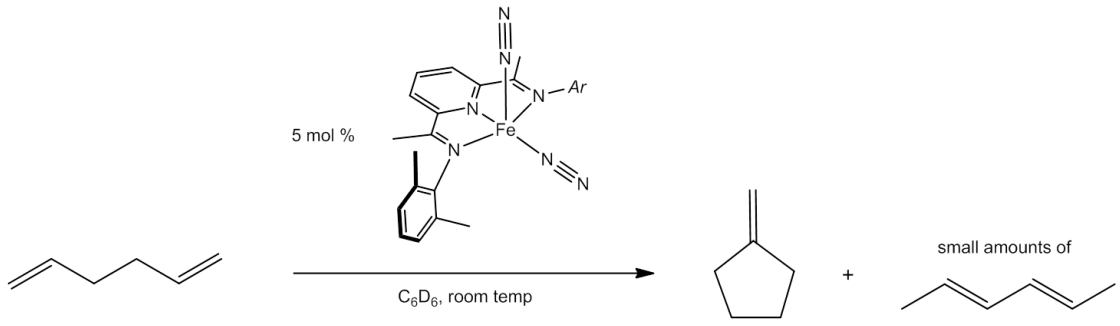

Figure 5.14 Cycloisomerization of 1,5-hexadiene by [(^{Me}PDI)Fe(N_2)]$_2$(μ_2-N_2).

As olefin isomerization reactions typically involve metal-hydride species, [40,41] this possibility was considered for the iron-catalyzed transformation of 1,5-hexadiene to methylenecyclopentane. While a bis(imino)pyridine iron hydride has yet to be definitively characterized, there is experimental evidence for it as a transient species in

solution.[25c] For example, the bis(imino)pyridine iron bis(dinitrogen) compound, (^{iPr}PDI)Fe(N_2)$_2$, isomerizes 1-butene and 1-hexene to the corresponding internal olefins in solution at ambient temperature. Furthermore, when (^{iPr}PDI)Fe(N_2)$_2$, is exposed to 4 atmospheres of D_2 gas, deuterium incorporation into the isopropyl methyl groups, but not into the methine position, is observed. The proposed mechanism for this ligand modification involves a cyclometalated iron alkyl hydride compound. Also, as the previous [2π+2π] labeling studies showed, addition of C_2D_4 to [(^{Me}PDI)Fe(N_2)]$_2$(μ_2-N_2) results in deuterium incorporation into the aryl methyl groups, providing evidence of a cyclometallation pathway for this compound (Section 5.3).

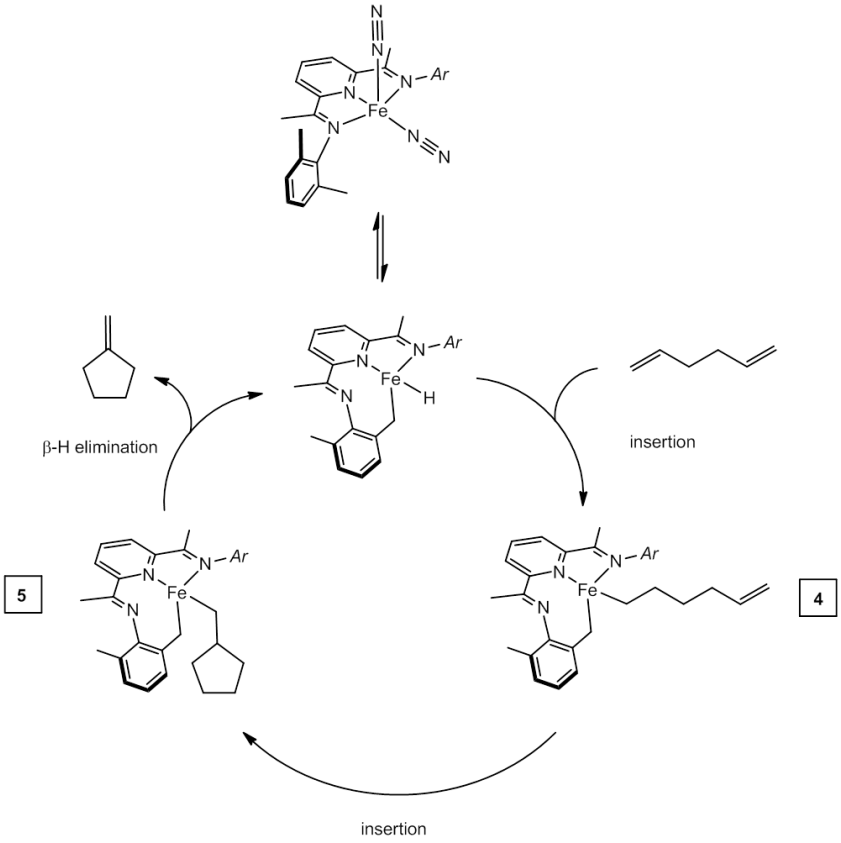

Figure 5.15 Possible mechanism of methylenecyclopentane formation based on an iron hydride.

Figure 5.15 depicts a possible mechanism for methylenecyclopentane formation if a bis(imino)pyridine iron cyclometallated hydride is present in solution. An olefin insertion of 1,5-hexadiene into the iron-hydride bond furnishes the iron alkyl, **4**. A second olefin insertion into the newly formed iron-carbon bond results in a new iron alkyl, **5**, with a methylcyclopentyl group. Subsequent β-hydrogen elimination furnishes methylenecyclopentane and reforms the iron hydride. During the reaction a second catalytic cycle appears to be occurring which isomerizes 1,5-hexadiene to 2,4-hexadiene (Figure 5.16). The difference between these two paths is formal 1,2 vs. 2,1 insertion of the first olefin into the iron-hydride. Cycloisomerization occurs following 1,2-insertion while internalization of the olefin follows 2,1-insertion. The steric hindrance of the aryl isopropyl groups of $(^{iPr}PDI)Fe(N_2)_2$ and the ethyl groups of $[(^{Et}PDI)Fe(N_2)]_2(\mu_2\text{-}N_2)$ likely prevent 2,1-insertion and inhibit 2,4-hexadiene formation.

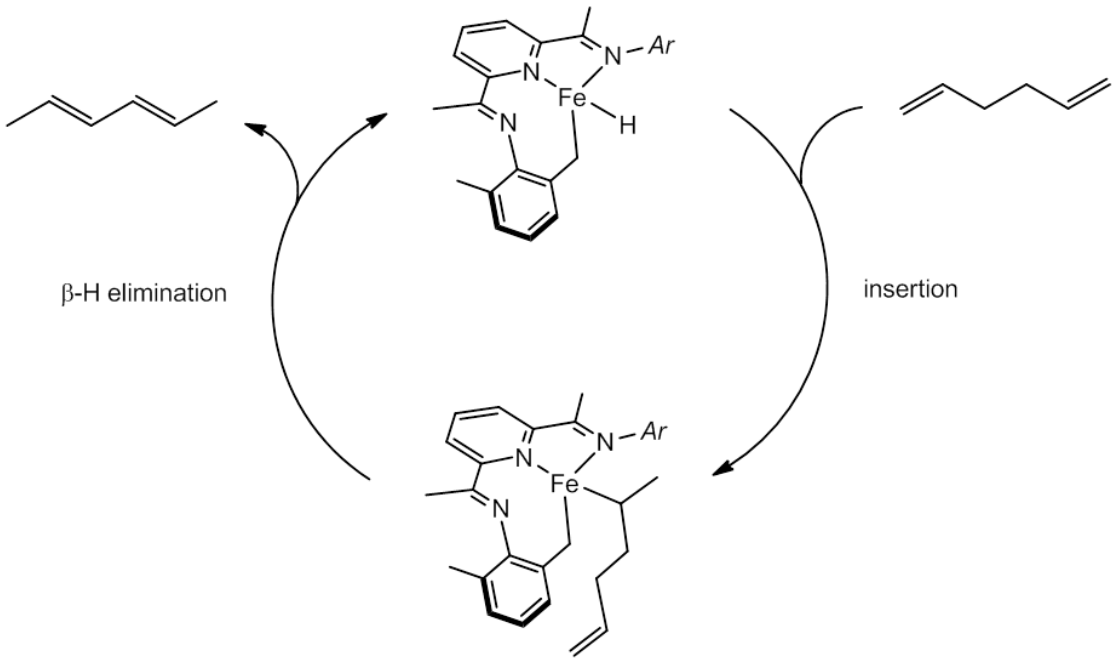

Figure 5.16 Mechanism for isomerization of 1,5-hexadiene to 2,4-hexadiene.

Deuterium labeling experiments were performed to probe the cyclometallation of the benzylic C-H bonds aryl methyl groups in $[(^{Me}PDI)Fe(N_2)]_2(\mu_2\text{-}N_2)$. Running the cyclization of 1,5-hexadiene with $[(*^{Me}PDI)Fe(N_2)]_2(\mu_2\text{-}N_2)$ ($*^{Me}PDI$ = 2,6-(2,6-$(CD_3)_2$-C_6H_3-N=CMe)$_2C_5H_3N$), resulted in deuterium incorporation into the α-CH_2 and the olefin positions of methylenecyclopentane. Small amounts of deuterium incorporation were also present in the methyl group of formed 2,4-hexadiene as well as into the terminal olefinic position of remaining 1,5-hexadiene (Figure 5.17). These observations can be explained by a reversible 2,1-insertion of 1,5-hexadiene into the iron-deuteride bond followed by β-hydride elimination to form either labeled 1,4-hexadiene or reform 1,5-hexadiene. The 1,4-hexadiene in then isomerized again to form 2,4-hexadiene and the 1,5-hexadiene can be transformed to methylenecyclopentane. A control experiment where 20 equivalents of 2,4-hexadiene were added to $[(*^{Me}PDI)Fe(N_2)]_2(\mu_2\text{-}N_2)$ resulted in no deuterium incorporation into the diene.

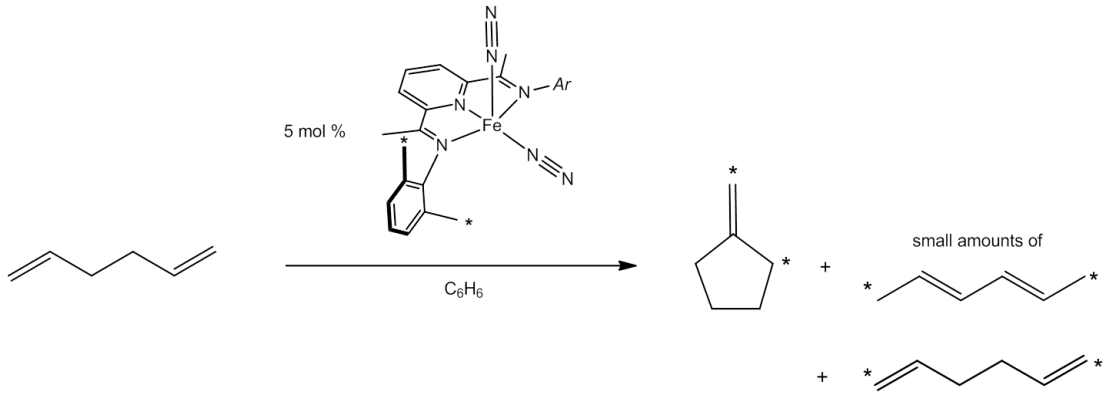

Figure 5.17 Deuterium labeling study with $[(*^{Me}PDI)Fe(N_2)]_2(\mu_2\text{-}N_2)$.

The deuterated olefin, 3-ethyl-1-pentene-d_1, has been used to probe whether metal-hydride catalyzed reactions occur by a metal hydride addition-elimination reaction or by a mechanism involving a metal allyl hydride intermediate.[31] The

fundamental difference between these two pathways is that the addition-elimination mechanism contains a 1,2-hydrogen migration while the metal allyl hydride mechanism results in a 1,3-hydrogen shift (Figure 5.18). Performing the cycloisomerization of 1,5-hexadiene with [(^{Me}PDI)Fe(N_2)]$_2$(μ_2-N_2) under the standard conditions in the presence of 3-ethyl-1-pentene-d_1 and analysis of the volatiles by ^{1}H and ^{2}H NMR spectroscopy revealed no isomerization of the deuterated olefin. The control reaction, addition of 3-ethyl-1-pentene-d_1 to [(^{Me}PDI)Fe(N_2)]$_2$(μ_2-N_2) without any 1,5-hexadiene, also produced no isomerization of the olefin. These results do not support an iron-hydride mechanism; however, they also do not eliminate it.

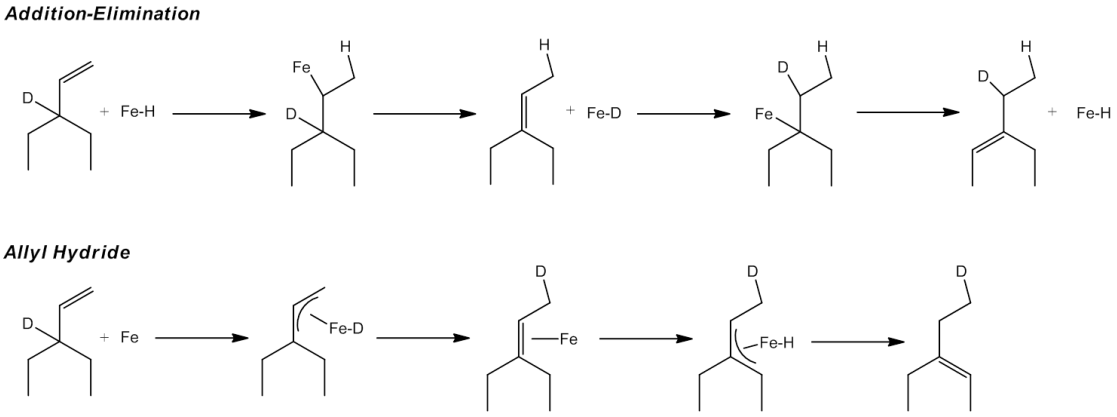

Figure 5.18 Metal hydride addition-elimination reaction vs. metal allyl hydride mechanism.

A second plausible mechanism is presented in Figure 5.19 and begins with metallacycle formation, which is also the first step proposed in the mechanism for bis(imino)pyridine iron-catalyzed α,ω-diene cycloisomerization.[22] It has been shown that when α,ω-dienes are added to [(^{Me}PDI)Fe(N_2)]$_2$(μ_2-N_2), methylenecyclopentane derivatives are formed along with the corresponding bicycle[0.2.3]heptane derivatives suggesting that β-hydrogen elimination is competitive with reductive elimination for this particular ligand.[42] Accordingly, the next step in the proposed mechanism is a β-

hydrogen elimination to form the iron methylene cyclobutane compound, **6**. Transition metal compounds with methylene cyclobutane rings have been shown to undergo β-alkyl elimination reactions to alleviate the strain of the cyclobutane ring.[43]

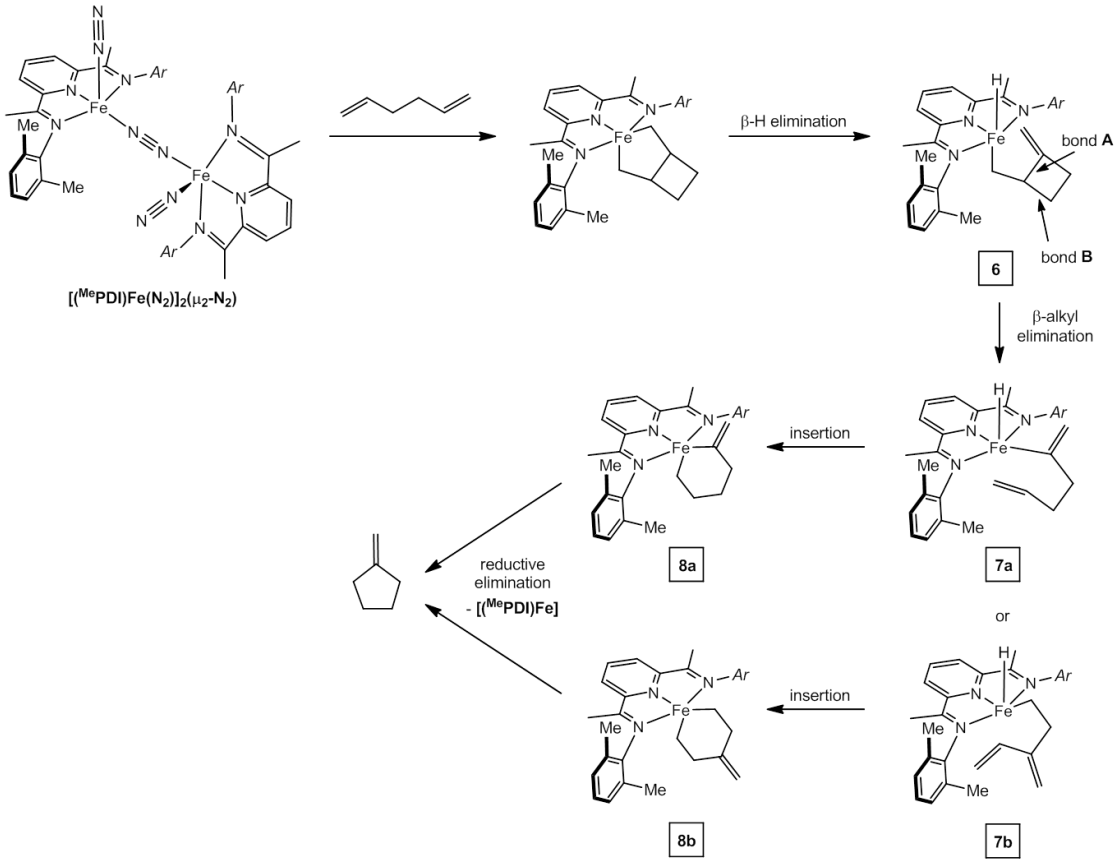

Figure 5.19 Possible mechanism of methylenecyclopentane formation involving a β-alkyl elimination reaction.

From compound **6** there are two options for β-alkyl elimination, one which breaks bond **A** and one which breaks bond **B** in Figure 5.19. The next intermediate on both pathways is an iron alkyl hydride, **7a** from breaking Bond A or **7b** from breaking Bond B, which can furnish the corresponding metallacycles, **8a** and **8b**, by an insertion reaction. Reductive elimination from both metallacycles affords

methylenecyclopentane and a formally iron(0) species that can enter back into the catalytic cycle by reaction with 1,5-hexadiene.

A ^{13}C-labeling experiment was performed in hopes of differentiating between the pathways. Forty equivalents of 1-^{13}C-1,5-hexadiene were added to [(^{Me}PDI)Fe(N_2)]$_2$(μ_2-N_2) (5 mol% [Fe]) and the product of the reaction was analyzed by ^{1}H and ^{13}C NMR spectroscopy. At > 95% conversion, the ^{13}C-label was detected in the terminal olefin of the carbon and in the 2-position of the cyclopentane ring (Figure 5.20). Two possible positions for the ^{13}C-label are expected because the two ends of the 1,5-hexadiene are otherwise identical. Unfortunately, this experiment does not rule out either mechanism as re-examining both possible mechanisms revealed that in each case, the carbon label will end up in one of these two positions.

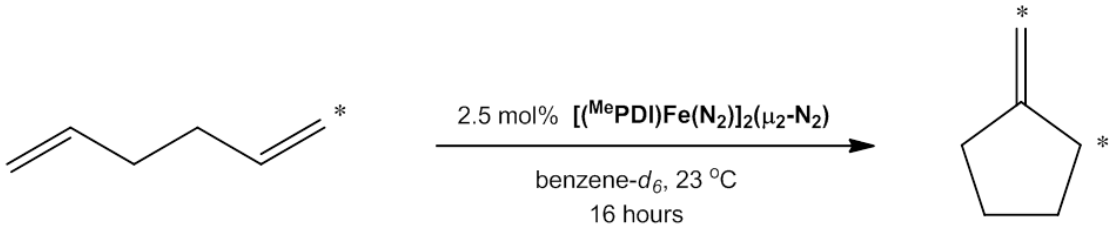

Figure 5.20 Results of the ^{13}C-labeled 1,5-hexadiene cyclization.

5.6 Conclusions

Several carbon-carbon bond forming reactions catalyzed by bis(imino)pyridine iron dinitrogen compounds were studied. The addition of ethylene to butadiene in the presence of 2.5 mol% [(^{Me}PDI)Fe(N_2)]$_2$(μ_2-N_2) afforded > 95% conversion to vinylcyclobutane after 16 hours at 23°C. Deuterium labeling studies with ethylene-d_4 and *cis*-d_2-ethylene were performed and revealed deuterium incorporation into only the 2 and 3 positions of the cyclobutane ring with no evidence for scrambling. An intermediate on the reaction pathway, the bis(imino)pyridine iron alkyl allyl

compound, (^{Me}PDI)Fe((CH$_2$)$_3$(CH)$_2$CH$_2$), was isolated and characterized by NMR and Mössbauer spectroscopies as well as X-ray diffraction. The electronic structure of (^{Me}PDI)Fe((CH$_2$)$_3$(CH)$_2$CH$_2$) likely exists as a resonance structure between an iron(II) diolefin complex and an iron(IV) alkyl allyl complex.

Different reactivity was observed when isoprene was used as the diene substrate. With [(^{Me}PDI)Fe(N$_2$)]$_2$(μ_2-N$_2$) as the catalyst, 1,4-hydrovinylation was observed and furnished the linear diene, 5-methyl-1,4-hexadiene. A deuterium labeling study was performed with ethylene-d_4 and showed deuterium incorporation into all three positions of the α-olefin and into one methyl group. When (^{iPr}PDI)Fe(N$_2$)$_2$ was employed as the catalyst,1,4-hydrovinylation was followed by the rapid isomerization of 5-methyl-1,4-hexadiene to 2-methyl-2,4-hexadiene. In this case, deuterium labeling studies with ethylene-d_4 showed incorporation into the 1, 5 and 6 positions of 2-methyl-2,4-hexadiene as well as some scrambling into the 4 position and into the isopropyl groups of (^{iPr}PDI)Fe(N$_2$)$_2$.

Finally, [(^{Me}PDI)Fe(N$_2$)]$_2$(μ_2-N$_2$) was revealed to catalyze the cycloisomerization of 1,5-hexadiene to methylenecyclopentane. Two mechanisms were proposed, one involving a transient bis(imino)pyridine iron hydride complex, and the second invoking a β-alkyl elimination reaction from a strained cyclobutane ring. Deuterium and ^{13}C-labeling studies were performed, but were not able to provide evidence against either mechanism.

5.7 Experimental Procedures

General Considerations. All air- and moisture-sensitive manipulations were carried out using standard vacuum line, Schlenk, and cannula techniques or in an MBraun inert atmosphere dry box containing an atmosphere of purified nitrogen. Solvents for air- and moisture-sensitive manipulations were initially dried and deoxygenated using

literature procedures. Benzene-d_6 was purchased from Cambridge Isotope Laboratories and dried over 4 Å molecular sieves. The compounds (^{iPr}PDI)Fe(N_2)$_2$,[22] [(^{Et}PDI)Fe(N_2)]$_2$(μ_2-N_2),[24] [(^{Me}PDI)Fe(N_2)]$_2$(μ_2-N_2),[24] and (^{Me}PDI)Fe(η^4-C_4H_6)[44] were prepared according to literature procedure. Ethylene was purchased from Sigma-Aldrich and passed through a column of molecular sieves before use. Isoprene and 1,3-butadiene were purchased from Sigma-Aldrich and dried over $LiAlH_4$ before use. 1,4-hexadiene and 1,5-hexadiene were purchased from Sigma-Aldrich and dried over CaH_2 before use. Ethylene-d_4 and *cis*-d_2-ethylene were purchased from Cambridge Isotope Laboratories, Inc. and used as purchased.

^{1}H NMR spectra were recorded on Varian Mercury 300, Inova 400, 500, and 600 spectrometers operating at 299.76, 399.78, 500.62, and 599.78 MHz, respectively. ^{13}C NMR spectra were recorded on an Inova 500 spectrometer operating at 125.893 MHz. All ^{1}H and ^{13}C NMR chemical shifts are reported relative to $SiMe_4$ using the ^{1}H (residual) and ^{13}C chemical shifts of the solvent as a secondary standard. For diamagnetic complexes, many assignments were made based on COSY and HSQC NMR experiments.

Single crystals suitable for X-ray diffraction were coated with polyisobutylene oil in a drybox, transferred to a nylon loop and then quickly transferred to the goniometer head of a Bruker X8 APEX2 diffractometer equipped with a molybdenum X-ray tube (λ = 0.71073 Å). Preliminary data revealed the crystal system. A hemisphere routine was used for data collection and determination of lattice constants. The space group was identified and the data were processed using the Bruker SAINT+ program and corrected for absorption using SADABS. The structures were solved using direct methods (SHELXS) completed by subsequent Fourier synthesis and refined by full-matrix least-squares procedures.

Zero-field ^{57}Fe Mössbauer spectra were recorded on a SEE Co. Mössbauer spectrometer (MS4) at 80 K in constant acceleration mode. ^{57}Co/Rh was used as the radiation source. WMOSS software was used for the quantitative evaluation of the spectral parameters (least-squares fitting to Lorentzain peaks). The minimum experimental line widths were 0.23 mm/s. The temperature of the sample was controlled by a Janis Research Co. CCS-850 He/N_2 cryostat within and accuracy of ± 0.3 K. Isomer shifts were determined relative to α-iron at 298 K.

Preparation of (^{Me}PDI)Fe($(CH_2)_3(CH)_2CH_2$). A thick walled glass vessel was charged with 0.200 g (0.42 mmol) of (^{Me}PDI)Fe(η^4-C_4H_6) in 20 mL of diethyl ether. The vessel was submerged in liquid nitrogen and degassed. Three equivalents (1.25 mmol) of ethylene were added to the vessel and the solution was warmed to room temperature. The reaction was stirred for 2 hours during which time the solution changed color from orange to yellow. The vessel was degassed and brought into the glove box where the solution was filtered through celite and concentrated. Recrystallization from diethyl ether at -35 °C afforded 0.099 g (47%) of a yellow-brown solid identified as (^{Me}PDI)Fe($(CH_2)_3(CH)_2CH_2$). Crystals suitable for X-ray diffraction were grown from a concentrated diethyl ether solution at -35 °C. Analysis for $C_{31}H_{37}N_3Fe$: Calc. C, 73.37; H, 7.35; N, 8.28. Found C, 72.99; H, 7.15; N, 7.88. ^{1}H NMR (benzene-d_6, 20 °C): δ = -0.12 (quart, 9.6 Hz, 1H, CH_2CH$_2$CH$_2$CHCHCH$_2$), 0.43 (td, 3.2 Hz and 9.6 Hz, 1H, CH_2CH$_2$CH$_2$CHCHCH$_2$), 1.20 (s, 3H, *Ar* CH_3), 1.37 (s, 3H, *Ar* CH_3), 1.78 (s, 3H, N=C(CH_3)), 1.82 (d, 12.0 Hz, 1H, CH$_2$CH$_2$CH$_2$CHCHCH_2), 1.87 (s, 3H, *Ar* CH_3), 1.88 (s, 3H, N=C(CH_3)), 2.05 (s, 3H, *Ar* CH_3), 2.68 (m, 1H, CH$_2$CH_2CH$_2$CHCHCH$_2$), 2.72 (d, 7.6 Hz, 1H, CH$_2$CH$_2$CH$_2$CHCHCH_2), 2.77 (m, 1H, CH$_2$CH$_2$CH_2CHCHCH$_2$), 2.99 (m, 1H, CH$_2$CH$_2$CH_2CHCHCH$_2$), 3.31 (m, 1H, CH$_2$CH_2CH$_2$CHCHCH$_2$), 5.60 (td, 7.6 Hz and

12 Hz, 1H, $CH_2CH_2CH_2CHCHCH_2$), 5.80 (td, 5.2 Hz and 11.6 Hz, 1H, $CH_2CH_2CH_2CHCHCH_2$), 6.75 (d, 7.6 Hz, 1H, *Ar*), 6.76 (m, 1H, *Ar*), 6.80 (t, 7.6 Hz, 1H, *Ar*), 6.88 (m, 3H, *Ar*), 7.28 (t, 7.6 Hz, 1H, *p-py*), 7.80 (d, 7.6 Hz, 1H, *m-py*), 8.0 (d, 7.6 Hz, 1H, *m-py*). ^{13}C NMR (benzene-d_6, 20 °C): δ = 17.35 (N=C(CH_3)), 19.34 (N=C(CH_3)), 18.35 (*Ar* CH_3), 18.45 (*Ar* CH_3), 19.07 (*Ar* CH_3), 19.41 (*Ar* CH_3), 39.37 ($CH_2CH_2CH_2CHCHCH_2$), 45.33 ($CH_2CH_2CH_2CHCHCH_2$), 47.58 ($CH_2CH_2CH_2CHCHCH_2$), 51.39 ($CH_2CH_2CH_2CHCHCH_2$), 105.51 ($CH_2CH_2CH_2CHCHCH_2$), 117.45 ($CH_2CH_2CH_2CHCHCH_2$), 117.54 (*p-py*), 117.62 (*m-py*), 119.57 (*m-py*), 125.75 (*Ar*), 125.85 (*Ar*), 128.72 (*Ar*), 128.91 (*Ar*), 129.07 (*Ar*), 129.11 (*Ar*), 130.09, 130.58, 130.68, 131.36, 149.46, 150.43, 150.75, 152.00, 156.75, 156.88 (quaternary carbons).

General Procedure for Butadiene/Isoprene and Ethylene Catalysis. A J Young tube was charged with 0.010 g (0.022 mmol of Fe) of [(^{Me}PDI)Fe(N_2)]$_2$(μ_2-N_2) and approximately 0.650 g of benzene-d_6. The J Young tube was submerged in liquid nitrogen and twenty equivalents (0.43 mmol) of diene, followed by twenty equivalents of ethylene (0.43 mmo), were added by gas-bulb transfer. The tube was warmed to room temperature resulting in a color change of the solution from brown to orange to yellow. After an allotted amount of time, the reaction was stopped by vac-transfering the volatiles into a second J Young tube.

NMR Spectroscopic Data for Vinylcyclobutane.

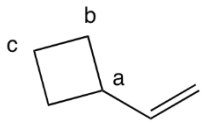

^{1}H NMR (benzene-d_6, 20 °C): δ = 1.71 (m, 4H, H_b and H_c), 1.96 (m, 2H, H_b), 2.81 (m, 1H, H_a), 4.92 (dt, 8.4 Hz and 1.2 Hz, 1H, CH=CH_2), 4.96 (dt, 14.0 Hz and 1.2 Hz, 1H,

CH=CH_2), 5.88 (ddd, 14.0 Hz and 8.4 Hz and 5.6 Hz, CH=CH_2). ^{13}C NMR (benzene-d_6, 20 °C): δ = 19.10 (C_c), 28.84 (C_b), 39.89 (C_a), 112.53 (CH=CH$_2$), 143.56 (CH=CH$_2$).

NMR Spectroscopic Data for 5-methylhexa-1,4-diene.

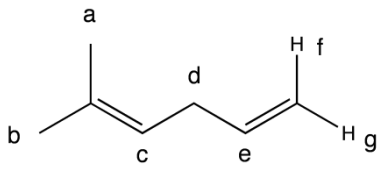

^{1}H NMR (benzene-d_6, 20 °C): δ = 1.48 (d, 1.2 Hz, 3H, H_a or H_b), 1.63 (d, 1.2 Hz, 3H, H_a or H_b), 2.70 (t, 6.8 Hz, 2H, H_d), 4.98 (ddd, 10 Hz and 1.8 Hz, 1H, H_g), 5.06 (ddd, 17 Hz and 1.8 Hz, 1H, H_f), 5.20 (t of sept, 6.8 Hz and 1.2 Hz, 1H, H_c), 5.79 (ddt, 17 Hz and 10 Hz and 6.8 Hz, 1H, H_e). ^{13}C NMR (benzene-d_6, 20 °C): δ = 17.92 (C_a or C_b), 26.09 (C_a or C_b), 33.14 (C_d), 114.66 ($C_{f/g}$), 122.50 (C_c), 132.91 (quaternary), 137.99 (C_e).

NMR Spectroscopic Data for (*E*)-2-methylhexa-1,4-diene.

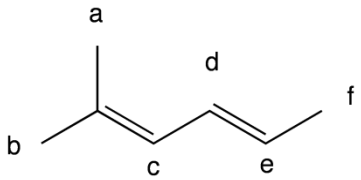

^{1}H NMR (benzene-d_6, 20 °C): δ = 1.61 (s, 3H, H_a or H_b), 1.65 (s, 3H, H_a or H_b), 1.67 (d, 7.0 Hz, 3H, H_f), 5.53 (dq, 15 Hz and 7.0 Hz, 1H, H_e), 5.90 (d, 11 Hz, 1H, H_c), 6.33 (dd, 15 Hz and 11 Hz, 1H, H_d). ^{13}C NMR (benzene-d_6, 20 °C): δ = 18.49 (C_f), 18.75 (C_a or C_b), 26.28 (C_a or C_b), 126.36 (C_e), 126.60 (C_c), 129.12 (C_d), 136.28 (quaternary).

General Procedure for 1,5-Hexadiene Catalytic Cycloisomerization. A 20 mL scintillation vial was charged with 0.010 g (0.017 mmol) of (^{iPr}PDI)Fe(N_2)$_2$ and approximately 0.650 g of benzene-d_6. To the vial was added 42 μL (20 equiv, 0.34 mmol) of 1,5-hexadiene by microsyringe. The solution was filtered into a J Young tube and the reaction monitored by ^{1}H NMR spectroscopy. After an allotted amount of time, the reaction was stopped by vacuum transferring the volatiles into a second J Young tube.

NMR Spectroscopic Data for (^{Me}PDI)Fe(η^4-C_6H_{10}). ^{1}H NMR (benzene-d_6, 20 °C): δ = 0.42 (d, 6.0 Hz, 6H, hexadiene CH_3), 1.59 (s, 18H, N=C(CH_3) and *Ar* CH_3), 4.03 (m, 2H, hexadiene C*H*), 4.62 (m, 2H, hexadiene C*H*), 6.83 (d, 7.6 Hz, 4H, *m-Ar*), 6.90 (t, 7.6 Hz, 2H, *p-Ar*), 7.43 (t, 7.6 Hz, 1H, *p-py*), 8.12 (d, 7.6 Hz, 2H, *m-py*).

NMR Spectroscopic Data for Methylenecyclopentane. ^{1}H NMR (benzene-d_6, 20 °C): 1.48 (m, 4H, cyclopentane β-CH_2), 2.18 (m, 4H, cyclopentane α-CH_2), 4.96 (quintet, 2.4 Hz, 2H, C=CH_2).

REFERENCES

[1] (a) Jolly, P. W.; Wilke, G. In *Applied Homogeneous Catalysis with Organometallic Compounds*; Cornils, B., Herrmann, W. A., Eds.; VCH: New York, 1996; Vol. 3, 1164. (b) Goossen, L. J. *Angew. Chem., Int. Ed.* **2002**, *41*, 3775. (c) RajanBabu, T. V. *Chem. Rev.* **2003**, *103*, 2845.

[2] Ni: (a) Saha, B; RajanBabu, t. V. *J. Org. Chem.* **2007**, *72*, 2357. (b) Zhang, A.; RajanBabu, T. V. *Org. Lett.* **2004**, *6*, 1515. (c) Zhang, A.; RajanBabu, T. V. *Org. Lett.* **2004**, *6*, 3159. (d) Kumareswaran, R.; Nandi, M.; RajanBabu, T. V.*Org. Lett.* **2003**, *5*, 4345. (e) RajanBabu, T. V.; Nomura, N. Jin, J. Nandi, M.; Park, H. Sun, X. *J. Org. Chem.* **2003**, *68*, 8431. (f) Park, H.; RajanBabu, T. V. *J. Am. Chem. Soc.* **2002**, *124*, 734.

[3] Ni: (a) Franciò, G.; Faraone, F; Leitner, W. *J. Am. Chem. Soc.* **2002**, *124*, 736. (b) Wegner, A.; Leitner, W. *Chem. Commun.* **1999**, 1583.

[4] Ni: (a) Wilke, G. *Angew. Chem., Int. Ed. Engl.* **1988**, *27*, 185. (b) Bogadanovi, B.; Pauling, H.; Wilke, G.; Meister, B.; Henc, B. *Angew. Chem., Int. Ed.* **1972**, *11*, 1023.
[5] Ru: Sanchez, R. P.; Connell, B. T. *Organometallics* **2008**, *27*, 2902.

[6] Pd: (a)Bayersdörfer, R.; Ganter, B.; Englert, W.; Keim, W.; Vogt, D. *J. Organomet. Chem.* **1998**, *552*, 187. (b) Englert, W.; Haerter, R.; Vasen, D.; Salzer, A.; Eggeling, E. B.; Vogt, D. *Organometallics* **1999**, *18*, 4390.

[7] Ru: (a) He, Z.; Yi, C. S.; Donaldson, W. A. *Synlett* **2004**, 1312. (b) He, Z.; Yi, C. S.; Donaldson, W. A. *Org. Lett.* **2003**, *5*, 1567. (c) Yi, C. S.; He, Z.; Lee, D. W. *Organometallics* **2001**, *20*, 802.

[8] Rh: Alderson, T.; Jenner, E. L.; Lindsey, R. V., Jr. *J. Am. Chem. Soc.* **1965**, *87*, 5638.

[9] Ir: Bhalla, G.; Oxgaard, J.; Goddard, W. A., III; Periana, R. A. *Organometallics* **2005**, *24*, 5499.

[10] Co: (a) Grutters, M. M. P.; Müller, C.; Vogt, D. *J. Am. Chem. Soc.* **2006**, *128*, 7414. (b) Grutters, M. M. P.; van der Vlugt, J. I.; Pei, Y.; Mills, A. M.; Lutz, M.; Spek, A. L.; Müller, C.; Mober, C.; Vogt, D. *Adv. Synth. Catal.* **2009**, *351*, 2199.

[11] Ni: (a) Zhang, A. B.; RajanBabu, T. V. *J. Am. Chem. Soc.* **2006**, *128*, 54. (b) Saha, B.; Smith, C. R.; RajanBabu, T. V. *J. Am. Chem. Soc.* **2008**, *130*, 9000.

[12] Co: (a) Hilt, G.; Danz, M.; Treutwein, J. *Org. Lett.* **2009**, *11*, 3322. (b) Hilt, G; Treutwein, J. *Chem. Commun.* **2009**, 1395. (c) Hilt, G.; Lüers, S.; Schmidt, F. *Synthesis* **2004**, 634. (d) Hilt, G.; Lüers, S. *Synthesis* **2002**, 609. (e) Hilt, G.; du Mesnil, F. X.; Lüers, S. *Angew. Chem. Int. Ed.* **2001**, *40*, 387.

[13] Co: Sharma, R. K.; RajanBabu, T. V. *J. Am. Chem. Soc.* **2010**, *132*, 3295.

[14] Bolm, C.; Legros, J.; Le-Paith, J.; Zani, L. *Chem. Rev.* **2004**, *104*, 6217.

[15] Enthaler, S.; Junge, K.; Beller, M. *Angew. Chem., Int. Ed.* **2008**, *47*, 3317.

[16] Correa, A.; Mancheño, O. G.; Bolm, C. *Chem. Soc. Rev.* **2008**, *37*, 1108.

[17] Sherry, B. D.; Fürstner, A. *Acc. Chem. Res.* **2008**, *41*, 1500.

[18] (a) Hata, G. *J. Am. Chem. Soc.* **1964**, *86*, 3903. (b) Hata, G.; Aoki, D. *J. Org. Chem.* **1967**, *32*, 3754.

[19] (a) Takacs, J. M.; Anderson, L. G.; Madhavan, g. V. B.; Creswell, M. W.; Seely, F. L.; Devroy, W. F. *Organometallics* **1986**, *5*, 2395. (b) Takacs, J. M.; Anderson, L. G.; Newsome, P. W. *J. Am. Chem. Soc.* **1987**, *109*, 2542. (c) Takacs, J. M.; Anderson, L. G.; Madhavan, g. V. B.; Seely, F. L. *Angew. Chem., Int. Ed.* **1987**, *26*, 1013.

[20] tom Dieck, H.; Dietrich, J. *Angew. Chem., Int. Ed. Engl.***1985**, *24*, 781.

[21] Moreau, B.; Wu, J. Y.; Ritter, T. *Org. Lett.* **2009**, *11*, 337.

[22] Bart, S. C.; Lobkovsky, E.; Chirik, P. J. *J. Am. Chem. Soc.* **2004**, *126*, 13794.

[23] Bouwkamp, M. W.; Bowman, A. C.; Lobkovsky, E.; Chirik, P. J. *J. Am. Chem. Soc.* **2006**, *128*, 13340.

[24] Russell, S. K.; Darmon, J. M.; Lobkovsky, E.; Chirik, P. J. *Inorg. Chem.* **2010**, *49*, 2782.

[25] (a) Sylvester, K. T.; Chirik, P. J. *J. Am. Chem. Soc.* **2009**, *131*, 8772. (b) Trovitch, R. J.; Lobkovsky, E.; Chirik, P. J. *J. Am. Chem. Soc.* **2008**, *130*, 11631. (c) Bart, S. C.; Lobkovsky, E.; Chirik, P. J. *J. Am. Chem. Soc.* **2007**, *129*, 7212.

[26] Bart, S. C.; Lobkovsky, E.; Bill, E.; Wieghardt, K.; Chirik, P. J. *Inorg. Chem.* **2007**, *46*, 7055.

[27] Trovitch, R. J.; Lobkovsky, E.; Bouwkamp, M. W.; Chirik, P. J. *Organometallics* **2008**, *27*, 6264.

[28] (a) Tondreau, A. M.; Milsmann, C.; Patrick, A. D.; Hoyt, H. M.; Lobkovsky, E.; Wieghardt, K.; Chirik, P. J. *J. Am. Chem. Soc.* **2010**, *312*, 15046. (b) Tondreau, A. M.; Lobkovsky, E.; Chirik, P. J. *Org. Lett.* **2008**, *10*, 2789. (c) Fernández, I.; Trovitch, R. J.; Lobkovsky, E.; Chirik, P. J. *Organometallics*, **2008**, *27*, 109. (d) Bouwkamp, M. W.; Bart, S. C.; Hawrelak, E. J.; Trovitch, R. J.; Lobkovsky, E.; Chirik, P. J. *Chem. Commun.* **2005**, 3406.

[29] (a) Knijnenburg, Q.; Gambarotta, S.; Budzelaar, P. H. M. *Dalton Trans.* **2006**, 5442. (b) Bart, S. C.; Chlopek, K.; Bill, E.; Bouwkamp, M. W.; Lobkovsky, E.; Neese, F.; Wieghardt, K.; Chirik, P. J. *J. Am. Chem. Soc.* **2006**, *128*, 13901.

[30] Aaron M. Tondreau, *Ph. D. Thesis*, Cornell University, 2011.

[31] Ziegler, K. *Angew. Chem.* **1956**, *68*, 721.

[32] Rienäcker, R.; Göthel, G. F. *Angew. Chem., Int. Ed. Engl.*, **1967**, *6*, 872.

[33] Chum, P. W.; Wilson, S. E. *Tetrahedron Lett.* **1976**, *16*, 1257.

[34] Lehmkuhl, H.; Tsien, Y. L. *Chem. Ber.* **1983**, *116*, 2437.

[35] Mach, K.; Sedmera, P.; Perusova, L.; Antropiusova, H.; Hanus, V.; Turecek, F. *Tetrahedron Lett.* **1982**, *23*, 1105.

[36] Bazan, G. C.; Rodriguez, G.; Ashe III, A. A.; Al-Ahmad, S.; Kampf, J. W. *Organometallics* **1997**, *16*, 2492.

[37] Kesti, M. R.; Waymouth, R. M. *J. Am. Chem. Soc.* **1992**, *114*, 3565.

[38] Walther, D.; Döhler, T.; Heubach, K.; Klobes, O.; Schweder, B.; Görls, H. *Z. Anorg. Allg. Chem.* **1999**, *625*, 923.

[39] Wasilke, J.; Komon, Z. J. A.; Bu, X.; Bazan, G. C. *Organometallics*, **2004**, *23*, 4174.

[40] Casey, C. P.; Cyr, C. R. *J. Am. Chem. Soc.* **1973**, *95*, 2248.

[41] Yue, C. J.; Liu, Y.; He, R. *J. Mol.Catal. A.: Chem.* **2006**, *259*, 17.

[42] Kevin T. Sylvester, *Ph. D. Thesis*, Cornell University, 2011.

[43] (a) Murakami, M.; Takahashi, K.; Amii, H.; Ito, Y. *J. Am. Chem. Soc.* **1997**, *119*, 9307. (b) Casey, C. P.; Hallenbeck, S. L.; Pollock, D. W.; Landis, C. R. *J. Am. Chem. Soc.* **1995**, *117*, 9770. (c) Ermer, S. P.; Struck, G. E.; Bitler, S. P.; Richards, R.; Bau, R.; Flood, T. C. *Organometallics* **1993**, *12*, 2634. (d) Bunel, E.; Burger, B. J.; Bercaw, J. E. *J. Am. Chem. Soc.* **1988**, *110*, 976.

[44] See Chapter 1.

CHAPTER 6

SYNTHESIS AND ELECTRONIC STRUCTURE INVESTIGATION OF REDUCED BIS(IMINO)PYRIDINE MANGANESE COMPLEXES

6.1 Abstract

The reduction chemistry of the bis(imino)pyridine manganese dichloride complex, (^{iPr}PDI)$MnCl_2$, was investigated in relation to the bis(imino)pyridine iron analog. The reduced compounds, (^{iPr}PDI)$Mn(THF)_2$, (^{iPr}PDI)$_2$Mn and (^{iPr}PDI)MnCl(THF), were synthesized and studied by a combination of ^{1}H NMR spectroscopy, magnetic susceptibility, X-ray diffraction and degradation experiments. The reduced manganese complexes, (^{iPr}PDI)$Mn(THF)_2$ and (^{iPr}PDI)$_2$Mn, both contain high spin manganese(II) centers antiferromagnetically coupled to bis(imino)pyridine chelate centered radicals. The bis(imino)pyridine manganese bis(THF) compound was also screened as a pre-catalyst for olefin hydrogenation and diene cycloisomerization reactions and exhibited no activity. A series of bis(imino)pyridine manganese carbonyl compounds, [(^{iPr}PDI)$Mn(CO)_2$][Na], (^{iPr}PDI)$Mn(CO)_2$ and [(^{iPr}PDI)$Mn(CO)_3$][BPh_4], was also prepared and studied by ^{1}H NMR, infrared and EPR spectroscopy as well as X-ray diffraction. These studies suggest that oxidation of a bis(imino)pyridine manganese carbonyl compound occurs at the bis(imino)pyridine chelate rather than at the metal center.

6.2 Introduction

Bis(imino)pyridine ligands (^{R}PDI = 2,6-(2,6-R-C_6H_3-N=CMe)$_2C_5H_3N$); R= ^{i}Pr, Et, Me, etc.) have become popular in the last two decades because of their ease of synthesis,[1] electronic[2] and structural modularity[3,4] and ability to support a range of transition metal and alkali metal ions,[5] including several dinitrogen complexes.[6,7,8,9,10]

The most notable feature of this ligand set is the ability of the π-system of the bis(imino)pyridine chelate to undergo reversible transfer of one to three electrons with the metal center.[11,12,13,14] In this manner, the chelate is able to stabilize reduced compounds whose low formal oxidation state assignments may be deceiving.[15] While bis(imino)pyridine iron and cobalt complexes are abundant in the literature, there are only a few accounts of similar chemistry with manganese.

In 2000, Wieghardt and coworkers investigated a series of first-row metal bis(chelate) complexes, including $[(^{4\text{-OMe}}PDI)_2Mn][PF_6]$ and $[(^{4\text{-OMe}}PDI)_2Mn][PF_6]_2$ ($^{4\text{-OMe}}PDI$ = 2,6-(4-OMe-C_6H_4-N=CMe)$_2C_5H_3N$), and addressed the question of spectroscopic oxidation states of both the metal center and the bis(imino)pyridine ligands.[16] Prior to this study, the only crystallographically characterized bis(imino)pyridine manganese derivative was $(^{H}PDI)MnBr_2$ (^{H}PDI = 2,6-(C_6H_5-N=CMe)$_2C_5H_3N$) reported by Edwards and coworkers in 1990.[17] The study by Wieghardt concluded that the dication, $[(^{4\text{-OMe}}PDI)_2Mn][PF_6]_2$, contains two neutral chelates and a high-spin manganese(II) center while the monocation, $[(^{4\text{-OMe}}PDI)_2Mn][PF_6]$, contains two monoanionic radical chelates and a low-spin manganese(III) center. Crystallographic characterization of these bis(chelate) manganese compounds also established some parameters for the average bond lengths of $[PDI]^0$ and $[PDI]^{1-}$ in manganese compounds.

Two years later, Gambarotta and coworkers described the synthesis and characterization of several bis(imino)pyridine manganese complexes.[18,19] Notably, they reported the bis(imino)pyridine manganese dichloride, the analog to the iron and cobalt ethylene polymerization catalysts popularized by Brookhart[20] and Gibson,[21] and demonstrated that unlike the other first row metal catalysts, $(^{iPr}PDI)MnCl_2$ (^{iPr}PDI = 2,6-(2,6-$^{i}Pr_2$-C_6H_3-N=CMe)$_2C_5H_3N$) is not active as an ethylene polymerization catalyst. The manganese compound was characterized by X-ray diffraction and

proposed to be a high spin manganese(II), $S = {}^5/_2$, compound, which is suggested to be the origin of the lack of reactivity. By addition of two equivalents of methyl lithium to (^{iPr}PDI)$MnCl_2$, the bis(imino)pyridine manganese methyl compound, (^{iPr}PDI)$MnCH_3$, was prepared; however, no attempts at probing its reactivity were reported.

Cámpora and coworkers have also recently reported the synthesis of the manganese(II) dialkyl complexes MnR_2L_2 (L = THF, pyridine) and their use in preparing bis(imino)pyridine ligands with *para*-pyridine substitutions.[22] However, the subsequent reactivity of the new bis(imino)pyridine manganese alkyl compounds was not described. Two bis(imino)pyridine manganese bis(triflate) complexes, (^{Mes}PDI)$Mn(OTf)_2$ (^{Mes}PDI = 2,6-(2,4,6-Me_3-C_6H_2-N=CMe)$_2C_5H_3N$) and (^{iPr}PDI)$Mn(OTf)_2$, were prepared by Britovsek and coworkers and studied for the catalytic oxidation of alkanes.[23] As in the attempted ethylene polymerization reactions, the bis(imino)pyridine manganese compounds were found to be inactive.

Our laboratory has previously reported the synthesis of bis(imino)pyridine iron[8] and cobalt[7] dinitrogen compounds from their corresponding dihalides and has shown that they serve as efficient pre-catalysts for the hydrogenation of olefins[8,24] and alkynes,[8b] the hydrosilylation of olefins,[8b] ketones and aldehydes,[25] the [$2\pi + 2\pi$] cycloisomerization of dienes[26] and the hydrogenative cyclization of enynes and diynes.[27] These successes led to the investigation of reduced bis(imino)pyridine manganese complexes for electronic structure comparisons and as possible pre-catalysts for organic transformations.

6.3 Two Electron Reduction of (^{iPr}PDI)$MnCl_2$

Stirring a tetrahydrofuran slurry of (^{iPr}PDI)$MnCl_2$ with 2 equivalents of sodium metal and 0.05 equivalents of naphthalene under a dinitrogen atmosphere for 16 hours furnished the brown bis(imino)pyridine manganese bis(tetrahydrofuran) compound,

(^{iPr}PDI)Mn(THF)$_2$ (Figure 6.1) Recrystallization of the crude solid from a diethyl ether solution did not yield the bis(imino)pyridine manganese bis(dinitrogen) complex as expected from related iron and cobalt chemistry,[8,9] but instead produced clean (^{iPr}PDI)Mn(THF)$_2$ in 61% yield. The ^{1}H NMR spectrum of (^{iPr}PDI)Mn(THF)$_2$ in benzene-d_6 is uninformative, exhibiting only very broad peaks. Without NMR and IR characterization techniques, degradation experiments were performed to help establish the composition of the compound. Addition of H_2O to (^{iPr}PDI)Mn(THF)$_2$ and analysis of the products by ^{1}H NMR spectroscopy yielded two equivalents of THF for every one bis(imino)pyridine ligand. Decomposition with D_2O produced no peaks in the ^{2}H NMR spectrum, confirming that the bis(imino)pyridine chelate is not altered during reduction.

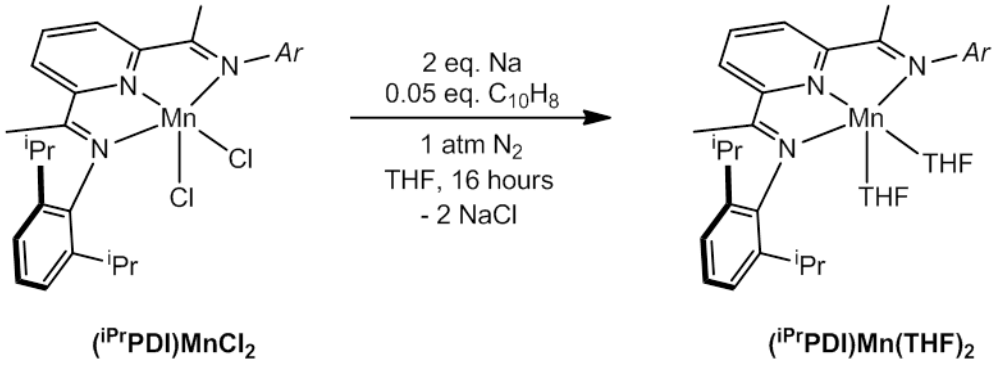

Figure 6.1 Synthesis of (^{iPr}PDI)Mn(THF)$_2$ from two electron reduction of (^{iPr}PDI)MnCl$_2$.

Single crystals of (^{iPr}PDI)Mn(THF)$_2$ suitable for X-ray diffraction were obtained from a concentrated diethyl ether solution as -35 °C. A representation of the solid state molecular structure is presented in Figure 6.2 and selected angles and bond distances are reported in Table 6.1. The solid state structure establishes an idealized square pyramidal geometry with a N(2)-Mn(1)-O(1) angle of 169.19(7)° and an O(1)-

Mn(1)-O(2) angle of 93.85(6)°. The bond distances of the bis(imino)pyridine chelate are consistent with two electron reduction.[12,16] The N_{imine}-C_{imine} bond distances are elongated to 1.367(3) and 1.340(3) Å while the C_{imine}-$C_{pyridine}$ bond distances are contracted to 1.441(3) and 1.421(3) Å. Although there is some asymmetry within the N_{imine}-C_{imine} and C_{imine}-$C_{pyridine}$ bond lengths, they all fall within the range for $[^{iPr}PDI]^{2-}$, suggesting that $(^{iPr}PDI)Mn(THF)_2$ contains a Mn(II) ion. Long Mn-N bond distances of 2.1213(15), 2.0514(17) and 2.1946(15) Å to the bis(imino)pyridine chelate indicate population of the d_{x2-y2} orbital, consistent with a high spin configuration at the manganese center.

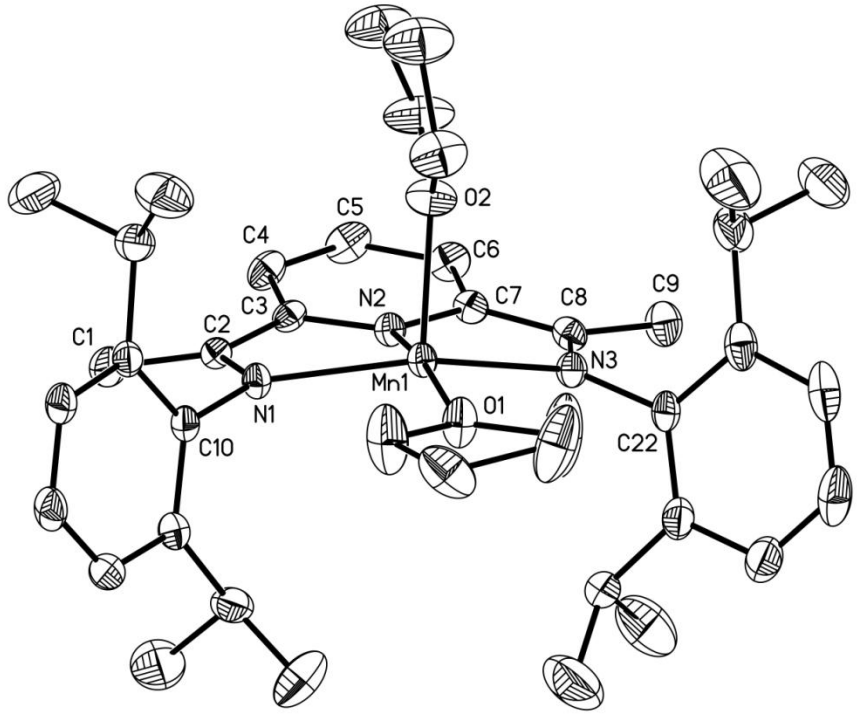

Figure 6.2 Solid state structure of $(^{iPr}PDI)Mn(THF)_2$ at 30% probability ellipsoids. Hydrogen atoms omitted for clarity.

Table 6.1 Selected bond distances (Å) and angles (°) for (^{iPr}PDI)Mn(THF)$_2$.

Mn(1)-N(1)	2.1213(15)	N(1)-C(2)	1.367(3)
Mn(1)-N(2)	2.0514(17)	N(3)-C(8)	1.340(3)
Mn(1)-N(3)	2.1946(15)	C(2)-C(3)	1.441(3)
Mn(1)-O(1)	2.1909(15)	C(7)-C(8)	1.421(3)
Mn(1)-O(2)	2.1998(16)	O(1)-Mn(1)-O(2)	93.85(6)
		N(2)-Mn(1)-O(1)	169.19(7)

The solid state magnetic moment of (^{iPr}PDI)Mn(THF)$_2$ at 23 °C was measured to be μ_{eff} = 3.7 μ_B by magnetic susceptibility balance, consistent with an overall $S = {}^3/_2$ spin state. This information, coupled with the solid state metrical parameters, suggest that the electronic structure of (^{iPr}PDI)Mn(THF)$_2$ is a high spin Mn(II) center ($S_{Mn} = {}^5/_2$) antiferromagnetically coupled to a triplet diradical bis(imino)pyridine chelate ($S_{PDI} = 1$), giving an overall spin state of $S = {}^3/_2$ for the molecule. To further substantiate this electronic structure, solution state EPR spectroscopic data was collected on (^{iPr}PDI)Mn(THF)$_2$. The experimental data is presented in Figure 6.3 along with the best fit that has been simulated to date. The EPR spectrum shows contamination from another manganese compound, likely a manganese oxide or hydroxide complex. However, the overall shape of the spectrum and the relatively high *g*-anisotropy are consistent with an $S = {}^3/_2$ compound with unpaired spins on the manganese center. The spectrum was simulated with the following parameters: D = 25.0 cm^{-1}, E/D = 0.20, g_x = 2.523, g_y = 2.615, g_z = 3.722, A_{xx} = 9.0 x 10^{-4} cm^{-1}, A_{yy} = 121.0 x 10^{-4} cm^{-1}, A_{zz} = 0.0 x 10^{-4} cm^{-1}. However, SQUID data is still needed to provide further evidence for the proposed electronic structure.

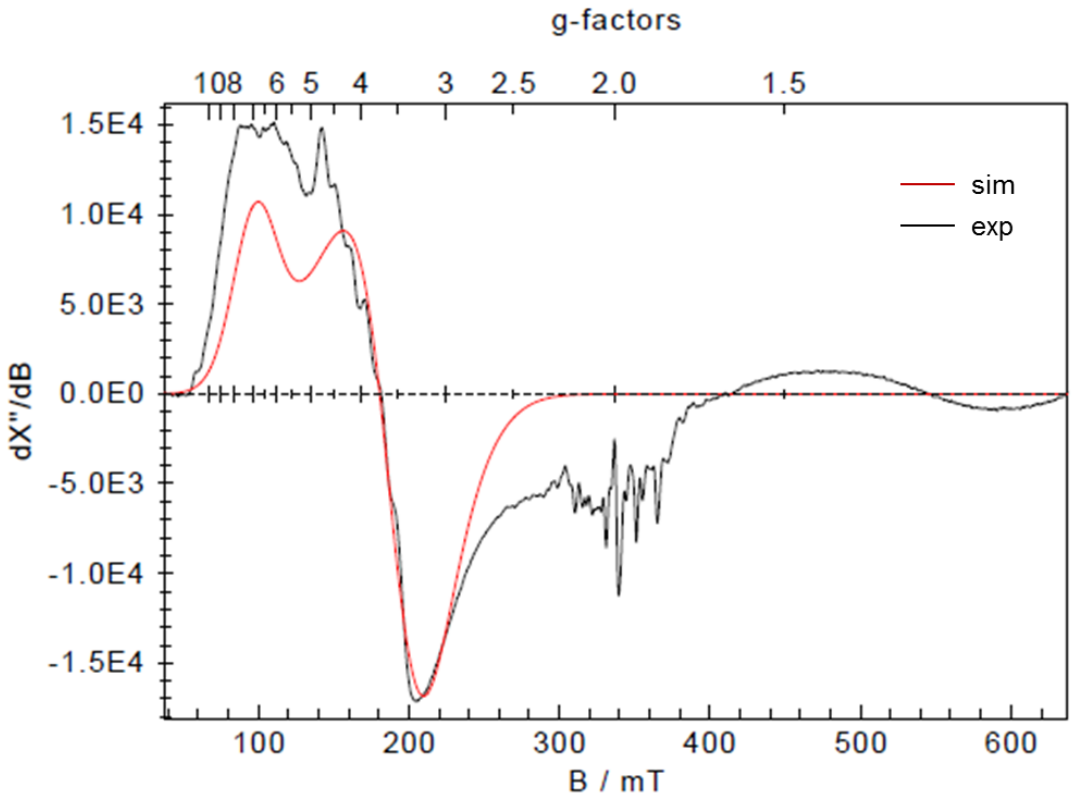

Figure 6.3 Experimental (10 K in 1:1 toluene/pentane solution) and simulated EPR spectra for (^{iPr}PDI)Mn(THF)$_2$; g_x = 2.523, g_y = 2.615, g_z = 3.722; A_{xx} = 9.0 x 10^{-4} cm^{-1}, A_{yy} =121 x 10^{-4} cm^{-1}, A_{zz} = 0.0 x 10^{-4} cm^{-1}.

In an attempt to isolate a bis(imino)pyridine manganese bis(dinitrogen) complex, a pentane slurry of (^{iPr}PDI)MnCl$_2$ was stirred with excess 0.5% sodium amalgam under a dinitrogen atmosphere for two days. Recrystallization from diethyl ether yielded the bis(chelate) manganese compound, (^{iPr}PDI)$_2$Mn, in 46% yield (Figure 6.4). Akin to (^{iPr}PDI)Mn(THF)$_2$, (^{iPr}PDI)$_2$Mn has a largely uninformative benzene-d_6 ^{1}H NMR spectrum with only broad peaks. Addition of 1 atmosphere of carbon monoxide to (^{iPr}PDI)$_2$Mn yielded the bis(imino)pyridine manganese dicarbonyl compound (*vide infra*), (^{iPr}PDI)Mn(CO)$_2$, and one equivalent of free ^{iPr}PDI.

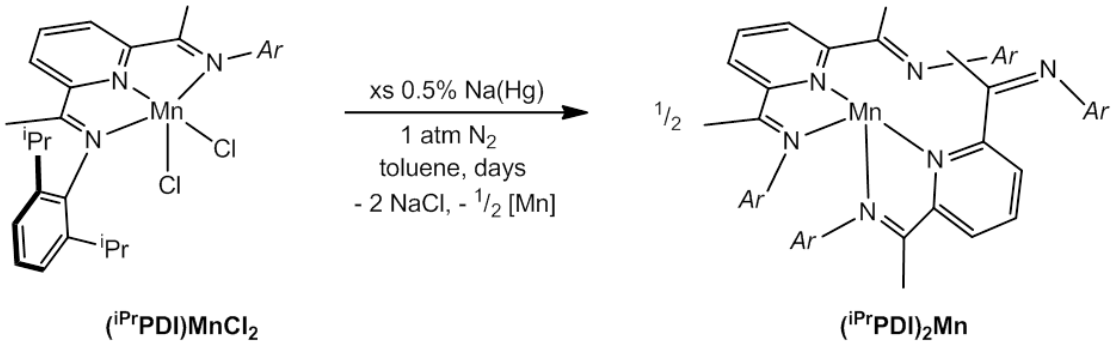

Figure 6.4 Synthesis of (^{iPr}PDI)$_2$Mn from two electron reduction of (^{iPr}PDI)MnCl$_2$.

Single crystals of (^{iPr}PDI)$_2$Mn suitable for X-ray diffraction were obtained from a concentrated diethyl ether solution at -35 °C. A representation of the solid state molecular structure is presented in Figure 6.5 and selected angles and bond distances are reported in Table 6.2. The solid state structure establishes two κ^2-coordinated chelates in an idealized *cis*-divacant octahedral geometry about the manganese center with the sites opposite to the coordinated N_{imine} atoms vacant. This geometry is in contrast to the idealized octahedral geometry observed for previously characterized [($^{4\text{-OMe}}$PDI)$_2$Mn][PF$_6$] and [($^{4\text{-OMe}}$PDI)$_2$Mn][PF$_6$]$_2$.[16] The κ^2- versus κ^3-chelate is likely steric in origin; the relatively large 2,6-diisopropyl aryl substituents prevent formation of a six-coordinate compound. This effect is also seen in bis(imino)pyridine iron compounds where the chelates in (^{Et}PDI)$_2$Fe are κ^2-coordinated while those in ($^{4\text{-OMe}}$PDI)$_2$Fe exhibit κ^3-coordination.[28]

As in (^{iPr}PDI)Mn(THF)$_2$, asymmetry in corresponding bond lengths is again observed; however, the average bond distances of each bis(imino)pyridine chelate are consistent with one electron reduction.[12,16] The N_{imine}-C_{imine} bond distances of the coordinated imine arms are elongated to 1.324(3) and 1.338(3) Å while the C_{imine}-$C_{pyridine}$ bond distances are contracted to 1.450(3) and 1.430(3) Å, respectively. The imine arms of the chelate that are not coordinated to the manganese center show very

little distortions in bond length with N_{imine}-C_{imine} distances of 1.298(3) and 1.281(3) Å and C_{imine}-$C_{pyridine}$ distances of 1.468(3) and 1.489(3) Å. Also like (^{iPr}PDI)Mn(THF)$_2$, the manganese bis(chelate) compound has long Mn-N_{PDI} bond lengths, indicating a probable high spin manganese(II) center.

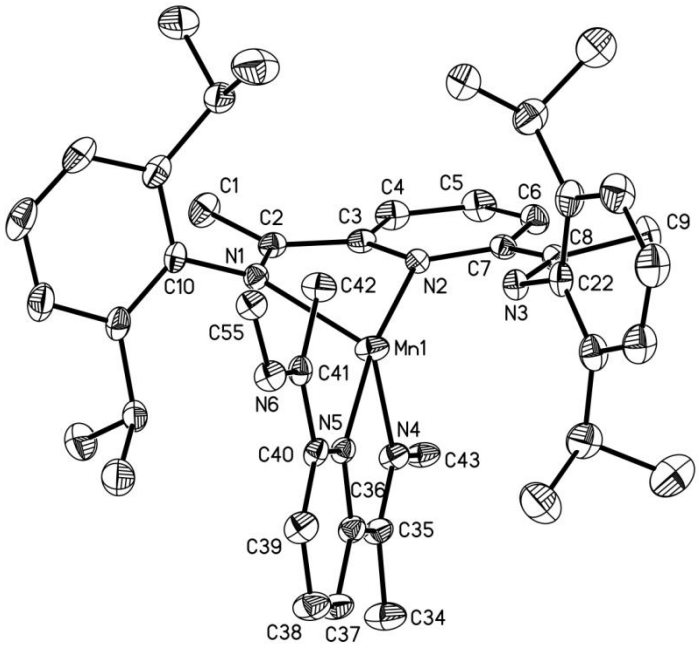

Figure 6.5 Solid state structure of (^{iPr}PDI)$_2$Mn at 30% probability ellipsoids. Hydrogen atoms and aryl groups omitted for clarity.

The solid state magnetic moment of (^{iPr}PDI)$_2$Mn was measured by magnetic susceptibility balance to be μ_{eff} = 3.9 μ_B at 23 °C, consistent with an overall spin state of $S = {}^3/_2$ for the molecule. Taking the molecular spin state and the solid state metrical parameters into account, an electronic structure for (^{iPr}PDI)$_2$Mn can be proposed. Similar to (^{iPr}PDI)Mn(THF)$_2$, the manganese bis(chelate) complex is likely a high spin Mn(II) center ($S_{Mn} = {}^5/_2$) antiferromagnetically coupled to, in this case, two one-electron reduced bis(imino)pyridine chelates ($S_{PDI} = {}^1/_2$), giving an overall spin state of $S = {}^3/_2$ for the molecule.

Table 6.2 Selected bond distances (Å) and angles (°) for (^{iPr}PDI)$_2$Mn.

Mn(1)-N(1)	2.2637(18)	N(3)-C(8)	1.298(3)
Mn(1)-N(2)	2.0320(16)	N(6)-C(41)	1.281(3)
Mn(1)-N(4)	2.1406(19)	C(2)-C(3)	1.450(3)
Mn(1)-N(5)	2.1311(16)	C(35)-C(36)	1.430(3)
N(1)-C(2)	1.324(3)	C(7)-C(8)	1.468(3)
N(4)-C(35)	1.338(3)	C(40)-C(41)	1.489(3)
N(2)-Mn(1)-N(5)	171.05(7)	N(1)-Mn(1)-N(2)	74.33(7)
N(2)-Mn(1)-N(4)	95.26(7)	N(1)-Mn(1)-N(5)	114.13(7)
N(4)-Mn(1)-N(5)	79.40(7)	N(1)-Mn(1)-N(4)	109.11(7)

To further substantiate this electronic structure, solution state EPR spectroscopic data was collected on (^{iPr}PDI)$_2$Mn. The experimental data is presented in Figure 6.6 along with the best fit that has been simulated to date. The EPR spectrum again shows contamination from another manganese compound, likely a manganese oxide or hydroxide complex. However, the overall shape of the spectrum and the relatively high *g*-anisotropy are consistent with an $S = {}^3/_2$ compound with unpaired spins on the manganese center. The spectrum was simulated with the following parameters: D = 26.0 cm^{-1}, E/D = 0.28, g_x = 1.715, g_y = 1.828, g_z = 2.294, A_{xx} = 250 x 10^{-4} cm^{-1}, A_{yy} = 200 x 10^{-4} cm^{-1}, A_{zz} = 200 x 10^{-4} cm^{-1}. However, SQUID data is still needed to provide further evidence for the proposed electronic structure.

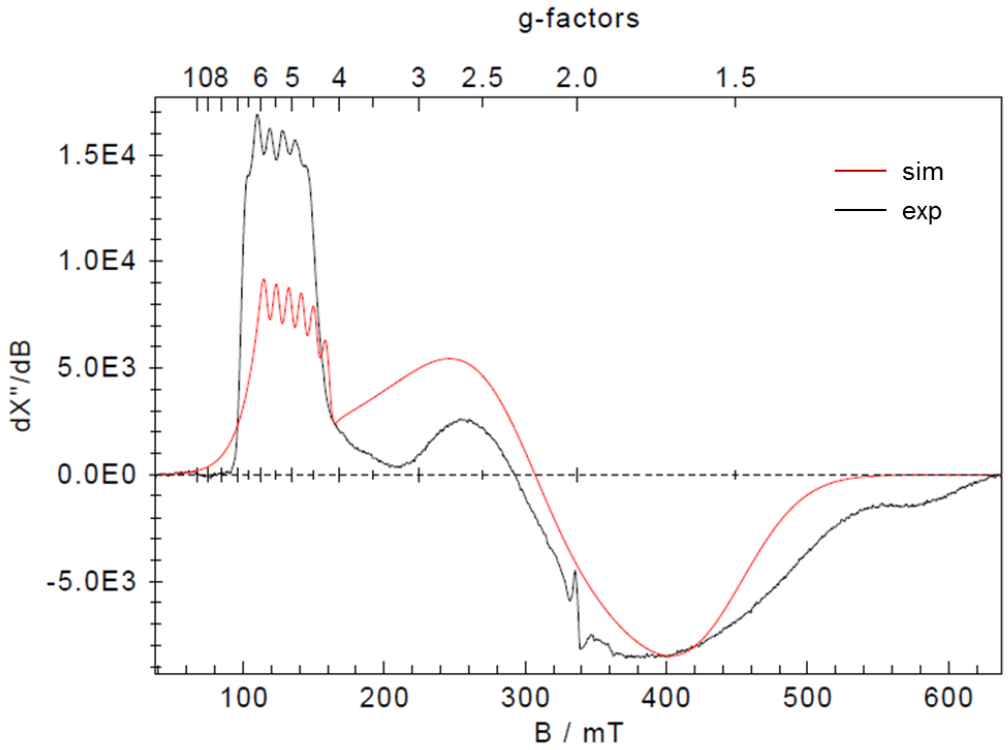

Figure 6.6 Experimental (10 K in 1:1 toluene/pentane solution) and simulated EPR spectra for (^{iPr}PDI)$_2$Mn; g_x = 1.715, g_y = 1.828, g_z = 2.294; A_{xx} =250 x 10^{-4} cm^{-1}, A_{yy} =200 x 10^{-4} cm^{-1}, A_{zz} = 200 x 10^{-4} cm^{-1}.

The bis(imino)pyridine manganese bis(THF) complex was screened as a pre-catalyst for olefin hydrogenation and diene cycloisomerization. Unfortunately, (^{iPr}PDI)Mn(THF)$_2$ produced no turnover for the hydrogenation of either 1-hexene or cyclohexene with up to 10 mol% catalyst loading at 23 °C or 65 °C and 4 atmospheres of H_2. Similarly, when the α,ω-substituted dienes diallyl-*tert*-butyl amine and diethyl diallyl malonate were exposed to 10 mol% (^{iPr}PDI)Mn(THF)$_2$ no reaction was observed, even upon heating to 65 °C. The lack of reactivity seen for (^{iPr}PDI)Mn(THF)$_2$ is not surprising given the failure of (^{iPr}PDI)MnCl$_2$ to polymerize ethylene when activated with methylaluminoxane (MAO).[18] Both compounds are proposed to have d^5 high spin manganese(II) centers which is thought to be the reason for, at least, the polymerization inactivity.

6.4 One Electron Reduction of (^{iPr}PDI)MnCl$_2$

An intermediate dark red-orange color was observed during the reduction of (^{iPr}PDI)MnCl$_2$ under both reduction conditions and is likely the bis(imino)pyridine manganese monochloride compound, (^{iPr}PDI)MnCl. Independent synthesis of (^{iPr}PDI)MnCl was achieved by two separate methods (Figure 6.7). Stirring a THF slurry of (^{iPr}PDI)MnCl$_2$ with one equivalent of sodium and 0.05 equivalents of naphthalene followed by a solvent switch to diethyl ether, filtration and removal of all solvent yielded a dark red solid identified as (^{iPr}PDI)MnCl(THF). Some decomposition occurred during work up of the reaction so a second method was investigated for the synthesis of the bis(imino)pyridine manganese monochloride. Stirring one equivalent of (^{iPr}PDI)MnCl$_2$ and (^{iPr}PDI)Mn(THF)$_2$ in THF for 16 hours followed by solvent removal furnished (^{iPr}PDI)MnCl(THF) in 91 % yield.

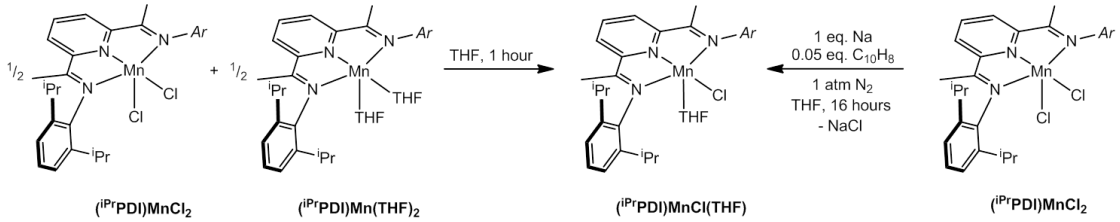

Figure 6.7 Synthetic routes to (^{iPr}PDI)MnCl(THF).

Surprisingly, (^{iPr}PDI)MnCl(THF) has a ^{1}H NMR spectrum that, while not readily assignable, can be used to positively identify the compound in a benzene-d_6 solution at 20 °C. The spectrum consists of 5 broad peaks ranging from -10 to 50 ppm. Addition of H_2O to the compound suggests that when synthesized in THF, a THF molecule coordinates to the manganese center. The THF ligand appears to stabilize the compound, as crystallization attempts from other solvents, such as diethyl ether or pentane, resulted in decomposition by the formation of a white powder.

Single crystals of (^{iPr}PDI)MnCl(THF) suitable for X-ray diffraction were obtained by layering pentane on a THF solution of the bis(imino)pyridine manganese monochloride. A representation of the solid state molecular structure is presented in Figure 6.8 and selected angles and bond distances are reported in Table 6.3. The solid state structure confirms the coordination of one molecule of THF and establishes an essentially square pyramidal geometry with the chelate and the chloride ligand in the basal positions and the THF ligand in the apical position. The unit cell contains one half of two independent (^{iPr}PDI)MnCl(THF) molecules and each molecule has a mirror plane containing the $N_{pyridine}$, Mn, Cl and O atoms.

The metrical parameters for (^{iPr}PDI)MnCl(THF) are consistent with either neutral or singly reduced bis(imino)pyridine chelate.[12,16] The N_{imine}-C_{imine} bond lengths of 1.293(2) and 1.296(3) Å are only slightly elongated from the values reported for (^{iPr}PDI)$MnCl_2$ (1.273(8) and 1.279(8) Å) and fall between the average values reported for the neutral and monoreduced chelate coordinated to a manganese center.[16] The bis(imino)pyridine iron monohalide complex, (^{iPr}PDI)FeBr(THF), has also been crystallographically characterized[29] and relevant bond lengths and angles are reported in Table 6.3 for comparison. For reference, the electronic structure of the iron monohalide compound is proposed to be a high spin iron(II) center antiferromagnetically coupled to a one-electron reduced chelate. The iron analog also has relatively short N_{imine}-C_{imine} bond lengths for a $[PDI]^{1-}$ assignment. This similarity, and the fact that the C_{imine}-$C_{pyridine}$ distances in (^{iPr}PDI)MnCl(THF) of 1.454(3) and 1.441(3) Å are much closer to the reported average value for a one-electron reduced chelate (1.442(1) Å) than an unreduced chelate (1.498(2) Å),[16] suggests that the bis(imino)pyridine manganese monohalide complex also contains a one-electron reduced chelate.

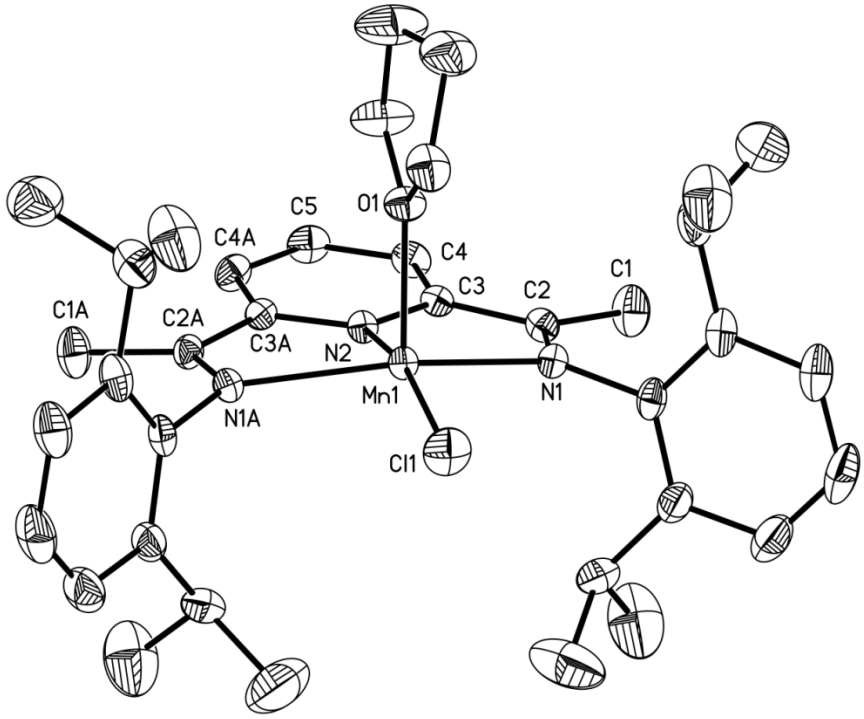

Figure 6.8 Solid state structure of (^{iPr}PDI)MnCl(THF) at 30% probability ellipsoids. Hydrogen atoms omitted for clarity.

The long Mn-N bond lengths in (^{iPr}PDI)MnCl(THF) again suggest a high spin manganese center similar to the corresponding bis(imino)pyridine iron monohalide. The solid state magnetic moment was measured by magnetic susceptibility balance at 23 °C to be 4.6 μ_B, consistent with an overall S = 2 spin state. The combination of the crystal structure data and the magnetic measurement suggest that (^{iPr}PDI)MnCl(THF) has an electronic structure similar to its iron analog with a high spin manganese(II) center ($S_{Mn} = {}^5/_2$) antiferromagnetically coupled to a monoreduced bis(imino)pyridine chelate (S_{PDI} = ½) for an overall S = 2 ground state.

Table 6.3 Selected bond distances (Å) and angles (°) for both molecules of (^{iPr}PDI)MnCl(THF) and for (^{iPr}PDI)FeBr(THF).[29]

	(^{iPr}PDI)MnCl(THF)	**(^{iPr}PDI)FeBr(THF)**
$Mn\text{-}N_{pyridine}$	2.065(2)	2.008(3)
	2.058(2)	
$Mn\text{-}N_{imine}$	2.283(2)	2.172(3)
	2.314(2)	2.150(3)
Mn-Cl	2.293(1)	2.416(1)
	2.298(1)	
Mn-O	2.162(2)	2.166(5)
	2.151(2)	
$N_{imine}\text{-}C_{imine}$	1.293(2)	1.299(4)
	1.296(3)	1.306(4)
$C_{imine}\text{-}C_{ipso}$	1.454(3)	1.446(5)
	1.441(3)	1.433(5)
$N_{pyridine}$-Mn-O	95.27(8)	92.64(15)
	102.39(9)	
$N_{pyridine}$-Mn-Cl	163.12(7)	167.89(9)
	160.63(7)	

6.5 Bis(imino)pyridine Manganese Carbonyl Complexes

Addition of 4 atmospheres of carbon monoxide to a toluene solution of (^{iPr}PDI)Mn(THF)$_2$ resulted in a color change from brown to dark pink. Solvent removal furnished the bis(imino)pyridine manganese dicarbonyl, (^{iPr}PDI)Mn(CO)$_2$, in 87 % yield as a dark purple solid (Figure 6.9). The infrared spectrum of (^{iPr}PDI)Mn(CO)$_2$ exhibits two strong carbonyl stretching bands centered at 1860 and 1915 cm^{-1} in pentane and 1836 and 1896 cm^{-1} in KBr. These frequencies are red-shifted from those observed for (^{iPr}PDI)Fe(CO)$_2$ which appear at 1914 and 1974 cm^{-1} in pentane,[8b] indicating that the manganese center in (^{iPr}PDI)Mn(CO)$_2$ is more reducing than the iron center in the corresponding iron dicarbonyl compound. As with the previously studied [^{iPr}PDIMn] compounds, only a few broad peaks are observed in the benzene-d_6 ^{1}H NMR spectrum of (^{iPr}PDI)Mn(CO)$_2$ collected at 20 °C; however,

the peaks are much sharper and within a much smaller range (from -5 to 15 ppm) compared to the bis(THF) and bis(chelate) manganese compounds.

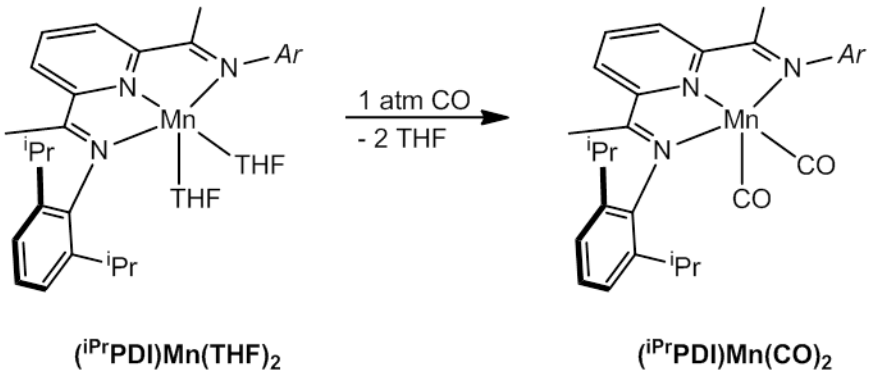

Figure 6.9 Synthesis of (^{iPr}PDI)Mn(CO)$_2$.

A solid state magnetic moment of 1.8 μ_B was measured for (^{iPr}PDI)Mn(CO)$_2$ by magnetic susceptibility balance at 23 °C, consistent with an $S = {}^1/_2$ ground state. To further study the electronic structure of (^{iPr}PDI)Mn(CO)$_2$, the bis(imino)pyridine manganese dicarbonyl compound was also studied by X-band EPR spectroscopy (Figure 6.10). The EPR spectrum was collected in toluene glass at 10K and confirms the S = ½ ground state measured by magnetic susceptibility balance. The g-values of 2.070, 2.202 and 1.998 are consistent with an organic centered radical as an unpaired spin in a metal-based orbital would have a g-value that deviates significantly from the ideal value of 2.002.[30] Simulating the experimental spectrum produced hyperfine coupling values to the manganese nucleus ($I = {}^5/_2$) of A_{xx} = 23 x 10^{-4} cm^{-1}, A_{yy} = 8.0 x 10^{-4} cm^{-1}, A_{zz} = 32.5 x 10^{-4} cm^{-1}. The relatively small hyperfine coupling constants are also indicative of bis(imino)pyridine chelate centered radical rather than a metal centered one. For comparison, low spin Mn(II) compounds which have an unpaired electron on the metal center have been studied by EPR spectroscopy and in all cases exhibit one A-value that is larger than 100 cm^{-1}.[31]

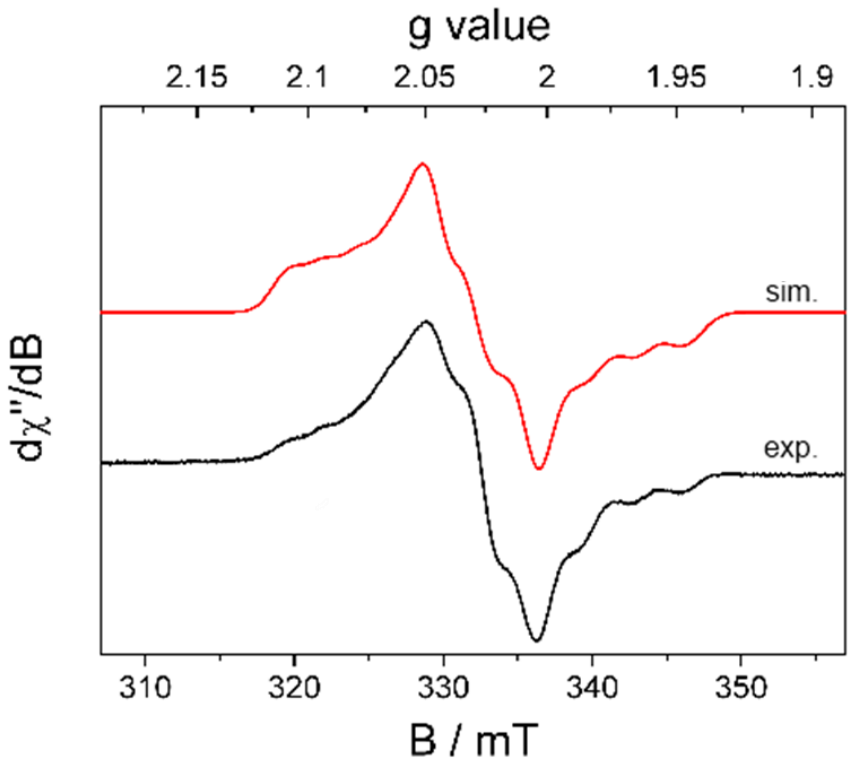

Figure 6.10 Experimental (10 K in toluene solution) and simulated EPR spectra for (^{iPr}PDI)Mn(CO)$_2$; g_x = 2.070, g_y = 2.202, g_z = 1.998; A_{xx} = 23 x 10^{-4} cm^{-1}, A_{yy} = 8.0 x 10^{-4} cm^{-1}, A_{zz} = 32.5 x 10^{-4} cm^{-1}.

Single crystals of (^{iPr}PDI)Mn(CO)$_2$ suitable for X-ray diffraction were obtained from a concentrated diethyl ether solution at -35 °C. A representation of the solid state molecular structure is presented in Figure 6.11 and selected bond distances and angles are reported in Table 6.4. The solid state structure of (^{iPr}PDI)Mn(CO)$_2$ establishes an idealized square pyramidal geometry with the chelate and one CO ligand forming the base and the other CO ligand occupying the apical position. The relatively short Mn-N bonds are consistent with a low spin manganese center. The N(1)-C(2) and N(3)-C(8) distances of 1.325(2) and 1.321(2) Å, respectively, fall nicely in the range of N_{imine}-C_{imine} bond distances for a monoreduced chelate. The

C(2)-C(3) and C(7)-C(8) distances of 1.443(2) and 1.445(2) Å are also consistent with one electron chelate reduction.

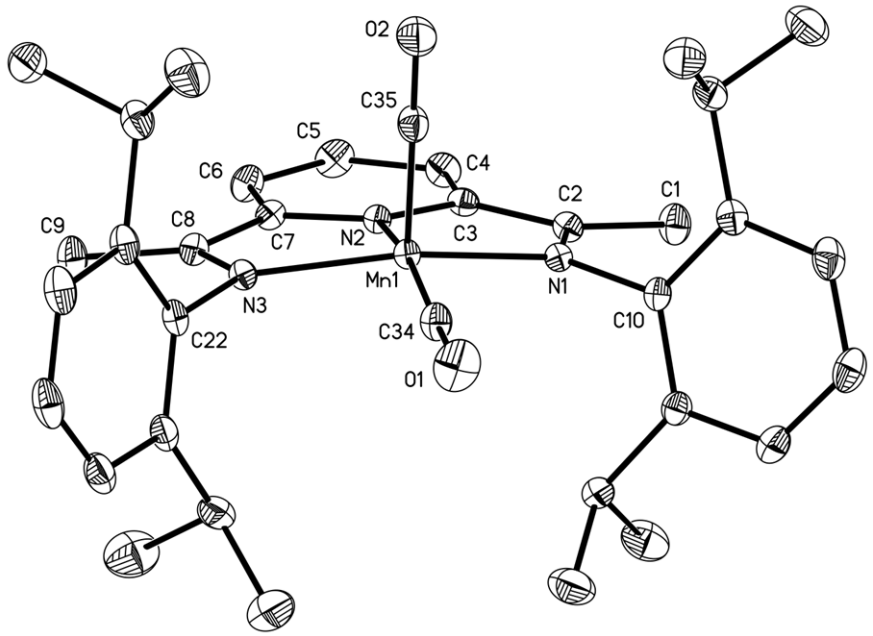

Figure 6.11 Solid state structure of (^{iPr}PDI)Mn(CO)$_2$ at 30% probability ellipsoids. Hydrogen atoms omitted for clarity.

Table 6.4 Selected bond distances (Å) and angles (°) for (^{iPr}PDI)Mn(CO)$_2$.

Mn(1)-N(1)	1.988(1)	N(1)-C(2)	1.325(2)
Mn(1)-N(2)	1.916(1)	N(3)-C(8)	1.321(2)
Mn(1)-N(3)	1.996(1)	C(2)-C(3)	1.443(2)
Mn(1)-C(34)	1.782(1)	C(7)-C(8)	1.445(2)
Mn(1)-C(35)	1.762(1)		
C(34)-Mn(1)-C(35)	90.30(6)	N(2)-Mn(1)-C(34)	165.42(5)

The EPR spectroscopy and X-ray diffraction data for (^{iPr}PDI)Mn(CO)$_2$ support a low spin manganese(I) center (S_{Mn} = 0) and a one-electron reduced bis(imino)pyridine chelate (S = ½) giving an S = ½ spin state for the overall molecule. Interestingly, this proposed electronic structure demonstrates a change in spin state as well as in the formal manganese oxidation state and amount of bis(imino)pyridine reduction by a ligand substitution reaction. The change from high spin to low spin at the manganese center can be explained by the fact that the weak σ-donor THF ligands are being replaced by strong σ-donor and π-acceptor carbon monoxide ligands. The π-accepting character of the CO ligands may also be the cause for the change in electron density distribution in the molecule. As stronger π-acceptors than the bis(imino)pyridine chelate, the carbon monoxide ligands pull electron density out of the PDI ligand and toward the manganese center and the Mn-CO bonds.

The proposed electronic structure of (^{iPr}PDI)Mn(CO)$_2$, with an uncoupled radical on the chelate, led to investigations of the reactivity of the bis(imino)pyridine manganese dicarbonyl compound. With the goal of observing radical reactivity at the backbone of the chelate, several substrates known to participate in radical reactions were added to (^{iPr}PDI)Mn(CO)$_2$. Unfortunately, addition of 2,2,6,6-tetramethylpiperidine-1-oxyl (TEMPO), TEMPOH, 1,4-cyclohexadiene, dihydroanthracene and ^{n}Bu$_3$SnH all resulted in no reaction even upon heating to 85 °C. The likely origin of the lack of radical reactivity is that the extra electron density is delocalized throughout the π-system of the bis(imino)pyridine chelate so that there is no true radical to react with.

Interestingly, attempts to prepare (^{iPr}PDI)Mn(CO)$_2$ by reduction of (^{iPr}PDI)MnCl$_2$ with excess 0.5% sodium amalgam under 4 atmospheres of carbon monoxide in toluene, standard conditions used to synthesize bis(imino)pyridine iron

dicarbonyl compounds, furnished the bis(imino)pyridine manganese dicarbonyl anion, [(^{iPr}PDI)Mn(CO)$_2$][Na(OEt$_2$)$_3$], instead of the neutral compound (Figure 6.12). Decreasing the amount of sodium amalgam to only two equivalents afforded only the manganese dicarbonyl anion and remaining (^{iPr}PDI)MnCl$_2$. Yellow [(^{iPr}PDI)Mn(CO)$_2$][Na(OEt$_2$)$_3$] was also prepared by reduction of (^{iPr}PDI)Mn(CO)$_2$ with one equivalent of sodium amalgam in toluene.

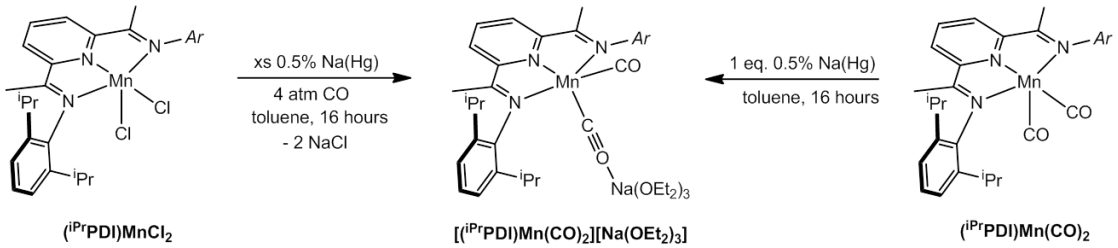

Figure 6.12 Synthetic routes to [(^{iPr}PDI)Mn(CO)$_2$][Na(OEt$_2$)$_3$].

The bis(imino)pyridine manganese dicarbonyl anion is isoelectronic with (^{iPr}PDI)Fe(CO)$_2$ and its facile synthesis demonstrates that the manganese compound prefers to have 18 electrons. The solid state infrared spectrum (KBr) of [(^{iPr}PDI)Mn(CO)$_2$][Na(OEt$_2$)$_3$] displays two strong ν(CO) bands at 1806 and 1719 cm^{-1}. These frequencies are red-shifted from those observed for the neutral compound and from those observed for the isoelectronic neutral iron dicarbonyl (Table 6.5), consistent with a more electron-rich manganese center in the anion. As expected for an 18 electron compound, [(^{iPr}PDI)Mn(CO)$_2$][Na(OEt$_2$)$_3$] is diamagnetic and displays an easily assignable solution ^{1}H NMR spectrum. Accordingly, the imine methyl backbone resonance appears at 2.62 ppm and the *meta*-pyridine resonance at 8.12 ppm in THF-d_8.

Table 6.5 Solid state infrared ν(CO) stretching frequencies for the bis(imino)pyridine manganese carbonyl series measured in KBr. Data for (^{iPr}PDI)Fe(CO)$_2$ taken from reference 8b.

Compound	ν(CO) (cm^{-1})
[(^{iPr}PDI)Mn(CO)$_2$][Na]	1806, 1719
(^{iPr}PDI)Mn(CO)$_2$	1896, 1836
	1915, 1860[a]
[(^{iPr}PDI)Mn(CO)$_3$][BPh$_4$]	2052, 1967, 1943
(^{iPr}PDI)Fe(CO)$_2$	1974, 1914[a]

[a] Recorded in pentane.

Single crystals of [(^{iPr}PDI)Mn(CO)$_2$][Na(OEt$_2$)$_3$] suitable for X-ray diffraction were obtained from a concentrated diethyl ether solution at -35 °C. A representation of the solid state structure is presented in Figure 6.13 and selected angles and bond distances are reported in Table 6.6. The solid state structure establishes an idealized trigonal bipyramidal geometry about the manganese center with a C(04)-Mn(1)-C(05) angle of 82.84(12)° and C(04)-Mn(1)-N(2) and C(05)-Mn(1)-N(2) angles of 141.11(11)° and 136.05(11)°, respectively. The sodium counterion is coordinated to the oxygen atom of one of the carbon monoxide ligands and the rest of its coordination sphere contains three disordered diethyl ether molecules. It is likely that the trigonal bipyramidal geometry is due to steric repulsion between the isopropyl aryl groups and the three diethyl ether molecules coordinated to the sodium.

The bond distances of the bis(imino)pyridine ligand are most consistent with a doubly reduced chelate. [12,16] The N(1)-C(2) and N(3)-C(8) bond distances are quite elongated to 1.343(3) and 1.351(3) Å, respectively, while the C(2)-C(3) and C(7)-C(8) distances are contracted to 1.411(4) and 1.399(4) Å, respectively. These bond distortions indicate that the added electron density resides on the bis(imino)pyridine ligand rather than the metal center while the short Mn-N bond lengths support a low-

spin manganese center. The solid state structure and the observed diamagnetism of [(^{iPr}PDI)Mn(CO)$_2$][Na(OEt$_2$)$_3$] suggest that the electronic structure of this compound is best described as a low-spin manganese(I) (S_{Mn} = 0) center with a singlet dianionic bis(imino)pyridine chelate (S_{PDI} = 0).

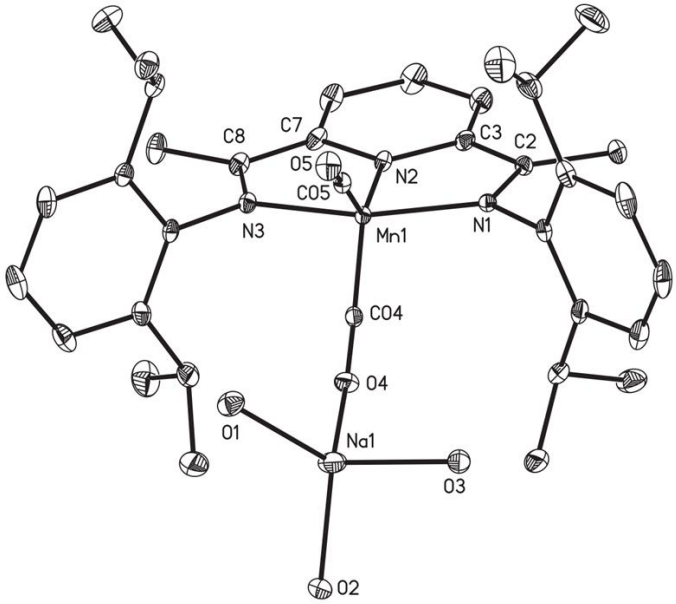

Figure 6.13 Solid state structure of [(^{iPr}PDI)Mn(CO)$_2$][Na(OEt$_2$)$_3$] at 30% probability ellipsoids. Hydrogen atoms and diethyl ether carbon atoms omitted for clarity.

Table 6.6 Select bond distances (Å) and angles (°) for [(^{iPr}PDI)Mn(CO)$_2$][Na(OEt$_2$)$_3$].

Mn(1)-N(1)	1.983(2)	N(1)-C(2)	1.343(3)
Mn(1)-N(2)	1.886(2)	N(3)-C(8)	1.351(3)
Mn(1)-N(3)	1.979(2)	C(2)-C(3)	1.411(4)
Mn(1)-C(04)	1.752(3)	C(7)-C(8)	1.399(4)
Mn(1)-C(05)	1.771(3)	C(04)-Mn(1)-C(05)	82.84(12)
C(04)-O(4)	1.190(3)	C(04)-Mn(1)-N(2)	141.11(11)
C(05)-O(5)	1.165(3)	C(05)-Mn(1)-N(2)	136.05(11)

The bis(imino)pyridine manganese dicarbonyl anion was easily oxidized to the neutral manganese dicarbonyl. Addition of one equivalent of silver tetrafluoroborate to [(^{iPr}PDI)Mn(CO)$_2$][Na(OEt$_2$)$_3$] followed by filtration to remove the silver metal afforded (^{iPr}PDI)Mn(CO)$_2$ in near quantitative yield, proving to be a second synthetic route to the neutral manganese dicarbonyl. To complete the bis(imino)pyridine manganese dicarbonyl series, the synthesis of the corresponding cation complex by further oxidation of the neutral compound was investigated.

Addition of one equivalent of [Cp$_2$Fe][BPh$_4$] to a benzene solution of (^{iPr}PDI)Mn(CO)$_2$ under a dinitrogen atmosphere followed by addition of pentane and collection of the tan solid afforded a new bis(imino)pyridine manganese compound in low yield. Interestingly, the solid state infrared spectrum displayed not two but three ν(CO) stretches centered at 2052, 1967 and 1943 cm^{-1}, identifying the new complex as the bis(imino)pyridine manganese tricarbonyl cation, [(^{iPr}PDI)Mn(CO)$_3$][BPh$_4$] (Figure 6.14). The first step in this transformation is likely oxidation of (^{iPr}PDI)Mn(CO)$_2$ to the corresponding manganese dicarbonyl cation, [(^{iPr}PDI)Mn(CO)$_2$][BPh$_4$]. The electron-poor manganese center then removes a carbon monoxide ligand from a second species in solution, probably (^{iPr}PDI)Mn(CO)$_2$ which then decomposes, resulting in the low yield of the reaction.

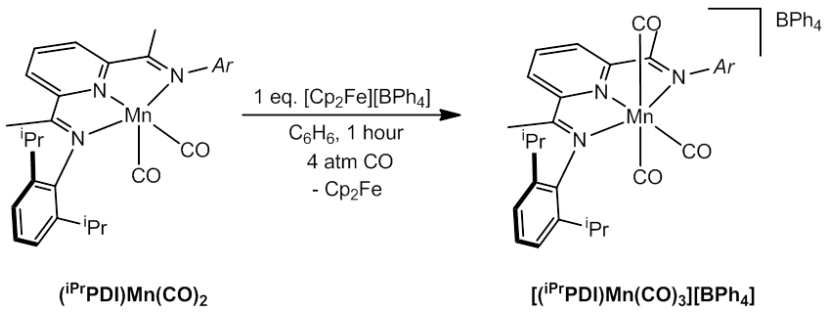

Figure 6.14 Synthesis of [(^{iPr}PDI)Mn(CO)$_3$][BPh$_4$].

The yield of [(^{iPr}PDI)Mn(CO)$_2$][BPh$_4$] was significantly increased by performing the oxidation under a carbon monoxide atmosphere instead of a dinitrogen one. Charging a thick-walled glass vessel with (^{iPr}PDI)Mn(CO)$_2$ and [Cp$_2$Fe][BPh$_4$] followed by addition of solvent by vacuum transfer and exposure to 4 atmospheres of carbon monoxide before warming to room temperature afforded [(^{iPr}PDI)Mn(CO)$_3$][BPh$_4$] in near quantitative yield. The cation, [(^{iPr}PDI)Mn(CO)$_3$][BPh$_4$], is also a diamagnetic 18 electron complex and accordingly displays a tetrahydrofuran-d_8 ^{1}H NMR spectrum with no evidence for temperature independent paramagnetism. The imine methyl group resonance appears at 2.17 ppm and the *meta*-pyridine resonance appears at 7.74 ppm.

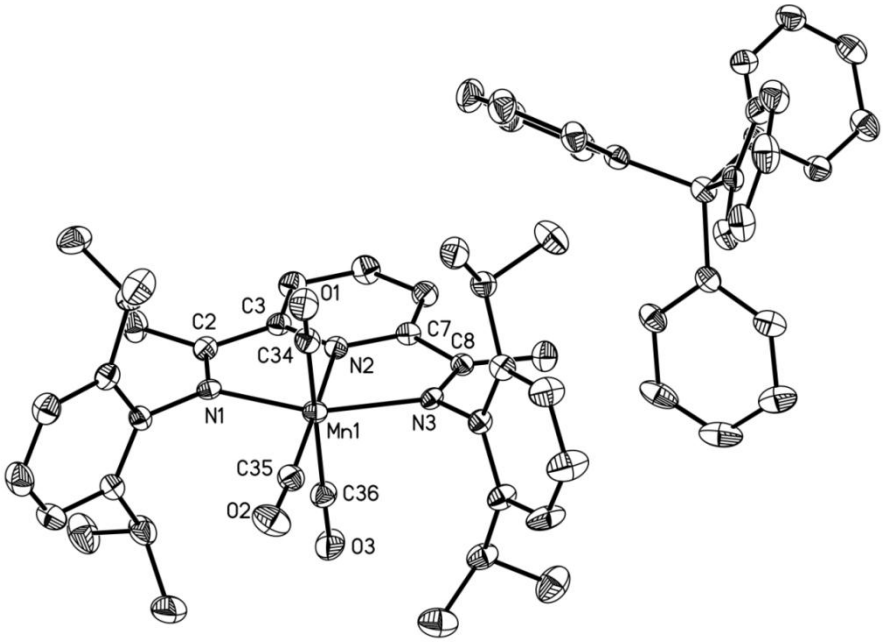

Figure 6.15 Solid state structure of [(^{iPr}PDI)Mn(CO)$_3$][BPh$_4$] at 30% probability ellipsoids. Hydrogen atoms omitted for clarity.

Single crystals suitable for X-ray diffraction were obtained from a fluorobenzene solution layered with pentane at -35 °C. A representative solid state structure is presented in Figure 6.15 and selected bond distances and angles are

reported in Table 6.7. The solid state geometry of [(^{iPr}PDI)Mn(CO)$_3$][BPh$_4$] is idealized octahedral with two carbon monoxide ligands *trans* to each other and the third *trans* to the pyridine nitrogen. The bis(imino)pyridine metrics are most consistent with a neutral chelate.[12,16] The C(2)-C(3) and C(7)-C(8) bond distances of 1.476(5) and 1.477(5) Å, respectively, are significantly longer than the corresponding bond distances of 1.443(2) and 1.445(2) Å in (^{iPr}PDI)Mn(CO)$_2$ and shorter than, but within statistical error of, those reported for (^{iPr}PDI)MnCl$_2$ (1.491(9) and 1.522(9) Å).[18] The bis(imino)pyridine manganese compounds, (^{iPr}PDI)MnCl$_2$ and (^{iPr}PDI)Mn(CO)$_2$, have neutral and one-electron reduced bis(imino)pyridine chelates, respectively. The C-N$_{imine}$ bond distances in [(^{iPr}PDI)Mn(CO)$_3$][BPh$_4$] also fall in the range between a neutral and monoreduced chelate. The N(1)-C(2) and N(3)-C(8) distances of 1.298(4) and 1.294(4) Å, respectively, are slightly longer than the corresponding distances in (^{iPr}PDI)MnCl$_2$, but shorter than those in (^{iPr}PDI)Mn(CO)$_2$.

Table 6.7 Selected bond distances (Å) and angles (°) for [(^{iPr}PDI)Mn(CO)$_3$][BPh$_4$].

Mn(1)-N(1)	2.054(3)	N(1)-C(2)	1.298(4)
Mn(1)-N(2)	1.961(3)	N(3)-C(8)	1.294(4)
Mn(1)-N(3)	2.093(3)	C(2)-C(3)	1.476(5)
Mn(1)-C(34)	1.858(4)	C(7)-C(8)	1.477(5)
Mn(1)-C(35)	1.784(4)		
Mn(1)-C(36)	1.861(4)	C(34)-Mn(1)-C(35)	84.54(16)
C(34)-O(1)	1.136(4)	C(35)-Mn(1)-C(36)	86.61(17)
C(35)-O(2)	1.169(4)	N(2)-Mn(1)-C(35)	173.43(14)
C(36)-O(3)	1.134(4)	C(34)-Mn(1)-C(36)	170.72(16)

The Mn-N bond distances are slightly longer than those observed for (^{iPr}PDI)Mn(CO)$_2$, a low spin manganese compound, but are still significantly shorter than the corresponding bond distances in (^{iPr}PDI)Mn(THF)$_2$ and (^{iPr}PDI)$_2$Mn which are both high spin manganese(II) species. These comparisons suggest that the manganese center in [(^{iPr}PDI)Mn(CO)$_3$][BPh$_4$] remains low spin manganese(I). The longer bond distances as compared to the neutral manganese dicarbonyl are possibly a result of the presence of the additional electron-withdrawing CO ligand. The solid state parameters coupled with the observed diamagnetism suggest that the electronic structure of [(^{iPr}PDI)Mn(CO)$_3$][BPh$_4$] is best described as a low spin Mn(I) center (S_{Mn} = 0) with a neutral bis(imino)pyridine chelate (S_{PDI} = 0).

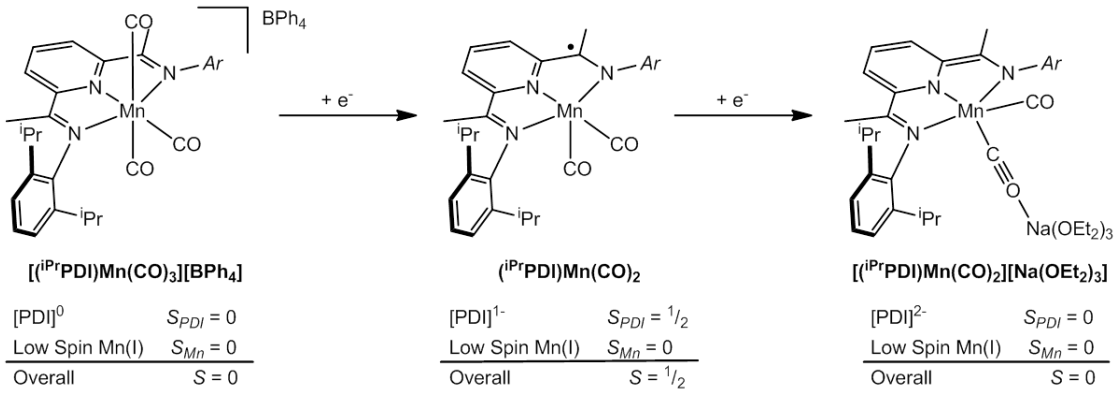

Figure 6.16 Proposed electronic structures of bis(imino)pyridine manganese carbonyl compounds.

Examining the proposed electronic structures of the series of bis(imino)pyridine manganese carbonyl compounds reveals that the oxidation and reduction events occur at the ligand, not the metal center (Figure 6.16). In reducing the cation, [(^{iPr}PDI)Mn(CO)$_3$][BPh$_4$], to the neutral compound, (^{iPr}PDI)Mn(CO)$_2$, the additional electron density is placed on the chelate and a reduction from [PDI]^0 to [PDI]$^{1-}$ is observed. Similarly, adding an addition electron to yield the anion,

[(^{iPr}PDI)Mn(CO)$_2$][Na(OEt2)3], results in further reduction of the bis(imino)pyridine chelate to [PDI]$^{2-}$. In all three compounds, the metal center remains in a d^6, low spin manganese(I) configuration.

6.6 Conclusions

The two electron reduction chemistry of (^{iPr}PDI)MnCl$_2$ was studied in comparison to its iron analog. Reduction of (^{iPr}PDI)MnCl$_2$ with excess 0.5 % sodium amalgam under a dinitrogen atmosphere did not yield the desired bis(imino)pyridine iron dinitrogen compound, but rather furnished the manganese bis(chelate) complex, (^{iPr}PDI)$_2$Mn. The room temperature electronic structure of (^{iPr}PDI)$_2$Mn is best described as a high spin manganese(II) center (S_{Mn} = $^5/_2$) antiferromagnetically coupled to two one-electron reduced bis(imino)pyridine chelates (S_{PDI} = ½) giving an overall quartet ground state. Similarly, reduction of (^{iPr}PDI)MnCl$_2$ in THF with sodium naphthalenide also did not furnish a dinitrogen compound, but rather the bis(imino)pyridine manganese bis(THF) complex, (^{iPr}PDI)Mn(THF)$_2$. The bis(THF) compound is also a quartet at room temperature, a result of a high spin manganese(II) center (S_{Mn} = $^5/_2$) antiferromagnetically coupling to a doubly reduced chelate (S_{PDI} = 1). Screening (^{iPr}PDI)Mn(THF)$_2$ as a pre-catalyst for olefin hydrogenation and diene cycloisomerization established that the reduced manganese compound is not catalytically active for either reaction.

One electron reduction of (^{iPr}PDI)MnCl$_2$ in THF afforded the bis(imino)pyridine manganese monochloride complex, (^{iPr}PDI)MnCl(THF). Similar to the iron analog, (^{iPr}PDI)FeBr(THF),[28] (^{iPr}PDI)MnCl(THF) appears to contain a one-electron reduced chelate antiferromagnetically coupled to a high spin metal(II) center. In the case of the manganese complex, the high spin manganese(II) (S_{Mn} = 5/2) and [^{iPr}PDI]$^{1-}$ result in an overall S = 2 ground state.

Finally, a series of bis(imino)pyridine manganese carbonyl complexes was synthesized and studied by NMR and EPR spectroscopy and X-ray diffraction. The data collected on the neutral compound, (^{iPr}PDI)Mn(CO)$_2$, establish a low spin manganese(I) center (S_{Mn} = 0) and a one-electron reduced chelate (S_{PDI} = ½) for an overall doublet ground state. Oxidation of (^{iPr}PDI)Mn(CO)$_2$ afforded the 18 electron bis(imino)pyridine manganese tricarbonyl cation, [(^{iPr}PDI)Mn(CO)$_3$][BPh$_4$]. The X-ray diffraction data support an unreduced bis(imino)pyridine chelate and a low spin manganese(I) center, suggesting that oxidation occurs at the ligand rather than the metal center. The corresponding 18 electron bis(imino)pyridine manganese dicarbonyl anion, [(^{iPr}PDI)Mn(CO)$_2$][Na(OEt$_2$)$_3$], was also synthesized and characterized by X-ray diffraction. The data support a singlet dianionic bis(imino)pyridine chelate coordinated to a low spin manganese(I) center, suggesting that reduction also occurs at the ligand rather than the metal center.

6.7 Experimental Procedures

General Considerations. All air- and moisture-sensitive manipulations were carried out using standard vacuum line, Schlenk, and cannula techniques or in an MBraun inert atmosphere dry box containing an atmosphere of purified nitrogen. Solvents for air- and moisture-sensitive manipulations were initially dried and deoxygenated using literature procedures.[32] Benzene-d_6 was purchased from Cambridge Isotope Laboratories and dried over 4 Å molecular sieves. The complexes: (^{iPr}PDI)MnCl$_2$[18] and [Cp$_2$Fe][BPh$_4$][33] were prepared according to literature procedures.

^{1}H NMR spectra were recorded on Varian Mercury 300, Inova 400, 500, and 600 spectrometers operating at 299.76, 399.78, 500.62, and 599.78 MHz, respectively. ^{13}C NMR spectra were recorded on an Inova 500 spectrometer operating at 125.893 MHz. All ^{1}H and ^{13}C NMR chemical shifts are reported relative to SiMe$_4$ using the ^{1}H

(residual) and ^{13}C chemical shifts of the solvent as a secondary standard. For diamagnetic complexes, many assignments were made based on COSY and HSQC NMR experiments. Solution magnetic moments were determined by Evans method[34] using a ferrocene standard and are the average value of at least two independent measurements. Gouy balance measurements were performed with a Johnson Matthey instrument that was calibrated with $HgCo(SCN)_4$. Peak widths at half heights are reported for paramagnetically broadened and shifted resonances. Infrared spectra were collected on a Thermo Nicolet spectrometer. Elemental analyses were performed at Robertson Microlit Laboratories, Inc., in Madison, NJ.

Single crystals suitable for X-ray diffraction were coated with polyisobutylene oil in a drybox, transferred to a nylon loop and then quickly transferred to the goniometer head of a Bruker X8 APEX2 diffractometer equipped with a molybdenum X-ray tube (λ = 0.71073 Å). Preliminary data revealed the crystal system. A hemisphere routine was used for data collection and determination of lattice constants. The space group was identified and the data were processed using the Bruker SAINT+ program and corrected for absorption using SADABS. The structures were solved using direct methods (SHELXS) completed by subsequent Fourier synthesis and refined by full-matrix least-squares procedures.

SQUID magnetization data of crystalline powdered samples were recorded with a SQUID magnetometer (Quantum Design) at 10 kOe between 5 and 300 K for all samples. Values of the magnetic susceptibility were corrected for the underlying diamagnetic increment by using tabulated Pascal constants and the effect of the blank sample holders (gelatin capsule/straw). Samples used for magnetization measurement were recrystallized multiple times and checked for chemical composition by ^1H NMR spectroscopy. The program julX written by E. Bill was used for (elements of) the simulation and analysis of magnetic susceptibility data.[35]

X-band EPR data were collected on a Bruker ELEXSYS E500 spectrometer equipped with the Bruker standard cavity (ER4102ST) and a helium flow cryostat (Oxford Instruments ESR 910). Microwave frequencies were calibrated with a Hewlett-Packard frequency counter (HP5352B), and the field control was calibrated with a Bruker NMR field probe (ER035M). The spectra were simulated with the program GFIT (by Eckhard Bill) for the calculation of powder spectra with effective g values and anisotropic line widths (Lorentzian line shapes were used). In each case, a 2 mM solution of the complex was prepared in toluene. Data was recorded at 296 K with a frequency of 9.43 GHz, a modulation amplitude of 10 G and a microwave power of 1.26 mW. Simulations were conducted using the W95EPR software package.

Preparation of (^{iPr}PDI)Mn(THF)$_2$. A 100 mL round bottom flask was charged with 1.00 g (^{iPr}PDI)$MnCl_2$ (1.65 mmol), 0.078 g sodium metal (3.37 mmol, 2.05 equivalents) and 0.010 g of naphthalene (0.082 mmol, 0.05 equivalents). To the flask was added approximately 20 mL of THF and the resulting reaction mixture was stirred for 16 hours. During this time, the solution changed color from orange to brown. After reduction was complete (indicated by the formation of the brown solution), the THF was removed *in vacuo*. The resulting solid was dissolved in diethyl ether and filtered through celite. The filtrate was collected and concentrated and stored at -35 ºC yielding 0.687 g (61 %) of a dark brown solid identified as (^{iPr}PDI)Mn(THF)$_2$. Crystals suitable for X-ray analysis were grown from a diethyl ether solution. Analysis for $C_{41}H_{59}N_3O_2Mn$: Calc. C, 75.89; H, 9.16; N, 6.48. Found C, 76.14; H, 9.20; N, 6.36. Magnetic susceptibility: μ_{eff} = 3.7 μ_B (Gouy balance, 23°C).

Preparation of (^{iPr}PDI)$_2$Mn. A 100 mL round bottom flask was charged with 45.41 g of mercury (226.38 mmol) and approximately 30 mL of pentane. Sodium metal

(0.227 g, 9.87 mmol) was cut into pieces and added to the round bottom. The amalgam was stirred for 10 minutes then solid (^{iPr}PDI)$MnCl_2$ (1.00 g, 1.65 mmol) was added to the flask. The reduction was stirred for 48 hours during which the color of the solution changed from orange to brown. After 48 hours, the solution was decanted away from the amalgam and filtered through celite. The remaining product was extracted into diethyl ether and filtered through celite. Recrystallization from diethyl ether at -35 ºC yielded 0.386 g (46 %) of a red solid identified as (^{iPr}PDI)$_2$Mn. Crystals suitable for X-ray analysis were grown from a diethyl ether solution. Analysis for $C_{66}H_{86}N_6Mn$: Calc. C, 77.84; H, 8.51; N, 8.25. Found C, 77.94; H, 8.52; N, 8.39. Magnetic susceptibility: $\mu_{eff} = 3.9\ \mu_B$ (Gouy balance, 23°C).

Preparation of (^{iPr}PDI)MnCl(THF). A 100 mL round bottom flask was charged with 0.500 g (0.734 mmol) of (^{iPr}PDI)Mn(THF)$_2$ and 0.450 g (0.741 mmol) of (^{iPr}PDI)$MnCl_2$. Approximately 20 mL of THF was added to the flask and the reaction was stirred for 16 hours resulting in a color change from brown to dark red. Following removal of the THF *in vacuo*, the product was taken up in diethyl ether and filtered through celite. The solution was evaporated to dryness to yield 0.673 g (91%) of a dark red solid identified as (^{iPr}PDI)MnCl(THF). Analysis for $C_{37}H_{51}N_3ClOMn$: Calc. C, 69.28; H, 7.58; N, 7.34. Found C, 69.01; H, 8.22; N, 7.32. Magnetic susceptibility: $\mu_{eff} = 4.6\ \mu_B$ (Gouy balance, 23°C). ^{1}H NMR (benzene-d_6, 20°C): δ = -7.91 (530 Hz), -1.80 (1013 Hz), 4.92 (656 Hz), 10.17 (954 Hz), 43.23 (1701 Hz).

Preparation of (^{iPr}PDI)Mn(CO)$_2$. A thick walled glass vessel was charged with 0.500 g (0.734 mmol) of (^{iPr}PDI)Mn(THF)$_2$ and approximately 20 mL of toluene. The vessel was brought out of the dry box and submerged in liquid nitrogen. On the high vacuum line, the vessel was evacuated and four atmospheres of CO were added. The

solution was warmed to room temperature and stirred for one hour turning dark pink in color. Excess CO was removed on the high vacuum line and the vessel brought back into the box. The solution was filtered through celite and all solvent removed *in vacuo* to yield 0.378 g (87 %) of a dark pink solid identified as (^{iPr}PDI)Mn(CO)$_2$. Crystals suitable for X-ray analysis were grown from a diethyl ether solution. Analysis for $C_{35}H_{43}N_3O_2Mn$: Calc. C, 70.93; H, 7.31; N, 7.09. Found C, 70.70; H, 7.37; N, 6.91. Magnetic susceptibility: $\mu_{eff} = 1.9\ \mu_B$ (benzene-d_6, 23°C). ^{1}H NMR (benzene-d_6, 20°C): δ = -2.41 (633 Hz), 3.52 (87 Hz), 5.98 (108 Hz), 7.24 (40 Hz), 13.34 (157 Hz). IR: ν(CO) 1836, 1896 cm^{-1} (KBr); 1860, 1915 cm^{-1} (pentane).

Preparation of [(^{iPr}PDI)Mn(CO)$_2$][Na(OEt$_2$)$_3$]. A thick-walled glass vessel was charged with 45.41 g of mercury (226.38 mmol) and approximately 50 mL of toluene. Sodium metal (0.227 g, 9.87 mmol) was cut into pieces and added to the vessel. The amalgam was stirred for 10 minutes then solid (^{iPr}PDI)MnCl$_2$ (1.00 g, 1.65 mmol) was added. The vessel was submerged in liquid nitrogen and 4 atmospheres of carbon monoxide were added on the high vacuum line. The reduction was warmed to room temperature and stirred for 48 hours during which the color of the solution changed from orange to dark yellow. After 48 hours, the vessel was degassed and brought into the glove box. The solution was decanted away from the amalgam and filtered through celite. The remaining product was extracted into diethyl ether and filtered through celite. Recrystallization from diethyl ether at -35 ºC yielded 0.772 g (92 %) of dark yellow crystals identified as [(^{iPr}PDI)Mn(CO)$_2$][Na(OEt$_2$)$_3$]. Crystals suitable for X-ray diffraction were grown from a concentrated diethyl ether solution at -35 ºC. ^{1}H NMR (benzene-d_6, 20°C): δ = 0.99 (d, 7.6 Hz, 12H, CH(C*H*$_3$)), 1.29 (d, 7.6 Hz, 12H, CH(C*H*$_3$)), 1.38 (bs, 8H, THF), 2.62 (s, 6H, C(C*H*$_3$)), 2.85 (sept, 7.6 Hz, 4H, C*H*(CH$_3$)), 3.49 (bs, 8H, THF), 7.09 (bs, 6H, *m-Ar* and *p-Ar*), 7.34 (t, 7.6 Hz, 1H, *p*-

py), 8.12 (d, 7.6 Hz, 2H, *m-py*) . ^{13}C NMR (benzene-d_6, 20°C): δ = 17.48 (C(*C*H$_3$)), 24.54 (CH(*C*H$_3$)$_2$), 25.54 (CH(*C*H$_3$)$_2$), 27.87 (*C*H(CH$_3$)$_2$), 117.47 (*m-py*), 123.02 (*m-Ar*), 124.85 (*p-Ar*), 126.41 (*p-py*), 140.09, 142.86, 146.81, 154.47 (quaternary carbons), 232.93 (*C*O) . IR(KBr): ν(CO) 1719, 1806 cm^{-1}.

Preparation of [(^{iPr}PDI)Mn(CO)$_3$][BPh$_4$]. A thick-walled glass vessel was charged with 0.200 g (0.337 mmol) of (^{iPr}PDI)Mn(CO)$_2$ and 0.170 g (0.337 mmol) of [Cp$_2$Fe][BPh$_4$]. The vessel was then evacuated on the high vacuum line and approximately 10 mL of benzene was added at liquid nitrogen temperature. Keeping the reaction frozen, 4 atmospheres of carbon monoxide was added. The solution was thawed to room temperature and stirred for 30 minutes during which time the color changed from purple to tan. The vessel was degassed and brought into the drybox where the solution was transferred to a vial and approximately 10 mL of pentane was added. Collection of the precipitate yielded 0.233 g (76 %) of a tan solid identified as [(^{iPr}PDI)Mn(CO)$_2$][BPh$_4$]. Analysis for $C_{60}H_{63}N_3O_3BMn$: Calc. C, 76.67; H, 6.67; N, 4.47. Found C, 76.39; H, 6.91; N, 4.38. ^{1}H NMR (tetrahydrofuran-d_8): δ = 1.08 (d, 5.2 Hz, 12H, CH(C*H*$_3$)$_2$), 1.36 (d, 5.2 Hz, 12H, CH(C*H*$_3$)$_2$), 2.17 (s, 6H, C(C*H*$_3$)), 2.57 (sept, 5.2 Hz, 4H, C*H*(CH$_3$)$_2$), 6.73 (bs, 8H, BPh$_4$), 6.87 (bs, 8H, BPh$_4$), 7.38 (bs, 4H, BPh$_4$), 7.07 (m, 6H, *Ar*), 7.74 (m, 3H, *m-py* and *p-py*). IR(KBr): ν(CO) 1943, 1967, 2052 cm^{-1}.

REFERENCES

[1] (a) Kleigrewe, N.; Steffen, W.; Blömker, T.; Kehr, G.; Fröhlich, R.; Wibbeling, B.; Erker, G.; Wasilke, J. –C.; Wu, G.; Bazan, G. C. *J. Am. Chem. Soc.* **2005**, *127*, 13955. (b) Bianchini, C.; Giambastiani, G.; Rios, I. G.; Mantovani, G.; Meli, A.; Segarra, A. M. *Coord. Chem. Rev.* **2006**, *250*, 1391.

[2] Zu, D.; Budzelaar, P. H. M. *Organometallics* **2008**, *27*, 2699.

[3] Gibson, V. C.; Redshaw, C.; Solan, G. A. *Chem. Rev.* **2007**, *107*, 1745.

[4] Matsugi, T.; Fujita, T. *Chem. Soc. Rev.* **2008**, *37*, 1264.

[5] Blackmore, I. J.; Gibson, V. C.; Hitchcock, P. B.; Rees, C. W.; Williams, D. J.; White, A. J. P. *J. Am. Chem. Soc.* **2005**, *127*, 6012.

[6] Vanadium: Vidyaratne, E.; Gambarotta, S.; Korobkov, E.; Budzelaar, P. H. M. *Inorg. Chem.* **2005**, *44*, 1187.

[7] Chromium: Vidyaratne, I.; Scott, j.; Bambarotta, S.; Budzelaar, P. H. M. *Inorg. Chem.* **2007**, *46*, 7040.

[8] Iron: (a) Russell, S. K.; Darmon, J. M.; Lobkovsky, E.; Chirik, P. J. *Inorg. Chem.* **2010**, *49*, 2782. (b) Bart, S. C.; Lobkovsky, E.; Chirik, P. J. *J. Am. Chem. Soc.* **2004**, *126*, 13794.

[9] Cobalt: (a) Bowman, A. C.; Milsmann, C.; Atienza, C. C. H.; Lobkovsky, E.; Wieghardt, K.; Chirik, P. J. *J. Am. Chem. Soc.* **2010**, *132*, 1676. (b) Gibson, V. C.; Humphries, M. J.; Tellmann, K. P.; Wass, D. F.; White, A. J. P.; Williams, D. J. *Chem. Commun.* **2001**, 2252.

[10] Ruthenium: Gallagher, M.; Wieder, N. L.; Dioumaev, V. K.; Carroll, P. J.; Berry, D. H. *Organometallics* **2010**, *29*, 591.

[11] Trovitch, R. J.; Lobkovsky, E.; Chirik, P. J. *Inorg. Chem.* **2006**, *45*, 7252.

[12] (a) Knijnenburg, Q.; Gambarotta, S.; Budzelaar, P. H. M. *Dalton Trans.* **2006**, 5442. (b) Bart, S. C.; Chlopek, K.; Bill, E.; Bouwkamp, M. W.; Lobkovsky, E.; Neese, F.; Wieghardt, K.; Chirik, P. J. *J. Am. Chem. Soc.* **2006**, *128*, 13901.

[13] Butin, K. P.; Beloglazkina, E. K.; Zyk, N. V. *Russ. Chem. Rev.* **2005**, *74*, 531.

[14] Knijnenburg, Q.; Hetterscheid, D.; Kooistra, T. M.; Budzelaar, P. H. M. *Eur. J. Inorg. Chem.* **2004**, 1204.

[15] Chaudhuri, P.; Wieghardt, K. *Prog. Inorg. Chem.* **2001**, *50*, 151.

[16] de Bruin, B.; Bill, E.; Bothe, E.; Weyhermüller, Wieghardt, K. *Inorg. Chem.* **2000**, *39*, 2936.

[17] Edwards, D. A.; Mahon, M. F.; Martin, W. R.; Molloy, K. C. *J. Chem. Soc., Dalton Trans.* **1990**, 3161.

[18] Reardon, D.; Aharonian, G.; Gambarotta, S.; Yap, G. P. A. *Organometallics* **2002**, *21*, 786.

[19] Sugiyama, H.; Aharonian, G.; Gambarotta, S.; Yap, G. P. A.; Budzelaar, P. H. M. *J. Am. Chem. Soc.* **2002**, *124*, 12268.

[20] (a) Small, B. M.; Brookhart, M. *J. Am. Chem. Soc.* **1998**, *120*, 7143. (b) Small, B. L.; Brookhart, M.; Bennett, A. M. A. *J. Am. Chem. Soc.* **1998**, *120*, 4049.

[21] (a) Britovsek, G. J. P.; Gibson, V. C.; Kimberley, B. S.; Maddox, S. J.; Solan, G. A.; White, A. J. P.; Williams, D. J. *Chem. Commun.* **1998**, 849. (b) Britovsek, G. J. P.; Bruce, M.; Gibson, V. C.; Kimberely, B. S.; Maddox, P. J.; Mastroianni, S.; McTavish, S. J.; Redshaw, C.; Solan, G. A.; Strömberg, S.; White, A. J. P.; Williams, D. J. *J. Am. Soc.* **1999**, *121*, 8728.

[22] (a) Cámpora, J.; Pérez, C. M.; Rodríguez-Delgado, A.; Naz, A. M.; Palma, P.; Álvarez, E. *Organometallics* **2007**, *26*, 1104. (b) Cámpora, J.; Palma, P.; Pérez, C. M.; Rodríguez-Delgado, A.; Álvarez, E.; Gutiérrez-Puebla, E. *Organometallics* **2010**, *29*, 2960.

[23] Britovsek, G. J. P.; England, J.; Spitzmesser, S. K.; White, A. J. P.; Williams, D. J. *Dalton Trans.* **2005**, 945.

[24] Trovitch, R. J.; Lobkovsky, E.; Bill, E.; Chirik, P. J. *Organometallics* **2008**, *27*, 1470.

[25] Tondreau, A. M.; Lobkovsky, E.; Chirik, P.J. *Org. Lett.* **2008**, *10*, 2789.

[26] Bouwkamp, M. W.; Bowman, A. C.; Lobkovsky, E.; Chirik, P. J. *J. Am. Chem. Soc.* **2006**, *128*, 13340.

[27] Sylvester, K. T.; Chirik, P. J. *J. Am. Chem. Soc.* **2009**, *131*, 8772.

[28] Wile, B. M.; Trovitch, R. J.; Bart, S. C.; Tondreau, A. M.; Lobkovsky, E.; Milsmann, C.; Bill, E.; Wieghardt, K.; Chirik, P. J. *Inorg. Chem.* **2009**, *48*, 4190.

[29] Trovitch, R. J.; Lobkovsky, E.; Chirik, P. J. *J. Am. Chem. Soc.* **2008**, *130*, 11631.

[30] Drago, R. S. *Physical Methods in Inorganic Chemistry*; Reinhold Publishing Co.: New York, 1965.

[31] Rieger, P. H. *Coord. Chem. Rev.* **1994**, *135-136*, 203.

[32] Pangborn, A. B.; Giardello, M. A.; Grubbs, R. H.; Rosen, R. K.; Timmers, F. J. *Organometallics* **1996**, *15*, 1518.

[33] Aggarwal, R. P.; Connelly, N. G.; Crespo, M. C.; Dunne, B. J.; Hopkins, P. M.; Orpen, A. G. *J. Chem. Soc. Dalton Trans.* **1992**, 655.

[34] Sur, S. K. *J. Mag. Res.* **1989**, *82*, 169-173.

[35] http://ewww.mpi-muelheim.mpg.de/bac/logins/bill/julX_en.php

APPENDIX A

CRYSTAL STRUCTURE DATA

Table A.1. Compilation of X-ray data for compounds discussed in this manuscript.

Compound	CU X-ray ID	Location
[(^{Et}PDI)Fe(N_2)]$_2$(μ_2-N_2)	skr2	CCDC 786285
(^{iPr}PDI)FeNHCHPh	sr1	CCDC 719827
(^{Et}PDI)FeCPh$_2$	sr2	APPENDIX A
(^{iPr}PDI)Mn(THF)$_2$	sr4	APPENDIX A
(^{iPr}PDI)$_2$Mn	sr5	APPENDIX A
(^{iPr}PDI)Mn(CO)$_2$	sr7	APPENDIX A
[(^{iPr}PDAI)Fe]$_2$	sr11	APPENDIX A
(^{iPr}PDAI)Fe(DMAP)	sr12	APPENDIX A
(^{iPr}PDAI)Fe(η^4-C_4H_6)	sr13	APPENDIX A
[(^{iPr}PDI)Mn(CO)$_3$][BPh$_4$]	sr14	APPENDIX A
(^{iPr}PDI)MnCl(THF)	sr15	APPENDIX A
(^{iPr}PDAI)FeN(2,4,6-Me$_3$-C_6H_2)	sr16	APPENDIX A
(^{Me}PDI)Fe((CH$_2$)$_3$(CH)$_2$CH$_2$)	sr18	APPENDIX A
[(^{iPr}PDI)Mn(CO)$_2$][Na(OEt$_2$)$_3$]	sr20[a]	APPENDIX A
^{iPr}PDAI	6996[b]	APPENDIX A

[a] Data collected at Princeton University.
[b] Data collected at MPI in Germany.

Table A.2. Crystal data and structure refinement for sr2.

Identification code	sr2	
Empirical formula	C42 H45 Fe N3	
Formula weight	647.66	
Temperature	173(2) K	
Wavelength	0.71073 Å	
Crystal system	Triclinic	
Space group	P-1	
Unit cell dimensions	a = 10.3857(5) Å	α= 80.960(2)°.
	b = 12.5498(6) Å	β= 86.060(2)°.
	c = 13.3966(6) Å	γ = 89.464(2)°.
Volume	1720.33(14) $Å^3$	
Z	2	
Density (calculated)	1.250 Mg/m^3	
Absorption coefficient	0.472 mm^{-1}	
F(000)	688	
Crystal size	0.60 x 0.25 x 0.15 mm^3	
Theta range for data collection	1.54 to 26.37°.	
Index ranges	-12<=h<=10, -15<=k<=15, -15<=l<=16	
Reflections collected	24375	
Independent reflections	6941 [R(int) = 0.0394]	
Completeness to theta = 26.37°	98.7 %	
Absorption correction	Semi-empirical from equivalents	
Max. and min. transmission	0.9326 and 0.7649	
Refinement method	Full-matrix least-squares on F^2	
Data / restraints / parameters	6941 / 33 / 472	
Goodness-of-fit on F^2	1.033	
Final R indices [I>2sigma(I)]	R1 = 0.0467, wR2 = 0.1037	
R indices (all data)	R1 = 0.0673, wR2 = 0.1142	
Largest diff. peak and hole	0.366 and -0.541 $e.Å^{-3}$	

Table A.3. Atomic coordinates (x 10^4) and equivalent isotropic displacement parameters ($Å^2$x 10^3) for sr2. U(eq) is defined as one third of the trace of the orthogonalized U^{ij} tensor.

	x	y	z	U(eq)
Fe(1)	1292(1)	2783(1)	7675(1)	30(1)
N(1)	1316(2)	4431(1)	7331(1)	33(1)
N(2)	-536(2)	3157(1)	7818(1)	41(1)
N(3)	361(2)	1443(1)	7301(1)	34(1)
C(1)	130(3)	6099(2)	7640(2)	63(1)
C(2)	222(2)	4921(2)	7567(2)	44(1)
C(3)	-878(2)	4220(2)	7745(2)	49(1)
C(4)	-2182(2)	4514(2)	7749(2)	69(1)
C(5)	-3116(2)	3743(2)	7755(2)	77(1)
C(6)	-2754(2)	2690(2)	7709(2)	64(1)
C(7)	-1455(2)	2413(2)	7705(2)	47(1)
C(8)	-903(2)	1408(2)	7505(2)	43(1)
C(9)	-1724(2)	434(2)	7501(2)	61(1)
C(10)	2495(2)	5041(2)	7121(1)	29(1)
C(12)	4147(2)	5822(2)	5895(2)	36(1)
C(13)	4837(2)	6105(2)	6655(2)	45(1)
C(14)	4361(2)	5856(2)	7642(2)	50(1)
C(15)	3191(2)	5310(2)	7908(2)	41(1)
C(11)	2971(2)	5293(2)	6109(1)	27(1)
C(16)	2213(2)	5062(2)	5252(2)	36(1)
C(17)	1295(2)	5981(2)	4904(2)	51(1)
C(18)	2903(5)	5072(4)	9004(3)	38(1)
C(19)	3994(4)	4925(4)	9706(3)	46(1)
C(18')	2483(7)	4943(5)	9011(4)	41(2)
C(19')	2247(6)	5876(4)	9583(3)	57(2)
C(20)	1005(2)	507(2)	7022(2)	37(1)
C(21)	1341(2)	517(2)	5998(2)	44(1)
C(22)	1945(3)	-399(2)	5717(2)	61(1)
C(23)	2233(3)	-1270(2)	6424(3)	75(1)
C(24)	1941(2)	-1242(2)	7423(3)	64(1)
C(25)	1314(2)	-365(2)	7763(2)	46(1)
C(26)	1182(6)	1570(5)	5310(5)	35(2)
C(27)	2136(6)	1982(5)	4407(5)	57(2)
C(26')	938(5)	1412(5)	5167(5)	57(2)
C(27')	1636(5)	1513(5)	4279(3)	64(2)
C(28)	976(7)	-350(6)	8879(5)	53(3)
C(29)	1614(6)	-981(4)	9779(4)	36(2)
C(28')	986(6)	-295(5)	8851(5)	59(2)
C(29')	1578(5)	-1326(4)	9493(4)	50(2)
C(30)	2809(2)	2233(2)	8322(1)	27(1)
C(31)	3728(2)	1774(2)	7633(1)	24(1)
C(32)	4013(2)	2306(2)	6642(2)	33(1)
C(33)	4711(3)	1806(2)	5935(2)	52(1)
C(34)	5143(3)	768(2)	6186(2)	54(1)
C(35)	4901(2)	231(2)	7156(2)	40(1)
C(36)	4228(2)	731(2)	7875(2)	27(1)
C(37)	3045(2)	2143(2)	9386(2)	31(1)
C(38)	4277(2)	2039(2)	9758(2)	38(1)
C(39)	4455(3)	2045(2)	10773(2)	53(1)
C(40)	3413(3)	2133(2)	11451(2)	60(1)
C(41)	2186(3)	2208(2)	11114(2)	58(1)

C(42)	2001(2)	2226(2)	10108(2)	44(1)

Table A.4. Bond lengths [Å] and angles [°] for sr2.

Fe(1)-C(30)	1.9205(19)	C(33)-C(34)	1.372(3)
Fe(1)-N(2)	1.9554(16)	C(34)-C(35)	1.373(3)
Fe(1)-N(1)	2.0467(16)	C(35)-C(36)	1.378(3)
Fe(1)-N(3)	2.0925(18)	C(37)-C(38)	1.402(3)
N(1)-C(2)	1.330(3)	C(37)-C(42)	1.416(3)
N(1)-C(10)	1.437(3)	C(38)-C(39)	1.387(3)
N(2)-C(3)	1.368(3)	C(39)-C(40)	1.380(4)
N(2)-C(7)	1.374(3)	C(40)-C(41)	1.378(4)
N(3)-C(8)	1.322(2)	C(41)-C(42)	1.371(3)
N(3)-C(20)	1.434(3)		
C(1)-C(2)	1.497(3)	C(30)-Fe(1)-N(2)	147.82(8)
C(2)-C(3)	1.432(3)	C(30)-Fe(1)-N(1)	112.04(7)
C(3)-C(4)	1.399(3)	N(2)-Fe(1)-N(1)	77.19(7)
C(4)-C(5)	1.375(4)	C(30)-Fe(1)-N(3)	105.91(7)
C(5)-C(6)	1.379(4)	N(2)-Fe(1)-N(3)	76.69(7)
C(6)-C(7)	1.390(3)	N(1)-Fe(1)-N(3)	140.43(7)
C(7)-C(8)	1.436(3)	C(2)-N(1)-C(10)	119.84(17)
C(8)-C(9)	1.499(3)	C(2)-N(1)-Fe(1)	115.49(14)
C(10)-C(11)	1.400(3)	C(10)-N(1)-Fe(1)	122.48(12)
C(10)-C(15)	1.403(3)	C(3)-N(2)-C(7)	118.89(18)
C(12)-C(13)	1.376(3)	C(3)-N(2)-Fe(1)	119.04(14)
C(12)-C(11)	1.387(3)	C(7)-N(2)-Fe(1)	119.57(15)
C(13)-C(14)	1.369(3)	C(8)-N(3)-C(20)	118.93(18)
C(14)-C(15)	1.397(3)	C(8)-N(3)-Fe(1)	115.34(15)
C(15)-C(18)	1.462(5)	C(20)-N(3)-Fe(1)	124.74(12)
C(15)-C(18')	1.606(6)	N(1)-C(2)-C(3)	113.89(19)
C(11)-C(16)	1.501(3)	N(1)-C(2)-C(1)	123.7(2)
C(16)-C(17)	1.525(3)	C(3)-C(2)-C(1)	122.4(2)
C(18)-C(19)	1.513(6)	N(2)-C(3)-C(4)	120.1(2)
C(18')-C(19')	1.506(8)	N(2)-C(3)-C(2)	112.08(18)
C(20)-C(21)	1.389(3)	C(4)-C(3)-C(2)	127.5(2)
C(20)-C(25)	1.408(3)	C(5)-C(4)-C(3)	120.0(2)
C(21)-C(22)	1.395(3)	C(4)-C(5)-C(6)	119.5(2)
C(21)-C(26)	1.503(6)	C(5)-C(6)-C(7)	119.6(3)
C(21)-C(26')	1.529(6)	N(2)-C(7)-C(6)	120.7(2)
C(22)-C(23)	1.374(4)	N(2)-C(7)-C(8)	112.59(17)
C(23)-C(24)	1.357(4)	C(6)-C(7)-C(8)	126.5(2)
C(24)-C(25)	1.395(4)	N(3)-C(8)-C(7)	114.06(19)
C(25)-C(28')	1.490(8)	N(3)-C(8)-C(9)	124.3(2)
C(25)-C(28)	1.516(7)	C(7)-C(8)-C(9)	121.56(19)
C(26)-C(27)	1.536(8)	C(11)-C(10)-C(15)	121.00(19)
C(26')-C(27')	1.339(7)	C(11)-C(10)-N(1)	117.69(17)
C(28)-C(29)	1.523(8)	C(15)-C(10)-N(1)	121.17(18)
C(28')-C(29')	1.582(7)	C(13)-C(12)-C(11)	121.2(2)
C(30)-C(37)	1.450(3)	C(14)-C(13)-C(12)	119.6(2)
C(30)-C(31)	1.460(3)	C(13)-C(14)-C(15)	121.9(2)
C(31)-C(36)	1.402(3)	C(14)-C(15)-C(10)	117.59(19)
C(31)-C(32)	1.403(3)	C(14)-C(15)-C(18)	112.8(3)
C(32)-C(33)	1.380(3)	C(10)-C(15)-C(18)	129.5(3)

C(14)-C(15)-C(18')	129.3(3)
C(10)-C(15)-C(18')	113.1(3)
C(18)-C(15)-C(18')	16.6(3)
C(12)-C(11)-C(10)	118.64(19)
C(12)-C(11)-C(16)	119.36(17)
C(10)-C(11)-C(16)	121.91(17)
C(11)-C(16)-C(17)	112.06(18)
C(15)-C(18)-C(19)	119.9(4)
C(19')-C(18')-C(15)	112.3(4)
C(21)-C(20)-C(25)	122.0(2)
C(21)-C(20)-N(3)	117.10(18)
C(25)-C(20)-N(3)	120.9(2)
C(20)-C(21)-C(22)	117.5(2)
C(20)-C(21)-C(26)	116.6(3)
C(22)-C(21)-C(26)	125.3(3)
C(20)-C(21)-C(26')	123.3(3)
C(22)-C(21)-C(26')	118.7(3)
C(26)-C(21)-C(26')	15.2(4)
C(23)-C(22)-C(21)	121.6(3)
C(24)-C(23)-C(22)	119.7(3)
C(23)-C(24)-C(25)	122.1(2)
C(24)-C(25)-C(20)	117.0(2)
C(24)-C(25)-C(28')	124.0(3)
C(20)-C(25)-C(28')	119.0(3)
C(24)-C(25)-C(28)	121.6(4)
C(20)-C(25)-C(28)	121.3(3)
C(28')-C(25)-C(28)	2.7(5)
C(21)-C(26)-C(27)	123.4(5)
C(27')-C(26')-C(21)	116.6(5)
C(25)-C(28)-C(29)	127.8(6)
C(25)-C(28')-C(29')	107.0(5)
C(37)-C(30)-C(31)	119.87(17)
C(37)-C(30)-Fe(1)	127.52(14)
C(31)-C(30)-Fe(1)	112.31(13)
C(36)-C(31)-C(32)	116.77(17)
C(36)-C(31)-C(30)	122.02(16)
C(32)-C(31)-C(30)	120.68(17)
C(33)-C(32)-C(31)	121.2(2)
C(34)-C(33)-C(32)	120.5(2)
C(33)-C(34)-C(35)	119.8(2)
C(34)-C(35)-C(36)	120.3(2)
C(35)-C(36)-C(31)	121.42(18)
C(38)-C(37)-C(42)	116.36(19)
C(38)-C(37)-C(30)	123.82(18)
C(42)-C(37)-C(30)	119.71(19)
C(39)-C(38)-C(37)	121.3(2)
C(40)-C(39)-C(38)	120.5(3)
C(41)-C(40)-C(39)	119.6(2)
C(42)-C(41)-C(40)	120.4(2)
C(41)-C(42)-C(37)	121.8(2)

Symmetry transformations used to generate equivalent atoms:

Table A.5. Crystal data and structure refinement for sr4.

Identification code	sr4	
Empirical formula	C41 H59	
Mn N3 O2		
Formula weight	680.85	
Temperature	173(2) K	
Wavelength	0.71073 Å	
Crystal system	Monoclinic	
Space group	P2(1)/c	
Unit cell dimensions	a = 11.4409(11) Å	α= 90°.
	b = 17.2188(15) Å	β= 110.977(4)°.
	c = 20.673(2) Å	γ = 90°.
Volume	3802.6(7) $Å^3$	
Z	4	
Density (calculated)	1.189 Mg/m^3	
Absorption coefficient	0.384 mm^{-1}	
F(000)	1468	
Crystal size	0.60 x 0.25 x 0.10 mm^3	
Theta range for data collection	1.91 to 26.65°.	
Index ranges	-14<=h<=13, -21<=k<=21, -17<=l<=25	
Reflections collected	27455	
Independent reflections	7840 [R(int) = 0.0437]	
Completeness to theta = 26.65°	97.8 %	
Absorption correction	Semi-empirical from equivalents	
Max. and min. transmission	0.9626 and 0.8022	
Refinement method	Full-matrix least-squares on F^2	
Data / restraints / parameters	7840 / 0 / 434	
Goodness-of-fit on F^2	1.055	
Final R indices [I>2sigma(I)]	R1 = 0.0516, wR2 = 0.1330	
R indices (all data)	R1 = 0.0868, wR2 = 0.1512	
Largest diff. peak and hole	0.650 and -0.527 $e.Å^{-3}$	

Table A.6. Atomic coordinates (x 10^4) and equivalent isotropic displacement parameters ($Å^2$x 10^3) for sr4. U(eq) is defined as one third of the trace of the orthogonalized U^{ij} tensor.

	x	y	z	U(eq)
Mn(1)	4227(1)	1971(1)	2868(1)	28(1)
O(1)	3535(1)	1285(1)	3549(1)	47(1)
O(2)	4663(2)	945(1)	2363(1)	50(1)
N(1)	6078(1)	2323(1)	3539(1)	30(1)
N(2)	4747(1)	2789(1)	2301(1)	29(1)
N(3)	2483(2)	2323(1)	2044(1)	31(1)
C(1)	7877(2)	3151(1)	3598(1)	47(1)
C(2)	6666(2)	2810(1)	3231(1)	30(1)
C(3)	5967(2)	3018(1)	2522(1)	30(1)
C(4)	6413(2)	3418(1)	2066(1)	41(1)
C(5)	5583(2)	3588(1)	1406(1)	46(1)
C(6)	4330(2)	3392(1)	1198(1)	41(1)
C(7)	3906(2)	2989(1)	1660(1)	31(1)
C(8)	2658(2)	2751(1)	1545(1)	33(1)
C(9)	1621(2)	3001(1)	899(1)	47(1)
C(10)	6737(2)	2157(1)	4253(1)	31(1)
C(11)	6497(2)	2592(1)	4763(1)	39(1)
C(12)	7114(2)	2410(1)	5452(1)	47(1)
C(13)	7964(2)	1812(1)	5650(1)	45(1)
C(14)	8205(2)	1387(1)	5152(1)	40(1)
C(15)	7609(2)	1540(1)	4455(1)	34(1)
C(16)	5592(2)	3279(2)	4578(1)	55(1)
C(17)	4533(3)	3161(2)	4846(2)	104(1)
C(18)	6268(3)	4032(2)	4850(2)	87(1)
C(19)	7922(2)	1057(1)	3934(1)	47(1)
C(20)	9270(2)	1177(2)	3974(2)	72(1)
C(21)	7716(3)	190(2)	4017(2)	79(1)
C(22)	1239(2)	2153(1)	2007(1)	34(1)
C(23)	579(2)	1516(1)	1624(1)	45(1)
C(24)	-556(2)	1314(2)	1681(1)	59(1)
C(25)	-1037(2)	1720(2)	2089(2)	65(1)
C(26)	-420(2)	2364(2)	2440(1)	59(1)
C(27)	729(2)	2592(2)	2408(1)	47(1)
C(28)	1070(2)	1049(1)	1153(2)	63(1)
C(29)	1247(4)	199(2)	1354(2)	112(2)
C(30)	198(3)	1123(2)	386(2)	83(1)
C(31)	1375(2)	3315(2)	2783(2)	69(1)
C(32)	777(4)	4039(2)	2385(2)	102(1)
C(33)	1380(4)	3357(2)	3518(2)	120(2)
C(34)	2293(3)	982(2)	3365(2)	103(1)
C(35)	2300(3)	373(2)	3823(2)	94(1)
C(36)	3463(3)	475(2)	4443(1)	74(1)
C(37)	4291(3)	947(2)	4198(1)	80(1)
C(38)	5110(3)	1038(2)	1800(2)	79(1)
C(39)	5859(3)	341(2)	1812(2)	87(1)
C(40)	5322(3)	-273(2)	2114(2)	91(1)
C(41)	4700(3)	147(1)	2532(2)	69(1)

Table A.7. Bond lengths [Å] and angles [°] for sr4.

Mn(1)-N(2)	2.0514(17)	C(40)-C(41)	1.488(4)
Mn(1)-N(1)	2.1613(15)		
Mn(1)-O(1)	2.1909(15)	N(2)-Mn(1)-N(1)	75.92(6)
Mn(1)-N(3)	2.1946(15)	N(2)-Mn(1)-O(1)	169.19(7)
Mn(1)-O(2)	2.1998(16)	N(1)-Mn(1)-O(1)	103.60(6)
O(1)-C(34)	1.431(3)	N(2)-Mn(1)-N(3)	74.68(6)
O(1)-C(37)	1.435(3)	N(1)-Mn(1)-N(3)	146.13(6)
O(2)-C(41)	1.414(3)	O(1)-Mn(1)-N(3)	102.13(6)
O(2)-C(38)	1.438(3)	N(2)-Mn(1)-O(2)	96.84(7)
N(1)-C(2)	1.367(3)	N(1)-Mn(1)-O(2)	101.15(6)
N(1)-C(10)	1.424(2)	O(1)-Mn(1)-O(2)	93.85(6)
N(2)-C(3)	1.363(2)	N(3)-Mn(1)-O(2)	98.69(6)
N(2)-C(7)	1.374(2)	C(34)-O(1)-C(37)	108.04(19)
N(3)-C(8)	1.340(3)	C(34)-O(1)-Mn(1)	125.34(16)
N(3)-C(22)	1.429(3)	C(37)-O(1)-Mn(1)	125.73(14)
C(1)-C(2)	1.444(3)	C(41)-O(2)-C(38)	108.7(2)
C(2)-C(3)	1.441(3)	C(41)-O(2)-Mn(1)	130.94(17)
C(3)-C(4)	1.403(3)	C(38)-O(2)-Mn(1)	120.11(14)
C(4)-C(5)	1.387(3)	C(2)-N(1)-C(10)	116.01(15)
C(5)-C(6)	1.382(3)	C(2)-N(1)-Mn(1)	113.91(12)
C(6)-C(7)	1.401(3)	C(10)-N(1)-Mn(1)	130.00(13)
C(7)-C(8)	1.421(3)	C(3)-N(2)-C(7)	122.02(18)
C(8)-C(9)	1.497(3)	C(3)-N(2)-Mn(1)	118.60(12)
C(10)-C(11)	1.399(3)	C(7)-N(2)-Mn(1)	118.51(13)
C(10)-C(15)	1.414(3)	C(8)-N(3)-C(22)	119.48(16)
C(11)-C(12)	1.381(3)	C(8)-N(3)-Mn(1)	113.89(13)
C(11)-C(16)	1.527(3)	C(22)-N(3)-Mn(1)	126.62(13)
C(12)-C(13)	1.374(3)	N(1)-C(2)-C(3)	116.09(16)
C(13)-C(14)	1.370(3)	N(1)-C(2)-C(1)	122.96(19)
C(14)-C(15)	1.380(3)	C(3)-C(2)-C(1)	120.79(19)
C(15)-C(19)	1.504(3)	N(2)-C(3)-C(4)	119.46(18)
C(16)-C(18)	1.512(4)	N(2)-C(3)-C(2)	113.45(18)
C(16)-C(17)	1.517(5)	C(4)-C(3)-C(2)	127.08(18)
C(19)-C(20)	1.528(4)	C(5)-C(4)-C(3)	118.7(2)
C(19)-C(21)	1.530(4)	C(6)-C(5)-C(4)	121.5(2)
C(22)-C(27)	1.394(3)	C(5)-C(6)-C(7)	118.9(2)
C(22)-C(23)	1.404(3)	N(2)-C(7)-C(6)	119.24(19)
C(23)-C(24)	1.389(4)	N(2)-C(7)-C(8)	113.83(18)
C(23)-C(28)	1.517(4)	C(6)-C(7)-C(8)	126.93(18)
C(24)-C(25)	1.355(4)	N(3)-C(8)-C(7)	116.55(17)
C(25)-C(26)	1.375(4)	N(3)-C(8)-C(9)	123.74(19)
C(26)-C(27)	1.396(3)	C(7)-C(8)-C(9)	119.69(19)
C(27)-C(31)	1.512(4)	C(11)-C(10)-C(15)	119.12(18)
C(28)-C(29)	1.515(4)	C(11)-C(10)-N(1)	119.94(18)
C(28)-C(30)	1.548(4)	C(15)-C(10)-N(1)	120.91(19)
C(31)-C(32)	1.514(4)	C(12)-C(11)-C(10)	119.4(2)
C(31)-C(33)	1.521(5)	C(12)-C(11)-C(16)	119.0(2)
C(34)-C(35)	1.411(4)	C(10)-C(11)-C(16)	121.59(19)
C(35)-C(36)	1.492(4)	C(13)-C(12)-C(11)	121.5(2)
C(36)-C(37)	1.468(4)	C(14)-C(13)-C(12)	119.2(2)
C(38)-C(39)	1.469(4)	C(13)-C(14)-C(15)	121.7(2)
C(39)-C(40)	1.470(4)	C(14)-C(15)-C(10)	119.0(2)
		C(14)-C(15)-C(19)	119.12(19)
		C(10)-C(15)-C(19)	121.84(18)

C(18)-C(16)-C(17)	110.3(3)	C(29)-C(28)-C(23)	112.3(3)
C(18)-C(16)-C(11)	111.2(2)	C(29)-C(28)-C(30)	109.5(2)
C(17)-C(16)-C(11)	111.3(2)	C(23)-C(28)-C(30)	111.3(2)
C(15)-C(19)-C(20)	112.4(2)	C(27)-C(31)-C(32)	110.9(2)
C(15)-C(19)-C(21)	111.9(2)	C(27)-C(31)-C(33)	112.2(3)
C(20)-C(19)-C(21)	108.7(2)	C(32)-C(31)-C(33)	110.1(3)
C(27)-C(22)-C(23)	120.2(2)	C(35)-C(34)-O(1)	109.0(2)
C(27)-C(22)-N(3)	118.55(18)	C(34)-C(35)-C(36)	106.2(3)
C(23)-C(22)-N(3)	121.0(2)	C(37)-C(36)-C(35)	104.9(2)
C(24)-C(23)-C(22)	118.6(2)	O(1)-C(37)-C(36)	107.4(2)
C(24)-C(23)-C(28)	119.5(2)	O(2)-C(38)-C(39)	105.6(2)
C(22)-C(23)-C(28)	121.9(2)	C(40)-C(39)-C(38)	105.3(3)
C(25)-C(24)-C(23)	121.6(2)	C(39)-C(40)-C(41)	104.9(2)
C(24)-C(25)-C(26)	119.9(3)	O(2)-C(41)-C(40)	107.9(2)
C(25)-C(26)-C(27)	121.1(3)		
C(26)-C(27)-C(22)	118.5(2)		
C(26)-C(27)-C(31)	120.2(2)		
C(22)-C(27)-C(31)	121.3(2)		

Symmetry transformations used to generate equivalent atoms:

Table A.8. Crystal data and structure refinement for sr5.

Identification code	sr5	
Empirical formula	C70 H96 Mn N6 O	
Formula weight	1092.47	
Temperature	173(2) K	
Wavelength	0.71073 Å	
Crystal system	Triclinic	
Space group	P-1	
Unit cell dimensions	a = 12.4246(8) Å	α= 79.966(2)°.
	b = 13.1877(8) Å	β= 88.926(2)°.
	c = 19.7294(11) Å	γ = 83.149(2)°.
Volume	3160.5(3) $Å^3$	
Z	2	
Density (calculated)	1.148 Mg/m^3	
Absorption coefficient	0.255 mm^{-1}	
F(000)	1182	
Crystal size	0.45 x 0.15 x 0.08 mm^3	
Theta range for data collection	1.58 to 24.71°.	
Index ranges	-14<=h<=14, -15<=k<=15, -23<=l<=12	
Reflections collected	21695	
Independent reflections	10395 [R(int) = 0.0367]	
Completeness to theta = 24.71°	96.4 %	
Absorption correction	Semi-empirical from equivalents	
Max. and min. transmission	0.9811 and 0.8938	
Refinement method	Full-matrix least-squares on F^2	
Data / restraints / parameters	10395 / 0 / 734	
Goodness-of-fit on F^2	1.020	
Final R indices [I>2sigma(I)]	R1 = 0.0530, wR2 = 0.1234	
R indices (all data)	R1 = 0.0961, wR2 = 0.1460	
Largest diff. peak and hole	0.444 and -0.530 $e.Å^{-3}$	

Table A.9. Atomic coordinates (x 10^4) and equivalent isotropic displacement parameters ($Å^2$x 10^3) for sr5. U(eq) is defined as one third of the trace of the orthogonalized U^{ij} tensor.

	x	y	z	U(eq)
O(1S)	318(3)	1995(2)	8296(2)	133(1)
Mn(1)	6012(1)	7506(1)	7008(1)	35(1)
N(1)	5189(1)	6723(1)	6261(1)	28(1)
N(2)	5802(1)	8566(1)	6127(1)	24(1)
N(3)	5505(2)	9360(1)	7256(1)	31(1)
N(4)	7732(2)	7196(2)	6904(1)	33(1)
N(5)	6416(1)	6538(1)	7972(1)	27(1)
N(6)	4064(2)	6008(2)	9015(1)	37(1)
C(1)	5205(2)	6673(2)	5002(1)	42(1)
C(2)	5414(2)	7146(2)	5623(1)	29(1)
C(3)	5830(2)	8142(2)	5533(1)	27(1)
C(4)	6180(2)	8689(2)	4917(1)	37(1)
C(5)	6453(2)	9678(2)	4888(1)	40(1)
C(6)	6339(2)	10133(2)	5474(1)	36(1)
C(7)	6018(2)	9573(2)	6084(1)	27(1)
C(8)	5797(2)	9990(2)	6722(1)	30(1)
C(9)	5877(2)	11122(2)	6713(1)	43(1)
C(10)	4466(2)	5941(2)	6363(1)	31(1)
C(11)	3369(2)	6212(2)	6158(1)	39(1)
C(12)	2678(2)	5447(2)	6278(1)	51(1)
C(13)	3037(2)	4448(2)	6591(1)	58(1)
C(14)	4092(2)	4197(2)	6807(1)	51(1)
C(15)	4831(2)	4932(2)	6704(1)	37(1)
C(16)	2897(2)	7317(2)	5836(1)	47(1)
C(17)	2139(3)	7799(3)	6345(2)	79(1)
C(18)	2285(2)	7353(2)	5169(1)	57(1)
C(19)	5992(2)	4602(2)	6937(1)	40(1)
C(20)	6583(2)	3947(2)	6444(2)	57(1)
C(21)	6090(3)	4006(2)	7677(1)	60(1)
C(22)	5073(2)	9804(2)	7839(1)	35(1)
C(23)	5693(2)	9696(2)	8437(1)	42(1)
C(24)	5263(2)	10168(2)	8979(1)	52(1)
C(25)	4255(3)	10722(2)	8933(1)	57(1)
C(26)	3627(2)	10793(2)	8353(1)	55(1)
C(27)	4012(2)	10324(2)	7799(1)	44(1)
C(28)	6827(2)	9125(2)	8512(1)	52(1)
C(29)	7660(3)	9885(3)	8564(2)	77(1)
C(30)	6934(3)	8249(2)	9132(2)	76(1)
C(31)	3260(2)	10403(2)	7185(1)	54(1)
C(32)	2265(3)	9833(2)	7409(2)	75(1)
C(33)	2868(3)	11515(2)	6867(1)	62(1)
C(34)	9407(2)	6193(2)	7484(1)	50(1)
C(35)	8207(2)	6563(2)	7447(1)	35(1)
C(36)	7532(2)	6217(2)	8015(1)	32(1)
C(37)	7993(2)	5566(2)	8611(1)	42(1)
C(38)	7366(2)	5237(2)	9160(1)	47(1)
C(39)	6253(2)	5539(2)	9111(1)	41(1)
C(40)	5802(2)	6166(2)	8530(1)	29(1)
C(41)	4602(2)	6426(2)	8503(1)	29(1)
C(42)	4078(2)	7141(2)	7893(1)	39(1)
C(43)	8381(2)	7585(2)	6321(1)	37(1)

C(44)	8585(2)	7039(2)	5774(1)	47(1)
C(45)	9143(2)	7484(3)	5196(1)	59(1)
C(46)	9487(3)	8425(3)	5150(2)	67(1)
C(47)	9319(2)	8955(2)	5688(2)	60(1)
C(48)	8767(2)	8559(2)	6284(1)	43(1)
C(49)	8256(3)	5981(3)	5776(2)	66(1)
C(50)	7913(3)	5827(3)	5065(2)	91(1)
C(51)	9199(4)	5137(3)	6001(2)	110(2)
C(52)	8655(2)	9154(2)	6871(1)	50(1)
C(53)	8717(3)	10322(2)	6639(2)	73(1)
C(54)	9523(3)	8744(3)	7428(2)	70(1)
C(55)	2923(2)	6169(2)	9076(1)	33(1)
C(56)	2437(2)	7000(2)	9372(1)	45(1)
C(57)	1326(2)	7056(2)	9503(1)	57(1)
C(58)	722(2)	6318(2)	9358(1)	55(1)
C(59)	1211(2)	5513(2)	9063(1)	46(1)
C(60)	2308(2)	5414(2)	8910(1)	36(1)
C(61)	3094(3)	7799(2)	9568(2)	65(1)
C(62)	2437(3)	8846(2)	9593(2)	88(1)
C(63)	3648(3)	7403(3)	10236(2)	107(1)
C(64)	2845(2)	4517(2)	8598(1)	45(1)
C(65)	3516(3)	3724(2)	9130(2)	71(1)
C(66)	2053(2)	3973(2)	8244(2)	65(1)
C(1S)	-132(5)	2659(4)	7156(4)	232(4)
C(2S)	-466(5)	2347(7)	7839(4)	230(4)
C(3S)	57(4)	1610(7)	8957(3)	287(4)
C(4S)	879(4)	1424(4)	9469(3)	149(2)

Table A.10. Bond lengths [Å] and angles [°] for sr5.

O(1S)-C(2S)	1.324(8)	C(6)-C(7)	1.376(3)
O(1S)-C(3S)	1.362(6)	C(7)-C(8)	1.468(3)
Mn(1)-N(2)	2.0320(16)	C(8)-C(9)	1.505(3)
Mn(1)-N(5)	2.1311(16)	C(10)-C(15)	1.408(3)
Mn(1)-N(4)	2.1406(19)	C(10)-C(11)	1.416(3)
Mn(1)-N(1)	2.2637(18)	C(11)-C(12)	1.388(4)
N(1)-C(2)	1.324(3)	C(11)-C(16)	1.535(4)
N(1)-C(10)	1.433(3)	C(12)-C(13)	1.379(4)
N(2)-C(7)	1.373(3)	C(13)-C(14)	1.370(4)
N(2)-C(3)	1.381(3)	C(14)-C(15)	1.401(4)
N(3)-C(8)	1.298(3)	C(15)-C(19)	1.512(3)
N(3)-C(22)	1.446(3)	C(16)-C(18)	1.524(4)
N(4)-C(35)	1.338(3)	C(16)-C(17)	1.530(4)
N(4)-C(43)	1.446(3)	C(19)-C(20)	1.532(4)
N(5)-C(40)	1.380(3)	C(19)-C(21)	1.532(3)
N(5)-C(36)	1.400(3)	C(22)-C(23)	1.399(3)
N(6)-C(41)	1.281(3)	C(22)-C(27)	1.408(4)
N(6)-C(55)	1.414(3)	C(23)-C(24)	1.395(3)
C(1)-C(2)	1.508(3)	C(23)-C(28)	1.513(4)
C(2)-C(3)	1.450(3)	C(24)-C(25)	1.369(4)
C(3)-C(4)	1.391(3)	C(25)-C(26)	1.381(4)
C(4)-C(5)	1.378(3)	C(26)-C(27)	1.397(4)
C(5)-C(6)	1.391(3)	C(27)-C(31)	1.526(4)

C(28)-C(30)	1.525(4)
C(28)-C(29)	1.541(4)
C(31)-C(33)	1.517(4)
C(31)-C(32)	1.540(4)
C(34)-C(35)	1.511(3)
C(35)-C(36)	1.430(3)
C(36)-C(37)	1.416(3)
C(37)-C(38)	1.362(3)
C(38)-C(39)	1.393(4)
C(39)-C(40)	1.377(3)
C(40)-C(41)	1.489(3)
C(41)-C(42)	1.499(3)
C(43)-C(44)	1.402(4)
C(43)-C(48)	1.414(4)
C(44)-C(45)	1.399(4)
C(44)-C(49)	1.500(4)
C(45)-C(46)	1.347(4)
C(46)-C(47)	1.370(4)
C(47)-C(48)	1.403(4)
C(48)-C(52)	1.505(4)
C(49)-C(50)	1.527(5)
C(49)-C(51)	1.532(5)
C(52)-C(54)	1.536(4)
C(52)-C(53)	1.539(4)
C(55)-C(56)	1.399(3)
C(55)-C(60)	1.409(3)
C(56)-C(57)	1.395(4)
C(56)-C(61)	1.511(4)
C(57)-C(58)	1.368(4)
C(58)-C(59)	1.372(4)
C(59)-C(60)	1.387(3)
C(60)-C(64)	1.508(4)
C(61)-C(63)	1.481(5)
C(61)-C(62)	1.526(4)
C(64)-C(65)	1.527(4)
C(64)-C(66)	1.529(4)
C(1S)-C(2S)	1.410(10)
C(3S)-C(4S)	1.421(7)

C(2S)-O(1S)-C(3S)	119.4(5)
N(2)-Mn(1)-N(5)	171.05(7)
N(2)-Mn(1)-N(4)	95.26(7)
N(5)-Mn(1)-N(4)	79.40(7)
N(2)-Mn(1)-N(1)	74.33(7)
N(5)-Mn(1)-N(1)	114.13(7)
N(4)-Mn(1)-N(1)	109.11(7)
C(2)-N(1)-C(10)	118.58(18)
C(2)-N(1)-Mn(1)	109.30(14)
C(10)-N(1)-Mn(1)	132.01(13)
C(7)-N(2)-C(3)	118.83(17)
C(7)-N(2)-Mn(1)	122.64(14)
C(3)-N(2)-Mn(1)	114.34(13)
C(8)-N(3)-C(22)	117.63(19)
C(35)-N(4)-C(43)	119.84(19)
C(35)-N(4)-Mn(1)	113.35(14)
C(43)-N(4)-Mn(1)	126.81(14)
C(40)-N(5)-C(36)	116.51(17)
C(40)-N(5)-Mn(1)	132.82(15)
C(36)-N(5)-Mn(1)	110.64(12)
C(41)-N(6)-C(55)	124.49(19)
N(1)-C(2)-C(3)	116.62(19)
N(1)-C(2)-C(1)	123.5(2)
C(3)-C(2)-C(1)	119.85(19)
N(2)-C(3)-C(4)	120.3(2)
N(2)-C(3)-C(2)	113.56(18)
C(4)-C(3)-C(2)	126.0(2)
C(5)-C(4)-C(3)	120.2(2)
C(4)-C(5)-C(6)	119.1(2)
C(7)-C(6)-C(5)	119.9(2)
N(2)-C(7)-C(6)	121.3(2)
N(2)-C(7)-C(8)	113.82(18)
C(6)-C(7)-C(8)	124.8(2)
N(3)-C(8)-C(7)	117.4(2)
N(3)-C(8)-C(9)	124.0(2)
C(7)-C(8)-C(9)	118.59(19)
C(15)-C(10)-C(11)	120.6(2)
C(15)-C(10)-N(1)	120.0(2)
C(11)-C(10)-N(1)	119.2(2)
C(12)-C(11)-C(10)	118.1(2)
C(12)-C(11)-C(16)	118.5(2)
C(10)-C(11)-C(16)	123.3(2)
C(13)-C(12)-C(11)	121.6(3)
C(14)-C(13)-C(12)	120.0(3)
C(13)-C(14)-C(15)	121.3(3)
C(14)-C(15)-C(10)	118.2(2)
C(14)-C(15)-C(19)	118.9(2)
C(10)-C(15)-C(19)	122.9(2)
C(18)-C(16)-C(17)	109.1(2)
C(18)-C(16)-C(11)	112.6(2)
C(17)-C(16)-C(11)	110.4(2)
C(15)-C(19)-C(20)	109.8(2)
C(15)-C(19)-C(21)	113.3(2)
C(20)-C(19)-C(21)	110.0(2)
C(23)-C(22)-C(27)	120.8(2)
C(23)-C(22)-N(3)	120.3(2)
C(27)-C(22)-N(3)	118.9(2)
C(24)-C(23)-C(22)	118.5(2)
C(24)-C(23)-C(28)	118.5(2)
C(22)-C(23)-C(28)	122.9(2)
C(25)-C(24)-C(23)	121.3(3)
C(24)-C(25)-C(26)	120.1(3)
C(25)-C(26)-C(27)	121.0(3)
C(26)-C(27)-C(22)	118.1(2)
C(26)-C(27)-C(31)	118.2(2)
C(22)-C(27)-C(31)	123.7(2)
C(23)-C(28)-C(30)	112.3(2)
C(23)-C(28)-C(29)	110.4(2)
C(30)-C(28)-C(29)	110.0(2)
C(33)-C(31)-C(27)	112.9(2)
C(33)-C(31)-C(32)	108.6(2)
C(27)-C(31)-C(32)	109.8(2)
N(4)-C(35)-C(36)	117.6(2)

N(4)-C(35)-C(34)	123.4(2)
C(36)-C(35)-C(34)	119.04(19)
N(5)-C(36)-C(37)	120.9(2)
N(5)-C(36)-C(35)	118.97(18)
C(37)-C(36)-C(35)	120.1(2)
C(38)-C(37)-C(36)	121.0(2)
C(37)-C(38)-C(39)	118.0(2)
C(40)-C(39)-C(38)	121.0(2)
C(39)-C(40)-N(5)	122.5(2)
C(39)-C(40)-C(41)	118.12(19)
N(5)-C(40)-C(41)	119.38(18)
N(6)-C(41)-C(40)	116.87(19)
N(6)-C(41)-C(42)	123.1(2)
C(40)-C(41)-C(42)	120.04(19)
C(44)-C(43)-C(48)	119.2(2)
C(44)-C(43)-N(4)	121.1(2)
C(48)-C(43)-N(4)	119.6(2)
C(45)-C(44)-C(43)	119.2(3)
C(45)-C(44)-C(49)	117.4(3)
C(43)-C(44)-C(49)	123.5(2)
C(46)-C(45)-C(44)	121.8(3)
C(45)-C(46)-C(47)	119.7(3)
C(46)-C(47)-C(48)	121.7(3)
C(47)-C(48)-C(43)	118.4(3)
C(47)-C(48)-C(52)	119.2(3)
C(43)-C(48)-C(52)	122.4(2)
C(44)-C(49)-C(50)	112.7(3)
C(44)-C(49)-C(51)	111.0(3)
C(50)-C(49)-C(51)	106.1(3)
C(48)-C(52)-C(54)	112.1(2)
C(48)-C(52)-C(53)	112.9(2)
C(54)-C(52)-C(53)	108.0(2)
C(56)-C(55)-C(60)	121.1(2)
C(56)-C(55)-N(6)	119.9(2)
C(60)-C(55)-N(6)	118.6(2)
C(57)-C(56)-C(55)	118.0(3)
C(57)-C(56)-C(61)	120.5(3)
C(55)-C(56)-C(61)	121.5(2)
C(58)-C(57)-C(56)	121.7(3)
C(57)-C(58)-C(59)	119.4(3)
C(58)-C(59)-C(60)	122.1(3)
C(59)-C(60)-C(55)	117.7(2)
C(59)-C(60)-C(64)	121.8(2)
C(55)-C(60)-C(64)	120.5(2)
C(63)-C(61)-C(56)	110.6(3)
C(63)-C(61)-C(62)	109.6(3)
C(56)-C(61)-C(62)	114.0(3)
C(60)-C(64)-C(65)	111.5(2)
C(60)-C(64)-C(66)	113.8(2)
C(65)-C(64)-C(66)	109.7(2)
O(1S)-C(2S)-C(1S)	116.1(6)
O(1S)-C(3S)-C(4S)	118.8(5)

Symmetry transformations used to generate equivalent atoms:

Table A.11. Crystal data and structure refinement for sr7.

Identification code	sr7	
Empirical formula	C35 H43 Mn N3 O2	
Formula weight	592.66	
Temperature	173(2) K	
Wavelength	0.71073 Å	
Crystal system	Triclinic	
Space group	P-1	
Unit cell dimensions	a = 8.7806(4) Å	α= 82.713(2)°.
	b = 10.0972(5) Å	β= 87.755(2)°.
	c = 19.8551(10) Å	γ = 65.193(2)°.
Volume	1584.81(13) $Å^3$	
Z	2	
Density (calculated)	1.242 Mg/m^3	
Absorption coefficient	0.451 mm^{-1}	
F(000)	630	
Crystal size	0.45 x 0.15 x 0.05 mm^3	
Theta range for data collection	2.07 to 29.13°.	
Index ranges	-11<=h<=11, -13<=k<=13, -27<=l<=27	
Reflections collected	27461	
Independent reflections	8253 [R(int) = 0.0321]	
Completeness to theta = 29.13°	97.2 %	
Absorption correction	Semi-empirical from equivalents	
Max. and min. transmission	0.9778 and 0.8228	
Refinement method	Full-matrix least-squares on F^2	
Data / restraints / parameters	8253 / 0 / 531	
Goodness-of-fit on F^2	1.026	
Final R indices [I>2sigma(I)]	R1 = 0.0368, wR2 = 0.0870	
R indices (all data)	R1 = 0.0515, wR2 = 0.0950	
Largest diff. peak and hole	0.357 and -0.301 $e.Å^{-3}$	

Table A.12. Atomic coordinates (x 10^4) and equivalent isotropic displacement parameters ($Å^2$x 10^3) for sr7. U(eq) is defined as one third of the trace of the orthogonalized U^{ij} tensor.

	x	y	z	U(eq)
Mn(1)	5899(1)	3346(1)	2324(1)	18(1)
O(1)	5914(2)	445(1)	2755(1)	50(1)
O(2)	2701(1)	4334(1)	1601(1)	49(1)
N(1)	5053(1)	4248(1)	3174(1)	19(1)
N(2)	6391(1)	5038(1)	2187(1)	19(1)
N(3)	7468(1)	2902(1)	1545(1)	20(1)
C(1)	4504(2)	6376(2)	3813(1)	31(1)
C(2)	5084(1)	5536(1)	3216(1)	22(1)
C(3)	5834(1)	6043(1)	2639(1)	21(1)
C(4)	6089(2)	7315(1)	2525(1)	27(1)
C(5)	6959(2)	7538(1)	1956(1)	31(1)
C(6)	7622(2)	6460(1)	1522(1)	28(1)
C(7)	7337(1)	5204(1)	1651(1)	22(1)
C(8)	7966(2)	3926(1)	1291(1)	23(1)
C(9)	9119(2)	3815(2)	706(1)	33(1)
C(10)	4476(1)	3586(1)	3756(1)	21(1)
C(11)	5682(2)	2519(1)	4207(1)	25(1)
C(12)	5134(2)	1897(2)	4778(1)	33(1)
C(13)	3447(2)	2329(2)	4904(1)	37(1)
C(14)	2286(2)	3360(2)	4452(1)	34(1)
C(15)	2752(2)	4000(1)	3863(1)	26(1)
C(16)	7546(2)	2060(2)	4107(1)	33(1)
C(17)	8525(2)	392(2)	4196(1)	51(1)
C(18)	8239(2)	2731(2)	4589(1)	46(1)
C(19)	1411(2)	5045(2)	3358(1)	32(1)
C(20)	35(2)	6290(2)	3686(1)	48(1)
C(21)	639(2)	4188(2)	3015(1)	44(1)
C(22)	8114(2)	1532(1)	1255(1)	23(1)
C(23)	7284(2)	1383(1)	700(1)	28(1)
C(24)	7961(2)	35(2)	439(1)	36(1)
C(25)	9380(2)	-1114(2)	722(1)	39(1)
C(26)	10156(2)	-952(2)	1270(1)	37(1)
C(27)	9556(2)	370(1)	1550(1)	29(1)
C(28)	5705(2)	2609(2)	382(1)	32(1)
C(29)	5982(2)	3151(2)	-347(1)	44(1)
C(30)	4264(2)	2137(2)	401(1)	52(1)
C(31)	10488(2)	523(2)	2139(1)	40(1)
C(32)	12031(2)	764(2)	1899(1)	61(1)
C(33)	10993(3)	-796(3)	2680(1)	67(1)
C(34)	5918(2)	1582(1)	2579(1)	28(1)
C(35)	3972(2)	3912(2)	1891(1)	29(1)

Table A.13. Bond lengths [Å] and angles [°] for sr7.

Mn(1)-C(35)	1.7624(13)	Mn(1)-N(3)	1.9956(10)
Mn(1)-C(34)	1.7816(14)	O(1)-C(34)	1.1587(17)
Mn(1)-N(2)	1.9161(10)	O(2)-C(35)	1.1610(16)
Mn(1)-N(1)	1.9884(10)	N(1)-C(2)	1.3252(16)
		N(1)-C(10)	1.4424(15)
		N(2)-C(7)	1.3604(15)

N(2)-C(3)	1.3633(15)
N(3)-C(8)	1.3208(16)
N(3)-C(22)	1.4428(15)
C(1)-C(2)	1.4939(17)
C(2)-C(3)	1.4432(17)
C(3)-C(4)	1.3833(18)
C(4)-C(5)	1.3862(19)
C(5)-C(6)	1.3908(19)
C(6)-C(7)	1.3842(18)
C(7)-C(8)	1.4448(17)
C(8)-C(9)	1.4935(17)
C(10)-C(11)	1.3992(16)
C(10)-C(15)	1.4059(17)
C(11)-C(12)	1.3941(18)
C(11)-C(16)	1.5148(18)
C(12)-C(13)	1.379(2)
C(13)-C(14)	1.369(2)
C(14)-C(15)	1.3947(19)
C(15)-C(19)	1.5121(18)
C(16)-C(18)	1.517(2)
C(16)-C(17)	1.526(2)
C(19)-C(20)	1.529(2)
C(19)-C(21)	1.534(2)
C(22)-C(27)	1.3995(17)
C(22)-C(23)	1.4026(18)
C(23)-C(24)	1.3964(19)
C(23)-C(28)	1.5111(18)
C(24)-C(25)	1.375(2)
C(25)-C(26)	1.368(2)
C(26)-C(27)	1.394(2)
C(27)-C(31)	1.513(2)
C(28)-C(30)	1.526(2)
C(28)-C(29)	1.528(2)
C(31)-C(33)	1.519(3)
C(31)-C(32)	1.522(3)

C(35)-Mn(1)-C(34)	90.30(6)
C(35)-Mn(1)-N(2)	104.26(5)
C(34)-Mn(1)-N(2)	165.42(5)
C(35)-Mn(1)-N(1)	99.21(5)
C(34)-Mn(1)-N(1)	98.99(5)
N(2)-Mn(1)-N(1)	78.21(4)
C(35)-Mn(1)-N(3)	100.09(5)
C(34)-Mn(1)-N(3)	100.50(5)
N(2)-Mn(1)-N(3)	77.99(4)
N(1)-Mn(1)-N(3)	152.36(4)
C(2)-N(1)-C(10)	117.65(10)
C(2)-N(1)-Mn(1)	117.04(8)
C(10)-N(1)-Mn(1)	125.26(8)
C(7)-N(2)-C(3)	120.47(11)
C(7)-N(2)-Mn(1)	119.85(8)
C(3)-N(2)-Mn(1)	119.65(8)
C(8)-N(3)-C(22)	118.44(10)
C(8)-N(3)-Mn(1)	117.22(8)
C(22)-N(3)-Mn(1)	124.32(8)
N(1)-C(2)-C(3)	113.79(10)
N(1)-C(2)-C(1)	124.64(11)
C(3)-C(2)-C(1)	121.48(11)
N(2)-C(3)-C(4)	120.29(11)
N(2)-C(3)-C(2)	110.81(10)
C(4)-C(3)-C(2)	128.83(11)
C(3)-C(4)-C(5)	119.43(12)
C(4)-C(5)-C(6)	119.83(13)
C(7)-C(6)-C(5)	119.08(12)
N(2)-C(7)-C(6)	120.57(11)
N(2)-C(7)-C(8)	111.01(11)
C(6)-C(7)-C(8)	128.39(11)
N(3)-C(8)-C(7)	113.60(10)
N(3)-C(8)-C(9)	125.51(11)
C(7)-C(8)-C(9)	120.85(12)
C(11)-C(10)-C(15)	121.17(11)
C(11)-C(10)-N(1)	117.97(10)
C(15)-C(10)-N(1)	120.86(10)
C(12)-C(11)-C(10)	118.32(12)
C(12)-C(11)-C(16)	119.35(11)
C(10)-C(11)-C(16)	122.30(11)
C(13)-C(12)-C(11)	121.24(12)
C(14)-C(13)-C(12)	119.58(13)
C(13)-C(14)-C(15)	121.98(12)
C(14)-C(15)-C(10)	117.63(11)
C(14)-C(15)-C(19)	119.33(11)
C(10)-C(15)-C(19)	122.99(11)
C(11)-C(16)-C(18)	110.95(12)
C(11)-C(16)-C(17)	111.97(14)
C(18)-C(16)-C(17)	109.89(13)
C(15)-C(19)-C(20)	112.49(12)
C(15)-C(19)-C(21)	109.49(12)
C(20)-C(19)-C(21)	109.85(13)
C(27)-C(22)-C(23)	121.66(12)
C(27)-C(22)-N(3)	118.32(11)
C(23)-C(22)-N(3)	120.01(10)
C(24)-C(23)-C(22)	117.71(12)
C(24)-C(23)-C(28)	119.54(12)
C(22)-C(23)-C(28)	122.74(11)
C(25)-C(24)-C(23)	121.24(14)
C(26)-C(25)-C(24)	120.09(13)
C(25)-C(26)-C(27)	121.54(13)
C(26)-C(27)-C(22)	117.75(13)
C(26)-C(27)-C(31)	119.91(12)
C(22)-C(27)-C(31)	122.32(12)
C(23)-C(28)-C(30)	111.15(13)
C(23)-C(28)-C(29)	111.99(11)
C(30)-C(28)-C(29)	110.08(13)
C(27)-C(31)-C(33)	112.07(16)
C(27)-C(31)-C(32)	111.28(14)
C(33)-C(31)-C(32)	109.84(15)
O(1)-C(34)-Mn(1)	178.76(12)
O(2)-C(35)-Mn(1)	177.60(14)

Symmetry transformations used to generate equivalent atoms:

Table A.14. Crystal data and structure refinement for sr11.

Identification code	sr11	
Empirical formula	C66 H88 Fe2 N6 O	
Formula weight	1093.12	
Temperature	173(2) K	
Wavelength	0.71073 Å	
Crystal system	Triclinic	
Space group	P-1	
Unit cell dimensions	a = 11.9873(9) Å	α= 90.002(3)°.
	b = 13.0557(10) Å	β= 98.795(3)°.
	c = 21.4760(17) Å	γ = 114.350(3)°.
Volume	3018.6(4) $Å^3$	
Z	2	
Density (calculated)	1.203 Mg/m^3	
Absorption coefficient	0.526 mm^{-1}	
F(000)	1172	
Crystal size	0.30 x 0.20 x 0.05 mm^3	
Theta range for data collection	1.72 to 26.62°.	
Index ranges	-15<=h<=15, -16<=k<=16, -26<=l<=26	
Reflections collected	40080	
Independent reflections	12238 [R(int) = 0.0405]	
Completeness to theta = 26.62°	96.6 %	
Absorption correction	Semi-empirical from equivalents	
Max. and min. transmission	0.9742 and 0.8581	
Refinement method	Full-matrix least-squares on F^2	
Data / restraints / parameters	12238 / 0 / 708	
Goodness-of-fit on F^2	1.011	
Final R indices [I>2sigma(I)]	R1 = 0.0460, wR2 = 0.1134	
R indices (all data)	R1 = 0.0772, wR2 = 0.1319	
Largest diff. peak and hole	0.784 and -0.554 $e.Å^{-3}$	

Table A.15. Atomic coordinates (x 10^4) and equivalent isotropic displacement parameters ($Å^2$x 10^3) for sr11. U(eq) is defined as one third of the trace of the orthogonalized U^{ij} tensor.

	x	y	z	U(eq)
Fe(1)	4021(1)	8606(1)	2525(1)	20(1)
Fe(2)	1722(1)	7856(1)	1719(1)	19(1)
N(1)	5881(2)	8779(2)	2767(1)	21(1)
N(2)	4603(2)	8777(2)	1707(1)	20(1)
N(3)	2915(2)	9444(2)	1954(1)	19(1)
N(4)	466(2)	6954(2)	879(1)	20(1)
N(5)	2093(2)	6540(2)	1611(1)	20(1)
N(6)	2384(2)	7552(2)	2718(1)	20(1)
C(1)	6291(2)	8578(2)	2262(1)	24(1)
C(2)	5611(2)	8568(2)	1663(1)	22(1)
C(3)	5912(3)	8425(2)	1072(1)	30(1)
C(4)	5189(3)	8540(3)	539(1)	35(1)
C(5)	4196(3)	8821(2)	589(1)	28(1)
C(6)	3922(2)	8931(2)	1182(1)	21(1)
C(7)	2942(2)	9233(2)	1322(1)	21(1)
C(8)	6696(2)	8893(2)	3353(1)	25(1)
C(9)	7474(3)	9978(2)	3630(1)	29(1)
C(10)	8278(3)	10083(3)	4187(1)	41(1)
C(11)	8323(3)	9145(3)	4465(2)	51(1)
C(12)	7554(3)	8086(3)	4195(1)	44(1)
C(13)	6723(3)	7930(2)	3636(1)	30(1)
C(14)	7463(3)	11017(2)	3318(1)	30(1)
C(15)	7788(3)	12018(3)	3790(2)	43(1)
C(16)	8329(3)	11362(3)	2832(2)	43(1)
C(17)	5889(3)	6749(2)	3358(1)	33(1)
C(18)	6640(3)	6168(3)	3141(2)	49(1)
C(19)	5079(3)	6053(3)	3823(2)	48(1)
C(20)	2622(2)	10377(2)	2091(1)	21(1)
C(21)	1477(2)	10230(2)	2243(1)	26(1)
C(22)	1261(3)	11188(2)	2343(1)	35(1)
C(23)	2146(3)	12257(2)	2293(2)	40(1)
C(24)	3286(3)	12391(2)	2168(1)	36(1)
C(25)	3560(2)	11474(2)	2072(1)	25(1)
C(26)	420(2)	9089(2)	2286(1)	29(1)
C(27)	-609(3)	8829(3)	1721(2)	40(1)
C(28)	-90(3)	8989(3)	2905(2)	41(1)
C(29)	4848(2)	11664(2)	1969(1)	29(1)
C(30)	5057(3)	11957(3)	1297(2)	43(1)
C(31)	5845(3)	12571(2)	2443(2)	46(1)
C(32)	860(2)	6254(2)	641(1)	23(1)
C(33)	1742(2)	5979(2)	1033(1)	22(1)
C(34)	2189(3)	5183(2)	890(1)	32(1)
C(35)	2975(3)	4962(2)	1352(1)	37(1)
C(36)	3291(3)	5506(2)	1953(1)	30(1)
C(37)	2841(2)	6292(2)	2073(1)	21(1)
C(38)	3053(2)	6909(2)	2671(1)	22(1)
C(39)	-522(2)	7104(2)	474(1)	22(1)
C(40)	-1733(2)	6569(2)	610(1)	25(1)
C(41)	-2684(3)	6729(2)	226(1)	32(1)
C(42)	-2454(3)	7381(2)	-286(1)	35(1)
C(43)	-1277(3)	7877(2)	-425(1)	31(1)

C(44)	-286(2)	7748(2)	-54(1)	25(1)
C(45)	-2023(3)	5778(2)	1139(1)	31(1)
C(46)	-3201(3)	5626(3)	1389(2)	43(1)
C(47)	-2121(3)	4618(2)	922(2)	44(1)
C(48)	989(3)	8322(2)	-232(1)	32(1)
C(49)	1402(3)	9600(3)	-233(2)	49(1)
C(50)	1034(4)	7841(3)	-870(2)	57(1)
C(51)	1897(2)	7523(2)	3288(1)	23(1)
C(52)	811(3)	6564(2)	3355(1)	30(1)
C(53)	289(3)	6526(3)	3892(1)	46(1)
C(54)	792(3)	7414(3)	4351(1)	51(1)
C(55)	1850(3)	8337(3)	4281(1)	47(1)
C(56)	2424(3)	8419(2)	3754(1)	34(1)
C(57)	225(3)	5576(2)	2866(1)	32(1)
C(58)	637(3)	4634(3)	3038(2)	55(1)
C(59)	-1175(3)	5110(3)	2737(2)	47(1)
C(60)	3649(3)	9420(3)	3747(1)	49(1)
C(61)	3621(4)	10554(3)	3892(2)	66(1)
C(62)	4668(3)	9264(4)	4196(2)	71(1)
O(1S)	7358(7)	15761(5)	5237(2)	180(3)
C(1S)	7405(16)	17275(8)	5844(4)	336(11)
C(2S)	7811(9)	16602(8)	5701(3)	151(3)
C(3S)	7595(10)	14958(8)	5127(4)	177(4)
C(4S)	6973(11)	14108(7)	4671(3)	207(5)

Table A.16. Bond lengths [Å] and angles [°] for sr11.

Fe(1)-N(2)	1.967(2)	C(4)-C(5)	1.401(4)
Fe(1)-N(6)	1.984(2)	C(5)-C(6)	1.384(3)
Fe(1)-C(38)	2.085(2)	C(6)-C(7)	1.454(4)
Fe(1)-N(1)	2.127(2)	C(8)-C(9)	1.404(4)
Fe(1)-N(3)	2.272(2)	C(8)-C(13)	1.406(4)
Fe(1)-Fe(2)	2.8047(5)	C(9)-C(10)	1.385(4)
Fe(2)-N(5)	1.967(2)	C(9)-C(14)	1.517(4)
Fe(2)-N(3)	1.9827(19)	C(10)-C(11)	1.380(4)
Fe(2)-C(7)	2.076(2)	C(11)-C(12)	1.372(4)
Fe(2)-N(4)	2.1489(19)	C(12)-C(13)	1.394(4)
Fe(2)-N(6)	2.2640(19)	C(13)-C(17)	1.510(4)
N(1)-C(1)	1.326(3)	C(14)-C(16)	1.521(4)
N(1)-C(8)	1.436(3)	C(14)-C(15)	1.532(4)
N(2)-C(6)	1.353(3)	C(17)-C(18)	1.515(4)
N(2)-C(2)	1.360(3)	C(17)-C(19)	1.528(4)
N(3)-C(7)	1.392(3)	C(20)-C(21)	1.396(4)
N(3)-C(20)	1.441(3)	C(20)-C(25)	1.416(4)
N(4)-C(32)	1.322(3)	C(21)-C(22)	1.401(4)
N(4)-C(39)	1.439(3)	C(21)-C(26)	1.520(4)
N(5)-C(33)	1.357(3)	C(22)-C(23)	1.378(4)
N(5)-C(37)	1.363(3)	C(23)-C(24)	1.373(4)
N(6)-C(38)	1.392(3)	C(24)-C(25)	1.389(4)
N(6)-C(51)	1.431(3)	C(25)-C(29)	1.510(4)
C(1)-C(2)	1.410(3)	C(26)-C(27)	1.519(4)
C(2)-C(3)	1.404(4)	C(26)-C(28)	1.530(4)
C(3)-C(4)	1.374(4)	C(29)-C(31)	1.526(4)

C(29)-C(30)	1.524(4)
C(32)-C(33)	1.412(3)
C(33)-C(34)	1.404(4)
C(34)-C(35)	1.376(4)
C(35)-C(36)	1.393(4)
C(36)-C(37)	1.381(4)
C(37)-C(38)	1.447(3)
C(39)-C(44)	1.404(4)
C(39)-C(40)	1.405(4)
C(40)-C(41)	1.390(4)
C(40)-C(45)	1.517(4)
C(41)-C(42)	1.381(4)
C(42)-C(43)	1.369(4)
C(43)-C(44)	1.397(4)
C(44)-C(48)	1.510(4)
C(45)-C(46)	1.525(4)
C(45)-C(47)	1.537(4)
C(48)-C(50)	1.526(4)
C(48)-C(49)	1.532(4)
C(51)-C(56)	1.402(4)
C(51)-C(52)	1.413(4)
C(52)-C(53)	1.384(4)
C(52)-C(57)	1.513(4)
C(53)-C(54)	1.385(5)
C(54)-C(55)	1.372(5)
C(55)-C(56)	1.393(4)
C(56)-C(60)	1.513(4)
C(57)-C(59)	1.510(4)
C(57)-C(58)	1.528(4)
C(60)-C(62)	1.520(5)
C(60)-C(61)	1.527(5)
O(1S)-C(3S)	1.225(8)
O(1S)-C(2S)	1.356(9)
C(1S)-C(2S)	1.225(11)
C(3S)-C(4S)	1.357(11)

N(2)-Fe(1)-N(6)	127.89(8)
N(2)-Fe(1)-C(38)	110.78(9)
N(6)-Fe(1)-C(38)	39.92(9)
N(2)-Fe(1)-N(1)	76.66(8)
N(6)-Fe(1)-N(1)	135.49(8)
C(38)-Fe(1)-N(1)	100.34(9)
N(2)-Fe(1)-N(3)	76.32(8)
N(6)-Fe(1)-N(3)	84.43(8)
C(38)-Fe(1)-N(3)	116.49(9)
N(1)-Fe(1)-N(3)	140.09(7)
N(2)-Fe(1)-Fe(2)	80.82(6)
N(6)-Fe(1)-Fe(2)	53.13(6)
C(38)-Fe(1)-Fe(2)	73.47(7)
N(1)-Fe(1)-Fe(2)	152.70(6)
N(3)-Fe(1)-Fe(2)	44.46(5)
N(5)-Fe(2)-N(3)	127.88(8)
N(5)-Fe(2)-C(7)	110.42(9)
N(3)-Fe(2)-C(7)	40.02(9)
N(5)-Fe(2)-N(4)	76.42(8)
N(3)-Fe(2)-N(4)	134.99(8)
C(7)-Fe(2)-N(4)	99.66(9)
N(5)-Fe(2)-N(6)	76.29(8)
N(3)-Fe(2)-N(6)	84.67(8)
C(7)-Fe(2)-N(6)	116.62(9)
N(4)-Fe(2)-N(6)	140.33(7)
N(5)-Fe(2)-Fe(1)	80.65(6)
N(3)-Fe(2)-Fe(1)	53.37(6)
C(7)-Fe(2)-Fe(1)	73.51(7)
N(4)-Fe(2)-Fe(1)	151.99(6)
N(6)-Fe(2)-Fe(1)	44.51(5)
C(1)-N(1)-C(8)	114.3(2)
C(1)-N(1)-Fe(1)	110.71(16)
C(8)-N(1)-Fe(1)	134.23(16)
C(6)-N(2)-C(2)	120.4(2)
C(6)-N(2)-Fe(1)	121.04(16)
C(2)-N(2)-Fe(1)	117.84(16)
C(7)-N(3)-C(20)	115.96(19)
C(7)-N(3)-Fe(2)	73.60(13)
C(20)-N(3)-Fe(2)	126.92(16)
C(7)-N(3)-Fe(1)	106.27(15)
C(20)-N(3)-Fe(1)	133.48(15)
Fe(2)-N(3)-Fe(1)	82.17(7)
C(32)-N(4)-C(39)	115.2(2)
C(32)-N(4)-Fe(2)	109.76(16)
C(39)-N(4)-Fe(2)	133.76(15)
C(33)-N(5)-C(37)	120.0(2)
C(33)-N(5)-Fe(2)	118.28(16)
C(37)-N(5)-Fe(2)	121.05(16)
C(38)-N(6)-C(51)	117.1(2)
C(38)-N(6)-Fe(1)	73.93(13)
C(51)-N(6)-Fe(1)	128.01(16)
C(38)-N(6)-Fe(2)	106.79(15)
C(51)-N(6)-Fe(2)	131.36(16)
Fe(1)-N(6)-Fe(2)	82.35(7)
N(1)-C(1)-C(2)	117.9(2)
N(2)-C(2)-C(3)	120.8(2)
N(2)-C(2)-C(1)	112.0(2)
C(3)-C(2)-C(1)	127.1(2)
C(4)-C(3)-C(2)	118.4(3)
C(3)-C(4)-C(5)	120.4(2)
C(6)-C(5)-C(4)	119.0(2)
N(2)-C(6)-C(5)	120.8(2)
N(2)-C(6)-C(7)	112.9(2)
C(5)-C(6)-C(7)	126.3(2)
N(3)-C(7)-C(6)	117.6(2)
N(3)-C(7)-Fe(2)	66.38(12)
C(6)-C(7)-Fe(2)	106.38(16)
C(9)-C(8)-C(13)	120.9(2)
C(9)-C(8)-N(1)	118.9(2)
C(13)-C(8)-N(1)	120.2(2)
C(10)-C(9)-C(8)	118.6(2)
C(10)-C(9)-C(14)	120.5(2)
C(8)-C(9)-C(14)	120.9(2)
C(11)-C(10)-C(9)	121.0(3)
C(12)-C(11)-C(10)	120.2(3)
C(11)-C(12)-C(13)	121.3(3)

C(12)-C(13)-C(8)	118.0(3)
C(12)-C(13)-C(17)	119.5(2)
C(8)-C(13)-C(17)	122.5(2)
C(9)-C(14)-C(16)	110.9(2)
C(9)-C(14)-C(15)	113.2(2)
C(16)-C(14)-C(15)	109.9(2)
C(13)-C(17)-C(18)	110.9(2)
C(13)-C(17)-C(19)	111.6(2)
C(18)-C(17)-C(19)	110.8(3)
C(21)-C(20)-C(25)	120.3(2)
C(21)-C(20)-N(3)	122.6(2)
C(25)-C(20)-N(3)	117.0(2)
C(20)-C(21)-C(22)	118.4(2)
C(20)-C(21)-C(26)	124.3(2)
C(22)-C(21)-C(26)	117.3(2)
C(23)-C(22)-C(21)	121.6(3)
C(24)-C(23)-C(22)	119.4(3)
C(23)-C(24)-C(25)	121.7(3)
C(24)-C(25)-C(20)	118.5(3)
C(24)-C(25)-C(29)	119.9(2)
C(20)-C(25)-C(29)	121.6(2)
C(27)-C(26)-C(21)	110.4(2)
C(27)-C(26)-C(28)	111.0(2)
C(21)-C(26)-C(28)	113.1(2)
C(25)-C(29)-C(31)	111.3(2)
C(25)-C(29)-C(30)	112.5(2)
C(31)-C(29)-C(30)	110.1(2)
N(4)-C(32)-C(33)	118.4(2)
N(5)-C(33)-C(34)	120.9(2)
N(5)-C(33)-C(32)	111.9(2)
C(34)-C(33)-C(32)	127.1(2)
C(35)-C(34)-C(33)	118.7(2)
C(34)-C(35)-C(36)	120.1(3)
C(37)-C(36)-C(35)	119.4(2)
N(5)-C(37)-C(36)	120.8(2)
N(5)-C(37)-C(38)	112.8(2)
C(36)-C(37)-C(38)	126.4(2)
N(6)-C(38)-C(37)	117.6(2)
N(6)-C(38)-Fe(1)	66.14(13)
C(37)-C(38)-Fe(1)	106.22(16)
C(44)-C(39)-C(40)	120.7(2)
C(44)-C(39)-N(4)	120.8(2)
C(40)-C(39)-N(4)	118.5(2)
C(41)-C(40)-C(39)	118.5(2)
C(41)-C(40)-C(45)	120.2(3)
C(39)-C(40)-C(45)	121.2(2)
C(42)-C(41)-C(40)	121.0(3)
C(43)-C(42)-C(41)	120.2(3)
C(42)-C(43)-C(44)	121.2(3)
C(43)-C(44)-C(39)	118.3(3)
C(43)-C(44)-C(48)	118.5(2)
C(39)-C(44)-C(48)	123.2(2)
C(40)-C(45)-C(46)	114.2(2)
C(40)-C(45)-C(47)	110.2(2)
C(46)-C(45)-C(47)	109.1(2)
C(44)-C(48)-C(50)	111.4(3)
C(44)-C(48)-C(49)	111.1(2)
C(50)-C(48)-C(49)	110.6(3)
C(56)-C(51)-C(52)	120.5(2)
C(56)-C(51)-N(6)	122.4(2)
C(52)-C(51)-N(6)	117.0(2)
C(53)-C(52)-C(51)	118.5(3)
C(53)-C(52)-C(57)	119.5(3)
C(51)-C(52)-C(57)	121.9(2)
C(52)-C(53)-C(54)	121.5(3)
C(55)-C(54)-C(53)	119.3(3)
C(54)-C(55)-C(56)	121.9(3)
C(55)-C(56)-C(51)	118.3(3)
C(55)-C(56)-C(60)	117.9(3)
C(51)-C(56)-C(60)	123.5(2)
C(59)-C(57)-C(52)	112.9(3)
C(59)-C(57)-C(58)	110.2(2)
C(52)-C(57)-C(58)	112.3(3)
C(56)-C(60)-C(62)	109.4(3)
C(56)-C(60)-C(61)	113.8(3)
C(62)-C(60)-C(61)	111.4(3)
C(3S)-O(1S)-C(2S)	133.8(8)
C(1S)-C(2S)-O(1S)	130.5(11)
O(1S)-C(3S)-C(4S)	127.3(9)

Symmetry transformations used to generate equivalent atoms:

Table A.17. Crystal data and structure refinement for sr12.

Identification code	sr12	
Empirical formula	C38 H49 Fe N5	
Formula weight	631.67	
Temperature	173(2) K	
Wavelength	0.71073 Å	
Crystal system	Monoclinic	
Space group	P2(1)	
Unit cell dimensions	a = 15.7617(4) Å	α= 90°.
	b = 11.4631(3) Å	β= 91.8290(10)°.
	c = 19.3934(5) Å	γ = 90°.
Volume	3502.18(16) $Å^3$	
Z	4	
Density (calculated)	1.198 Mg/m^3	
Absorption coefficient	0.463 mm^{-1}	
F(000)	1352	
Crystal size	0.45 x 0.30 x 0.15 mm^3	
Theta range for data collection	1.64 to 28.74°.	
Index ranges	-21<=h<=20, -15<=k<=12, -25<=l<=24	
Reflections collected	33485	
Independent reflections	9223 [R(int) = 0.0358]	
Completeness to theta = 28.74°	96.6 %	
Absorption correction	Semi-empirical from equivalents	
Max. and min. transmission	0.9338 and 0.8186	
Refinement method	Full-matrix least-squares on F^2	
Data / restraints / parameters	9223 / 1 / 806	
Goodness-of-fit on F^2	1.020	
Final R indices [I>2sigma(I)]	R1 = 0.0319, wR2 = 0.0764	
R indices (all data)	R1 = 0.0404, wR2 = 0.0807	
Absolute structure parameter	?	
Largest diff. peak and hole	0.310 and -0.216 $e.Å^{-3}$	

Table A.18. Atomic coordinates (x 10^4) and equivalent isotropic displacement parameters ($Å^2$x 10^3) for sr12. U(eq) is defined as one third of the trace of the orthogonalized U^{ij} tensor.

	x	y	z	U(eq)
Fe(2)	6976(1)	4785(1)	1290(1)	20(1)
N(6)	6766(1)	3214(2)	1578(1)	22(1)
N(7)	5878(1)	4647(2)	959(1)	19(1)
N(8)	6867(1)	6248(2)	848(1)	22(1)
N(9)	8058(1)	4991(2)	1828(1)	27(1)
N(10)	10303(2)	4821(3)	3050(2)	60(1)
C(39)	5974(1)	2826(2)	1425(1)	23(1)
C(40)	5438(1)	3627(2)	1076(1)	21(1)
C(41)	4591(2)	3531(2)	843(1)	25(1)
C(42)	4207(1)	4467(2)	500(1)	27(1)
C(43)	4653(1)	5494(2)	381(1)	25(1)
C(44)	5502(1)	5577(2)	621(1)	21(1)
C(45)	6099(1)	6480(2)	561(1)	23(1)
C(46)	7369(1)	2457(2)	1921(1)	24(1)
C(47)	8100(2)	2145(2)	1560(1)	29(1)
C(48)	8751(2)	1563(3)	1922(2)	35(1)
C(49)	8679(2)	1283(3)	2612(2)	38(1)
C(50)	7960(2)	1549(3)	2943(1)	36(1)
C(51)	7289(2)	2158(2)	2617(1)	28(1)
C(52)	8144(2)	2404(3)	795(1)	36(1)
C(53)	7600(2)	1526(3)	377(2)	50(1)
C(54)	9052(2)	2418(4)	530(2)	55(1)
C(55)	6520(2)	2470(3)	3032(1)	35(1)
C(56)	5982(2)	1385(3)	3156(2)	43(1)
C(57)	6760(2)	3040(3)	3727(2)	49(1)
C(58)	7525(1)	7104(2)	794(1)	26(1)
C(59)	8033(2)	7107(3)	212(1)	34(1)
C(60)	8727(2)	7862(3)	214(2)	42(1)
C(61)	8905(2)	8601(3)	764(2)	44(1)
C(62)	8382(2)	8606(3)	1324(2)	40(1)
C(63)	7687(2)	7857(2)	1351(1)	30(1)
C(64)	7857(2)	6312(3)	-398(2)	50(1)
C(65)	7881(3)	6926(4)	-1078(2)	74(1)
C(66)	8437(5)	5281(4)	-401(2)	116(2)
C(67)	7094(2)	7907(3)	1951(1)	36(1)
C(68)	6433(2)	8863(4)	1830(2)	59(1)
C(69)	7555(2)	8061(3)	2652(2)	49(1)
C(70)	8818(2)	5204(2)	1568(2)	35(1)
C(71)	9572(2)	5153(3)	1947(2)	43(1)
C(72)	9575(2)	4885(3)	2650(2)	41(1)
C(73)	8777(2)	4694(3)	2930(1)	39(1)
C(74)	8063(2)	4760(3)	2512(1)	31(1)
C(75)	11114(2)	5052(4)	2753(3)	82(2)
C(76)	10268(2)	4546(4)	3778(2)	81(2)
Fe(1)	12475(1)	7277(1)	4002(1)	21(1)
N(1)	13271(1)	6009(2)	4075(1)	25(1)
N(2)	11966(1)	6432(2)	4678(1)	22(1)
N(3)	11551(1)	8296(2)	4171(1)	24(1)
N(4)	12913(1)	7990(2)	3155(1)	24(1)
N(5)	13987(2)	9271(2)	1357(1)	34(1)
C(1)	13080(2)	5198(2)	4543(1)	29(1)

C(2)	12321(2)	5387(2)	4890(1)	26(1)
C(3)	11911(2)	4710(3)	5379(1)	34(1)
C(4)	11143(2)	5087(3)	5627(1)	36(1)
C(5)	10792(2)	6137(3)	5419(1)	33(1)
C(6)	11215(2)	6819(2)	4937(1)	26(1)
C(7)	11004(2)	7907(2)	4644(1)	28(1)
C(8)	14026(2)	5837(2)	3682(1)	28(1)
C(9)	14678(2)	6677(3)	3752(1)	33(1)
C(10)	15379(2)	6549(3)	3334(2)	45(1)
C(11)	15437(2)	5646(3)	2871(2)	51(1)
C(12)	14798(2)	4842(3)	2811(2)	44(1)
C(13)	14073(2)	4909(3)	3214(1)	32(1)
C(14)	14634(2)	7642(3)	4271(2)	38(1)
C(15)	14910(2)	7192(4)	4985(2)	57(1)
C(16)	15124(2)	8743(3)	4085(2)	59(1)
C(17)	13376(2)	4005(3)	3104(2)	36(1)
C(18)	13641(2)	2811(3)	3393(2)	57(1)
C(19)	13105(2)	3881(4)	2339(2)	57(1)
C(20)	11397(1)	9426(2)	3879(1)	27(1)
C(21)	11617(2)	10434(3)	4250(1)	32(1)
C(22)	11507(2)	11504(3)	3922(2)	40(1)
C(23)	11192(2)	11585(3)	3251(2)	46(1)
C(24)	10978(2)	10583(3)	2889(2)	40(1)
C(25)	11070(2)	9494(2)	3189(1)	32(1)
C(26)	12007(2)	10376(3)	4976(2)	39(1)
C(27)	11674(4)	11335(4)	5439(2)	101(2)
C(28)	12958(2)	10362(6)	4953(2)	103(2)
C(29)	10810(2)	8393(3)	2803(1)	34(1)
C(30)	9891(2)	8063(3)	2958(2)	42(1)
C(31)	10929(2)	8490(4)	2026(2)	52(1)
C(32)	13150(2)	9113(2)	3093(1)	27(1)
C(33)	13509(2)	9566(2)	2514(1)	29(1)
C(34)	13634(2)	8851(2)	1935(1)	25(1)
C(35)	13367(2)	7694(2)	1994(1)	29(1)
C(36)	13029(1)	7310(3)	2595(1)	26(1)
C(37)	14340(2)	10424(3)	1346(1)	36(1)
C(38)	14119(2)	8511(3)	774(1)	45(1)

Table A.19. Bond lengths [Å] and angles [°] for sr12.

Fe(2)-N(7)	1.8330(17)	N(10)-C(75)	1.443(5)
Fe(2)-N(8)	1.889(2)	N(10)-C(76)	1.450(5)
Fe(2)-N(6)	1.917(2)	C(39)-C(40)	1.406(3)
Fe(2)-N(9)	1.9850(19)	C(40)-C(41)	1.400(3)
N(6)-C(39)	1.349(3)	C(41)-C(42)	1.391(4)
N(6)-C(46)	1.435(3)	C(42)-C(43)	1.394(4)
N(7)-C(44)	1.376(3)	C(43)-C(44)	1.406(3)
N(7)-C(40)	1.382(3)	C(44)-C(45)	1.406(3)
N(8)-C(45)	1.343(3)	C(46)-C(51)	1.402(3)
N(8)-C(58)	1.435(3)	C(46)-C(47)	1.413(3)
N(9)-C(70)	1.337(3)	C(47)-C(48)	1.396(4)
N(9)-C(74)	1.352(3)	C(47)-C(52)	1.515(4)
N(10)-C(72)	1.367(3)	C(48)-C(49)	1.383(4)
		C(49)-C(50)	1.355(4)

C(50)-C(51)	1.400(3)	C(20)-C(25)	1.421(4)
C(51)-C(55)	1.519(3)	C(21)-C(22)	1.389(4)
C(52)-C(54)	1.535(4)	C(21)-C(26)	1.522(4)
C(52)-C(53)	1.537(5)	C(22)-C(23)	1.382(5)
C(55)-C(56)	1.529(4)	C(23)-C(24)	1.382(5)
C(55)-C(57)	1.534(4)	C(24)-C(25)	1.382(4)
C(58)-C(63)	1.400(4)	C(25)-C(29)	1.517(4)
C(58)-C(59)	1.404(4)	C(26)-C(28)	1.501(5)
C(59)-C(60)	1.395(4)	C(26)-C(27)	1.523(5)
C(59)-C(64)	1.513(4)	C(29)-C(31)	1.529(4)
C(60)-C(61)	1.384(5)	C(29)-C(30)	1.535(4)
C(61)-C(62)	1.385(4)	C(32)-C(33)	1.374(3)
C(62)-C(63)	1.393(4)	C(33)-C(34)	1.409(3)
C(63)-C(67)	1.516(4)	C(34)-C(35)	1.398(4)
C(64)-C(65)	1.496(5)	C(35)-C(36)	1.369(3)
C(64)-C(66)	1.494(6)		
C(67)-C(68)	1.526(5)	N(7)-Fe(2)-N(8)	81.18(9)
C(67)-C(69)	1.532(4)	N(7)-Fe(2)-N(6)	81.45(9)
C(70)-C(71)	1.379(4)	N(8)-Fe(2)-N(6)	162.21(8)
C(71)-C(72)	1.397(4)	N(7)-Fe(2)-N(9)	168.50(8)
C(72)-C(73)	1.404(4)	N(8)-Fe(2)-N(9)	101.34(8)
C(73)-C(74)	1.367(3)	N(6)-Fe(2)-N(9)	96.44(8)
Fe(1)-N(2)	1.8357(19)	C(39)-N(6)-C(46)	119.9(2)
Fe(1)-N(3)	1.904(2)	C(39)-N(6)-Fe(2)	114.34(16)
Fe(1)-N(1)	1.922(2)	C(46)-N(6)-Fe(2)	125.80(15)
Fe(1)-N(4)	1.978(2)	C(44)-N(7)-C(40)	121.58(18)
N(1)-C(1)	1.339(3)	C(44)-N(7)-Fe(2)	119.15(16)
N(1)-C(8)	1.447(3)	C(40)-N(7)-Fe(2)	119.23(15)
N(2)-C(6)	1.373(3)	C(45)-N(8)-C(58)	118.6(2)
N(2)-C(2)	1.379(3)	C(45)-N(8)-Fe(2)	115.58(16)
N(3)-C(7)	1.355(3)	C(58)-N(8)-Fe(2)	125.83(15)
N(3)-C(20)	1.431(3)	C(70)-N(9)-C(74)	115.3(2)
N(4)-C(32)	1.347(3)	C(70)-N(9)-Fe(2)	126.05(18)
N(4)-C(36)	1.354(3)	C(74)-N(9)-Fe(2)	118.09(16)
N(5)-C(34)	1.355(3)	C(72)-N(10)-C(75)	120.2(3)
N(5)-C(37)	1.435(4)	C(72)-N(10)-C(76)	120.4(3)
N(5)-C(38)	1.447(4)	C(75)-N(10)-C(76)	119.4(3)
C(1)-C(2)	1.407(4)	N(6)-C(39)-C(40)	115.4(2)
C(2)-C(3)	1.399(4)	N(7)-C(40)-C(41)	119.4(2)
C(3)-C(4)	1.385(4)	N(7)-C(40)-C(39)	109.54(19)
C(4)-C(5)	1.380(4)	C(41)-C(40)-C(39)	131.0(2)
C(5)-C(6)	1.404(3)	C(42)-C(41)-C(40)	119.3(2)
C(6)-C(7)	1.406(4)	C(41)-C(42)-C(43)	121.1(2)
C(8)-C(13)	1.402(4)	C(42)-C(43)-C(44)	118.8(2)
C(8)-C(9)	1.412(4)	N(7)-C(44)-C(45)	109.36(19)
C(9)-C(10)	1.399(4)	N(7)-C(44)-C(43)	119.7(2)
C(9)-C(14)	1.499(4)	C(45)-C(44)-C(43)	130.9(2)
C(10)-C(11)	1.375(5)	N(8)-C(45)-C(44)	114.6(2)
C(11)-C(12)	1.368(5)	C(51)-C(46)-C(47)	121.1(2)
C(12)-C(13)	1.406(3)	C(51)-C(46)-N(6)	121.0(2)
C(13)-C(17)	1.521(4)	C(47)-C(46)-N(6)	117.5(2)
C(14)-C(15)	1.529(5)	C(48)-C(47)-C(46)	117.9(2)
C(14)-C(16)	1.529(5)	C(48)-C(47)-C(52)	122.0(2)
C(17)-C(18)	1.531(5)	C(46)-C(47)-C(52)	120.0(2)
C(17)-C(19)	1.538(4)	C(49)-C(48)-C(47)	121.1(3)
C(20)-C(21)	1.399(4)	C(50)-C(49)-C(48)	120.1(2)

C(49)-C(50)-C(51)	122.0(3)
C(50)-C(51)-C(46)	117.7(2)
C(50)-C(51)-C(55)	118.8(2)
C(46)-C(51)-C(55)	123.4(2)
C(47)-C(52)-C(54)	113.8(2)
C(47)-C(52)-C(53)	110.2(3)
C(54)-C(52)-C(53)	109.9(3)
C(51)-C(55)-C(56)	110.3(2)
C(51)-C(55)-C(57)	112.8(2)
C(56)-C(55)-C(57)	109.3(2)
C(63)-C(58)-C(59)	121.6(2)
C(63)-C(58)-N(8)	118.7(2)
C(59)-C(58)-N(8)	119.5(2)
C(60)-C(59)-C(58)	117.8(3)
C(60)-C(59)-C(64)	120.1(2)
C(58)-C(59)-C(64)	122.1(2)
C(61)-C(60)-C(59)	121.4(3)
C(62)-C(61)-C(60)	119.8(3)
C(61)-C(62)-C(63)	121.0(3)
C(62)-C(63)-C(58)	118.3(2)
C(62)-C(63)-C(67)	120.7(3)
C(58)-C(63)-C(67)	120.9(2)
C(65)-C(64)-C(66)	109.7(3)
C(65)-C(64)-C(59)	113.3(3)
C(66)-C(64)-C(59)	112.4(3)
C(63)-C(67)-C(68)	110.1(3)
C(63)-C(67)-C(69)	113.5(2)
C(68)-C(67)-C(69)	110.8(3)
N(9)-C(70)-C(71)	124.0(3)
C(70)-C(71)-C(72)	120.3(3)
N(10)-C(72)-C(71)	122.8(3)
N(10)-C(72)-C(73)	121.3(3)
C(71)-C(72)-C(73)	115.9(2)
C(74)-C(73)-C(72)	119.5(3)
N(9)-C(74)-C(73)	124.9(3)
N(2)-Fe(1)-N(3)	81.18(9)
N(2)-Fe(1)-N(1)	81.24(9)
N(3)-Fe(1)-N(1)	162.27(8)
N(2)-Fe(1)-N(4)	169.47(9)
N(3)-Fe(1)-N(4)	100.25(8)
N(1)-Fe(1)-N(4)	97.45(8)
C(1)-N(1)-C(8)	118.0(2)
C(1)-N(1)-Fe(1)	114.45(16)
C(8)-N(1)-Fe(1)	127.59(16)
C(6)-N(2)-C(2)	121.2(2)
C(6)-N(2)-Fe(1)	119.45(17)
C(2)-N(2)-Fe(1)	119.22(16)
C(7)-N(3)-C(20)	117.5(2)
C(7)-N(3)-Fe(1)	114.93(18)
C(20)-N(3)-Fe(1)	127.52(16)
C(32)-N(4)-C(36)	115.6(2)
C(32)-N(4)-Fe(1)	125.07(17)
C(36)-N(4)-Fe(1)	119.20(17)
C(34)-N(5)-C(37)	120.6(2)
C(34)-N(5)-C(38)	120.4(2)
C(37)-N(5)-C(38)	118.5(2)
N(1)-C(1)-C(2)	115.5(2)
N(2)-C(2)-C(3)	119.4(2)
N(2)-C(2)-C(1)	109.5(2)
C(3)-C(2)-C(1)	131.1(3)
C(4)-C(3)-C(2)	119.3(3)
C(5)-C(4)-C(3)	121.2(2)
C(4)-C(5)-C(6)	119.0(3)
N(2)-C(6)-C(5)	119.8(3)
N(2)-C(6)-C(7)	109.6(2)
C(5)-C(6)-C(7)	130.6(2)
N(3)-C(7)-C(6)	114.7(2)
C(13)-C(8)-C(9)	121.7(2)
C(13)-C(8)-N(1)	120.4(2)
C(9)-C(8)-N(1)	117.7(2)
C(10)-C(9)-C(8)	117.3(3)
C(10)-C(9)-C(14)	121.4(3)
C(8)-C(9)-C(14)	121.2(2)
C(11)-C(10)-C(9)	121.8(3)
C(12)-C(11)-C(10)	120.0(3)
C(11)-C(12)-C(13)	121.6(3)
C(8)-C(13)-C(12)	117.6(3)
C(8)-C(13)-C(17)	123.7(2)
C(12)-C(13)-C(17)	118.7(3)
C(9)-C(14)-C(15)	109.9(3)
C(9)-C(14)-C(16)	114.6(2)
C(15)-C(14)-C(16)	111.2(3)
C(13)-C(17)-C(18)	111.7(2)
C(13)-C(17)-C(19)	112.0(3)
C(18)-C(17)-C(19)	109.5(3)
C(21)-C(20)-C(25)	121.0(2)
C(21)-C(20)-N(3)	120.5(2)
C(25)-C(20)-N(3)	118.3(2)
C(22)-C(21)-C(20)	118.0(3)
C(22)-C(21)-C(26)	120.2(3)
C(20)-C(21)-C(26)	121.7(3)
C(23)-C(22)-C(21)	121.8(3)
C(24)-C(23)-C(22)	119.8(3)
C(23)-C(24)-C(25)	121.1(3)
C(24)-C(25)-C(20)	118.4(3)
C(24)-C(25)-C(29)	121.4(2)
C(20)-C(25)-C(29)	120.2(2)
C(28)-C(26)-C(21)	110.3(2)
C(28)-C(26)-C(27)	112.9(4)
C(21)-C(26)-C(27)	112.2(3)
C(25)-C(29)-C(31)	112.7(3)
C(25)-C(29)-C(30)	110.5(2)
C(31)-C(29)-C(30)	110.9(2)
N(4)-C(32)-C(33)	123.9(2)
C(32)-C(33)-C(34)	120.2(2)
N(5)-C(34)-C(35)	122.5(2)
N(5)-C(34)-C(33)	121.7(2)
C(35)-C(34)-C(33)	115.8(2)
C(36)-C(35)-C(34)	120.1(2)
N(4)-C(36)-C(35)	124.3(3)

Symmetry transformations used to generate eq. atoms

Table A.20. Crystal data and structure refinement for sr13.

Identification code	sr13	
Empirical formula	C38 H52 Fe N3	
Formula weight	606.68	
Temperature	173(2) K	
Wavelength	0.71073 Å	
Crystal system	Triclinic	
Space group	P-1	
Unit cell dimensions	a = 9.0851(4) Å	α= 94.958(2)°.
	b = 12.1329(6) Å	β= 104.666(2)°.
	c = 16.6443(7) Å	γ = 109.051(2)°.
Volume	1648.76(13) $Å^3$	
Z	2	
Density (calculated)	1.222 Mg/m^3	
Absorption coefficient	0.487 mm^{-1}	
F(000)	654	
Crystal size	0.40 x 0.15 x 0.10 mm^3	
Theta range for data collection	1.29 to 27.48°.	
Index ranges	-11<=h<=11, -15<=k<=15, -21<=l<=21	
Reflections collected	23513	
Independent reflections	7429 [R(int) = 0.0408]	
Completeness to theta = 27.48°	98.2 %	
Absorption correction	Semi-empirical from equivalents	
Max. and min. transmission	0.9529 and 0.8289	
Refinement method	Full-matrix least-squares on F^2	
Data / restraints / parameters	7429 / 112 / 484	
Goodness-of-fit on F^2	1.001	
Final R indices [I>2sigma(I)]	R1 = 0.0446, wR2 = 0.1148	
R indices (all data)	R1 = 0.0632, wR2 = 0.1314	
Largest diff. peak and hole	0.673 and -0.389 $e.Å^{-3}$	

Table A.21. Atomic coordinates (x 10^4) and equivalent isotropic displacement parameters ($Å^2$x 10^3) for sr13. U(eq) is defined as one third of the trace of the orthogonalized U^{ij} tensor.

	x	y	z	U(eq)
Fe(1)	9890(1)	8376(1)	3020(1)	17(1)
N(1)	9521(2)	8949(2)	1940(1)	20(1)
N(2)	9960(2)	7156(2)	2298(1)	21(1)
N(3)	9550(2)	7108(1)	3690(1)	19(1)
C(1)	9755(3)	8331(2)	1316(1)	26(1)
C(2)	10047(3)	7295(2)	1503(1)	24(1)
C(3)	10375(3)	6473(2)	1004(2)	33(1)
C(4)	10587(4)	5497(2)	1327(2)	39(1)
C(5)	10423(3)	5326(2)	2116(2)	33(1)
C(6)	10087(3)	6158(2)	2598(1)	23(1)
C(7)	9802(3)	6154(2)	3387(1)	23(1)
C(8)	9169(3)	9989(2)	1745(1)	22(1)
C(9)	7565(3)	9966(2)	1626(1)	26(1)
C(10)	7263(3)	10985(2)	1458(2)	36(1)
C(11)	8479(3)	11991(2)	1397(2)	41(1)
C(12)	10028(3)	11989(2)	1498(2)	35(1)
C(13)	10409(3)	10991(2)	1674(1)	25(1)
C(14)	6166(3)	8846(2)	1608(2)	29(1)
C(15)	4943(3)	9063(3)	2015(2)	42(1)
C(16)	5289(4)	8200(3)	695(2)	58(1)
C(17)	12125(3)	11021(2)	1734(2)	27(1)
C(18)	12401(3)	11033(3)	865(2)	40(1)
C(19)	13459(3)	12073(2)	2376(2)	38(1)
C(20)	9188(3)	7072(2)	4484(1)	20(1)
C(21)	10428(3)	7193(2)	5228(1)	21(1)
C(22)	10034(3)	7121(2)	5983(2)	28(1)
C(23)	8467(3)	6923(2)	6006(2)	34(1)
C(24)	7267(3)	6810(2)	5268(2)	32(1)
C(25)	7583(3)	6884(2)	4496(2)	24(1)
C(26)	12167(3)	7362(2)	5238(2)	24(1)
C(27)	12585(3)	6295(2)	5503(2)	36(1)
C(28)	13409(3)	8510(2)	5823(2)	38(1)
C(29)	6195(3)	6692(2)	3701(2)	29(1)
C(30)	5247(4)	5366(3)	3370(2)	52(1)
C(31)	5011(3)	7297(3)	3831(2)	47(1)
C(32)	12456(19)	9259(16)	3557(13)	23(3)
C(33)	11588(4)	9991(3)	3645(3)	23(1)
C(34)	10383(5)	9613(3)	4071(3)	24(1)
C(35)	8790(9)	9471(15)	3650(10)	25(3)
C(32')	12520(30)	9360(30)	3562(19)	25(4)
C(33')	11573(7)	9579(5)	4052(4)	22(2)
C(34')	10361(7)	10040(5)	3669(4)	24(2)
C(35')	8775(13)	9390(20)	3617(14)	27(5)
C(1S)	4388(8)	4810(6)	229(4)	128(2)
C(2S)	6004(8)	4373(8)	1264(4)	150(3)
C(3S)	5150(13)	5041(10)	1144(6)	190(4)

Table A.22. Bond lengths [Å] and angles [°] for sr13.

Fe(1)-N(2)	1.8523(17)	C(1S)-C(1S)#1	1.478(12)
Fe(1)-N(3)	1.9657(17)	C(2S)-C(3S)	1.288(10)
Fe(1)-N(1)	1.9728(18)		
Fe(1)-C(33)	2.041(3)	N(2)-Fe(1)-N(3)	79.41(7)
Fe(1)-C(33')	2.049(5)	N(2)-Fe(1)-N(1)	78.89(7)
Fe(1)-C(34)	2.055(3)	N(3)-Fe(1)-N(1)	151.92(7)
Fe(1)-C(34')	2.062(5)	N(2)-Fe(1)-C(33)	132.59(12)
Fe(1)-C(32')	2.19(3)	N(3)-Fe(1)-C(33)	116.05(14)
Fe(1)-C(32)	2.129(18)	N(1)-Fe(1)-C(33)	91.82(14)
Fe(1)-C(35)	2.240(14)	N(2)-Fe(1)-C(33')	133.44(17)
Fe(1)-C(35')	2.16(2)	N(3)-Fe(1)-C(33')	91.37(19)
N(1)-C(1)	1.329(3)	N(1)-Fe(1)-C(33')	116.55(19)
N(1)-C(8)	1.443(3)	C(33)-Fe(1)-C(33')	24.73(17)
N(2)-C(2)	1.366(3)	N(2)-Fe(1)-C(34)	162.08(13)
N(2)-C(6)	1.377(3)	N(3)-Fe(1)-C(34)	90.33(14)
N(3)-C(7)	1.333(3)	N(1)-Fe(1)-C(34)	114.90(14)
N(3)-C(20)	1.441(3)	C(33)-Fe(1)-C(34)	40.71(16)
C(1)-C(2)	1.410(3)	C(33')-Fe(1)-C(34)	31.18(18)
C(2)-C(3)	1.397(3)	N(2)-Fe(1)-C(34')	162.03(19)
C(3)-C(4)	1.391(4)	N(3)-Fe(1)-C(34')	114.8(2)
C(4)-C(5)	1.385(4)	N(1)-Fe(1)-C(34')	90.3(2)
C(5)-C(6)	1.393(3)	C(33)-Fe(1)-C(34')	32.42(19)
C(6)-C(7)	1.402(3)	C(33')-Fe(1)-C(34')	40.6(2)
C(8)-C(13)	1.400(3)	C(34)-Fe(1)-C(34')	24.68(18)
C(8)-C(9)	1.410(3)	N(2)-Fe(1)-C(32')	98.7(5)
C(9)-C(10)	1.388(3)	N(3)-Fe(1)-C(32')	101.2(9)
C(9)-C(14)	1.519(3)	N(1)-Fe(1)-C(32')	99.5(9)
C(10)-C(11)	1.385(4)	C(33)-Fe(1)-C(32')	36.7(6)
C(11)-C(12)	1.376(4)	C(33')-Fe(1)-C(32')	38.2(5)
C(12)-C(13)	1.397(3)	C(34)-Fe(1)-C(32')	68.7(5)
C(13)-C(17)	1.525(3)	C(34')-Fe(1)-C(32')	68.7(5)
C(14)-C(15)	1.519(4)	N(2)-Fe(1)-C(32)	97.1(3)
C(14)-C(16)	1.527(4)	N(3)-Fe(1)-C(32)	99.1(6)
C(17)-C(18)	1.529(3)	N(1)-Fe(1)-C(32)	101.0(6)
C(17)-C(19)	1.530(3)	C(33)-Fe(1)-C(32)	38.8(4)
C(20)-C(21)	1.407(3)	C(33')-Fe(1)-C(32)	39.1(4)
C(20)-C(25)	1.406(3)	C(34)-Fe(1)-C(32)	69.9(4)
C(21)-C(22)	1.392(3)	C(34')-Fe(1)-C(32)	70.7(4)
C(21)-C(26)	1.521(3)	C(32')-Fe(1)-C(32)	2.4(12)
C(22)-C(23)	1.376(3)	N(2)-Fe(1)-C(35)	158.0(3)
C(23)-C(24)	1.383(4)	N(3)-Fe(1)-C(35)	97.3(4)
C(24)-C(25)	1.390(3)	N(1)-Fe(1)-C(35)	96.2(4)
C(25)-C(29)	1.518(3)	C(33)-Fe(1)-C(35)	68.4(3)
C(26)-C(28)	1.531(3)	C(33')-Fe(1)-C(35)	67.9(3)
C(26)-C(27)	1.532(3)	C(34)-Fe(1)-C(35)	37.3(3)
C(29)-C(30)	1.528(4)	C(34')-Fe(1)-C(35)	36.5(4)
C(29)-C(31)	1.533(4)	C(32')-Fe(1)-C(35)	103.2(5)
C(32)-C(33)	1.388(11)	C(32)-Fe(1)-C(35)	104.9(4)
C(33)-C(34)	1.425(6)	N(2)-Fe(1)-C(35')	156.7(4)
C(34)-C(35)	1.385(9)	N(3)-Fe(1)-C(35')	96.6(6)
C(32')-C(33')	1.394(15)	N(1)-Fe(1)-C(35')	96.3(6)
C(33')-C(34')	1.428(8)	C(33)-Fe(1)-C(35')	69.8(5)
C(34')-C(35')	1.373(13)	C(33')-Fe(1)-C(35')	69.1(5)
C(1S)-C(3S)	1.464(10)	C(34)-Fe(1)-C(35')	38.4(5)

C(34')-Fe(1)-C(35')	37.9(5)
C(32')-Fe(1)-C(35')	104.6(6)
C(32)-Fe(1)-C(35')	106.2(5)
C(35)-Fe(1)-C(35')	1.4(7)
C(1)-N(1)-C(8)	115.30(18)
C(1)-N(1)-Fe(1)	114.74(14)
C(8)-N(1)-Fe(1)	129.74(14)
C(2)-N(2)-C(6)	120.24(18)
C(2)-N(2)-Fe(1)	120.22(14)
C(6)-N(2)-Fe(1)	119.23(15)
C(7)-N(3)-C(20)	114.61(17)
C(7)-N(3)-Fe(1)	114.47(15)
C(20)-N(3)-Fe(1)	130.76(13)
N(1)-C(1)-C(2)	114.9(2)
N(2)-C(2)-C(3)	120.8(2)
N(2)-C(2)-C(1)	109.72(19)
C(3)-C(2)-C(1)	129.4(2)
C(4)-C(3)-C(2)	118.6(2)
C(5)-C(4)-C(3)	120.5(2)
C(4)-C(5)-C(6)	119.5(2)
N(2)-C(6)-C(5)	120.1(2)
N(2)-C(6)-C(7)	110.03(18)
C(5)-C(6)-C(7)	129.9(2)
N(3)-C(7)-C(6)	115.09(19)
C(13)-C(8)-C(9)	121.46(19)
C(13)-C(8)-N(1)	119.83(19)
C(9)-C(8)-N(1)	118.71(18)
C(10)-C(9)-C(8)	117.7(2)
C(10)-C(9)-C(14)	120.0(2)
C(8)-C(9)-C(14)	122.13(19)
C(11)-C(10)-C(9)	121.7(2)
C(12)-C(11)-C(10)	119.8(2)
C(11)-C(12)-C(13)	121.2(2)
C(12)-C(13)-C(8)	118.2(2)
C(12)-C(13)-C(17)	118.7(2)
C(8)-C(13)-C(17)	123.06(19)
C(15)-C(14)-C(9)	114.0(2)
C(15)-C(14)-C(16)	109.6(2)
C(9)-C(14)-C(16)	109.4(2)
C(13)-C(17)-C(18)	110.22(19)
C(13)-C(17)-C(19)	113.0(2)
C(18)-C(17)-C(19)	110.0(2)
C(21)-C(20)-C(25)	121.1(2)
C(21)-C(20)-N(3)	119.72(18)
C(25)-C(20)-N(3)	119.17(18)
C(22)-C(21)-C(20)	118.6(2)
C(22)-C(21)-C(26)	118.67(19)
C(20)-C(21)-C(26)	122.74(19)
C(23)-C(22)-C(21)	121.3(2)
C(22)-C(23)-C(24)	119.2(2)
C(23)-C(24)-C(25)	122.4(2)
C(24)-C(25)-C(20)	117.5(2)
C(24)-C(25)-C(29)	119.7(2)
C(20)-C(25)-C(29)	122.7(2)
C(21)-C(26)-C(28)	112.14(19)
C(21)-C(26)-C(27)	110.11(18)
C(28)-C(26)-C(27)	110.1(2)
C(25)-C(29)-C(30)	110.27(19)
C(25)-C(29)-C(31)	113.2(2)
C(30)-C(29)-C(31)	109.2(2)
C(33)-C(32)-Fe(1)	67.2(6)
C(32)-C(33)-C(34)	116.9(9)
C(32)-C(33)-Fe(1)	74.0(8)
C(34)-C(33)-Fe(1)	70.2(2)
C(35)-C(34)-C(33)	118.4(7)
C(35)-C(34)-Fe(1)	78.6(7)
C(33)-C(34)-Fe(1)	69.1(2)
C(34)-C(35)-Fe(1)	64.1(5)
C(33')-C(32')-Fe(1)	65.4(9)
C(34')-C(33')-C(32')	116.8(14)
C(34')-C(33')-Fe(1)	70.2(3)
C(32')-C(33')-Fe(1)	76.4(13)
C(35')-C(34')-C(33')	117.0(11)
C(35')-C(34')-Fe(1)	74.8(11)
C(33')-C(34')-Fe(1)	69.2(3)
C(34')-C(35')-Fe(1)	67.3(8)
C(3S)-C(1S)-C(1S)#1	111.8(8)
C(2S)-C(3S)-C(1S)	105.2(9)

Symmetry transformations used to generate equivalent atoms:
#1 -x+1,-y+1,-z

Table A.23. Crystal data and structure refinement for sr14.

Identification code	sr14	
Empirical formula	C60 H63 B Mn N3 O3	
Formula weight	939.88	
Temperature	173(2) K	
Wavelength	0.71073 Å	
Crystal system	Monoclinic	
Space group	P2(1)/n	
Unit cell dimensions	a = 10.3963(6) Å	α= 90°.
	b = 35.987(2) Å	β= 98.485(2)°.
	c = 15.3682(8) Å	γ = 90°.
Volume	5686.8(5) $Å^3$	
Z	4	
Density (calculated)	1.098 Mg/m^3	
Absorption coefficient	0.275 mm^{-1}	
F(000)	1992	
Crystal size	0.30 x 0.10 x 0.02 mm^3	
Theta range for data collection	1.13 to 22.98°.	
Index ranges	-11<=h<=11, -39<=k<=36, -16<=l<=16	
Reflections collected	30820	
Independent reflections	7901 [R(int) = 0.0731]	
Completeness to theta = 22.98°	99.9 %	
Absorption correction	Semi-empirical from equivalents	
Max. and min. transmission	0.9945 and 0.9220	
Refinement method	Full-matrix least-squares on F^2	
Data / restraints / parameters	7901 / 0 / 615	
Goodness-of-fit on F^2	0.998	
Final R indices [I>2sigma(I)]	R1 = 0.0571, wR2 = 0.1272	
R indices (all data)	R1 = 0.1010, wR2 = 0.1410	
Largest diff. peak and hole	0.299 and -0.480 $e.Å^{-3}$	

Table A.24. Atomic coordinates (x 10^4) and equivalent isotropic displacement parameters ($Å^2$x 10^3) for sr14. U(eq) is defined as one third of the trace of the orthogonalized U^{ij} tensor.

	x	y	z	U(eq)
B(1)	8608(4)	7616(1)	12471(3)	35(1)
Mn(1)	8942(1)	8967(1)	8013(1)	30(1)
O(1)	11672(3)	9187(1)	8702(2)	50(1)
O(2)	8772(3)	9759(1)	7514(2)	60(1)
O(3)	6088(3)	8922(1)	7353(2)	57(1)
N(1)	9381(3)	8760(1)	6846(2)	27(1)
N(2)	8900(3)	8429(1)	8206(2)	27(1)
N(3)	8610(3)	8927(1)	9321(2)	26(1)
C(1)	9643(4)	8185(1)	5979(2)	45(1)
C(2)	9388(3)	8401(1)	6771(2)	30(1)
C(3)	9085(4)	8196(1)	7547(2)	29(1)
C(4)	8944(4)	7818(1)	7634(2)	37(1)
C(5)	8605(4)	7679(1)	8407(2)	41(1)
C(6)	8414(4)	7918(1)	9086(2)	37(1)
C(7)	8558(3)	8295(1)	8962(2)	29(1)
C(8)	8396(3)	8595(1)	9592(2)	28(1)
C(9)	7972(4)	8496(1)	10451(2)	40(1)
C(10)	9638(4)	8993(1)	6117(2)	30(1)
C(11)	10920(4)	9121(1)	6107(2)	34(1)
C(12)	11113(4)	9372(1)	5456(2)	46(1)
C(13)	10078(5)	9488(1)	4839(3)	53(1)
C(14)	8861(5)	9352(1)	4853(2)	49(1)
C(15)	8606(4)	9097(1)	5487(2)	37(1)
C(16)	12092(4)	8979(1)	6721(2)	41(1)
C(17)	12996(4)	9292(1)	7112(3)	58(1)
C(18)	12865(4)	8708(1)	6240(3)	56(1)
C(19)	7244(4)	8944(1)	5436(2)	49(1)
C(20)	6891(5)	8709(1)	4598(3)	70(2)
C(21)	6244(5)	9252(1)	5488(3)	76(2)
C(22)	8645(4)	9235(1)	9942(2)	30(1)
C(23)	7562(4)	9469(1)	9907(2)	36(1)
C(24)	7644(4)	9765(1)	10487(3)	55(1)
C(25)	8745(5)	9827(1)	11081(3)	63(1)
C(26)	9790(4)	9594(1)	11112(3)	53(1)
C(27)	9780(4)	9294(1)	10549(2)	35(1)
C(28)	6297(4)	9402(1)	9295(2)	43(1)
C(29)	5917(4)	9732(1)	8680(3)	63(1)
C(30)	5206(4)	9309(1)	9815(3)	63(1)
C(31)	10967(4)	9045(1)	10646(2)	36(1)
C(32)	11061(5)	8805(1)	11470(2)	62(1)
C(33)	12241(4)	9265(1)	10691(2)	50(1)
C(34)	10667(4)	9075(1)	8439(2)	34(1)
C(35)	8830(4)	9448(1)	7737(2)	39(1)
C(36)	7171(4)	8940(1)	7595(2)	38(1)
C(37)	7131(4)	7770(1)	12105(2)	33(1)
C(38)	6417(4)	7963(1)	12657(3)	45(1)
C(39)	5173(5)	8104(1)	12400(3)	56(1)
C(40)	4592(5)	8053(1)	11539(3)	61(1)
C(41)	5229(4)	7862(1)	10964(3)	52(1)
C(42)	6473(4)	7721(1)	11243(2)	40(1)
C(43)	8506(4)	7232(1)	13037(2)	33(1)

C(44)	7452(4)	7147(1)	13461(2)	38(1)
C(45)	7394(4)	6833(1)	13981(2)	48(1)
C(46)	8421(5)	6589(1)	14094(3)	47(1)
C(47)	9482(5)	6658(1)	13687(2)	46(1)
C(48)	9518(4)	6972(1)	13164(2)	40(1)
C(49)	9421(4)	7520(1)	11654(2)	33(1)
C(50)	9098(4)	7215(1)	11104(2)	42(1)
C(51)	9775(5)	7111(1)	10439(3)	52(1)
C(52)	10829(5)	7314(1)	10280(3)	57(1)
C(53)	11181(4)	7621(1)	10798(3)	56(1)
C(54)	10488(4)	7722(1)	11470(2)	43(1)
C(55)	9432(4)	7931(1)	13096(2)	32(1)
C(56)	10493(4)	7842(1)	13713(2)	41(1)
C(57)	11313(4)	8106(1)	14162(2)	54(1)
C(58)	11063(5)	8476(1)	14020(3)	55(1)
C(59)	10009(5)	8580(1)	13434(2)	51(1)
C(60)	9213(4)	8310(1)	12978(2)	41(1)

Table A.25. Bond lengths [Å] and angles [°] for sr14.

B(1)-C(55)	1.643(5)	C(12)-C(13)	1.389(6)
B(1)-C(43)	1.646(5)	C(13)-C(14)	1.361(6)
B(1)-C(49)	1.651(6)	C(14)-C(15)	1.390(5)
B(1)-C(37)	1.651(6)	C(15)-C(19)	1.512(5)
Mn(1)-C(35)	1.784(4)	C(16)-C(18)	1.523(5)
Mn(1)-C(34)	1.858(4)	C(16)-C(17)	1.533(5)
Mn(1)-C(36)	1.861(4)	C(19)-C(21)	1.529(6)
Mn(1)-N(2)	1.961(3)	C(19)-C(20)	1.540(5)
Mn(1)-N(1)	2.054(3)	C(22)-C(23)	1.400(5)
Mn(1)-N(3)	2.093(3)	C(22)-C(27)	1.408(5)
O(1)-C(34)	1.136(4)	C(23)-C(24)	1.384(5)
O(2)-C(35)	1.169(4)	C(23)-C(28)	1.520(5)
O(3)-C(36)	1.134(4)	C(24)-C(25)	1.373(5)
N(1)-C(2)	1.298(4)	C(25)-C(26)	1.369(6)
N(1)-C(10)	1.455(4)	C(26)-C(27)	1.382(5)
N(2)-C(3)	1.350(4)	C(27)-C(31)	1.514(5)
N(2)-C(7)	1.352(4)	C(28)-C(30)	1.518(6)
N(3)-C(8)	1.294(4)	C(28)-C(29)	1.534(5)
N(3)-C(22)	1.460(4)	C(31)-C(32)	1.525(5)
C(1)-C(2)	1.500(5)	C(31)-C(33)	1.536(5)
C(2)-C(3)	1.476(5)	C(37)-C(38)	1.393(5)
C(3)-C(4)	1.374(5)	C(37)-C(42)	1.409(5)
C(4)-C(5)	1.382(5)	C(38)-C(39)	1.390(6)
C(5)-C(6)	1.388(5)	C(39)-C(40)	1.383(6)
C(6)-C(7)	1.383(5)	C(40)-C(41)	1.366(6)
C(7)-C(8)	1.477(5)	C(41)-C(42)	1.398(6)
C(8)-C(9)	1.495(5)	C(43)-C(44)	1.389(5)
C(10)-C(15)	1.386(5)	C(43)-C(48)	1.398(5)
C(10)-C(11)	1.412(5)	C(44)-C(45)	1.390(5)
C(11)-C(12)	1.385(5)	C(45)-C(46)	1.375(6)
C(11)-C(16)	1.517(5)	C(46)-C(47)	1.369(6)
		C(47)-C(48)	1.389(5)
		C(49)-C(54)	1.392(5)

C(49)-C(50)	1.394(5)
C(50)-C(51)	1.376(5)
C(51)-C(52)	1.369(6)
C(52)-C(53)	1.378(6)
C(53)-C(54)	1.392(6)
C(55)-C(56)	1.382(5)
C(55)-C(60)	1.390(5)
C(56)-C(57)	1.391(5)
C(57)-C(58)	1.368(6)
C(58)-C(59)	1.365(6)
C(59)-C(60)	1.396(5)

C(55)-B(1)-C(43)	109.9(3)
C(55)-B(1)-C(49)	108.0(3)
C(43)-B(1)-C(49)	107.7(3)
C(55)-B(1)-C(37)	110.3(3)
C(43)-B(1)-C(37)	109.4(3)
C(49)-B(1)-C(37)	111.4(3)
C(35)-Mn(1)-C(34)	84.54(16)
C(35)-Mn(1)-C(36)	86.61(17)
C(34)-Mn(1)-C(36)	170.72(16)
C(35)-Mn(1)-N(2)	173.43(14)
C(34)-Mn(1)-N(2)	101.34(14)
C(36)-Mn(1)-N(2)	87.65(14)
C(35)-Mn(1)-N(1)	99.16(14)
C(34)-Mn(1)-N(1)	93.22(13)
C(36)-Mn(1)-N(1)	90.94(13)
N(2)-Mn(1)-N(1)	77.72(11)
C(35)-Mn(1)-N(3)	106.28(14)
C(34)-Mn(1)-N(3)	87.94(13)
C(36)-Mn(1)-N(3)	91.87(14)
N(2)-Mn(1)-N(3)	77.10(11)
N(1)-Mn(1)-N(3)	154.51(11)
C(2)-N(1)-C(10)	120.0(3)
C(2)-N(1)-Mn(1)	116.3(2)
C(10)-N(1)-Mn(1)	123.6(2)
C(3)-N(2)-C(7)	120.6(3)
C(3)-N(2)-Mn(1)	119.4(2)
C(7)-N(2)-Mn(1)	119.7(2)
C(8)-N(3)-C(22)	118.6(3)
C(8)-N(3)-Mn(1)	115.7(2)
C(22)-N(3)-Mn(1)	125.7(2)
N(1)-C(2)-C(3)	115.0(3)
N(1)-C(2)-C(1)	126.3(3)
C(3)-C(2)-C(1)	118.8(3)
N(2)-C(3)-C(4)	120.7(3)
N(2)-C(3)-C(2)	111.5(3)
C(4)-C(3)-C(2)	127.8(3)
C(3)-C(4)-C(5)	119.2(3)
C(4)-C(5)-C(6)	120.2(3)
C(7)-C(6)-C(5)	118.4(3)
N(2)-C(7)-C(6)	120.9(3)
N(2)-C(7)-C(8)	112.0(3)
C(6)-C(7)-C(8)	127.1(3)
N(3)-C(8)-C(7)	114.9(3)
N(3)-C(8)-C(9)	126.4(3)
C(7)-C(8)-C(9)	118.7(3)
C(15)-C(10)-C(11)	122.5(3)
C(15)-C(10)-N(1)	118.9(3)
C(11)-C(10)-N(1)	118.5(3)
C(12)-C(11)-C(10)	117.3(3)
C(12)-C(11)-C(16)	118.7(4)
C(10)-C(11)-C(16)	123.8(3)
C(11)-C(12)-C(13)	120.6(4)
C(14)-C(13)-C(12)	120.6(4)
C(13)-C(14)-C(15)	121.5(4)
C(10)-C(15)-C(14)	117.4(4)
C(10)-C(15)-C(19)	124.0(3)
C(14)-C(15)-C(19)	118.5(3)
C(11)-C(16)-C(18)	110.3(3)
C(11)-C(16)-C(17)	112.6(3)
C(18)-C(16)-C(17)	109.0(4)
C(15)-C(19)-C(21)	111.8(4)
C(15)-C(19)-C(20)	110.5(3)
C(21)-C(19)-C(20)	111.2(4)
C(23)-C(22)-C(27)	121.6(3)
C(23)-C(22)-N(3)	119.3(3)
C(27)-C(22)-N(3)	119.1(3)
C(24)-C(23)-C(22)	117.8(3)
C(24)-C(23)-C(28)	119.1(4)
C(22)-C(23)-C(28)	123.0(3)
C(25)-C(24)-C(23)	121.3(4)
C(26)-C(25)-C(24)	120.2(4)
C(25)-C(26)-C(27)	121.6(4)
C(26)-C(27)-C(22)	117.5(4)
C(26)-C(27)-C(31)	118.0(3)
C(22)-C(27)-C(31)	124.5(3)
C(30)-C(28)-C(23)	110.7(3)
C(30)-C(28)-C(29)	110.6(4)
C(23)-C(28)-C(29)	112.3(3)
C(27)-C(31)-C(32)	111.6(3)
C(27)-C(31)-C(33)	112.6(3)
C(32)-C(31)-C(33)	107.8(3)
O(1)-C(34)-Mn(1)	171.4(3)
O(2)-C(35)-Mn(1)	176.5(3)
O(3)-C(36)-Mn(1)	179.0(4)
C(38)-C(37)-C(42)	114.0(4)
C(38)-C(37)-B(1)	120.8(3)
C(42)-C(37)-B(1)	125.2(4)
C(39)-C(38)-C(37)	124.5(4)
C(40)-C(39)-C(38)	118.7(4)
C(41)-C(40)-C(39)	120.0(4)
C(40)-C(41)-C(42)	120.0(4)
C(41)-C(42)-C(37)	122.8(4)
C(44)-C(43)-C(48)	114.7(3)
C(44)-C(43)-B(1)	123.3(4)
C(48)-C(43)-B(1)	122.0(4)
C(43)-C(44)-C(45)	123.5(4)
C(46)-C(45)-C(44)	119.6(4)
C(47)-C(46)-C(45)	119.2(4)
C(46)-C(47)-C(48)	120.3(4)
C(47)-C(48)-C(43)	122.7(4)

C(54)-C(49)-C(50)	114.6(4)	C(55)-C(56)-C(57)	123.4(4)
C(54)-C(49)-B(1)	123.8(3)	C(58)-C(57)-C(56)	119.9(4)
C(50)-C(49)-B(1)	121.5(3)	C(59)-C(58)-C(57)	119.2(4)
C(51)-C(50)-C(49)	124.1(4)	C(58)-C(59)-C(60)	119.9(4)
C(52)-C(51)-C(50)	119.9(4)	C(55)-C(60)-C(59)	122.9(4)
C(51)-C(52)-C(53)	118.3(4)		
C(52)-C(53)-C(54)	121.1(4)		
C(49)-C(54)-C(53)	121.9(4)		
C(56)-C(55)-C(60)	114.7(3)		
C(56)-C(55)-B(1)	122.3(3)		
C(60)-C(55)-B(1)	122.6(3)		

Symmetry transformations used to generate equivalent atoms:

Table A.26. Crystal data and structure refinement for sr15.

Identification code	sr15	
Empirical formula	C37 H51 Cl Mn N3 O	
Formula weight	644.20	
Temperature	173(2) K	
Wavelength	0.71073 Å	
Crystal system	Orthorhombic	
Space group	Pnma	
Unit cell dimensions	a = 17.726(2) Å	α= 90°.
	b = 23.893(3) Å	β= 90°.
	c = 18.322(2) Å	γ = 90°.
Volume	7760.0(15) $Å^3$	
Z	8	
Density (calculated)	1.103 Mg/m^3	
Absorption coefficient	0.438 mm^{-1}	
F(000)	2752	
Crystal size	0.40 x 0.30 x 0.30 mm^3	
Theta range for data collection	1.60 to 27.32°.	
Index ranges	-22<=h<=22, -30<=k<=21, -23<=l<=21	
Reflections collected	34838	
Independent reflections	8831 [R(int) = 0.0328]	
Completeness to theta = 27.32°	98.5 %	
Absorption correction	Semi-empirical from equivalents	
Max. and min. transmission	0.8799 and 0.8443	
Refinement method	Full-matrix least-squares on F^2	
Data / restraints / parameters	8831 / 0 / 472	
Goodness-of-fit on F^2	1.070	
Final R indices [I>2sigma(I)]	R1 = 0.0460, wR2 = 0.1365	
R indices (all data)	R1 = 0.0671, wR2 = 0.1480	
Largest diff. peak and hole	0.333 and -0.268 $e.Å^{-3}$	

Table A.27. Atomic coordinates (x 10^4) and equivalent isotropic displacement parameters ($Å^2$x 10^3) for sr15. U(eq) is defined as one third of the trace of the orthogonalized U^{ij} tensor.

	x	y	z	U(eq)
Mn(1)	1328(1)	2500	1734(1)	26(1)
Mn(2)	5295(1)	7500	2046(1)	28(1)
Cl(1)	1890(1)	2500	607(1)	56(1)
Cl(2)	4775(1)	7500	897(1)	50(1)
O(1)	2297(1)	2500	2450(1)	38(1)
O(2)	4250(1)	7500	2644(1)	42(1)
N(1)	952(1)	3405(1)	1896(1)	29(1)
N(2)	538(1)	2500	2564(1)	26(1)
N(3)	5663(1)	6581(1)	2222(1)	30(1)
N(4)	6086(1)	7500	2868(1)	28(1)
C(1)	262(1)	4053(1)	2707(2)	51(1)
C(2)	537(1)	3487(1)	2466(1)	31(1)
C(3)	317(1)	2991(1)	2875(1)	28(1)
C(4)	-106(1)	2996(1)	3508(1)	37(1)
C(5)	-313(2)	2500	3831(2)	40(1)
C(6)	1104(1)	3864(1)	1421(1)	36(1)
C(7)	612(1)	3967(1)	849(1)	46(1)
C(8)	764(2)	4417(1)	392(2)	64(1)
C(9)	1384(2)	4746(1)	497(2)	70(1)
C(10)	1871(2)	4629(1)	1049(2)	60(1)
C(11)	1752(1)	4188(1)	1520(2)	44(1)
C(12)	-69(2)	3601(1)	714(2)	61(1)
C(13)	-21(2)	3308(2)	-33(2)	120(2)
C(14)	-781(2)	3907(2)	768(3)	114(2)
C(15)	2309(1)	4063(1)	2110(2)	56(1)
C(16)	2315(2)	4528(2)	2693(2)	85(1)
C(17)	3093(2)	3986(1)	1801(3)	92(1)
C(18)	2233(2)	2500	3225(2)	69(1)
C(19)	3001(2)	2500	3510(3)	93(2)
C(20)	3499(3)	2662(3)	2919(4)	75(3)
C(21)	3080(2)	2500	2240(3)	53(1)
C(22)	6402(1)	5953(1)	3014(2)	50(1)
C(23)	6105(1)	6512(1)	2778(1)	32(1)
C(24)	6332(1)	7008(1)	3169(1)	31(1)
C(25)	6773(1)	7001(1)	3787(1)	39(1)
C(26)	6984(2)	7500	4108(2)	45(1)
C(27)	5462(1)	6105(1)	1791(1)	34(1)
C(28)	5880(1)	5979(1)	1176(1)	43(1)
C(29)	5678(2)	5510(1)	771(1)	51(1)
C(30)	5089(2)	5181(1)	973(2)	54(1)
C(31)	4674(2)	5314(1)	1574(2)	52(1)
C(32)	4845(1)	5777(1)	1994(1)	42(1)
C(33)	6540(2)	6329(1)	934(2)	59(1)
C(34)	7252(2)	5981(2)	838(2)	98(1)
C(35)	6367(2)	6621(2)	210(2)	97(1)
C(36)	4354(2)	5918(1)	2641(2)	64(1)
C(37)	4395(2)	5480(2)	3240(2)	96(1)
C(38)	3545(2)	5986(2)	2413(3)	96(1)
C(39)	3504(2)	7500	2338(2)	50(1)
C(40)	2978(2)	7500	2970(3)	71(1)
C(41)	3466(3)	7281(3)	3613(3)	65(2)

C(42)	4204(2)	7500	3425(2)	54(1)

Table A.28. Bond lengths [Å] and angles [°] for sr15.

Mn(1)-N(2)	2.065(2)	C(26)-C(25)#2	1.382(3)
Mn(1)-O(1)	2.1615(19)	C(27)-C(28)	1.382(3)
Mn(1)-N(1)#1	2.2825(16)	C(27)-C(32)	1.396(3)
Mn(1)-N(1)	2.2825(16)	C(28)-C(29)	1.389(3)
Mn(1)-Cl(1)	2.2927(9)	C(28)-C(33)	1.506(3)
Mn(2)-N(4)	2.058(2)	C(29)-C(30)	1.360(4)
Mn(2)-O(2)	2.151(2)	C(30)-C(31)	1.362(4)
Mn(2)-Cl(2)	2.2977(9)	C(31)-C(32)	1.381(3)
Mn(2)-N(3)	2.3135(16)	C(32)-C(36)	1.508(4)
Mn(2)-N(3)#2	2.3135(16)	C(33)-C(34)	1.520(4)
O(1)-C(18)	1.424(5)	C(33)-C(35)	1.529(4)
O(1)-C(21)	1.440(4)	C(36)-C(37)	1.519(5)
O(2)-C(39)	1.436(4)	C(36)-C(38)	1.503(4)
O(2)-C(42)	1.434(4)	C(39)-C(40)	1.487(6)
N(1)-C(2)	1.293(2)	C(40)-C(41)	1.552(7)
N(1)-C(6)	1.425(3)	C(40)-C(41)#2	1.552(7)
N(2)-C(3)#1	1.362(2)	C(41)-C(41)#2	1.048(13)
N(2)-C(3)	1.362(2)	C(41)-C(42)	1.451(6)
N(3)-C(23)	1.296(3)	C(42)-C(41)#2	1.451(6)
N(3)-C(27)	1.429(3)		
N(4)-C(24)	1.370(2)	N(2)-Mn(1)-O(1)	95.27(8)
N(4)-C(24)#2	1.370(2)	N(2)-Mn(1)-N(1)#1	72.98(4)
C(1)-C(2)	1.503(3)	O(1)-Mn(1)-N(1)#1	98.81(4)
C(2)-C(3)	1.454(3)	N(2)-Mn(1)-N(1)	72.99(4)
C(3)-C(4)	1.381(3)	O(1)-Mn(1)-N(1)	98.81(4)
C(4)-C(5)	1.375(3)	N(1)#1-Mn(1)-N(1)	142.80(7)
C(5)-C(4)#1	1.375(3)	N(2)-Mn(1)-Cl(1)	163.12(7)
C(6)-C(7)	1.384(3)	O(1)-Mn(1)-Cl(1)	101.60(6)
C(6)-C(11)	1.396(3)	N(1)#1-Mn(1)-Cl(1)	104.08(4)
C(7)-C(8)	1.389(4)	N(1)-Mn(1)-Cl(1)	104.08(4)
C(7)-C(12)	1.511(4)	N(4)-Mn(2)-O(2)	102.39(9)
C(8)-C(9)	1.366(4)	N(4)-Mn(2)-Cl(2)	160.63(7)
C(9)-C(10)	1.360(4)	O(2)-Mn(2)-Cl(2)	96.98(6)
C(10)-C(11)	1.378(3)	N(4)-Mn(2)-N(3)	72.89(4)
C(11)-C(15)	1.494(4)	O(2)-Mn(2)-N(3)	99.93(4)
C(12)-C(14)	1.462(4)	Cl(2)-Mn(2)-N(3)	103.91(4)
C(12)-C(13)	1.540(5)	N(4)-Mn(2)-N(3)#2	72.89(4)
C(15)-C(17)	1.512(4)	O(2)-Mn(2)-N(3)#2	99.92(4)
C(15)-C(16)	1.541(4)	Cl(2)-Mn(2)-N(3)#2	103.91(4)
C(18)-C(19)	1.458(5)	N(3)-Mn(2)-N(3)#2	143.31(8)
C(19)-C(20)#1	1.450(8)	C(18)-O(1)-C(21)	110.0(3)
C(19)-C(20)	1.450(8)	C(18)-O(1)-Mn(1)	122.83(19)
C(20)-C(20)#1	0.777(15)	C(21)-O(1)-Mn(1)	127.2(2)
C(20)-C(21)	1.500(8)	C(39)-O(2)-C(42)	109.7(3)
C(21)-C(20)#1	1.500(8)	C(39)-O(2)-Mn(2)	126.4(2)
C(22)-C(23)	1.499(3)	C(42)-O(2)-Mn(2)	123.86(18)
C(23)-C(24)	1.441(3)	C(2)-N(1)-C(6)	119.08(16)
C(24)-C(25)	1.375(3)	C(2)-N(1)-Mn(1)	114.37(13)
C(25)-C(26)	1.382(3)	C(6)-N(1)-Mn(1)	126.48(12)

C(3)#1-N(2)-C(3)	119.0(2)
C(3)#1-N(2)-Mn(1)	120.19(11)
C(3)-N(2)-Mn(1)	120.19(11)
C(23)-N(3)-C(27)	118.99(16)
C(23)-N(3)-Mn(2)	113.58(13)
C(27)-N(3)-Mn(2)	127.42(12)
C(24)-N(4)-C(24)#2	118.2(2)
C(24)-N(4)-Mn(2)	120.79(11)
C(24)#2-N(4)-Mn(2)	120.79(11)
N(1)-C(2)-C(3)	116.54(17)
N(1)-C(2)-C(1)	123.81(19)
C(3)-C(2)-C(1)	119.62(18)
N(2)-C(3)-C(4)	121.03(19)
N(2)-C(3)-C(2)	114.12(17)
C(4)-C(3)-C(2)	124.80(18)
C(5)-C(4)-C(3)	119.9(2)
C(4)-C(5)-C(4)#1	119.2(3)
C(7)-C(6)-C(11)	121.3(2)
C(7)-C(6)-N(1)	118.63(19)
C(11)-C(6)-N(1)	120.1(2)
C(6)-C(7)-C(8)	118.1(2)
C(6)-C(7)-C(12)	121.7(2)
C(8)-C(7)-C(12)	120.2(2)
C(9)-C(8)-C(7)	121.1(3)
C(8)-C(9)-C(10)	119.8(2)
C(9)-C(10)-C(11)	121.8(3)
C(10)-C(11)-C(6)	117.9(2)
C(10)-C(11)-C(15)	120.2(2)
C(6)-C(11)-C(15)	121.9(2)
C(14)-C(12)-C(7)	112.9(3)
C(14)-C(12)-C(13)	109.5(3)
C(7)-C(12)-C(13)	111.4(3)
C(11)-C(15)-C(17)	111.2(3)
C(11)-C(15)-C(16)	111.2(2)
C(17)-C(15)-C(16)	110.0(2)
O(1)-C(18)-C(19)	106.5(3)
C(20)#1-C(19)-C(20)	31.1(6)
C(20)#1-C(19)-C(18)	107.5(4)
C(20)-C(19)-C(18)	107.5(4)
C(20)#1-C(20)-C(19)	74.5(3)
C(20)#1-C(20)-C(21)	75.0(3)
C(19)-C(20)-C(21)	104.4(4)
O(1)-C(21)-C(20)	104.9(4)
O(1)-C(21)-C(20)#1	104.9(4)
C(20)-C(21)-C(20)#1	30.0(6)
N(3)-C(23)-C(24)	117.11(17)
N(3)-C(23)-C(22)	123.48(19)
C(24)-C(23)-C(22)	119.38(18)
N(4)-C(24)-C(25)	121.55(19)
N(4)-C(24)-C(23)	114.58(17)
C(25)-C(24)-C(23)	123.86(19)
C(24)-C(25)-C(26)	119.6(2)
C(25)-C(26)-C(25)#2	119.3(3)
C(28)-C(27)-C(32)	120.9(2)
C(28)-C(27)-N(3)	119.37(19)
C(32)-C(27)-N(3)	119.70(19)
C(27)-C(28)-C(29)	118.3(2)
C(27)-C(28)-C(33)	122.4(2)
C(29)-C(28)-C(33)	119.3(2)
C(30)-C(29)-C(28)	121.2(2)
C(31)-C(30)-C(29)	120.1(2)
C(30)-C(31)-C(32)	121.2(2)
C(31)-C(32)-C(27)	118.3(2)
C(31)-C(32)-C(36)	119.3(2)
C(27)-C(32)-C(36)	122.4(2)
C(28)-C(33)-C(34)	112.1(2)
C(28)-C(33)-C(35)	110.7(2)
C(34)-C(33)-C(35)	108.4(3)
C(37)-C(36)-C(32)	112.7(3)
C(37)-C(36)-C(38)	108.7(3)
C(32)-C(36)-C(38)	110.9(3)
O(2)-C(39)-C(40)	105.9(3)
C(39)-C(40)-C(41)	103.9(3)
C(39)-C(40)-C(41)#2	103.9(3)
C(41)-C(40)-C(41)#2	39.5(5)
C(41)#2-C(41)-C(42)	68.8(3)
C(41)#2-C(41)-C(40)	70.3(2)
C(42)-C(41)-C(40)	101.6(4)
O(2)-C(42)-C(41)	106.7(3)
O(2)-C(42)-C(41)#2	106.7(3)
C(41)-C(42)-C(41)#2	42.4(5)

Symmetry transformations used to generate equivalent atoms:
#1 x,-y+1/2,z #2 x,-y+3/2,z

Table A.29. Crystal data and structure refinement for sr16.

Identification code	sr16	
Empirical formula	C40 H50 Fe N4	
Formula weight	642.69	
Temperature	173(2) K	
Wavelength	0.71073 Å	
Crystal system	Triclinic	
Space group	P-1	
Unit cell dimensions	a = 8.6946(7) Å	α= 89.518(4)°.
	b = 12.1958(10) Å	β= 76.783(3)°.
	c = 18.0040(15) Å	γ = 77.426(4)°.
Volume	1812.2(3) $Å^3$	
Z	2	
Density (calculated)	1.178 Mg/m^3	
Absorption coefficient	0.448 mm^{-1}	
F(000)	688	
Crystal size	0.40 x 0.40 x 0.30 mm^3	
Theta range for data collection	1.71 to 29.57°.	
Index ranges	-10<=h<=12, -16<=k<=16, -24<=l<=22	
Reflections collected	37462	
Independent reflections	9939 [R(int) = 0.0198]	
Completeness to theta = 29.57°	97.8 %	
Absorption correction	Semi-empirical from equivalents	
Max. and min. transmission	0.8773 and 0.8411	
Refinement method	Full-matrix least-squares on F^2	
Data / restraints / parameters	9939 / 0 / 485	
Goodness-of-fit on F^2	1.009	
Final R indices [I>2sigma(I)]	R1 = 0.0340, wR2 = 0.0906	
R indices (all data)	R1 = 0.0412, wR2 = 0.0953	
Largest diff. peak and hole	0.404 and -0.305 $e.Å^{-3}$	

Table A.30. Atomic coordinates (x 10^4) and equivalent isotropic displacement parameters ($Å^2$x 10^3) for sr16. U(eq) is defined as one third of the trace of the orthogonalized U^{ij} tensor.

	x	y	z	U(eq)
Fe(1)	3159(1)	7357(1)	2107(1)	22(1)
N(1)	3551(1)	5922(1)	1569(1)	23(1)
N(2)	4634(1)	7577(1)	1223(1)	22(1)
N(3)	2920(1)	8954(1)	2183(1)	22(1)
N(4)	2402(2)	7074(1)	3010(1)	37(1)
C(1)	4710(1)	5752(1)	928(1)	25(1)
C(2)	5348(1)	6702(1)	690(1)	23(1)
C(3)	6457(2)	6855(1)	27(1)	30(1)
C(4)	6829(2)	7903(1)	-96(1)	32(1)
C(5)	6066(2)	8800(1)	430(1)	27(1)
C(6)	4955(1)	8627(1)	1087(1)	22(1)
C(7)	3939(1)	9401(1)	1668(1)	24(1)
C(8)	2793(1)	4993(1)	1789(1)	25(1)
C(9)	1187(2)	5092(1)	1724(1)	28(1)
C(10)	519(2)	4149(1)	1869(1)	34(1)
C(11)	1383(2)	3155(1)	2078(1)	36(1)
C(12)	2932(2)	3089(1)	2165(1)	35(1)
C(13)	3670(2)	4004(1)	2028(1)	30(1)
C(14)	227(2)	6177(1)	1482(1)	35(1)
C(15)	725(2)	6315(2)	621(1)	51(1)
C(16)	-1608(2)	6292(2)	1730(1)	51(1)
C(17)	5373(2)	3890(1)	2148(1)	42(1)
C(18)	5453(3)	3538(2)	2959(1)	63(1)
C(19)	6615(2)	3061(2)	1556(1)	62(1)
C(20)	1644(1)	9716(1)	2710(1)	24(1)
C(21)	1882(2)	10077(1)	3402(1)	29(1)
C(22)	600(2)	10849(1)	3867(1)	39(1)
C(23)	-844(2)	11231(1)	3659(1)	41(1)
C(24)	-1072(2)	10834(1)	2985(1)	35(1)
C(25)	156(2)	10060(1)	2500(1)	28(1)
C(26)	-106(2)	9597(1)	1771(1)	35(1)
C(27)	381(2)	10310(2)	1092(1)	53(1)
C(28)	-1834(2)	9461(2)	1842(1)	53(1)
C(29)	3460(2)	9666(1)	3646(1)	33(1)
C(30)	4466(2)	10564(2)	3540(1)	49(1)
C(31)	3174(2)	9308(1)	4474(1)	47(1)
C(32)	1907(2)	6829(1)	3742(1)	36(1)
C(33)	225(2)	6995(1)	4095(1)	45(1)
C(34)	-201(3)	6663(2)	4845(1)	59(1)
C(35)	944(3)	6206(1)	5254(1)	61(1)
C(36)	2556(3)	6099(1)	4915(1)	58(1)
C(37)	3084(2)	6404(1)	4173(1)	46(1)
C(38)	-999(3)	7514(2)	3661(1)	68(1)
C(39)	411(4)	5863(2)	6067(1)	93(1)
C(40)	4851(3)	6326(2)	3834(1)	62(1)

Table A.31. Bond lengths [Å] and angles [°] for sr16.

Fe(1)-N(4)	1.6728(11)
Fe(1)-N(2)	1.8598(10)
Fe(1)-N(3)	1.9160(10)
Fe(1)-N(1)	1.9323(10)
N(1)-C(1)	1.3303(15)
N(1)-C(8)	1.4394(14)
N(2)-C(6)	1.3773(14)
N(2)-C(2)	1.3785(14)
N(3)-C(7)	1.3306(14)
N(3)-C(20)	1.4412(14)
N(4)-C(32)	1.3419(16)
C(1)-C(2)	1.4129(16)
C(2)-C(3)	1.3925(16)
C(3)-C(4)	1.3887(18)
C(4)-C(5)	1.3954(18)
C(5)-C(6)	1.3922(16)
C(6)-C(7)	1.4123(16)
C(8)-C(13)	1.4011(17)
C(8)-C(9)	1.4073(17)
C(9)-C(10)	1.3947(18)
C(9)-C(14)	1.5207(19)
C(10)-C(11)	1.379(2)
C(11)-C(12)	1.376(2)
C(12)-C(13)	1.3968(18)
C(13)-C(17)	1.521(2)
C(14)-C(15)	1.529(2)
C(14)-C(16)	1.530(2)
C(17)-C(19)	1.530(3)
C(17)-C(18)	1.532(3)
C(20)-C(21)	1.3990(17)
C(20)-C(25)	1.4057(17)
C(21)-C(22)	1.3996(18)
C(21)-C(29)	1.5164(19)
C(22)-C(23)	1.375(2)
C(23)-C(24)	1.382(2)
C(24)-C(25)	1.3938(17)
C(25)-C(26)	1.5164(19)
C(26)-C(28)	1.524(2)
C(26)-C(27)	1.528(2)
C(29)-C(30)	1.529(2)
C(29)-C(31)	1.531(2)
C(32)-C(33)	1.425(2)
C(32)-C(37)	1.429(2)
C(33)-C(34)	1.398(2)
C(33)-C(38)	1.490(3)
C(34)-C(35)	1.389(3)
C(35)-C(36)	1.373(3)
C(35)-C(39)	1.516(2)
C(36)-C(37)	1.386(2)
C(37)-C(40)	1.501(3)
N(4)-Fe(1)-N(2)	160.64(6)
N(4)-Fe(1)-N(3)	101.65(5)
N(2)-Fe(1)-N(3)	79.33(4)
N(4)-Fe(1)-N(1)	102.85(5)
N(2)-Fe(1)-N(1)	79.54(4)
N(3)-Fe(1)-N(1)	154.80(4)
C(1)-N(1)-C(8)	115.71(9)
C(1)-N(1)-Fe(1)	116.04(8)
C(8)-N(1)-Fe(1)	128.19(8)
C(6)-N(2)-C(2)	120.16(9)
C(6)-N(2)-Fe(1)	119.85(7)
C(2)-N(2)-Fe(1)	119.93(8)
C(7)-N(3)-C(20)	117.46(9)
C(7)-N(3)-Fe(1)	117.01(8)
C(20)-N(3)-Fe(1)	125.29(7)
C(32)-N(4)-Fe(1)	175.79(13)
N(1)-C(1)-C(2)	114.77(10)
N(2)-C(2)-C(3)	120.51(11)
N(2)-C(2)-C(1)	109.20(10)
C(3)-C(2)-C(1)	130.23(11)
C(4)-C(3)-C(2)	119.29(11)
C(3)-C(4)-C(5)	120.27(11)
C(6)-C(5)-C(4)	119.36(11)
N(2)-C(6)-C(5)	120.32(10)
N(2)-C(6)-C(7)	109.27(9)
C(5)-C(6)-C(7)	130.28(11)
N(3)-C(7)-C(6)	114.04(10)
C(13)-C(8)-C(9)	121.46(11)
C(13)-C(8)-N(1)	120.30(11)
C(9)-C(8)-N(1)	118.18(10)
C(10)-C(9)-C(8)	117.64(12)
C(10)-C(9)-C(14)	121.03(12)
C(8)-C(9)-C(14)	121.30(11)
C(11)-C(10)-C(9)	121.68(13)
C(12)-C(11)-C(10)	119.70(12)
C(11)-C(12)-C(13)	121.37(13)
C(12)-C(13)-C(8)	118.05(12)
C(12)-C(13)-C(17)	119.07(12)
C(8)-C(13)-C(17)	122.88(11)
C(9)-C(14)-C(15)	111.81(12)
C(9)-C(14)-C(16)	113.21(12)
C(15)-C(14)-C(16)	109.90(13)
C(13)-C(17)-C(19)	111.28(14)
C(13)-C(17)-C(18)	110.95(14)
C(19)-C(17)-C(18)	110.67(15)
C(21)-C(20)-C(25)	121.97(11)
C(21)-C(20)-N(3)	121.01(11)
C(25)-C(20)-N(3)	117.01(10)
C(20)-C(21)-C(22)	117.33(13)
C(20)-C(21)-C(29)	122.10(11)
C(22)-C(21)-C(29)	120.57(12)
C(23)-C(22)-C(21)	121.62(13)
C(22)-C(23)-C(24)	120.08(13)
C(23)-C(24)-C(25)	120.92(13)
C(24)-C(25)-C(20)	117.98(12)
C(24)-C(25)-C(26)	121.06(12)
C(20)-C(25)-C(26)	120.96(11)
C(25)-C(26)-C(28)	113.10(13)
C(25)-C(26)-C(27)	111.71(12)

C(28)-C(26)-C(27)	110.13(13)
C(21)-C(29)-C(30)	111.02(12)
C(21)-C(29)-C(31)	111.90(13)
C(30)-C(29)-C(31)	109.95(12)
N(4)-C(32)-C(33)	120.79(15)
N(4)-C(32)-C(37)	119.41(14)
C(33)-C(32)-C(37)	119.79(13)
C(34)-C(33)-C(32)	117.61(18)
C(34)-C(33)-C(38)	122.77(18)
C(32)-C(33)-C(38)	119.61(14)
C(35)-C(34)-C(33)	122.59(19)
C(36)-C(35)-C(34)	118.78(15)
C(36)-C(35)-C(39)	121.0(2)
C(34)-C(35)-C(39)	120.2(2)
C(35)-C(36)-C(37)	122.4(2)
C(36)-C(37)-C(32)	118.69(18)
C(36)-C(37)-C(40)	120.82(19)
C(32)-C(37)-C(40)	120.46(14)

Symmetry transformations used to generate equivalent atoms:

Table A.32. Crystal data and structure refinement for sr18.

Identification code	sr18	
Empirical formula	C31 H37 Fe N3	
Formula weight	507.49	
Temperature	173(2) K	
Wavelength	0.71073 Å	
Crystal system	Orthorhombic	
Space group	Pbca	
Unit cell dimensions	a = 17.5522(6) Å	α= 90°.
	b = 10.4649(4) Å	β= 90°.
	c = 28.3624(9) Å	γ = 90°.
Volume	5209.7(3) $Å^3$	
Z	8	
Density (calculated)	1.294 Mg/m^3	
Absorption coefficient	0.603 mm^{-1}	
F(000)	2160	
Crystal size	0.45 x 0.30 x 0.20 mm^3	
Theta range for data collection	1.85 to 29.13°.	
Index ranges	-19<=h<=24, -14<=k<=10, -38<=l<=22	
Reflections collected	23930	
Independent reflections	6984 [R(int) = 0.0258]	
Completeness to theta = 29.13°	99.6 %	
Absorption correction	Semi-empirical from equivalents	
Max. and min. transmission	0.8889 and 0.7730	
Refinement method	Full-matrix least-squares on F^2	
Data / restraints / parameters	6984 / 4 / 357	
Goodness-of-fit on F^2	1.014	
Final R indices [I>2sigma(I)]	R1 = 0.0413, wR2 = 0.1067	
R indices (all data)	R1 = 0.0581, wR2 = 0.1165	
Largest diff. peak and hole	0.391 and -0.435 $e.Å^{-3}$	

Table A.33. Atomic coordinates (x 10^4) and equivalent isotropic displacement parameters ($Å^2$x 10^3) for sr18. U(eq) is defined as one third of the trace of the orthogonalized U^{ij} tensor.

	x	y	z	U(eq)
Fe(1)	263(1)	1467(1)	1173(1)	21(1)
N(1)	1075(1)	154(1)	1246(1)	26(1)
N(2)	710(1)	1993(1)	1728(1)	25(1)
N(3)	-491(1)	2727(1)	1403(1)	25(1)
C(1)	2279(1)	-394(2)	1674(1)	52(1)
C(2)	1590(1)	410(2)	1578(1)	32(1)
C(3)	1406(1)	1492(2)	1857(1)	30(1)
C(4)	1804(1)	1991(2)	2238(1)	38(1)
C(5)	1516(1)	3034(2)	2482(1)	40(1)
C(6)	846(1)	3591(2)	2334(1)	36(1)
C(7)	443(1)	3064(2)	1956(1)	28(1)
C(8)	-271(1)	3437(2)	1768(1)	30(1)
C(9)	-750(1)	4486(2)	1983(1)	43(1)
C(10)	1138(1)	-1111(2)	1043(1)	28(1)
C(11)	810(1)	-2126(2)	1296(1)	37(1)
C(12)	869(2)	-3354(2)	1113(1)	47(1)
C(13)	1244(1)	-3578(2)	695(1)	48(1)
C(14)	1581(1)	-2584(2)	457(1)	41(1)
C(15)	1541(1)	-1333(2)	626(1)	32(1)
C(16)	432(2)	-1928(2)	1768(1)	56(1)
C(17)	1951(1)	-291(2)	371(1)	46(1)
C(18)	-1277(1)	2870(2)	1264(1)	30(1)
C(19)	-1819(1)	2096(2)	1489(1)	40(1)
C(20)	-2573(1)	2154(3)	1334(1)	56(1)
C(21)	-2790(2)	2971(3)	985(1)	64(1)
C(22)	-2264(2)	3786(3)	789(1)	60(1)
C(23)	-1493(1)	3756(2)	921(1)	41(1)
C(24)	-1604(2)	1261(3)	1897(1)	55(1)
C(25)	-929(2)	4675(2)	713(1)	59(1)
C(26)	998(1)	2780(2)	863(1)	31(1)
C(27)	989(2)	2892(3)	334(1)	63(1)
C(28)	366(2)	2207(3)	111(1)	58(1)
C(29)	163(4)	1084(6)	429(2)	33(1)
C(30)	-521(3)	913(5)	655(2)	37(2)
C(28')	366(2)	2207(3)	111(1)	58(1)
C(29')	-170(3)	1675(5)	442(1)	38(1)
C(30')	-134(3)	435(5)	588(2)	41(1)
C(31)	-569(1)	38(2)	999(1)	42(1)

Table A.34. Bond lengths [Å] and angles [°] for sr18.

Fe(1)-N(2)	1.8407(14)	Fe(1)-C(29)	2.155(5)
Fe(1)-N(3)	1.9785(15)	Fe(1)-C(29')	2.221(4)
Fe(1)-N(1)	1.9895(15)	N(1)-C(2)	1.333(2)
Fe(1)-C(26)	2.0797(19)	N(1)-C(10)	1.448(2)
Fe(1)-C(30)	2.096(4)	N(2)-C(7)	1.377(2)
Fe(1)-C(30')	2.100(4)	N(2)-C(3)	1.379(2)
Fe(1)-C(31)	2.149(2)	N(3)-C(8)	1.330(2)

N(3)-C(18)	1.443(2)
C(1)-C(2)	1.498(3)
C(2)-C(3)	1.419(3)
C(3)-C(4)	1.388(3)
C(4)-C(5)	1.387(3)
C(5)-C(6)	1.377(3)
C(6)-C(7)	1.399(3)
C(7)-C(8)	1.417(3)
C(8)-C(9)	1.511(3)
C(10)-C(15)	1.399(3)
C(10)-C(11)	1.405(3)
C(11)-C(12)	1.390(3)
C(11)-C(16)	1.507(3)
C(12)-C(13)	1.377(3)
C(13)-C(14)	1.373(3)
C(14)-C(15)	1.395(3)
C(15)-C(17)	1.493(3)
C(18)-C(23)	1.398(3)
C(18)-C(19)	1.403(3)
C(19)-C(20)	1.397(3)
C(19)-C(24)	1.499(3)
C(20)-C(21)	1.362(4)
C(21)-C(22)	1.375(4)
C(22)-C(23)	1.405(4)
C(23)-C(25)	1.501(4)
C(26)-C(27)	1.505(3)
C(27)-C(28)	1.453(4)
C(28)-C(29)	1.524(7)
C(29)-C(30)	1.372(10)
C(30)-C(31)	1.341(6)
C(29')-C(30')	1.364(8)
C(30')-C(31)	1.454(6)

N(2)-Fe(1)-N(3)	78.74(6)
N(2)-Fe(1)-N(1)	79.23(6)
N(3)-Fe(1)-N(1)	154.83(6)
N(2)-Fe(1)-C(26)	84.31(7)
N(3)-Fe(1)-C(26)	96.55(7)
N(1)-Fe(1)-C(26)	93.22(7)
N(2)-Fe(1)-C(30)	164.03(17)
N(3)-Fe(1)-C(30)	88.60(17)
N(1)-Fe(1)-C(30)	110.61(17)
C(26)-Fe(1)-C(30)	107.00(17)
N(2)-Fe(1)-C(30')	166.02(16)
N(3)-Fe(1)-C(30')	112.37(14)
N(1)-Fe(1)-C(30')	87.97(14)
C(26)-Fe(1)-C(30')	102.16(17)
C(30)-Fe(1)-C(30')	23.78(15)
N(2)-Fe(1)-C(31)	133.96(9)
N(3)-Fe(1)-C(31)	94.86(8)
N(1)-Fe(1)-C(31)	91.72(8)
C(26)-Fe(1)-C(31)	141.59(9)
C(30)-Fe(1)-C(31)	36.80(17)
C(30')-Fe(1)-C(31)	40.00(17)
N(2)-Fe(1)-C(29)	157.92(19)
N(3)-Fe(1)-C(29)	113.04(19)
N(1)-Fe(1)-C(29)	91.81(19)
C(26)-Fe(1)-C(29)	76.02(18)
C(30)-Fe(1)-C(29)	37.6(3)
C(30')-Fe(1)-C(29)	26.24(17)
C(31)-Fe(1)-C(29)	65.76(19)
N(2)-Fe(1)-C(29')	156.14(14)
N(3)-Fe(1)-C(29')	90.75(16)
N(1)-Fe(1)-C(29')	114.17(16)
C(26)-Fe(1)-C(29')	75.59(12)
C(30)-Fe(1)-C(29')	31.44(18)
C(30')-Fe(1)-C(29')	36.7(2)
C(31)-Fe(1)-C(29')	67.69(14)
C(29)-Fe(1)-C(29')	22.37(15)
C(2)-N(1)-C(10)	114.35(15)
C(2)-N(1)-Fe(1)	114.86(12)
C(10)-N(1)-Fe(1)	130.17(12)
C(7)-N(2)-C(3)	119.08(15)
C(7)-N(2)-Fe(1)	119.97(12)
C(3)-N(2)-Fe(1)	119.43(12)
C(8)-N(3)-C(18)	115.53(15)
C(8)-N(3)-Fe(1)	115.75(12)
C(18)-N(3)-Fe(1)	128.25(12)
N(1)-C(2)-C(3)	113.56(16)
N(1)-C(2)-C(1)	124.32(18)
C(3)-C(2)-C(1)	122.03(18)
N(2)-C(3)-C(4)	120.67(18)
N(2)-C(3)-C(2)	110.87(16)
C(4)-C(3)-C(2)	128.30(19)
C(3)-C(4)-C(5)	120.0(2)
C(6)-C(5)-C(4)	119.53(18)
C(5)-C(6)-C(7)	119.86(19)
N(2)-C(7)-C(6)	120.62(18)
N(2)-C(7)-C(8)	110.39(16)
C(6)-C(7)-C(8)	128.90(18)
N(3)-C(8)-C(7)	113.27(16)
N(3)-C(8)-C(9)	123.98(18)
C(7)-C(8)-C(9)	122.65(17)
C(15)-C(10)-C(11)	120.91(17)
C(15)-C(10)-N(1)	121.77(17)
C(11)-C(10)-N(1)	117.24(16)
C(12)-C(11)-C(10)	118.51(19)
C(12)-C(11)-C(16)	119.5(2)
C(10)-C(11)-C(16)	121.94(19)
C(13)-C(12)-C(11)	121.0(2)
C(14)-C(13)-C(12)	120.0(2)
C(13)-C(14)-C(15)	121.4(2)
C(14)-C(15)-C(10)	118.10(19)
C(14)-C(15)-C(17)	119.70(19)
C(10)-C(15)-C(17)	122.15(18)
C(23)-C(18)-C(19)	121.05(19)
C(23)-C(18)-N(3)	121.21(19)
C(19)-C(18)-N(3)	117.73(17)
C(18)-C(19)-C(20)	118.3(2)
C(18)-C(19)-C(24)	121.13(19)
C(20)-C(19)-C(24)	120.5(2)
C(21)-C(20)-C(19)	121.4(3)

C(20)-C(21)-C(22)	119.7(2)
C(21)-C(22)-C(23)	121.7(2)
C(18)-C(23)-C(22)	117.5(2)
C(18)-C(23)-C(25)	121.3(2)
C(22)-C(23)-C(25)	121.1(2)
C(27)-C(26)-Fe(1)	117.91(14)
C(28)-C(27)-C(26)	113.7(2)
C(27)-C(28)-C(29)	107.4(3)
C(30)-C(29)-C(28)	125.6(6)
C(30)-C(29)-Fe(1)	68.9(3)
C(28)-C(29)-Fe(1)	114.7(3)
C(31)-C(30)-C(29)	118.9(6)
C(31)-C(30)-Fe(1)	73.7(2)
C(29)-C(30)-Fe(1)	73.5(3)
C(30')-C(29')-Fe(1)	66.8(2)
C(29')-C(30')-C(31)	119.5(4)
C(29')-C(30')-Fe(1)	76.5(2)
C(31)-C(30')-Fe(1)	71.82(18)
C(30)-C(31)-C(30')	35.8(3)
C(30)-C(31)-Fe(1)	69.5(2)
C(30')-C(31)-Fe(1)	68.18(17)

Symmetry transformations used to generate equivalent atoms:

Table A.35. Crystal data and structure refinement for sr20.

Identification code	sr20	
Empirical formula	C47 H73 Mn N3 Na O5	
Formula weight	838.01	
Temperature	173(2) K	
Wavelength	0.71073 Å	
Crystal system	Monoclinic	
Space group	P2(1)/n	
Unit cell dimensions	a = 10.2439(10) Å	α= 90°.
	b = 22.017(2) Å	β= 98.091(2)°.
	c = 20.880(2) Å	γ = 90°.
Volume	4662.5(8) $Å^3$	
Z	4	
Density (calculated)	1.194 Mg/m^3	
Absorption coefficient	0.338 mm^{-1}	
F(000)	1808	
Crystal size	0.32 x 0.09 x 0.07 mm^3	
Theta range for data collection	1.85 to 28.39°.	
Index ranges	-13<=h<=13, -29<=k<=28, -27<=l<=27	
Reflections collected	77275	
Independent reflections	11556 [R(int) = 0.0500]	
Completeness to theta = 28.39°	98.7 %	
Absorption correction	Semi-empirical from equivalents	
Max. and min. transmission	0.9767 and 0.8995	
Refinement method	Full-matrix least-squares on F^2	
Data / restraints / parameters	11556 / 100 / 606	
Goodness-of-fit on F^2	1.139	
Final R indices [I>2sigma(I)]	R1 = 0.0590, wR2 = 0.1559	
R indices (all data)	R1 = 0.0704, wR2 = 0.1605	
Largest diff. peak and hole	0.327 and -0.437 $e.Å^{-3}$	

Table A36. Atomic coordinates (x 10^4) and equivalent isotropic displacement parameters ($Å^2$x 10^3) for sr20. U(eq) is defined as one third of the trace of the orthogonalized U^{ij} tensor.

	x	y	z	U(eq)
Mn(1)	3276(1)	2479(1)	4249(1)	13(1)
Na(1)	-569(1)	1798(1)	2633(1)	32(1)
N(1)	3867(2)	1682(1)	4627(1)	14(1)
N(2)	5063(2)	2630(1)	4564(1)	15(1)
N(3)	3465(2)	3344(1)	4021(1)	15(1)
C(04)	2260(3)	2233(1)	3552(1)	17(1)
O(4)	1489(2)	2073(1)	3104(1)	26(1)
C(05)	1757(3)	2533(1)	4559(1)	17(1)
O(5)	724(2)	2557(1)	4730(1)	27(1)
C(1)	5773(3)	1064(1)	5200(1)	23(1)
C(2)	5130(3)	1631(1)	4900(1)	17(1)
C(3)	5850(3)	2175(1)	4873(1)	18(1)
C(4)	7170(3)	2280(1)	5108(2)	24(1)
C(5)	7706(3)	2857(2)	5047(2)	30(1)
C(6)	6920(3)	3317(1)	4748(2)	25(1)
C(7)	5595(3)	3205(1)	4511(1)	19(1)
C(8)	4657(3)	3604(1)	4191(1)	18(1)
C(9)	4989(3)	4257(1)	4061(2)	26(1)
C(10)	3077(3)	1143(1)	4635(1)	17(1)
C(11)	3027(3)	722(1)	4130(1)	21(1)
C(12)	2334(3)	182(1)	4172(2)	29(1)
C(13)	1696(3)	60(1)	4699(2)	34(1)
C(14)	1726(3)	482(2)	5186(2)	32(1)
C(15)	2402(3)	1030(1)	5169(1)	23(1)
C(16)	3754(3)	823(1)	3556(1)	26(1)
C(17)	2873(4)	712(2)	2914(2)	39(1)
C(18)	4978(3)	418(2)	3595(2)	35(1)
C(19)	2433(3)	1473(2)	5726(2)	30(1)
C(20)	1052(4)	1578(2)	5917(2)	45(1)
C(21)	3377(5)	1259(2)	6318(2)	53(1)
C(22)	2449(3)	3725(1)	3689(1)	17(1)
C(23)	1676(3)	4090(1)	4045(1)	19(1)
C(24)	770(3)	4489(1)	3708(2)	28(1)
C(25)	606(3)	4522(2)	3040(2)	33(1)
C(26)	1340(3)	4150(2)	2697(2)	30(1)
C(27)	2276(3)	3749(1)	3007(1)	22(1)
C(28)	1815(3)	4065(1)	4780(1)	21(1)
C(29)	2567(3)	4615(2)	5089(2)	35(1)
C(30)	474(3)	4021(1)	5017(2)	29(1)
C(31)	3124(4)	3385(1)	2607(2)	31(1)
C(32)	4194(4)	3788(2)	2380(2)	45(1)
C(33)	2321(5)	3078(2)	2023(2)	51(1)
O(1)	-2155(5)	2470(3)	2929(2)	29(1)
C(34)	-1494(10)	2924(4)	3343(5)	37(2)
C(35)	-2082(7)	3547(3)	3228(3)	36(2)
C(36)	-3442(6)	2340(3)	3104(3)	34(2)
C(37)	-4141(11)	1919(4)	2613(5)	48(2)
O(1')	-2522(6)	2208(3)	2898(3)	26(1)
C(34')	-2612(8)	2837(4)	3044(5)	44(2)
C(35')	-1272(13)	3093(6)	3199(8)	52(4)

C(36')	-3709(8)	1873(5)	2951(5)	43(2)
C(37')	-4793(9)	1987(5)	2413(5)	38(2)
O(2)	35(2)	1694(1)	1613(1)	28(1)
C(38)	-828(3)	1877(2)	1046(1)	31(1)
C(39)	-2190(3)	1940(2)	1230(2)	37(1)
C(40)	1343(3)	1568(2)	1477(2)	35(1)
C(41)	1482(5)	926(2)	1231(2)	52(1)
O(3)	-1327(6)	823(2)	3039(3)	25(1)
C(42)	-1135(10)	741(5)	3727(5)	28(2)
C(43)	-760(20)	1319(8)	4069(8)	36(3)
C(44)	-1629(7)	250(3)	2716(3)	35(2)
C(45)	-2062(9)	359(4)	2008(4)	40(2)
O(3')	-942(6)	854(2)	2828(3)	30(1)
C(42')	-1064(11)	648(5)	3460(6)	37(2)
C(43')	-725(18)	1161(7)	3928(8)	36(3)
C(44')	-953(7)	393(3)	2358(4)	37(2)
C(45')	-2286(8)	111(4)	2185(5)	44(2)

Table A.37. Bond lengths [Å] and angles [°] for sr20.

Mn(1)-C(04)	1.752(3)	C(11)-C(16)	1.514(4)
Mn(1)-C(05)	1.771(3)	C(12)-C(13)	1.384(5)
Mn(1)-N(2)	1.886(2)	C(13)-C(14)	1.374(5)
Mn(1)-N(3)	1.979(2)	C(14)-C(15)	1.393(4)
Mn(1)-N(1)	1.983(2)	C(15)-C(19)	1.515(4)
Na(1)-O(3')	2.161(6)	C(16)-C(17)	1.527(4)
Na(1)-O(4)	2.278(2)	C(16)-C(18)	1.532(4)
Na(1)-O(2)	2.313(2)	C(19)-C(21)	1.532(5)
Na(1)-O(1')	2.332(5)	C(19)-C(20)	1.541(4)
Na(1)-O(1)	2.344(5)	C(22)-C(27)	1.409(4)
Na(1)-O(3)	2.472(6)	C(22)-C(23)	1.412(4)
Na(1)-C(43')	3.069(18)	C(23)-C(24)	1.396(4)
Na(1)-C(34)	3.104(8)	C(23)-C(28)	1.521(4)
N(1)-C(2)	1.343(3)	C(24)-C(25)	1.382(5)
N(1)-C(10)	1.437(3)	C(25)-C(26)	1.381(5)
N(2)-C(3)	1.388(3)	C(26)-C(27)	1.393(4)
N(2)-C(7)	1.389(3)	C(27)-C(31)	1.517(4)
N(3)-C(8)	1.351(3)	C(28)-C(29)	1.528(4)
N(3)-C(22)	1.437(3)	C(28)-C(30)	1.526(4)
C(04)-O(4)	1.190(3)	C(31)-C(33)	1.530(5)
C(05)-O(5)	1.165(3)	C(31)-C(32)	1.537(5)
C(1)-C(2)	1.506(4)	O(1)-C(34)	1.429(10)
C(2)-C(3)	1.411(4)	O(1)-C(36)	1.445(7)
C(3)-C(4)	1.391(4)	C(34)-C(35)	1.504(9)
C(4)-C(5)	1.398(4)	C(36)-C(37)	1.489(9)
C(5)-C(6)	1.386(4)	O(1')-C(34')	1.423(8)
C(6)-C(7)	1.400(4)	O(1')-C(36')	1.440(9)
C(7)-C(8)	1.399(4)	C(34')-C(35')	1.478(11)
C(8)-C(9)	1.512(4)	C(36')-C(37')	1.484(10)
C(10)-C(11)	1.400(4)	O(2)-C(38)	1.431(3)
C(10)-C(15)	1.415(4)	O(2)-C(40)	1.435(4)
C(11)-C(12)	1.393(4)	C(38)-C(39)	1.504(5)
		C(40)-C(41)	1.516(5)

O(3)-C(42)	1.434(8)	O(4)-C(04)-Mn(1)	174.9(2)
O(3)-C(44)	1.443(7)	C(04)-O(4)-Na(1)	152.8(2)
C(42)-C(43)	1.484(11)	O(5)-C(05)-Mn(1)	176.2(2)
C(44)-C(45)	1.500(9)	N(1)-C(2)-C(3)	113.0(2)
O(3')-C(44')	1.411(8)	N(1)-C(2)-C(1)	125.7(2)
O(3')-C(42')	1.419(9)	C(3)-C(2)-C(1)	121.3(2)
C(42')-C(43')	1.501(11)	N(2)-C(3)-C(4)	121.1(2)
C(44')-C(45')	1.497(9)	N(2)-C(3)-C(2)	111.0(2)
		C(4)-C(3)-C(2)	127.9(3)
C(04)-Mn(1)-C(05)	82.84(12)	C(3)-C(4)-C(5)	119.6(3)
C(04)-Mn(1)-N(2)	141.11(11)	C(6)-C(5)-C(4)	119.7(3)
C(05)-Mn(1)-N(2)	136.05(11)	C(5)-C(6)-C(7)	120.2(3)
C(04)-Mn(1)-N(3)	99.45(11)	N(2)-C(7)-C(8)	111.1(2)
C(05)-Mn(1)-N(3)	98.25(10)	N(2)-C(7)-C(6)	120.3(2)
N(2)-Mn(1)-N(3)	77.92(9)	C(8)-C(7)-C(6)	128.7(3)
C(04)-Mn(1)-N(1)	99.80(11)	N(3)-C(8)-C(7)	113.2(2)
C(05)-Mn(1)-N(1)	98.57(10)	N(3)-C(8)-C(9)	125.0(2)
N(2)-Mn(1)-N(1)	77.90(9)	C(7)-C(8)-C(9)	121.8(2)
N(3)-Mn(1)-N(1)	155.80(9)	C(11)-C(10)-C(15)	120.4(3)
O(3')-Na(1)-O(4)	110.59(18)	C(11)-C(10)-N(1)	120.0(2)
O(3')-Na(1)-O(2)	99.0(2)	C(15)-C(10)-N(1)	119.5(2)
O(4)-Na(1)-O(2)	94.13(9)	C(12)-C(11)-C(10)	118.9(3)
O(3')-Na(1)-O(1')	98.5(2)	C(12)-C(11)-C(16)	119.1(3)
O(4)-Na(1)-O(1')	124.57(18)	C(10)-C(11)-C(16)	121.9(2)
O(2)-Na(1)-O(1')	127.32(16)	C(13)-C(12)-C(11)	121.1(3)
O(3')-Na(1)-O(1)	114.2(2)	C(14)-C(13)-C(12)	119.5(3)
O(4)-Na(1)-O(1)	110.65(15)	C(13)-C(14)-C(15)	121.8(3)
O(2)-Na(1)-O(1)	126.16(15)	C(14)-C(15)-C(10)	118.2(3)
O(1')-Na(1)-O(1)	16.84(13)	C(14)-C(15)-C(19)	119.7(3)
O(3')-Na(1)-O(3)	13.76(15)	C(10)-C(15)-C(19)	122.1(3)
O(4)-Na(1)-O(3)	113.55(16)	C(11)-C(16)-C(17)	112.0(3)
O(2)-Na(1)-O(3)	111.57(17)	C(11)-C(16)-C(18)	111.3(3)
O(1')-Na(1)-O(3)	86.2(2)	C(17)-C(16)-C(18)	109.4(2)
O(1)-Na(1)-O(3)	101.2(2)	C(15)-C(19)-C(21)	111.4(3)
O(3')-Na(1)-C(43')	50.4(3)	C(15)-C(19)-C(20)	112.0(3)
O(4)-Na(1)-C(43')	84.4(3)	C(21)-C(19)-C(20)	109.6(3)
O(2)-Na(1)-C(43')	145.2(3)	C(27)-C(22)-C(23)	120.7(2)
O(1')-Na(1)-C(43')	79.4(3)	C(27)-C(22)-N(3)	119.3(2)
O(1)-Na(1)-C(43')	86.1(3)	C(23)-C(22)-N(3)	120.0(2)
O(3)-Na(1)-C(43')	40.9(3)	C(24)-C(23)-C(22)	118.3(3)
O(3')-Na(1)-C(34)	127.2(3)	C(24)-C(23)-C(28)	119.5(2)
O(4)-Na(1)-C(34)	84.73(19)	C(22)-C(23)-C(28)	122.2(2)
O(2)-Na(1)-C(34)	131.1(2)	C(25)-C(24)-C(23)	121.4(3)
O(1')-Na(1)-C(34)	41.2(2)	C(24)-C(25)-C(26)	119.7(3)
O(1)-Na(1)-C(34)	25.9(2)	C(25)-C(26)-C(27)	121.6(3)
O(3)-Na(1)-C(34)	113.5(2)	C(26)-C(27)-C(22)	118.3(3)
C(43')-Na(1)-C(34)	83.5(3)	C(26)-C(27)-C(31)	119.2(3)
C(2)-N(1)-C(10)	115.9(2)	C(22)-C(27)-C(31)	122.4(3)
C(2)-N(1)-Mn(1)	117.69(17)	C(23)-C(28)-C(29)	111.6(2)
C(10)-N(1)-Mn(1)	126.39(17)	C(23)-C(28)-C(30)	111.6(2)
C(3)-N(2)-C(7)	119.1(2)	C(29)-C(28)-C(30)	109.7(2)
C(3)-N(2)-Mn(1)	120.43(17)	C(27)-C(31)-C(33)	112.8(3)
C(7)-N(2)-Mn(1)	120.38(18)	C(27)-C(31)-C(32)	110.7(3)
C(8)-N(3)-C(22)	116.5(2)	C(33)-C(31)-C(32)	109.6(3)
C(8)-N(3)-Mn(1)	117.41(18)	C(34)-O(1)-C(36)	110.9(6)
C(22)-N(3)-Mn(1)	126.11(17)	C(34)-O(1)-Na(1)	108.3(4)

C(36)-O(1)-Na(1)	129.3(4)	C(42)-O(3)-C(44)	110.4(6)
O(1)-C(34)-C(35)	113.4(7)	C(42)-O(3)-Na(1)	116.5(5)
O(1)-C(34)-Na(1)	45.8(3)	C(44)-O(3)-Na(1)	131.0(5)
C(35)-C(34)-Na(1)	142.6(6)	O(3)-C(42)-C(43)	111.4(10)
O(1)-C(36)-C(37)	108.4(6)	O(3)-C(44)-C(45)	109.5(6)
C(34')-O(1')-C(36')	113.7(6)	C(44')-O(3')-C(42')	115.1(7)
C(34')-O(1')-Na(1)	120.8(5)	C(44')-O(3')-Na(1)	123.0(5)
C(36')-O(1')-Na(1)	125.5(6)	C(42')-O(3')-Na(1)	121.5(6)
O(1')-C(34')-C(35')	109.4(8)	O(3')-C(42')-C(43')	108.8(10)
O(1')-C(36')-C(37')	113.9(7)	C(42')-C(43')-Na(1)	78.9(8)
C(38)-O(2)-C(40)	112.1(2)	O(3')-C(44')-C(45')	112.5(6)
C(38)-O(2)-Na(1)	121.29(19)		
C(40)-O(2)-Na(1)	125.41(18)		
O(2)-C(38)-C(39)	107.6(2)		
O(2)-C(40)-C(41)	112.5(3)		

Symmetry transformations used to generate equivalent atoms:

Table A.38. Crystal data and structure refinement for 6996.

Identification code	6996	
Empirical formula	C33.5 H45 N3	
Formula weight	489.73	
Temperature	100(2) K	
Wavelength	0.71073 Å	
Crystal system	Monoclinic	
Space group	P21/n, No. 14	
Unit cell dimensions	a = 8.4772(12) Å	α= 90°.
	b = 29.510(4) Å	β= 91.744(4)°.
	c = 24.084(3) Å	γ = 90°.
Volume	6022.1(14) $Å^3$	
Z	8	
Density (calculated)	1.080 Mg/m^3	
Absorption coefficient	0.63 mm^{-1}	
F(000)	2136	
Crystal size	0.03 x 0.02 x 0.02 mm	
Theta range for data collection	2.18 to 25.50°.	
Index ranges	-10<=h<=10, -35<=k<=35, -29<=l<=29	
Reflections collected / unique	95705	
Independent reflections	10934 [R(int) = 0.0530]	
Completeness to theta = 29.13°	97.5%	
Absorption correction	Gaussian	
Max. and min. transmission	0.9987 and 0.9981	
Refinement method	Full-matrix least-squares on F^2	
Data / restraints / parameters	10934 / 7 / 690	
Goodness-of-fit on F^2	1.055	
Final R indices [I>2sigma(I)]	R1 = 0.0438, wR2 = 0.1097	
R indices (all data)	R1 = 0.0593, wR2 = 0.1198	
Largest diff. peak and hole	0.293 and -0.299 $e.Å^{-3}$	

Table A.39. Atomic coordinates (x 10^4) and equivalent isotropic displacement parameters (A^2 x 10^3) for 6996. U(eq) is defined as one third of the trace of the orthogonalized Uij tensor.

	x	y	z	U(eq)
C(1)	4462(2)	3109(1)	7693(1)	25(1)
C(2)	5094(2)	3046(1)	8229(1)	28(1)
C(3)	6478(2)	2806(1)	8319(1)	29(1)
C(4)	7275(2)	2626(1)	7874(1)	27(1)
C(5)	6678(2)	2670(1)	7330(1)	23(1)
C(6)	5245(2)	2907(1)	7252(1)	21(1)
N(7)	4604(2)	2974(1)	6703(1)	22(1)
C(8)	3663(2)	2679(1)	6504(1)	21(1)
C(9)	2896(2)	2729(1)	5950(1)	19(1)
C(10)	3118(2)	3111(1)	5621(1)	22(1)
C(11)	2339(2)	3132(1)	5108(1)	25(1)
C(12)	1389(2)	2773(1)	4936(1)	23(1)
C(13)	1245(2)	2403(1)	5291(1)	19(1)
C(15)	256(2)	2004(1)	5154(1)	20(1)
N(14)	1971(2)	2380(1)	5793(1)	20(1)
N(16)	-413(1)	1950(1)	4681(1)	20(1)
C(17)	-1386(2)	1558(1)	4597(1)	21(1)
C(18)	-733(2)	1123(1)	4548(1)	24(1)
C(19)	-1775(2)	764(1)	4442(1)	31(1)
C(20)	-3384(2)	833(1)	4384(1)	34(1)
C(21)	-3998(2)	1265(1)	4429(1)	32(1)
C(22)	-3024(2)	1637(1)	4532(1)	25(1)
C(23)	2957(2)	3384(1)	7596(1)	32(1)
C(24)	1528(2)	3118(1)	7767(1)	62(1)
C(25)	3015(2)	3840(1)	7894(1)	47(1)
C(26)	7538(2)	2482(1)	6831(1)	27(1)
C(27)	8259(2)	2869(1)	6495(1)	34(1)
C(28)	8812(2)	2133(1)	6984(1)	36(1)
C(29)	1042(2)	1032(1)	4587(1)	29(1)
C(30)	1629(2)	866(1)	4029(1)	34(1)
C(31)	1490(2)	698(1)	5051(1)	46(1)
C(32)	-3658(2)	2115(1)	4599(1)	30(1)
C(33)	-3831(2)	2235(1)	5216(1)	34(1)
C(34)	-5227(2)	2199(1)	4286(1)	42(1)
C(41)	5036(2)	-833(1)	3548(1)	26(1)
C(42)	5777(2)	-1233(1)	3722(1)	32(1)
C(43)	7298(2)	-1338(1)	3574(1)	34(1)
C(44)	8117(2)	-1042(1)	3245(1)	31(1)
C(45)	7438(2)	-637(1)	3056(1)	26(1)
C(46)	5889(2)	-540(1)	3206(1)	23(1)
N(47)	5181(2)	-118(1)	3036(1)	23(1)
C(48)	4278(2)	-119(1)	2608(1)	23(1)
C(49)	3425(2)	292(1)	2415(1)	20(1)
C(50)	3485(2)	698(1)	2714(1)	22(1)
C(51)	2611(2)	1065(1)	2518(1)	23(1)
C(52)	1717(2)	1017(1)	2030(1)	21(1)
C(53)	1735(2)	602(1)	1754(1)	19(1)
N(54)	2565(2)	241(1)	1941(1)	21(1)
C(55)	798(2)	527(1)	1237(1)	21(1)
N(56)	17(2)	843(1)	1001(1)	21(1)

C(57)	-931(2)	739(1)	517(1)	21(1)
C(58)	-247(2)	705(1)	-7(1)	23(1)
C(59)	-1258(2)	611(1)	-459(1)	27(1)
C(60)	-2870(2)	554(1)	-399(1)	30(1)
C(61)	-3517(2)	607(1)	118(1)	29(1)
C(62)	-2565(2)	711(1)	582(1)	24(1)
C(63)	3391(2)	-705(1)	3730(1)	32(1)
C(64)	2454(2)	-1100(1)	3961(1)	40(1)
C(65)	3492(3)	-320(1)	4157(1)	43(1)
C(66)	8389(2)	-305(1)	2717(1)	30(1)
C(67)	9462(3)	-23(1)	3100(1)	47(1)
C(68)	9350(3)	-539(1)	2277(1)	54(1)
C(69)	1510(2)	793(1)	-69(1)	28(1)
C(70)	1864(2)	1302(1)	2(1)	37(1)
C(71)	2143(2)	619(1)	-614(1)	40(1)
C(72)	-3250(2)	796(1)	1153(1)	29(1)
C(73)	-4858(2)	1028(1)	1123(1)	37(1)
C(74)	-3331(2)	359(1)	1491(1)	39(1)
C(81)	2690(30)	-1209(10)	1724(15)	81(2)
C(82)	3912(9)	-1517(2)	1451(3)	61(1)
C(83)	5427(12)	-1545(6)	1801(6)	57(1)
C(84)	6664(8)	-1840(2)	1491(3)	52(1)
C(85)	8171(10)	-1844(4)	1820(4)	70(1)
C(81')	2944(12)	-1291(4)	1801(6)	81(2)
C(82')	4468(5)	-1473(1)	2087(2)	61(1)
C(83')	5719(6)	-1564(3)	1672(2)	57(1)
C(84')	7163(4)	-1797(1)	1962(1)	52(1)
C(85')	8445(5)	-1871(2)	1556(2)	70(1)

Table A.40. Bond lengths [A] and angles [°] for 6996.

C(1)-C(2)	1.394(2)	C(18)-C(19)	1.398(2)
C(1)-C(6)	1.404(2)	C(18)-C(29)	1.529(2)
C(1)-C(23)	1.524(2)	C(19)-C(20)	1.382(3)
C(2)-C(3)	1.381(2)	C(20)-C(21)	1.384(3)
C(3)-C(4)	1.391(2)	C(21)-C(22)	1.391(2)
C(4)-C(5)	1.396(2)	C(22)-C(32)	1.520(2)
C(5)-C(6)	1.408(2)	C(23)-C(24)	1.511(3)
C(5)-C(26)	1.529(2)	C(23)-C(25)	1.525(3)
C(6)-N(7)	1.4284(19)	C(26)-C(28)	1.528(2)
N(7)-C(8)	1.265(2)	C(26)-C(27)	1.536(2)
C(8)-C(9)	1.475(2)	C(29)-C(30)	1.528(2)
C(9)-N(14)	1.3422(19)	C(29)-C(31)	1.529(3)
C(9)-C(10)	1.394(2)	C(32)-C(34)	1.529(2)
C(10)-C(11)	1.385(2)	C(32)-C(33)	1.538(2)
C(11)-C(12)	1.386(2)	C(41)-C(42)	1.395(2)
C(12)-C(13)	1.396(2)	C(41)-C(46)	1.409(2)
C(13)-N(14)	1.3403(19)	C(41)-C(63)	1.523(2)
C(13)-C(15)	1.476(2)	C(42)-C(43)	1.383(3)
C(15)-N(16)	1.2655(19)	C(43)-C(44)	1.380(2)
N(16)-C(17)	1.4312(19)	C(44)-C(45)	1.397(2)
C(17)-C(18)	1.404(2)	C(45)-C(46)	1.402(2)
C(17)-C(22)	1.411(2)	C(45)-C(66)	1.522(2)

C(46)-N(47)	1.436(2)
N(47)-C(48)	1.266(2)
C(48)-C(49)	1.480(2)
C(49)-N(54)	1.345(2)
C(49)-C(50)	1.397(2)
C(50)-C(51)	1.386(2)
C(51)-C(52)	1.385(2)
C(52)-C(53)	1.395(2)
C(53)-N(54)	1.3458(19)
C(53)-C(55)	1.475(2)
C(55)-N(56)	1.269(2)
N(56)-C(57)	1.430(2)
C(57)-C(62)	1.401(2)
C(57)-C(58)	1.407(2)
C(58)-C(59)	1.394(2)
C(58)-C(69)	1.524(2)
C(59)-C(60)	1.390(2)
C(60)-C(61)	1.383(2)
C(61)-C(62)	1.393(2)
C(62)-C(72)	1.529(2)
C(63)-C(64)	1.527(2)
C(63)-C(65)	1.532(3)
C(66)-C(67)	1.522(3)
C(66)-C(68)	1.523(3)
C(69)-C(71)	1.522(2)
C(69)-C(70)	1.540(2)
C(72)-C(73)	1.525(2)
C(72)-C(74)	1.527(2)
C(81)-C(82)	1.539(14)
C(82)-C(83)	1.517(10)
C(83)-C(84)	1.570(9)
C(84)-C(85)	1.483(8)
C(81')-C(82')	1.541(10)
C(82')-C(83')	1.504(5)
C(83')-C(84')	1.552(6)
C(84')-C(85')	1.499(5)

C(2)-C(1)-C(6)	117.78(15)
C(2)-C(1)-C(23)	120.68(14)
C(6)-C(1)-C(23)	121.54(14)
C(3)-C(2)-C(1)	120.98(15)
C(2)-C(3)-C(4)	120.32(15)
C(3)-C(4)-C(5)	121.12(15)
C(4)-C(5)-C(6)	117.30(14)
C(4)-C(5)-C(26)	122.34(15)
C(6)-C(5)-C(26)	120.35(14)
C(1)-C(6)-C(5)	122.39(14)
C(1)-C(6)-N(7)	117.80(14)
C(5)-C(6)-N(7)	119.66(13)
C(8)-N(7)-C(6)	118.14(13)
N(7)-C(8)-C(9)	121.93(14)
N(14)-C(9)-C(10)	123.22(14)
N(14)-C(9)-C(8)	114.60(13)
C(10)-C(9)-C(8)	122.18(14)
C(11)-C(10)-C(9)	118.33(14)
C(10)-C(11)-C(12)	119.33(14)
C(11)-C(12)-C(13)	118.39(14)
N(14)-C(13)-C(12)	123.04(14)
N(14)-C(13)-C(15)	113.91(13)
C(12)-C(13)-C(15)	123.04(13)
N(16)-C(15)-C(13)	122.60(13)
C(13)-N(14)-C(9)	117.68(13)
C(15)-N(16)-C(17)	118.09(13)
C(18)-C(17)-C(22)	122.05(14)
C(18)-C(17)-N(16)	121.54(14)
C(22)-C(17)-N(16)	116.31(14)
C(19)-C(18)-C(17)	117.36(15)
C(19)-C(18)-C(29)	119.51(15)
C(17)-C(18)-C(29)	123.09(14)
C(20)-C(19)-C(18)	121.54(16)
C(19)-C(20)-C(21)	120.00(16)
C(20)-C(21)-C(22)	121.25(16)
C(21)-C(22)-C(17)	117.79(15)
C(21)-C(22)-C(32)	122.73(15)
C(17)-C(22)-C(32)	119.44(14)
C(24)-C(23)-C(1)	110.80(16)
C(24)-C(23)-C(25)	110.12(16)
C(1)-C(23)-C(25)	112.47(15)
C(28)-C(26)-C(5)	113.99(14)
C(28)-C(26)-C(27)	109.69(14)
C(5)-C(26)-C(27)	110.53(13)
C(30)-C(29)-C(18)	110.47(14)
C(30)-C(29)-C(31)	110.86(14)
C(18)-C(29)-C(31)	112.31(15)
C(22)-C(32)-C(34)	113.77(16)
C(22)-C(32)-C(33)	111.12(14)
C(34)-C(32)-C(33)	109.42(14)
C(42)-C(41)-C(46)	117.49(15)
C(42)-C(41)-C(63)	122.14(14)
C(46)-C(41)-C(63)	120.34(14)
C(43)-C(42)-C(41)	121.73(15)
C(44)-C(43)-C(42)	119.71(16)
C(43)-C(44)-C(45)	121.27(16)
C(44)-C(45)-C(46)	118.09(15)
C(44)-C(45)-C(66)	120.40(15)
C(46)-C(45)-C(66)	121.45(14)
C(45)-C(46)-C(41)	121.70(14)
C(45)-C(46)-N(47)	119.38(13)
C(41)-C(46)-N(47)	118.81(14)
C(48)-N(47)-C(46)	117.83(13)
N(47)-C(48)-C(49)	122.10(14)
N(54)-C(49)-C(50)	122.98(14)
N(54)-C(49)-C(48)	114.88(13)
C(50)-C(49)-C(48)	122.12(14)
C(51)-C(50)-C(49)	118.85(14)
C(52)-C(51)-C(50)	118.91(14)
C(51)-C(52)-C(53)	118.58(14)
N(54)-C(53)-C(52)	123.38(14)
N(54)-C(53)-C(55)	115.25(13)
C(52)-C(53)-C(55)	121.36(13)
C(49)-N(54)-C(53)	117.28(13)
N(56)-C(55)-C(53)	121.90(14)

C(55)-N(56)-C(57)	118.59(13)	C(45)-C(66)-C(67)	110.15(15)
C(62)-C(57)-C(58)	122.18(14)	C(45)-C(66)-C(68)	112.62(15)
C(62)-C(57)-N(56)	117.01(13)	C(67)-C(66)-C(68)	110.31(16)
C(58)-C(57)-N(56)	120.59(14)	C(71)-C(69)-C(58)	113.45(14)
C(59)-C(58)-C(57)	117.04(14)	C(71)-C(69)-C(70)	110.67(14)
C(59)-C(58)-C(69)	122.44(14)	C(58)-C(69)-C(70)	110.11(13)
C(57)-C(58)-C(69)	120.44(14)	C(73)-C(72)-C(74)	110.44(14)
C(60)-C(59)-C(58)	121.65(14)	C(73)-C(72)-C(62)	113.30(14)
C(61)-C(60)-C(59)	119.95(16)	C(74)-C(72)-C(62)	111.39(14)
C(60)-C(61)-C(62)	120.71(15)	C(83)-C(82)-C(81)	111.3(14)
C(61)-C(62)-C(57)	118.24(14)	C(82)-C(83)-C(84)	109.4(9)
C(61)-C(62)-C(72)	122.05(14)	C(85)-C(84)-C(83)	109.1(7)
C(57)-C(62)-C(72)	119.71(14)	C(83')-C(82')-C(81')	111.3(6)
C(41)-C(63)-C(64)	113.90(15)	C(82')-C(83')-C(84')	110.1(4)
C(41)-C(63)-C(65)	110.18(15)	C(85')-C(84')-C(83')	110.4(3)
C(64)-C(63)-C(65)	109.95(14)		